Investigation and Application of γH2AX as a Potential Biomarker of DNA Double-Strand Breaks in Insect and Human cells

A thesis submitted to the University of Adelaide

for the degree of Doctor of Philosophy

Mohammad Sabbir Siddiqui

Discipline of Science

School of Agriculture Food and Wine, University of Adelaide

&

Nutritional Genomics & Genome Health Diagnostics Research Laboratory

Commonwealth Scientific & Industrial Research Organization (CSIRO)

Health and Biosecurity

August 2016

Abstract

Double strand breaks (DSBs) are one of the most biologically significant DNA damage lesions. Replication stress, endogenous reactive oxygen species, exogenous sources of DNA damage such as ionizing radiation (IR), and genotoxic compounds are key causes of DNA breaks in living systems. An early known response to DNA DSBs in the cell is the phosphorylation of the C-terminal of the core histone protein H2AX (termed γH2AX when phosphorylated). It is accepted that with the passage of time, the level of γH2AX declines as repair of DSBs is completed; however, DSBs can remain unrepaired and may result in persistent γH2AX signals and the knowledge of persistent γH2AX signals remain relatively unexplored. DNA damage has been associated with some age-related diseases, including the neurodegenerative disorder, Alzheimer's disease (AD). The aim of this PhD thesis was to (i) investigate IR-induced persistent γH2AX responses in Queensland fruit fly (Q-fly) (*Bactrocera tryoni*), and human buccal cell as a model system (ii) quantify endogenous γH2AX levels in buccal cells and lymphocytes of individuals with mild cognitive impairment (MCI) and AD relative to healthy controls in the Australian Imaging, Biomarkers and Lifestyle Flagship Study of Ageing (AIBL) and the South Australian Alzheimer's Nutrition and DNA Damage (SAND) studies. Persistent and dose-dependent γH2AB (a homologue of γH2AX) signals were detected and quantified either by Western blot or laser scanning cytometry (LSC) for up to 17 days post-IR exposure in adult Q-flies (when irradiated as pupae). In human buccal cells irradiated (up to 4 Gy), LSC and visual scoring demonstrated a significant increase in γH2AX (n=6 individuals). Twenty-four hours after IR exposure the γH2AX levels remained significantly higher than baseline. The frequency of visually scored

γH2AX in human buccal cell nuclei showed a strong positive correlation (up to r=0.999) with automated LSC scored γH2AX signals.

In the SAND study, the endogenous γH2AX levels were significantly higher in lymphocytes from AD (n=20) compared to MCI (n=18) and controls (n=40). Plasma homocysteine, creatinine, and chitinase-3-like protein 1 (CHI3L1) were positively correlated with lymphocyte γH2AX signals, whilst glomerular filtration rate (GFR) was negatively correlated. In buccal cells, the endogenous γH2AX levels were significantly elevated in AD (n=16), compared to MCI (n=18) and controls (n=17), from the AIBL study. Nuclear circularity (irregular nuclear shapes) was significantly higher in buccal cell nuclei from AD compared to MCI and controls and there was a positive correlation between nuclear circularity and γH2AX signals. The elevated γH2AX levels in lymphocytes and buccal cells of AD patients may indicate defects in the efficiency of repairing the chronic endogenous DNA DSBs contributing to the accumulation of unrepaired or persistent DSBs. The measurement of persistent and endogenous γH2AX may have application in radiation biodosimetry as well as a potential biomarker in AD.

Declaration of Originality

I certify that this thesis does not, to the best of my knowledge and belief:

i. incorporate without acknowledgment any material previously submitted for a degree of diploma in any institution of higher education;

ii. contain any material previously published or written by another person except where due reference is made in the text of this thesis; or

iii. contain any defamatory material

Mohammad Sabbir Siddiqui (August, 2016)

Acknowledgments

I would like to express my special thanks to Dr. Wayne Leifert for his contributions of time, scientific ideas, and especially encouraging me to improve my scientific writing skills in English during my PhD pursuit. I find myself so fortunate to have such a lively, enthusiastic, and energetic supervisor like you. Your valuable guidance and precious lesson of life have contributed immensely to my personal and professional time throughout my PhD journey.

I would also like to thank Professor Michael Fenech for encouraging my research and for his scientific advice, knowledge and many insightful discussions and suggestions. Your advice on both research as well as on my career have been invaluable.

I would especially like to thank Dr. Richard Glatz for his helpful career advice and being supportive in every steps of my PhD journey. I genuinely appreciate your response in signing all my PhD related official documents in a timely manner.

Very special thanks is extended to Dr. Maxime François who set up the laser scanning cytometry protocol. I am especially grateful to Dr. Maxime François and Tori Nguyen for processing buccal sample onto microscopic slide.

I also thank the wonderful staff in the CSIRO Nutrigenomics lab, in particular Tori Nguyen, Tina Mccarthy, Ms Maryam Hor, and Ms Theodora for always being so helpful and friendly. People here are genuinely nice and helpful. I will always remember this gesture of yours throughout my life.

Words cannot express how grateful I am to my family- Dad, Mom, siblings for their love and encouragement. Special thanks goes to my wife Shanjeeda Shafi who is also doing PhD. Your sacrifices and controlling temper during tuff period of our PhD journey was instrumental in instilling confidence. You are the one who let me finish my degree. To my beloved daughter Sharnaz Shehrin Siddiqui and Suvaina Zerzain Siddiqui, I would like to express my thanks for being such a good girl always cheering

me up and listening to my words. Finally, I thank my God, for letting me through all the difficulties in my PhD journey.

Publication Arising from This Thesis

Mohammad Sabbir Siddiqui, Maxime François, Michael F. Fenech & Wayne R. Leifert. (2015) Persistent γH2AX: A promising molecular marker of DNA Damage. Mutation Research Reviews in Mutation Research. 2015 Oct-Dec;766:1-19. dOI: 10.1016/j.mrrev.2015.07.001

Mohammad Sabbir Siddiqui, Maxime François, Michael Fenech, Wayne R. Leifert. (2014) γH2AX responses in human buccal cells exposed to ionizing radiation. Cytometry A. 2015 Apr;87(4):296-308. doi: 10.1002/cyto.a.22607.

Mohammad Sabbir Siddiqui, Erika Filomeni, Maxime François, Sam R Collins, Tamara cooper, Richard V Glatz, Phil W Taylor, Michael Fenech, Wayne R Leifert. (2013) Exposure of insect cells to ionizing radiation in vivo induces persistent phosphorylation of a H2AX homologue (H2AvB). Mutagenesis. 2013 Sep;28(5):531-41. doi: 10.1093/mutage/get030.

Mohammad Sabbir Siddiqui, Maxime François, Ralph N. Martins, Stephanie R. Rainey-Smith, Colin L. Masters, David Ames, Christopher C. Rowe, S. Lance Macaulay, Michael Fenech, Wayne R Leifert. γH2AX in human buccal cells is significantly associated with Alzheimer's disease in the Australian Imaging, Biomarkers and Lifestyle Flagship Study of Ageing (AIBL). **In preparation.**

Mohammad Sabbir Siddiqui, Maxime François, Jane Hecker, Jeffrey Faunt, Sau Lai Lee, Philip Thomas, Michael Fenech, Wayne Leifert. Elevated γH2AX Level in Peripheral Blood Lymphocytes Identifies Alzheimer's Disease in the South Australian

Neurodegeneration, Nutrition and DNA Damage (SAND) Study of Aging. **In preparation.**

Presentation Arising from This Thesis

Mohammad Sabbir Siddiqui, Maxime François Michael Fenech and Wayne R. Leifert. γH2AX responses in human buccal cells exposed to ionizing radiation. 14th IWRDD (2016), Melbourne.

Mohammad Sabbir Siddiqui, Erika Filomeni, Maxime François, Samuel R. Collins, Richard V.Glatz, Phillip W. Taylor, Michael Fenech and Wayne R. Leifert. Exposure of Insect Cells to Ionizing Radiation in vivo Induces Persistent Phosphorylation of Histone (H2AvB), *Bactrocera tryoni*. FAOBMB, (2013), Singapore.

Mohammad Sabbir Siddiqui, Erika Filomeni, Maxime François, Samuel R. Collins, Richard V. Glatz, Phillip W. Taylor, Michael Fenech and Wayne R. Leifert. (2012) γH2AX is a biomarker of ionizing radiation induced DNA damage in the fruit fly, *Bactrocera tryoni*. ComBio 2012. Adelaide, Australia.

Award Arising from This Thesis

AINSE Young Investigator Awards at the international workshop on radiation damage to DNA (14th IWRDD- 2016).

$21,000 allowance + $45,000 operational - Top-up PhD scholarship from CSIRO P-Health Flagship – 2013-2015.

$1000 Travel award to attend FAOBMB conference in Singapore.

Abbreviations

Alzheimer's disease (AD)
Amyloid β peptides (Aβ)
Area under the curve (AUC)
Ataxia Telangiectasia (AT)
Ataxia Telangiectasia and Rad3- related protein (ATR)
Ataxia telangiectasia mutated (ATM)
Australian Imaging Biomarkers and Lifestyle Flagship Study of Ageing (AIBL)

Bovine serum albumin (BSA)
Buccal micronucleus cytome (BMCyt)

Cerebrospinal fluid (CSF)
Computed tomography (CT) scan
Cytolethal distending toxin (CDT)

Dimethylamino benzoylphenylurea (BPU)
DNA damage response (DDR)
DNA protein kinase catalytic subunit (DNA-PKcs)
DNA-dependent protein kinase (DNA-PK).
Double-strand breaks (DSBs)
Dulbecco's phosphate buffered saline (DBPS)

Enhanced chemi luminescence (ECL)

Fanconi anemia (FA)
^{18}F-Fluorodeoxyglucose (FDG)
Foetal bovine serum (FBS)

Guggulsterone (GS)

Herpes simplex virus thymidine kinase (HSV-TK)
Histone protein H2AX (termed γH2AX)
HuaChanSu (HCS)
Human embryonic stem cells (hES)

Ionising radiation (IR)

Laser scanning cytometry (LSC)

Mediator of DNA damage checkpoint (MDC1)

Mild cognitive impairment (MCI)
Mini-mental state examination (MMSE)
Mitomycin C (MMC)
MRE11-RAD50-NBS1 (MRN)

Nijmegen breakage syndrome (NBS)
Non-fanconi anemia bone marrow failure (non-FABMF)
Normal tissue toxicity (NTT)

Paraformaldehyde (PFA)
Peptide receptor radionuclide therapy (PRRT)
Percutaneous transluminal angioplasty (PTA)
Peripheral blood lymphocytes (PBLs)
Peripheral blood mononuclear cells (PBMCs)
Phosphate-buffered saline (PBS)
Phosphatidyl insositol 3'-kinase related protein kinase (PIKK)
Pittsburgh B (PiB)
Positron emission tomography (PET)
Protein phosphatase 2A (PP2A)

Queensland fruit fly ('Q-fly' *Bactrocera tryoni*)

RABiT (Rapid Automated Biodosimetry Tool for Radiological Triage)
Radio-immune precipitation assay (RIPA)
Radiotherapy (RT)
RCT (radiotherapy in combination with chemotherapy)
Receiver-operating characteristic curves (ROC)

Roswell Park Memorial Institute (RPMI)

Senescence-associated secretory phenotype (SASP)
Senescence-associated β-galactosidase (SA- β -gal)
Shwachman–Diamond syndrome (SDS)
Standard error of the mean (SEM)
Sterile insect technique (SIT)
Structural magnetic resonance imaging (MRI)
South Australian Neurodegeneration, Nutrition, and DNA damage (SAND)

Tris buffer saline (TBS)

Werner syndrome (WS)

β-amyloid precursor protein (APP)

4’,6-diamidino-2-phenylindole (DAPI)

Table of Contents

List of Tables

List of Figures

Statement of Authorship

Publication

Mohammad Sabbir Siddiqui, Maxime François, Michael F. Fenech & Wayne R. Leifert. (2015) Persistent γH2AX: A promising molecular marker of DNA damage and aging. ***Mutation Research Reviews in Mutation Research***. 2015 Oct-Dec;766:1-19. doi: 10.1016/j.mrrev.2015.07.001.

Mohammad Sabbir Siddiqui (PhD candidate)

Wrote manuscript and contributed to planning of article.

Signed Date 10.08.2016

Maxime François

Contribute to planning of article and provide critical evaluation of the manuscript.

Signed . Date 13.07.2016

Michael Fenech

Contribute to planning of article and provide critical evaluation of the manuscript.

Signed .. Date 10-08-2016

Wayne R. Leifert

Contribute to planning of article and provide critical evaluation of the manuscript.

Signed

Date 13/7/2016

Chapter 1: Persistent γH2AX: A Promising Molecular Marker of DNA Damage and Aging

Authors:

Mohammad Sabbir Siddiqui [1, 2], Maxime François [1], Michael F. Fenech [1] and Wayne R. Leifert [1].

Affiliations:

[1] CSIRO Food and Nutrition Flagship, Genome Health and Healthy Aging, Adelaide, South Australia, 5000, Australia.

[2] University of Adelaide, School of Agriculture, Food & Wine, Urrbrae, South Australia, 5064, Australia.

Keywords: γH2AX, ionizing radiation, DNA damage, aging

Running title:

Persistence of γH2AX

Abstract

One of the earliest cellular responses to DNA double strand breaks (DSBs) is the phosphorylation of the core histone protein H2AX (termed γH2AX). Persistent γH2AX is the level of γH2AX above baseline, measured at a given time-point beyond which DNA DSBs are normally expected to be repaired (and usually persist for days to months). This review summarises the concept of persistent γH2AX in the context of exogenous source induced DNA DSBs (e.g. ionizing radiation (IR), chemotherapeutic drugs, genotoxic agents), and endogenous γH2AX levels in normal aging and accelerated aging disorders. Summary of the current literature demonstrates the following (i) γH2AX persistence is a common phenomenon that occurs in humans and animals; (ii) nuclei retain persistent γH2AX foci for up to several months after IR exposure, allowing for retrospective biodosimetry; (iii) the combination of various radiosensitizing drugs with ionizing radiation exposure leads to persistent γH2AX response, thus enabling the potential for monitoring cancer patients' response to chemotherapy and radiotherapy as well as tailoring cancer treatments; (iv) persistent γH2AX accumulates in telomeric DNA and in cells undergoing cellular senescence; and (v) increased endogenous γH2AX levels may be associated with diseases of accelerated aging. In summary, measurement of persistent γH2AX could potentially be used as a marker of radiation biodosimetry, evaluating sensitivity to therapeutic genotoxins and radiotherapy, and exploring the association of unrepaired DNA DSBs on telomeres with diseases of accelerated aging.

1.1 Introduction

Double strand breaks (DSBs) in DNA may lead to genetic instabilities and gene mutation resulting in reduced integrity of the genome and survival of the organism (Dugle, Gillespie & Chapman 1976, Olive 1998). Replication stress, endogenous reactive oxygen species, exogenous sources of DNA damage such as ionizing radiation (IR), and genotoxic compounds are key causes of DNA breaks in living systems (Mah, El-Osta & Karagiannis 2010). To repair these lesions, the DNA damage response (DDR) is initiated at the site of DNA damage (Sharpless, DePinho 2007, Ward, Chen 2004). An early known response to DNA DSBs in the cell is the phosphorylation of the C-terminal of the core histone protein H2AX (termed γH2AX when phosphorylated) (Rogakou et al. 1998, Savic et al. 2009). The phosphorylation of H2AX occurs at the highly conserved amino acid Ser139 contained in the SQ (serine/glutamine) motif near the carboxy-terminus of H2AX (Redon et al. 2002, Kinner et al. 2008). The phosphoinositide 3-kinase-related protein kinase (PIKK) family which includes Ataxia Telangiectasia Mutated (ATM), Ataxia Telangiectasia and Rad3-related protein (ATR) and DNA protein kinase catalytic subunit (DNA-PKcs) have all been implicated in H2AX phosphorylation (Redon et al. 2002, Kinner et al. 2008). However, ATM is considered as the main kinase for H2AX phosphorylation in response to DSBs under normal physiological conditions and to a greater extent when a cell is exposed to ionizing radiation, such as γ-radiation (Rogakou et al. 1998, Redon et al. 2002, Burma et al. 2001). On the other hand, during replication stress, ATR appears to be involved in H2AX phosphorylation at the site of stalled ‘replication forks’ and DNA-PKcs respond to DSBs during the non-homologous end joining process (Burma et al. 2001, Ward, Chen 2001, McManus, Hendzel 2005, Durocher, Jackson 2001). The role of γH2AX is to recruit associated DDR proteins and ensure the retention of those proteins in the

vicinity of DSB sites (Celeste et al. 2003, Bhogal, Jalali & Bristow 2009, Nakamura et al. 2010, Paull et al. 2000). γH2AX interacts with the mediator of DNA damage check point (MDC1), which in turn recruits p53 binding protein 1 (53BP1) at the vicinity of DNA DSB sites. MDC1 and 53BP1 then interact with the MRE11-RAD50-NBS1 (MRN) complex, and contribute to efficient ATM attachment at the DNA DSBs site (Goodarzi, Jeggo & Lobrich 2010). Phosphorylation of H2AX is an important step in the DDR process and has widely been used as a marker of DNA damage (Bhogal, Jalali & Bristow 2009, Nakamura et al. 2010, Paull et al. 2000, Lou et al. 2006, Kobayashi 2004, Anderson, Henderson & Adachi 2001, Furuta et al. 2003).

It has been previously estimated in human fibroblasts that approximately 1% of H2AX becomes phosphorylated (γH2AX) per 1 Gy of IR (Rogakou et al. 1998). This appears to approximate 35 DNA DSBs, and hence one might expect 35 γH2AX foci. An antibody for γH2AX was designed to recognize the last nine residues of H2AX including the phosphorylated serine at position 139 (Rogakou et al. 1999). γH2AX signals appear as individual foci when cells are immunostained against fluorescence-coupled antibodies and visualized by fluorescence microscopy. γH2AX is formed in the close vicinity to DSBs within seconds after cells are exposed to IR, and an individual γH2AX foci represents a single DSB with a ratio of 1:1 (Rogakou et al. 1998, Sedelnikova et al. 2002, Rothkamm, Lobrich 2003). After successful repair of DSBs, the γH2AX molecules are dephosphorylated by protein phosphatase 2A (PP2A) and γH2AX foci are no longer detectable with the γH2AX antibody (Paull et al. 2000, Doida, Okada 1969, Chowdhury et al. 2005, Stiff et al. 2004).

The kinetics of γH2AX foci formation and loss have been widely investigated in different cell and tissue types in the context of DSBs induced after exposure *ex vivo* and

in vivo to exogenous DNA damaging agents (Rogakou et al. 1998, Madigan, Chotkowski & Glaser 2002, Roch-Lefevre et al. 2010, Olive, Banath 2004, Sedelnikova et al. 2004). Two types of γH2AX foci have been found in cells: Firstly, transient γH2AX foci that are associated with rapid DSB repair and dephosphorylation of γH2AX to H2AX, usually within minutes to hours. The second type of γH2AX foci are residual and tend to persist for days to months (Figure 1.1). The long-term persistence of "residual γH2AX" has been also termed "excess γH2AX" foci by different groups (Moroni et al. 2013, Lobrich et al. 2005). In this review, we have chosen to use the term "persistent γH2AX" (i.e. the γH2AX level assessed at a given time-point beyond which DSBs are expected to be repaired after initial exposures to DNA damaging agents such as IR, chemotherapeutic drugs, and genotoxic agent minus the baseline γH2AX level). Persistent γH2AX may indicate DNA DSBs that are either in the process of slow, ongoing repair, or DSBs that remain permanently unrepaired due to cellular senescence, apoptosis, or DSBs that remain unrepaired in specific genome sequences such as telomeres (Sedelnikova et al. 2004, Fumagalli et al. 2012, Hewitt et al. 2012, Torudd et al. 2005). DNA DSBs also occur during normal cellular processes including DNA replication, cellular senescence, and exposure to reactive oxygen species. Therefore, endogenous γH2AX foci are formed even in the absence of external DNA damaging agents such as radiation (Bonner et al. 2008). Humans and other mammals follow an intrinsic DNA repair mechanism to repair these endogenous DNA DSBs. However, small defects in the efficiency of repairing the chronic endogenous DNA DSBs for long periods (days, weeks, months and even years) may contribute to the accumulation of unrepaired DSBs on telomeres which can be reflected as persistent γH2AX (Figure 1.2). Measurement of persistent γH2AX in different cell and tissue types could therefore be

used in radiation biodosimetry and cellular radiosensitivity responses during chemo- and radiotherapy, and to identify regions of the genome where DSB fails to repair.

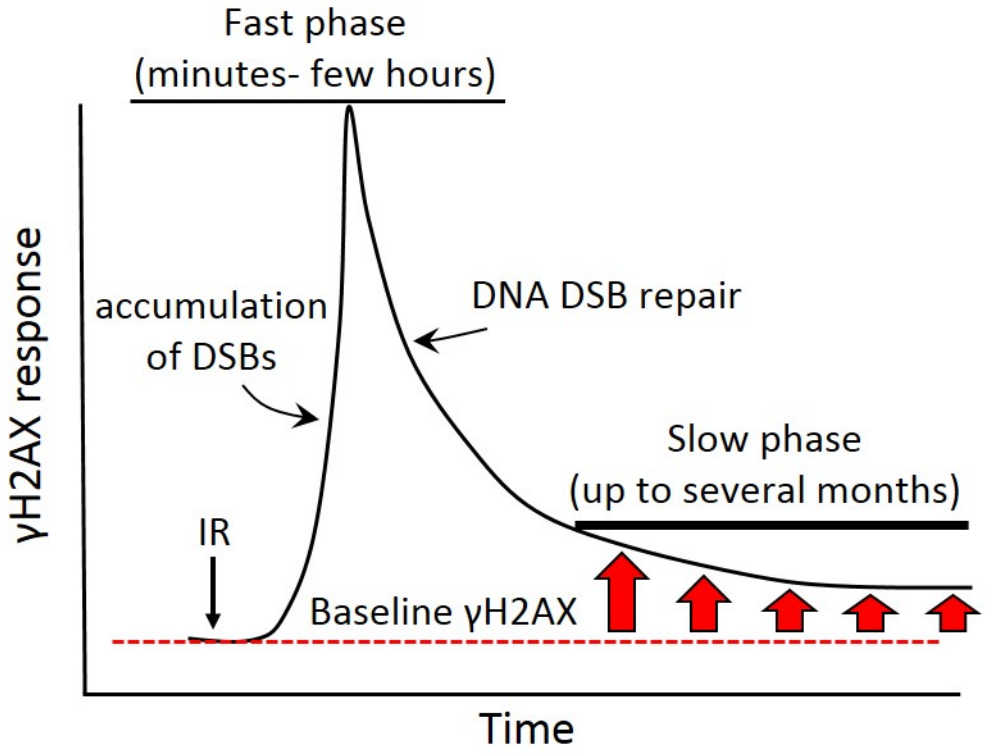

Figure 1.1: Schematic representation of the short-term kinetics and persistent γH2AX response in relation to DSB repair. The kinetics of DNA DSB repair follows two phases, a fast phase lasting up to a few hours which is followed by a slower phase that may persist for several hours to days. Upon exposure to DNA damaging agents such as ionizing radiation (IR), the γH2AX foci appear in the fast phase within minutes after the DSBs are formed, and reach a maximum level after about 30 min. This level then declines rapidly, and corresponds to repair of DNA DSBs. A small portion of γH2AX (above baseline, as indicated by the dashed line) may persist for up to several months (slower phase) after the initial DSB-induction event is known as the persistent γH2AX response (as indicated by the bold red arrows). Persistent γH2AX may represent unrepaired DSBs which are either in the process of slow ongoing repair, that are too complex to repair or associated with telomere DNA DSBs.

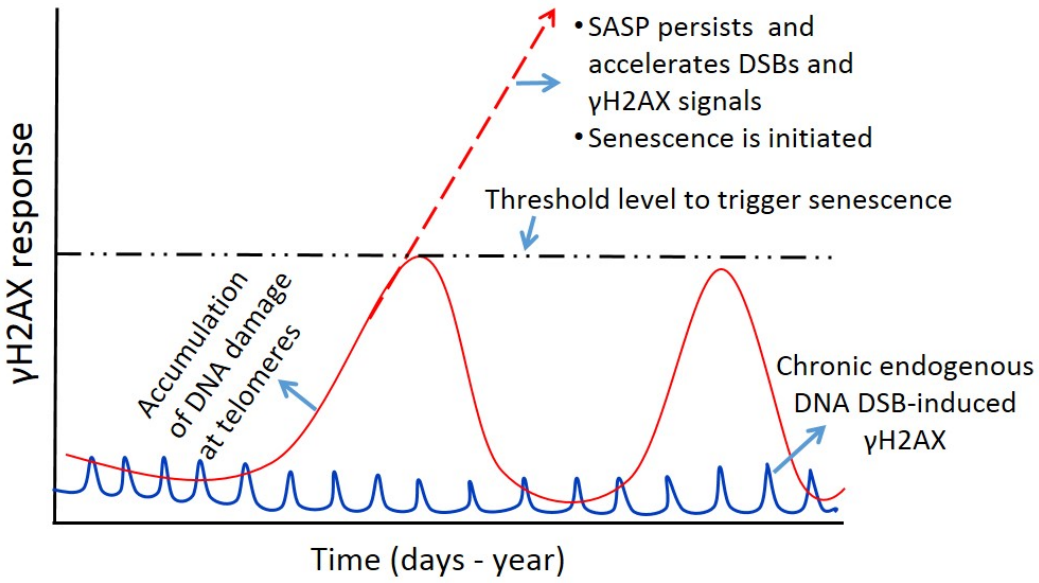

Figure 1.2: Model depicting the possible cause of chronic endogenous DSB-induced persistent γH2AX. The intrinsic DNA repair mechanisms to repair endogenous DSBs occur during common cellular processes, including DNA replication, exposure to reactive oxygen species and cellular senescence. The repair of endogenous DSBs is continuous and rapid, involving recurring transient γH2AX responses. DSBs and γH2AX accumulate in telomere sequences within cells and may ultimately reach a threshold that triggers SASP which put into action the senescence process by which such cells are eliminated. There is therefore two recurring waves of γH2AX foci expression in tissues: the first with short amplitude involving disappearance of γH2AX due to DSB repair and the second with wider amplitude involving elimination of cells with accumulated persistent γH2AX by cellular senescence processes. **Abbreviations:** DSBs, double-strand breaks; SASP, senescence associated secretory phenotype.

IR-induced γH2AX foci formation and loss have been extensively investigated (Rogakou et al. 1998, Madigan, Chotkowski & Glaser 2002, Roch-Lefevre et al. 2010), whereas comparatively few studies have investigated endogenous γH2AX levels in normal aging and accelerated aging disorders. H2AX phosphorylation and DDR have been implicated in diseases of accelerated aging (e.g. Werner syndrome, Alzheimer's disease, obesity, diabetes, sleep apnoea, prostate cancer, cataract disease, hypertension, and Hutchinson-Gilford progeria syndrome) in recent studies (Myung et al. 2008, Sedelnikova et al. 2008, Schurman et al. 2012), suggesting that lack of DNA integrity

due to DNA damage progressively increases with age and may contribute to or be caused by these accelerated aging disorders. To date, no review has explored persistence of γH2AX in different cell and tissue types and discussed the importance of endogenous levels of γH2AX, in human aging and diseases of accelerated aging. The aims of this review are to summarise the findings of persistence of γH2AX in the context of exogenous source induced DSBs in different cell and tissue types, and to further discuss human diseases of accelerated aging that have reported endogenous γH2AX levels as a marker of unrepaired DNA damage.

1.2 Bibliographic Search

The identification and selection of studies reported in this review was carried out through an extensive literature search using the PubMed database (National Library of Medicine, National Institutes of Health, Bethesda, MD, USA; http:// www.ncbi.nih.gov/PubMed, and was up-to date as on April 30th 2015. The search strategy was based on the following keywords: ‘‘persistent gammaH2AX”, “residual gammaH2AX”, “gammaH2AX kinetics”, “unrepaired DNA damage”, “irreparable DNA damage”, “human endogenous gammaH2AX”, “gammaH2AX in age-related diseases”. Eligible studies included in this review were those conducted in humans, or animals, written in English, reporting long-term (>4 hours) persistence of residual or excess γH2AX levels as a marker of either DNA damage or DNA repair (i.e. after *in vitro* or *in vivo* exposure to IR, and after chemotherapeutic or genotoxic drug treatment). Studies in blood cells or other surrogate cells, cancer tissues, biopsies, established cell lines or in cultured cells after treatments were included.

1.3 γH2AX Detection Methods

γH2AX foci can be observed with fluorescence microscopy by immunostaining cells with primary γH2AX antibodies coupled with fluorescent labelled secondary antibodies. The discernible hallmark of γH2AX foci counting is the ability to detect a single DSB in an individual cell (Pilch et al. 2004, Nakamura et al. 2006, Hamasaki et al. 2007). The use of fluorescence can be extended to the measurement of total γH2AX protein level, in particular types of cells and tissues using western blot and flow cytometry techniques (Pilch et al. 2004, Nakamura et al. 2006, Hamasaki et al. 2007). The γH2AX foci counting approach has been used in numerous studies to assess the relationship between γH2AX foci removal and the rate of DSBs repair (Rothkamm, Lobrich 2003, Lassmann et al. 2010, Bouquet, Muller & Salles 2006, Taneja et al. 2004, Siddiqui et al. 2015). In radiation biology the number of DSBs positively correlates with γH2AX foci formation (Rogakou et al. 1998, Rogakou et al. 1999, Sedelnikova et al. 2002). A linear increase of γH2AX foci per cell was proportional to the initial radiation dose 24 h and 48 h after exposure to IR doses ranging from 0.2 to 5 Gy in human blood samples and skin cells (Redon et al. 2009). The highly dynamic changes of foci number and foci size over time after treatment with radiation or cytotoxic compounds can make the visual scoring time-consuming, potentially subjective, operator-dependent, and may involve fluorescence bleaching due to extended evaluation time, therefore making visual scoring unsuitable for high-throughput applications. Several image analysis solutions for automated foci scoring have been developed, but were limited to low IR dose exposure resulting in discrete scoreable foci within the nuclei (Willitzki et al. 2013, Runge et al. 2012). Visual and automated scoring of γH2AX foci formation in rat thyroid cells (PC Cl3) demonstrated a direct correlation between γH2AX foci and radiation dose but was restricted up to 1 Gy of IR (Runge et al. 2012). Following exposure of cells to a dose of

5 Gy, visual scorers were unable to score γH2AX foci due to high density of DSBs which lead to γH2AX foci overlap (diffuse foci). Thus, one of the main issues when scoring multiple foci after exposure to a high radiation dose is the phenomenon of foci overlap that makes it more difficult to distinguish γH2AX as discrete entities (foci) (Willitzki et al. 2013). In that case, measurement of total γH2AX intensity using western blot or flow cytometry image analysis techniques may be sufficient to measure DNA damage levels by quantifying the total fluorescence for γH2AX signals.

Flow cytometry, allows rapid measurement of total γH2AX intensity in a large number of heterogeneous cell populations while enabling assessment of γH2AX intensity in different cell cycle phases and simultaneous measurement of other cellular proteins/markers involved in DNA damage/repair signalling process (Brzozowska et al. 2012). The γH2AX intensity in lymphocytes measured by flow cytometry quantitatively correlated with the number and size of γH2AX foci scored visually by fluorescence microscopy (Brzozowska et al. 2012). The IR-induced γH2AX quantification in the lymphocytes of prostate cancer patients during radiotherapy showed significant differences between patients and healthy donors by use of flow cytometry analysis; however, these results were not always in close agreement with results from fluorescence microscopy (Brzozowska et al. 2012). More recently, the use of laser scanning cytometry has also been proposed as a useful tool to measure cellular DNA content for cell cycle stage evaluation in conjunction with multiple γH2AX parameters (e.g. area, integral, MaxPixel) after inducing DNA damage (Siddiqui et al. 2015, Zhao et al. 2009, Tanaka et al. 2007). The frequency of visually scored γH2AX in human buccal cell nuclei showed a strong correlation with LSC measured γH2AX integral (Siddiqui et al. 2015). Taken together, both microscopy and cytometry-based methods are suitable to evaluate γH2AX formation and loss and the choice of the best γH2AX

assay will depend on the purpose of the study. The image cytometry and LSC methods have an advantage over flow cytometry because they enable counting and sizing of γH2AX foci but they are slower to perform.

1.4 Long-Term Persistence of Residual γH2AX

The decline kinetics of DNA DSB repair appears to follow two distinct phases: a fast phase generally lasting a few hours followed by a slower phase that may persist for several hours or days and may extend to several months (Riballo et al. 2004, Lobrich et al. 2010) (a schematic is shown in Fig. 1.1). The majority of DSBs (~80%) are repaired during the first phase of the repair process and the remaining portion (~20%) repair at a slower pace during the slower phase (Riballo et al. 2004, Lobrich et al. 2010). The slow γH2AX repair kinetics reported in lymphocytes from healthy donors following exposure to IR is consistent with the findings that showed ~25% of residual γH2AX foci at 7 hours after exposure to 4 Gy of IR in lymphocytes (Goodhead 1994, Sharma et al. 2015). Evidence from several studies suggests that 60% of initial IR-induced DSBs are transient and repair in a relatively fast manner, often with half-lives of approximately 1-18 minutes (Kodym, Horth 1995, Nunez et al. 1995). The remaining 40% of DSBs repair slowly, with a repairing half-life in the range of 1.5-8 hours (Kodym, Horth 1995, Nunez et al. 1995, MacPhail et al. 2003b, Ward 1988, Ward 1990). DSBs measured several hours after an initial radiation exposure that still remain unrepaired, may be predictive of individual radiosensitivity to complex DNA lesions that can be lethal (Banath et al. 2010, Bhogal et al. 2010, Djuzenova et al. 2013). The rate of γH2AX foci loss and the presence of residual foci has also been correlated with cellular radiosensitivity and absorbed radiation dose (Taneja et al. 2004, Lobrich et al. 2010, Jeggo, Geuting & Lobrich 2011, MacPhail et al. 2003a, Dikomey et al. 1998, Redon et

al. 2010, Qvarnstrom et al. 2004). Estimation of DSB repair rate from the decline kinetics of γH2AX foci was reported as a useful parameter to evaluate cellular radiosensitivity (Sharma et al. 2015). The persistent γH2AX foci may be present in the form of large foci. For example, in spermatids, the persistent γH2AX foci appeared as larger foci at 48 h after IR exposure (Paris et al. 2011). Large persistent γH2AX foci were also observed in normal human fibroblasts (VH-10) and in HeLa cells after exposure to IR (Markova, Schultz & Belyaev 2007). Additionally, a recent study reported the persistence and larger size of γH2AX foci 6 hours after 3 Gy of high linear energy transfer radiation in a cell line lacking DNA-dependent protein kinase activity (Bracalente et al. 2013). Clinical studies have demonstrated that the stochastic γH2AX foci induction and loss after external and internal radiation exposure in different types of cell depend on (i) the amount or type of IR (e.g high dose (radiotherapy), low dose X-ray examination, or computed tomography (CT) scan), chemotherapeutic drug and genotoxic compound used; (ii) type of sample or part of body exposed to IR; (iii) duration or fractionation of exposure; (iv) inter individual radiosensitivity or damage response; (v) methods to measure γH2AX immunoreactivity; (vi) time-points for the kinetics of γH2AX foci formation and loss; (vii) time elapsed between the exposure and the γH2AX analysis, particularly if genotoxic exposure is acute rather than chronic (Sharma et al. 2015, Zalenskaya, Bradbury & Zalensky 2000, Ismail, Wadhra & Hammarsten 2007).

In the following sections we discuss persistence of γH2AX following *in vitro* and *in vivo* exposure to IR, chemotherapeutic drugs, and genotoxic agents among animals in different cell and tissue types (summarised in Table 1.1).

Table 1.1: Persistent γH2AX response among animals in different cell and tissue types following ionizing radiation

Cells/tissues analysed	Treatment	Cohort/ characteristic of cells	Outcome of γH2AX response	Technique used	Ref
Human					
Lymphocytes	γ rays 2 Gy	Cancer patients: (n=12) with severe NTT after RT (n=10) with little or no NTT and (n=7) healthy, non-cancer control	24 h post-IR γH2AX ↑ by ~ 4x in cancer patients with NTT compared with cancer patients with low NTT or non-cancer control	Flow cytometry	(Bourton et al. 2011)
Lymphocytes	X-rays 1 – 2 Gy	Children with solid tumors received chemotherapy (n=23), Healthy children (n=24)	24h post-IR ↑ foci/nucleus in children with solid tumours compared with age-matched healthy children ↑ foci/nucleus enables identification of children at risk with high-grade toxicities	Visually scored by fluorescence microscopy	(Rube et al. 2010)
Lymphocytes	γ rays 2 Gy	Healthy donor (n=4), AT (n=6) and NBS (n=4) patients	72 h post IR ↑ foci/nucleus by ~ 4-8x in AT and NBS patient's cells	Visually scored by fluorescence microscopy	(Porcedda et al. 2006)
Lymphocytes	X-rays 4 Gy	Breast cancer patient after radiotherapy Control: very little or no damage in normal tissue (n=7), Case: marked damage in normal tissue (n =7)	24 h post-IR ↑ foci/nucleus in case compared with control	Visually scored by fluorescence microscopy	(Chua et al. 2011)
PBMCs	X-rays 4 Gy	Control: healthy donors (n=12) Case: Breast cancer patients undergoing radiotherapy (n=57)	24 h post-IR ↑ foci/nucleus in case compared with untreated healthy control	Visually scored using fluorescence images	(Djuzenova et al. 2013)
Lymphocytes	X-rays 2 Gy	Head and neck cancer patients undergoing radiotherapy (n=54) Untreated control (n=26)	6 h post IR ↑ foci/nucleus in lymphocytes of head-and-neck cancer patients compared with untreated control group	Image captured by fluorescence microscopy followed by foci counting using olympus microimage software.	(Goutham et al. 2012)
Lymphocytes	low dose rate (14.7 cGy/h) and high dose rate (0.5 Gy/min)	Cervix cancer patients (n=12) or endometrial cancer patients (n=17)	24 h post-IR No significant changes in non to mild and moderate to severe late radiotoxicity	Visually scored using fluorescence images	(Werbrouck et al. 2010)

Cells/tissues analysed	Treatment	Cohort/ characteristic of cells	Outcome of γH2AX response	Technique used	Ref
Leucocytes	Radionuclide therapy with the isotope I^{131}	26 Patients with differentiated thyroid carcinoma (7 men, 19 women)	6 days after administration ↑ foci/nucleus	Visually scored using fluorescence images	(Lassmann et al. 2010)
Lymphocytes	Radionuclide therapy with the isotope I^{131}	15 patients with differentiated thyroid carcinoma (8 women, 7 men)	4 days after administration ↑ foci/nucleus	Visually scored using fluorescence images	(Doai et al. 2013)
Lymphocytes	X-rays 60–66 Gy (single dose 2 Gy, five fractions per week)	Head and neck cancer patients (n=31)	24 h post-IR ↑ foci/nucleus predisposed to increased incidence of severe oral mucositis	Visually scored using fluorescence images	(Fleckenstein et al. 2011)
Lymphocytes	CT- 157 to 1,514 mGy·cm	Benign diseases (n=13) and known malignant neoplasms (n= 10)	24 h after CT ↑ foci/nucleus in one patient with rectal cancer showed exceptionally severe side effects after radiotherapy	Visually scored using fluorescence images	(Lobrich et al. 2005)
Lymphocytes	PET involving the use of ^{18}F-fluorodeoxy glucose, and whole-body CT scan	Patients with history of lymphoma or leukaemia (n=33)	24 h after combined PET/CT ↑ foci/nucleus	Visually scored using fluorescence images	(May et al. 2012)
Lymphocytes	PRRT	Neuroendocrine tumors patients undergoing PRRT (n=11)	72 h after treatment foci/nucleus ↓ close to baseline and correlated with absorbed dose to tumors and bone marrow ↓ number of lymphocytes	Visually scored using fluorescence images	(Denoyer et al. 2015)
Lymphocytes	CT- 7.78 per 1 Gy·cm and PTA of lower limb arteries	Patients scheduled for CT (n=5) and patients scheduled for PTA (n=20)	24 h after treatment ↑ foci/nucleus	Visually scored using fluorescence images	(Geisel et al. 2008)
Lymphocytes	γ rays 4 Gy	Healthy donors (n=94)	24 h after treatment ↑ foci/nucleus	Fluorescence microscopy, Image J	(Sharma et al. 2015)
Lymphocytes	γ rays 2 Gy	Healthy donors	24 h to 4 weeks post-treatment ↑foci/nucleus	Fluorescence microscopy, and LSM 510 software	(Markova, Torudd & Belyaev 2011)
Cell lines after isolation of lymphocytes from SDS patients	X-rays 4 10 Gy	SDS patients (n=2) and SDS patient's heterozygous father (n=1)	↑ foci/nucleus in SDS patients compared with sham irradiated control	Visually scored using fluorescence images	(Morini et al. 2015)

Cells/tissues analysed	Treatment	Cohort/ characteristic of cells	Outcome of γH2AX response	Technique used	Ref
Fibroblasts	γ rays 0.6 Gy	Normal human fibroblast cells (IMR90)	270 min post-IR 4.5 foci/nucleus compared to 1.5 foci/nucleus at baseline	Laser scanning confocal microscopy	(Rogakou et al. 1999)
Fibroblasts	γ rays 0.6 Gy	WS patients (n=4) Control donors (n=4)	24 h post-IR ↑ foci/nucleus by ~1.5x in 60 year old WS patients compared with controls	Visually scored by fluorescence microscopy	(Sedelnikova et al. 2008)
Fibroblasts	γ rays 2 Gy	FA patients (n=10) Healthy donor (n=6)	24 h post-IR foci/nucleus ↑ by ~2.5-8x in FA cells compared with non-irradiated control and non-FABMF cells	Fluorescence microscopy, Image J	(Cantor, Brosh 2014)
Fibroblasts	X-rays 10 Gy	Foreskin fibroblasts (HCA2)	6 weeks post-exposure ↑ foci/nucleus	Fluorescence microscopy, Photoshop CS2	(Rodier et al. 2009)
Fibroblasts	Potent human carcinogen chromium Cr(VI) 20 μM	SV40-transformed WRN fibroblasts cell line (AG11395)	24 h after treatment ↑ foci/nucleus	Fluorescence microscopy, Phoenix software	(Lan et al. 2005)
Embryonic stem cells	γ rays 5 Gy	H1 hES cell lines	24 h post-IR dephosphorylation rate was slower in irradiated hES compared with normal somatic lung fibroblasts ↑ foci/nucleus in hES in irradiated hES compared with normal somatic lung fibroblasts	Western blot	(Filion et al. 2009)
Stem cells	X-rays 2 Gy	Healthy volunteers (n = 68) and umbilical cord blood (n = 34)	24 h post-IR Identical decline of foci/nucleus in all cells analysed	Visually scored by fluorescence microscopy	(Rube et al. 2011)
Buccal cells	γ rays 2 Gy	5 healthy individuals (3 females, 2 males, aged 26-47 years)	5 h post-IR ↑ foci/nucleus by ~4x in irradiated cells compared with non-irradiated control	Immunofluorescence and Histolab™ software	(Gonzalez et al. 2010)
Buccal cells	γ rays 4 Gy	6 healthy individuals (3 females and 3 males, aged from 25-44 years)	24 h post-IR Visually scored: % of cell containing foci ↑ by ~3x LSC: integral ↑ by ~3x	Visually scored and laser scanning cytometry	(Siddiqui et al. 2015)

Cells/tissues analysed	Treatment	Cohort/ characteristic of cells	Outcome of γH2AX response	Technique used	Ref
Mouse					
Germ cells	X-rays 4 Gy	10- to 12-week-old C57Bl/6J male mice	% of cell containing foci ↑ by ~6-10x 48 h post IR	Visually scored using fluorescence microscopy	(Paris et al. 2011)
Heart and kidney	X-rays 3 Gy	3 months old C57Bl/6 female mice	23h post-IR % of nuclei containing foci ↑ by ~5-10x	Confocal microscope	(Gavrilov et al. 2006)
Skin biopsies	γ rays 10 Gy	(n=2) 4–6 week old radiosensitive strains (SCID and BALB/c) and (n=2) radioresistant strains (C57BL/6 and C3H/HeJ) male mice	7 days post-IR Radioresistant strains (13-15 foci/100-μm^2 area) > Radiosensitive strains (~4-6 γH2AX foci/ 100-μm^2 area)	Confocal microscopy	(Bhogal et al. 2010)
Spinal cord	X-rays 17 Gy followed by an immediate additional dose of 19 Gy	12 weeks old C3H/N female mice	1 year post-IR Foci were detected	Flow cytometry	(Andratsch ke et al. 2011)
Spleen, thymus, liver, lung, kidney, cerebellum, hippocampus, frontal cortex and olfactory bulb	X-rays 1 Gy	Very young (7 and 14 days old), adolescent (24 days old), young adult (30 days old) and sexually mature adult (45 days old) male and female mice	24 h post-IR Average number of foci/nucleus ↑in Spleen>Thymus> Liver>Lung Average number of foci/nucleus↑ after 7 days > 14 days>24 days >30 days > 45 days	Visually scored using fluorescence microscopy	(Hudson et al. 2011)
Small intestine, lung, brain, heart and kidney	Whole body X-rays 2 Gy	C57BL/6 mice	48 h post-IR ~0.5 foci/nucleus, similar DNA repair kinetics were observed in all tissues.	Visually scored using fluorescence microscopy	(Rube et al. 2008)
Heart, small intestine, and kidney	X-rays 10 mGY,100 mGy, and 1 Gy	C57BL/6 mouse	24 h post-IR 1 Gy: ~< 1 foci/nucleus 100 mGy: ~< 0.2 foci/nucleus 10 mGy: ~< 0.06 foci/nucleus	Visually scored using fluorescence images	(Grudzensk i et al. 2010)
Minipig					
Skin biopsy	γ rays ~50 Gy	14 to 16 months old (n=7) female Göttingen minipig	70 days post-IR Irradiated cells: 0.14 foci/nucleus, non Irradiated cells: 0.05 foci/nucleus	Visually scored using fluorescence images	(Ahmed et al. 2012)

Cells/tissues analysed	Treatment	Cohort/ characteristic of cells	Outcome of γH2AX response	Technique used	Ref
(1)Lymphocytes (2)Fibroblasts	γ rays 1.8 Gy (2) 2 Gy	4 months old male Gottingen minipigs	24 h post-IR ↑ foci/nucleus by up to ~11x ↑ foci/nucleus	Visually scored using fluorescence images	(Moroni et al. 2013)
Fruit Fly					
Pupae	γ rays 0-400 Gy	Pupae were allowed to emerge as adults 17 days post-IR	17 days post-IR 25% of nuclei contained ↑ γH2AvB compared with non-irradiated controls	Western Blot, ImageJ and LSC	(Siddiqui et al. 2013)
Syrian hamsters					
Heart, Brain, liver	X-rays 5 Gy	Male Syrian hamsters	20 h post-IR ↑ foci positive nuclei in heart, brain (not liver) by 3- 4.5x	Visually scored following laser scanning confocal microscopy	(Firsanov et al. 2012)

Abbreviations: AT - Ataxia telangiectasia, ATM - Ataxia telangiectasia mutated, CT - Computed tomography, FA - Fanconi anaemia, hES - Human embryonic stem cells, IR - Ionizing radiation, LSC - Laser scanning cytometry, NTT - Normal tissue toxicity, NBS - Nijmegen breakage syndrome, Non-FABMF - Non Fanconi anemia bone marrow failure, PBMC - Peripheral blood mononuclear cells, PET - Positron emission tomography, PRRT - Peptide receptor radionuclide therapy, PTA - Percutaneous transluminal angioplasty, RT - Radiotherapy, SDS - Shwachman–diamond syndrome, WS - Werner syndrome

1.5 Persistent γH2AX in Human Cells

1.5.1 Peripheral Blood Mononuclear Cells

Human blood lymphocytes have several advantages that make them suitable for evaluating γH2AX foci formation and loss: (i) a limited quantity of blood containing lymphocytes is required for γH2AX assay (1-2 ml) (Sak et al. 2007); (ii) lymphocytes have low γH2AX background levels (0.05 to 0.1 foci/nucleus) (Rogakou et al. 1998, Lobrich et al. 2005, Kasten-Pisula et al. 2007); (iii) the majority of cells are in the G_0 phase of the cell cycle (Ivashkevich et al. 2012); (iv) there is minimal intra-individual variation in the level of γH2AX foci in different subsets of lymphocytes (Andrievski, Wilkins 2009); (v) there is minimal intra-individual variation in γH2AX foci number per lymphocytes, and therefore the assay is relatively efficient at measuring differences

in γH2AX between individuals (Lobrich et al. 2005, Kasten-Pisula et al. 2007, Andrievski, Wilkins 2009).

Radiation therapy used in cancer treatment is applied either alone or in combination with chemotherapy; however, radiation therapy induces severe side-effects (acute effects such as erythema, edema, mucositis, dry or moist desquamation, severe skin changes, and late effects such as telangiectasia, fibrosis, cancer induction, brachial plexopathy, neurological effects) due to normal tissue toxicity (NTT) (Bourton et al. 2011, Werbrouck et al. 2010, Fleckenstein et al. 2011, Turesson et al. 1996, Tucker et al. 1996). NTT has been graded by the Radiation Therapy Oncology Group into a standardized scale of acute and late responses after radiotherapy treatment for all tissue types and these scales are used to avoid severe sequelae of radiotherapy (Cox, Stetz & Pajak 1995). Induction and persistence of γH2AX were assessed in peripheral blood lymphocytes (PBLs) of cancer patients with tumors in breast, thyroid, colon, brain, pituitary, prostate, cervix, and larynx for up to 24 h after 2 Gy of IR exposure (Bourton et al. 2011). The level of γH2AX response remained elevated in lymphocytes of cancer patients who had experienced acute NTT as a consequence of earlier radiotherapy compared to cancer patients who had little or no tissue toxicity as well as non-cancer controls, for up to 24 h after exposure to IR (Bourton et al. 2011). Persistence of γH2AX was significantly higher in lymphocytes from children with pediatric cancer compared with age-matched control children 8 h after exposure of whole blood with 1 Gy and 2 Gy of X-rays. While all healthy children exhibited efficient DNA repair, three children with pediatric cancer had impaired DNA repair capacity and two out of these three children developed acute normal tissue toxicity which may be indicative of impaired DNA repair (Rube et al. 2010). The measure of persistence of γH2AX can be a predictive assay in identifying those individuals at the greatest risk for the development

of adverse effects to radiotherapy or chemotherapy. Additionally the γH2AX assay may be clinically useful to monitor NTT, thus will allow fine-tuning of the applied radiation dose during radiotherapy for improved cancer treatments. Another study reported higher levels of persistence of γH2AX foci per cell in blood lymphocytes of breast cancer patients with chronic late toxicities after radiotherapy compared with minimal late toxicities up to 24 h after exposure to 4 Gy of X-rays (Chua et al. 2011). This result indicates that the persistence of γH2AX is likely associated with breast cancer patients' radiosensitivity. In another study, the mean number of γH2AX foci per cell analyzed in peripheral blood mononuclear cells (PBMCs) of breast cancer patients undergoing radiotherapy was significantly higher compared with untreated healthy controls with respect to the initial (30 min after 0.5 Gy of X-rays) and residual (24 h after exposure to 2 Gy X-rays) γH2AX foci, indicating potential use of γH2AX assay for screening radiosensitivity of breast cancer patients (Djuzenova et al. 2013). The level of γH2AX foci has also been previously measured to predict the side effects of radiotherapy among head and neck cancer patients (Goutham et al. 2012). Persistence of γH2AX was higher in lymphocytes of head and neck cancer patients compared with the untreated control group for up to 6 h after exposure to 2 Gy of X-rays (Goutham et al. 2012). Thus γH2AX would be a useful measure to identify individuals' radiosensitivity in advance so that customized radiation therapy may be applied to avoid severe side-effects due to radiation therapy. Persistence of γH2AX was also significantly higher in lymphocytes of Shwachman–Diamond syndrome individuals (an autosomal-recessive disorder characterized by bone marrow failure and a cumulative risk of progression to acute myeloid leukaemia) compared to sham-irradiated cells 4 h after exposure to 4 Gy and 10 Gy of X-rays or γ-rays (Morini et al. 2015). Interestingly, another group (Werbrouck et al. 2010) found no difference in the persistence of γH2AX foci in T-lymphocytes 24 h

after *ex vivo* exposure (up to 2.2 Gy) when comparing (1) none to mild and (2) moderate to severe, late normal tissue radiotoxicity in gynecological cancer patients (Werbrouck et al. 2010). Persistent γH2AX was assessed in T lymphocytes from Ataxia Telangiectasia (AT) patients and patients with Nijmegen breakage syndrome (NBS), a disease associated with the mutation in nibrin proteins (coded by *NBN* gene). Seventy two hours after exposure to 2 Gy of IR the number of γH2AX foci per cell increased in AT and NBS cells approximately 8- and 4-fold, respectively, compared with non-irradiated control cells (Porcedda et al. 2006).

γH2AX as a biomarker of toxicity and as a biodosimeter after systemic administration of radionuclide was investigated *in vivo* in several clinical studies (Lassmann et al. 2010, Fleckenstein et al. 2011). For example, γH2AX induction and loss were assessed in a recent clinical study where radionuclide I^{131} therapy for thyroid cancer was used (Lassmann et al. 2010). The leucocytes were irradiated *in vivo* by the β-particles emitting from circulating ^{131}I. γH2AX was quantified in leukocytes at different times and the highest number of γH2AX foci was observed at 2 h after administration of radionuclide therapy and thereafter declined with time; however, persistence of γH2AX was higher for up to 6 days compared with the number of γH2AX foci in the samples taken immediately before radionuclide therapy (Lassmann et al. 2010). This result indicates that persistence of γH2AX is a promising marker to estimate the absorbed radiation dose *in vivo* after radionuclide therapy. Another study (Doai et al. 2013) reported elevated persistence of γH2AX foci in lymphocytes of thyroid cancer patients 4 days following *in vivo* isotope ^{131}I radionuclide therapeutic administration, allowing estimation of the radiation doses absorbed with this therapy. One important factor to consider on the interpretation of radionuclide induced *in vivo* γH2AX is that radionuclides may be continuously present in the body and induce DSBs chronically.

Typically, other radiation exposures are acute and would likely represent a different kinetic profile of DSB formation and repair. It is also important to note that external irradiation treatment generally involves partial body irradiation whereas radionuclide therapy involves whole body exposure to irradiation. Another study showed that individuals who had higher levels of persistent γH2AX in PBMCs observed 24 h after *in vivo* exposure to X-rays (a single dose of 2 Gy, given once daily for 5 days per week) or RCT (radiotherapy in combination with chemotherapy) are likely to have an increased incidence of severe oral mucositis (Fleckenstein et al. 2011). Following a computed tomography (CT) examination, γH2AX levels in normal individuals reached baseline levels 24 h after the CT scan. However, one patient who had previously shown severe side effects after radiotherapy and had a DSB repair defect displayed a very much higher persistence of γH2AX foci (Lobrich et al. 2005). This result suggests that individuals with a defect in DSB repair may exhibit impaired γH2AX foci loss thereby resulting in an increased persistence of γH2AX after CT (Lobrich et al. 2005). The kinetics of γH2AX formation and loss were also assessed in blood lymphocytes of patients undergoing positron emission tomography (PET) involving the use of ^{18}F-Fluorodeoxyglucose (FDG), and whole body CT scan (May et al. 2012). Radiation-induced γH2AX foci peaked 30 min after ^{18}F-FDG administration and 5 min after CT. After 24 h the number of γH2AX foci per cell decreased but remained higher compared to the pre-exposure level suggesting γH2AX as a useful marker to monitor radiation-induced *in vivo* DNA DSBs by ^{18}F-FDG and CT separately in patients undergoing combined PET/CT (May et al. 2012). In a similar manner, the average number of γH2AX foci per lymphocyte increased in the first 30 min after LuTate administration (for neuroendocrine tumors) and peaked at 2 h (Denoyer et al. 2015). The number of γH2AX foci decreased close to the baseline value 24-72 h after treatment. The γH2AX

foci number in the interval from 10 min to 72 h after therapy correlated with the absorbed dose to tumor and bone marrow and subsequently resulted in a reduced number of lymphocytes. This result suggests γH2AX as a biomarker to assess lymphocyte cytotoxicity (Denoyer et al. 2015). Immunofluorescence was used to demonstrate DSB induction (γH2AX foci) and repair in individuals exposed to IR during percutaneous transluminal angioplasty (PTA) (Geisel et al. 2008). γH2AX levels were approximately 1.7 fold higher in lymphocytes after PTA treatment compared to lymphocytes before PTA treatment. Thus γH2AX can be used as a marker to assess *in vivo* induction and repair of DSB in individuals exposed to radiation at PTA (Geisel et al. 2008). Persistence of 53BP1/γH2AX was also reported in human G_0 lymphocytes obtained from healthy volunteers 24 h to 4 weeks after exposure to 2 Gy of IR (Markova, Torudd & Belyaev 2011), indicating the potential use of γH2AX in biological dosimetry (Markova, Torudd & Belyaev 2011). Therefore, persistence of γH2AX following the exposure to IR in human lymphocytes could be used as a maker to identify the radiosensitivity and the ability of individuals to recover from IR related damage. The effect of age, gender, race, ethnicity, and alcohol use was investigated on IR-induced persistent γH2AX (24 h) in lymphocytes from healthy adults (Sharma et al. 2015). Of these demographic variables, there was a decline of persistent γH2AX in lymphocytes with increasing age, although age and race influenced the early γH2AX responses (Sharma et al. 2015).

1.5.2 Fibroblasts

Persistence of γH2AX has been investigated in human fibroblasts after exposure to IR. In one study, γH2AX foci formed 3 min after exposure to 0.6 Gy of IR in human fibroblasts, γH2AX foci numbers then peaked at 30 min (11.6 foci/nucleus), and at 4.5 h

this level declined to 4.5 foci/nucleus which was higher compared to the level in non-irradiated control fibroblasts (Rogakou et al. 1999). In another study, persistence of γH2AX was reported in human diploid fibroblasts for up to 6 days after exposure to 10 Gy of IR (X-rays) (Rodier et al. 2009). However, the initial dose used in this study was very high (Rodier et al. 2009). The level of γH2AX was also tested in fibroblasts from Werner Syndrome patients (a disease associated with premature aging) to determine whether premature aging diseases is associated with a higher level of persistent γH2AX (Sedelnikova et al. 2008). Twenty-four hours after exposure to 0.6 Gy of IR, the level of γH2AX foci in the fibroblasts from a 61 year old healthy individual returned close to the values observed in non-irradiated controls. However, fibroblasts from a 60 year old Werner Syndrome patient had approximately 1.5 fold increased levels of γH2AX foci/nucleus compared with the non-irradiated controls (Sedelnikova et al. 2008). WRN protein exhibits both helicase and exonuclease activities and is mutated in Werner Syndrome (Baynton et al. 2003, Huang et al. 2006). WRN interacts with several proteins involved in the repair of DNA DSB and localizes to the sites of laser-induced DSB in live cells (Lan et al. 2005). A recent study reported a higher persistence of γH2AX/53BP1 foci in human WRN-deficient fibroblasts compared with controls for up to 24 h after being treated with 20 μM of the potent human carcinogen, chromium Cr(VI), indicating impaired DSB repair due to abnormal mismatched repair (Zecevic et al. 2009). This result suggests that the WRN protein may play an important role in repairing a specific class of DSB in human cells. Fanconi anemia is a blood disorder associated with a genetic defect in a cluster of proteins responsible for DNA repair and results in bone marrow failure (Cantor, Brosh 2014). The repair kinetics of radiation-induced DSBs were assessed in primary fibroblasts from Fanconi anemia, non-fanconi anemia bone marrow failure (non-FABMF) and control cell lines based on a γH2AX

assay. Twenty four hours after exposure to 2 Gy of IR, the level of γH2AX foci per cell in Fanconi anemia cell lines was approximately 2.5 fold higher compared to that in non-FABMF patients and approximately 8 fold higher when compared with non-irradiated controls (Leskovac et al. 2010). Fanconi anemia fibroblasts retained an elevated level of residual γH2AX foci after 24 h IR exposure, suggesting that the persistence of γH2AX foci could be a reliable measure to diagnose Fanconi anemia from non-FABMF and controls. These data suggest that persistence of γH2AX indicates impaired repair of a subset of IR-induced DNA DSBs in human fibroblasts and can be a useful marker to identify individuals with diseases of accelerated aging.

1.5.3 Buccal Cells

Buccal cells are an easily accessible source of tissue and have been investigated for radiation biodosimetry (Siddiqui et al. 2015, Gonzalez et al. 2010). The kinetics of γH2AX induction and loss in buccal cells were investigated by counting γH2AX foci for up to 5 h after exposure to 2 Gy of IR (Gonzalez et al. 2010). γH2AX signals in nuclei peaked at 30 min after exposure to IR, and subsequently declined over a period of 5 h. However, the level of γH2AX remained elevated in irradiated buccal cells for 5 h compared to non-irradiated control cells. In a recent study by our group, γH2AX levels remained elevated in γ-irradiated human buccal cells compared with non-irradiated control cells for up to 24 h following exposure to 4 Gy of IR as measured by quantitative laser scanning cytometry (Siddiqui et al. 2015). These results suggest that radiation induced γH2AX levels in human buccal cells may remain elevated above the baseline γH2AX level for a relatively long time (up to 24 h). Measurement of persistent γH2AX responses in human buccal cells could therefore be used as a powerful and reliable biomarker to assess DNA damage status of individuals exposed to IR during

accidental catastrophic radiation exposure, or during radiation therapy, or possibly as a result of a DNA damaging disease process. However, the variable response to IR exposure between individuals should be taken into consideration when using the γH2AX assay for radiation biodosimetry.

1.5.4 Stem Cells

The kinetics of DSB repair have been investigated in IR-induced human embryonic stem cells (hES) by measuring the persistence of γH2AX (Filion et al. 2009). γH2AX levels decreased at a slower rate in hES after exposure to 5 Gy of IR, over a period of 24 h compared with normal somatic lung fibroblasts. This result suggests that hES retain persistent γH2AX and are possibly less efficient at repairing DSBs (Filion et al. 2009). Another study quantified γH2AX foci numbers per cell after exposure to 2 Gy of IR in various subpopulations of stem cells (CD34+CD38-, CD34+CD38+, CD34-) derived from umbilical cord blood (newborn) and the bone marrow of healthy elderly individuals (>70 years) (Rube et al. 2011). In all cell types examined, there was a similar increase in the frequency of γH2AX foci numbers per cell at both 8 h and 24 h after 2 Gy of IR exposure (Rube et al. 2011). These results suggest that γH2AX response may persist in irradiated stem cells and DSBs repair efficiency could be similar between the stem cell populations analyzed, irrespective of the wide difference in donor age.

1.5.5 Monitoring Effects of Radiotherapy on Cell Lines Using Persistent γH2AX Response

Measurement of persistent γH2AX in human cell lines could be used as a powerful and reliable marker to identify the radiosensitivity of cells or to evaluate DNA damage repair capacity of cells undergoing radiotherapy treatment (Klokov et al. 2006). The

combination of various radiosensitizing drugs with ionizing radiation exposure leads to persistent DNA damage compared with radiation or drug treatment alone (summarized in Table 1.2). The number of persistent γH2AX foci at 12 and 24 h after irradiation was found to correlate with clonogenic cell survival (an *in vitro* cell survival assay based on the ability of a single cell to grow into a colony) (Smogorzewska et al. 2002, Menegakis et al. 2009). Since radiotherapy treatment of cancer cells is aimed to kill cancer cells with a minimum side effects to normal cells, measurement of persistent γH2AX *in vitro* in different cell lines has a great potential for monitoring cancer patients' response to chemotherapy and radiotherapy as well as to enable tailored cancer treatments.

Table 1.2: Persistent γH2AX response following exposure to IR, chemotherapeutic drugs and genotoxic agents in human cell lines

Cell lines	Treatment	Outcome of γH2AX response	Technique used	Ref
Cervical carcinoma (SiHa) Colon carcinoma (WiDr) SiHa and WiDr xenograft tumors	X-rays Single dose: 4 Gy, 6 Gy, and 10 Gy Fractionated dose: 1 Gy daily for 5 days 2 Gy daily for 5 days	24 h post-IR ↑foci/nucleus correlated with the clonogenic cell survival % of cells with < 3 foci predicts cell survival	Visually scored by fluorescence microscopy Flow cytometry	(Klokov et al. 2006)
Radiosensitive head and neck squamous cell carcinoma (SCC-61), and prostate cancer (PC-3) Radioresistant head and neck squamous cell carcinoma (SQ-20b) and prostate cancer (DU- 145) (SCC-61) and (SQ-20b) xenograft tumors	X-rays 3 Gy	24 h post-IR ↑ foci & ↓ viability and clonogenic survival in radiosensitive cells compared with radioresistant cells	Immunoblot Fluorescence microscopy	(Taneja et al. 2004)
Cervical cancer (HeLa, Caski, MS751, C33A,SW756,SiHA)	X-rays 2 Gy	24 h post-IR ↑ intensity and foci/nucleus correlated with clonogenic surviving fraction, indicates ↑ cellular radiosensitivity	Flow cytometry and Visually scored by fluorescence microscopy	(Banath, Macphail & Olive 2004)
Melanoma (HT144) Colon carcinoma (WiDr) Cervical carcinoma (SiHa) Glioma (U87) Breast cancer (HCC1937) Prostate cancer (DU145) B lymphoblastoid (WIL-2NS) Normal cell strains	X-rays 10 Gy	6 h post-IR ↑ γH2AX intensity in radiosensitive cells lines compared with radioresistant cells	Flow cytometry	(MacPhail et al. 2003a)

Cell lines	Treatment	Outcome of γH2AX response	Technique used	Ref
(HFL1)				
Squamous cell carcinoma cells of head and neck (FaDu and SKX)	X-rays 4 Gy	24 h post-IR ↑ foci/nucleus correlated with the clonogenic cell survival % of cells with < 3 foci predicts cell survival	Visually scored by fluorescence microscopy	(Menegakis et al. 2009)
Normal 48BR fibroblasts Patient-derived Artemis-deficient (CJ179 hTERT) fibroblasts	γ-rays 2 Gy	18 h post-IR ↑ foci/nucleus in CJ179 hTERT than in 48BR. Time dependent ↑ in γH2AX foci size (0.8 μm at 30 min to 1.4 μm at 12–18 h post -IR)	Confocal microscopy	(Mohapatra et al. 2011)
Cervical carcinoma HeLa cells Hepatoma (HepG2) Mucoepidermoid carcinoma (MEC-1)	($^{12}C^{6+}$) and X-rays 2 and 4 Gy of radiation using carbon ions	24 h post-IR↑ foci/nucleus ↓ clonogenic survival for ($^{12}C^{6+}$) radiation than for X-rays radiation indicates ↑ cellular radiosensitivity	Visually scored by fluorescence microscopy	(Zhao et al. 2013)
Adenocarcinoma (A549) Squamous cell carcinoma (NCI-H226) Adenosquamous carcinoma (NCI-H596)	BPU + X-rays (4 Gy) 4 Gy alone	24 h post- treatment foci/nucleus ↑ ~2 times in cells pre-treated with BPU + X-rays compared with X-rays alone ↑ foci/nucleus, ↓ clonogenic survival, indicates ↑ cellular radiosensitivity	Flow cytometry	(Balcer-Kubiczek, Attarpour & Edelman 2007)
Bronchial carcinoma (A549) Squamous cell carcinoma head and neck (FaDu) Breast carcinoma (MCF7) Lung carcinoma (H1299) Prostate carcinoma (Du145)	Gossypol + X-ray (2-8) Gy 2-8 Gy alone	24 h post-treatment ↑ foci/nucleus in cells pre-treated with Gossypol + X-rays than in X-rays alone ↑ foci/nucleus with ↓ clonogenic survival indicates ↑ cellular radiosensitivity	Visually scored by fluorescence microscopy	(Kasten-Pisula et al. 2007)
Breast cancer brain metastatic (MDA–MB-231-BR) Breast cancer brain metastatic (MDA– MB– 231-BR) xenograft tumors	Vorinostat + X-rays (2 Gy) for 16 h 2 Gy alone	48 h post-treatment ↑ foci/nucleus with ↓ clonogenic survival in cells pre-treated with vorinostat + X-rays compared with X-rays alone	Visually scored by fluorescence microscopy	(Baschnagel et al. 2009)
Breast cancer (MCF7) Astrocytoma (SF268)	γ rays 0.6 Gy	270 min post-IR 4.5 foci/nucleus compared to 1.5 foci/nucleus at baseline	Laser scanning confocal microscopy	(Rogakou et al. 1999)
SV40-transformed WRN fibroblast (AG11395)	Potent human carcinogen chromium Cr(VI) 20 μM	24 h after treatment ↑ foci/nucleus	Fluorescence microscopy, Phoenix software	(Lan et al. 2005)
Human colorectal cancer (HT-29) Human colorectal cancer (HT-29) xenograft tumors	JP-1201 + X-rays (2 Gy) 2 Gy alone	24 h post-treatment ↑ foci/nucleus with ↓ clonogenic survival in cells pre-treated with JP1201 + X-rays compared with X-rays alone	Visually scored by fluorescence microscopy	(Huerta et al. 2010)
Colon carcinoma (HT29) Breast Carcinoma (MCF7) Pancreatic Carcinoma (MIA PaCa-2) Pancreatic carcinoma (Bx-PC3)	Guggulsterone + X-rays (6 Gy) 6 Gy alone	24 h post-treatment ↑ foci/nucleus with ↓ clonogenic survival in cells pre-treated with GS + X-rays compared with IR alone	Flow cytometry	(Choudhuri et al. 2011)

Cell lines	Treatment	Outcome of γH2AX response	Technique used	Ref
Lung cancer: p53 wild-type (H460 and A549) p53 null (H1299)	HuaChanSu + γ-rays (2 Gy)	24 h post-treatment ↑ foci/nucleus with ↓ clonogenic survival in cells treated with HCS + IR compared with IR alone	Visually scored by fluorescence microscopy	(Wang et al. 2011)
HeLa cells ATM deficient (AT5BIVA) DNA-PKcs deficient ((M059J)	Wortmannin, caffeine or UCN-01+X- rays (10 Gy)	24 h post-treatment ↑ foci/nucleus in HeLa and ATM deficient cell lines but not in DNA-PKcs cell lines	Western blot, Visually scored by fluorescence microscopy	(Wang et al. 2005)
Cervical carcinoma (SiHa)	DNA damaging drugs Camptothecin, cisplatin, doxorubicin, etoposide, hydrogen peroxide, MNNG, temozolomide, and tirapazamine	24 h post-treatment ↑ foci/nucleus with ↓ clonogenic survival	Visually scored by fluorescence microscopy	(Banath et al. 2010)
Prostate cancer (DU145)	Drugs + X-rays MS0019266 or MS0017509 + 4 Gy IR	6 and 24 h post-treatment ↑ foci/nucleus, ↓ cell survival in cells treated with MS0019266 or MS0017509 + X-rays compared with radiation alone	Visually scored by fluorescence microscopy	(Fu et al. 2012)
Primary skin fibroblasts: Wild-type-(48BR) ATM-deficient - (AT7BI) DNA ligase IV-deficient-(411BR) nonhomologous end-joining-deficient cells - (2BN)	γ rays 2 Gy IR	14 days post-IR ↑ level of foci/nucleus (representing 3-6% of unrepaired DSBs) in patient with mutation in ATM and DNA ligase IV	Visually scored by fluorescence microscopy	(Kuhne et al. 2004)
Colorectal adenocarcinomas cancer model (DLD-1 and HT-29) Colorectal adenocarcinomas cancer model (DLD-1 and HT-29) tumor xenograft	Sorafenib + X-rays (2 Gy) Sorafenib alone 2 Gy alone	6 and 24 h post-treatment ↑ foci/nucleus, ↓ cell survival in cells after treatment with Sorafenib + X-rays compared with radiation alone or drug alone cells	Visually scored by fluorescence microscopy	(Kim et al. 2013)
Bone marrow mesenchymal stem cells (U2OS and CALU-1)	Actinomycin D	21 days post-treatment ↑ foci/nucleus	Visually scored using fluorescence images	(Minieri et al. 2015)
Pulmonary carcinoma (A549)	Mitomycin (0.01 and 0.02 μg/ml)	3 to 6 days after treatment Concentration dependent ↑ of γH2AX intensity	Laser scanning cytometry	(McKenna et al. 2012)
Pancreatic cancer (Panc-1) Pancreatic cancer MiaPaCa-2 (PPP2R1A depleted by siRNA)	LB100+ X-rays 7.5 Gy + LB100 for 2 h	24 h post-treatment ↑ γH2AX intensity	Immunoblots	(Wei et al. 2013)
Breast cancer (MCF-7)	Barberine + X-rays 15 μM barberine for 24 h + 1 Gy	12 h post-treatment ↑ foci/nucleus in cells pre-treated with barberine + radiation compared with radiation alone	Visually scored using fluorescence images	(Wang, Liu & Yang 2012)
Fibroblasts (GM637)	CDT + X-rays 0.5 μg/ml CDT and 5 Gy of IR	24 h post-treatment ↑ foci/nucleus and ↑ intensity in cells treated with CDT compared with IR treated cells	Western blot and Fluorescence microscopy, ImageJ	(Fahrer et al. 2014)

Cell lines	Treatment	Outcome of γH2AX response	Technique used	Ref
Colorectal cancer (HCT116)	Oxaliplatin (1–10 μM) treatment for 6-24 h	24 h post-treatment ↑ intensity in a time- and concentration dependent manner	Western blot	(Chiu et al. 2008)
Human pancreatic cancer (MiaPaCa-2)	AZD7762 (Chk1/2 inhibitor) and gemcitabine	48 h post-treatment ↑intensity in 56% of cells	Flow cytometry	(Morgan et al. 2010)
The normal human fibroblasts AGO1522B (AGO) Normal peripheral blood lymphocytes from patients with advanced cancer	SJG-136 (crosslinking agent)	8 and 15 days post-treatment ↑ foci/nucleus	Visually scored using fluorescence images	(Wu et al. 2013)
Glioblastoma (U251)	HSV-TK + antiviral drug Ganciclovir	24 h post-treatment ↑ foci/nucleus	Visually scored using fluorescence images	(Ladd et al. 2011)
Bone marrow mesenchymal stromal (MSC)	X-rays 40 and 2000 mGy	48 h post-treatment ↑ foci/nucleus	Visually scored using fluorescence images	(Alessio et al. 2015)
Human mammary epithelial (HMEC)	Iron-ion and γ-rays 1 Gy and 2 Gy	72 h post-treatment ↑ foci/nucleus in non-proliferative cells than in proliferative cells ↑ foci/nucleus after iron-ion exposure than after γ-rays exposure	Visually scored using fluorescence	(Groesser et al. 2011)
Normal diploid cells (HE49)	X-rays 4 Gy	5 days post-IR ↑ foci size and ↑% of positive nuclei	Fluorescence microscopy, IP lab software	(Suzuki et al. 2006)

Abbreviations: Cytolethal distending toxin (CDT), Dimethylamino benzoylphenylurea (BPU), Guggulsterone (GS), HuaChanSu (HCS), Herpes simplex virus thymidine kinase (HSV-TK), Mitomycin C (MMC).

1.6 Persistent γH2AX in Mouse Cells and Tissues

1.6.1 Germ Cells

The persistence of γH2AX has been investigated in mouse germ cells after whole- body exposure to X-rays (Paris et al. 2011). Round spermatids and primary spermatocytes had a higher proportion of cells containing γH2AX foci (around 50% and 30%, respectively) compared to non-irradiated controls, 48 h after exposure to 4 Gy IR. The pattern of γH2AX foci within these cells changed from many innumerable foci at early time points (1 h) to a pattern of fewer discrete foci at 48 h post-IR (Paris et al. 2011). Another study showed the presence of Mdc1, 53BP1 and Rad51 proteins that are expressed in conjunction with γH2AX in male germ cell types for up to 16 h after

exposure to 4 Gy of X-rays (Ahmed et al. 2007). These results suggest that mouse germ cells display persistence of γH2AX following IR.

1.6.2 Skin Biopsies

An *in vivo* investigation of persistent γH2AX as a biodosimeter of initial radiation dose has been carried out in keratinocytes within the epidermis of radiosensitive and radioresistant murine skin biopsies (Bhogal et al. 2010). In this study, γH2AX foci/100 μm^2 areas of irradiated tissue sections were quantified for up to 7 days after exposure to a dose ranging from 1 to 10 Gy using 3D confocal microscopy. γH2AX foci were more persistent in radiosensitive strains compared with radioresistant strains and respective non-irradiated time-matched controls. Therefore, confocal microscopy may enable high resolution 3D image acquisition of γH2AX foci in different depths of skin biopsies, thereby making it possible to measure IR induced persistent γH2AX levels for many days after radiation exposure which could have practical application in radiation biodosimetry.

1.6.3 Spinal Cord

γH2AX induction and loss have been investigated in murine spinal cord for 1 year after topical application of spinal cord to an acute IR dose of 17 Gy of X-rays followed by an immediate additional dose of 19 Gy of X-rays (Andratschke et al. 2011). The frequency of γH2AX foci was higher in the blood vessel endothelium of irradiated spinal cord compared with non-irradiated controls where γH2AX was virtually absent. The higher levels of γH2AX foci were still detectable 1 year after IR exposure suggesting that the IR-induced γH2AX response can persist in murine spinal cord for a very long time after a radiation exposure event (Andratschke et al. 2011).

1.6.4 Other Tissues and Organs

Variations in IR-induced DNA breaks in different animal tissues were first observed in 1983 (Meyn, Jenkins 1983). Although, the levels of H2AX protein have been reported in similar amounts among mouse thymus, testis and small intestine, the proportion of phosphorylated H2AX differed between tissues after 30 Gy IR exposure (Yoshida et al. 2003). It was observed that 17% of H2AX were phosphorylated in the epithelial cells in the villi of the small intestine compared to 37% and 94 % in thymus and testis respectively (Yoshida et al. 2003). This result suggests that H2AX does not always phosphorylate to the same extent in all tissues after exposure to IR. γH2AX has been previously measured in heart and kidney sections of mice after their whole body was exposed to 3 Gy of X-rays (Gavrilov et al. 2006). The maximum frequency of γH2AX positive nuclei was found in heart and kidney sections at 20 and 40 min, respectively, then slowly declined. After a further 23 h the number of γH2AX positive nuclei (in about 50% of γH2AX positive nuclei in cardiomyocytes of heart) remained persistent; however γH2AX positive nuclei decreased in kidney cells to the values observed in the control (Gavrilov et al. 2006). Furthermore, the γH2AX response was tested in mouse heart, brain, kidney and liver tissues for up to 5 h after whole-body exposures to 3 Gy of IR. The amount of γH2AX observed was lowest in the heart compared with brain, kidney and liver at 5 h post-IR (Firsanov et al. 2012).

Persistence of γH2AX has been investigated in mouse spleen, thymus, liver, lung, kidney, cerebellum, hippocampus, frontal cortex and olfactory bulb of 7, 14, 24, 30 and 45 day old mice (Hudson et al. 2011). The number of γH2AX foci per cell peaked at 30 min after exposure to 1 Gy of X-rays and then declined in most tissues within 24 h.

However, IR-induced γH2AX foci were more persistent in the thymus and spleen of 7 and 14 day old mice compared with mice from the older age categories.

One study has reported that the kinetics of γH2AX foci loss were almost similar in small intestine, lung, brain, heart, and kidney tissues of mice 48 h after whole-body exposure to 2 Gy of IR (Rube et al. 2008). Similar results on the kinetics of γH2AX foci loss were also observed in mouse heart, small intestine, and kidney tissues for 24 h following whole-body exposure to 0.01, 0.1, and 1 Gy of X-rays (Grudzenski et al. 2010). Taken together, these data suggest that the rate of initial γH2AX induction as well as the rate of γH2AX loss after X-ray exposure significantly varies in non-proliferating mammalian tissues and should be taken into account when comparing radiation induced γH2AX responses between various tissues and species.

1.7 Persistent γH2AX in Cells and Tissues of Other Animals

1.7.1 Minipig Skin, Lymphocytes and Fibroblasts

A recent study showed the presence of IR-induced γH2AX foci in ~60% of cells in keratinocytes within the epidermis of Göttingen minipig skin biopsies 4 h after exposure to 50 Gy of IR (Ahmed et al. 2012). The average radiation induced γH2AX foci number per epidermal keratinocyte then declined after 70 days; however, the average numbers of residual γH2AX foci per epidermal keratinocyte at 70 days were significantly higher compared to non-irradiated controls (Ahmed et al. 2012). Twenty four hours after *ex vivo* exposure to 1.8 Gy of IR, both human and minipig lymphocytes exhibited ~15% of the maximal γH2AX response observed at 30 min (Moroni et al. 2013). Furthermore, approximately 3% residual γH2AX foci were found in human and minipig fibroblasts for up to 24 h after 2 Gy of IR exposure. γH2AX kinetics in minipig lymphocytes after

exposure to different total body irradiation doses showed that persistent γH2AX foci per cell were proportional to the initial IR dose thus suggesting that a portion of IR-induced DSBs remains unrepaired (Moroni et al. 2013).

1.7.2 Fruit Fly Pupae

Our previous study on the Queensland fruit fly (*Bactrocera tryoni*) demonstrated that IR exposure leads to a persistent γH2AvB response (a fruit fly variant of γH2AX) that could be assessed during the adult phase of the life cycle when the IR exposure was carried out at the pupal stage (Siddiqui et al. 2013). Queensland fruit flies are able to withstand high doses of IR, and we reported a linear dose-response of γH2AvB (0–400 Gy IR) 24 h after IR exposure. γH2AvB signal peaked at approximately 20 min after IR exposure. At 24 h post IR, the signal remained elevated but was substantially reduced after 5 days compared with 1 day post-IR exposure. γH2AvB response in adult Queensland fruit flies was persistent and dose-dependent up to 17 days after IR exposure. The persistent γH2AvB response can therefore be utilized as a biomarker of prior IR exposure of fruit flies (Siddiqui et al. 2013). This finding has several potential applications for the management of economically important insects, such as the sterile insect technique, where fruit flies are irradiated at ~70 Gy to induce reproductive sterility but not death of the organism or to determine whether fruit containing fruit fly larvae was irradiated with an appropriate dose of radiation (Siddiqui et al. 2013).

1.7.3 Macaque Lymphocytes and Plucked Hair Bulbs

Persistence of γH2AX was observed in lymphocytes from macaque after whole body irradiation with doses from 1 to 8.5 Gy (Redon et al. 2010). The number of γH2AX foci per cell were elevated in lymphocytes by approximately 16-fold for up to 14 days after exposure to 8.5 Gy of IR when compared with non-irradiated controls. Similarly,

γH2AX foci from plucked hair bulbs of macaques were approximately 14-fold increased per cell compared with non-irradiated controls up to 9 days after 8.5 Gy IR exposures (Redon et al. 2010). This study suggests that plucked hair bulbs are an easily accessible source of sample to measure persistence of γH2AX for many days after radiation exposure and may be adopted as a strategy for early triage during accidental catastrophic radiation incidents.

1.7.4 Syrian Hamster Heart, Brain, and Liver Tissues

The kinetics of γH2AX induction and loss were tested in heart, brain, and liver tissues of adult Syrian hamsters following whole-body exposure to 5 Gy of X-rays (Firsanov et al. 2012). The γH2AX response 24 h after IR was more persistent in heart and brain tissues compared with liver (Firsanov et al. 2012). These results suggest that the kinetics of IR-induced γH2AX induction and loss is tissue specific, being less efficient in heart and brain in comparison with liver (Firsanov et al. 2012).

The results of these studies, suggest that (i) γH2AX persistence is a common phenomenon across species, and (ii) nuclei may retain persistent γH2AX foci for up to several months after IR exposure, allowing for retrospective biodosimetry.

1.8 Persistence of γH2AX Associated with Telomeres

Telomeres are evolutionarily conserved, specific, repetitive hexameric nucleotide sequences (TTAGGG) located at the end of each chromosome (Zalenskaya, Bradbury & Zalensky 2000) and are responsible for protecting chromosomes from improper recombination and degradation (McEachern, Krauskopf & Blackburn 2000). These repetitive sequences bind to proteins forming a protein–DNA complex known as Shelterin (de Lange 2005). This complex caps the end of the chromosome and prevents

DNA repair machinery from misidentifying the overhang located at chromosome-ends as a DSB. A previous study reported that Shelterin components such as telomeric repeat-binding factor 2 inhibits DNA end-joining by DSB repair mechanisms and therefore prevents end-to-end fusions of chromosomes, thus allowing DNA damage to accumulate at telomeres (Smogorzewska et al. 2002, McEachern, Krauskopf & Blackburn 2000, Bae, Baumann 2007, Passos et al. 2010). For this reason, it has been suggested that telomeric DNA may accumulate DSBs and could be a preferred location for formation of persistent DDR foci (Fumagalli et al. 2012, Hewitt et al. 2012). At 4 days post-IR exposure, approximately 10% of γH2AX foci were co-localized at telomeres, whilst at 10 and 30 days post-IR, 20% and 40% of γH2AX foci were co-localized at telomeres, respectively (Fumagalli et al. 2012). Co-localization between γH2AX foci and telomeres was also higher in X-ray-treated senescent human fibroblasts for up to 26 days after exposure to 20 Gy of IR (Hewitt et al. 2012). Findings from this study suggest that while the mean number of γH2AX foci per cell in the non-telomeric region progressively declined, the percentage of γH2AX foci co-localizing with a telomere signal gradually increased for up to 26 days (Hewitt et al. 2012). In order to demonstrate that γH2AX binds telomeric repeats and not only the sub-telomeric regions; quantitative real-time PCR of sub-telomeric regions were performed on chromatin immunoprecipitation of human dipoloid fibroblasts with an anti-γH2AX antibody 10 days after exposure to 20 Gy of IR. There was a strong enrichment of γH2AX at the sub-telomeric region of fibroblasts exposed to IR compared to non-irradiated controls. The enrichment of γH2AX increased from the centromere towards the direction of the chromosome terminal region and represented an approximate 14-fold enrichment of γH2AX at the telomere repeats, in irradiated human fibroblasts compared to non-irradiated human fibroblasts (Hewitt et al. 2012). The enrichment of

γH2AX at the telomere repeats has also been confirmed using a chromatin immunoprecipitation procedure followed by next generation sequencing and real-time PCR (Fumagalli et al. 2012). Both studies suggest that persistent γH2AX foci are not only associated with cytological close proximity with telomeres (the association observed when viewed by a microscope), but also physically associated (as measured by chromatin immunoprecipitation and real-time PCR) with telomeres. A schematic of the accumulation of γH2AX at telomeres is shown in Figure 1.3. This result supports the paradigm that DNA damage at telomeres may not be repaired after exposure to DNA damaging agents such as IR. The irreparable telomeres may therefore, trigger persistent DDR (reflected by persistent γH2AX response) which is associated with the formation of cellular senescence processes.

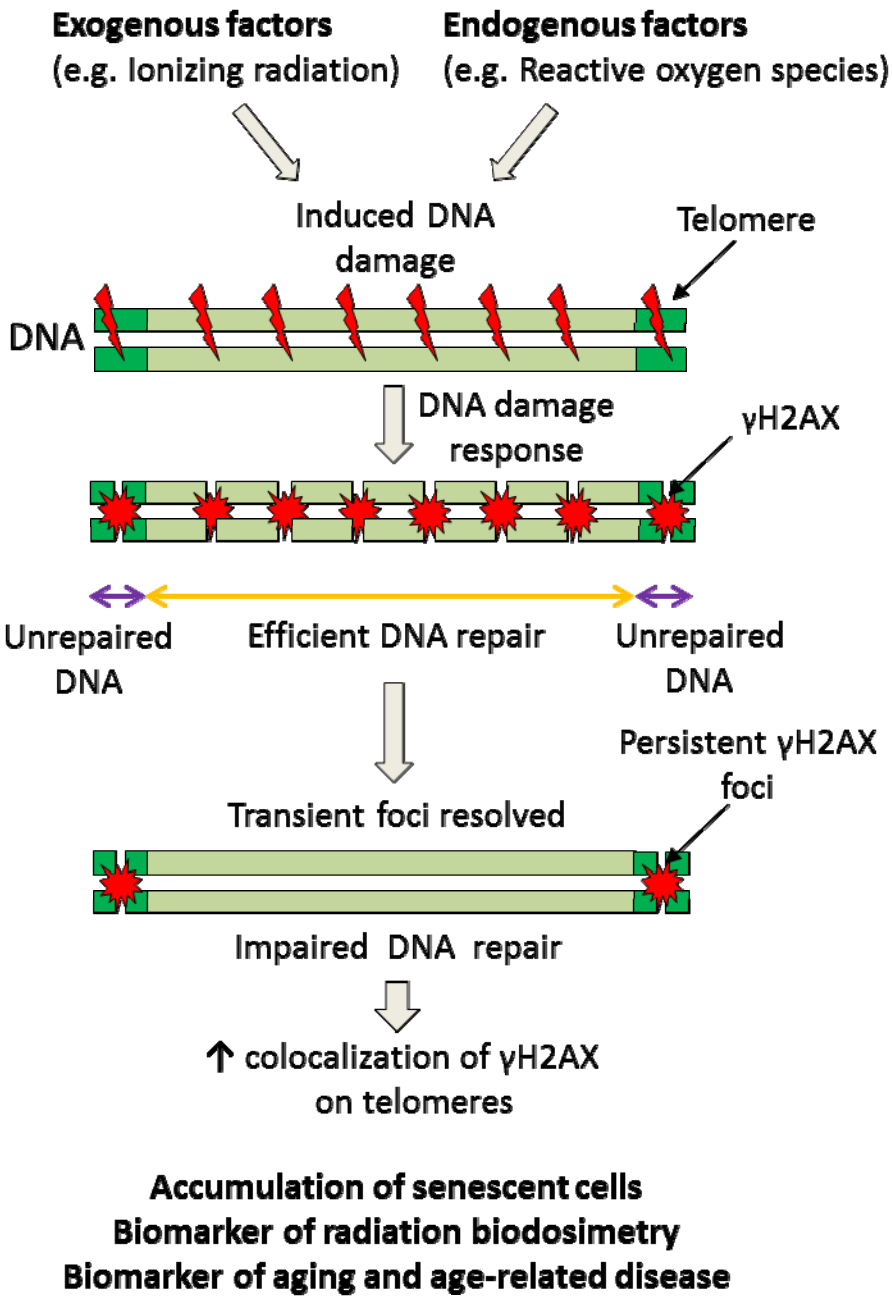

Figure 1.3: Model of persistent γH2AX as a result of endogenous and exogenous factors. Exogenous and endogenous factors induce DNA damage throughout the genome. While the DNA DSBs in non-telomere regions are efficiently repaired, DNA DSBs generated in telomeres are not repaired leading to persistent γH2AX. These unrepaired DNA DSBs likely result in the accumulation of senescent cells. The accumulation of senescent cells may be involved in accelerated aging processes. Measurement of the persistent γH2AX could potentially be used as a biomarker of radiation biodosimetry, radiosensitivity and accelerated aging. Adapted from (Fumagalli et al. 2012).

1.9 Senescence-Associated Persistence of γH2AX

Unrepaired DSBs could result in either cell death or in a form of cell cycle arrest known as cellular senescence (d'Adda di Fagagna 2008). Cellular senescence is an irreversible process where cells remain alive but are unable to proliferate (Campisi, d'Adda di Fagagna 2007). Senescent cells can be detected by histochemical staining for senescence-associated β-galactosidase (SA-β-gal) activity (Dimri et al. 1995). Senescence-associated persistent γH2AX foci were present for up to 24 h after exposure to 1 Gy of IR in senescent cultured human fibroblasts, human prostate epithelial cells, human fibroblasts with elongated telomeres and in nuclei of whole tissues from mice (i.e. liver, testis, kidney, lung) (Sedelnikova et al. 2004). To characterize persistent γH2AX foci, a further radiation dose was applied to the same cells (i.e. mouse and human cells already containing IR-induced foci). After 30 min post-IR, the newly formed γH2AX foci were eliminated 24h post IR whilst the persistent foci, i.e. those from the first dose of IR, were still present 24 h after IR exposure (Sedelnikova et al. 2004). Additionally, persistent γH2AX has been demonstrated in human diploid fibroblasts after exposure to 20 Gy of IR for up to 4 months (Fumagalli et al. 2012). In a separate experiment, senescent cells that already contained persistent γH2AX foci from prior IR as well as normal human diploid fibroblast cells (that were not exposed to IR) were irradiated to investigate the nature of persistent γH2AX foci. Whilst the newly formed IR-induced transient γH2AX foci were repaired, γH2AX foci in senescent cells (from prior treatment) remained unresolved (Fumagalli et al. 2012). This evidence suggests that senescent cells are associated with the accumulation of persistent γH2AX, which represents a subset of DSBs that are resistant to repair processes. The criteria of senescent-associated persistence of γH2AX after exposure to IR needs to be further investigated in order to be used as a potential marker of radiation biodosimetry.

1.10 γH2AX Responses in Aging

Aging is a process that alters cellular function of most living organisms and is influenced by environmental and genetic factors (Li, Mitchell & Hasty 2008, Aubert, Lansdorp 2008, Lopez-Otin et al. 2013). The aging process is regulated by the accumulation of genetic alterations and dysregulation in epigenetic fingerprints, which may ultimately contribute to genomic instability, cellular senescence, apoptosis and/or cancer (Sinclair, Oberdoerffer 2009, Gedik et al. 2005). Imperfections or defects in pathways repairing DNA DSBs may either trigger the aging process or indirectly regulate it by cellular senescence or apoptosis (Li, Mitchell & Hasty 2008). DSBs may cause progressive shortening or dysfunction of telomeres when left unrepaired and may play a major role in the aging process of somatic cells (Harley, Futcher & Greider 1990, Hastie et al. 1990, Campisi 2013). This accumulation of DSBs causes persistent DDR coupled with p53 activation and may contribute to cellular senescence (Aubert, Lansdorp 2008, Sinclair, Oberdoerffer 2009, Campisi 2013, d'Adda di Fagagna et al. 2003), a key factor in healthy and pathological aging (Campisi, d'Adda di Fagagna 2007, Stein et al. 1991, Baker et al. 2011). Senescent cells characterized by the presence of γH2AX, including activity of SA-β-gal, accumulate in tissues of aged animals and are thought to increase during aging and age-related diseases (Dimri et al. 1995, Wang et al. 2009, Sikora et al. 2011). In addition to the arrest of cell proliferation, senescent cells display altered chromatin organization and gene expression. These changes involve the secretion of different proteins (such as proinflammatory cytokines, chemokines, growth factors, and proteases), the so-called senescence associated secretory phenotype (SASP) (Campisi et al. 2011, Freund et al. 2010). The secretion of SASP proteins by senescent cells ultimately results in chronic inflammation which is a cause of, or important contributor to multiple age-related diseases (Campisi et al. 2011,

Chung et al. 2009, Franceschi 2007). It has been reported that persistent DDR signalling (observed by increased γH2AX levels) can fuel the secretion of SASP cytokines (e.g. IL-6) as compared with transient DDR signalling and is summarized in Figure 1.4 (Rodier et al. 2009). It is likely that accumulation of persistent DSBs may be strongly involved during aging and diseases of accelerated aging.

1.10.1 Endogenous Levels of γH2AX in Individuals of Different Ages

Several studies have examined whether endogenous levels of γH2AX is altered by the age of individuals. (Sedelnikova et al. 2008, Garm et al. 2013). For example, the frequency of γH2AX foci were measured to investigate the presence of unrepaired DSBs in human fibroblasts and lymphocytes from healthy young donors and older donors in the age range from 21 to 72 years (Sedelnikova et al. 2008). The endogenous γH2AX foci per cell were higher in fibroblasts and lymphocytes from older donors compared with younger donors (Sedelnikova et al. 2008). Studies on aging and senescing cell lines of epithelial and fibroblastic origin (including mice), also showed an increase in γH2AX foci with age (Sedelnikova et al. 2004, Sedelnikova et al. 2008, Wang et al. 2009, Endt et al. 2011). Recently, a longitudinal study of aging also tested the hypothesis that the frequency of γH2AX foci correlates with age in leukapheresis-derived mononuclear cells from patients in the age range of 37 to 83 years; with 37 patients over the age of 50 and 13 patients over the age of 72 (Schurman et al. 2012). The average number of γH2AX foci per cell was increased with age up to 57 years and then remained relatively stable up to the age of 83. This result was in agreement with other observations whereby the number of γH2AX foci per cell increased with age up to approximately 50 years and then subsequently plateaued (Sedelnikova et al. 2008). However, it is important to note in that study only 8 donors were examined in the 50

year old group. A more recent study (Sharma et al. 2015) reported a trend of linear increase in endogenous γH2AX level with age in lymphocytes from 94 healthy adults with the age range from 19 to 50 years. Another study investigated the presence of endogenous levels of γH2AX in PBMCs from a population-based sample of twins ranging in age from 40 to 77 years (Garm et al. 2013). In that study, γH2AX levels decreased with increasing donor age in human PBMCs. The reason for the discrepancies in the γH2AX levels with age is not known but may be partly due to the differences in the study populations. Interindividual variability of endogenous γH2AX response is known, although the effect of modulators such as age, genotype, ethnicity and race, hormonal responses, gender, environmental factors, and alcohol intake may impact on the base-line endogenous γH2AX responses, but this is not completely understood (Sharma et al. 2015). The endogenous γH2AX foci frequency (per cell) increased with age in CD34+ and CD34- stem/progenitor cells derived from both growth-factor mobilized peripheral blood and bone marrow cells compared to cells derived from umbilical cord blood (Rube et al. 2011). Furthermore, endogenous γH2AX foci were approximately two times higher in CD34+CD38-, CD34+CD38+ and CD34- cells derived from bone marrow samples of healthy elderly individuals (>70 years) compared with cells from umbilical cord blood (Rube et al. 2011). This indicates that different subtypes of stem cells and progenitor cells may accumulate unrepaired DSBs with age. Additionally, the frequencies of the senescent cell marker, i.e SA-β-gal activity, and γH2AX foci positive cells increased in the heart, skeletal muscle, kidney, eye lens, testis, liver, skin, lung, spleen and small intestine of 42 month old male mice compared with 12 month old mice (Wang et al. 2009). The levels of persistent γH2AX foci that co-localize with telomeres also increased with age in senescent primate fibroblasts (Herbig et al. 2006). These studies suggest that γH2AX response may be indirectly

involved in the process of normal physiological aging but its use as a robust biomarker of biological aging remains uncertain.

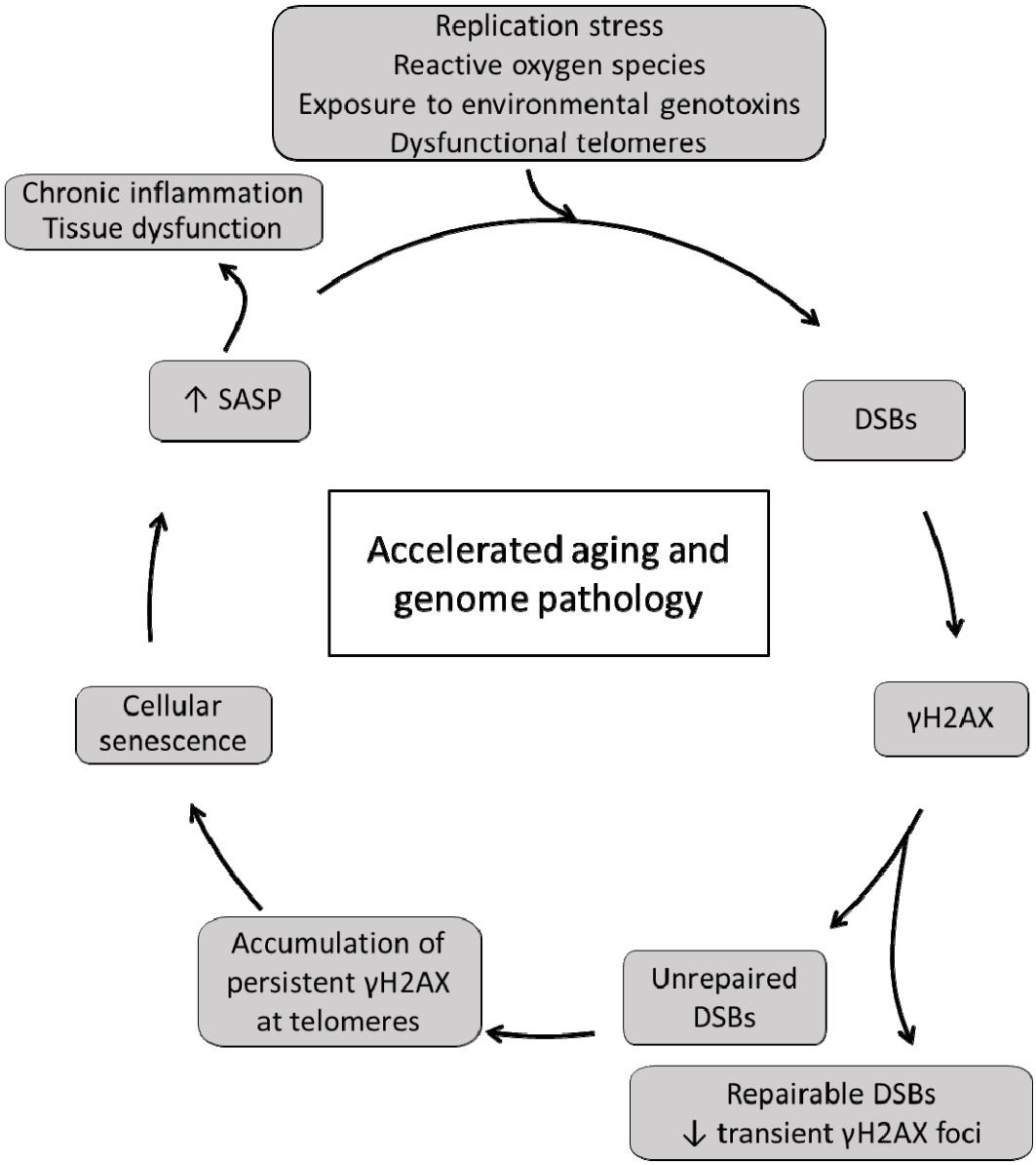

Figure 1.4: Model depicting the possible role of persistent γH2AX/unrepaired DSBs in aging and diseases of accelerated aging. Replication stress, environmental genotoxins, dysfunctional telomeres and dysregulation in epigenetic fingerprints induce DSBs. When DSBs are repairable, transient γH2AX foci are removed; however, unrepaired DSBs marked by persistent γH2AX foci lead to cellular senescence. The persistence of γH2AX is also associated with increased expression of SASP. The deleterious effect of senescent cells and SASP includes chronic inflammation, tissue dysfunction promoting aging and fuelling the development of age-related disease. Abbreviations: DSBs, double-strand breaks; SASP, senescence associated secretory phenotype.

1.10.2 γH2AX in Chronic Diseases of Aging

The association between the levels of γH2AX foci and age-related disease have been investigated in several studies (Sedelnikova et al. 2008, Schurman et al. 2012). For example, the frequency of γH2AX foci was apparently higher in PBMCs of hypertensive patients when compared to the cells from their respective controls (Schurman et al. 2012). However, the analysis was only significant when restricted to hypertensive patients that were aged more than 57 years old. In that study, the γH2AX foci per cell was 36% higher in hypertensive patients compared with non-hypertensive study participants (Schurman et al. 2012). A trend of increasing γH2AX foci per cell has also been reported in patients with sleep apnoea, prostate cancer and cataract disease patients compared to those without history of these respective conditions, although it should be noted that the increase observed did not reach statistical significance (Schurman et al. 2012). In another study, senescent fibroblasts from Werner Syndrome patients exhibited a higher number of γH2AX foci per cell compared to senescent fibroblasts from healthy donors (Sedelnikova et al. 2008). The rate of recruitment of DDR proteins such as Mre11 and 53BP1 to γH2AX foci was inversely correlated with age in both healthy and Werner Syndrome donors (Sedelnikova et al. 2008). Thus, recruitment of DDR proteins at the DSBs site may be less efficient with age, leading to accumulation of DSBs during the aging process (Sedelnikova et al. 2008, Gorbunova, Seluanov 2005). In a study of obesity in children, γH2AX in lymphocytes of obese children (n=81) and healthy controls (n=38) was 8-fold higher in obese children compared with non-obese children (Scarpato et al. 2011). The level of γH2AX was also measured in lymphocytes of adolescents with type 1 diabetes mellitus (T1DM) (n=35) and healthy controls (n=19) (Giovannini et al. 2014). The number of γH2AX foci per nucleus was approximately 50 fold higher in T1DM patients compared with healthy

controls (Giovannini et al. 2014). γH2AX staining has been shown to be higher in the nuclei of astrocytes from Alzheimer's disease patients relative to healthy controls as determined by immunocytochemical techniques (Myung et al. 2008). This result suggests that DSBs measured by γH2AX positive immunostaining in the nuclei of astrocytes may be associated with impaired neuronal function and contribute to the pathogenesis of Alzheimer's disease (Myung et al. 2008). Fibroblasts from patients with Hutchinson-Gilford progeria syndrome (a disease associated with accelerated aging) also reported increased amounts of endogenous γH2AX levels compared with controls (Liu et al. 2006). Overall, these studies show that accumulation of γH2AX foci is marginally increased in individuals with increased morbidity and supports the hypothesis of accumulation of unrepaired DSBs in pathological aging.

1.10.3 Biomarker search for the diagnosis of Alzheimer's Disease

AD is the most common cause of dementia in old age, representing approximately 60–80% of all dementia cases (Lobo et al. 2000, Tijms et al. 2013, Forlenza et al. 2013). According to the World Health Organization, 46.8 million people were affected by dementia in the year 2015 (Prince et al. 2015). Increasing rate of AD is expected to reach at a level of one new case at every 33 seconds by 2050 (Alzheimer's Association, Thies & Bleiler 2011). Currently, AD has come to a global prevalence of approximately 24.3 million with 4.6 million new cases being diagnosed worldwide each year (Smith 2008, Ferri et al. 2005). Furthermore, increasing trends of AD not only causes loss of the quality of life, health and wellbeing of those affected but also create a significant financial burden at both the social and government level. AD is characterized clinically by abnormal behavioral and mental effects that include loss of memory, tremors, and absent-mindedness, and is the most common cause of dementia (Alzheimer's Association, Thies & Bleiler 2011, Fernandez et al. 2010, Burns, Byrne & Maurer 2002). The onset of AD involves the accumulation of increasingly severe cognitive deficits, progressing from mild cognitive impairment (MCI) to AD. MCI is characterized by deterioration in cognitive ability that; however, does not affect the individuals' ability to carry out their activities of daily living. Individuals affected by MCI have a higher risk of developing AD with advancing age, with estimates that vary between 14 and 18 percent of those over 70 years of age suffering from this condition (Grundman et al. 2004, Petersen et al. 2009). Currently, the ability to detect the early stages of AD and differentiate the stages of AD progression to guide the choice of therapy is limited. The Mini-Mental State Examination (MMSE) is a validated research-based set of 30 questions considering memory loss, cognitive decline, visuospatial and language impairment that is currently used as a standard tool for the clinical diagnosis

of AD (Tombaugh, McIntyre 1992, Mitchell 2009). However, this test lacks accuracy for the diagnosis of AD in living subjects, and diagnostic confirmation can only be achieved post mortem by the examination of the senile plaques and neurofibrillary tangles in brain tissue from the patient (Armstrong 2006). Therefore, identification of other biomarkers in easily accessible tissue that can aid the diagnosis of AD may be useful to identify individuals at an increased risk of AD while they are still in the early stages of illness.

1.10.4 Why peripheral tissue biomarkers of Alzheimer's disease are important for diagnosis

The identification of biomarkers to enable the early diagnosis of Alzheimer's disease (AD) is one of the major challenges for researchers in this area. AD is characterised by major lesions in the brain, comprising (i) aggregated extracellular amyloid plaques around the neuronal bodies and (ii) neurofibrillary tangles that appear within the neurons. Most methods for the investigation of AD are invasive and expensive and are unable to establish biomarkers (Thambisetty, Lovestone 2010, Hampel & Prvulovic 2012, Blennow & Zetterberg 2009). A successful population-based screening programme will require less invasive, easily accessible and inexpensive samples as well as a robust diagnostic test with high specificity and sensitivity at much lower cost than is currently available. At present investigators rely on blood, cerebrospinal fluid (CSF) or brain imaging for diagnosis of AD. The Pittsburgh B (PiB) compound has been used detect the β-amyloid protein aggregates that form senile plaques in specific regions of the brains of AD patients, which are readily detectable with this technique. However, some reports have shown that useful imaging with PiB can only be done once there has

been significant plaque accumulation (i.e., when the disease is already quite advanced) Cairns et al. 2009, Leinonen et al. 2008).

Micronuclei are abnormal DNA fragments associated with chromosomal aberrations produced during cell division and are widely recognised as a biomarker for the assessment of genomic instability. The propensity for micronuclei formation increases with advancing age, and fibroblasts, a type of peripheral tissue, have displayed these changes in relation to AD (Migliore et al. 2011, Trippi et al. 2001).

One of the major proteins involved in AD is the amyloid precursor protein (APP), which encoded on Chromosome 21 (Selkoe 2001). APP is widely expressed in many tissues, but is more concentrated in the synapses of neurons and plays a vital role in neurite growth, cell adhesion, synaptic functions and the induction of apoptosis (Thomas, Fenech 2007).

Oxidative stress, which is followed by oxidised DNA base adduct 8-hydroxy-2 dexyguanosine (8-OHdG) accumulation, is also a leading cause of neurodegenerative disease (Giasson et al. 2002, Migliore & Coppede 2002, Perry et al. 2002). It has been suggested that elevated urinary (8-OHdG) levels and serum Paraoxonase 1 (PON1) activity can be used to monitor disease progression in AD (Zengi et al. 2011).

Significant telomere shortening has been observed in lymphocyte samples from AD patients (Jenkins et al. 2006, Panossian et al. 2003). White blood cells from AD patients were tested for telomere shortening and showed a significantly higher level of shortening in AD patients in comparison to that seen in young and healthy elderly controls ($P<0.0001$) (Thomas, O'Callaghan, Fenech 2008). Taken together, the evidence outlined above suggests that AD is a systemic disorder that is mirrored in various peripheral tissues, thereby rationalising the approach of investigating less

invasive cellular biomarker for the diagnosis of mild cognitive impairment (MCI) or AD risk.

1.10.5 Why buccal cell is important as a material for the diagnosis of Alzheimer's disease

The buccal mucosa (BM) is of ectodermal origin, and defects in BM cells may potentially reflect the pathology in other tissues of ectodermal origin, such as the nervous system. Buccal cells could, therefore, be a potential source for the diagnosis of the fundamental pathological changes that occur in AD. It has been suggested that the ubiquitous presence and different expression levels of APP in BM could be a useful means to estimate the regenerative status of tissue (Kummer et al. 2002). The amounts of buccal cell tau protein (responsible for AD) significantly correlates with the tau levels in cerebrospinal fluid (CSF) and is also present at higher levels in AD subjects (Hattori et al. 2002). Methods like cotton swabs (Richards et al. 1993), cytobrushes (Richards et al. 1993, Garcia-Closas et al. 2001, King et al. 2002, Patten et al. 1996), 'swish and spit' (Hayney, Poland & Lipsky 1996; Lum & Le Marchand 1998; Feigelson et al. 2001), a modified Guthrie card (Harty et al. 2000) and a method of rubbing the cheeks against the teeth to exfoliate cells (King et al. 2002) are all well-known techniques for buccal cell collection. These methods allow the collection of large quantities of buccal cells (more than 106 cells) that can subsequently be used for DNA analysis using PCR or other genotype tests (Hayney, Poland & Lipsky 1996, Lum & Le Marchand 1998, de Vries et al. 1996; Myerson et al. 1999; Guangda et al. 1999; Le Marchand et al. 2001) and Western blots and immunocytochemistry for the detection of proteins (Hattori et al. 2002, Michalczyk et al. 2004, Spivack et al. 2004). Moreover, buccal cells have certain important features such as stability in hypotonic solutions,

including water (Lee et al. 1994), and a lower propensity to disruption, which makes them a potential source of samples without the risk of losing their intracellular contents.

AD is associated with genomic DNA damage, and a lack of repair capacity could potentially lead to genomic instability (Thomas & Fenech 2007, Fraga et al. 1990; Goukassian et al. 2000; Wilson, Bohr & McKinnon 2008). The buccal micronucleus cytome assay (BMCyte) has been developed to score DNA damage, cell death and regenerative potential (Thomas et al. 2007, 2009). A higher frequency of micronuclei ($P<0.0001$) in comparison with that seen in young and older controls has been observed in a Down's syndrome (DS) cohort, which represents a model for premature ageing (Thomas et al. 2008). However, the same assay did not show a statistically significant micronuclei score in an AD cohort (Thomas et al. 2007). Consistent micronuclei frequencies were obtained when the same slides from the DS cohort were analysed by laser scanning cytometry (Leifert et al. 2011), a technology able to provide micronuclei scores in a fully automated fashion (Darzynkiewicz et al. 2011).

Aneuploidy is an abnormal chromosomal state that has been investigated in the buccal cells of AD and DS patients, and in comparison, with healthy controls, both the AD and DS cohorts showed higher levels of aneuploidy of Chromosomes 17 and 21, which encode tau and APP respectively (Iqbal et al. 1989; Koo 2002; Thomas & Fenech 2008). Additionally, the double-strand break (DSB) marker γH2AX has also been detected in human buccal cells following radiation (Gonzalez et al. 2010). Buccal samples from AD patients were tested for telomere shortening and showed significant shorter telomere lengths in an older AD group in comparison to that seen in older controls (Thomas, O'Callaghan & Fenech 2008). Taken together, this evidence forms a

basis to suggest that micronuclei, γH2AX, and variation in telomere length may be reflected in buccal cells once AD develops.

1.10.6 Why measuring persistent γH2AX response in Q-fly is important

Q-fly is a major insect pest in Australia. Between 2006 and 2009, the average value of fruit fly susceptible production in Australia was approximately $5.3 billion/year, and exports of susceptible crops were worth around $750 million/year. Since standard post-harvest disinfestation insecticides such as fenthion and dimethoate have been withdrawn, irradiation is likely to become the method of choice for disinfestation. There is a need to certify exported produce as having been irradiated to assess quarantine interceptions of live insect pests. Radiation is currently being used to sterilise Q-fly in the sterile insect technique (SIT) programme. The widespread use of SIT for the eradication of fruit fly outbreaks in some areas in Australia (e.g., South Australia) has resulted in them being designated as 'fruit fly free'. The use of fluorescent dye is not reliable in trapped flies, and other approaches are indirect and/or inflexible (rely on testing the strain) and therefore require a molecular marker of prior irradiation that is dose-dependent across disinfestation and SIT doses. A reliable test to retrospectively assess radiation exposure is lacking, which reduces confidence in the context of live pests being detected in exported/imported fruit. In addition, the appropriate radiation dose to induce sterility should be optimised to achieve adequate sterility, while minimising the potentially deleterious effects of irradiation to Q-flies. A test that assesses the prior radiation dose of irradiated fruit would improve and facilitate commercial irradiation treatments in Australia, giving Australian producers potential production and market access advantages. Additionally, retrospective assessment of irradiation in flies used for SIT eradication programmes is another key challenge, and a

reliable test delivering this capacity would be of great benefit. Since persistent γH2AX responses have been reported in different cell and tissue types, an assay based on measuring, persistent γH2AX responses may be investigated for its potential as a method to detect and quantify prior irradiation exposure and to discriminate released irradiated flies from the wild population.

1.10.7 Aim

The aim of this PhD thesis was to (i) investigate IR-induced persistent γH2AX responses in Q-fly and human buccal cells (ii) investigate endogenous γH2AX level in buccal cells and lymphocytes of individuals with MCI and AD relative to control.

1.10.8 Hypotheses:

1. γH2AX signals persist in emergent adult Q-fly and serve as an indicator of previous acute radiation exposure.

2. Lymphocytes and buccal cells of individuals with MCI and AD exhibit a higher level of DNA DSBs relative to healthy controls.

3. Increased endogenous γH2AX signals in lymphocytes and buccal cells of individuals with MCI and AD is associated with other known biomarkers of MCI and AD.

Statement of Authorship

Publication

Mohammad Sabbir Siddiqui, Erika Filomeni, Maxime François, Sam R Collins, Tamara cooper, Richard V Glatz, Phil W Taylor, Michael Fenech, Wayne R Leifert. Exposure of insects cells to ionizing radiation in vivo induces persistent phosphorylation of a H2AX homologue (H2AvB). **Mutagenesis.** 2013 Sep;28(5):531-41. doi: 10.1093/mutage/get030

Mohammad Sabbir Siddiqui (PhD candidate)

Collected the samples and data, conducted all experimental work, analysed and interpreted data, wrote manuscript and contributed to planning of article.

Signed ..... Date 10.08.2016

Erika F

Contributed to experimental protocol and critical evaluation of manuscript.

Signed ..... Date 20/07/2016

Maxime François

Contributed to experimental protocol and critical evaluation of manuscript.

Signed ..... Date 13.07.2016

Sam R Collins

Contributed to experimental protocol and critical evaluation of manuscript.

Signed ..... Date 7/8/16

Tamara cooper

Contributed to experimental protocol and critical evaluation of manuscript.

Signed Date 21/7/16

Richard V Glatz

Contribute to planning of article and provide critical evaluation of the manuscript.

Signed Date 23 July 2016

Phil W Taylor

Contribute to planning of article and provide critical evaluation of the manuscript.

Signed Date 27/07/16

Michael Fenech

Supervised study, contribute to planning of article and provide critical evaluation of the manuscript.

Signed Date 10/08/16

Wayne R. Leifert

Supervised study, development of work, contribute to analysing and interpreting data, wrote manuscript and contributed to planning of article.

Signed

Date ..13./7./2016...

Chapter 2: Exposure of Insect Cells to Ionizing Radiation *In Vivo* Induces Persistent Phosphorylation of a H2AX Homolog (H2avB)

Authors/Affiliations:

Mohammad Sabbir Siddiqui [1], Erika Filomeni [1], Maxime François [1], Samuel R. Collins [2], Tamara Cooper [3], Richard V. Glatz [3, 4], Phillip W. Taylor [2], Michael Fenech [1] and Wayne R. Leifert [1 *]

[1] CSIRO Animal, Food & Health Sciences, Nutritional Genomics & Genome Health Diagnostics, Adelaide, SA, 5000, Australia.

[2] Department of Biological Sciences, Macquarie University, NSW, 2109, Australia.

[3] SARDI Sustainable Systems, Entomology, Waite Building, SA, 5064, Australia.

[4] School of Food, Agriculture and Wine, University of Adelaide, Urrbrae, SA, Australia, 5064, Australia.

Running title:

Persistent γH2AX response to ionizing radiation in Q-fly

Abstract

The response of eukaryotic cells to ionizing radiation (IR)-induced double strand DNA breaks is highly conserved and involves a DNA repair mechanism characterized by the early phosphorylation of histone protein H2AX (producing the active form γH2AX). Although the expression of an induced γH2AX variant has been detected in *Drosophila melanogaster*, the expression and radiation response of a γH2AX homolog has not been reported in economically important fruit flies. We use *Bactrocera tryoni* (Diptera: Tephritidae, Queensland fruit fly or "Q-fly") to investigate this response with a view to developing molecular assays to detect/quantify exposure of fruit flies to IR and consequent DNA damage. Deep sequencing confirmed the presence of a H2AX homolog that we have termed H2AvB (and has an identical sequence to a histone reported from the human disease vector *Glossina morsitans*). A linear dose-response of γH2AvB (0–400 Gy IR) was observed in whole Q-fly pupal lysates 24 h post-IR and was detected at doses as low as 20 Gy. γH2AvB signal peaked at approximately 20 min after IR exposure and at 24 h post IR the signal remained elevated but declined significantly by 5 days. Persistent and dose-dependent γH2AvB signal could be detected and quantified either by Western blot or laser scanning cytometry up to 17 days post IR exposure in histone extracts or isolated nuclei from adult Q-flies (irradiated as pupae). We conclude that IR exposure in Q-fly leads to persistent γH2AvB signals (over a period of days) that can easily be detected by Western blot or quantitative immunohistochemistry techniques. These approaches have potential as the basis for assays for detection and quantification of prior IR exposure in pest fruit flies.

2.1 Introduction

Double strand breaks (DSBs) in chromosomal DNA may lead to genetic instabilities and gene mutations resulting in reduced integrity of the genome but also impaired health and survival (Dugle, Gillespie & Chapman 1976, Olive 1998). Phosphorylation of the C-terminal tails of H2AX histones in nucleosomes which are located in the vicinity of the break (Rogakou et al. 1998, Savic et al. 2009), is one of the earliest known responses to DNA DSB formation in cells. The nucleosome complex comprises DNA wrapped around eight histone proteins, two from each of the four core histone families (H4, H3, H2B, H2A), and is essential for genome health in terms of normal regulation of gene expression, and genome maintenance and replication (Rogakou et al. 1999, Goll, Bestor 2002, Mendez-Acuna et al. 2010). Induction of DSBs in live mammalian cells triggers the phosphorylation of Ser139 contained in the SQ motif near the carboxy-terminus of H2AX, resulting in the formation of phosphorylated H2AX, termed γH2AX (Redon et al. 2002, Kinner et al. 2008). Whilst H2AX is distributed uniformly throughout chromatin, only H2AX molecules located in close vicinity to DSBs become phosphorylated (Rogakou et al. 1998, Savic et al. 2009, Rogakou et al. 1999). Several kinase proteins are known to phosphorylate H2AX including phosphatidylinositol 3-OH serine/threonine protein kinase-like kinases (PIKKs), ataxia telangiectasia mutated (ATM), ATM and Rad-3-related (ATR) and DNA-dependent protein kinase (DNA-PK). However, only ATM and DNA-PKs have been shown to phosphorylate H2AX in response to ionizing radiation (IR) (Rogakou et al. 1998, Redon et al. 2002, Burma et al. 2001, Stiff et al. 2004, Olive, Banath 2004, Park et al. 2003, Fernandez-Capetillo et al. 2004).

The SQ motif in H2AX is highly conserved among animals, plants, and fungi (Downs, Lowndes & Jackson 2000, Friesner et al. 2005, Lang et al. 2012). This evolutionary conservation of the phosphorylation of the core histone protein H2AX suggests the DSB damage-response mechanism is a fundamental process in DNA repair, that arose prior to the evolutionary divergence of fungi, plants and animals. This is partly evidenced by the fact that SQ-specific antibodies raised against the mammalian γH2AX sequence can recognize DSBs in the frog *Xenopus laevis,* vinegar fly *Drosophila melanogaster* and bread/wine yeast *Saccharomyces cerevisiae,* after exposure to IR or other genotoxic agents (Redon et al. 2002, Rogakou et al. 1999). Antibodies that recognise phosphorylated H2AX in mammals have also been shown to recognise IR-induced H2Av (H2AX variant) in *D. melanogaster* (H2AvD) and binding has been shown to be dependent on the presence of the SQ motif (Rogakou et al. 1999, Madigan, Chotkowski & Glaser 2002).

Irradiation-induced genetic damage and repair processes involving γH2AX, are relevant to two very different control measures applicable to management of Queensland fruit fly ('Q-fly' *Bactrocera tryoni*), Australia's most economically damaging insect pest of horticultural crops; post-harvest irradiation and Sterile Insect Technique (SIT). Currently, a generic dose of 150 Gy is applied to exterminate fruit flies in infested produce (Follett, Armstrong 2004, Follett et al. 2011), however assurance of irradiation treatment of produce relies solely on certification. There are currently no routine assays available to detect and/or quantify prior IR exposure in economically important fruit flies or other insects. A direct and reliable assay to confirm irradiation would be of substantial value to export horticulture. In SIT, millions of Q-flies are irradiated as pupae (70 Gy) to induce reproductive sterility and released into the environment as adults where they mate with pest populations and induce reproductive failure, thereby

reducing pest numbers in the next generation. Fruit flies captured in monitoring traps then need to be assessed as being part of the SIT release or part of the outbreak. A generic biomarker based on the distinctive molecular processes of irradiation-induced DNA damage and repair would be a useful tool for this purpose. SIT is also the focus of various ongoing or proposed programs across the globe, aimed at a range of fly species (and other insects) of economic and medical concern (Oliva et al. 2012, Mastrangelo et al. 2012, Ant et al. 2012, Mutika et al. 2013, Kumano, Haraguchi & Kohama 2008, Soopaya et al. 2011) and so a biomarker for identifying sterilized insects would have internationally broad application.

In the present study we identified the sequence of a H2AX protein variant from deep sequencing analysis of Q-fly transcripts and mass spectrometry of the irradiation-induced protein (we have termed this variant H2AvB and the sequence has been deposited into the NCBI Short Read Archive; BankIt1580860 isotig00988 KC161252). We found that H2AvB amino acid sequence is 96.4% similar to the homolog found in the genetic model *D. melanogaster*, 54.8% similar to human H2AX, and identical in comparison with *Glossina morsitans morsitans* (the Savannah tsetse fly). Using Western blotting and laser scanning cytometry (LSC) techniques, we demonstrate an irradiation-induced short-term rapid increase in γH2AvB followed by a long-term (persistent) and dose-dependent γH2AvB response in Q-fly. This assay has practical application to confirm irradiation status of live Q-fly found in exported fruits and to confirm the identity of unmarked flies captured in monitoring traps during SIT releases.

2.2 Materials and Methods

2.2.1 Pupal and Adult Preparation and Irradiation

Bactrocera tryoni (Q-fly) pupae were obtained from the NSW Department of Primary Industries Fruit Fly Production Facility at Elizabeth Macarthur Agricultural Institute (EMAI, New South Wales, Australia). Pupae from this facility are routinely sent to the Australian Nuclear Science and Technology Organisation (ANSTO, Lucas Heights, NSW, Australia) for irradiation as part of the SIT control program to suppress outbreak populations of wild Q-flies. Individual 'zip-lock' plastic bags (100 x 150 mm) containing approximately 8,000 pupae were sealed and packed at EMAI, and transported directly to ANSTO in an air-conditioned vehicle. All pupae were packed on the day of pupation and all irradiated pupae were treated one-day post the onset of pupation. Bags of control and test pupae were packed together at all times during transport and storage to ensure that all pupae received similar conditions. To achieve a hypoxic atmosphere prior to irradiation, the sealed bags were held overnight at ANSTO in a temperature-controlled room at approximately 18ºC. The following day, pupae were treated with IR using ANSTO's ^{60}Co GATRI facility delivering final doses of 0-400 Gy at a dose rate of 5 Gy/min. We investigated doses greater than the standard disinfestations dose of 150 Gy up to 400 Gy, since *Bactrocera* fruit flies appear to be considerably more tolerant to IR compared with other fruit fly genera such as *Ceratitis*, *Anastrepha* and *Rhagoletis* (Follett et al. 2011).

After irradiation, pupae were immediately transported in a closed styrofoam box in an air conditioned vehicle to a laboratory at Macquarie University, Sydney, where they were housed to emerge in 5 L plastic cages, each with a large mesh-covered ventilation hole in the top. Pupae were held in a laboratory maintained at 25 ± 1ºC and 70 ± 5%

relative humidity, on a 14:10 day:night cycle including one hour dawn and dusk periods during which the lights turned on and off intermittently. At one and five days post IR, a sample of Q-fly pupae was frozen and stored at -80°C until required for assays. Other IR-treated pupae were allowed to emerge as adults, then collected using an aspirator and frozen at -80ºC at 17 days post IR. Adult flies were maintained on a standard diet of granular sucrose and yeast hydrolysate, with water provided in soaked cotton wool.

2.2.2 Egg Collection and Irradiation

Adult Q-flies were housed in 5 L plastic cages with one side replaced with mesh screen for ventilation. Approximately 150 flies were kept per cage. After observed mating (post 10 days of age), each cage was provided with an egging dish comprising of a 55 mm Petri dish containing a solution of lemon essence and water in a 140:1 ratio, covered with a layer of parafilm. The parafilm was pierced 5-6 times with an entomological pin to release the odour of lemon. After 2 days the egging dishes were collected and a plastic 5 ml pipette was used to transfer eggs to a 10 ml vial of water. Each vial contained approximately 500 eggs. Vials were then exposed to either 0 or 150 Gy ionising radiation and then frozen at -80ºC 2 h post IR.

2.2.3 Larvae Collection and Irradiation

Adult Q-flies were housed in 5 L plastic cages with one side replaced with mesh screen for ventilation. Approximately 150 flies were kept per cage. After observed mating (post 10 days of age), each cage was provided a collection of fresh organic chillies resting on a 15 cm plate. After 4 days the chillies were inspected for the presence of larvae. All chillies were then left a further 4 days to allow larvae to mature to 3rd instar. Chillies were placed into separate ‘zip-lock’ bags and then exposed to 0 or 150 Gy ionising radiation and maintained at 25 ± 1ºC and 70 ± 5% relative humidity for 24 h.

Chillies were then gently sliced longitudinally in half and larvae were gently removed using a pair of forceps. Collected larvae were frozen at -80ºC in 10 ml vials containing water.

2.2.4 Whole Pupal Lysate Preparation for Western Blotting

Whole pupae were thawed from -80°C at room temperature for 5 min. 10 pupae of each IR dose being investigated were placed in cold (4°C) TBS solution (50 mM Trizma Base, 150 mM NaCl, pH 8.0) in a Petri dish on ice. The pupae were then added to 1 ml lysis buffer comprising RIPA buffer (Sigma) with additional 0.9 % SDS, phosphatase inhibitors (25 mM NaF, 0.25 mM sodium orthovanadate, 1 mM EDTA, 1 mM phenylmethylsulfonylfluoride, 1 mM dithiothreitol) and a protease inhibitor cocktail (Sigma), and their tissues disrupted in a glass tissue homogenizer on ice until a clear suspension was achieved (usually ~15 passes). Lysates were centrifuged at 4°C for 5 min at 300 x*g* to remove debris. Total protein from the pupal samples was quantified using the QuantiPro^{TM} BCA Assay kit (Sigma) as per manufacturer's instructions, using bovine serum albumin (BSA) as a standard. Sample concentrations were adjusted to the same total protein concentration prior to gel electrophoresis. Samples were stored at -20°C until used for Western blotting. Various amounts of total protein were added depending on the assay conducted and this is indicated in relevant figures.

2.2.5 Acid Extraction of Histone Protein from Pupae and Subsequent Dephosphorylation

To obtain histone proteins from pupal samples, an acid extraction technique was performed essentially as previously described (Shechter et al. 2007) with some modification. Pupae were washed twice with TBS and placed in 3 ml of hypotonic lysis buffer (10 mM Trizma Base pH 8.0, 1 mM KCl, 1.5 mM $MgCl_2$, 1 mM dithiothreitol), a

commercial protease inhibitor cocktail and other phosphatase inhibitors (as above), in a glass homogenizer on ice. Pupae were then homogenized until a clear suspension was produced, followed by filtration with nylon net filters (filter type: 100 µm NY1H) and then incubation for 30 min (on a rotator at 4°C) to allow hypotonic swelling and lysis of cells. The crude extract was then centrifuged at 15000 x*g* for 10 min at 4°C to separate the pellet (containing nuclei) from the soluble cytosol. The pellet was then resuspended in 400 µl of 0.8 M H_2SO_4 and vortexed thoroughly until aggregates were dispersed in the solution. This solution was vortexed gently overnight at 4°C using a minishaker. After centrifugation at 15000 x*g* for 10 min at 4°C the pellet was discarded and the acid-soluble histone proteins in the supernatant were then precipitated with a 33% trichloroacetic acid solution. The solution containing precipitated histones was mixed several times producing a milky suspension. Subsequently, the histone solution was incubated at 4ºC overnight and then again centrifuged at 15000 x*g* for 10 min at 4°C; the supernatant was then carefully discarded. The pellet of precipitated histones was washed 3 times with 1 ml ice-cold acetone to remove the acid from the protein sample. The acetone supernatant was removed and the protein pellet was air dried for 30 min at RT and then dissolved in 150 µl of purified H_20. Finally, the histone extract was stored at -20°C for subsequent analyses. In some experiments, dephosphorylation of the purified proteins was achieved by dissolving the extracted protein pellet in 100 mM NaCl, 50 mM Tris-HCl, 10 mM $MgCl_2$, 1 mM dithiothreitol (pH 7.9) and incubated with (or without for negative control) 1000 U/ml calf intestinal alkaline phosphatase (New England Biolabs, USA) overnight at 37ºC.

2.2.6 Total Lysates and Histone Extracts from Individual Pupae

Total lysates or histone extracts were prepared from individual pupae by a modification of the above method. For total lysates, the lysis volume was decreased to 150 µl of RIPA buffer (final volume), and for histone extracts of single pupae the hypotonic buffer was decreased to 150 µl. For the single pupae total lysates, 180 µg total protein was used for SDS-PAGE and analysed by Western blotting, while 1.3 µg total protein was loaded for the histone extracts from individual pupae.

2.2.7 Total Lysates from Irradiated Eggs and Larvae

Samples of irradiated Q-fly eggs were homogenised in liquid nitrogen and subsequently lysed in 150 µl RIPA buffer giving a final protein concentration of approximately 400 µg/ml. 3rd instar larvae (collected from 0 or 150 Gy irradiated chillies) were lysed (using the same method as for pupae) giving a final total protein concentration of approximately 7 mg/ml.

2.2.8 Antibodies

Anti γH2AX was prepared by Biosensis Pty Ltd. (Thebarton, South Australia, Australia). Affinity purified KKAATQA[PSer]QEY (human sequence) peptide conjugated with KLH was used as antigen to generate high titer polyclonal antiserum in rabbit against γH2AX. Drosophila Anti-Histone H2AvD pS137 rabbit polyclonal antibody (Rockland Immunochemicals Inc. Gilbertsville, PA, USA) (Madigan, Chotkowski & Glaser 2002) was also used to detect IR-induced histone in Q-fly. Both antibodies (γH2AX and H2AvD pS137) recognized a 15 kDa protein in Western blot analyses. Cytochrome C oxidase subunit II and β-actin antibodies (Abcam). Alexa Fluor

488-conjugated goat IgG was from Invitrogen (Vic, Australia) and horseradish peroxidase-labelled secondary antibodies were from Perkin Elmer (Vic, Australia).

2.2.9 Western Blotting

Whole and histone-extracted lysates were diluted in Laemmli buffer (1:2 vol:vol) containing β-mercaptoethanol followed by heating at 95°C for 5 min, before being loaded on a Criterion^{TM}-TGX^{TM} precast polyacrylamide gels (BioRad) and subjected to electrophoresis. Gels were then stained with Coomassie Blue to ensure the electrophoresis had been successful and that similar amounts of protein were loaded in each well. A separate (duplicate) gel was used for Western blotting onto a 0.2 μm pore nitrocellulose membrane (BioRad) for 1 h at 100 V in chilled transfer buffer (25 mM Trizma base, 190 mM glycine, 20% methanol, pH 8.5). The membrane was washed 3 times (5 min each) in TBST (TBS containing 0.5% Tween-20) and then blocked for one h at RT in TBST containing 5% BSA. Membranes were then incubated overnight at 4°C in γH2AX primary antibody diluted 1:1000 in TBST containing 5% BSA. Membranes were then thoroughly washed 3 times in TBST for 5 min each time, then incubated with anti–rabbit horseradish peroxidase–linked secondary antibody (PerkinElmer) at a dilution of 1:2000 in TBST containing 5% BSA for 2 h at RT. Probed membranes were then finally washed 3 times with TBST prior to imaging by enhanced chemiluminescence (ECL) (Western Lightning® Plus-ECL, PerkinElmer) using an ImageQuant LAS 4000 imager (GE Health Care). Images were saved as 8-bit TIFF files and band intensities (as integrals) were quantified with ImageJ software (Abramoff, Magalhaes & Ram 2004). Data were normalised to β-actin (loading controls) where possible i.e. in histone extracts this was not possible since actin was removed during the processing of the samples. In Western blots showing histone extracts containing

γH2AvB where β-actin could not be used, we also show Coomassie-stained gel bands at approximately 15 kDa to demonstrate similar loading of histone proteins.

2.2.10 Immunocytochemistry to Quantify γH2AX Response Foci in Q-Fly Nuclei

Cell nuclei obtained from adult Q-fly were extracted using a similar protocol as described above with the following modifications: adult Q-flies (17 days post-IR) were thawed from -80ºC at RT for 5 min and suspended in 1.5 ml of hypotonic lysis buffer containing 10 mM Tris-HCl pH 8.0, 1 mM KCl, 1.5 mM $MgCl_2$, phosphatase inhibitors (as above) and protease inhibitor cocktail, in a glass tissue homogenizer. Tissues were homogenized on ice until a clear suspension was achieved (usually 5 passes). The suspension was filtered using nylon net filters (filter type 100 μm NY1H) to remove most of the particles and then incubated for 30 min on a rotator at 4°C to allow the hypotonic swelling and lysis of cells, which were subsequently fixed in 1% formaldehyde in the same tube for 15 min at RT. Nuclei were then spotted on slides (using 10 μl of the suspension) and air-dried for 20 min at RT. Spotted nuclei were re-hydrated in phosphate-buffered saline (PBS) for 15 min. Slides were then incubated in pre-chilled 70% ethanol for at least 20 min and washed in PBS for 15 min. Cell nuclei were "blocked" using TBST containing 5% BSA for 30 min at RT, and slides were then washed once in PBS. Primary antibody (anti-γH2AX) was added at 1:500 dilution in TBST containing 5% BSA and slides were incubated overnight at 4°C under a parafilm cover. Slides were then washed three times in PBS for 5 min each to remove unbound antibody, and then incubated with secondary antibody (Alexa Fluor 488-conjugated) at a dilution of 1:500 in TBST containing 5% BSA for 1 h at RT. Slides were again washed three times in PBS for 5 min each to remove unbound, or non-specifically bound, antibody. Nuclei staining was achieved using 4',6-diamidino-2-phenylindole

(DAPI) at a concentration of 0.2 µg/ml for 7 min at RT and then washed in a solution containing 300 mM NaCl and 30 mM trisodium citrate (pH 7.0). Spotted, DAPI-stained nuclei were subsequently mounted under a cover slip using mounting medium consisting of PBS and glycerol (1:1) and sealed to prevent desiccation prior to analysis by laser scanning cytometry.

2.2.11 Laser Scanning Cytometry

Microscope slides containing fluorescently stained nuclei were inserted into a standard four-slide carrier and analyzed using an iCyte® Automated Imaging Cytometer (CompuCyte Corporation, Westwood, MA, USA) with full autofocus function, and inverted fluorescence microscope with laser excitation (Argon 488 nm, and Violet 405 nm) for quantitation of blue and green fluorescence emission. 2000–3000 nuclei were analyzed using iCyte cytometric analysis software version 3.4.10. The ‘‘CompuColor’’ feature in iCyte was used to provide nuclear staining as blue and γH2AX signal as green. The slides were scanned using a 40x objective and a 0.25 µm resolution step. Two lasers (405 nm and 488 nm) were used to excite the dyes DAPI and Alexa Fluor 488, respectively. The two lasers were scanned over the samples in separate passes, one immediately following the other, to prevent any overlapping (thus compensation) of fluorescence signals. The emitted and filtered fluorescence was then detected by photomultiplier tubes in separate channels (blue and green). The nuclei and γH2AX events were contoured using empirically determined thresholds to exclude the scoring of false positives (e.g. small fluorescent debris). Any small debris or larger blue-emitting particulate matter (which was rarely observed) was excluded from the analyses. Individual data points for each nuclear event were automatically generated using the iCyte® software and transferred to statistical analysis software (see below).

2.2.12 mRNA Isolation, cDNA Synthesis and 454 Sequencing

Frozen pupae that had been irradiated with 150 Gy were divided into 3 replicate groups, each weighing 0.1g (10-11 pupae). mRNA was purified using a GenElute^{TM} Direct mRNA miniprep kit (Sigma) according to the manufacturer's directions. Briefly, tissues were homogenized and lysed using liquid nitrogen with mortar and pestle and 1 ml of lysis solution containing proteinase K. mRNA extraction proceeded using oligo(dT) beads and eluted mRNA was precipitated overnight at -20°C using 1 µl of 20 µg/µl glycogen, 0.1 volumes of 3 M sodium acetate pH 5.2, and 3 volumes of ice cold ethanol. Precipitated mRNA was centrifuged and the pellet washed in 70% ethanol. mRNA was then resuspended in 19 µl of elution buffer and checked for quantity and quality using a NanoDrop1000 spectrophotometer (Thermo Fisher, USA) and gel electrophoresis. The cDNA library was then generated according to the cDNA Rapid Library Preparation Method Manual (Roche). Each replicate group was ligated with different MID adaptors (RL 13, 14, 15; manufactured by Integrated DNA Technologies). Following library quantitation using a FLURO Star Optima (BMG Labtech, Germany), 20 µl of each replicate was then pooled together and the combined library diluted to a final concentration of $1x10^6$ molecules/µl. Emulsion PCR and bead enrichment was performed as per the emPCR amplification method manual –Lib-L (Roche Applied Science, USA) using 2 library molecules per bead. Approximately 500,000 of the enriched beads were loaded onto a PicoTiter-Plate (Roche Applied Science, USA) and pyrosequencing was performed using a 454 GS Junior (Roche Applied Science, USA) according to the manufacturer's sequencing method manual (Roche) using the default parameters for cDNA.

2.2.13 Sequence Analysis and Homology Search

454 sequencing of the cDNA library generated 3,166,947 bases from 91,349 reads. These reads were assembled into 2,512 contigs, 2,258 isotigs and 21,950 singletons using de novo assembly by Newbler version 2.0.1 (Roche Applied Science). Isotig sequences were compared to sequences in the NCBI database by BLASTn using Blast2goPro (www.Blast2GO.org) (Gotz et al. 2008). E-values lower than 1.0E-3 were considered significant. Isotig00988 (GenBank Acc No. KC161252) was found to be most similar to H2A of Glossina morsitans. Isotig00988 contained 748 bp and the nucleotide sequence was submitted to the ORF finder at NCBI (http://www.ncbi.nlm.nih.gov/gorf/gorf.html). The longest ORF was found to be the candidate H2A protein coding region. Clustal Omega (accessed through http://www.uniprot.org/) was used to compare the resulting amino acid sequence to Drosophila (accession no. P0895), Human (accession no. P16104) and Glossina (accession no. D3PTWO) H2A sequences.

2.2.14 Statistical Analyses

GraphPad Prism 5 was used to analyse data using the student's t-test or to determine the correlation coefficients. Data were expressed as mean ± standard error of the mean. GraphPad InStat 3.1 was used for other statistical analyses.

2.3 Results

Our preliminary studies used an antibody that was prepared based on the human γH2AX sequence KKAATQA[PSer]QEY. The antibody recognized a nuclear protein of approximately 15 kDa that was evident in irradiated pupal samples (not shown) and is consistent with the molecular weight of γH2AX as observed in other species (Redon et

al. 2002, Rogakou et al. 1999). Although the (human) antibody provided a clear band at approximately 15 kDa, there was some non-specific binding detected at approximately 75 kDa. Since there was no available γH2AX antibody specific to *B. tryoni*, we used an antibody specific to the *D. melanogaster* γH2AX sequence (γH2AvD) that resulted in a single band of approximately 15 kDa in irradiated samples. Figure 2.1, shows that 454 sequencing revealed a H2AX protein sequence that was identical to that found in *G. mortisans*, was 96.4% similar to *D. melanogaster*, and only 54.8% similar to human H2AX. We have termed the *B. tryoni* H2AX homolog "H2AvB". The SQ motif of H2AvB was conserved as for all other species in which the histone has been sequenced.

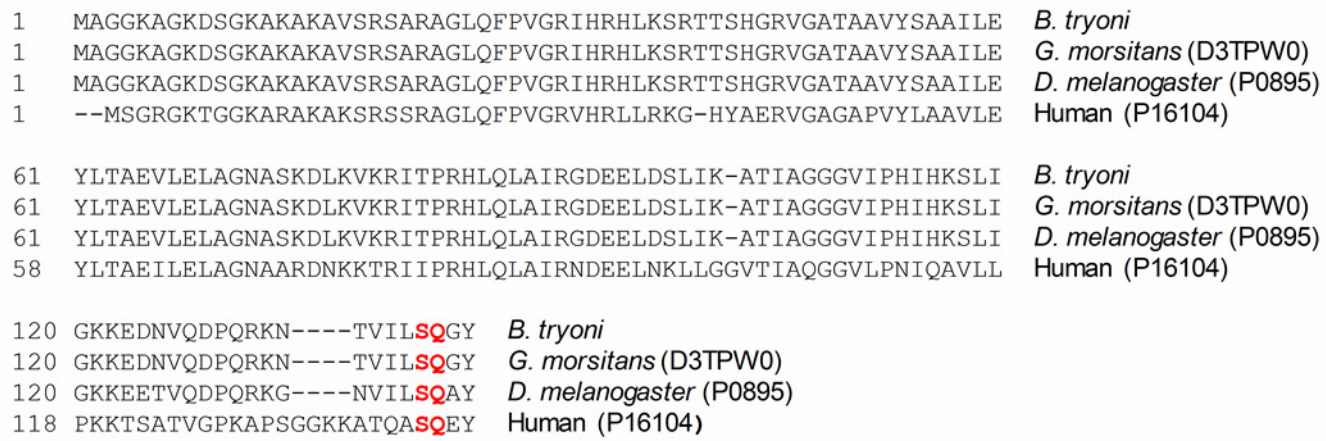

Figure 2.1: Amino acid sequence and alignment of H2A histone variants. The conserved SQ motif is highlighted in red text. The sequence of a H2AX homolog protein was identified from deep sequencing transcript analyses and mass spectrometry of Q-fly (*B. tryoni*) cells. The Q-fly H2A variant is termed H2AvB (GenBank Accession #KC161252). We found that H2AvB is 96.4% similar to that of the vinegar fly (genetic model species) *D. melanogaster* (H2AvD), 54.8% similar to human H2AX, and identical to *G. morsitans* (the Savannah tsetse fly). The numbers in parentheses represents the UniProtKB accession numbers for each sequence. Figures at the left of sequences represent the first amino acid position of each line.

Phosphorylated H2AvB (γH2AvB) was detected following exposure of pupae to doses as low as 10 Gy of IR (Figure 2.2A). The phosphorylation of H2AvB occurred rapidly and could be detected at 5 min post-IR exposure, peaking at approximately 20 min post IR exposure (Figure 2.2B). There was a gradual decline of γH2AvB over a period of 24 h, however, there was still significant γH2AvB present 24 h post IR exposure, indicating that only a proportion of γH2AvB was dephosphorylated within 24 h. As expected, 60 Gy IR exposure led to a higher level of γH2AvB relative to the pupae exposed to 10 Gy. Alkaline phosphatase treatment of a histone extract from IR-treated (70 Gy, 24 h post IR) pupae abolished γH2AvB detection (Figure 2.2C), confirming the antibody was detecting only the phosphorylated form of the H2AvB, at the SQ-motif. Confirming that irradiated samples at other life stages (egg versus larvae) of *B. tryoni* also elicit a γH2AvB response we have also shown an increase in γH2AvB response

following IR exposure at 150 Gy, the standard dose used for Q-fly post-harvest disinfestation (Figure 2.2D).

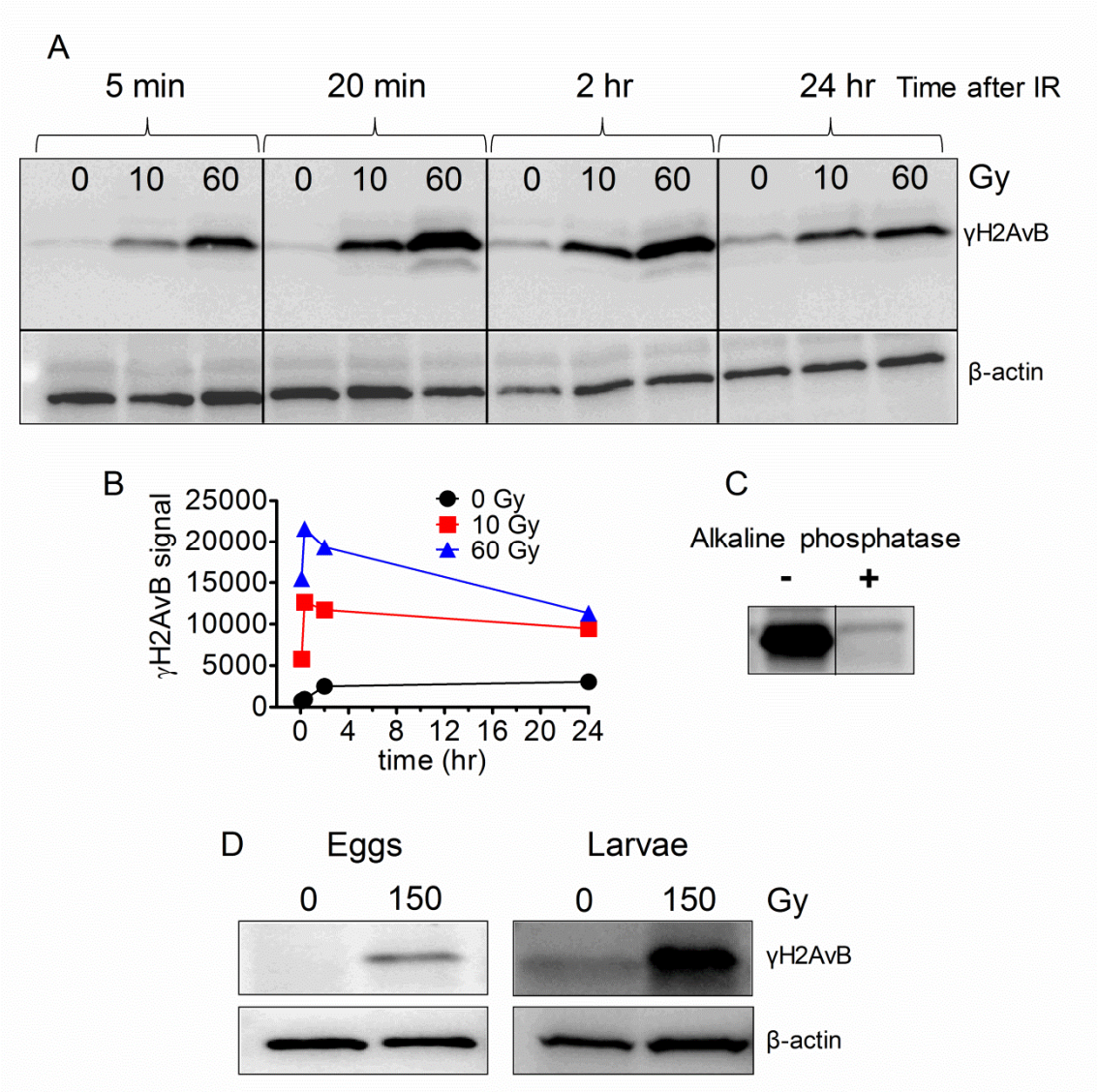

Figure 2.2: Short-term kinetics of H2AvB phosphorylation in Q-fly. (A) Total pupae lysates were prepared and γH2AvB responses are shown to 0, 10, and 60 Gy IR at 5 min, 20 min, 2 h, or 24 h following IR exposure. β-actin is shown on the lower panels to demonstrate loading controls (225 µg protein on each lane). (B) The γH2AvB signal from (A) was quantified using ImageJ and the data were plotted with the following symbols. 0 Gy (filled circles), 10 Gy (filled squares), and 60 Gy (filled triangles). (C) 24 h post-IR exposed pupae were subjected to the acid precipitation method to extract histones. Treatment of samples with alkaline phosphatase (+) abolished the γH2AvB signal, which remained in non-treated samples (-). The data shown confirmed the IR-induced H2AvB is in the phosphorylated form that is detected by the primary antibody. (D) Western blot analyses of Q-fly eggs (73 µg protein loaded; left panel) or larvae right

panel (105 μg protein loaded) demonstrating detectable γH2AvB signal in different Q-fly life stages.

The above data indicate a clear phosphorylation-dependent γH2AvB signal following IR exposure compared with non-irradiated samples. To further investigate the effect of IR on Q-fly pupae at different doses, particularly covering and exceeding the range most often used for SIT and to disinfest produce, pupae were exposed to a wide dose range (up to 400 Gy) and then frozen at -80ºC 24 h post-IR. Figure 2.3A shows a representative Western blot demonstrating a dose-dependent increase in the γH2AvB signal. The maximum signal was produced at the highest tested dose of 400 Gy and yielded an approximate 20-fold increase above non-irradiated pupae. γH2AvB signal was detected in Q-fly pupae at doses as low as 20 Gy, however, in Figure 2.3A this is not particularly clear since this Western blot was exposed for ECL under conditions that would clearly show the higher end doses (>80 Gy) of the Western blot. To compare the results of 3 separate assays, data were normalized by using β-actin as a loading control. Since there were differences between imaging exposure times and therefore the band intensities between separate assays, the data were then further corrected to the "maximum" signal (i.e. at 400 Gy) to account for these potential differences in imaging and incubation conditions. This allowed the slope and fit of the lines of γH2AvB responses to be compared appropriately in separate assays as shown in Figure 2.3B inset. This figure also demonstrates the high linear correlation of γH2AvB with IR dose ($r^2 > 0.9$).

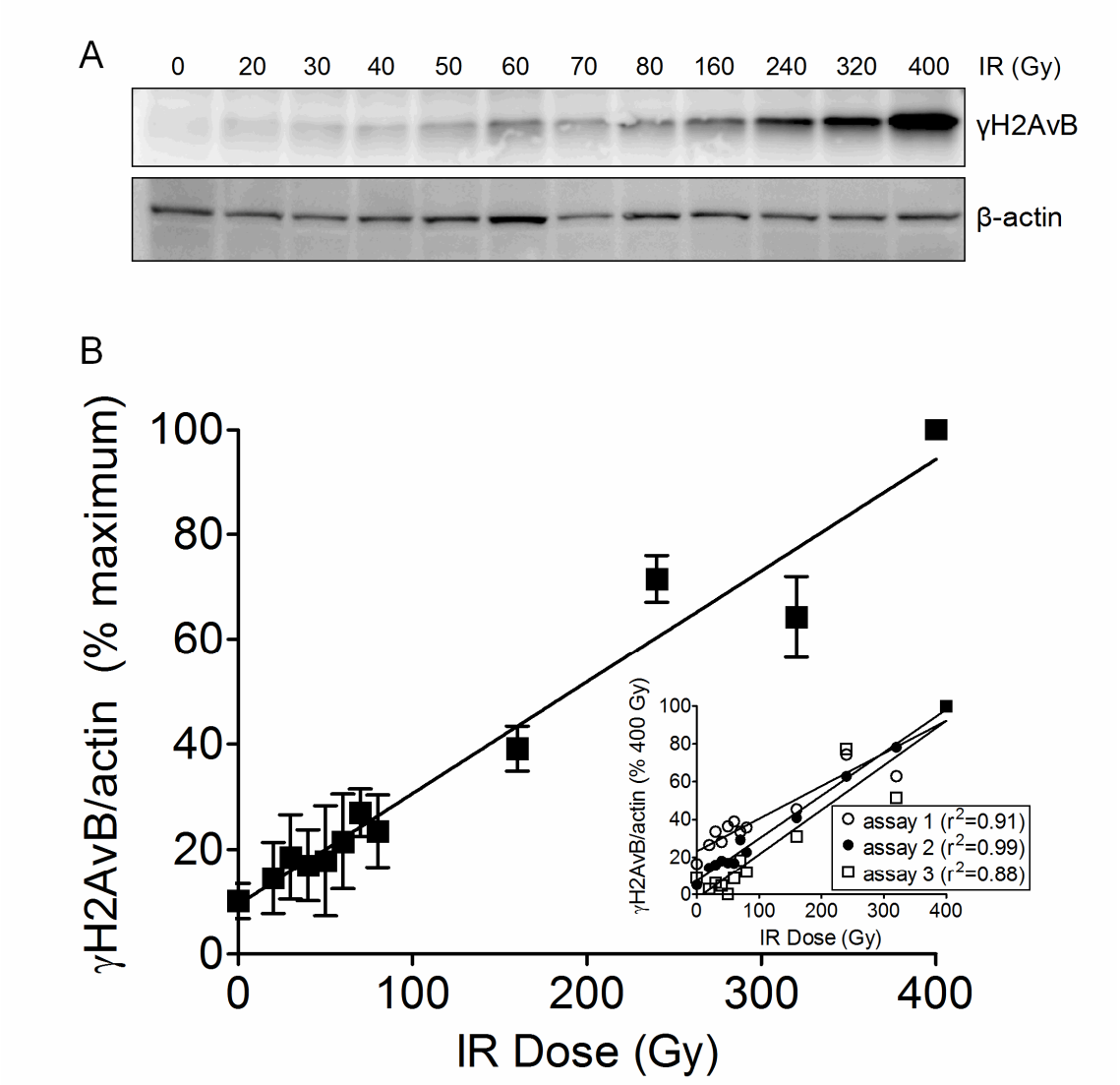

Figure 2.3: The intensity of γH2AvB signal in Q-fly pupae (24 h post IR) is proportional to IR exposure. (A) Western blot showing the γH2AvB signal at approximately 15 kDa (upper panel) increases in proportion to the IR dose up to the maximum exposure of 400 Gy tested for this assay. The lower panel shows the β-actin loading controls. (B) ImageJ software was used to quantify the integral of the bands in (A) upper and lower panels. γH2AvB signal from three independent assays (see inset) was corrected for the amount of β-actin loaded and data (as % of maximum) was plotted against IR dose to allow for differences in incubating conditions and imaging exposure times. Data are mean ± SEM.

Interestingly, our data show a very strong γH2AvB signal in Q-fly pupal lysates from exposures as low as 20 Gy, at least 24 h post-IR (Figure 2.3). This led us to examine whether the γH2AvB signal was evident at even longer time points post-IR, as this would potentially provide a useful biomarker to demonstrate prior IR exposure. Figure

2.4 demonstrates that the dose effect of IR on γH2AvB signal was clearly observed at 24 h post-IR (for doses of 0, 70 & 240 Gy), however, at five days post–IR the γH2AX signal in pupal lysates was substantially reduced compared with one day post-IR (the same amount of total protein was loaded in all samples to allow direct comparisons). It should be noted that in some of our earlier Western blot assays we did occasionally observe a very low amount of γH2AvB signal (approximately 15 kDa) after 70 Gy exposure at five days post-IR, when higher amounts of total protein were loaded and when longer ECL exposure times were used. These preliminary observations led us to believe that there was indeed a measureable persistent γH2AvB signal even 5 days post-IR exposure. Figure 2.4A (lower right panel, labelled "overexposed") shows a longer development time on the same Western blot membrane and a dose-responsive γH2AvB signal became more evident, albeit not as intensely as achieved when analyzed at one day post-IR. This suggests that despite a large decline in phosphorylated γH2AvB levels between one and five days post-IR exposure in Q-fly pupae, a persistent or residual γH2AvB signal remained.

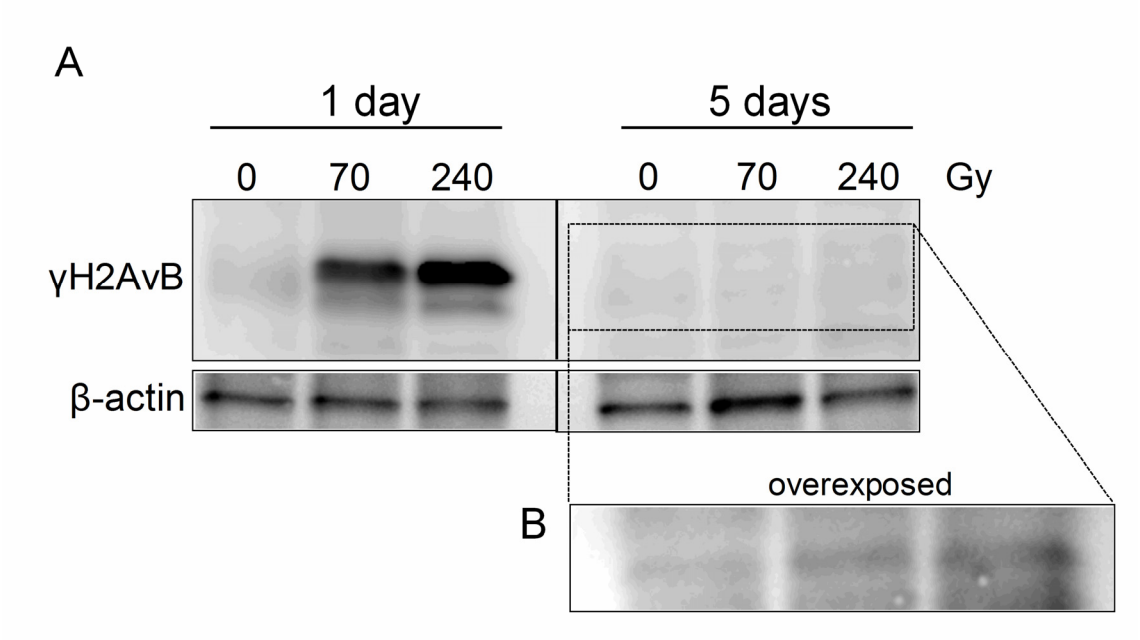

Figure 2.4: γH2AvB signal in Q-fly pupae was reduced at five days post-IR. (A) Western blot showing a dose-dependent increase in γH2AvB signal one day after IR exposure (0, 70 and 240 Gy). However, at five days post IR, the γH2AvB response was not easily visible in this representative assay until the Western blot membrane was allowed to develop with a longer imaging time ("overexposed") as shown in (B). 100 µg protein was loaded in all lanes.

To further examine whether we could detect γH2AvB signal at least 5 days after IR exposure (at the standard dose used for SIT), we investigated the effect of 70 Gy IR on γH2AvB signal using whole Q-fly pupal lysates 1 day and 5 days post-IR. The γH2AvB response was quantified by Western blot as shown in Figure 2.5A (left "pupal lysate" panels, lanes 1 and 2) demonstrating a significant γH2AvB signal at approximately 15 kDa. β-actin and cytochrome c oxidase subunit II were used as loading controls and confirmed that equivalent amounts of protein had been loaded for each treatment. To confirm the specific association of the γH2AvB signal with cell nuclei and to improve the γH2AvB signal we isolated nuclear proteins by an acid precipitation method as described previously (Shechter et al. 2007). When 15 µg total nuclear protein extract was examined by Western blot analysis (shown in lane 5 and 6 of Figure 2.5A, labeled "histone extract") the γH2AvB signal following 70 Gy IR clearly yielded a higher signal

than that of the equivalent amount of protein from the whole "pupal lysate" when either 15 µg or 150 µg protein was loaded (Figure 2.5A). This enrichment of nuclear γH2AvB protein observed was also associated with a higher γH2AvB signal at 0 Gy. Nevertheless, the IR response of γH2AvB signal was clearly distinguishable from background levels and several fold more intense at 70 Gy compared with 0 Gy. The absence of any detectable signal coming from β-actin (cytoplasm) and cytochrome C oxidase subunit II (a mitochondrial protein) in the histone extract (Figure 2.5A, lanes 5 and 6) demonstrate that the histone extract was relatively free from these latter proteins as expected, and confirmed that the nuclear extract method employed did not result in significant cytoplasmic or mitochondrial contamination, whilst significantly enriching the histone fraction. Therefore, it appears that the nuclear histone extraction method offers a convenient way to partially purify and concentrate low levels of persistent IR-induced γH2AvB signal from Q-fly. Since our objective was to detect any long-term persistent γH2AvB signal in irradiated Q-fly pupae we subsequently used the histone extract method to concentrate the γH2AvB signal as outlined earlier. Figure 2.5B shows a representative Western blot experiment using whole lysate from Q-fly pupae (120 µg protein) and nuclear extracts (6 µg protein), five days post-IR. Under the same duration of exposure times using ECL, Figure 2.5B left panels (lane 1 and 2) show no apparent γH2AvB signal response to 70 Gy IR using 120 µg total protein loaded, compared to a strong signal using the histone extract with only 6 µg total nuclear protein loaded (i.e. 20 times less protein, compare lanes 2 and 4 of Figure 2.5B). The IR-induced signal (70 Gy) was clearly evident and significantly higher than the background (0 Gy) signal. Since Q-fly are able to survive and withstand relatively high doses of IR, we hypothesized that adult Q-fly specimens produced from irradiated pupae would contain persistent γH2AvB (as has been observed recently with minipig skin samples after

receiving a dose of 50 Gy IR (Ahmed et al. 2012). Figure 2.5C demonstrates that persistent IR-responsive γH2AvB signal was observed in adult Q-fly at 17 days post-IR, in nuclear extract samples. Although we did not investigate later time points, this may be a convenient method to identify prior IR exposure of Q-fly pupae and therefore, may have application for SIT. To address whether individual pupae show variation in their γH2AvB response following IR exposure, we scaled down the total lysate and histone extraction techniques in order to examine γH2AvB responses of individual pupae. Figure 2.5D demonstrates that when replicate individual pupae were lysed and used for Western blot analyses, there was some variation of the γH2AvB produced in response to IR as would be expected. However, on the whole, all pupae from the 0 Gy group (individual pupae lysates were loaded in lanes 1-6, Figure 2.5D) had significantly less γH2AvB signal compared individual pupae exposed to 70 Gy IR (24 h post IR), as shown in Figure 2.5D, lanes 7-12. The γH2AvB signal was quantified using ImageJ and results are shown on the right panel of Figure 2.5D, with 70 Gy (n=6) significantly higher ($P<0.001$) than 0 Gy (n=6). Furthermore, we were able to scale down the histone extraction method in a similar manner so that individual pupae could be subjected to the nuclear extraction method to increase the γH2AvB signal per total protein tested. Pupae exposed to 70 Gy had a significantly higher amount of γH2AvB signal ($P<0.001$) in the individual histone preparations as demonstrated by the Western blot from the single pupae replicates compared with 0 Gy (Figure 2.5E).

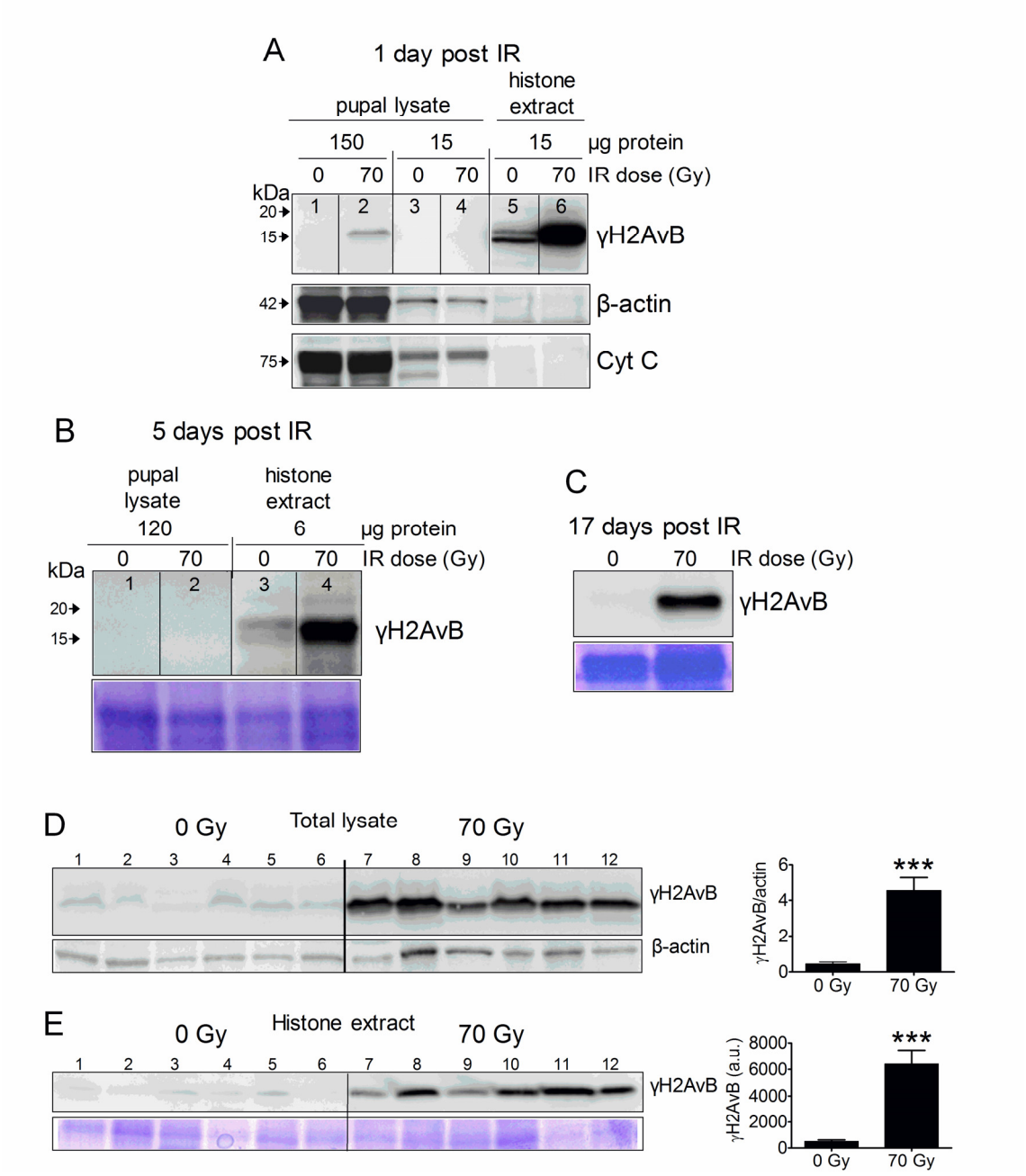

Figure 2.5: γH2AvB response in Q-fly pupae following 70 Gy exposure at different times post-IR. (A) Left panel show γH2AvB response from whole pupal lysates (150 µg protein loaded; 0 vs 70 Gy; lanes 1 and 2). There was no clear signal at 15 kDa in the non-irradiated control. At 10-fold dilution of the same sample to 15 µg, the γH2AX was not observed in the same Western blot membrane at the same imaging exposure time using the ECL technique (lanes 3 and 4). However, in the same Western blot membrane when 15 µg total protein from the histone extract was loaded, two bands appeared at approximately 15 kDa in the non-irradiated sample, which likely represent phosphorylated and non phosphorylated H2AvB, respectively. The 70 Gy sample showed a far more intense signal even exceeding that observed when 10 times the amount of whole pupal lysate was analyzed demonstrating that nuclear extraction may provide a good method to concentrate the histone proteins and increase the related signal, for analysis of γH2AvB. The absence of cytoplasmic proteins including β-actin and cytochrome C oxidase subunit II proteins in the histone extract preparation

confirmed the relative purity of the histone extract. (B) γH2AvB signal in Q-fly pupae was reduced at 5 days post-IR as confirmed by analyses of total pupal lysates (lanes 1 and 2). However, significant γH2AvB signal was observed in the histone extract from Q-fly pupae five days post-IR (70 Gy; lanes 3 and 4), even when probing 20 times less total protein. (C) 17 days post-IR (70 Gy) significant γH2AvB signal was observed in the histone fraction. (D) Variability in individual pupae responding to IR. Individual pupae were exposed to 0 Gy (n=6; lanes 1-6) or 70 Gy (n=6; lanes 7-12) and γH2AvB is shown for each. (E) Variation in response of individual pupae responding to IR using histone extracts. Individual pupae were exposed to 0 Gy (n=6; lanes 1-6) or 70 Gy (n=6; lanes 7-12) and the individual γH2AvB responses are shown for each. For both (D) and (E) all histone extracts shown were run on the same Western blot to allow direct comparison. Bar charts to the right represent the mean ± SEM of the band intensities (integral) as determined by ImageJ analyses. Lower panels in (B), (C) and (E) are loading controls showing the Coomassie-stained gels have equivalent amount of protein loaded. ***P<0.001.

To further validate the long-term (17 days) post IR γH2AvB response (as shown in the Western blot in Figure 2.5C), we employed immunohistochemical methods using nuclear extracts in combination with laser scanning cytometry (LSC). LSC is a very accurate cytometric method to colocalise and quantify fluorescent events in thousands of nuclei (Zhao et al. 2009, Zhao, Traganos & Darzynkiewicz 2009) (which is not practical with visual scoring), therefore we used this method to quantify the γH2AvB signal in nuclei fixed on microscope slides. Representative LSC images of adult Q-fly nuclei stained with DAPI (blue) and demonstrating the γH2AvB signal are shown in Figure 2.6 (A–C). To determine whether long-term persistent γH2AvB signal could be observed at low and high doses, Q-fly pupae were exposed to 0, 20 or 240 Gy and then allowed to emerge as adults. The γH2AvB signal (green) was observed within nuclei 17 days post-IR, in doses as low as 20 Gy. Figure 2.6D shows the mean (± SEM) integral fluorescence (from LSC) was significantly increased (P<0.001) following 20 Gy IR (n = 3078 nuclei) or 240 Gy IR (n = 3571 nuclei) compared with 0 Gy IR (n = 2656 nuclei). Figure 2.6E demonstrates that 240 Gy IR exposure resulted in a significantly higher (P<0.001) percentage of nuclei containing a γH2AvB signal compared with 0 Gy (24% and 7%, respectively). The fluorescence integral of those nuclei with a positive γH2AvB

signal identified from Figure 2.6E were quantified and then reported in Figure 2.6F (as mean ± SEM). Figure 2.6F demonstrates that the γH2AvB signal (integral) was also significantly elevated in adult Q-fly nuclei 17 days post IR at the low dose of 20 Gy ($P<0.01$) as well as the higher dose of 240 Gy ($P<0.05$). The area of the γH2AvB signal in nuclei was examined as shown in Figure 2.6G. Although the area of γH2AvB signal appeared to be dose-dependent at 20 and 240 Gy, this increase was not statistically significant. The overall findings illustrated in Figure 2.6 further confirmed that γH2AvB signals persisted in emergent adult Q-flies for at least 17 days post IR (irradiated as pupae).

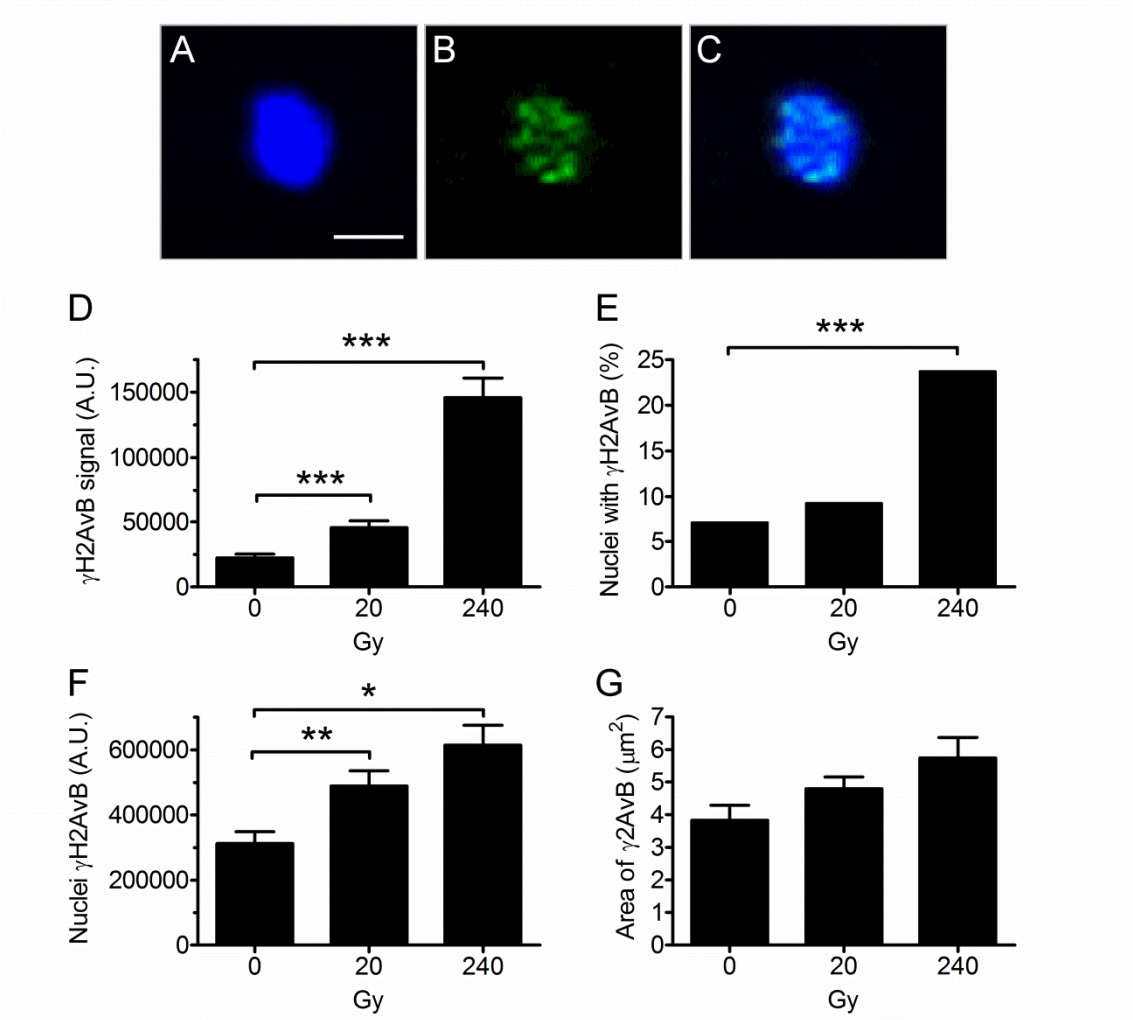

Figure 2.6: Quantification of γH2AvB signal in isolated adult Q-fly nuclei by laser scanning cytometry (LSC). Q-fly pupae were exposed to 0, 20 or 240 Gy IR and allowed to emerge as adults. At 17 days post-IR they were frozen at -80ºC. Following hypotonic lysis and extraction of nuclei, LSC was performed on samples. Representative LSC images of Q-fly nuclei showing (A) DAPI only (blue), (B) γH2AvB signal only (green) and (C) "merged" images which show the DAPI and γH2AvB signal overlaid. The scale bar in (A) represents 5 μm. (D) Mean (± SEM) of the integral fluorescence per nucleus of all nuclei examined including nuclei that lacked any measurable γH2AvB signal; n = 2656, 3078 and 3571 nuclei for 0, 20 and 240 Gy samples, respectively. (E) The percentage of nuclei examined that contain a measurable γH2AvB signal above background, increased significantly from approximately 7% in 0 Gy samples to almost 25% of nuclei in 240 Gy samples ($P<0.001$ by chi-squared). To further examine if there was a greater γH2AvB signal in the 20 and 240 Gy samples compared with 0 Gy samples, only those nuclei with a measurable γH2AvB signal were analyzed and this is reported in (F) as the mean integral (± SEM). Finally, the mean contoured areas of the total γH2AX signal per nucleus are shown in (G). *$P<0.05$, **$P<0.01$, ***$P<0.001$.

2.4 Discussion

Phosphorylation of the C-terminal tail of H2AX proteins in nucleosomes located in the vicinity of DSBs is one of the earliest responses to IR-induced DNA damage (Rogakou et al. 1998, Olive, Banath 2004). A γH2AX homolog has not been reported previously in tephritid fruit flies, including the commercially important Q-fly (*B. tryoni*), although the expression of a H2AX variant (H2AvD) has been reported in the vinegar fly *D. melanogaster* (Madigan, Chotkowski & Glaser 2002). In this study we show that Q-fly pupae exposed to IR had an elevated level of phosphorylated H2A protein (termed γH2AvB). Consistent with reports for other species (Rogakou et al. 1999), irradiated Q-fly pupae showed a strong γH2AvB signal of approximately 15 kDa when examined using Western blot. The γH2AvB sequence was identified using 454 sequencing and found to be identical to *G. morsitans.* The identity and partial sequence of the IR-induced, phosphorylated histone was also confirmed by LC-ESI-MS/MS (data not shown, mass spectrometry was carried out by the Adelaide Proteomics Centre, University of Adelaide, SA, Australia). Twenty-four hours post-IR we observed a linear dose-response of γH2AvB up to our maximum tested dose of 400 Gy in Q-fly pupae. However, after 5–17 days post IR, the γH2AvB signal had declined significantly when analysing whole pupal lysates. In contrast, the persistent (5 days post-IR and beyond) γH2AvB response remained dose-responsive and was easily measurable by either Western blot or immunohistochemical methods such as LSC when analysing enriched nucleosome extracts. The dose-dependent response over doses used for SIT (70 Gy) and disinfestation of fruit (up to 400 Gy), shows that γH2AvB may be useful as a marker of previous IR exposure in assays that support these commercially important applications.

γH2AX is highly conserved across a wide taxonomic range of organisms (Redon et al. 2002, Friesner et al. 2005) and is a well-characterized histone protein that is known to be responsive to IR-induced DSBs (Roch-Lefevre et al. 2010, Olive, Banath 2004, Huang, Halicka & Darzynkiewicz 2004). We identified the sequence of a H2AX homolog protein in the Q-fly, *B. tryoni* (termed H2AvB; GenBank Accession #KC161252). We found that H2AvB is approximately 96% similar to the vinegar fly *D. melanogaster* H2AvD, approximately 54.8% similar to human H2AX and interestingly, identical to the human disease vector *G. morsitans* (which is also the subject of SIT (Mutika et al. 2013)). Our preliminary experiments demonstrated that an antibody designed to the human c-terminal tail sequence of γH2AX, KKAATQA[PSer]QEY, showed similar IR-induced γH2AvB signal compared with the antibody used for detection of *D. melanogaster* γH2Av as used in this study, which revealed a protein of approximately 15 kDa. The C-terminal amino acid sequence of human histone H2AX consists of ASQEY whereas for *D. melanogaster* the equivalent sequence is LSQAY. Although the C-terminal sequence for *B. tryoni* is slightly different from both human and *Drososphila*, it therefore appears that the antibody recognition site is likely to be mostly targeted towards recognizing the SQ phosphorylation motif, which is conserved across species. Indeed, others have used antibodies based on the human sequence of phosphorylated H2AX and found that it cross-reacts with histone H2A (phosphorylated) variants from many diverse taxa, including plants (Rogakou et al. 1999, Friesner et al. 2005). Therefore, it was not surprising in this study that the H2AvD antibody (based on the *Drosophila* sequence) yielded a single intense band on Western blots (following IR) corresponding to phosphorylated H2AvB in the *B. tryoni* samples.

Many studies have analyzed the kinetics of phosphorylation and dephosphorylation of H2AX, with IR shown to induce maximal amounts of γH2AX in cells at times often less

than 10 min after exposure to IR followed by a decline in γH2AX signal over a period of hours (Rogakou et al. 1998, Madigan, Chotkowski & Glaser 2002, Roch-Lefevre et al. 2010, Olive, Banath 2004). Previous reports using *Drosophila* S2 tissue culture cells have suggested that the phosphorylation of H2Av increases within minutes following IR exposure, but then declines significantly after several hours (Madigan, Chotkowski & Glaser 2002). The rapid loss of the phosphorylated H2Av was likely due to regulated dephosphorylation of H2Av and was similar to that reported for radiation-induced phosphorylation/dephosphorylation kinetics in mammals (Rogakou et al. 1998). Indeed, γH2AX quantification assays have been proposed as the basis of protocols for biological dosimetry following IR events (Roch-Lefevre et al. 2010). Although the absolute number of phosphorylated γH2AX molecules declines over a period of hours and days post-IR, a recent study in mice showed a dose-dependent response of γH2AX foci in nuclei up to 7 days after exposure to IR (Bhogal et al. 2010). The residual γH2AX foci at 24-72 h post-IR are believed to represent misrepaired DSBs, unrepaired DNA with ongoing genomic instability, S-phase cells or apoptotic cells (Liu, Olive & Bristow 2008). In *Drosophila* S2 cultured cells, the percentage of phosphorylated H2AX variant (H2Av) was shown to have reduced almost to non-irradiated levels within 3 h after the initial IR dose (Madigan, Chotkowski & Glaser 2002). Similarly, in cultured human microvascular endothelial cells exposed to 2–16 Gy IR, a transient increase in γH2AX signal was observed to peak at 1 h post IR and return to background levels 24 h post IR (Kataoka et al. 2006). The γH2AvB response we observed in whole tissue displayed kinetics that were less transient than that of cultured cells and persisted at measurable levels for at least 17 days, although the signal was considerably reduced even 1-5 days post IR. It should be noted that doses used in human studies are generally much less than applied here, as the doses used for SIT and disinfestation of insects are well

beyond what can be tolerated by humans. Thus, the persistence of the phosphorylated protein may be related to the higher IR-doses we have tested. The basis for the relatively high IR-tolerance of insects is not clear, however, it is conceivable that it may be partly related to the persistence of the phosphorylated histone. A recent study that used Göttingen minipig skin biopsies found that radiation induced γH2AX foci (50 Gy) were observed in approximately 60% of cells 4 h after IR. The number of γH2AX foci was found to be significantly less after 70 days following IR exposure; however, there remained a significantly higher number of γH2AX foci per epidermal keratinocyte compared with controls (Ahmed et al. 2012). In our study there was a strong positive linear correlation (r^2>0.9) in γH2AX signal over a dose range of 0–400 Gy, corresponding to a 20-fold increase in signal above the background (non-irradiated) level. It is therefore likely that high IR doses are necessary to observe the long–term persistent γH2AX signals. Indeed, after 17 days post IR (240 Gy) we found that approximately 25% of nuclei had a measurable signal γH2AvB as determined by LSC. Although LSC detected a small amount of measurable background signal in 0 Gy Q-fly adults in approximately 7% of nuclei, we did not observe a 0 Gy γH2AvB signal by Western blotting (Figure 2.5C). Therefore, it appears LSC may prove to be a more sensitive method to detect and quantify γH2AvB signal in nuclei that are persistent many days after exposure to the IR event. Bonner et al. (Rogakou et al. 1999) previously suggested there is potentially a low level of γH2AX in non-irradiated cells. This is in agreement with our study (see discussion below) in which we additionally confirmed the necessity for the phosphorylation of putative Ser137 within the SQ motif of γH2AvB to allow detection by our primary antibody, through abolishing the signal via treatment of the histone extract with alkaline phosphatase.

At five days post IR exposure, we occasionally observed an IR-induced γH2AX signal in whole pupal lysates via Western blotting (depending on amount of protein loaded on gels and imaging exposure times). Therefore, the nucleosome (histone) extraction procedure was used and this resulted in a substantial enrichment of the γH2AvB signal compared with the use of the whole pupal lysates. In the non-irradiated whole pupal lysate we did not detect any γH2AvB. However, in the non-irradiated histone fraction, we observed a basal γH2AvB signal in the non-irradiated 5 day samples. However, at 17 days (Q-fly adults) we did not observe a γH2AvB signal in the 0 Gy samples, possibly indicating that "basal" level of γH2AvB is life-stage specific and is dependent on the level of cellular differentiation.

LSC was a successful technique for quantitation of IR-induced γH2AvB signal in Q-fly showing the localisation within nuclei as well as its quantitative increase in adult Q-fly 17 days post-IR as pupae. Our LSC results support data obtained by Western blot analyses and also provide a visualisation of the signal, although visual scoring of foci was not practical. The iCyte® software allows for automated scoring and quantitation of nuclei and events within them, and therefore LSC could be useful for future studies to investigate additional parameters associated with IR induction of γH2AvB (e.g. γH2AvB signal related to cell cycle phases) at a tissue-specific level. Additionally, LSC could be used to simultaneously detect γH2AvB signal with a dependant DNA repair mechanism protein such as ATM or other markers such as caspases (for apoptosis), to yield more information on cell-cycle dynamics.

Our work has identified γH2AvB as a potential biomarker and biodosimeter of prior IR exposure in Q-fly. This finding has several potential applications for the management of these economically important insects. Firstly, with chemical approaches facing

increasing restrictions, IR treatment is quickly becoming an internationally accepted alternative for disinfestation of horticultural produce (IAEA-TECDOC-1427 2004). Secondly, doses of 70 Gy applied to pupae are used to induce reproductive sterility in flies released during SIT pest management programs that are used to reduce Q-fly populations (Collins et al. 2009). The γH2AvB assay presented here (or modifications thereof) may have applications in both these contexts for detecting IR-induced DNA damage in Q-fly specimens. Given that *G. mortisans* is an important human disease vector for which SIT is being investigated, and that its homologous histone protein is apparently identical to γH2AvB, the assays developed here may also be applicable for monitoring in *G. mortisans* SIT programs. In addition, given that many of the DNA-repair and apoptotic biochemical pathways are conserved between mammals and insects (Song 2005, Steller 2008, Sun et al. 2010), insect-based assays may be useful for detecting DNA-damage processes occurring in the environment as insects are widespread and abundant, and some species can be efficiently trapped using highly specific chemical lures. Tephritid fruit flies also generally meet these criteria. Future studies that focus on γH2AvB as a potential biomarker of IR-induced DNA damage in Q-fly should extend the time course following IR exposure and use tissue section immunohistochemistry techniques that will allow identification of tissue-specificity of γH2AvB signals in Q-fly. The kinetics of γH2AvB phosphoylation/dephosphoryhlation in different life stages of Q-fly would also be of benefit.

Statement of authorship

Publication

Mohammad Sabbir Siddiqui, Maxime François, Michael Fenech, Wayne R. Leifert. (2014) γH2AX responses in human buccal cells exposed to ionizing radiation. **Cytometry** A. 2015 Apr;87(4):296-308. doi: 10.1002/cyto.a.22607.

Mohammad Sabbir Siddiqui (PhD candidate)

Collected the samples and data, conducted all experimental work, analysed and interpreted data, wrote manuscript and contributed to planning of article.

Signed ..... Date 10.08.2016

Maxime François

Contributed to experimental protocol and critical evaluation of manuscript.

Signed ..... Date 13.07.2016

Michael Fenech

Supervised study, contribute to planning of article and provide critical evaluation of the manuscript.

Signed ..... Date 10-08-2016

Wayne R. Leifert

Supervised study, development of work, contribute to analysing and interpreting data, wrote manuscript and contributed to planning of article

Signed [redacted] Date 13/7/2016

Chapter 3: γH2AX Responses in Human Buccal Cells Exposed to Ionizing Radiation

Authors:

Mohammad Sabbir Siddiqui [1, 2], Maxime François [1], Michael Fenech [1] and Wayne R Leifert [1].

Affiliations:

[1] CSIRO Food & Nutrition Flagship, Nutrigenomics & DNA Damage, Adelaide, South Australia 5000, Australia.

[2] University of Adelaide, School of Agriculture, Food & Wine, Urrbrae, South Australia 5064, Australia.

Keywords for title: γH2AX, buccal cells, ionizing radiation

Running title:

γH2AX response to ionizing radiation in buccal cells

Abstract

DNA double strand breaks are induced by ionizing radiation (IR), leading to the phosphorylation of the core histone protein H2AX (termed γH2AX). The understanding of the γH2AX responses in irradiated human buccal cells is still very limited. We used visual scoring and laser scanning cytometry (LSC) methods to investigate γH2AX signalling following exposure of human buccal cells (from six individuals) to ionizing radiation at 0-4 Gy. The frequency of nuclei containing 15-30 γH2AX foci was significantly elevated 30 min post-IR exposure (by visual scoring). Concomitantly, there was a significant decrease in the frequency of cells without foci following exposure to IR. IR-induced γH2AX signal as determined by laser scanning cytometry (which included γH2AX integral and MaxPixel value) increased significantly in all individual's 2N nuclei 30 min post-IR and was similar for all 3 nuclear shapes identified. Individuals with the lowest baseline γH2AX integral (i.e. in non-irradiated cells) showed the greatest fold stimulation of γH2AX and significant dose-responses to IR doses of 1, 2, and 4 Gy. In 5 out of 6 individuals, the frequency of visually scored γH2AX in nuclei showed a strong correlation (up to $r = 0.999$) with LSC scored γH2AX integrals. The γH2AX response and subsequent decline varied between individuals but remained elevated above baseline levels 24 h post IR exposure. γH2AX response in irradiated human buccal cells has potential to be used as an index of baseline DNA damage in population studies. The variable response to IR exposure between individuals should be taken into consideration when using the γH2AX assay for radiation biodosimetry.

3.1 Introduction

DNA Double strand breaks (DSBs) are one of the most biologically significant DNA damage lesions that leads to chromosome breakage and/or rearrangement, mutagenesis and loss or gain of genetic information (Dugle, Gillespie & Chapman 1976, Olive 1998). DSBs are directly generated by exogenous agents such as ionizing radiation (IR) (Ismail, Wadhra & Hammarsten 2007, Riches, Lynch & Gooderham 2008), antitumor drugs (bleomycin, mitoxantrone, etoposide) (Tanaka et al. 2009, Turner et al. 2001) or by endogenously generated reactive oxygen species (Pilch et al. 2003). Mammalian cells respond to DSBs by activating a multitude of proteins involved in signalling and DNA repair pathways. Although the majority of lesions are efficiently repaired, the very nature of DSBs poses such a threat to cell survival that DNA damage checkpoint proteins may be activated to initiate cellular division arrest. This provides time for DNA repair to proceed before mitosis is completed or in the case of overwhelming damage, apoptosis ensues (Rogakou et al. 2000). Therefore, DSBs in chromosomal DNA may lead to reduced integrity of the genome but also impaired health and survival of mammalian cells (Dugle, Gillespie & Chapman 1976, Olive 1998).

The histone proteins are intricate components of the nucleosome complex and are essential for genome integrity in terms of normal regulation of gene expression, genome maintenance and replication (Rogakou et al. 1999, Goll, Bestor 2002, Mendez-Acuna et al. 2010). Induction of DNA DSBs in live mammalian cells triggers the phosphorylation of Ser139 in the SQ motif near the C-terminal of H2AX, which results in the phosphorylated form of H2AX, termed γH2AX (Redon et al. 2002, Kinner et al. 2008). The phosphorylation of H2AX histone proteins which are located in the vicinity of the DSBs (Rogakou et al. 1998, Savic et al. 2009) is known as one of the earliest responses

to DNA DSBs in cells. Therefore, γH2AX quantification may prove to be a sensitive biomarker of DNA DSBs in human cells.

Studies of the kinetics of phosphorylation and dephosphorylation of H2AX after exposure of cells to IR have shown induction of maximal amounts of γH2AX in cells in a few minutes after exposure to IR (Rogakou et al. 1998, Madigan, Chotkowski & Glaser 2002, Roch-Lefevre et al. 2010, Olive, Banath 2004). Subsequently, the γH2AX signals decline over a period of hours. However, radiation induced γH2AX signals have been observed to persist after 70 days post IR exposure to skin cells (Ahmed et al. 2012). Our previous study using Queensland fruit fly (*Bactrocera tryoni*) demonstrated that IR exposure leads to persistent γH2AvB signals (a variant of γH2AX) that could be measured during the adult stage of the life cycle when the IR exposure was conducted at the pupal stage (Siddiqui et al. 2013). Therefore, it is plausible that persistent γH2AX may represent prior DNA damage due to misrepaired DSBs, unrepaired DSBs in specific sequences such as telomeric DNA, S-phase cells or apoptotic cells (Liu, Olive & Bristow 2008).

Human buccal mucosa has considerable potential as an easily accessible source of cells to determine endogenous- or exogenous-induced DNA damage (Leifert et al. 2011, Darzynkiewicz et al. 2011) and has been used successfully to measure IR-induced γH2AX signals (Gonzalez et al. 2010, Yoon et al. 2009). In one recent study, a sub-population of 50-100 buccal cells were scored from microscope images by semi-automation for the presence of γH2AX foci (Gonzalez et al. 2010). Another study measured the absorbance of diffuse γH2AX staining in nuclei from individuals exposed to a low dose of ionizing radiation by examining only 25-30 cells from each individual (Yoon et al. 2009). However, our previous studies have demonstrated that there are

multiple sub-populations of buccal cell types present (Thomas et al. 2007, Thomas et al. 2009, Francois et al. 2014a) and therefore in both of those earlier studies (Gonzalez et al. 2010, Yoon et al. 2009), it was likely that insufficient cells were scored to give an accurate representation of the entire sample population's γH2AX response. Moreover, different nuclear shapes have been used as criteria to identify nuclear abnormalities in buccal cells (Torres-Bugarin et al. 2014). The aim of this study was to determine whether LSC could be used to measure multiple parameters (area, integral, MaxPixel) of γH2AX signals as well as the ploidy and nuclear shapes in thousands of cells. Use of the proposed LSC γH2AX method can overcome limitations of visual scoring methods by increasing scoring speed, increasing cell number measured, eliminating variation due to differences between scorers and scorer fatigue, and enabling the possibility of higher statistical power and high content analysis of multiple nuclear parameters.

3.2 Materials and Methods

3.2.1 Chemicals and Reagents

Roswell Park Memorial Institute (RPMI)-1640, Fetal Bovine Serum (FBS), sodium pyruvate, L-glutamine/penicillin/streptomycin mix and all other chemicals were purchased from Sigma-Aldrich (Castle Hill, NSW, Australia) unless otherwise stated. Mouse monoclonal antibody anti-γH2AX (clone JBW301) was obtained from Millipore (Kilsyth, VIC, Australia). Dulbecco's Phosphate Buffered Saline (DPBS) and secondary antibody Alexa Fluor 488 Goat anti-mouse were purchased from Life Technologies (Mulgrave, VIC, Australia).

3.2.2 Participants

Buccal cells were collected from six healthy individuals (three females and three males) aged from 25 to 44 years. Participants were healthy non-smokers, not taking vitamin supplements and were informed of the purpose of the study. Approval for this study was obtained from the CSIRO Human Research Ethics Committee.

3.2.3 Buccal Cell Collection

Prior to buccal cell collection, each participant was first required to rinse their mouth twice with water. Small flat headed toothbrushes were rotated 20 times against the inner part of the cheeks in a circular motion. Both cheeks were sampled using separate toothbrushes. Heads of the brushes were transferred into 20 ml conical screw cap tubes (one tube per participant) each containing 15 ml of fresh pre-warmed complete medium (RPMI with 10% FBS, 2 mM L-Glutamine, 1 mM sodium pyruvate, 100 U penicillin and 100 µg/ml streptomycin) and vigorously agitated to dislodge the cells. Cells were centrifuged at 1000 x*g* for 10 min before discarding and replacing supernatant with fresh DPBS. This washing procedure was carried out twice. The cells were then resuspended in 10 ml of fresh pre-warmed (37ºC) complete medium. Cell concentration was assessed using a haemocytometer and diluted with complete medium to reach a final concentration of 50,000 cells/ml. The cell suspension was then divided into four 10 ml aliquots in 20 ml conical screw cap tubes.

3.2.4 Buccal Cell Irradiation

Cell aliquots were exposed to 0, 1, 2, or 4 Gy ionizing radiation (IR) using a ^{137}Cs-γ IBL 437 irradiator 5 Gy/min at 25ºC (Shering CIS bio international) and immediately incubated for 30 min at 37ºC in complete medium using a portable tissue incubator. For

kinetics experiments, post-irradiated cells (4 Gy) and non-irradiated cells (0 Gy) were incubated at 37ºC in complete medium for 30 min, 3 h or 24 h. Following incubation, cells were centrifuged at 1000 x*g* for 10 min and supernatant was discarded. Cells were then resuspended in 10 ml of 4% formaldehyde in DPBS for 15 min at room temperature. Following fixation cells were centrifuged at 1000 x*g* for 10 min and supernatant was removed before washing cells in 10 ml of buccal cell buffer (10 mM Tris, 0.1 M ethylenediaminetetraacetic, 20 mM NaCl, pH 7.0). The washing procedure was carried out twice, and cells were then cytocentrifuged for 5 min at 600 rpm onto microscopic slides to a final number of 5000 cells per cytospot using a Shandon Cytospin®4 (Thermo Scientific, USA). Slides were washed once with distilled water and air-dried for 15 min at room temperature.

3.2.5 Staining of Buccal Cells

A circle was drawn around each cytospot using a hydrophobic PAP pen (Dako, Australia) and air-dried for 10 min. Slides were rinsed in DBPS for 15 min, incubated in chilled 70% ethanol for 20 min and washed in DPBS for 15 min. Buccal cell cytospots were then treated with 150 µl of pre-warmed (37°C) pepsin solution (containing 750 U/ml of porcine gastric mucosa pepsin) in 0.01 M HCl and then covered with parafilm for 30 min at 37°C in a humidified box. The slides were then washed twice with DPBS for 5 min. Buccal cells were then permeabilized with 1% Triton X-100 for 15 min at room temperature and subsequently quenched of any trace of formaldehyde by dipping slides into 0.1 M glycine in DPBS twice for 2 min. Slides were then rinsed three times in DPBS and a blocking step was performed by incubating cells in 10% goat serum for 1 h at room temperature before being washed once with DPBS. The anti-γH2AX antibody was added to each cytospot at a dilution of 1:100 in DPBS containing 10%

goat serum and covered with parafilm overnight at 4°C in a humidified box. Slides were washed three times in DPBS for 5 min and a secondary antibody Alexa Fluor 488 Goat anti-mouse was added to each cytospot at a dilution of 1:500 in DPBS containing 10% FBS and covered with parafilm for 1 h at room temperature. Slides were washed three times in DPBS for 5 min and nuclei were counterstained with 4, 6-diamidino-2-phenylindole (DAPI) at a concentration of 1 μg/ml for 10 min at room temperature. The excess DAPI was removed by rinsing the slides with a solution containing 300 mM NaCl and 34 mM sodium citrate. Slides were then mounted with coverslips and DPBS:glycerol (1:1) medium. The edges of coverslips were sealed with nail polish to prevent drying prior to performing LSC and visual scoring.

3.2.6 Visual Scoring of γH2AX Foci

Visual scoring of γH2AX foci was performed immediately after the staining procedure was applied using a florescence microscope (ZEISS Metasystems, Althusheim, Germany) under a 63x oil objective. DAPI (nuclei) and Alexa Fluor 488 (γH2AX) fluorescence was viewed using a blue and green filter, respectively. A minimum of 375 cells per cytospot were scored for γH2AX foci. Since we observed three distinct shapes of nuclei (which may represent different stages of post-mitotic differentiation), they were classified into three groups based upon their morphological features i.e. round nuclei, long nuclei and oval nuclei. γH2AX appeared as discrete foci or as diffuse staining within nuclei (see Figure 3.1), therefore we categorized γH2AX scores for each nucleus as follows; no foci, 1-14 foci per nucleus, 15-30 foci per nucleus and diffuse foci (either >30 foci or diffuse nuclear staining of γH2AX i.e. wide-spread and uniform presence of γH2AX signal within nucleus).

3.2.7 Laser Scanning Cytometry Measurements of γH2AX

Laser scanning cytometry (LSC) measurements were carried out with an iCyte® Automated Imaging Cytometer (Thorlabs, Sterling Virginia, USA) with full autofocus function as well as 405 nm and 488 nm lasers for excitation of DAPI and Alexa Fluor 488, respectively. Fluorescence from DAPI (blue) and Alexa Fluor 488 (green) was collected with a photomultiplier tube. Samples were scanned in separate passes (consecutively) to prevent spectral overlap. The nuclei and γH2AX events were contoured using empirically determined thresholds to exclude the scoring of false positives (e.g. small fluorescent debris). The frequency (%) of nuclei containing γH2AX signal was recorded as well as multiple parameters within each nucleus; including the total γH2AX integral (a function of γH2AX intensity and size) and the MaxPixel value (the value of the most intense γH2AX signal/pixel within nuclei). These parameters were generated using the iCyte® 3.4 software and subsequently transferred into excel for further statistical analyses. Nuclei were also classified into round, long or oval shapes (Figure 3.2) by utilizing the iCyte software parameters which included area, circularity, perimeter and diameter as described in detail of figure legend (Figure 3.2)**.** Additionally, all nuclei were separated according to their ploidy status (DNA content) as follows; <2N, 2N and >2N, where 2N was defined as the mean integral signal of the population of nuclei ± 1 standard deviation. For 2N nuclei, the peak of the nuclei count coincided with the mean DAPI integral.

3.2.8 Statistical Analyses

GraphPad Prism 6.01 (GraphPad Prism, San Diego, CA, USA) was used to analyse data. For visual scoring comparison of the frequency of DNA damaged cells at IR doses 1, 2, and 4 Gy were compared to control (0 Gy) using one-way ANOVA followed by

Dunnett's multiple comparison test. For LSC analyses, γH2AX data were checked for normality using D'Agostino and Pearson omnibus normality test. Comparison of the frequency of DNA damaged cells at IR doses 1, 2, and 4 Gy were compared to control (0 Gy) using the Kruskal-Wallis test followed by the Dunn's multiple comparisons test. Correlation coefficients were obtained using the Pearson correlation coefficient (r). Data were expressed as mean ± standard error of the mean (SEM). $P<0.05$ was considered statistically significant.

3.3 Results

3.3.1 Visual Scoring of γH2AX in Buccal Cells

Representative images of nuclei are shown in Figure 3.1. Nuclei were classified into 3 groups based upon the nuclear shape; either round, long or oval as shown in Figure 3.1A, B and C, respectively. γH2AX foci were observed in buccal cell nuclei as shown in Figure 3.1A-D, even at baseline i.e. 0 Gy. The frequency (%) of buccal cell nuclei in 6 individuals that had no γH2AX foci at baseline (0 Gy) was 11.70 ± 3.52%, 13.60 ± 3.92% and 10.89 ± 2.80% for round, long and oval nuclei, respectively (totalling 36% of all nuclei) as shown in Table 3.1. Following exposure to IR the frequency of nuclei (all three types) containing no foci significantly decreased with increasing dose of IR exposure (Table 3.1). This suggested that IR exposure caused an increase in the levels of γH2AX in the buccal cell nuclei. On further examination, the frequency of long nuclei containing 15-30 γH2AX foci was significantly increased following IR exposure to 1 Gy ($P<0.05$), 2 Gy ($P<0.001$) and 4 Gy ($P<0.0001$) as shown in Table 3.1. Additionally, there was a significant increase in the frequency of round nuclei containing 15-30 γH2AX foci at 2 Gy ($P<0.05$) and 4 Gy ($P<0.01$). The frequency of oval nuclei containing no foci (10.89 ± 2.80%) significantly decreased to 4.04 ± 0.92%,

2.22 ± 0.54% and 1.69 ± 0.59% for 1 Gy ($P<0.05$), 2 Gy ($P<0.01$) and 4 Gy ($P<0.01$), respectively. i.e. there were dose-related increases in the frequency of nuclei with 15-30 γH2AX foci across all nuclear types. However, there was no statistically significant increase in the frequency of oval nuclei containing 1-14 γH2AX foci, 15-30 γH2AX foci or diffuse γH2AX. In fact, regardless of nuclear type, there was no significant change in the frequency of nuclei containing diffuse γH2AX or 1-14 γH2AX foci following IR exposure (Table 3.1).

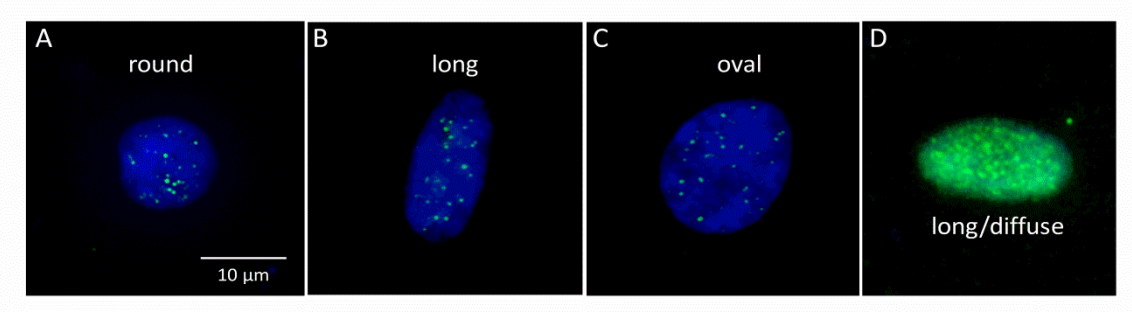

Figure 3.1: Fluorescence images of buccal cell nuclei containing discrete or diffuse γH2AX foci. Buccal cell nuclei were visualised (stained with DAPI) with a fluorescence microscope as described in the Materials and Methods section. Nuclei were classified into 3 categories i.e. round nuclei (A), long nuclei (B) and oval nuclei (C). Discrete γH2AX foci were observed in A-C, however approximately 25% of nuclei at baseline demonstrated a diffuse pattern of γH2AX signal within nuclei (D).

Table 3.1: Visually scored γH2AX in buccal cells

Nucleus shape	γH2AX foci	Radiation Dose			
ROUND		**0 Gy**	**1 Gy**	**2 Gy**	**4 Gy**
	0 foci	11.70 ± 3.52	4.13 ± 0.90[A]	1.82 ± 0.39[B]	1.20 ± 0.23[B]
	1-14 foci	3.20 ± 0.86	2.40 ± 0.91	1.69 ± 0.38	1.24 ± 0.64
	15-30 foci	10.20 ± 2.33	12.40 ± 2.54	17.87 ± 1.57[A]	20.00 ± 1.74[B]
	>30 diffuse foci	9.09 ± 1.52	10.71 ± 1.75	8.18 ± 1.70	7.78 ± 1.61
LONG		**0 Gy**	**1 Gy**	**2 Gy**	**4 Gy**
	0 foci	13.60 ± 3.92	6.76 ± 1.97	2.49 ± 0.89[B]	0.71 ± 0.21[B]
	1-14 foci	1.92 ± 0.48	2.67 ± 0.93	1.82 ± 0.45	0.93 ± 0.33
	15-30 foci	9.14 ± 2.94	19.02 ± 1.40[A]	24.62 ± 1.36[C]	28.27 ± 2.64[D]
	>30 diffuse foci	8.93 ± 1.47	11.96 ± 1.67	12.40 ± 2.67	9.20 ± 3.07
OVAL		**0 Gy**	**1 Gy**	**2 Gy**	**4 Gy**
	0 foci	10.89 ± 2.80	4.04 ± 0.92[A]	2.22 ± 0.54[B]	1.69 ± 0.59[B]
	1-14 foci	2.73 ± 0.55	2.18 ± 0.62	2.62 ± 0.69	0.76 ± 0.27
	15-30 foci	11.45 ± 2.91	14.22 ± 2.95	17.56 ± 1.37	15.73 ± 3.11
	>30 diffuse foci	7.15 ± 0.95	9.51 ± 1.30	6.71 ± 1.98	12.49 ± 3.46
All nuclei types (round + long + oval)		**0 Gy**	**1 Gy**	**2 Gy**	**4 Gy**
	0 foci	36.17 ± 9.94	14.93 ± 2.80[A]	6.53 ± 0.90[B]	3.6 ± 0.60[C]
	1-14 foci	7.85 ± 1.66	7.23 ± 1.97	6.13 ± 1.39	2.93 ± 0.98
	15-30 foci	30.80 ± 7.72	45.63 ± 2.81	60.03 ± 2.55[B]	64.00 ± 6.45[C]
	>30 diffuse foci	25.18 ± 2.84	32.18 ± 1.97	27.28 ± 1.99	29.46 ± 7.54

Frequency (%) of the different nuclear types classified (round, long and oval nuclei) containing γH2AX signals (n=6 individuals, 375 cells scored for each individual) at 0, 1, 2 and 4 Gy in the 6 individuals A-E is shown. Data are presented as Mean ± SE. [A]P<0.05, [B]P<0.01, [C]P<0.001, [D]P<0.0001.

3.3.2 Scoring of γH2AX in Buccal Cells by LSC

Figure 3.3 shows a representative example of the data obtained from a single individual's preliminary LSC assay (from "individual B"). To demonstrate the distribution of DNA content in the buccal cells, nuclei count versus DAPI integral (equivalent to DNA content) was plotted as shown in Figure 3.3A, whereby 2634 nuclei were examined. Nuclei were then classified as <2N, 2N or >2N prior to further analyses. Figure 3.3B shows the DAPI integral was correlated with nuclear area for the same 2634 nuclei as in Figure 3.3A. Figure 3.3C and 3.3D shows the γH2AX integral of individual B when plotted against DNA content (DAPI integral) for 0 Gy (mean = 0.131

x 10^6 a.u., n=2634 nuclei) and 4 Gy (mean = 3.25 x 10^6 a.u., n=1060 nuclei), respectively.

3.3.2.1 2N nuclei

Table 3.2 summarizes γH2AX integral measurements in buccal cells exposed to 0, 1, 2 or 4 Gy for six individuals. All 6 individuals demonstrated a significant increase in γH2AX integral in buccal nuclei following exposure to IR as low as 1 Gy. The variation of baseline (0 Gy) γH2AX signals were variable between individuals. For example, 2 individuals (B and E) had γH2AX signals that were less than 1 x 10^6 a.u. at 0 Gy, whereas the remaining 4 individuals had values that ranged from 1.209 to 6.067 x 10^6 a.u. There was also considerable variation in the response of buccal cells to radiation exposure; indeed, the individuals with the lowest baseline γH2AX values (B and E) also showed the greatest fold increase in IR-induced γH2AX signal. For example, the γH2AX integral in individual B significantly increased from 0.132 x 10^6 a.u. at 0 Gy to 1.009 x 10^6 a.u. ($P<0.0001$) at 1 Gy, 1.954 x 10^6 a.u. ($P<0.0001$) at 2 Gy and 2.673 x 10^6 a.u. at 4 Gy ($P<0.0001$), representing up to a 20-fold increase of γH2AX signal in 2N nuclei. Conversely, the individuals with the highest γH2AX integral at baseline (0 Gy) showed the least IR-induced γH2AX signal response, although the responses were statistically significant. Although each individual had a significantly increased γH2AX integral following IR exposure; however, when the 4 IR doses were averaged (n=6 per IR dose), there was no significant difference between IR exposure doses compared to 0 Gy, which was likely due to the large amount of inter-individual variation, particularly at baseline (0 Gy).

Consistent with the increase in γH2AX integral post-IR as discussed above, both the γH2AX area (data not shown) and γH2AX MaxPixel values also increased significantly

with IR dose (Table 3.3). Additionally, both parameters (γH2AX area and MaxPixel) correlated well with the γH2AX integral values (γH2AX integral and γH2AX area correlation coefficients were R^2=0.979 and R^2=0.960 for γH2AX area and γH2AX MaxPixel, respectively) in buccal cell nuclei exposed to 0, 1, 2 and 4 Gy in all individuals (n=6) (Figure 3.4).

3.3.2.2 <2N nuclei and >2N nuclei

Tables 3.2 and Table 3.3 summarize γH2AX integral and MaxPixel, respectively for <2N and >2N nuclei from six individuals. For <2N nuclei, 3 out of 6 individuals showed a significant increase in γH2AX integral (Table 3.2) whereas for >2N nuclei 4 out of 6 individuals had significantly increased γH2AX integral values at 4 Gy compared with 0 Gy. As expected, both the γH2AX area (not shown) and γH2AX MaxPixel (Table 3.3) values also increased significantly with IR dose.

3.3.2.3 Inter- and intra-individual variation

The variation between the six individuals examined for 2N nuclei ranged from 2.326 to 8.942 x 10^6 a.u. at 4 Gy (Table 3.2). When a single individual's γH2AX integral (2N) was measured on 6 separate occasions (individual B), the 4 Gy γH2AX integral ranged from 2.67 - 4.74 x 10^6 a.u. with a coefficient of variation of 20.5%.

3.3.2.4 Nuclear shape

In an attempt to score nuclear shape by LSC (as was done for visual scoring of buccal cell nuclei), we categorized nuclei as either round, long or oval by using several iterative processes in iCyte as shown in Figure 3.2. By using some of the features available within the iCyte software (area, perimeter, diameter and circularity), we empirically classified the buccal cell nuclei shapes and quantified the γH2AX MaxPixel

values as shown in (Table 3.4). For each individual, the dose-response data for each nuclear shape are shown at 0 – 4 Gy. For round nuclei, all 6 individuals showed a significant IR-induced increase in γH2AX MaxPixel values. For long nuclei, 3 out of 6 individuals showed a significant increase, whilst for oval nuclei, 4 out of 6 individuals showed significant increases in MaxPixel values at 4 Gy compared with 0 Gy.

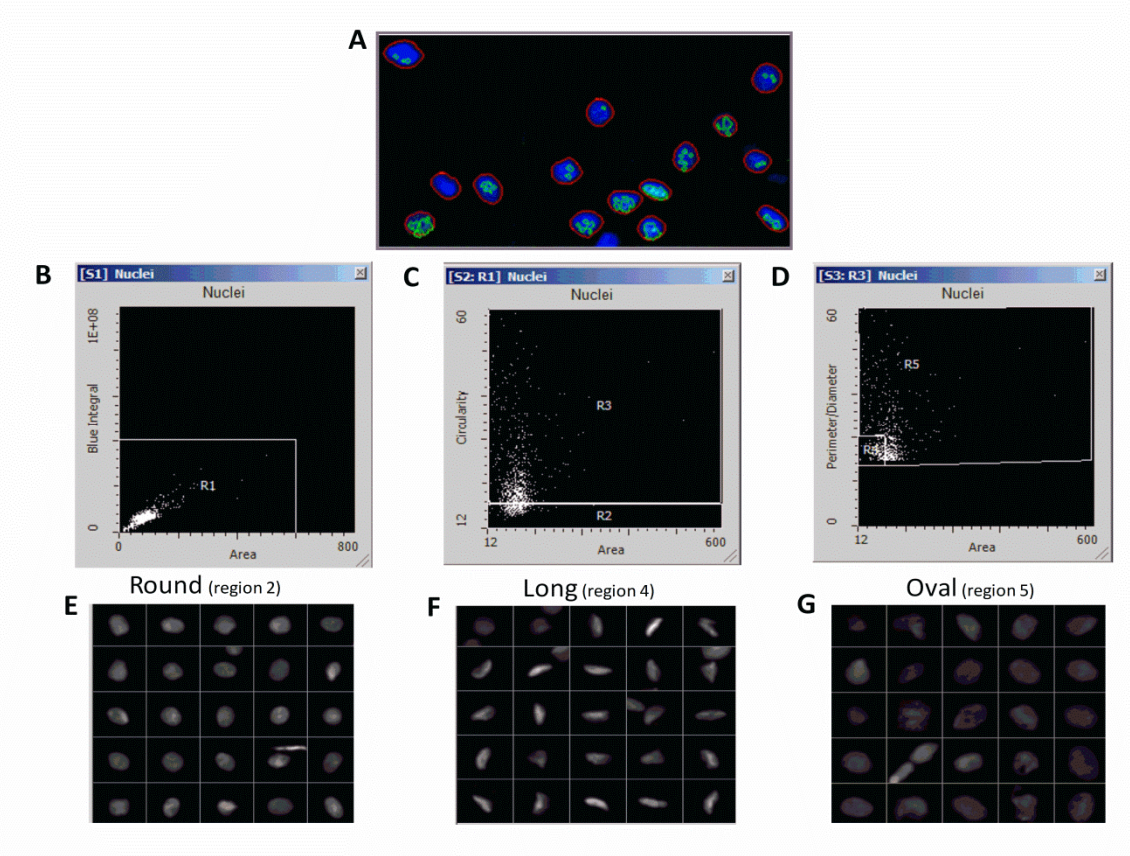

Figure 3.2: Identification of buccal cell nuclear shapes; round, long and oval, by laser scanning cytometry. The events from different scattergram regions were relocated and imaged (using an imaging gallery) to empirically identify the 3 different nuclear shapes present. (A) Individual nuclei were automatically contoured (red contour lines) as described in methods based on a thresholding procedure. γH2AX signal (green contour lines) was detected and quantified (integral or MaxPixel) within the nuclei following exposure to 0 – 4 Gy. (B) Nuclei having area values that ranged from 0-600 μm^2 and blue integral values that ranged from 0-4x10^7 (arbitrary units) in region 1 (R1) were analyzed in (C) by plotting their circularity (y-axis) versus nuclear area (x-axis) where "Round" nuclei were identified in region 2 (R2). (D) Nuclei from region 3 (R3) were further analyzed by plotting their perimeter/diameter ratio (y-axis) versus nuclear area (x-axis). Two new groups were established from R3; long nuclei were identified in R4 and oval nuclei in R5. Representative galleries of nuclear shape are shown for (E) round, (F) long and (G) oval nuclei.

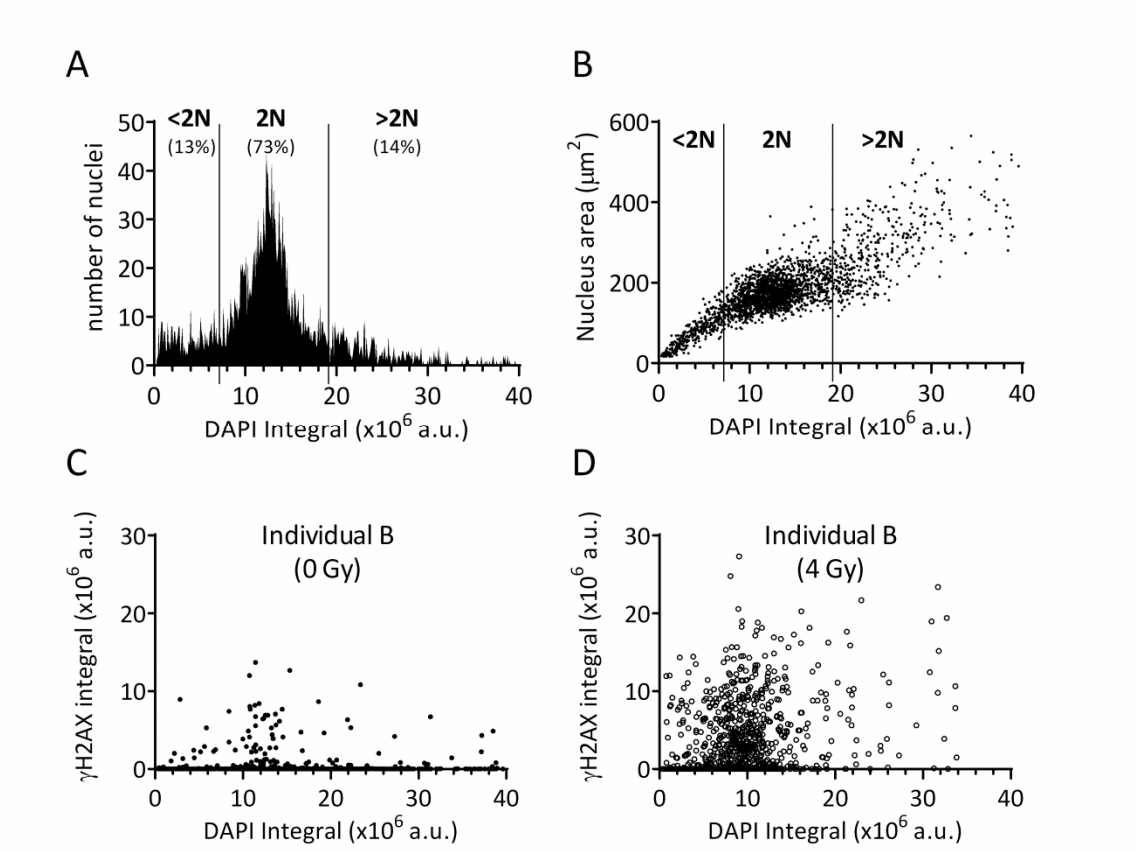

Figure 3.3: DNA content and γH2AX quantification in buccal cell nuclei by laser scanning cytometry (LSC). A representative example from individual B showing: (A) buccal cell DNA content was calculated automatically from all nuclei by using the DAPI integral feature within the iCyte software; the DNA content was determined by categorizing nuclei as <2N, 2N and >2N. 2N was defined as the mean integral ± 1 S.D. Sub-2N and >2N were less and greater than 1 S.D. from the mean, respectively. Numbers in parentheses represent the percentage of nuclei. (B) The correlation of DAPI integral with nuclear area. γH2AX integral in buccal cells from individual B exposed to either 0 Gy (C) or 4 Gy (D) IR and γH2AX signal was plotted for all nuclei versus DNA content; the number of nuclei examined by LSC was n=2634 at 0 Gy and n=1060 nuclei at 4 Gy.

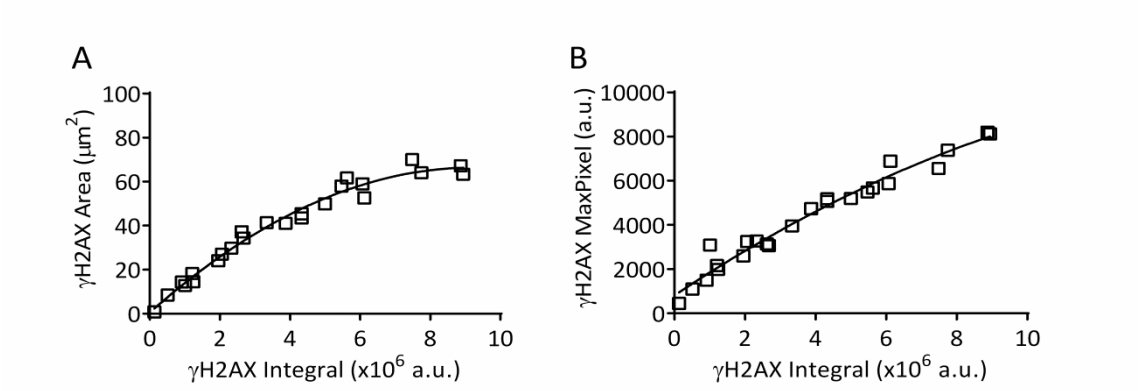

Figure 3.4: Correlation of γH2AX integral with γH2AX area and γH2AX MaxPixel by LSC. (A) Correlation of γH2AX foci area and γH2AX integral or (B) correlation of γH2AX MaxPixel and γH2AX integral, per nucleus scored by LSC in buccal cell nuclei exposed to 0, 1, 2 and 4 Gy in all individuals (n=6). The relationship of the two parameters fitted a second order polynomial (quadratic) resulting in correlation coefficients (R^2) for γH2AX foci area = 0.979 and for γH2AX MaxPixel = 0.960).

Table 3.2: Summary of γH2AX integral (a.u. X10^6) by LSC in <2N, 2N or >2N buccal cells exposed to 0, 1, 2, or 4 Gy

<2N	Individuals	0 Gy	1 Gy	2 Gy	4 Gy
	A	1.967 ± 0.293 (*n*=108)	3.509 ± 0.663 (*n*=88)	3.127 ± 0.518 (*n*=102)	4.152 ± 0.491^A (*n*=111)
	B	0.092 ± 0.033 (*n*=353)	0.438 ± 0.101^D (*n*=70)	1.984 ± 0.203^D (*n*=320)	2.724 ± 0.540^D (*n*=101)
	C	2.902 ± 0.570 (*n*=102)	3.500 ± 0.399 (*n*=187)	2.814 ± 0.264 (*n*=366)	2.278 ± 0.340 (*n*=122)
	D	1.121 ± 0.119 (*n*=313)	2.915 ± 0.825 (*n*=33)	2.153 ± 0.237^A (*n*=216)	2.641 ± 0.332^D (*n*=215)
	E	1.528 ± 0.873 (*n*=155)	2.090 ± 0.906 (*n*=129)	2.958 ± 2.327 (*n*=70)	1.057 ± 0.239 (*n*=85)
	F	4.388 ± 0.516 (*n*=74)	5.227 ± 1.065 (*n*=25)	3.657 ± 0.458 (*n*=99)	6.440 ± 0.715 (*n*=73)
	Mean ± SE	**2.000 ± 0.610**	**2.946 ± 0.655**	**2.782 ± 0.255**	**3.215 ± 0.761**
2N	**Individuals**	**0 Gy**	**1 Gy**	**2 Gy**	**4 Gy**
	A	6.067 ± 0.298 (*n*=586)	7.484 ± 0.395^A (*n*=397)	7.745 ± 0.352^C (*n*=498)	8.942 ± 0.455^D (*n*=388)
	B	0.132 ± 0.021 (*n*=1913)	1.009 ± 0.076^D (*n*=751)	1.954 ± 0.078^D (*n*=2466)	2.673 ± 0.122^D (*n*=1312)
	C	3.337 ± 0.191 (*n*=810)	5.469 ± 0.179^D (*n*=1626)	4.333 ± 0.119^D (*n*=3218)	4.329 ± 0.229^B (*n*=777)
	D	1.209 ± 0.059 (*n*=1847)	2.059 ± 0.221^D (*n*=209)	2.619 ± 0.114^D (*n*=1444)	3.877 ± 0.170^D (*n*=976)
	E	0.511 ± 0.073 (*n*=433)	0.913 ± 0.105^B (*n*=473)	1.242 ± 0.418^A (*n*=213)	2.326 ± 0.622^D (*n*=211)
	F	4.998 ± 0.337 (*n*=379)	6.122 ± 0.546^B (*n*=148)	5.627 ± 0.323^A (*n*=433)	8.872 ± 0.490^D (*n*=326)
	Mean ± SE	**2.709 ± 1.010**	**3.843 ± 1.168**	**3.920 ± 1.007**	**5.170 ± 1.220**
>2N	**Individuals**	**0 Gy**	**1 Gy**	**2 Gy**	**4 Gy**
	A	10.620 ± 1.536 (*n*=58)	12.040 ± 2.190 (*n*=44)	8.364 ± 1.147 (*n*=73)	9.229 ± 1.550 (*n*=56)
	B	0.164 ± 0.047 (*n*=368)	3.052 ± 0.738^D (*n*=59)	3.478 ± 0.270^D (*n*=441)	7.388 ± 1.103^D (*n*=108)
	C	5.389 ± 0.834 (*n*=89)	9.216 ± 1.053^B (*n*=122)	8.329 ± 0.624^B (*n*=326)	7.520 ± 0.952 (*n*=89)
	D	1.070 ± 0.229 (*n*=262)	2.019 ± 0.527^C (*n*=30)	3.567 ± 0.456^D (*n*=276)	3.829 ± 0.451^D (*n*=177)
	E	0.762 ± 0.286 (*n*=61)	0.640 ± 0.193 (*n*=69)	1.088 ± 0.612 (*n*=33)	2.739 ± 1.138^A (*n*=34)
	F	4.367 ± 0.804 (*n*=55)	4.349 ± 0.941 (*n*=30)	8.736 ± 1.957 (*n*=65)	7.250 ± 0.854^B (*n*=58)
	Mean ± SE	**3.729 ± 1.625**	**5.219 ± 1.818**	**5.594 ± 1.341**	**6.326 ± 1.015**

Letters denote the *p*-values when comparing 1, 2 or 4 Gy IR relative to 0 Gy for each individual. Data are presented as Mean ± SE. Numbers in parentheses represent the total number of nuclei that were scored at each IR dose. ^{A}P<0.05, ^{B}P<0.01, ^{C}P<0.001, ^{D}P<0.0001.

Table 3.3: Summary of γH2AX MaxPixel (a.u.) by LSC in <2N, 2N or >2N buccal cells exposed to 0, 1, 2, or 4 Gy

<2N	Individuals	0 Gy	1 Gy	2 Gy	4 Gy
	A	2994 ± 337 (*n*=108)	4241 ± 485 (*n*=88)	3728 ± 473 (*n*=102)	5614 ± 544^{B} (*n*=111)
	B	332 ± 100 (*n*=353)	1820 ± 283^{D} (*n*=70)	2373 ± 217^{D} (*n*=320)	2698 ± 352 ^{D} (*n*=101)
	C	4092 ± 524 (*n*=102)	5356 ± 431^{A} (*n*=187)	4148 ± 263 (*n*=366)	4520 ± 460 (*n*=122)
	D	2289 ± 203 (*n*=313)	3436 ± 782 (*n*=33)	2768 ± 241 (*n*=216)	3820 ± 323^{C} (*n*=215)
	E	2023 ± 325 (*n*=155)	1913 ± 326 (*n*=129)	1897 ± 470 (*n*=70)	2279 ± 356 (*n*=85)
	F	4680 ± 475 (*n*=74)	6560 ± 981 (*n*=25)	3932 ± 381 (*n*=99)	7449 ± 605^{B} (*n*=73)
	Mean ± SE	2735 ± 636	3887 ± 770	3141 ± 376	4396 ± 785
2N	**Individuals**	**0 Gy**	**1 Gy**	**2 Gy**	**4 Gy**
	A	5874 ± 206 (*n*=586)	6552 ± 247 (*n*=397)	7381 ± 250^{D} (*n*=498)	8124 ± 303^{D} (*n*=388)
	B	445 ± 54 (*n*=1913)	3085 ± 152^{D} (*n*=751)	2593 ± 79^{D} (*n*=2466)	3062 ± 103^{D} (*n*=1312)
	C	3598 ± 150 (*n*=810)	5484 ± 120^{D} (*n*=1626)	5185 ± 87^{D} (*n*=3218)	5064 ± 178^{D} (*n*=777)
	D	2163 ± 84 (*n*=1847)	3242 ± 251^{C} (*n*=209)	3141 ± 100^{D} (*n*=1444)	4738 ± 142^{D} (*n*=976)
	E	1092 ± 132 (*n*=433)	1498 ± 126^{B} (*n*=473)	1989 ± 289^{A} (*n*=213)	3274 ± 344^{D} (*n*=211)
	F	5195 ± 274 (*n*=379)	6886 ± 414^{C} (*n*=148)	5673 ± 202 (*n*=433)	8199 ± 306^{D} (*n*=326)
	Mean ± SE	3121 ± 909	4457 ± 884	4327 ± 851	5410 ± 927
>2N	**Individuals**	**0 Gy**	**1 Gy**	**2 Gy**	**4 Gy**
	A	9212 ± 804 (*n*=58)	8786 ± 1025 (*n*=44)	8161 ± 819 (*n*=73)	9451 ± 1194 (*n*=56)
	B	587 ± 120 (*n*=368)	6664 ± 984^{D} (*n*=59)	4012 ± 232^{D} (*n*=441)	6316 ± 583^{D} (*n*=108)
	C	6575 ± 572 (*n*=89)	10772 ± 814^{C} (*n*=122)	10690 ± 426^{D} (*n*=326)	10658 ± 1060^{A} (*n*=89)
	D	1793 ± 244 (*n*=262)	3632 ± 609 ^{C} (*n*=30)	3759 ± 292^{D} (*n*=276)	5311 ± 440^{D} (*n*=177)
	E	1608 ± 380 (*n*=61)	1841 ± 431 (*n*=69)	2182 ± 959 (*n*=33)	5027 ± 1410^{A} (*n*=34)
	F	4938 ± 536 (*n*=55)	5210 ± 798 (*n*=30)	6983 ± 695 (*n*=65)	8133 ± 603^{C} (*n*=58)
	Mean ± SE	4118 ± 1376	6150 ± 1346	5964 ± 1306	7482 ± 939

Letters denote the *p*-values when comparing 1, 2 or 4 Gy IR relative to 0 Gy for each individual. Data are presented as Mean ± SE. Numbers in parentheses represent the total number of nuclei that were scored at each IR dose. ^{A}P<0.05, ^{B}P<0.01, ^{C}P<0.001, ^{D}P<0.0001.

Table 3.4: Summary of γH2AX MaxPixel (a.u.) by LSC in round, long and oval shaped nuclei of buccal cells exposed to 0, 1, 2, or 4 Gy

Round	Individuals	0 Gy	1 Gy	2 Gy	4 Gy
	A	6435 ± 200 (*n*=576)	7443 ± 306^{A} (*n*=277)	7619 ± 256^{B} (*n*=429)	8376 ± 312^{D} (*n*=366)
	B	1319 ± 54 (*n*=623)	3450 ± 143^{D} (*n*=494)	3686 ± 83^{D} (*n*=1817)	5223 ± 157^{D} (*n*=625)
	C	4093 ± 131 (*n*=792)	5453 ± 117^{D} (*n*=1484)	5409 ± 82^{D} (*n*=3227)	5382 ± 134^{D} (*n*=1227)
	D	2510 ± 52 (*n*=1963)	3339 ± 352 (*n*=60)	3534 ± 107^{D} (*n*=866)	5315 ± 136^{D} (*n*=1015)
	E	1912 ± 88 (*n*=431)	2193 ± 105 (*n*=323)	2170 ± 140 (*n*=133)	3115 ± 184^{D} (*n*=227)
	F	5372 ± 284 (*n*=282)	7727 ± 653^{B} (*n*=62)	5876 ± 220 (*n*=378)	8878 ± 305^{D} (*n*=322)
	Mean ± SE	3667 ± 857	4934 ± 942	4716 ± 800	6050 ± 888
Long	**Individuals**	**0 Gy**	**1 Gy**	**2 Gy**	**4 Gy**
	A	4286 ± 638 (*n*=34)	5941 ± 633 (*n*=60)	5662 ± 690 (*n*=55)	7061 ± 714^{A} (*n*=53)
	B	1400 ± 90 (*n*=60)	2846 ± 236^{B} (*n*=137)	3690 ± 259^{D} (*n*=198)	3169 ± 281^{C} (*n*=148)
	C	4334 ± 872 (*n*=25)	5207 ± 695 (*n*=46)	5541 ± 411 (*n*=133)	3870 ± 453 (*n*=56)
	D	2519 ± 373 (*n*=55)	4150 ± 473 (*n*=57)	4537 ± 340^{B} (*n*=116)	4671 ± 427^{B} (*n*=84)
	E	2473 ± 375 (*n*=44)	3666 ± 494 (*n*=44)	2894 ± 554 (*n*=30)	2753 ± 318 (*n*=34)
	F	6951 ± 951 (*n*=26)	6936 ± 827 (*n*=40)	4682 ± 705 (*n*=28)	8880 ± 949 (*n*=34)
	Mean ± SE	3672 ± 803	4791± 621	4501 ± 436	5280 ± 984
Oval	**Individuals**	**0 Gy**	**1 Gy**	**2 Gy**	**4 Gy**
	A	6049 ± 464 (*n*=124)	6855 ± 388 (*n*=167)	7000 ± 450 (*n*=155)	7334 ± 545 (*n*=106)
	B	1456 ± 50 (*n*=1812)	2698 ± 175^{D} (*n*=210)	3626 ± 114^{D} (*n*=1030)	3989 ± 234^{D} (*n*=240)
	C	5418 ± 339 (*n*=162)	6371 ± 259 (*n*=341)	6774 ± 228^{B} (*n*=478)	6564 ± 298^{A} (*n*=268)
	D	2578 ± 125 (*n*=353)	4030 ± 316^{D} (*n*=115)	3703 ± 106^{D} (*n*=866)	4656 ± 293^{D} (*n*=220)
	E	2469 ± 166 (*n*=143)	2540 ± 142 (*n*=249)	2426 ± 247 (*n*=128)	2988 ± 339 (*n*=54)
	F	4627 ± 284 (*n*=178)	6282 ± 551^{B} (*n*=84)	5071 ± 279 (*n*=158)	7836 ± 561^{D} (*n*=91)
	Mean ± SE	3310 ± 673	4384 ± 762	4320 ± 678	5206 ± 803

Letters denote the *p*-values when comparing 1, 2 or 4 Gy IR relative to 0 Gy for each individual. Data are presented as Mean ± SE. Numbers in parentheses represent the total number of nuclei that were scored at each IR dose. ^{A}P<0.05, ^{B}P<0.01, ^{C}P<0.001, ^{D}P<0.0001.

3.3.3 Correlation of Visually Scored γH2AX and γH2AX Integral by LSC

The frequency of visually scored long nuclei (containing 15-30 foci) was strongly correlated with LSC scored γH2AX integrals in 5 out of 6 individuals (Figure 3.5). The Pearson correlation coefficients from individuals A-E were r = 0.945, 0.930, 0.608, 0.964, 0.999 and one individual (individual F) showed no correlation. Indeed, for individual F, the LSC measured γH2AX integrals (including area and MaxPixel) significantly increased with IR dose (see Table 3.2, 2N nuclei, individual F). However, using the visual scoring criteria used here, we were unable to demonstrate significant differences between the frequency (%) of nuclei containing 15-30 foci at the different IR doses for individual F. This suggests that LSC was more sensitive to quantifying the small changes in IR-induced γH2AX signals in nuclei.

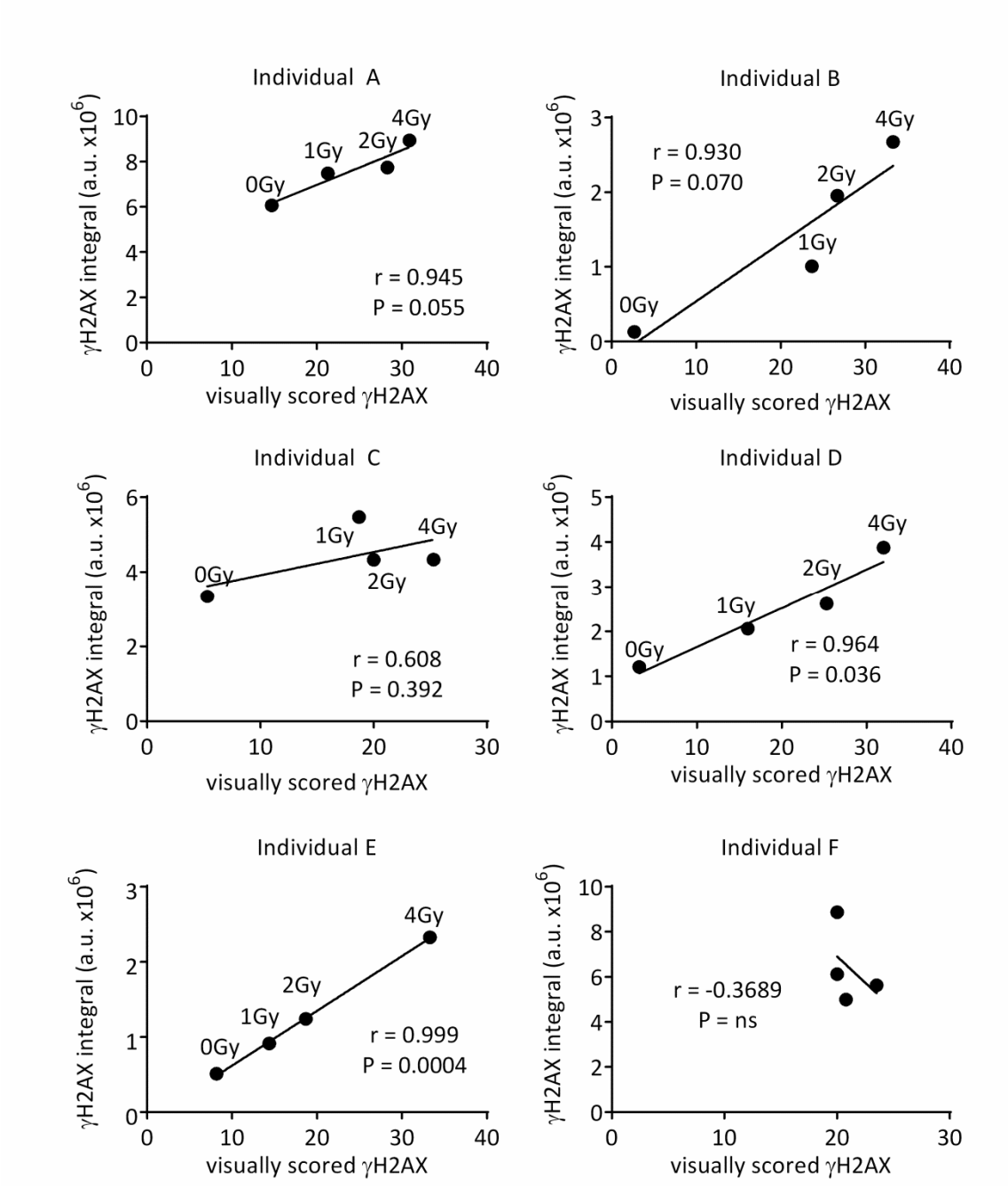

Figure 3.5: Correlation of visually scored and LSC quantified γH2AX signals in buccal cell nuclei exposed to 0, 1, 2 or 4 Gy IR. The frequency (%) of visually scored buccal nuclei containing 15-30 γH2AX foci are shown on the x-axis and the mean γH2AX integrals (by LSC) per 2N nuclei are shown on the y-axis for all individuals A-E (n=6). Pearson correlation coefficients (r) and p-values are shown as insets within each graph.

3.3.4 Kinetics of γH2AX in Buccal Cells

The time course of γH2AX was monitored at 0, 0.5, 3 and 24 h after the exposure of buccal cells to 4 Gy IR in 3 individuals (B, D and E). These individuals were chosen for γH2AX kinetics analyses since they had the greatest dose-response to irradiation at 0 - 4 Gy. Figure 3.6A demonstrates that the mean frequency (%) of nuclei containing 15-30 γH2AX foci, when scored visually, remained elevated for a period of up to 24 h post IR. A peak was reached at 30 min post IR exposure (4 Gy) and subsequently declined by 40% at 24 h post IR (4 Gy); however, this remained significantly ($P<0.0001$) higher than the baseline value. A similar result was obtained by LSC as shown in Figure 3.6B. The γH2AX integral significantly increased ($P<0.05$) 30 minutes post IR exposure and then subsequently declined by 82% 24 h post IR which was not significantly different from the baseline value.

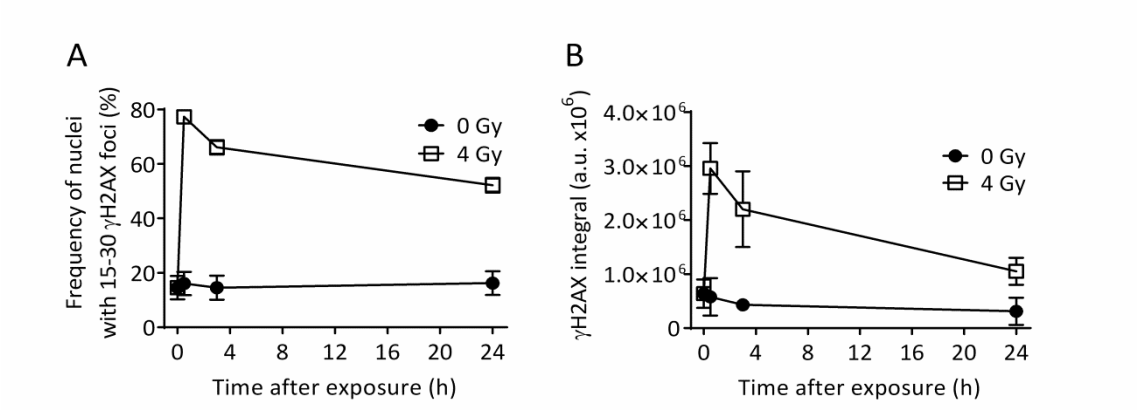

Figure 3.6: 24 h kinetics of γH2AX foci in buccal cell nuclei assessed by visual scoring method or LSC. Buccal cells were exposed to 4 Gy IR and then subsequently incubated for 0, 0.5, 3 or 24 h prior to fixation. (A) The frequency (%) of buccal cell nuclei containing 15-30 γH2AX foci per nucleus was visually scored as described in methods. (B) γH2AX integral in 2N nuclei was determined by LSC.

3.4 Discussion

The objective of the present study was to investigate the induction and persistence of DNA DSBs in irradiated human buccal cells. We used two scoring protocols to quantify ionizing radiation-induced γH2AX, a marker of DNA DSBs. Visual scoring of nuclei was correlated with the automated laser scanning cytometry (LSC) method developed here to quantify γH2AX integral (and MaxPixel) in each nucleus examined in thousands of buccal cells for each individual. Additionally, these LSC measurements were combined with quantitation of nuclear DNA content to classify cells depending on their DNA content (ploidy status) as well as nuclear shapes based on their area, perimeter, diameter and circularity. Our experimental results demonstrated that buccal cells exposed to IR have the capacity to accumulate γH2AX which partially remained up to 24 h post IR exposure suggesting buccal cells have diminished capacity to repair DNA DSBs. We also observed a large variation in baseline levels of γH2AX and in γH2AX response to IR exposure.

In the visual scoring study, we aimed to classify buccal cells into separate groups based upon their nuclear shapes. Since the buccal mucosa is known to consist of heterogeneous cell types that may have discrete functions within the mucosa (Patten et al. 1996, Thomas et al. 2008, Leifert et al. 2011, Darzynkiewicz et al. 2011, Francois et al. 2014a, Torres-Bugarin et al. 2014, Hosoya et al. 2008, Lavker, Sun 1982), we therefore hypothesized that our defined categories may also exhibit differences in their response to DNA damage induction and subsequent repair. In fact, our results demonstrated that γH2AX could be measured in buccal cells and that γH2AX response following IR varied between nuclei types as has been observed in previous studies (Gonzalez et al. 2010, Yoon et al. 2009, Mondal, Ghosh & Ray 2011). Long nuclei, for

instance, showed the largest dose response (up to 3-fold) to increasing radiation exposure (0, 1, 2 and 4 Gy) with a higher frequency of nuclei containing 15-30 foci. In contrast, no significant difference was observed for oval shaped nuclei, and a weaker dose response (up to 2-fold) was found in round nuclei containing 15-30 foci. Interestingly, there was no change in the the frequency of cells with diffuse foci following exposure to IR. It is likely that these "diffuse" nuclei we categorized here (approximately 25%) represent the necrotic or non-viable cell population expressing a phenotype of reduced response efficiency to DNA damage. This notion is consistent with previous studies showing that a relatively high proportion (up to 20%) of buccal cells are non-viable, necrotic, or apoptotic at baseline (Gonzalez et al. 2010, Schwartz et al. 2003, de Oliveira et al. 2008). For a more complete understanding of the DNA damage response biology of buccal cells, it would therefore be valuable in future studies to combine γH2AX detection with a cytoplasmic marker of cell sub-types present (if compatible with the current immunofluorescence protocol). Such markers could be met, for example, by the detection of cytokeratin proteins or other markers of epithelial cells, which are expressed differentially between buccal mucosa cell types depending on their differentiation status (Hosoya et al. 2008, Moll et al. 1982, Vaidya et al. 1989, Purkis et al. 1990).

LSC has previously been shown as a useful tool to measure cellular DNA content for cell cycle stage evaluation in conjunction with γH2AX after inducing DNA damage (Zhao et al. 2009, Tanaka et al. 2007, Huang et al. 2004). It was therefore decided to include DNA content (measured by nuclear DAPI integral) as an additional measurement in our LSC protocol allowing us to classify nuclei as <2N, 2N or >2N. Previously, we demonstrated that approximately 60% of buccal cells are likely to be post-mitotic 2N nuclei (Francois et al. 2014a) which is similar to the results obtained in

this study (see Figure 3.3A). Our current findings support previous observations in that significant increases of γH2AX in buccal cell nuclei are induced by exposure to IR (Gonzalez et al. 2010). A significant increase in γH2AX signal in 2N nuclei up to 4 Gy was observed in all individuals and dose responses measured by LSC correlated with those measured visually. For <2N nuclei only three out of six individuals showed a significant increase in γH2AX at a dose of 4 Gy. Alternatively, four out of six individuals showed a significant increase in γH2AX at a dose of 4 Gy in >2N nuclei. We believe that the buccal cell <2N and >2N populations are mainly composed of apoptotic cells, condensed chromatin cells or cells immobilized at a cell cycle check point due to mitotic defects or abnormal nuclear DNA content (Francois et al. 2014a, Kirsch-Volders, Fenech 2001). The nature of the <2N and >2N population of cells may partly explain their somewhat lower response to radiation compared to the 2N cell population.

Although all individuals showed an increase in γH2AX following IR exposure, when the individual data obtained for the six individuals was averaged, the significant differences between IR exposure doses compared to 0 Gy was absent in all three populations of nuclei (i.e. <2N, 2N and >2N). However, we believe this is due to the substantial differences observed in the γH2AX baseline levels at 0 Gy between the individuals in this study. Such variation in baseline γH2AX signal in human buccal cells has been observed previously when the γH2AX foci were scored. Indeed, values ranged from 0.08 γH2AX foci/nucleus (Gonzalez et al. 2010) to 4.08 γH2AX foci/nucleus (Mondal, Ghosh & Ray 2011); however, the former study excluded some buccal cell types from their analyses, which may partly explain the differences observed between previous studies. In our study, the LSC protocol was also utilized to extract data on γH2AX integral, MaxPixel and area measurements from within the contoured nuclei.

Both γH2AX MaxPixel and area correlated well with the γH2AX integral as expected, since the integral is a function of both γH2AX total intensity and γH2AX area. Furthermore, the increase in γH2AX MaxPixel and area indicates that the abundance of phosphorylated histone H2AX proteins accumulated at sites of DNA breakage, and that the accumulation of γH2AX was dose-dependent and readily quantifiable by LSC. Therefore, these types of quantifiable parameters (integral, intensity, area) could prove useful as alternative measures to quantify γH2AX responses within buccal cells that may be achieved with the use of other automated imaging platforms.

Different nuclear shape morphology has been used as one of the criteria to distinguish nuclear abnormalities and has been used in patients with oral squamous cell carcinoma to assess radiosensitivity (Torres-Bugarin et al. 2014, Raj, Mahajan 2011). In this study, we assessed the γH2AX MaxPixel response to IR in different shaped buccal cell nuclei (round, long and oval). Although γH2AX MaxPixel dose-dependently increased there appeared to be no particular nuclear shape that was more responsive than the other. Nuclear shape could be a parameter used in future studies when comparing buccal cell nuclei at “baseline” (e.g. in studies comparing populations or disease states) as it may provide information on long-term (chronic) DNA damage. One advantage of LSC (compared with visual scoring) is that multiple parameters can be examined and quantified in cells (high content) simultaneously which may provide more information on cellular signaling. Ideally, this approach could be combined with cell morphology parameters to accurately identify the buccal cell-subtypes present.

The kinetics of γH2AX response in buccal cells were investigated by measuring DNA damage levels up to 24 h post-IR. LSC and visual scoring demonstrated that γH2AX signals in nuclei peaked at 30 min after exposure to IR, which subsequently declined

over a period of 24 h. In some individuals the level of γH2AX remained higher than baseline levels 24 h after exposure, suggesting persistent DNA damage occurred. In a previous study investigating DNA DSBs in buccal cells, the longest time point following IR exposure was 5 h (Gonzalez et al. 2010). Our study, therefore, demonstrates for the first time that buccal cells express variable but persistent γH2AX responses up to 24 h post-IR. The kinetics of γH2AX can be rapid, with γH2AX declining over a period of hours (Rogakou et al. 1998, Madigan, Chotkowski & Glaser 2002, Roch-Lefevre et al. 2010, Olive, Banath 2004). Persistence of DNA damage has also been observed in different models. For instance, a recent study that used Göttingen minipig skin biopsies found that IR-induced γH2AX foci was found to be significantly lower after 70 days post-IR exposure; however, a significantly higher number of γH2AX foci still remained in irradiated epidermal keratinocytes compared with controls (Ahmed et al. 2012). Most recently, γH2AX formation and removal in heart, brain and liver tissue following X-ray exposure was tested in adult Syrian hamsters; it was found that all tissues accumulated γH2AX but heart and brain tissues contained more persistent γH2AX 24 h post-IR indicating the presence of unrepaired DNA DSBs. This result suggested that kinetics of IR-induced H2AX phosphorylation (and γH2AX dephosphorylation) is tissue specific, being less efficient in heart and brain in comparison with liver and kidney (Firsanov et al. 2012). Since different tissues can have distinct γH2AX responses, it may not be possible to extrapolate buccal cell data generated from our study to investigations carried out on other tissues. Moreover, the high level of γH2AX still present in cells after 24 h suggest that buccal cells may simply not repair DNA damage as efficiently as other cell types. The persistent γH2AX signal after 24 hours could be explored for radiation biodosimetry purpose following a radiation accident. However, this may be limited by the large variation in baseline

γH2AX signal in cells not exposed to IR between individuals. Understanding the dietary, life-style, genotoxic exposure and genetic factors is essential prior to considering the possibility of using γH2AX assay in buccal cells for human biodosimetry.

Although a better understanding of the biology of γH2AX response in buccal cells is needed, our findings suggest that buccal mucosa may be a tissue of interest in monitoring radiation exposure in humans or monitoring levels of DNA damage in patients undergoing radiotherapy. Such large-scale monitoring may be made possible with the use of LSC. Indeed, the full automation of this LSC method offers an efficient unbiased and quantifiable measure of γH2AX abundance in a large number of cells (thousands of cells per individual) and should be considered as an alternative method to visual scoring, which is labor-intensive and subject to bias. Additionally, the LSC protocol presented here can combine accurate measurement of γH2AX signal with nuclei ploidy status and by its design, can potentially incorporate the simultaneous measurement of other cellular proteins/markers involved in DNA damage/repair signaling processes.

Chapter 4: γH2AX Levels in Human Buccal Cells is Significantly Associated with Alzheimer's Disease in the Australian Imaging, Biomarkers and Lifestyle Flagship Study of Ageing (AIBL)

Abstract

In response to double-stranded breaks (DSBs) in chromosomal DNA, H2AX (a member of histone H2A family) becomes phosphorylated to form γH2AX. Although increased level of γH2AX has been reported in the neuronal nuclei of Alzheimer's disease (AD) patients, the understanding of γH2AX responses in buccal nuclei of individuals with Mild cognitive impairment (MCI) and AD remain unexplored. In the current study, endogenous γH2AX level was measured in the buccal nuclei from MCI (n=18) or AD (n=16) patients and in healthy controls (n=17) using laser scanning cytometry (LSC). The γH2AX level was significantly elevated in nuclei of the AD group compared to the MCI and control group, and there was a concomitant increase with a significant trend for increase in γH2AX from the control group through MCI to the AD group. Receiver-Operating Characteristic (ROC) curves were carried out for different γH2AX parameters, and γH2AX MaxPixel resulted in the greatest area under the curve (AUC) value of 0.7794 (p=0.0062) with 75% sensitivity and 70 % specificity for the identification of AD patients from control. In addition, nuclear circularity (irregular nuclear shapes) was significantly higher in the buccal nuclei from AD group compared to the MCI and control groups. This result was further supported by a positive correlation between the nuclear circularity and γH2AX signals. The results indicated that γH2AX level in buccal nuclei could be used as a potential diagnostic in identifying individuals with increased risk of developing MCI and AD.

4.1 Introduction

Alzheimer's disease (AD) is a neurodegenerative disease that is characterised clinically by severe memory loss, cognitive deterioration and behavioural changes (Alzheimer's Association, Thies & Bleiler 2011, Burns, Byrne & Maurer 2002). AD is the most common cause of dementia in old age, representing approximately 60–80% of all dementia cases (Lobo et al. 2000, Tijms et al. 2013, Forlenza et al. 2013). According to the World Health Organization, 46.8 million people were affected by dementia in the year 2015 (Prince et al. 2015). It has been estimated that by the year 2030, 74.7 million people will be affected by AD unless effective interventions are implemented (Prince et al. 2015). This increase in the prevalence of AD not only reduces the quality of life, health and wellbeing of those affected but also causes a significant financial burden at both the social and economic levels (Sloane et al. 2002).

The classic neuropathological lesions in AD consist of (i) aggregated amyloid plaques containing extracellular hydrophobic deposition of amyloid β peptides (Aβ) in the neuronal body, and (ii) neurofibrillary tangles composed of aggregates of hyperphosphorylated and misfolded tau protein (a microtubule-associated protein) that appear within the neurons (Ittner, Gotz 2011). Alzheimer's patients are usually identified by neuropsychological assessment when the disease has progressed to an advanced stage of cognitive impairment when it is already too late to cure (Weintraub, Wicklund & Salmon 2012, Storandt 1991). Currently the ability to detect the early stage of AD and track the different stages of AD progression to guide the choice of therapy is limited. The Mini-Mental State Examination (MMSE) is a validated research-based set of 30 questions assessing memory loss, cognitive decline, visuospatial and language impairment that is currently used as a standard tool for the clinical diagnosis of AD

(Tombaugh, McIntyre 1992, Mitchell 2009). However, the test lacks accuracy for the diagnosis of AD in living subjects, and diagnostic confirmation can only be achieved post-mortem by the examination of the senile plaques and neurofibrillary tangles in the cerebral tissue (Armstrong 2006, Nelson et al. 2012). The most validated AD disease-related established diagnostic biomarkers are cerebrospinal fluid (CSF) (aβ1-42, total tau, and phosphorylated tau), structural magnetic resonance imaging (MRI) (e.g., hippocampal volumetry), amyloid-positron emission tomography and fluorodeoxyglucose-positron emission tomography imaging (Humpel 2011, Henry et al. 2012). Mild cognitive impairment (MCI) is an intermediate state between the cognitive changes of normal aging and the earliest clinical signs of dementia and is represented as a declining cognition that does not meet the diagnostic criteria for dementia (Gauthier et al. 2006). Individuals affected by MCI have a higher risk of developing AD with an annual conversion rate of approximately 10-15% per year (Petersen et al. 2009, Fischer et al. 2007, Farias et al. 2009). Recent evidence indicates that AD is a systemic disorder that can be mirrored by subclinical pathologies in various peripheral tissues other than the brain, thereby rationalising the grounds for investigating cellular biomarkers in peripheral tissues for the diagnosis of MCI/AD risk (Gasparini et al. 1998, Joachim, Mori & Selkoe 1989, Soininen et al. 1992, Khan, Alkon 2015, Goldstein et al. 2003). There is a need for non-invasive biomarkers and inexpensive diagnostic approaches with high specificity and sensitivity to identify individuals at increased risk of developing MCI and AD so that early diagnosis and the initiation of preventative therapy is commenced to halt progression to irreversible neurological impairment.

Human buccal mucosa has considerable potential as an easily accessible source of cells that can be collected in a minimally invasive manner. Defects in buccal mucosa cells may reflect systemic changes in pathology in other tissues of ectodermal origin, such as

the nervous system (Leifert et al. 2011, Francois et al. 2014a, Francois et al. 2014b). It has been suggested that the ubiquitous presence and different expression of β-amyloid precursor protein (APP) in the buccal mucosa could be a useful means to estimate the regenerative status of tissue (Kummer et al. 2002). Accumulation of tau protein in the brain is the major component of neurofibrillary tangles and is the hallmark of AD pathogenesis (Braak, Braak 1991, Khan, Bloom 2016). The amount of buccal cell tau protein was observed at higher levels in AD subjects and correlated with the levels of tau protein in the CSF (Hattori et al. 2002). AD is associated with genomic DNA damage, and lack of DNA repair capacity could potentially lead to genomic instability (Fraga et al. 1990, Goukassian et al. 2000, Wilson, Bohr & McKinnon 2008, Thomas, Fenech 2008, Bucholtz, Demuth 2013, Lovell, Xie & Markesbery 2000).

The buccal micronucleus cytome (BMCyt) assay has been developed to score the cytological marker of DNA damage, cell death, and regenerative capacity of buccal mucosa cells (Thomas et al. 2009, Thomas, Fenech 2008). Individuals who had just been diagnosed with AD, but had not yet taken medication for their condition, had significantly reduced basal buccal cells frequency compared to unaffected age-matched controls suggesting reduced regenerative capacity. Aneuploidy (abnormal chromosomal number), has been investigated in buccal cells of AD patients in comparison with respective controls, with the results showing a higher aneuploidy level in chromosomes 17 and 21, which are known to encode Tau and APP, respectively (Iqbal et al. 1989, Koo 2002, Thomas, Fenech 2008). A recent study showed abnormal DNA content (e.g., hyperploidy in nuclei; a marker of aneuploidy) in buccal mucosa cells of AD patients (Francois et al. 2014a). The same study also demonstrated decreased amount of neutral lipids as measured by Oil Red-O staining in buccal cells from MCI patients (Francois et al. 2014a). Buccal samples of AD patients were tested for telomere shortening and

displayed a significantly shorter telomere length when compared to healthy older controls (Thomas, O'Callaghan & Fenech 2008). A previous study suggested that DNA strand breaks may be increased in MCI and AD patients (Migliore et al. 2005).

In response to double-stranded breaks (DSBs) in chromosomal DNA, H2AX (a member of histone H2A family and part of the chromatin structure) becomes phosphorylated to form γH2AX (Rogakou et al. 1998). γH2AX has also been found to be increased in neuronal cells of AD and with ageing in lymphocytes (Myung et al. 2008, Schurman et al. 2012, Silva et al. 2014). While H2AX is distributed uniformly throughout chromatin, only H2AX molecules located in close vicinity to DSBs become phosphorylated (Rogakou et al. 1998, Savic et al. 2009, Rogakou et al. 1999). The association of astrocyte degeneration and DNA damage with AD has been elucidated by investigating γH2AX signals in astrocytes from the hippocampus, which is known to be the most vulnerable region affected by AD (Myung et al. 2008). The results showed a significantly increased amount of γH2AX-immunopositive nuclei in the astrocytes of AD patients in comparison to healthy controls, suggesting that astrocytes may be associated with impaired neuronal function and contribute to the pathogenesis of AD (Myung et al. 2008). Additionally, a recent study reported elevated γH2AX levels in the hippocampal tissue of individuals with both AD pathology and clinical dementia than those seen in a normal ageing group (Silva et al. 2014). γH2AX has been used as a DSB marker in irradiated human buccal cells and was found to be dose responsive in different buccal cell types (Siddiqui et al. 2015, Gonzalez et al. 2010). However, buccal cell DNA damage involving γH2AX, an important marker of DNA damage and DNA damage response, has not been reported in neurodegenerative disorders such as AD.

Taken together, the evidence outlined above forms the basis of the hypothesis we tested that buccal cells from individuals with MCI and AD exhibit elevated levels of γH2AX compared to buccal cells from healthy controls. To test this hypothesis, the endogenous levels of γH2AX in buccal cells from participants in the Australian Imaging, Biomarkers and Lifestyle Flagship Study of Ageing (AIBL) who were either healthy controls, MCI cases or AD cases were measured. An automated laser scanning cytometry (LSC) γH2AX protocol was used to measure multiple parameters (area, integral, MaxPixel) of γH2AX signals, as well as the ploidy and nuclear shapes and senescent cells in thousands of buccal cells.

4.2 Methods and Materials

4.2.1 Human Ethics and Clinical Assessment of the Participants

Approval for the Australian Imaging, Biomarkers and Lifestyle Flagship Study of Ageing (AIBL) was from the institutional ethics committees of Austin Health (Parkville, Vic, Australia), St Vincent's Health (Fitzroy, Vic, Australia), Hollywood Private Hospital (Nedlands, WA, Australia), Edith Cowan University (Perth, WA, Australia) and CSIRO Australia. All volunteers were informed of the purpose of the study and gave written consent before participating in the study. The demographic and health characteristics of participants included in this study have been well characterized and reported previously (Ellis et al. 2009). Diagnosis of MCI and AD was performed and confirmed by experienced AIBL clinicians using a battery of neuropsychological tests that were selected on the basis that together then covered the main domains of cognition that are affected by AD and other dementias (Ellis et al. 2009). Data reported in this study are from a total of 51 randomly sub-sampled participants, including: (1) the cognitively healthy control (C) group (n=17); the MCI group (n=18) clinically

diagnosed with MCI; and the (3) AD group (n=16) clinically diagnosed with AD. Full blood pathology testing was conducted as described previously (Doecke et al. 2012, Faux et al. 2011). There were no blood pathology data available for 10 participants.

4.2.2 Buccal Cell Collection and Microscopic Slide Preparation

Prior to buccal cell collection, each participant was first required to rinse their mouth twice with water. Small flat headed toothbrushes were rotated 20 times against the inner part of the cheeks in a circular motion. Both cheeks were sampled using separate toothbrushes. Heads of the brushes were transferred into a 25 mL tube containing 20 mL of Saccomano's fixative solution and agitated vigorously to dislodge cells into the solution. Cells were then centrifuged at 1000g for 10 min before discarding and replacing supernatant with fresh 5 mL of buccal cell buffer (10mM Tris, 0.1 M ethylenediaminetetraacetic, 20 mM NaCl, i.e. pH 7.0. The cell suspension was drawn up and down for 5 times into a 10 mL syringe using 21 G needle in order to maximize the likelihood of getting single cells in suspension. The cell suspension was then passed through a 100 µm filter in a Swinex filter holder to remove clumps of cells. Cell concentration was assessed using a haemocytometer and cells were then cytocentrifuged for 5 min at 600 rpm onto microscope slides to a final number of 3,000 cells per cytospot using a Shandon CytospinVR 4 (Thermo Scientific, USA). Slides were washed once with distilled water and air-dried for 1 h and subsequently transferred to ethanol: acetic acid (3:1) fixative for 10 min. The slides were air-dried for 1 h and stored in sealed microscope boxes with desiccant at -80°C until the staining procedure was performed.

4.2.3 Preparation of Buccal Cells for Immunofluorescence

A circle was drawn around each cytospot using a hydrophobic PAP pen (Dako, Australia) and air-dried for 10 min. Slides were rinsed in Dulbecco's phosphate buffered saline (DBPS) for 15 min, incubated in chilled 70% ethanol for 20 min and washed in DPBS for 15 min. Buccal cell cytospots were then treated with 150 µl of prewarmed (37°C) pepsin solution (containing 750 U/ml of porcine gastric mucosa pepsin) in 0.01 M HCl and then covered with parafilm for 30 min at 37°C in a humidified box. The slides were then washed twice with DPBS for 5 min. Buccal cells were then permeabilized with 1% Triton X-100 for 15 min at room temperature. Slides were then rinsed three times in DPBS, and a blocking step was performed by incubating cells in 10% goat serum for 1 h at room temperature before being washed once with DPBS. The anti-γH2AX antibody was added to each cytospot at a dilution of 1:100 in DPBS containing 10% goat serum and covered with parafilm overnight at 4 ^{0}C in a humidified box. Slides were washed three times in DPBS for 5 min and a secondary antibody Alexa Fluor 488 Goat antimouse was added to each cytospot at a dilution of 1:500 in DPBS containing 10% FBS and covered with parafilm for 1 h at room temperature. Slides were washed three times in DPBS for 5 min and nuclei were counterstained with 4,6-diamidino-2-phenylindole (DAPI) at a concentration of 1 µg/ml for 10 min at room temperature. The excess DAPI was removed by rinsing the slides with a solution containing 300 mM NaCl and 34 mM sodium citrate. Slides were then mounted with coverslips and DPBS: glycerol (1:1) medium. The edges of coverslips were sealed with nail polish to prevent drying prior to performing LSC.

4.2.4 Laser scanning cytometry measurements of γH2AX

Laser scanning cytometry (LSC) measurements were carried out with an iCyte® Automated Imaging Cytometer (Thorlabs, Sterling Virginia, USA) with full autofocus function as well as 405 nm and 488 nm lasers for excitation of DAPI and Alexa Fluor 488, respectively. Fluorescence from DAPI (blue) and Alexa Fluor 488 (green) was collected with a photomultiplier tube. Samples were scanned in separate passes (consecutively) to prevent spectral overlap. The nuclei and γH2AX events were contoured using empirically determined thresholds to exclude the scoring of false positives (e.g., small fluorescent debris). The frequency (%) of nuclei containing γH2AX signal was recorded as well as multiple parameters within each nucleus; including the total γH2AX integral (a function of γH2AX intensity and size) and the MaxPixel value (the value of the most intense γH2AX signal/pixel within nuclei). These parameters were generated using the iCyte® 3.4 software and subsequently transferred into excel for further statistical analyses. Nuclei were also classified into round, long, or oval shapes by utilizing the iCyte software parameters which included area, circularity, perimeter and diameter as described in the legend of Figure 4.1. Additionally, all nuclei were separated according to their ploidy status (DNA content) as follows; <2N, 2N, and >2N and cellular senescence status. For 2N nuclei, the peak of the nuclei count coincided with the mean DAPI integral.

4.2.5 Statistical Analysis

GraphPad Prism 6.01 (GraphPad Prism, San Diego, CA) was used to statistically analyse the data. LSC γH2AX data were checked for normality using the D'Agostino and Pearson omnibus normality test. Differences in relative γH2AX signals in the lymphocytes from control, MCI, and AD groups were compared using the Kruskal-

Wallis test for non-Gaussian distributed data followed by Dunn's multiple comparisons test. Correlation coefficients were obtained using Pearson's correlation coefficients for Gaussian distributed data and Spearman's rho for non-Gaussian distributed data. Analysed data are reported as mean ± standard error of the mean (SEM) with $p<0.05$ considered statistically significant. Receiver-operating characteristic curves (ROC) were prepared for selected γH2AX parameters between the control and MCI or AD groups to obtain the area under the curve (AUC), sensitivity, specificity, confidence interval and p-value.

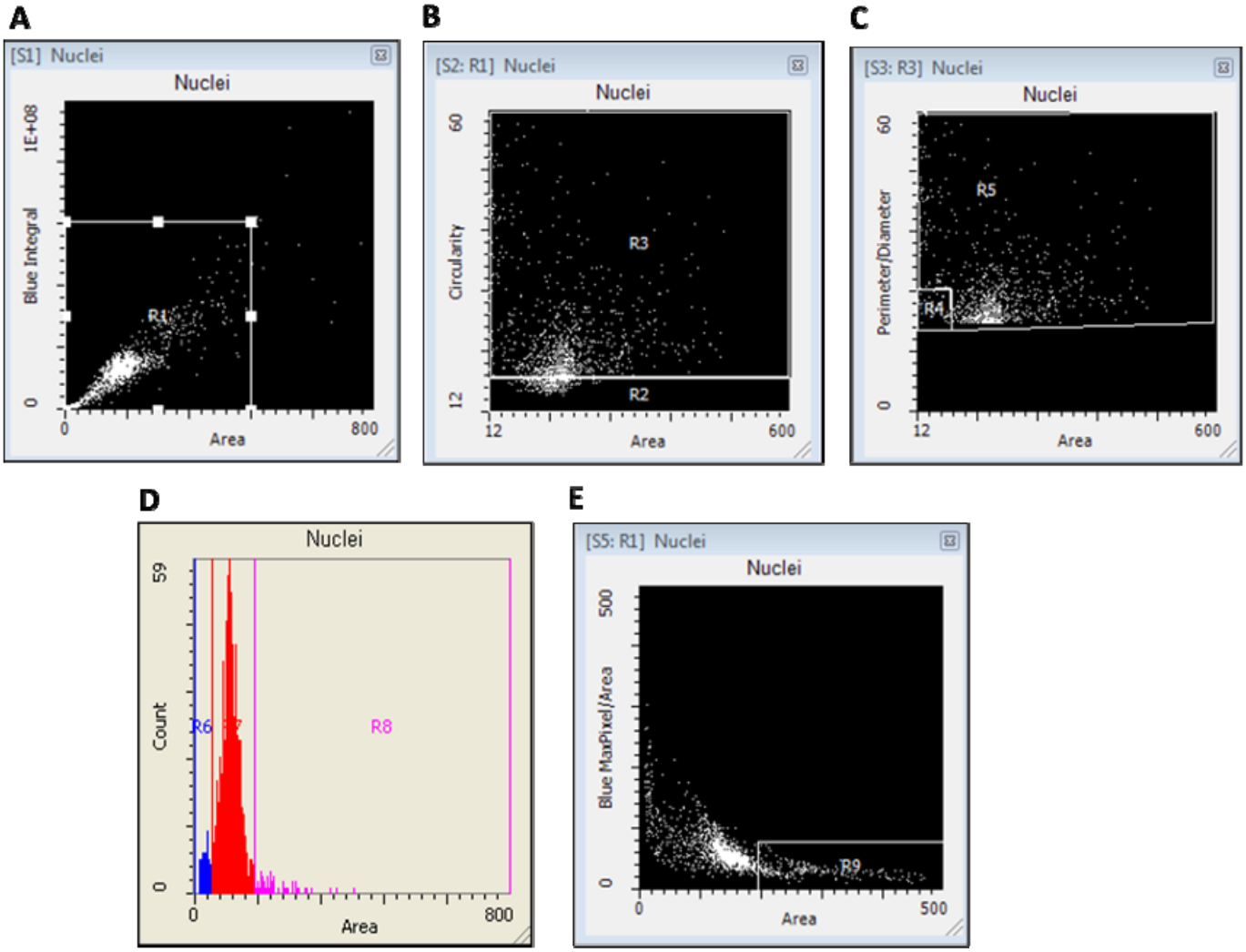

Figure 4.1: Scattergram and histogram for separation of buccal cell nuclei types by LSC. A representative example of DNA content scattergram and histogram for a participant from the control group. (A) A scattergram was generated to separate cells based on differences in nuclear staining and area by plotting their blue integral versus the area. Nuclei having area values that ranged from 0 to 600 μm^2 and blue integral values that ranged from 0 to 4 X 10^7 (arbitrary units) were separated in Region 1 (R1). (B) Nuclei in R1 were analyzed by plotting their circularity (y-axis) versus nuclear area (x-axis) where "Round" nuclei were identified in Region 2 (R2). (C) Nuclei from Region 3 (R3) were further analyzed by plotting their perimeter/diameter ratio (y-axis) versus nuclear area (x-axis). Two new groups were identified from R3; long nuclei were identified in R4 and oval nuclei in R5. Representative galleries of round, long, and oval nuclei different buccal cell nuclear shapes are shown in Chapter 3 Section 3.2.2.4 and Figure 3.2. A histogram plot of the same data in R1 showing the <2N, 2N and >2N peaks as represented in R6, R7, and R8, respectively, and the respective frequency of DNA content events scored, with the majority of buccal cells being scored as 2N. (E). Nuclei in R1 were plotted against nuclear area versus the ratio of the maximal pixel intensity /area of DAPI fluorescence per nucleus. These cells had morphometric characteristics of cellular senescence [i.e., increased nuclear size (area) combined with decreased intensity of MaxPixel of DNA-associated fluorescence per nucleus, after DNA staining with DAPI] were separated in R9.

4.3 Results

4.3.1 Clinical Characteristics of Participants

The mean age, gender distribution (male/female), body mass index (BMI) and MMSE score of AIBL participants in the control, MCI and AD groups is shown in Table 4.1. There were no significant differences for gender ratio and BMI between the groups, while there was a significant difference in age (p=0.0039) between control and AD group. As expected, there was a significant decrease in the MMSE scores of both the MCI (p=0.0126) and AD (p=<0.0001) groups compared with the control group.

Table 4.1: Clinical characteristics of participants

	Control n=18	MCI n=17	AD n=16
Sex (M:F)	12:6	11:6	9:7
Age (years)	72.2 ± 1.5	78.7 ± 1.9	81.0 ± 1.8 **
BMI	27.0 ± 1.3	23.4 ± 1.3	24.8 ± 1.1
MMSE score	29.1 ± 0.2	26.0 ± 0.8 *	12.8 ± 1.8 ****

Means and standard error of the mean (SEM) are reported for each group. Significance was accepted at p<0.05. Abbreviations: AD, Alzheimer's disease; F, Female; M, Male; MCI, Mild cognitive impairment; MMSE, Mini-Mental State Examination score. *p<0.05, **p<0.01, ****p<0.0001.

4.3.2 Scoring of γH2AX Signals in Buccal Cells by LSC

The endogenous γH2AX levels in buccal cells from control, MCI, and AD cases were measured by LSC assay in order to investigate whether the γH2AX level is significantly increased in AD compared to control cells. Multiple parameters of γH2AX signals, including the total γH2AX integral (a function of γH2AX intensity and size), γH2AX MaxPixel (the value of the most intense γH2AX signal/pixel within a nucleus), γH2AX area, and the number of γH2AX events (foci) per cell were measured in all nuclei and/or

in cells with different DNA content (ploidy status), different nuclear shapes as well as in senescent cells.

4.3.2.1 γH2AX in All Nuclei

Table 4.2 summarises the one-way ANOVA results for the different γH2AX parameters (integral, MaxPixel, area and foci/nucleus) for all nuclei, which included <2N nuclei, 2N nuclei, and >2N nuclei analysed from the control, MCI and AD groups. There was a significant increase in the γH2AX integral (p=0.0332) in AD cells compared to control cells in all nuclei (Table 4.2, 1A, and Figure 4.2, A). Consistent with the increase in the γH2AX integral, a significant increase in the γH2AX MaxPixel value (p=0.0199) and the numbers of γH2AX foci/nucleus (p=0.0234) were also observed in AD cells compared to control cells (Table 4.2, 1A and Figure 4.2, B and 4.2, D). Although all nuclei had a higher level of γH2AX (MaxPixel, foci/nucleus) in MCI cells compared to control cells, there was no statistically significant differences in these parameters. However, a significant increase in the linear trend for the γH2AX MaxPixel value (p=0.0124) was observed across the groups (i.e., AD > MCI > control) in all nuclei (Figure 4.2, B). There was also significant increase in the γH2AX MaxPixel value (p=0.0458) in AD cells compared to MCI cells (Table 4.2, 1A, Figure 4.2, B). Individual data are also presented in [Figure 4.3 (A-D)].

4.3.2.2 γH2AX in 2N Nuclei

There was a significant increase in the γH2AX integral value (p=0.0485), γH2AX MaxPixel value (p=0.0159) and number of γH2AX foci/nucleus (p=0.0211) in AD cells compared to control cells (Table 4.2, 1C)). No significant increase in any of the γH2AX parameters was seen between the control and MCI cells and between MCI and AD cells.

In addition, a significant increase in the γH2AX MaxPixel value (p=0.0281) was observed in AD cells compared to MCI cells (Table 4.2, 1C).

4.3.2.3 γH2AX in <2N and >2N Nuclei

For the <2N nuclei, a significant increase in the γH2AX signals (integral, MaxPixel, area, foci/nucleus) was observed in AD compared to control cells, at p=0.0406, p=0.0216, p=0.0498 and p=0.0064, respectively (Table 4.2, 1B). The >2N nuclei showed significantly increased γH2AX integral, γH2AX MaxPixel, γH2AX area, γH2AX foci/nucleus in AD compared to control cells (Table 4.2, 1D). Additionally, both the γH2AX integral and γH2AX area values also increased significantly (p=0.0174 and p=0.0414, respectively) in AD compared to MCI cells for >2N nuclei (Table 4.2,1D).

Table 4.2: Summary of one-way ANOVA tests for different γH2AX parameters measured using LSC in different types of buccal cell nuclei

LSC	Con	MCI	AD	Con v MCI	Con vs AD	MCI vs AD
	Mean+/-SEM	Mean+/-SEM	Mean+/-SEM	p-value	p-value	p-value
1A: All nuclei						
γH2AX integral (x10^6 a.u.)	3.873+/- 1.733	2.280+/-0.6092	5.088+/-1.611	NS	**0.0332**	0.0512
γH2AX MaxPixel (a.u.)	3365+/-458.5	3931+/-673.5	6477+/-1244	NS	**0.0199**	**0.0458**
γH2AX area (μm)	51.47+/- 21.94	29.34+/-6.624	51.62+/-9.776	NS	0.0645	0.1633
γH2AX foci/nucleus	1.510+/-0.2912	1.943+/-0.3310	2.940+/-0.3316	NS	**0.0234**	0.1176
1B: < 2N nuclei						
γH2AX integral	2.827+/-1.105	2.098+/-0.559	4.253+/-0.983	NS	**0.0406**	0.0619
γH2AX MaxPixel	3459+/-476.9	3922+/-629.8	6498+/-1263	NS	**0.0216**	0.0745
γH2AX area	40.29+/-16.22	27.72+/-5.742	46.54+/-7.902	NS	**0.0498**	0.1975
γH2AX foci/nucleus	0.8886+/-0.1652	1.366+/-0.1802	1.851+/-0.2257	NS	**0.0064**	0.6317
1C: 2N nuclei						
γH2AX integral	3.954+/-1.914	2.201+/-0.592	5.057+/-1.788	NS	**0.0485**	0.1273
γH2AX MaxPixel	3309+/-445.8	3764+/-625.2	6465+/-1266	NS	**0.0159**	**0.0281**
γH2AX area	51.56+/-23.32	29.29+/-6.655	50.13+/-10.96	NS	0.1018	0.2603
γH2AX foci/nucleus	1.660+/-0.3251	2.068+/-0.3792	3.145+/-0.3631	NS	**0.0211**	0.1173
1D: <2N nuclei						
γH2AX integral	12.58+/-6.035	3.842+/-1.039	18.20+/-4.103	NS	**0.0069**	**0.0174**
γH2AX MaxPixel	3580+/-728.9	4879+/-921.7	8227+/-1388	NS	**0.0008**	0.0552
γH2AX area	128.8+/-53.45	52.24+/-16.46	195.4+/-40.74	NS	**0.0187**	**0.0414**
γH2AX foci/nucleus	2.891+/-0.7799	4.246+/-1.499	5.711+/-0.795	NS	**0.0176**	0.0792

Parameters highlighted in bold text were considered statistically significant. Data were expressed as mean ± SEM. Abbreviations: a.u., Arbitrary units; AD, Alzheimer's disease; MCI, Mild cognitive impairment; NS= non-significant.

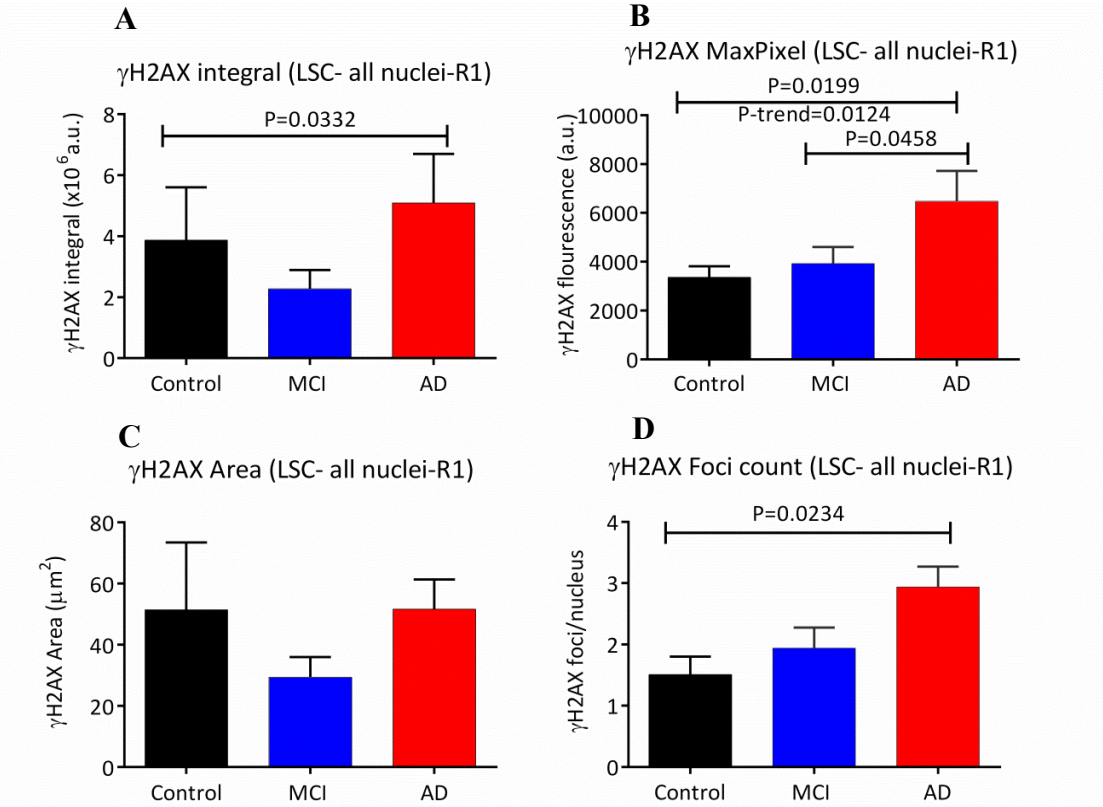

Figure 4.2: γH2AX signals (integral, MaxPixel, area, foci/nucleus) in all nuclei.

A: γH2AX integral; B: γH2AX MaxPixel; C: γH2AX area; D: γH2AX foci/nucleus. These parameters were measured by LSC for control (n=17), MCI (n=18), AD (n=16). Abbreviations: a.u., Arbitrary units; AD, Alzheimer's disease; MCI, Mild cognitive impairment. Data are means ± SEM.

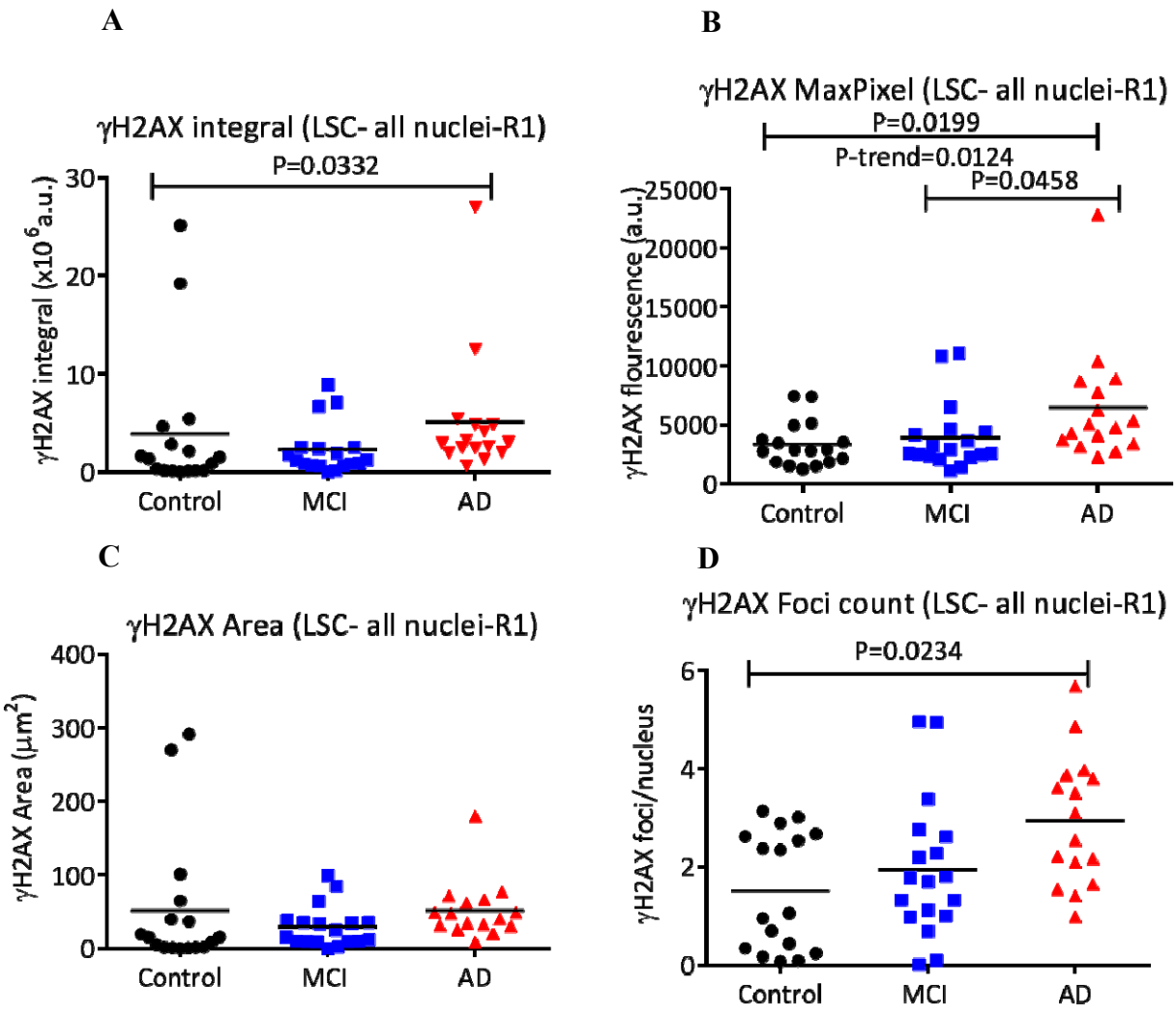

Figure 4.3: Individual data of γH2AX parameters (integral, MaxPixel, area, foci/nucleus) in all nuclei.

A: γH2AX integral; B: γH2AX MaxPixel; C: γH2AX area; D: γH2AX foci/nucleus. These parameters were measured by LSC for control (n=17), MCI (n=18), AD (n=16). Abbreviations: a.u., Arbitrary units; AD, Alzheimer's disease; MCI, Mild cognitive impairment. Data are means. Lines within data points indicate mean.

Nuclear Shape

In the previous study (see Section 3.3.2.4, Figure 3.2) we demonstrated morphological changes in nuclear shape parameters such as round, long, and oval (Siddiqui et al. 2015). Therefore, in this study round, long and oval nuclei were investigated from control, MCI and AD cases using LSC. Table 4.3 summarises the one-way ANOVA results for the different γH2AX parameters (integral, MaxPixel, area and foci/nucleus) for round, long and oval nuclei analysed from the control, MCI and AD groups.

4.3.3 γH2AX in round Nuclei

There was a significant increase in the γH2AX MaxPixel value (p=0.0207) and numbers of γH2AX foci/nucleus (p=0.0420) in round nuclei of AD cells compared to control cells (Table 4.3, 1A). No significant increase of any of the γH2AX parameters was seen between the control and MCI cells and between MCI and AD cells.

4.3.4 γH2AX in long Nuclei

For long nuclei, significant increases in the γH2AX MaxPixel value (p=0.0119) and numbers of γH2AX foci/nucleus (0.0209) were observed in AD cells compared to control cells. As seen in the round nuclei, no significant increase of any of the γH2AX parameters was seen between the control and MCI cells and between MCI and AD cells (Table 4.3, 1B)

4.3.5 γH2AX in oval Nuclei

For oval nuclei, a significant increase in the γH2AX integral value (p=0.0264), γH2AX MaxPixel value (p=0.0135) and numbers of γH2AX foci/nucleus (0.0091) were observed in AD cells compared to control cells. However, no significant increase of any

of the γH2AX parameters was seen between the control and MCI cells and between MCI and AD cells (Table 4.3, 1C).

It does not appear that nuclear shape substantially alters or influences the relative differences in the buccal cell γH2AX parameters in AD cases versus controls.

Table 4.3: Summary of one-way ANOVA tests for different γH2AX parameters measured using LSC in round, long and oval nuclei from buccal cells

LSC	Con	MCI	AD	Con v MCI	Con vs AD	MCI vs AD
	Mean+/-SEM	Mean+/-SEM	Mean+/-SEM	p-value	p-value	p-value
1A. Round						
γH2AX integral (x10^6 a.u.)	3.440+/-1.820	2.182+/-0.669	4.514+/-1.722	NS	0.1424	0.4755
γH2AX MaxPixel (a.u.)	3414+/-449.2	4061+/-695	6673+/-1274	NS	**0.0207**	0.0586
γH2AX area (μm)	35.76+/-17.92	22.85+/-6.45	42.71+/-10.41	NS	0.2046	0.1749
γH2AX foci/nucleus	1.552+/-0.287	1.716+/-0.313	2.934+/-0.403	NS	**0.0420**	0.0703
1B. Long						
γH2AX integral	2.266+/-0.9230	2.168+/-0.6196	4.487+/-1.253	NS	0.0804	0.2344
γH2AX MaxPixel	3631+/-586.4	3911+/-647.2	7692+/-1437	NS	**0.0119**	0.2690
γH2AX area	35.76+/-15.19	27.54+/-6.82	42.02+/-8.43	NS	0.1659	0.5273
γH2AX foci/nucleus	1.095+/-0.2044	1.522+/-0.6077	2.132+/-0.2940	NS	**0.0209**	0.5141
1C. Oval						
γH2AX integral	3.917+/-1.734	2.341+/-0.608	5.407+/-1.635	>0.9999	**0.0264**	0.0574
γH2AX MaxPixel	3398+/-495.1	3885+/-655.5	6366+/-1123	>0.9999	**0.0135**	0.0527
γH2AX area	56.62+/-23.98	30.40+/-6.755	58.62+/-12.99	>0.9999	0.0535	0.1500
γH2AX foci/nucleus	1.580+/-0.3293	2.061+/-0.3624	3.248+/-0.3491	>0.9999	**0.0091**	0.0862

Parameters highlighted in bold text were considered statistically significant. Data were expressed as mean ± SEM. Abbreviations: a.u., Arbitrary units; AD, Alzheimer's disease; MCI, Mild cognitive impairment; NS= non-significant.

4.3.6 Frequency (%) of Round, Long, and Oval Nuclei Across Control, MCI and AD groups.

There was a no significant changes in the frequency (%) of round long, and oval shaped nuclei between control, MCI and AD group [Figure 4.4, (A-C)].

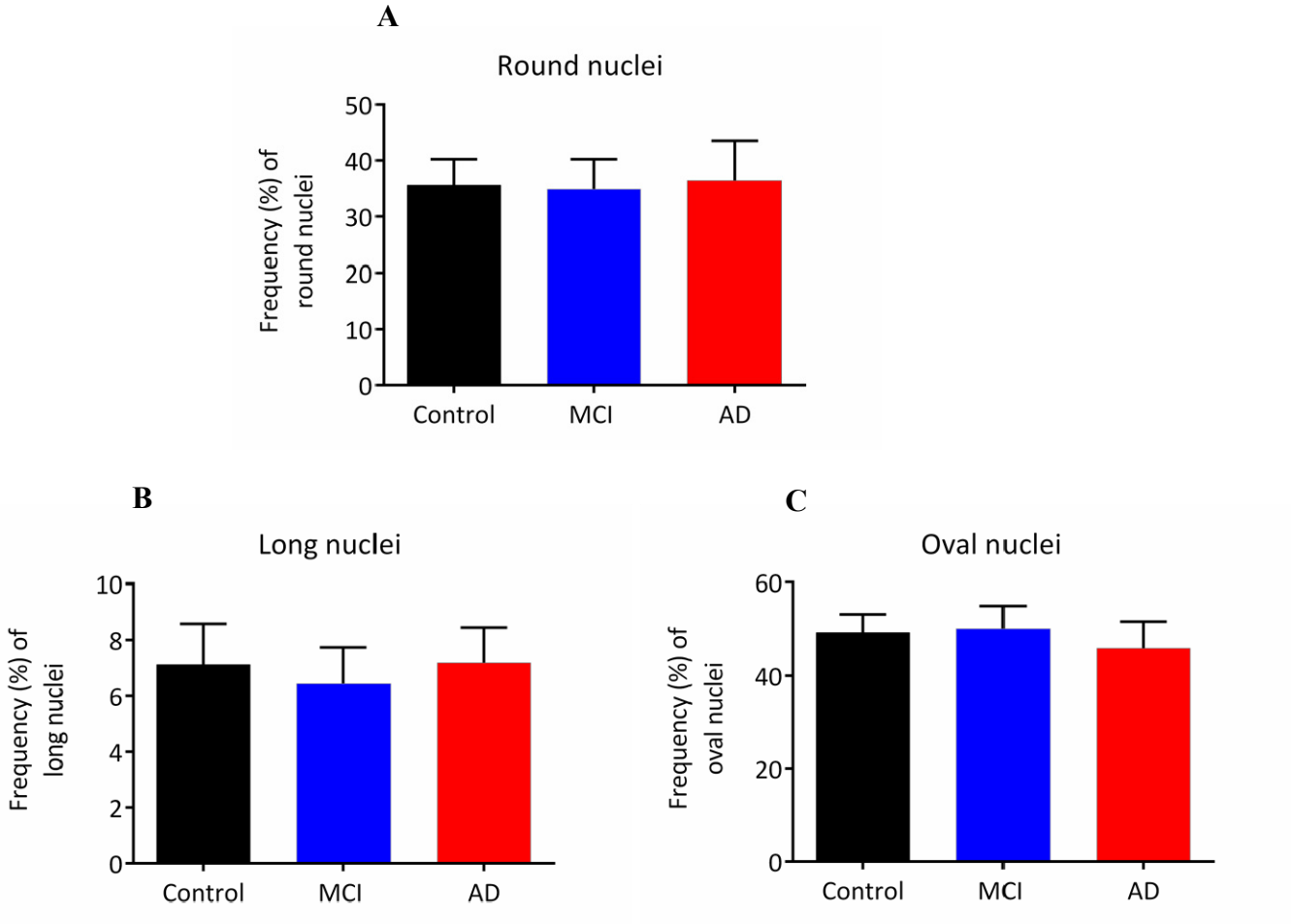

Figure 4.4: Frequency (%) of round long, and oval shaped nuclei.

Frequency (%) of different shaped buccal cell nuclei in the control (n=17), MCI (n=18), AD (n=16) groups. A: Round nuclei; B: long nuclei; C: Oval nuclei. Abbreviations: AD, Alzheimer's disease; MCI, Mild cognitive impairment. Data are means ± SEM.

4.4 γH2AX in Senescent Nuclei

The nuclear area and nuclear MaxPixel features available within iCyte were used to empirically classify senescent buccal cells and their γH2AX parameter (integral, MaxPixel, area foci/nucleus) values as shown in Table 4.4. There were no differences in the percentage of senescent cells across the groups (Table 4.5). Significant increase was observed for the γH2AX integral (p=0.0123) γH2AX MaxPixel (p=0.0014), γH2AX area (p=0.0062) and γH2AX foci/nucleus (p=0.0015) in AD senescent cells compared to control senescent cells. The significant increase was also observed for the γH2AX integral (p=0.0349), γH2AX MaxPixel (p=0.0134), and γH2AX area (p=0.0345) in AD senescent cells compared to MCI senescent cells (Table 4.4).

Table 4.4: Summary of the one-way ANOVA tests for different γH2AX parameters in senescent nuclei

Senescent nuclei	Con	MCI	AD	Con vs MCI	Con vs AD	MCI vs AD
	Mean+/-SEM	Mean+/-SEM	Mean+/-SEM	p-value	p-value	p-value
γH2AX integral (x10^6 a.u.)	6.921+/-2.693	3.590+/-0.864	12.87+/-2.87	NS	**0.0123**	**0.0349**
γH2AX MaxPixel (a.u.)	3611+/-594	4342+/-734	7613+/-1058	NS	**0.0014**	**0.0134**
γH2AX area (μm^2)	73.18+/-27.08	49.93+/-13.34	152.8+/-30.1	NS	**0.0062**	**0.0345**
γH2AX foci/nucleus	2.181+/-0.599	3.635+/-1.027	5.571+/-0.671	NS	**0.0015**	0.0761

Parameters highlighted in bold text were considered statistically significant. Data were expressed as mean ± SEM. Abbreviations: a.u., Arbitrary units; AD, Alzheimer's disease; MCI, Mild cognitive impairment; NS= non-significant.

Table 4.5: Summary of the one-way ANOVA tests for % of senescent nuclei across Control, MCI, and AD

Senescent nuclei	Con	MCI	AD	Con vs MCI	Con vs AD	MCI vs AD
	Mean+/-SEM	Mean+/-SEM	Mean+/-SEM	p-value	p-value	p-value
Frequency (%) of cells	14.59 +/- 4.047	16.11 +/- 4.430	11.13 +/- 3.150	NS	NS	NS

Data were expressed as mean ± SEM. Abbreviations: a.u., Arbitrary units; AD, Alzheimer's disease; MCI, Mild cognitive impairment; NS= non-significant.

4.5 Nuclear Circularity, Integral, and Area in Buccal Cells

Other nuclear parameters, such as circularity, integral and area were also measured by LSC in order to investigate whether there are other significant changes in nuclei from AD and MCI cells compared to control cells. For the nuclear integral and area, no significant difference was found between the control, MCI and AD groups. The nuclear circularity of different types of buccal cell nuclei in the control, MCI and AD groups was also measured using the circularity feature available with the iCyte. A high circularity value indicates more irregular shaped nuclei; in contrast, the lowest circularity value indicates a perfect circle.

4.5.1 All Nuclei

There was a significant increase in nuclear circularity ($p=0.0075$) in all nuclei of AD cells compared to control cells. In addition, a significant increase of nuclear circularity ($p=0.0257$) was also observed in AD cells compared to MCI cells. Circularity was also investigated in the different nuclear types (Figure 4.5, A). A significant increase in the linear trend for the nuclear circularity value ($p=0.0027$) was observed across the groups (i.e., AD > MCI > control) in all nuclei

4.5.2 2N Nuclei

For 2N nuclei, no statistically significant increase in nuclear circularity was observed between control and AD cells and between MCI and AD cells (Figure 4.5, C). However, significant increase in the linear trend for the nuclear circularity value ($p=0.0315$) was observed across the groups (i.e., AD > MCI > control) in 2N nuclei.

4.5.3 <2N and >2N Nuclei

No significant differences in circularity in <2N nuclei was observed between the groups, while a significant increase was observed in >2N nuclei of AD cells ($p=0.0411$) compared to control cells, as well as in MCI cells ($p=0.0254$) compared to AD cells (Figure 4.5, B and D).

4.5.4 Senescent Nuclei

Nuclear circularity was also measured in senescent nuclei, which were identified using the nuclear area and MaxPixel features available within iCyte. There was a significant increase in circularity in senescent nuclei ($p=0.0483$) of AD cells compared to control cells. In addition, a significant increase of circularity ($p=0.0240$) was observed in AD cells compared with control cells (Figure 4.5, E).

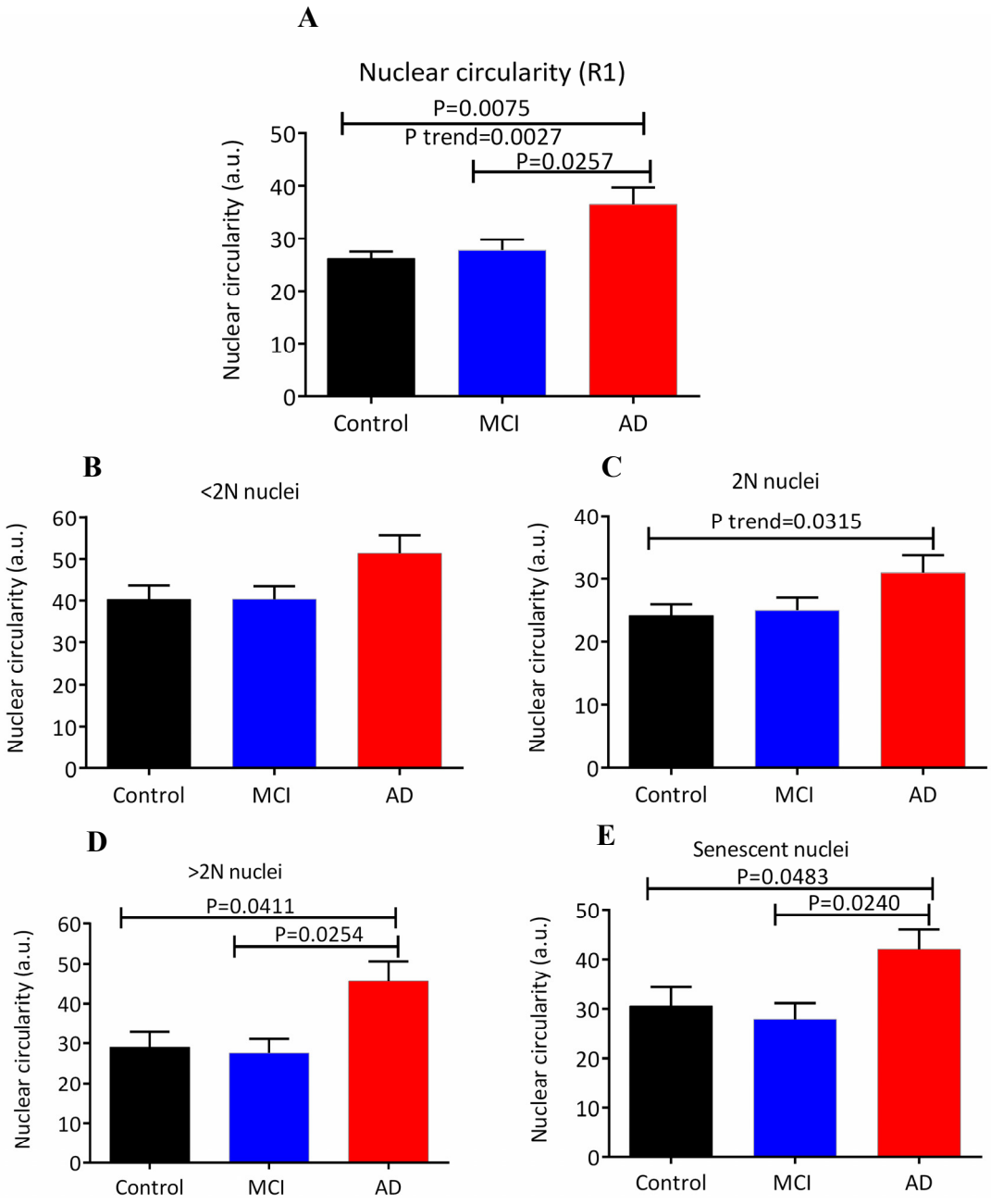

Figure 4.5: Circularity of different types of buccal cell nuclei.

Circularity of nuclei was measured in different types of buccal cell nuclei in the control (n=17), MCI (n=18), AD (n=16) groups. (A) all nuclei; (B) <2N nuclei; (C) 2N nuclei; (D) >2N nuclei and (E) senescent nuclei. Abbreviations: a.u., Arbitrary units; AD, Alzheimer's disease; MCI, Mild cognitive impairment. Data are means ± SEM.

4.6 Receiver-Operating Characteristic Curve

Since the γH2AX parameters (e.g., integral, γH2AX MaxPixel, γH2AX foci/nucleus) were significantly higher in AD compared to the control group for each category of nuclei, evaluation of diagnostic value of these parameters for discriminating AD patients from controls, receiver operating characteristic (ROC) curves were generated. The area under the curve (AUC) values for γH2AX integral, MaxPixel, and foci/nucleus were 0.7353 (p=0.2118), 0.7794 (p=0.0062) and 0.7684 (p=0.0086), respectively (Figure 4.6, A–C). Of all parameters analysed using ROC curves, the γH2AX MaxPixel value showed the greatest value for the identification of AD, with 75% sensitivity and 70 % specificity.

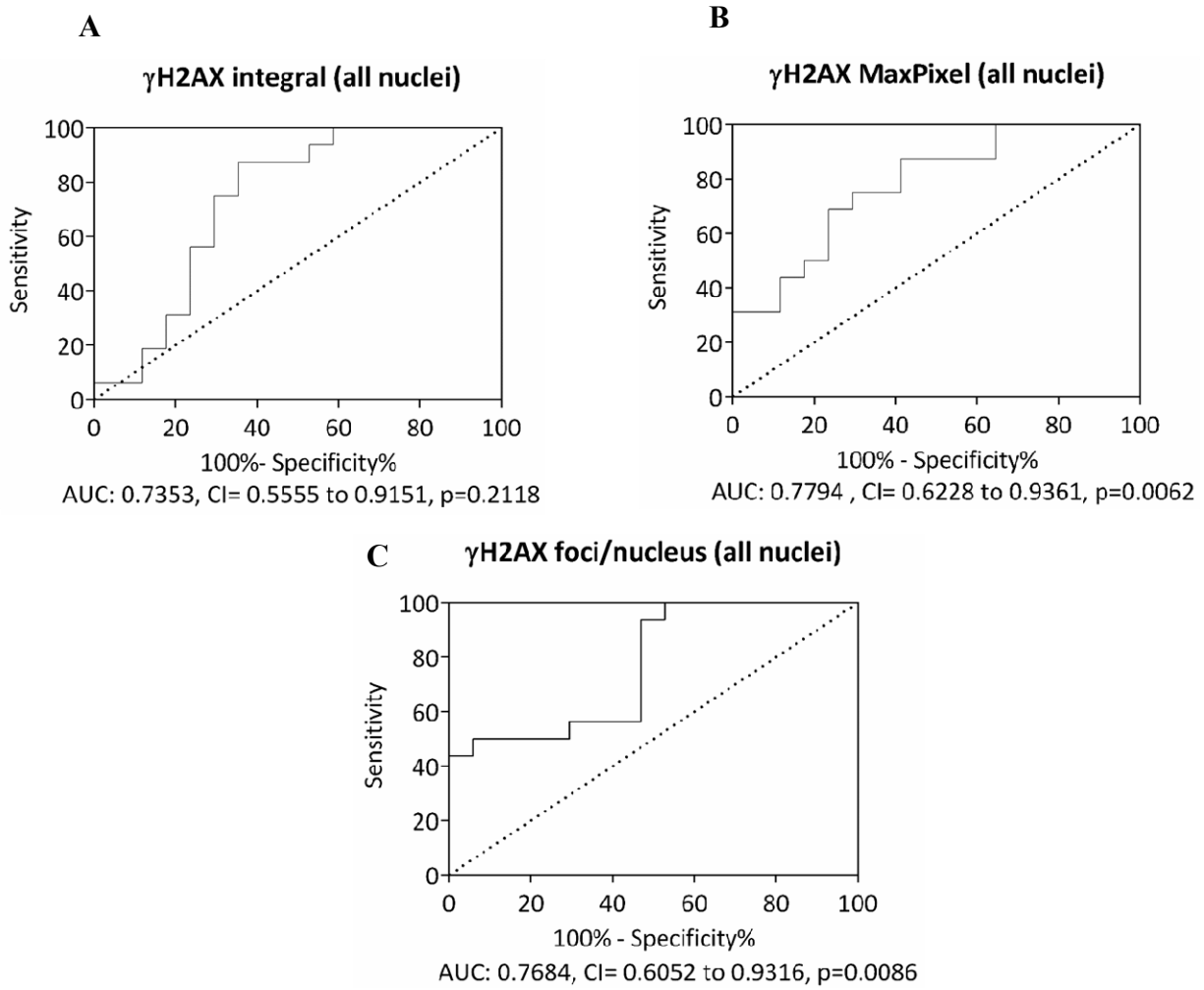

Figure 4.6: ROC curves for selected LSC-measured γH2AX parameters for control and AD nuclei. ROC curves were generated for the γH2AX integral, γH2AX MaxPixel and γH2AX foci/nucleus using measurements in buccal cells from control and AD cells.

4.6.1 Correlation of the γH2AX Integral and Other γH2AX Parameters by Laser Scanning Cytometry

To investigate the correlation between different γH2AX parameters measured by LSC, γH2AX integral in all nuclei was selected for investigating correlations with γH2AX MaxPixel, γH2AX Area, and γH2AX foci/nucleus. γH2AX MaxPixel, γH2AX Area, γH2AX foci/nucleus strongly correlated with γH2AX integral. Table 4.6 summarises the r and p-values for each of the γH2AX parameters analysed. The parameters highlighted in bold indicates different γH2AX parameters correlated with γH2AX integral.

Table 4.6: Summary of correlations tested between γH2AX integral and other γH2AX parameters in different types of buccal cell nuclei from the AIBL study

Cell Types	Parameters	Correlation (r)	CI	p-value
All nuclei	γH2AX MaxPixel	0.7945	0.6643–0.8779	**<0.0001**
	γH2AX area	0.9264	0.8740–0.9576	**<0.0001**
	γH2AX foci/nucleus	0.3386	0.06947–0.5618	**0.0151**
<2N nuclei	γH2AX MaxPixel	0.8345	0.7258–0.9025	**<0.0001**
	γH2AX area	0.9254	0.8722–0.9569	**<0.0001**
	γH2AX foci/nucleus	0.3704	0.1056–0.5862	**0.0075**
2N nuclei	γH2AX MaxPixel	0.7795	0.6417–0.8685	**<0.0001**
	γH2AX area	0.9336	0.8859–0.9617	**<0.0001**
	γH2AX foci/nucleus	0.2804	0.0052–0.5162	**0.0462**
>2N nuclei	γH2AX MaxPixel	0.5874	0.3719–0.7428	**<0.0001**
	γH2AX area	0.8986	0.8280–0.9411	**<0.0001**
	γH2AX foci/nucleus	0.2943	0.02031–0.5272	**<0.0361**
Senescent nuclei	γH2AX MaxPixel	0.7643	0.6190–0.8589	**<0.0001**
	γH2AX area	0.9142	0.8536–0.9503	**<0.0001**
	γH2AX foci/nucleus	0.4159	0.1583–0.6204	**0.0002**
Round	γH2AX MaxPixel	0.7423	0.5867–0.8451	**<0.0001**
	γH2AX area	0.9495	0.9127–0.9710	**<0.0001**
	γH2AX foci/nucleus	0.2950	0.02105–0.5277	**0.0356**
Long	γH2AX MaxPixel	0.8961	0.8240–0.9397	**<0.0001**
	γH2AX area	0.8673	0.7775–0.9224	**<0.0001**
	γH2AX foci/nucleus	0.1422	-0.1389–0.4021	**0.3196**
Oval	γH2AX MaxPixel	0.8053	0.6808–0.8846	**<0.0001**
	γH2AX area	0.9455	0.9060–0.9687	**<0.0001**
	γH2AX foci/nucleus	0.4033	0.1436–0.6110	**0.0033**

Parameters highlighted in bold text were considered statistically significant. CI; 95% confidence interval.

4.6.2 Correlation of γH2AX Signals (Integral, MaxPixel) in Different Types of Buccal Cell Nuclei with the MMSE Score

To investigate whether the γH2AX signals in different types of buccal cell nuclei were related to the advancement of cognitive decline in the subjects (a low MMSE score represents more cognitive decline), the correlations between the γH2AX integral,

γH2AX MaxPixel and MMSE scores were tested. Table 4.7 summarises the r and p-values for each of the γH2AX parameters analysed in different types of buccal cell nuclei. The parameters highlighted in bold indicate that the γH2AX integral or MaxPixel negatively correlated with the MMSE score.

Table 4.7: Summary of correlations between LSC scored γH2AX signals vs the MMSE score available from the AIBL study

	Parameters	Correlation (r)	CI	p-value
All nuclei	γH2AX integral	-0.1899	-0.4014–0.0408	**0.0959**
	γH2AX MaxPixel	-0.2266	-0.4331–0.0024	**0.0460**
<2N nuclei	γH2AX integral	-0.3059	-0.5452 to -0.0205	**0.0365**
	γH2AX MaxPixel	-0.4402	-0.6458 to -0.1751	**0.0020**
2N nuclei	γH2AX integral	-0.3227	-0.5582 to -0.0391	**0.0269**
	γH2AX MaxPixel	-0.4477	-0.6512 to -0.1841	**0.0016**
>2N nuclei	γH2AX integral	-0.4616	-0.6671 to -0.1908	**0.0016**
	γH2AX MaxPixel	-0.5200	-0.7023 to -0.2737	**0.0002**
Round	γH2AX integral	-0.3535	-0.5816 to -0.0737	**0.0148**
	γH2AX MaxPixel	-0.4550	-0.6565 to -0.1930	**0.0013**
Long	γH2AX integral	-0.3039	-0.5437 to -0.0183	**0.0378**
	γH2AX MaxPixel	-0.4141	-0.6268 to -0.1440	**0.0038**
Oval	γH2AX integral	-0.3534	-0.5816 to -0.0736	**0.0148**
	γH2AX MaxPixel	-0.4678	-0.6656 to -0.2086	**0.0009**
Senescent	γH2AX integral	-0.5229	-0.7044 to -0.2773	**0.0002**
	γH2AX MaxPixel	-0.5156	-0.6993 to -0.2680	**0.0002**

Parameters highlighted in bold text were considered statistically significant. All are Spearman's rho correlation. CI; 95% confidence interval.

4.6.3 Correlation of γH2AX Signals (Integral, Maxpixel) with Nuclear Circularity in Different Types of Buccal Cell Nuclei

Since increased nuclear circularity was observed in AD cells compared to control and MCI cells, the correlation between γH2AX signals (γH2AX integral or γH2AX MaxPixel) and nuclear circularity was investigated in order to determine if there was a relationship between nuclear circularity and γH2AX signals. Table 4.8 summarises the r and p-values for each of the γH2AX parameters analysed in different types of buccal

cell nuclei. The parameters highlighted in bold indicate that the γH2AX integral and MaxPixel values positively correlated with nuclear circularity in the different type of buccal cell nuclei analysed.

Table 4.8: Summary of correlations between LSC-scored γH2AX signals versus the nuclear circularity score available from the AIBL study

	Parameters	Correlation (r)	CI	p-value
All nuclei	γH2AX integral	0.3246	0.05378 to 0.5510	**0.0201**
	γH2AX MaxPixel	0.3554	0.08843 to 0.5748	**0.0105**
<2N nuclei	γH2AX integral	0.3737	0.1093 to 0.5887	**0.0069**
	γH2AX MaxPixel	0.3489	0.08101 to 0.5697	**0.0121**
2N nuclei	γH2AX integral	0.2971	0.02340 to 0.5294	**0.0342**
	γH2AX MaxPixel	0.3699	0.1049 to 0.5858	**0.0076**
>2N nuclei	γH2AX integral	0.5128	0.2614 to 0.6991	**0.0003**
	γH2AX MaxPixel	0.4389	0.1702 to 0.6468	**0.0023**
Round nuclei	γH2AX integral	0.4567	0.2071 to 0.6504	**0.0008**
	γH2AX MaxPixel	0.3700	0.1051 to 0.5859	**0.0075**
Long nuclei	γH2AX integral	0.3982	0.1377 to 0.6072	**0.0038**
	γH2AX MaxPixel	0.5460	0.3183 to 0.7142	**< 0.0001**
Oval nuclei	γH2AX integral	0.4644	0.2165 to 0.6561	**0.0006**
	γH2AX MaxPixel	0.6152	0.4090 to 0.7617	**< 0.0001**
Senescent nuclei	γH2AX integral	0.6050	0.3952 to 0.7548	**< 0.0001**
	γH2AX MaxPixel	0.6004	0.3891 to 0.7516	**< 0.0001**

Parameters highlighted in bold text were considered statistically significant. All are Spearman's rho correlation. CI; 95% confidence interval.

4.6.4 Correlation of γH2AX Integral in All Nuclei with Blood Parameters

Many blood parameters have been analysed in the AIBL cohort, and the data for these are stored in the AIBL database. Correlation tests were carried out between each of these blood parameters and the γH2AX integral values in all nuclei. Table 4.9 summarises the r and p-values obtained for each of the parameters examined. p-values highlighted in bold text correlated with the γH2AX integral. Total protein positively correlated with γH2AX integral, but there was no correlation between the γH2AX integral and the rest of the blood parameters. In addition, correlation tests were also

performed between each of these blood parameters and the γH2AX MaxPixel values. There was no correlation of γH2AX MaxPixel with any blood parameters when data from all nuclei were analysed.

Table 4.9: Summary of the correlations tested between the γH2AX integral in buccal cells and blood measurements from the AIBL cohort

	Blood measurements		
Parameters	**Correlation (r)**	**95% confidence interval**	**p-value**
Homocysteine	0.0092	-0.1537–0.4472	0.9541
Serum folate	0.1617	-0.377–0.198	0.3125
Vitamin B12	-0.1295	-0.4205–0.1856	0.4195
Red cell folate	0.0005	-0.3151–0.3161	0.9975
Calcium	0.0422	-0.2770–0.3531	0.7985
Cholesterol	-0.0270	-0.1924–0.4290	0.4261
Triglycerides	-0.118	-0.3397–0.2911	0.8704
HDL	-0.1846	-0.4726–0.1391	0.2606
LDL	0.2371	-0.08484–0.5142	0.1461
Albumin	0.0305	-0.2879–0.3428	0.8539
Bilirubin	-0.2013	-0.4860–0.1220	0.2191
Urea	-0.0181	-0.3318–0.2992	0.9131
Creatinine	0.0134	-0.3035–0.3276	0.9354
eGFR	0.0427	-0.2766–0.3535	0.7964
Glucose	-0.2302	-0.5088–0.09207	0.1586
Total protein	**0.332**	**0.01837–0.5862**	**0.0389**
ALT	0.0088	-0.3077–0.3234	0.9579
AP	0.0101	-0.3065–0.3247	0.9514
GGT	0.0708	-0.2504–0.3779	0.6684
Ceruloplasmin	-0.2476	-0.5224–0.07374	0.1286
Fe	-0.2834	-0.5498–0.03533	0.0804
Transferrin	0.170	-0.1539–0.4608	0.3009
Trsat	-0.2688	-0.5387–0.05111	0.0980
Ferritin	-0.0201	-0.3336–0.2973	0.9031
Insulin	-0.1066	-0.4084–0.2163	0.5185
Testosterone	0.1546	-0.1692–0.4483	0.3472
LH	0.0245	-0.2933–0.3375	0.8822
FT4	0.1808	-0.1429–0.4696	0.2707
TSH	0.1425	-0.1812–0.4384	0.3868
FT3	0.1999	-0.1234–0.4849	0.2223
Cl	0.04746	-0.2722–0.3577	0.7742
AST	-0.1123	-0.4132–0.2108	0.4961

	Blood measurements		
Parameters	**Correlation (r)**	**95% confidence interval**	**p-value**
PCV	-0.0888	-0.3933–0.2334	0.5911
Mg	0.1919	-0.1317–0.4785	0.2418
RCC	-0.0009	-0.3165–0.3147	0.9952
MCV	-0.226	-0.5055–0.09647	0.1665
MCH	-0.2427	-0.5185–0.07897	0.1366
MCHC	-0.1327	-0.4303–0.1909	0.4206
RDW	-0.208	-0.4913–0.1152	0.2039
ESR	-0.1164	-0.4167–0.2068	0.4803
Platelets	-0.05805	-0.3669–0.2623	0.7255
MPV	-0.1251	-0.4239–0.1983	0.4481
WCC	-0.2584	-0.5307–0.06222	0.1122
Neutrophils	-0.2226	-0.5028–0.1001	0.1733
Lymphocytes	-0.1001	-0.4030–0.2225	0.5442
Monocytes	-0.2631	-0.5343–0.05722	0.1056
Eosinophils	-0.1277	-0.4261–0.1958	0.4386
Basophils	-0.2012	-0.4859–0.1222	0.2194

Parameters highlighted in bold text were considered statistically significant. Abbreviations: ALT, alanine aminotransferase; AP, alkaline phosphatase; AST, aspartate aminotransferase; Cl, chloride; eGFR, estimated glomerular filtration rate; ESR, erythrocyte sediment rate; Fe, iron; FT3, free thyroxine; FT4, free triiodothyronine; GGT, gamma-glutamyl transferase; HDL, high-density lipoprotein; LDL, low-density lipoprotein; LH, luteinising hormone; MCH, mean cell haematocrit; MCHC, mean corpuscular haemoglobin concentration; MCV, mean corpuscular volume; Mg, magnesium; MPV, mean platelet volume; PCV, packed cell volume; RCC, red blood cell count; RDW, red cell volume distribution; Trsat, transferrin saturation; TSH, thyroid stimulation hormone; WCC, white cell count.

4.6.5 Correlation of γH2AX Signals in Control, MCI and AD Nuclei with Blood Parameters

Correlation tests were carried out between each of these blood parameters in the AIBL database and the γH2AX integral or the γH2AX MaxPixel values in control, MCI and AD nuclei. Table 4.10 summarises the r and p-values obtained for γH2AX integral with each of the blood parameters. p-values highlighted in bold text indicates significant correlations. Correlation tests were also performed between each of these blood parameters and the γH2AX MaxPixel values in control, MCI and AD nuclei (Table 4.11). Albumin, AP, Testosterone and MCV positively correlated with γH2AX integral (Table 4.10) and γH2AX MaxPixel (Table 4.11) in MCI nuclei. In addition, MCH

positively correlated with γH2AX MaxPixel (Table 4.11) in MCI nuclei. Total protein, Transferrin, LH, FT4, MCH, MCHC correlated with γH2AX integral or γH2AX MaxPixel in control nuclei. There was no correlation of γH2AX integral or γH2AX MaxPixel with any blood parameters when data from AD nuclei were analysed (Table 4.10 and Table 4.11).

Table 4.10: Summary of the correlations tested between γH2AX integral scores in buccal cells and blood parameters in the control, MCI, and AD groups from the AIBL cohort

	Control	MCI	AD
Homocysteine	r= -0.070, p = 0.804	r= 0.514, p = 0.106	r = -0.175, p = 0.518
Serum folate	r = 0.193, p = 0.491	r= 0.256, p = 0.448	r = 0.134, p= 0.635
Vitamin B12	r = -0.041, p = 0.883	r = -0.293, p = 0.382	r = -0.243, p = 0.383
Red cell folate	r = 0.288, p = 0.299	r = 0.003, p = 0.993	r = -0.149, p = 0.595
Calcium	r = -0.041, p = 0.884	r = -0.433, p = 0.244	r = 0.065, p = 0.817
Cholesterol	r = 0.467, p = 0.079	r = -0.279, p = 0.467	r = -0.072, p = 0.799
Triglycerides	r = 0.114, p = 0.685	r = -0.516, p = 0.155	r = -0.033, p = 0.906
HDL	r = 0.194, p = 0.489	r = -0.266, p = 0.488	r = -0.292, p = 0.292
LDL	r = 0.465, p = 0.080	r = -0.016, p = 0.968	r = 0.292, p = 0.802
Albumin	r = 0.209, p = 0.454	**r = 0.724, p = 0.027**	r = -0.018, p = 0.951
Bilirubin	r = -0.286, p = 0.300	r = -0.173, p = 0.656	r = -0.187, p = 0.504
Urea	r = 0.500, p = 0.058	r = -0.181, p = 0.640	r = -0.326, p = 0.236
Creatinine	r = -0.276, p = 0.320	r = 0.407, p = 0.277	r = -0.038, p = 0.893
eGFR	r = 0.186, p = 0.508	r =-0.259, p = 0.502	r = 0.092, p = 0.745
Glucose	r = -0.457, p = 0.087	r = 0.112, p = 0.775	r = -0.175, p = 0.534
Total protein	**r = 0.557, p = 0.031**	r = 0.127, p = 0.745	r = 0.133, p = 0.636
ALT	r = -0.224, p = 0.421	r = 0.109, p = 0.779	r = -0.035, p = 0.901
AP	r = -0.189, p = 0.498	**r = 0.681, p = 0.043**	r = -0.046, p = 0.870
GGT	r = -0.108, p = 0.700	r = -0.087, p = 0.824	r = 0.025, p = 0.931
Ceruloplasmin	r = -0.133, p = 0.638	r = -0.149, p = 0.703	r = -0.294, p = 0.287
Fe	r= -0.298, p = 0.280	r= -0.385, p=0.306	r = -0.309, p = 0.261
Transferrin	**r = 0.628, p = 0.012**	r = -0.225, p = 0.560	r = -0.034, p = 0.904
Trsat	r = -0.344, p = 0.209	r = -0.294, p = 0.442	r = -0.282, p = 0.308
Ferritin	r = -0.252, p = 0.366	r = 0.025, p = 0.949	r = -0.100, p = 0.721
Insulin	r = -0.162, p = 0.565	r = 0.013, p= 0.975	r = 0.280, p = 0.310
Testosterone	r = -0.162, p = 0.565	**r = 0.684, p= 0.042**	r = 0.175, p = 0.532
LH	**r = 0.522, p = 0.046**	r = -0.235, p= 0.542	r = -0.177, p = 0.527
FT4	**r = 0.648, p = 0.009**	r = -0.078, p= 0.842	r = 0.155, p = 0.582
TSH	r = 0.228, p = 0.411	r = 0.056, p= 0.887	r = 0.146, p = 0.603
FT3	r = 0.431, p = 0.109	r = -0.014, p= 0.972	r = 0.115, p = 0.684
Cl	r = -0.173, p = 0.650	r = -0.269, p= 0.485	r = 0.173, p = 0.538
AST	r = -0.173, p = 0.536	r = 0.032, p= 0.935	r = -0.185, p = 0.508
PCV	r = -0.267, p = 0.335	r = 0.074, p= 0.850	r = -0.061, p = 0.829
Mg	r = -0.016, p = 0.954	r = 0.263, p= 0.495	r = 0.255, p = 0.359
RCC	r = -0.081, p = 0.773	r = 0.279, p= 0.467	r = -0.071, p = 0.799
MCV	r = -0.425, p = 0.115	**r = -0.678, p= 0.045**	r = -0.045, p = 0.871

MCH	**r = -0.658, p = 0.008**	r = -0.657, p= 0.055	r = 0.054, p = 0.848
MCHC	**r = -0.689, p = 0.005**	r = -0.479, p= 0.193	r = 0.307, p = 0.265
RDW	r = -0.197, p = 0.481	r = 0.213, p= 0.582	r = -0.378, p = 0.165
ESR	r = -0.157, p = 0.577	r = -0.209, p= 0.589	r = -0.186, p = 0.507
Platelets	r = 0.049, p = 0.861	r = 0.265, p= 0.490	r =-0.158, p = 0.576
MPV	r = 0.057, p = 0.844	r = -0.143, p= 0.713	r = -0.438, p = 0.103
WCC	r = -0.163, p = 0.563	r = 0.369, p= 0.327	r = -0.473, p = 0.075
Neutrophils	r = -0.292, p = 0.291	r = 0.588, p= 0.096	r = -0.496, p = 0.059
Lymphocytes	r = 0.412, p = 0.127	r = -0.356, p= 0.347	r = -0.206, p = 0.460
Monocytes	r = -0.420, p = 0.119	r = 0.091, p= 0.815	r = -0.335, p = 0.223
Eosinophils	r = 0.015, p = 0.958	r = -0.517, p= 0.154	r = -0.218, p = 0.435
Basophils	r = -0.171, p = 0.542	r = 0.408, p= 0.275	r = -0.331, p = 0.226

Parameters highlighted in bold text were considered statistically significant. See abbreviations in table 4.9.

Table 4.11: Summary of the correlations tested between γH2AX MaxPixel scores in buccal cells and blood parameters in the control, MCI, and AD groups from the AIBL cohort

	Control	MCI	AD
Homocysteine	r= 0.082, p=0.769	r= 0.487, p=0.129	r= -0.169, p=0.532
Serum folate	r = 0.107, p=0.705	r= 0.243, p=0.471	r = 0.157, p=0.576
Vitamin B12	r = -0.073, p=0.796	r = -0.250, p=0.457	r = -0.089, p=0.750
Red cell folate	r = 0.267, p=0.336	r = 0.077, p=0.843	r = 0.054, p=0.847
Calcium	r = -0.135, p=0.631	r = -0.397, p=0.289	r = 0.105, p=0.709
Cholesterol	r = 0.322, p=0.242	r = -0.422, p=0.257	r = -0.004, p=0.988
Triglycerides	r = 0.008, p=0.975	r = -0.626, p=0.071	r = 0.145, p=0.606
HDL	r = -0.001, p=0.9990	r = -0.258, p=0.503	r = -0.299, p=0.279
LDL	r = 0.379, p=0.279	r = -0.165, p=0.672	r = 0.102, p=0.717
Albumin	r = 0.112, p=0.692	**r = 0.704, p=0.034**	r = 0.046, p=0.872
Bilirubin	r = -0.097, p=0.732	r = -0.174, p=0.655	r = -0.170, p=0.543
Urea	r = 0.513, p=0.050	r = -0.169, p=0.664	r = -0.374, p=0.1701
Creatinine	r = -0.186, p=0.507	r = 0.309, p=0.418	r = -0.132, p=0.6392
eGFR	r = 0.259, p=0.3511	r =-0.020, p=0.959	r = 0.205, p=0.462
Glucose	r = -0.359, p=0.1883	r = 0.347, p=0.360	r = -0.083, p=0.767
Total protein	r = 0.357, p=0.192	r = -0.048, p=0.903	r = 0.235, p=0.398
ALT	r = -0.295, p=0.2863	r = -0.025, p=0.949	r = 0.094, p=0.738
AP	r = -0.126, p=0.6545	**r = 0.696, p=0.038**	r = 0.090, p=0.749
GGT	r = -0.171, p=0.542	r = -0.066, p=0.865	r = 0.145, p=0.605
Ceruloplasmin	r = -0.187, p=0.504	r = -0.264, p=0.4925	r = 0.201, p=0.4725
Fe	r= -0.302, p=0.275	r= -0.564, p=0.114	r= -0.233, p=0.403
Transferrin	**r = 0.550, p=0.034**	r = -0.101, p=0.795	r = 0.027, p=0.924
Trsat	r = -0.354, p=0.195	r = -0.485, p=0.186	r = -0.252, p=0.364
Ferritin	r = -0.159, p=0.569	r = -0.150, p=0.699	r = -0.066, p=0.816
Insulin	r = -0.188, p=0.500	r = -0.091, p=0.815	r = 0.335, p=0.222
Testosterone	r = -0.024, p=0.932	r = 0.789, p=0.012	r = 0.152, p=0.589
LH	r = 0.280, p=0.311	r = -0.269, p=0.485	r = -0.162, p=0.563
FT4	**r = 0.604, p=0.017**	r = -0.107, p=0.783	r = 0.275, p=0.322
TSH	r = -0.099, p=0.724	r = -0.131, p=0.7368	r = 0.085, p=0.763
FT3	**r = 0.557, p=0.0308**	r = 0.000, p=0.999	r = 0.151, p=0.589
Cl	r = -0.197, p=0.479	r = -0.313, p=0.412	r = 0.034, p=0.905
AST	r = -0.167, p=0.553	r = -0.020, p=0.959	r = -0.092, p=0.745
PCV	r = -0.249, p=0.372	r = -0.056, p=0.885	r = -0.059, p=0.834
Mg	r = -0.284, p=0.305	r = 0.212, p=0.584	r = 0.248, p=0.372
RCC	r = -0.027, p=0.925	r = 0.200, p=0.605	r = -0.095, p=0.734
MCV	r = -0.509, p=0.053	**r = -0.772, p= 0.015**	r = 0.012, p=0.968
MCH	**r = -0.6469, p= 0.0091**	**r = -0.747, p= 0.020**	r = 0.131, p= 0.641
MCHC	r = -0.482, p= 0.069	r = 0.519, p=0.1517	r = 0.365, p=0.1811

	Control	MCI	AD
RDW	r = -0.334, p=0.224	r = 0.375, p=0.319	r = -0.448, p=0.093
ESR	r = -0.211, p=0.449	r = -0.096, p=0.805	r = -0.171, p= 0.541
Platelets	r =-0.100, p=0.721	r =0.332, p=0.382	r =-0.175, p=0.532
MPV	r =0.111, p=0.693	r =-0.039, p=0.9216	r =-0.494, p=0.0613
WCC	r =-0.282, p=0.309	r =0.418, p=0.263	r =-0.442, p=0.099
Neutrophils	r =-0.334, p=0.224	r =0.632, p=0.068	r =-0.439, p=0.101
Lymphocytes	r =0.227, p=0.415	r =-0.308, p=0.419	r =-0.212, p=0.449
Monocytes	r =-0.479, p=0.071	r =-0.016, p=0.967	r =-0.349, p=0.201
Eosinophils	r =0.029, p=0.918	r =-0.470, p=0.202	r =-0.243, p=0.382
Basophils	r =-0.196, p=0.482	r =0.371, p=0.326	r =-0.297, p= 2891

Parameters highlighted in bold text were considered statistically significant. See abbreviations in Table 4.9.

4.7 Discussion

The objective of this study was to investigate whether buccal cells from MCI and AD patients have higher levels of endogenous γH2AX (a biomarker of double strand DNA breaks) compared with healthy controls, with the ultimate aim of testing whether the buccal cell γH2AX assay might be useful as a diagnostic test for those with cognitive impairment and or AD. The γH2AX assay offers an excellent opportunity to robustly measure the levels of DNA DSBs and cellular response in individuals or populations and test its suitability for clinical purposes (Shukkur et al. 2006, Bader Lange et al. 2010, Delledonne et al. 2009). The LSC method was used to quantify endogenous γH2AX in buccal cells from individuals who met the clinical criteria for MCI or AD and in healthy controls. The results of this study showed increased levels of γH2AX in the buccal cells of patients with AD compared to those in cells from MCI patients or healthy controls, and there was a concomitant increase with a linear trend from the control group through MCI to the AD group. This result was further supported by the significantly increased negative correlation between γH2AX signals and MMSE scores when the analysis included all subjects. The LSC protocol developed here simultaneously quantifies different γH2AX parameters (integral, MaxPixel, area, foci/nucleus) in cells with different nuclear DNA content (ploidy status) as well cells with different nuclear shapes, based on their area, perimeter, diameter and circularity. Nuclear circularity (irregular nuclear shape) was increased significantly in AD cells compared to control cells and there was a concomitant increase with a linear trend from controls through MCI to AD. A significant positive correlation was also observed between nuclear circularity and γH2AX signals in the different types of nuclei analysed. The results of this study demonstrate that buccal cells exhibit increased levels of endogenous γH2AX in AD cells relative to those from MCI patients and healthy

controls, and suggest the possibility of using γH2AX as a marker for determining those individuals with MCI that may be progressing to AD.

At present the analysis of Aβ (1-42), total tau and phospho-tau-181 in CSF allows reliable, sensitive and specific diagnosis of AD, but the collection of CSF is an invasive procedure with potential random variation in AD specific biomarkers measurements (Fagan et al. 2007, Ingber et al. 2016, Zetterberg 2015). Thus, there is a clear need to search for inexpensive and minimally invasive surrogate markers to diagnose and monitor AD progression. The use of surrogate cells, and particularly exfoliated buccal cells, is of particular interest since buccal cell collection is reliable, fast, relatively simple, cheap, minimally invasive and painless. Since the both the human nervous system and buccal cells are of ectodermal origin, the regenerative potential of the brain, which has been found to be altered in AD, may be mirrored in the buccal mucosa. Studying the buccal mucosa cells from healthy individuals revealed decreased nuclear diameter and cell diameter with increasing age (Donald et al. 2013). Another study showed a decrease in the thickness of the epidermis and underlying cell layer with increasing age (Williams, Cruchley 1994). It is possible that the lack of regenerative potential of buccal cells from MCI and AD patients may be a consequence of accelerated ageing. A previous study has investigated the formation of micronuclei (a cytogenetic marker of either chromosome segregation or breakage) in buccal mucosa cells. An increased MN frequency was observed in patients with AD compared to age- and gender-matched controls (Thomas et al. 2007). The same study also reported an abnormal cytome profile characterised by a lower frequency of basal cells, condensed chromatin and karyorrhectic cells in AD patients, suggesting reduced regenerative capacity in buccal cells from AD patients. Another study showed a significant 1.5-fold increase in trisomy 21 and a significant 1.2-fold increase in trisomy 17 in buccal cells of

AD patients compared to matched controls (Thomas, Fenech 2008), providing further evidence of abnormalities in buccal cells in AD patients.

LSC is a microscope-based quantitative image analysis technique that combines the advantages of flow cytometry and image analysis (Kamentsky, Kamentsky 1991, Henriksen et al. 2011). LSC allows the quantifiable measurement of γH2AX signals in large numbers of cells per sample (thousands of cells per individual) with the same LSC settings, making it a useful method to assess subtle cellular and nuclear changes between individuals. The γH2AX signals (integral, MaxPixel, area, foci/nucleus) were measured in nuclei from the control, MCI, and AD groups. The results from all nuclei demonstrated that the γH2AX signal was significantly higher in AD cells compared to cells from the control group, and also significantly increased in AD cells compared to cells from MCI patients. LSC has previously been shown to be a useful tool that simultaneously measures cellular DNA content for the evaluation of cell cycle stage and γH2AX signals after DNA damage (Zhao et al. 2009, Tanaka et al. 2007, Huang et al. 2004). Therefore, γH2AX signals in nuclei with different DNA contents (measurement of the nuclear DAPI integral allows classification of nuclei as <2N, 2N, and >2N) were measured using the LSC protocol. The results from this study demonstrated a significant increase in the γH2AX signal in 2N nuclei from AD patients compared to those from the control and MCI groups. A number of studies have been conducted to assess the association between astrocyte degeneration and DNA damage in AD by investigating the γH2AX signals in astrocytes from the hippocampal region (Myung et al. 2008, Silva et al. 2014). The results from these studies demonstrated strong γH2AX staining in the nuclei of cells from AD patients compared to those from healthy controls. To the best of the researcher's understanding, there are no earlier reports investigating the levels of γH2AX in buccal cells and their ability to distinguish those individuals with MCI and

AD from those of control patients. Since the level of DNA DSBs in buccal cells, as marked by γH2AX immunostaining, has not been previously used to investigate the pathogenesis of AD, the findings from this study support the previous observation of increased γH2AX signals in nuclei of astrocytes from AD patients relative to those of healthy controls (Myung et al. 2008, Silva et al. 2014). While the <2N and >2N nuclei showed a significant increase in all γH2AX parameters in AD buccal cells compared to control cells, no statistical significance was observed for the γH2AX area in 2N nuclei. In the present study, a statistically significant association of γH2AX signals (integral, MaxPixel, area, foci/nucleus) was not observed in MCI cells compared to control cells; however, there was an increasing linear trend in the γH2AX MaxPixel values observed in control cells, through MCI cells to AD cells, suggesting that buccal cells from MCI patients may be more susceptible to DNA damage than those from healthy controls. There are no reports investigating γH2AX in buccal cells from MCI patients compared to those from healthy controls; however, the insights from previous studies carried out in lymphocytes are in line with the observations of the current study, and demonstrate a significant increase in oxidative DNA damage (oxidised DNA bases) in lymphocytes from an MCI group compared with a control group (Migliore et al. 2005). It is of interest to explore whether MaxPixel γH2AX in AD nuclei represent some unique type of DNA damage (e.g. a site of clustered DSBs).

ROC curve analysis was carried out to assess the diagnostic accuracy of γH2AX assay in identifying individuals with AD from controls. ROC curve for LSC scored γH2AX MaxPixel yielded the area under the ROC curve value of 0.7794 with 75% sensitivity and 70 % specificity for the AD ($p=0.0062$) group suggesting that measurement of γH2AX MaxPixel in the buccal cell might be useful in discriminating AD and control. Although the good sensitivity and specificity achieved in this study are promising for

the value of γH2AX assay in identifying AD from control, given the relatively low number of participants tested within each group, and the lack of defined γH2AX thresholds for determining of test positivity, we cannot recommend its routine use in clinical practice. Therefore, it is important to clearly demonstrate its accuracy involving larger numbers of participants tested within each group and standardize the γH2AX assay by validating the stringent cut-off point of test positivity prior to it being widely used routinely for differentiating AD from non-AD and from control.

The buccal mucosa is known to consist of heterogenous cell types that may have discrete functions within this tissue. Different nuclear shape morphology has been used to distinguish nuclear abnormalities and has been used in patients with oral squamous carcinoma to assess radiosensitivity (Torres-Bugarin et al. 2014, Raj, Mahajan 2011). Therefore, the current study aimed to classify buccal cells based on their nuclear shapes using the features available with LSC. The results from this study demonstrated for the first time that the γH2AX signal was significantly higher in the round, long and oval nuclei of cells from AD patients compared to those from the control group, and also significantly increased in AD cells compared to those from patients with MCI. While the oval nuclei from AD cells showed the most significant increase in γH2AX signal (integral, MaxPixel and foci/nucleus) compared to those from control and MCI cells, round and long nuclei had significantly increased γH2AX MaxPixel values and numbers of γH2AX foci/nucleus, but this was not the case for the γH2AX integral value. Overall, regardless of the different nuclei with different nuclear shapes analysed, there was a significant increase of γH2AX signals in AD cells compared to control and MCI cells. For a better understanding of the DNA damage response in buccal cells with different nuclear shapes, it will, therefore, be valuable to combine γH2AX assays, other cellular markers of apoptosis and cellular signaling using the LSC protocol.

In this study, irregular nuclear shapes (circularity) were measured using the circularity parameter of LSC in different types of nuclei (e.g., all nuclei, <2N nuclei, 2N nuclei, > 2N nuclei). A higher circular value indicates a more irregular nuclear shape. The results showed a significantly higher circularity in all nuclei of AD cells compared to control cells, as well as in AD cells compared to MCI cells. Nuclear circularity was also significantly higher in AD cells compared to control cells as well as in AD cells compared to MCI cells when analysed for >2N nuclei and senescent nuclei. The higher circularity in AD cells compared to control and MCI cells might be due partly to the accumulation of DNA damage leading to morphometric and cytometric alterations in the buccal mucosa cells of AD patients. Previously, the morphological and cytometric parameters of buccal cells have been assessed using microscopy and Image J analysis, respectively, following Papanicolaou staining (de Oliveira et al. 2008). The results from this study showed a significant decrease in the number of intermediate buccal cells in the AD group compared to the control group (de Oliveira et al. 2008). Another study reported an increase in trisomy 21 and trisomy 17 in buccal cells in AD cases compared to their respective controls (Thomas, Fenech 2008). In addition, evidence of increased levels of DNA damage, indicated by the formation of micronuclei (a biomarker of chromosome missegregation) has been previously detected in buccal cells from AD patients and Down Syndrome cases who have a high risk of developing AD (Thomas et al. 2007, Thomas et al. 2008). In this study, the γH2AX integral and MaxPixel values were positively correlated with nuclear circularity in the different types of buccal cell nuclei analysed, which may reflect the fact that DNA damage in these cells is associated with an irregular nuclear shape. It is possible that the increased DNA damage in those irregularly shaped nuclei is associated with altered nuclear lamina structure. The nuclear lamina is a filamentous structure under the inner nuclear membrane composed of A-type

and B-type lamins (Hozak et al. 1995, Dechat et al. 2008). Recent studies show that the deficient A-type lamin is associated with altered structural nuclear proteins with a variety of human diseases, including severe premature aging syndromes (Broers et al. 2006). A-type-lamin-deficient cells have been associated with impaired DNA repair capacity and maintaining telomere localization, structure, length and function (Gonzalo 2014, Gonzalez-Suarez et al. 2009). Moreover, loss of A-type-lamin-leads to localization of telomeres away from the nuclear membrane towards the center of the nucleus (Gonzalez-Suarez et al. 2009). The colocalization of γH2AX can easily visualize dysfunctional telomeres with a telomere DNA probe (Fumagalli et al. 2012, Hewitt et al. 2012, Smogorzewska et al. 2002). A previous report in human buccal cells of AD patients showed significantly shortened telomeres in an older AD group in comparison with older controls (Thomas, O'Callaghan & Fenech 2008). Therefore, it is plausible that the positive correlation between nuclear circularity and γH2AX in buccal cells of AD patients observed in this study may be linked with deficient nuclear lamin contributing to telomere dysfunction. Future studies should explore whether the γH2AX signals in buccal cells of AD patients are mostly in the nuclear periphery or aggregated centrally and associated with dysfunctional telomeres which may be due to deficient A-type lamin coupled with increased nuclear circularity. It is possible that irregular nuclear shape caused by a defect in lamines lead to telomere dysfunction and/or shortening. Taken together, altered nuclear morphology, cellular structure and increased levels of DNA damage associated with dysfunctional telomeres in buccal cells may contribute to the irregular nuclear shape observed in buccal cells of AD patients. A further study of changes in nuclear circularity coupled with multiple DNA damage markers (e.g., γH2AX, 8HOdG) associated with telomere dysfunction and AD-specific markers (e.g., putative tau, Aβ) in buccal cells from a large patient cohort will better

assess the likelihood of discriminating AD and MCI patients from healthy controls using these tests.

Cellular senescence is elicited in damaged cells and characterised by the presence of γH2AX, and senescence-associated β-galactosidase (SA- β -gal) activity, detectable by immunocytochemistry (Dimri et al. 1995, Sikora et al. 2011). Previous studies have shown increased number of senescent nuclei during ageing and in age-related diseases (Dimri et al. 1995, Sikora et al. 2011). It is accepted that older animals exhibit more senescence cell than younger animals as demonstrated by increased p16 (INK4a), senescence associated β-galactosidase activity, and γH2AX positive signals (Fumagalli et al. 2012, Wang et al. 2009, Berkenkamp et al. 2014). The morphological features of senescent nuclei in cultured fibroblasts after methotrexate (Mtx) treatment have been assessed using the features available in the iCyteR software for LSC (Zhao, Darzynkiewicz 2013, Zhao et al. 2010). In this study, senescent nuclei were isolated based on the criteria of decreased levels of DAPI staining (MaxPixel staining) paralleled by increases in nuclear size (area) and the simultaneous expression of senescence markers (e.g., the p21WAF1, p16INK4a or p27KIP1 cyclin kinase inhibitors), and demonstrating that senescent nuclei are flattened and larger in size. To date, the morphological features of senescent nuclei in buccal cells have not been assessed using the features available in LSC. In this study, senescent nuclei were identified by plotting the ratio of MaxPixel intensity of DAPI fluorescence per nucleus to nuclear area versus the nuclear size (area). A significant increase in the γH2AX signal was observed in senescent nuclei of AD cells compared to control and MCI cells for all individual γH2AX parameters measured by LSC, suggesting that accumulation of DNA DSBs may contribute to cellular senescence and impaired repairing capacity of senescent nuclei may ultimately contribute to the risk of developing AD. Although previous studies in

cultured fibroblasts have characterised the morphological features of senescent nuclei using immunocytochemical analysis of the expression of additional senescent markers, such as the p21WAF1, p16INK4a or p27KIP1 cyclin kinase inhibitors, this study did not confirm this, but rather attempted for the first time to identify senescent nuclei of control, MCI and AD cells by their morphometric features alone. It is important to note that senescent cell showed the strongest negative correlation for γH2AX integral and γH2AX MaxPixel in relation to MMSE scores. While investigating the morphological features of senescent buccal cells is important, it is also important for future research to simultaneously measure the expression of senescence markers in conjunction with DNA damage markers (e.g., γH2AX) and AD-specific markers (e.g., aβ1-42, total tau, and phosphorylated-tau) in buccal cells in order to discriminate AD and MCI patients from healthy controls.

In the present study, from all of the blood parameters examined only total protein showed a positive correlation with buccal cell γH2AX signals when all samples were analysed together. Correlations between blood parameters and buccal cell γH2AX signals in the control, MCI and AD groups were further assessed in three separate tests. Although a significant correlation between buccal cell γH2AX signals and several blood parameters (e.g., albumin, total protein, transferrin, FT4, FT3, MCH, MCV) in control and MCI group was observed, in the AD group, no blood parameters showed a significant correlation with buccal cell γH2AX signals. The negative correlation with MCV and MCH are important because these are biomarkers of anemia, which was previously shown to be a risk factor for MCI and AD in AIBL (Faux et al. 2014). In this study, the positive correlation between transferrin and γH2AX signals suggests that the plasma transferrin levels may have a role in increasing γH2AX signals in AD. However, previous study showed that plasma transferrin levels decline with age in AD. These

results strongly suggest that the development of pathological features of AD is not restricted to the brain, but is associated with multiple metabolic changes occurring in peripheral cells (Francois et al. 2014b).

Senescent cells are characterized by the presence of γH2AX, including the activity of SA-β-gal, accumulate in tissues of aged animals and are thought to increase during aging and age-related diseases (Dimri et al. 1995, Sikora et al. 2011). In this study, the senescent nuclei were identified based on morphometric features of nuclei., showing a significant increase in the γH2AX signal in senescent nuclei of AD cells compared to control and MCI cells, suggesting an added value of the evaluation of the different cellular biomarkers for identifying individuals at risk of developing AD. To better understand these results, the experiment should be performed to confirm that the senescent nuclei we identified have increased SA-β-gal activity. Further improvements of LSC protocol in identifying and scoring γH2AX in senescent nuclei are required before its use can be recommended without reservation. It is important to investigate whether sample storage condition, sample processing, slide preparation, use of γH2AX staining techniques and differences in the scoring criteria have an impact on the variable baseline γH2AX level observed within individuals.

Evidence suggests that when the AD diagnosis is made the pathological features of AD are already well advanced. Early diagnosis of AD allows immediate access to medications and medical attention. Therefore, it is important to identify individuals during the pre-dementia phase where treatments may be taken in advance. The early treatments of AD include (i) prompt access to currently available medications for AD (ii) initiation of health management involving management of person depression and irritability (iii) remembering patient to take medications such as for diabetes, heart

disease or high blood pressure (iv) lowering elevated levels of raised blood homocysteine levels by applying high dose B-vitamins or antioxidant N-acetyl cysteine. These early treatments may play a significant role possibly in inhibiting or delaying the progression of the AD pathology.

To date, no studies have assessed the presence of γH2AX in the buccal cells of AD patients relative to control and MCI patients, and the available literature on the use γH2AX as a DNA DSB marker in ageing populations is not yet sufficient to understand the association between DNA DSBs and AD. The current study is the first to demonstrate that buccal cells from AD patients exhibit elevated levels of DNA DSBs and irregular nuclear shapes relative to control and MCI cells, and support the potential use of γH2AX as a marker to identify individuals with an increased risk of developing MCI or AD. Identification of reliable biomarkers in non-invasive samples will be useful for early diagnosis and treatment of AD, which may prevent the onset of irreversible AD and reduce the overall economic and human cost of the disease. Buccal cells offer a sample source that is easily obtained in a relatively non-invasive manner. The LSC-based γH2AX protocol provides a practical and inexpensive tool for assessing DNA DSBs in buccal cells of control, MCI and AD patients. The levels of γH2AX in buccal cells quantified by LSC may have prognostic implications to understand the pathogenesis of AD better, and offer the opportunity to monitor disease progression and the bioefficacy of potential preventative measure (i.e., diet, lifestyle, and therapeutics). Moreover, LSC provides identification and quantification of buccal cell sub-types based on cellular features that were previously not measurable (e.g., nuclear shape, DNA content, nucleus size, nucleus MaxPixel value). Scoring of buccal cell nuclear parameters in conjunction with multiple DNA damage parameters and AD-specific markers will be useful to establish a potential biomarker panel with high specificity for

AD patients. Thus, the combination of cytome and proteome approaches to a single sampling of buccal cells may significantly increase the sensitivity and/or specificity for AD diagnosis, which will have relevance not only for future clinical practice but also for the reliable prediction of those individuals who are likely to develop MCI and AD and also to monitor the bio-efficacy of preventative strategy. The buccal cell γH2AX assay may provide a useful method for AD and MCI diagnosis, particularly when sample collection must occur remotely and/or in disadvantaged communities unable to attend more expensive prognostic or diagnostic tests. In this study, a small number of populations were analysed, and there was lack of replication. Therefore, comprehensive studies using large prospective cohorts are warranted in order to validate the suitability of the LSC-based buccal cell γH2AX assay, particularly to identify those in the early stages of AD.

4.8 Acknowledgement

I thank Tori Nguyen, Maryam Hor for assisting with the preparation of microscope slides. I thank all the participants who took part in this study and the clinicians who referred participants. The Australian Imaging, Biomarker & Lifestyle Flagship Study of Ageing (AIBL) study is a collaboration between CSIRO Australia, Edith Cowan University (Perth, WA, Australia), The Florey Institute of Neuroscience and Mental Health (Melbourne, Victoria, Australia), National Ageing Research Institute and Austin Health (Parkville, Vic, Australi a). It also involves support from CogState Ltd. (Melbourne, Vic, Australia), Hollywood Private Hospital and Sir Charles Gairdner Hospital (Nedlands, WA, Australia). The AIBL study received funding support from the Science and Industry Endowment Fund, National Health and Medical Research Council (NHMRC) and Dementia Collaborative Research Centres (DCRC), Alzheimer's Australia and the McCusker Alzheimer's Research Foundation, as well as Industry, including Pfizer, Merck, Janssen and GE Healthcare. Thanks to University of Adelaide registered editing service (Elite Editing) to help to edit this chapter. Financial support from the CSIRO's Preventative Health Flagship is gratefully acknowledged. WRL received a grant from The JO & JR Wicking Trust, which is managed by ANZ Trustees (Australia). The authors thank all the AIBL investigators (https://aibl.csiro.au/).

Chapter 5: Elevated γH2AX Level in Peripheral Blood Lymphocytes Identifies Alzheimer's Disease in the South Australian Neurodegeneration, Nutrition and DNA Damage (SAND) Study of Aging

Abstract

The initial cellular response to repair DNA double-stranded breaks (DSBs) is the phosphorylation of H2AX (a member of histone H2A family) to from γH2AX. Although increased level of γH2AX has been reported in neuronal nuclei of Alzheimer's disease (AD) patients, the understanding of γH2AX responses in lymphocytes of individuals with Mild cognitive impairment (MCI) and AD remain unexplored. In the current study, endogenous γH2AX level was measured in lymphocytes nuclei from MCI (n=18), or AD (n=20) patients and in healthy controls (n=40) using laser scanning cytometry (LSC) and visual scoring. The endogenous γH2AX levels were significantly elevated in nuclei of AD group compared to MCI and control group, and there was a concomitant increase with a significant trend for an increase in γH2AX from the control group through MCI to the AD group. The visually scored % cell containing overlapping γH2AX foci displayed the best area under the Receiver Operation Characteristic (ROC) curve value of 0.9081 with 85 % sensitivity and 92 % specificity for the AD (p=<0001) group. This result was further supported by the significant negative correlation between the γH2AX signals and MMSE score when the analysis included all subjects. Plasma homocysteine, creatinine, and chitinase-3-like protein 1 (CHI3L1) were positively correlated with lymphocyte γH2AX signals, while glomerular filtration rate (GFR) was negatively correlated. Finally, there was a blunted γH2AX response in the MCI and AD group compared to control group following X-ray radiation exposure. The results indicated that γH2AX level in lymphocytes nuclei could be used as a potential diagnostic in identifying individuals with increased risk of developing MCI and AD.

5.1 Introduction

Alzheimer's disease (AD) is a neurodegenerative disease that is characterised clinically by abnormal behavioural and mental effects that include loss of memory, tremors, and absent-mindedness, and is the most common cause of dementia (Alzheimer's Association, Thies & Bleiler 2011, Fernandez et al. 2010, Burns, Byrne & Maurer 2002). The brains of patients with AD are histopathologically characterised by two hallmark lesions—deposition of amyloid-β (Aβ) plaques and the development of neurofibrillary tangles composed of hyperphosphorylated protein tau (Ittner, Gotz 2011). Currently, AD has reached a global prevalence of approximately 24.3 million, with 4.6 million new cases being diagnosed worldwide each year (Smith 2008, Ferri et al. 2005). The increasing rate of AD is expected to reach a level of one new case every 33 seconds by 2050 (Alzheimer's Association, Thies & Bleiler 2011). Furthermore, this increase in the prevalence of AD not only reduces the quality of life, health and wellbeing of those affected but also causes a significant financial burden at both the social and economic levels (Sloane et al. 2002).

The onset of AD involves the accumulation of increasingly severe cognitive deficits, progressing from mild cognitive impairment (MCI) to AD. MCI is characterised by deterioration in cognitive ability that; however, does not affect the individual's ability to carry out their activities of daily living. Individuals affected by MCI have a higher risk of developing AD with advancing age, with estimates that vary between 14 and 18 per cent of those over 70 years of age suffering from this condition (Grundman et al. 2004, Petersen et al. 2009). Currently, the ability to detect the early stages of AD and differentiate the stages of AD progression to guide the choice of therapy is limited. The Mini Mental State Examination (MMSE) is a validated research-based set of 30

questions considering memory loss, cognitive decline, visuospatial and language impairment that is currently used as a standard tool for the clinical diagnosis of AD (Tombaugh, McIntyre 1992, Mitchell 2009). However, this test lacks accuracy for the diagnosis of AD in living subjects, and diagnostic confirmation can only be achieved post mortem by the examination of the senile plaques and neurofibrillary tangles in brain tissue from the patient (Armstrong 2006). Therefore, identification of other biomarkers in easily accessible tissue that can aid the diagnosis of AD may be useful to identify individuals at an increased risk of AD while they are still in the early stages of illness.

The identification of biomarkers that can be used for the early detection of AD is challenging for the scientific fraternity. Most methods for the investigation of AD are too invasive and expensive and are unable to identify biomarkers (Thambisetty, Lovestone 2010, Hampel, Prvulovic 2012, Blennow, Zetterberg 2009). Successful population-based screening requires readily available, minimally invasive and inexpensive samples for a robust, low-cost diagnostic test that has high specificity and sensitivity. To detect amyloid-β protein aggregation forming senile plaques in specific regions of the brain, the Pittsburgh B (PiB) compound was used and found to be able to detect these plaques readily. However, some study reports showed that useful imaging with PiB depends on the accumulation of large plaques (Cairns et al. 2009, Leinonen et al. 2008). Although the formation of plaques containing Aβ peptides is a hallmark of AD (Ittner, Gotz 2011), these have also previously been detected in non-neural tissues such as blood, saliva, skin and other peripheral tissues (Gasparini et al. 1998, Joachim, Mori & Selkoe 1989, Soininen et al. 1992, Goldstein et al. 2003, Citron et al. 1994), suggesting that abnormalities in Aβ processing may be exhibited in peripheral tissues other than the brain. Several studies have reported abnormalities in platelets, red blood

cells, and white blood cells due to AD pathology (Tang et al. 2006, Janoshazi et al. 2006, Hye et al. 2005).

Previous studies have shown loss of genome integrity due to increased DNA damage levels in neurodegenerative disease (Migliore et al. 2011, Thomas et al. 2007, Migliore et al. 2005, Wang, Markesbery & Lovell 2006, Wang et al. 2005). Furthermore, several studies have reported increased levels of DNA damage in conjunction with elevated oxidative stress and a lack of DNA repair capacity in the peripheral lymphocytes of AD individuals compared to age-matched controls (Migliore et al. 2005, Migliore et al. 1999). DNA double strand breaks (DSBs) are considered to be the most lethal form of DNA lesions, which if left unrepaired or misrepaired can alter the integrity of the genome and affect the survival of the organism (Dugle, Gillespie & Chapman 1976, Olive 1998). Phosphorylation of the C-terminal tails of the H2AX histones in the nucleosomes located in the vicinity of the break (Rogakou et al. 1998, Savic et al. 2009) is one of the earliest known responses to DNA DSB formation in cells. The nucleosome complex comprises DNA wrapped around eight histone proteins, two from each of the four core histone families (H4, H3, H2B, H2A), and is essential for normal genome function in terms of normal regulation of gene expression, DNA repair, maintenance of DNA methylation and accurate replication (Rogakou et al. 1999, Goll, Bestor 2002, Mendez-Acuna et al. 2010). Induction of DSBs in live cells triggers the phosphorylation of Ser139 contained in the SQ motif near the carboxy-terminus of H2AX, resulting in the formation of phosphorylated H2AX, termed γH2AX (Redon et al. 2002, Kinner et al. 2008). While H2AX is distributed uniformly throughout chromatin, only H2AX molecules located in close vicinity to DSBs become phosphorylated to form γH2AX (Rogakou et al. 1998, Savic et al. 2009, Rogakou et al. 1999). H2AX is phosphorylated by the ATM protein following ionising radiation (IR)-induced DNA damage (Rogakou

et al. 1998, Redon et al. 2002, Burma et al. 2001, Olive, Banath 2004, Fernandez-Capetillo et al. 2004).

The association of astrocyte degeneration and DNA damage with Alzheimer's disease has been elucidated by investigating the γH2AX signal in astrocytes from the hippocampal region (known to be the most vulnerable region of the brain in AD). γH2AX staining has been shown to be stronger in the nuclei of astrocytes from AD patients compared to healthy controls, as determined by immunocytochemical techniques (Myung et al. 2008). This suggests that the DSBs measured by γH2AX positive immunostaining in the nuclei of astrocytes may be associated with impaired neuronal function and contribute to the pathogenesis of AD (Myung et al. 2008). Additionally, a recent study reported higher γH2AX levels in hippocampal tissue of individuals with both AD pathology and clinical dementia than was seen in a normal ageing group (Silva et al. 2014).

Growing evidence shows that high blood pressure, midlife obesity, stroke and Type 2 diabetes are associated with the risk of developing AD (Soto-Gordoa et al. 2015, Kivipelto et al. 2006, Li, Holscher 2007, Peters et al. 2008, Sery et al. 2014). Few studies have investigated endogenous γH2AX levels in normal ageing and accelerated ageing disorders. H2AX phosphorylation and the DNA damage response (DDR) have been implicated in diseases of accelerated ageing (e.g., Werner syndrome, AD, obesity, diabetes, sleep apnea, prostate cancer, cataract disease, hypertension and Hutchinson–Gilford progeria syndrome) in recent studies (Myung et al. 2008, Sedelnikova et al. 2008, Schurman et al. 2012), suggesting that lack of DNA integrity due to accumulating DNA damage progressively increases with age and may contribute to, or be caused by, these accelerated ageing disorders. Overall, these studies show that accumulation of

γH2AX foci is increased in individuals with greater morbidity and pathological ageing. This led to the hypothesis that individuals with MCI and AD may exhibit increased levels of γH2AX compared to healthy controls.

Identification of susceptibility to DSBs of lymphocytes after exposure to IR may provide valuable information about the risk of developing diseases. Previous study has reported that lymphocytes from bladder cancer patients are highly susceptible to DSBs (i.e. measured using γH2AX assay) than control (Fernandez et al. 2013). Another study on mouse model has reported low induction of DNA damage responses (e.g. γH2AX foci and ATM protein levels) in old mice than young and mature mice suggesting inefficient DNA damage recognition or defect in recruiting and functioning of DNA repair machineries (Kovalchuk et al. 2014). In a study of obesity in children, the fold increase of γH2AX induction was higher in lymphocytes of obese subjects than in overweight subjects after treating the lymphocytes with radiomimetic mutagen bleomycin (Scarpato et al. 2011). We hypothesize that lymphocytes from MCI, and AD groups exhibit higher levels of endogenous γH2AX. We also hypothesize that lymphocytes from MCI, and AD groups are not able to respond to radiation-induced damage as efficiently as the control group.

To test these hypotheses, (i) the endogenous levels of γH2AX in lymphocytes from participants in the South Australian Neurodegeneration Nutrition and DNA Damage study (SAND) were assessed to determine whether they could be used for identifying those at risk of developing AD and (ii) radiation-induced γH2AX levels in control, MCI and AD groups were assessed. To the researcher's knowledge, this is the first study that correlates H2AX phosphorylation with the risk of developing AD in a single cohort study. This was done by (i) visually scoring of γH2AX foci in lymphocytes from

control, MCI and AD patients, and (ii) developing and utilising an automated laser scanning cytometry (LSC) γH2AX protocol in which multiple γH2AX parameters (area, integral, MaxPixel), as well as the ploidy, was measured in thousands of lymphocytes from control, MCI and AD patients to identify whether increased levels of γH2AX were associated with those who were diagnosed with MCI or AD as compared to healthy age- and - gender matched controls.

5.2 Materials and Methods

5.2.1 Human Ethics and Clinical Assessment of the Participants

This cross-sectional study was approved by the institutional ethics committees of CSIRO Food and Nutrition, Adelaide University, and the Calvary Hospital Human Research Ethics Committee. All volunteers gave written informed consent before participating in the study. The participants included in this study have been well characterised and reported previously (Lee et al. 2015). Diagnosis of MCI or AD was made based on the criteria outlined by the National Institute of Neurological and Communicative Disorders and the Stroke-Alzheimer's Disease and Related Disorders Association (NINCDS-AD&DA), which are well-recognised standards used for MCI and AD diagnosis. Data reported in this study are from a total of 78 participants, including: (1) the control (C) group (n=40), which consisted of healthy age- and gender-matched participants; (2) the MCI group (n=18), clinically diagnosed with MCI; and the (3) AD group (n=20) clinically diagnosed with AD. It is important to note that SAND cohort is completely separate from AIBL cohort.

5.2.2 Chemicals and Reagents

Roswell Park Memorial Institute (RPMI) 1640, foetal bovine serum (FBS), sodium pyruvate, L-glutamine/penicillin/streptomycin mix, Hank's balanced salt solution (HBSS), sodium citrate, 4',6-diamidino-2-phenylindole (DAPI), Paraformaldehyde (PFA), glycerol and all other chemicals were purchased from Sigma-Aldrich (Castle Hill, NSW, Australia) unless otherwise stated. Ficoll–Paque, sterile was purchased from (Amersham Pharmacia Biotech). Mouse monoclonal antibody anti-γH2AX (clone JBW301) was obtained from Millipore (Kilsyth, VIC, Australia). Dulbecco's phosphate-buffered saline (DPBS) and the secondary antibody Alexa Fluor 488 goat anti-mouse were purchased from Life Technologies (Mulgrave, VIC, Australia).

5.2.3 Peripheral Blood Lymphocyte Isolation

Whole blood was diluted in HBSS at a ratio of 1:1 and gently inverted to mix. The diluted blood was carefully layered on top of Ficoll solution in a TV10 tube (Techno Plas, S9716VSU, Australia) using a ratio of 1(Ficoll):3 (diluted blood) to minimise any mixing of blood with the Ficoll, as described previously (Fenech 2007). The tube containing diluted blood overlaid on Ficoll was centrifuged once at 400 x g for 30 min at 18–20ºC to separate the lymphocytes. Lymphocytes are typically found at the interface between the plasma and the Ficoll solution, and were carefully recovered using a sterile plugged Pasteur pipette to avoid uptake of Ficoll. The lymphocyte suspension was washed three times with HBSS by gentle pipetting and then centrifuged at 180 x g for 10 min at room temperature to remove any residual Ficoll and plasma. The supernatant was removed and the pellet resuspended in 1 mL of tissue culture freezing medium (90 per cent FBS + 10 per cent DMSO cooled to 4°C). The lymphocyte suspensions were then transferred to cryovials and placed in a StrataCooler Cryo

preservation module (Cat #400005 32) that had been precooled to 4°C by refrigeration and placed in a -80°C freezer. After 24 hours, the vials were transferred to a box in the -80°C freezer until required.

Cryovials containing frozen lymphocytes were swabbed with 70 per cent v /v ethanol and thawed rapidly by agitation in pre-warmed (37ºC) Milli Q water for 2–3 mins and removed from the water as soon as the cell suspension was thawed. The cell suspension was gently mixed to maximise the number of single cells in the suspension, centrifuged at 180 x g for 10 min and supernatant was discarded. The pellets containing lymphocytes were washed twice with 1 mL of DPBS, centrifuged at 180 x g for 10 min, and the supernatant was discarded. The cell pellet was then resuspended in 1 mL DPBS and divided into three aliquots: (1) 700 µL was fixed in 1 per cent PFA for 10 min in a cryovial at room temperature; (2) 10 µL was used to measure cell concentration and cell viability (Trypan blue dye exclusion assay) using a haemocytometer; and (3) the remaining 290 µL cell aliquot was used for radiation treatment.

Following fixation, cells were centrifuged at 100 x g for 10 min and the supernatant was removed before the cells were washed with DPBS. The washing procedure was carried out twice, and the cell concentration was measured using a haemocytometer and the cell suspension was diluted with DPBS to reach a final concentration of 40,000 cells/mL. The lymphocytes were finally cytocentrifuged for 3 min at 200 rpm onto microscope slides at a concentration of 4,000 cells per cytospot using a Shandon CytospinVR 4 (Thermo Scientific, USA). The slides were washed once with distilled water and air-dried for 1 h at room temperature and subsequently stored in sealed microscope boxes with dessicant at -80°C until the staining procedure was performed.

For the irradiation experiments, 290 µL of the cell aliquot was centrifuged, the supernatant discarded and the cells resuspended in complete medium (RPMI with 10 % FBS, 2 mM L-glutamine, 1 mM sodium pyruvate, 100 U penicillin and 100 mg/mL streptomycin). The cell aliquot was exposed to 1 Gy of X-rays (Faxitron Bioptics LLC, USA) with a dose rate of 1 Gy/ min and 44 kVp at 25°C then immediately incubated for 30 min at 37ºC in an incubator and stored at -80°C.

5.2.4 Staining of Lymphocytes for LSC and Visual Scoring

Microscope slides containing lymphocytes were randomly selected, thawed at room temperature for 20 min and air-dried in a fume hood and then stained in random batches of six, including a positive control slide (to confirm all staining procedures were positive in each batch). A circle was drawn around each cytospot using a hydrophobic PAP pen (Dako, Australia) and air-dried for 10 min. Lymphocyte cytospots were permeabilised in PBS + 0.1 %Triton X-100 for 10 min. Following two washes with DPBS for 5 min each, the cells were blocked in PBS with 20 % goat serum for 30 min at room temperature and then washed once with DPBS. The anti-γH2AX antibody was added to each cytospot at a dilution of 1/500 in DPBS containing 10 per cent goat serum for 60 min. Slides were washed three times in DPBS for 5 min each time, and a secondary antibody, Alexa Fluor 488 goat anti-mouse, was added to each cytospot at a dilution of 1/1,500 in DPBS containing 20 per cent goat serum, for 60 min at room temperature. Finally, the slides were washed three times in DPBS for 5 min per wash, and nuclei were counterstained with 4,6-diamidino-2-phenylindole (DAPI) at a concentration of 1 mg/mL for 10 min at room temperature. The excess DAPI was removed by rinsing the slides with a solution containing 300 mM NaCl and 34 mM sodium citrate. Slides were then mounted with coverslips and DPBS:glycerol (1:1)

medium. The edges of the coverslips were sealed with nail polish to prevent drying prior to performing LSC and visual scoring. All the quantitative γH2AX experiments were done using reagents from the same batches to minimise inter-experimental variation.

5.2.5 Laser Scanning Cytometry Measurements of γH2AX

Microscope slides with lymphocytes were inserted in a four-slide carrier and analysed immediately after the staining procedure using an iCyte® automated imaging cytometer (Thorlabs, Sterling Virginia, USA) featuring a full autofocus function as well as 405 nm and 488 nm lasers for excitation of DAPI and Alexa Fluor 488, respectively. The blue and green photomultiplier tubes were used to collect fluorescence from DAPI (blue) and Alexa Fluor 488 (green), respectively. LSC parameters such as voltage, gain, offset values, contour, and threshold were determined and kept unchanged for all batch-to-batch analyses. Samples were scanned consecutively in separate passes to prevent spectral overlap and nuclei, and γH2AX events were contoured using empirically determined thresholds to exclude the scoring of false positives (e.g., small fluorescent debris). The DAPI fluorescence integral of nuclei (for DNA content and nuclear ploidy), as well as multiple parameters within each nucleus, including the total γH2AX integral (a function of γH2AX intensity and size) and the MaxPixel value (the value of the most intense γH2AX signal/pixel within nuclei) and frequency (percentage) of cells containing γH2AX signals, were recorded and generated using the iCyteVR 3.4 software and subsequently transferred into Microsoft Excel for further statistical analyses. Using the features available in the iCyte® software, the senescence characteristics of nuclei were classified to identify senescent cells as described in details in Section 5.2.6 and Figure 5.1.

5.2.6 Identification of Different Lymphocyte Nuclei by LSC

Following a high - resolution scan using the LSC protocol as described in Section 5.2.6 and Figure 5.1, nuclei were separated based on their DNA content (the DAPI integral) and the nuclear area. Nuclei with area values ranging from 0 to 210 μm^2 and blue integral values ranging from 0 to 4 x 10^7 arbitrary units (a.u.) were separated in Region 1 (R1) when plotted against the nuclear area (X-axis) and blue integral (Y-axis). The nuclei in R1 were denoted as 'all nuclei' (A). This scattergram plot separated cells from clumps of cells as well as from false positive events. In this version of the iCyte® software, cells falling outside the scan boundaries were excluded from the analysis. The R1 cells (Figure 5.1) were then separated based on differences in their nuclear staining by plotting a frequency histogram showing the number of nuclei ('count') versus the blue integral. Three regions were identified from the different peaks obtained: Region 2 (R2, black) separated <2N nuclei from the 2N nuclei in Region 3 (R3, red), and Region 4 (R4, magenta) indicating >2N nuclei. Gallery images of <2N, 2N, and >2N nuclei are shown in Figure 5.2. Nuclei in R1 were then plotted against the nuclear area (X-axis) versus the ratio of the maximal pixel intensity of DAPI fluorescence per nucleus to the nuclear area (y-axis) (Figure 5.1, C and D). Senescent nuclei were then identified based on the criteria of decreased levels of DAPI staining (maximal pixel intensity) paralleled by an increase in nuclear size (area), shown in Region 5 (R5). Gallery images R5 (senescent nuclei) are shown in Figure 5.2 (Zhao, Darzynkiewicz 2013, Zhao et al. 2010). Multiple parameters within each nucleus, including the γH2AX integral (a function of γH2AX intensity and size), the γH2AX MaxPixel value (the value of the most intense γH2AX signal/pixel within nuclei) and the γH2AX area, as well as nuclear parameters such as integral, area and circularity, were generated for R1, R2, R3, R4, and

R5 using the iCyte® 3.4 software and subsequently transferred into Excel for further statistical analyses.

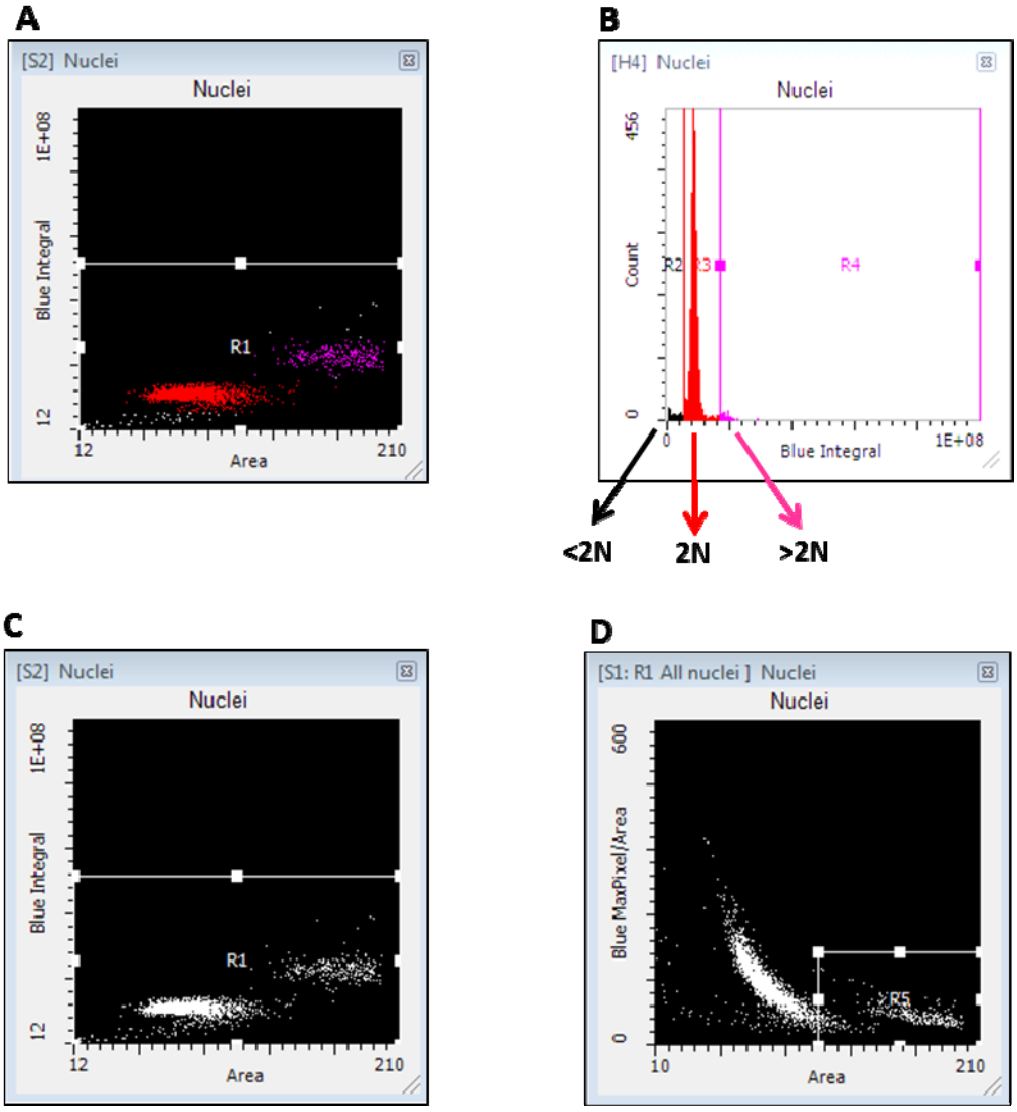

Figure 5.1: Scattergram and histogram for Identification of cell types. A representative example of DNA content scattergram and histogram for a participant from the control group. A scattergram was generated to separate cells based on differences in nuclear staining and area by plotting their blue integral versus the area. (A) Nuclei having area values that ranged from 0 to 210 μm^2 and blue integral values that ranged from 0 to 4 x 10^7 a.u. were separated in R1. (B) A histogram plot of the same data in the right panel showing the <2N, 2N and >2N peaks as represented in black, red, and magenta, respectively, and the respective frequency of DNA content events scored, with the majority of lymphocytes being scored as 2N. (C) A scattergram was generated to separate cells based on differences in nuclear staining and area by plotting their blue integral versus the area. (D) Nuclei in R1 were plotted against nuclear area versus the ratio of the maximal pixel intensity of DAPI fluorescence per nucleus to the nuclear area and the nuclei with morphometric characteristics of cellular senescence [i.e., increased nuclear size (area) combined with decreased intensity of MaxPixel of DNA-associated fluorescence per nucleus, after DNA staining with DAPI] were separated in R5.

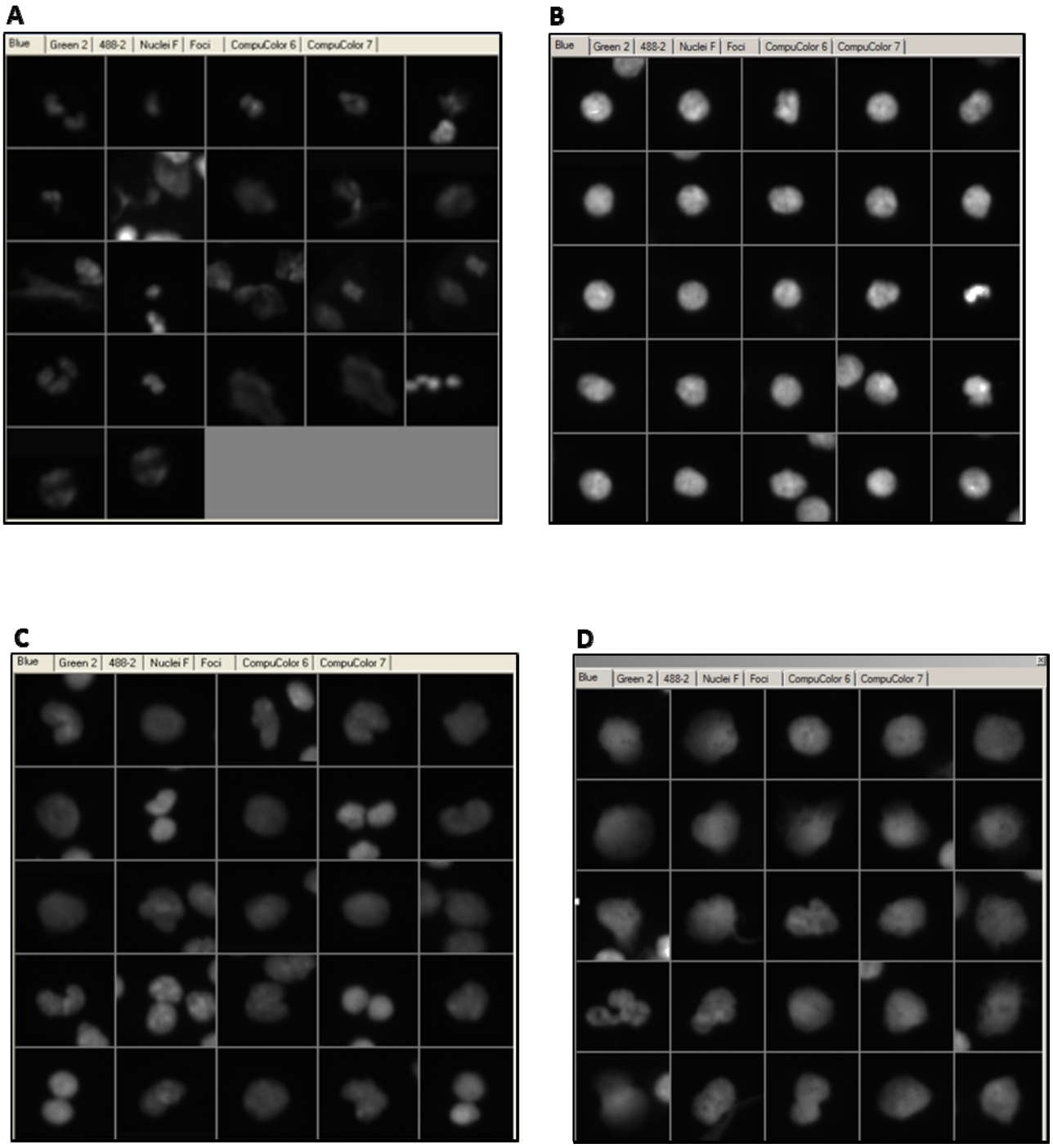

Figure 5.2: Gallery of images generated by LSC of <2N nuclei, 2N nuclei, >2N nuclei and senescent nuclei. Gallery images of lymphocytes nuclei A: (R2: <2N nuclei), B: (R3: 2N nuclei), C: (R4: >2N nuclei) and D: (R5: senescent nuclei) were checked using the 'Image Gallery' function in the iCyte® 3.4 software. Gallery images of lymphocytes senescent nuclei showing increased nuclear size (area) and decreased DAPI staining (D).

5.2.7 Visual Scoring of γH2AX Foci

Visual scoring of γH2AX foci was performed on microscope slides containing lymphocytes immediately after LSC scanning using a fluorescence microscope (ZEISS Metasystems, Althusheim, Germany) under a 63x oil objective. DAPI (nuclei) and Alexa Fluor 488 (γH2AX) fluorescence was viewed using blue and green filters, respectively. The presence of γH2AX foci were visualised as green fluorescence spots in the blue counterstained nuclei. A minimum of 400 nuclei were scored per cytospot. Since both discrete and overlapped γH2AX foci were observed within nuclei (Figure 5.3), the visual scoring of γH2AX foci for each nucleus was performed as follows: no foci, discrete foci (e.g., nuclei containing 1 focus, 2 foci, 3 foci, >5 foci, and overlapping foci (likely containing >5 large γH2AX foci overlapping each other or diffuse nuclear staining of γH2AX foci., i.e., widespread and uniform presence of γH2AX signal within the nucleus). The frequency (percentage) of nuclei containing γH2AX foci, as well as the frequency of nuclei containing overlapped foci representing nuclei with severe DNA damage, were recorded.

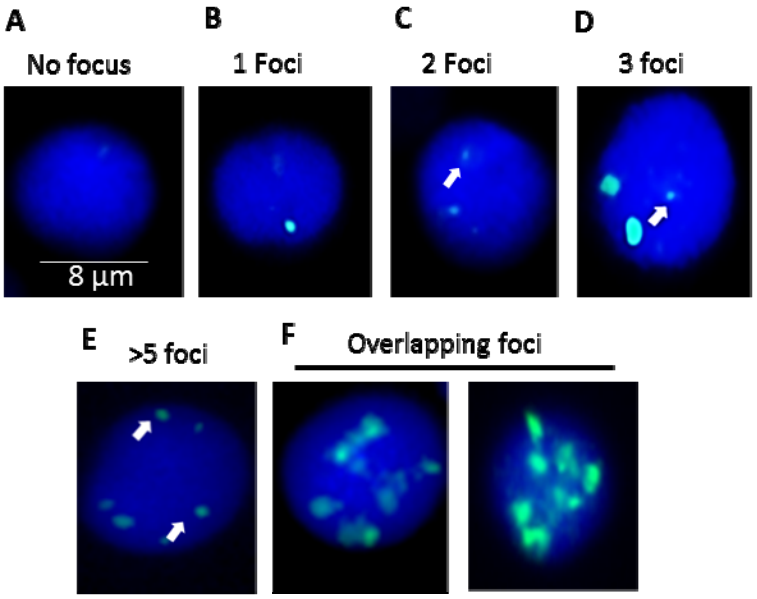

Figure 5.3: Fluorescence images of lymphocytes nuclei containing discrete or diffuse γH2AX foci. DAPI stained nuclei were visualised with a fluorescence microscope as described in Section 5.2.7. Discrete γH2AX foci in each nucleus were scored according to six categories: No focus (A), 1 foci (B), 2 foci (C), 3 foci (D), > 5 foci (E); however, some nuclei demonstrated an overlapping pattern of γH2AX signal (F). The arrow indicates discrete γH2AX foci. The scale bar in (A) represents 8 µm.

Since overlapping γH2AX foci were observed during visual scoring, it was difficult to distinguish overlapping γH2AX foci from discrete γH2AX foci. Counting overlapping γH2AX foci may not give an accurate representation of the entire sample populations' γH2AX signal or an actual number of foci/nuclei. Therefore, for visual scoring, as an alternative to counting γH2AX foci/nucleus, counting numbers of nuclei with clear bright γH2AX foci was chosen to obtain (i) % cell containing γH2AX foci and (ii) % cell containing overlapping γH2AX foci (Figure 5.4). It is important to note that total fluorescence signals (e.g. total integral or intensity of discrete and overlapping foci) were measured through the nuclei using LSC allowing detection of any subtle changes in γH2AX signals among individuals.

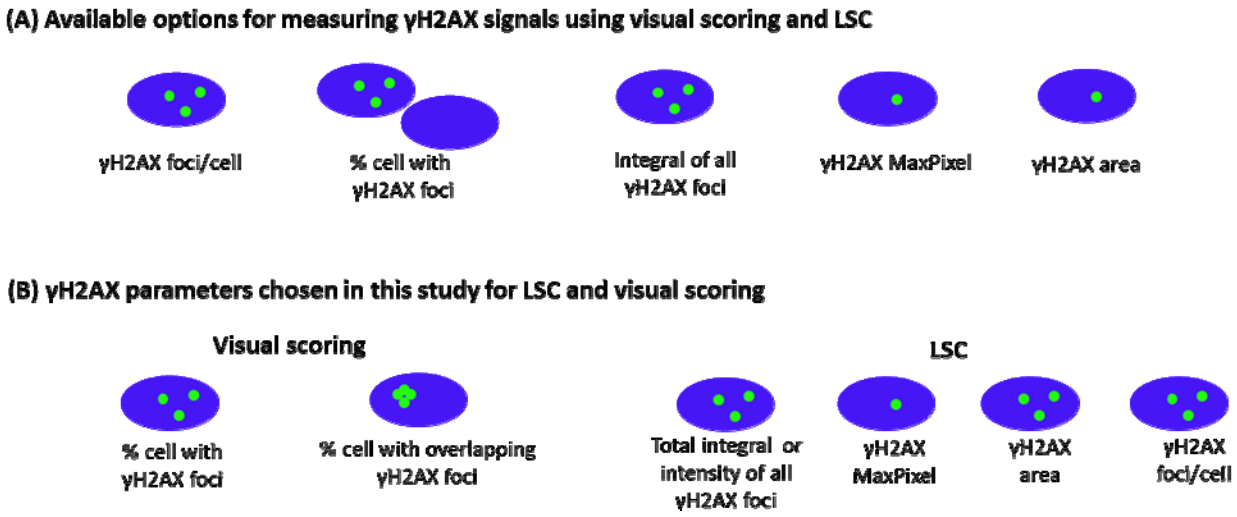

Figure 5.4: γH2AX parameters analysed by LSC and visual scoring. (A) Schematic showing an example of the different γH2AX parameters measured by LSC and visual scoring. In the schematic, the various types of γH2AX parameters are shown (γH2AX foci/nucleus, % cell containing γH2AX foci, γH2AX integral, γH2AX MaxPixel, and γH2AX area) (B) Schematic showing an example of the different γH2AX parameters those were chosen in this study for LSC and visual scoring. Note the blue indicating the nuclei and the green indicating γH2AX signal.

5.2.8 Statistical Analysis

GraphPad Prism 6.01 (GraphPad Prism, San Diego, CA) was used to analyse the data. Visual and LSC γH2AX data were checked for normality using the D'Agostino and Pearson omnibus normality test. Differences in relative γH2AX signals in the lymphocytes from control, MCI, and AD groups were compared using the Kruskal-Wallis test for non-Gaussian distributed data followed by Dunn's multiple comparisons test. In addition, for LSC and visually scored γH2AX data, comparison of the γH2AX signals between (i) MCI cases and age- and gender-matched controls (CON-MCI), and (ii) AD cases and age- and gender-matched controls (CON-AD) groups were performed using paired t-tests (Wilcoxon matched paired signed rank test) for non-Gaussian distributed data. The effect of X-irradiation on the γH2AX response in radiated and non-irradiated lymphocytes from the control, MCI and AD group was evaluated using a t-test for non-Gaussian distributed data (the Mann-Whitney test), which allows a

comparison of the γH2AX integrals between irradiated control versus non-irradiated control groups, irradiated MCI cells versus non-irradiated MCI cells and irradiated AD cells versus non-irradiated AD cells. Correlation coefficients were obtained using Pearson's correlation coefficients for Gaussian distributed data and Spearman's rho for non-Gaussian distributed data. Analysed data are reported as mean ± standard error of the mean (SEM) with $p<0.05$ considered statistically significant. Receiver-operating characteristic curves (ROC) were calculated for selected γH2AX parameters between the control and MCI or AD groups to obtain the area under the curve (AUC), sensitivity, specificity, confidence interval and p-value. p values <0.05 were considered to be statistically significant.

5.3 Results

5.3.1 Optimization of nuclear fixation to remove lymphocytes clumping

To determine which fixative method was the most suitable to provide isolated single cells on the microscope slides, two fixation methods were tested. Cells were either fixed with 0.1 per cent PFA in PBS or with methanol, both for 10 min at room temperature. When lymphocytes were fixed with methanol, the majority of cells clumped, as visualised by bright-field microscopy, while PFA-fixed lymphocytes appeared as isolated single cells (Figure 5.5). Since cells in small clusters of 2–6 cells on the microscope slide could not be contoured separately for LSC analysis, PFA was considered to be the most suitable fixative to ensure isolated single lymphocyte nuclei were present on the microscope slides for γH2AX assays using LSC and visual scoring.

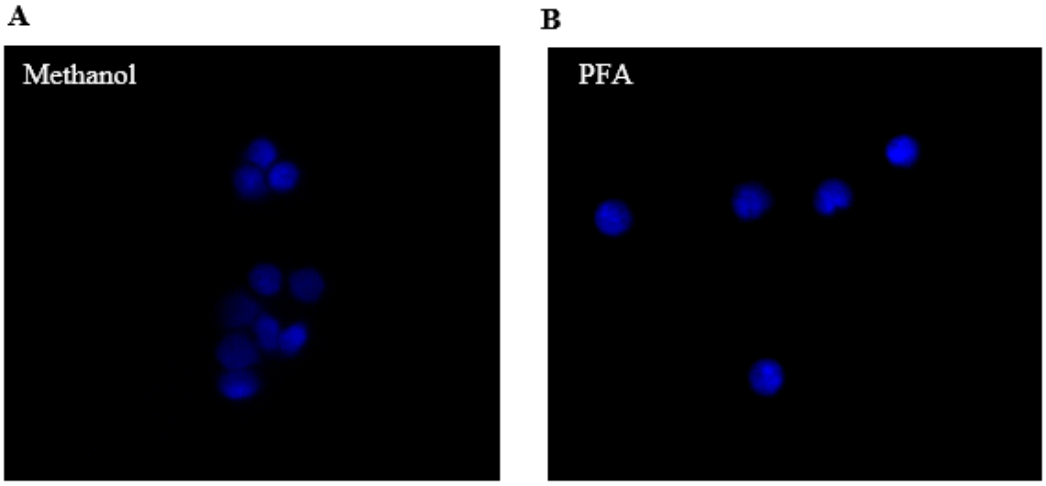

Figure 5.5: PFA and methanol fixation of lymphocytes for γH2AX staining and LSC. Lymphocyte staining was compared using two different cell fixation methods; **A:** Methanol-fixed lymphocytes appeared as clumped or a group of cell in close proximity. **B:** PFA fixation gave isolated single cells and was considered as the most suitable fixative for the LSC protocol.

5.3.2 Variation of γH2AX Data

Microscope slides containing lymphocytes previously fixed with 1 per cent PFA were defrosted at room temperature and stained for γH2AX analysis by LSC in batches of 12, including a positive control slide carrying X-irradiated (1 Gy) lymphocytes sampled from an individual (healthy male aged 34). The use of a control slide in each batch scan confirmed that all steps of γH2AX staining protocol were performed accurately in all batches analysed in this study. Additionally, prior to each batch scan, the same regions from a γH2AX positive stained slide (carrying 1 Gy exposed lymphocytes) were scanned using the γH2AX protocol by LSC to ensure that all settings and measurements of nuclei and γH2AX had not varied over the course of the study.

The coefficient of variation of γH2AX signals (γH2AX integral by LSC, and percentage of cells containing γH2AX foci as determined by visual scoring) was examined in non-irradiated lymphocytes as well as in lymphocytes exposed to 1 Gy of X-irradiation. Microscope slides were prepared from a single sampling of a healthy control (34 years

old), and cells were subsequently scored for γH2AX signals using LSC and visual scoring.

When a single individual's γH2AX integral was measured by LSC in non-irradiated control lymphocytes (all nuclei) slide in four separate experiments, the γH2AX integral ranged from 2.05 x 10^4 to 3.2 x 10^4 a.u. with a coefficient of variation of 20.5%. Additionally, the γH2AX integral in irradiated (1 Gy) lymphocytes (all nuclei) was measured by LSC in six separate experiments (within the same individual), and ranged from 1.27 x 10^6 to 2.5 x 10^6 a.u. with a coefficient of variation of 24.5%.

For non-irradiated lymphocytes (all nuclei) the coefficient of variation of the percentage of cells containing γH2AX foci by visual scoring on four separate experiments was 18.3%. For irradiated (1Gy) lymphocytes, the coefficient of variation of the percentage of cells containing γH2AX foci in six separate experiments was 11.8%.

5.3.3 Effect of Radiation Doses on γH2AX Response in Lymphocytes

Once the LSC and visual scoring protocols were validated, the γH2AX response for different doses was determined. The aim of this experiment was to determine if this protocol was suitable for distinguishing γH2AX signals at doses as low as 0.2 Gy X-irradiation from the basal levels of γH2AX signals in non-irradiated samples. Within the dose range tested (0.2, 0.5, and 1 Gy) with a dose rate of 1 Gy/ min and 44 kVp, the γH2AX integral measured by LSC and the percentage of cells containing γH2AX increased linearly with increasing radiation doses. For visual scoring, correlation was r=0.9712, (p=0.0288), and for LSC measurement correlation was r=0.9961, (p=0.0039) (Figure 5.6).

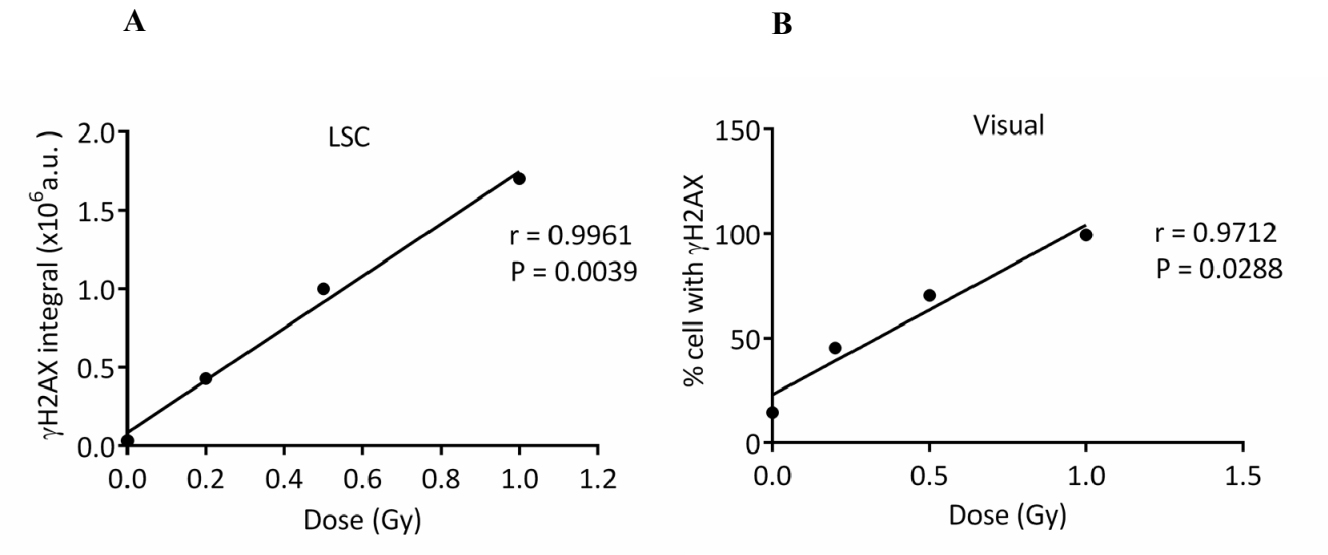

Figure 5.6: Dose response of lymphocytes population using LSC measurement and visual scoring. Lymphocytes from an individual (healthy male aged 34) were exposed to three doses: 0 Gy, 0.2 Gy, 0.5 Gy, 1 Gy and γH2AX response was measured 30 min after X-irradiation in a single experiment. A: γH2AX response was measured using LSC and an increase linear trend of γH2AX integral with radiation dose was observed. B: Linear increase of % of cells containing γH2AX with radiation was also observed when the same slides were visually scored. A minimum of 400 nuclei were counted for each condition regardless of scoring method.

5.3.4 Correlation of Visual and LSC Scored γH2AX Responses

The frequency (%) of visually scored nuclei strongly correlated with the automated LSC method developed here to quantify γH2AX integral (and MaxPixel) as shown in Figure 5.7. The correlation coefficients of visually scored γH2AX and the γH2AX integrals by LSC was r=0.9898, p=0.0102. This suggests that LSC was sensitive enough to quantify the small changes in IR-induced γH2AX signals in nuclei.

.

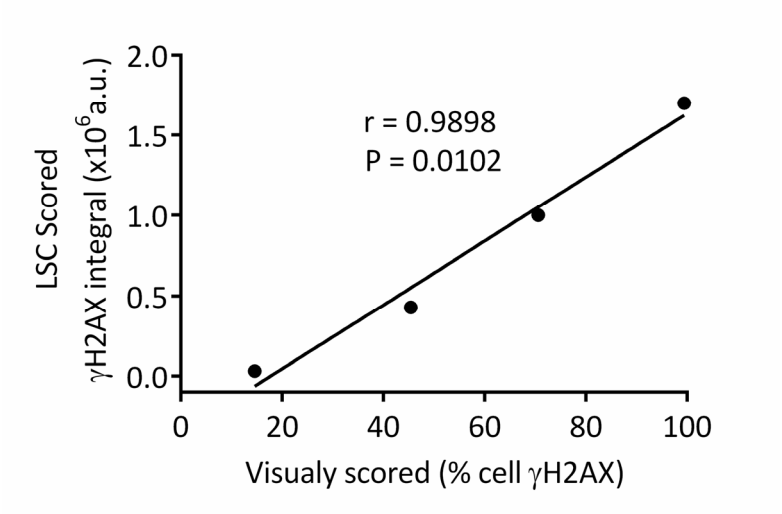

Figure 5.7: Correlation of visually scored and LSC quantified γH2AX signals in lymphocytes exposed to 0, 1, 2, or 4 Gy IR. The frequency (%) of cells containing γH2AX foci is shown on the X-axis and the mean γH2AX integrals (by LSC) in all nuclei are shown on the Y-axis for an individual. The Pearson correlation coefficient (r) and p-value are shown as an inset within the graph.

5.3.5 Clinical Characteristics of Participants

The mean age, gender and MMSE score of the SAND participants in the control, MCI, and AD groups is shown in Table 5.1. There were no statistically significant differences for age and gender ratios between the groups. As expected, there was a significant decrease in the MMSE scores of both the MCI and AD groups compared with the control group.

Table 5.1: Clinical characteristics

Means, standard error of the mean (SEM) are reported for each group. Significance was accepted at $p<0.05$. Abbreviations: AD, Alzheimer's disease; F, Female; M, Male; MCI, Mild cognitive impairment; MMSE, Mini Mental State Examination. *p<0.05, **p<0.01, ****p<0.0001.

	Control	MCI	AD
Sex (M:F)	11:28	7:13	5:15
Age (years)	75.75±1.575 (72.57-78.93)	74.60±1.955 (78.69-70.51)	76.85±2.450 (71.72-81.98)
MMSE score	28.60±0.211 (28.17-29.03)	26.28±0.559 (25.10-27.46)**	21.00±0.8645 (19.19-22.81)***

5.3.6 Scoring of γH2AX Signals in Lymphocytes by LSC

To investigate whether the endogenous γH2AX level is significantly increased in AD compared to control, γH2AX protein was measured in lymphocytes from control, MCI and AD cases by immunofluorescence. LSC measured multiple γH2AX parameters within each nucleus, including the total γH2AX integral (a function of γH2AX intensity and size), γH2AX MaxPixel (the value of the most intense γH2AX signal/pixel within each nuclei), γH2AX area, and the number of γH2AX events (foci) per cell in all nuclei and/or in cells with different DNA content (ploidy status) and senescent cells.

5.3.6.1 γH2AX results using all nuclear types

Table 5.2 summarises the one-way ANOVA results for the different γH2AX parameters (integral, MaxPixel, area and foci/nucleus) for each nuclear type analysed from the control, MCI and AD groups. There was a significant increase in the γH2AX integral ($p=0.0023$) in AD nuclei compared to control nuclei in all nuclei [Table 5.2, 1A, Figure 5.8 (A)]. Consistent with the increase in the γH2AX integral, significant increases in γH2AX MaxPixel ($p=0.0006$), γH2AX area ($p=0.0045$), and γH2AX foci/nucleus ($p=0.0080$) were also observed in AD cells compared to control cells [Table 5.2, 1A,

Figure 5.8 (B–D)]. Although all nuclei had a higher level of γH2AX signal (integral, MaxPixel, area and foci/nucleus) in MCI cells compared to control cells, there was no statistically significant difference in these γH2AX parameters between control nuclei and MCI nuclei or between MCI nuclei and AD nuclei. Additionally, there was no statistically significant difference in any of the γH2AX parameters in MCI nuclei compared to AD nuclei. However, a significant increase in the linear trend for the γH2AX integral ($p = 0.0005$), γH2AX MaxPixel ($p = 0.0002$) and γH2AX area ($p = 0.0007$) as well as for γH2AX foci/nucleus ($p = 0.0262$) was observed across the groups (i.e., AD > MCI > control) in all nuclei [Figure 5.8 (A-D)]. Individual data are also presented in Figure 5.9 (A-D).

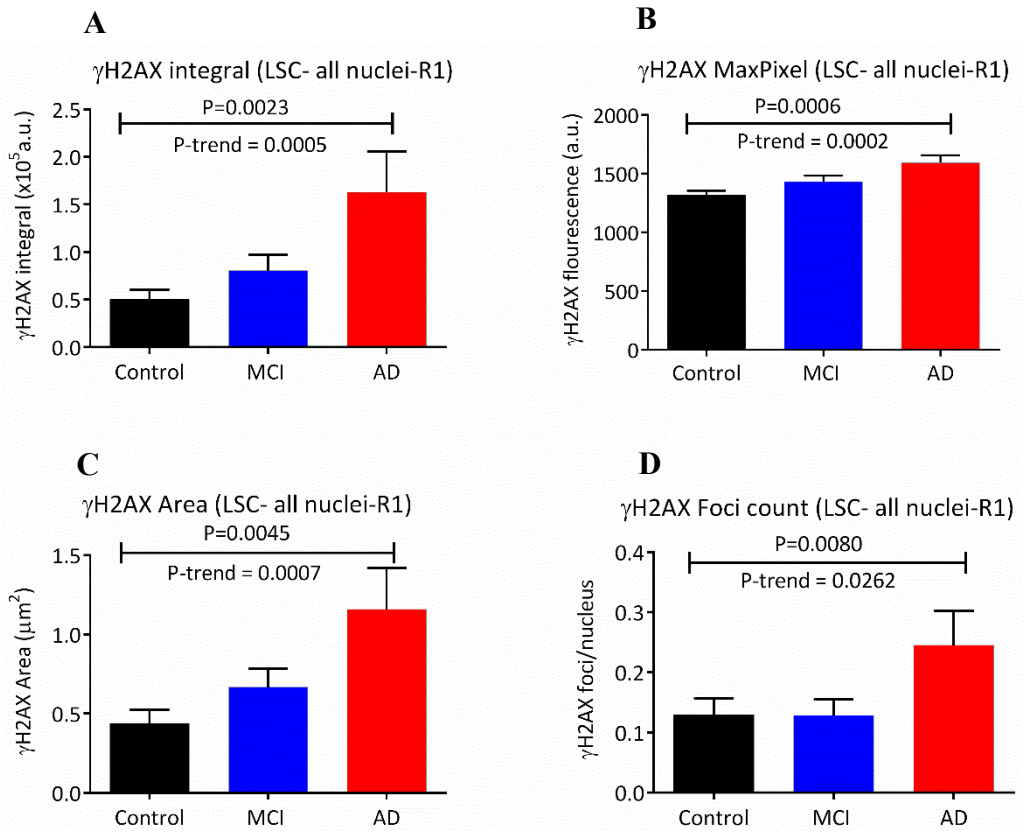

Figure 5.8: Different γH2AX parameters (integral, MaxPixel, area, foci/nucleus) in all nuclei. A: γH2AX integral. B: γH2AX MaxPixel. C: γH2AX area. D: γH2AX foci/nucleus. These parameters were measured for control (n=40), MCI (n=18) and AD (n=20) groups in all cells. *, $p<0.05$. Abbreviations: a.u., Arbitrary units; AD, Alzheimer's disease; MCI, Mild cognitive impairment. Data are means ± SEM.

In an attempt to score the γH2AX signals in nuclei with different DNA contents, nuclei were categorised as 2N, <2N and >2N by plotting the nuclei count versus the DAPI integral (equivalent to DNA content) as described in Section 5.2.6 and Figure 5.1.

5.3.6.2 γH2AX in 2N nuclei

There was a significant increase in the γH2AX integral (p=0.0020) in 2N nuclei from AD cells compared with control cells. Similarly, significant increases in the γH2AX MaxPixel (p=0.0020), γH2AX area (p=0.0047) and γH2AX foci/nucleus (p=0.0103) were also observed in AD cells compared to control cells (Table 5.2, 1C). No significant increase of any of the γH2AX parameters was seen between the control and MCI cells

or between MCI and AD cells. Additionally, a significant increase in the linear trend was observed across the groups (i.e., AD > MCI > control in the 2N nuclei).

5.3.6.3 γH2AX in <2N and >2N nuclei

For <2N nuclei, no significant increase in the γH2AX signals (integral, MaxPixel, area, foci/nucleus) was observed between the three groups, whereas the >2N nuclei showed significantly increased γH2AX integral, γH2AX MaxPixel, γH2AX area, γH2AX foci/nucleus in AD compared to control cells (Table 5.2, 1B, 1D). As expected, both the γH2AX area and γH2AX MaxPixel values also increased significantly in AD compared to control cells for >2N nuclei.

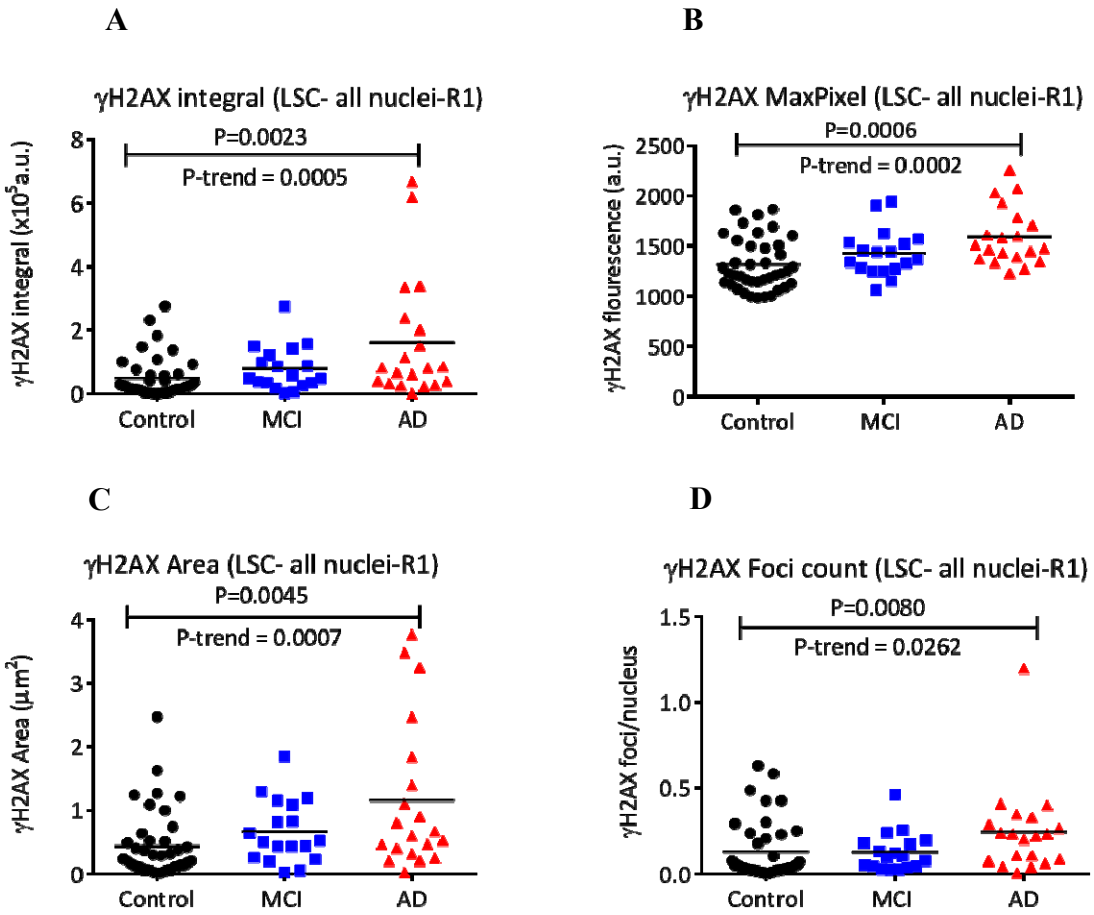

Figure 5.9: Individual data of γH2AX parameters (integral, MaxPixel, area, foci/nucleus) measured by LSC in all nuclei.

A: γH2AX integral. B: γH2AX MaxPixel. C: γH2AX area. D: γH2AX foci/nucleus. These parameters were measured for control (n=40), MCI (n=18) and AD (n=20) groups in all cells. *, $p<0.05$. Abbreviations: a.u., Arbitrary units; AD, Alzheimer's disease; MCI, Mild cognitive impairment. Data are means. Lines within data points indicate mean.

Table 5.2: Summary of one-way ANOVA tests for different γH2AX parameters measured using LSC in different types of lymphocyte nuclei

LSC	Con	MCI	AD	Con v MCI	Con vs AD	MCI vs AD
	Mean+/-SEM	Mean+/-SEM	Mean+/-SEM	p-value	p-value	p-value
1A. All nuclei						
γH2AX integral (x105a.u.)	0.5020+/-0.1027	0.8062+/-0.1633	1.627+/-0.429	0.0757	**0.0023**	>0.9999
γH2AX MaxPixel (a.u.)	1315+/-40.6	1430+/-54.8	1593+/-64.2	0.2693	**0.0006**	0.1370
γH2AX area (μM)	0.4398+/-0.0833	0.6672+/-0.1161	1.158+/-0.2618	0.0985	**0.0045**	>0.9999
γH2AX foci/nucleus	0.1295+/-0.0271	0.1283+/-0.0265	0.2452+/-0.0572	0.6248	**0.0080**	0.4551
1B. <2N nuclei						
γH2AX integral	0.6040+/-0.1674	1.389+/-0.6546	2.896+/-1.634	>0.9999	0.3486	>0.9999
γH2AX MaxPixel	1183+/-35.1	1394+/-165.8	1488+/-167.0	0.3424	0.0948	0.8475
γH2AX area	0.5893+/-0.1613	1.217+/-0.5427	1.982+/-1.016	>0.9999	0.3838	>0.9999
γH2AX foci/nucleus	0.1483+/-0.0317	0.08229+/-0.0254	0.1209+/-0.0297	>0.9999	>0.9999	0.9999
1C. 2N nuclei						
γH2AX integral	0.4369+/-0.0962	0.7152+/-0.1741	1.447+/-0.3876	0.1756	**0.0020**	0.6717
γH2AX MaxPixel	1309+/-40.8	1421+/-56.1	1577+/-62.1	0.2883	**0.0009**	0.1572
γH2AX area	0.3808+/-0.0765	0.5851+/-0.1264	1.025+/-0.2371	0.2601	**0.0047**	0.7275
γH2AX foci/nucleus	0.1204+/-0.0273	0.1245+/-0.0279	0.2267+/-0.0568	0.8300	**0.0103**	0.3870
1D. >2N nuclei						
γH2AX integral	1.108+/-0.3259	1.704+/-0.5788	3.420+/-0.7982	0.4210	**0.0009**	0.2393
γH2AX MaxPixel	1422+/-80.49	1852+/-282.7	1867+/-89.79	0.2945	**0.0008**	0.3129
γH2AX area	1.034+/-0.2705	1.369+/-0.2995	2.697+/-0.5447	0.5536	**0.0016**	0.2358
γH2AX foci/nucleus	0.2443+/-0.0503	0.3063+/-0.0747	0.7305+/-0.2383	0.9603	**0.0029**	0.1671

Parameters highlighted in bold text were considered statistically significant. Data were expressed as mean ± SEM. Statistical significance was accorded for p-values <0.05.

In addition to one-way ANOVA tests for LSC and visually scored γH2AX parameters, comparison of the γH2AX signals between age and gender matched (i) AD and CON-AD (ii) MCI and CON-MCI groups were performed using paired T-test. For all nuclei,

significant increase in the γH2AX integral (p=0.0007) was observed in AD cells compared to matched control cells, whereas visually scored cells showed a significant increase in the % of cells containing γH2AX foci (p=0.0001) and the percentage of cells containing overlapping γH2AX foci (p=0.0001) in AD cells compared to and CON-AD cells. No significant increase of any of the γH2AX parameters was seen in MCI cells compared to CON-MCI cells (Table 5.3).

Table 5.3: Comparison of AD and CON-AD and MCI and CON-MCI in regards to γH2AX signals measured by LSC and visual scoring

	AD	CON-AD	p-value	MCI	CON-MCI	p-value
Integral Mean±SEM	16273±4294 (n=20)	49730±1445 (n=20)	**0.0007**	8063±1634 (n=18)	53002±1645 6(n=18)	0.30
Percentage of cells containing γH2AX foci (Mean±SEM)	16.65±2.67 (n=20)	6.60±1.31 (n=20)	**0.0001**	8.68±1.24 (n=18)	6.35±1.30 (n=18)	0.138
Percentage of cells containing overlapping γH2AX foci (Mean±SEM)	1.31±0.30 (n=20)	0.02±0.02 (n=20)	**0.0001**	0.32±0.15 (n=18)	0.02±0.02 (n=18)	0.09

Parameters highlighted in bold text were considered statistically significant. Data were expressed as mean ± SEM. Statistical significance was accorded for p-values <0.05.

5.3.6.4 Effect of Age and Gender- on visually scored and LSC quantified γH2AX signals

Paired T-tests and Pearson's or Spearman's rho tests were performed to find whether visually scored and LSC quantified γH2AX signals were affected by gender and/or correlated with age when combining the data from all of the groups. The % of cells containing overlapping γH2AX foci were significantly affected by gender but not age. The percentage of cells containing overlapping γH2AX foci was significantly higher (P=0.01) in females compared with males. The LSC quantified γH2AX integral and visually scored percentage of cells containing γH2AX foci was not affected by age and gender. γH2AX integral (all nuclei), % of cells containing γH2AX foci, % of cells containing overlapping γH2AX foci had no significant correlation with age (Table 5.4).

Table 5.4: Effect of Age and Gender on visually scored and LSC quantified γH2AX signals based on combined data from all groups (N=78)

	γH2AX integral (all nuclei)	Percentage of cells containing γH2AX foci	Percentage of cells containing overlapping γH2AX foci
Comparison of male vs. female			
Male (N=23) (Mean ± SEM)	112707±28944	13.16±1.84	0.20±0.08
Female (N=55) (Mean ± SEM)	74940±15014	7.92±1.11	0.50±0.14
P-value	NS	NS	**0.01**
Correlation with age			
R-value	0.14	0.21	0.023
p-value	NS	NS	NS

Parameters highlighted in bold text were considered statistically significant. Data were expressed as mean ± SEM. Statistical significance was accorded for p-values <0.05.

5.3.6.5 Senescent nuclei

The Nuclear Area and Nuclear MaxPixel features available within iCyte were used to empirically classify senescent lymphocytes, and their γH2AX parameters (integral, MaxPixel, area foci/nucleus) values are shown in Table 5.5. There were no differences in the % of senescent cells across the groups. The γH2AX integral was significantly increased (p=0.0092) in AD cells compared to control cells, while a significant increase was also observed for the γH2AX MaxPixel (p=0.0008), γH2AX area (p=0.0157) and γH2AX foci/nucleus (p=0.0056) in AD cells compared to control cells (Table 5.5).

Table 5.5: Summary of the one-way ANOVA tests for different γH2AX parameters in senescent nuclei

Senescent nuclei	Con	MCI	AD	Con vs MCI	Con vs AD	MCI vs AD
	Mean+/-SEM	Mean+/-SEM	Mean+/-SEM	p-value	p-value	p-value
γH2AX integral	0.1170+/-0.0297	0.1307+/-0.0345	0.2743+/-0.0758	0.4677	**0.0092**	0.6265
γH2AX MaxPixel	1315+/-40.6	1430+/-54.8	1593+/-64.2	0.2380	**0.0008**	0.3634
γH2AX area	1.110+/-0.2939	1.150+/-0.2540	2.153+/-0.5009	0.4013	**0.0157**	0.8897
γH2AX foci/nucleus	0.2456+/-0.0698	0.2341+/-0.0545	0.3777+/-0.0681	0.4749	**0.0056**	0.4938

Parameters highlighted in bold text were considered statistically significant. Data were expressed as mean ± SEM. Statistical significance was accorded for p-values <0.05.

5.3.7 Visual Scoring of γH2AX Foci

Microscope slides containing lymphocytes stained as described in Section 5.2.4 were visually assessed using the criteria described in Section 5.2.7. Representative images of nuclei with discrete and overlapped γH2AX foci are shown in Figure 5.3 (A–F). The % of cells containing γH2AX foci was significantly higher (p=0.0003) in AD compared to those from the control group. Additionally, the percentage of cells containing γH2AX foci was significantly increased (p=0.0212) in AD compared to MCI. Data are summarised in Figure 5.10 and Table 5.6.

There was also significant increase in the frequency (%) of nuclei containing overlapping γH2AX foci in AD cells compared to control cells (p=0.0001), as well as in AD cells compared to MCI cells (p=0.0007). In fact, regardless of the different γH2AX parameters analysed, this significant increase in the frequency of nuclei containing overlapping foci was observed in AD cells compared to control cells as well as in AD cells compared to MCI cells [Table 5.6, Figure 5.10, (B)]. Individual data are also presented in Figure 5.10 (A-B).

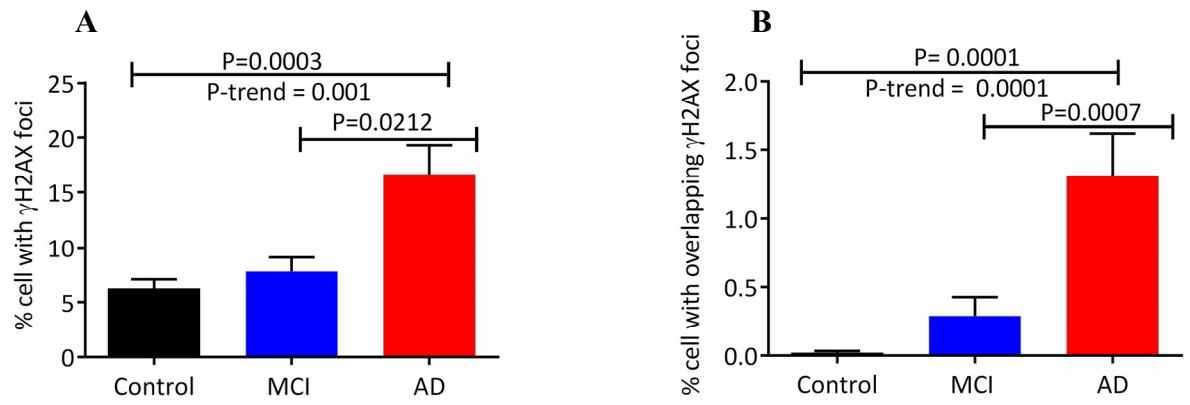

Figure 5.10: Different γH2AX parameters scored visually in all cells. A: Percentage of cells containing γH2AX foci. B: Percentage of cells containing overlapping γH2AX foci in the control (n=40), MCI (n=18) and AD (n=20) groups. *P<0.05. Abbreviations: a.u., Arbitrary units; AD, Alzheimer's disease; MCI, Mild cognitive impairment. Data are means ± SEM.

Table 5.6: Summary of one-way ANOVA tests for different γH2AX parameters measured by visual scoring in lymphocyte nuclei

Visual Scoring	Con	MCI	AD	Con v MCI	Con vs AD	MCI vs AD
	Mean+/-SEM	Mean+/-SEM	Mean+/-SEM	p-value	p-value	p-value
% of cells with γH2AX foci	6.230+/-0.889	7.820+/-1.271	16.65+/-2.671	>0.9999	**0.0003**	**0.0212**
% of cells with overlapping γH2AX foci	0.020+/-0.012	0.2900+/-0.1372	1.310+/-0.308	0.1447	**0.0001**	**0.0007**

Parameters highlighted in bold text were considered statistically significant. Data were expressed as mean ± SEM. Statistical significance was accorded for p-values <0.05.

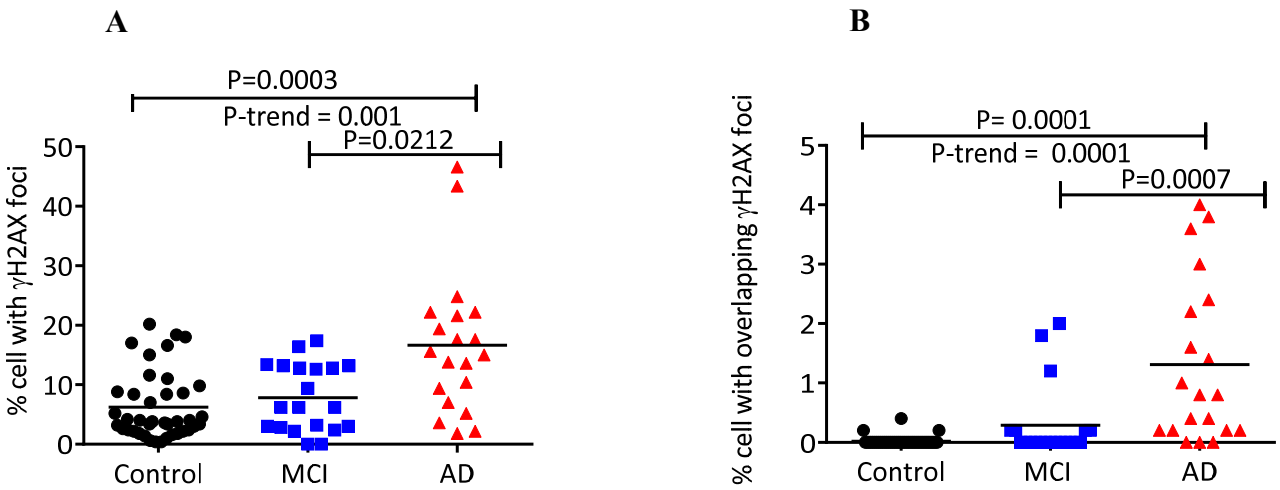

Figure 5.10: Individual data of γH2AX parameters scored visually in all cells.

A: Percentage of cells containing γH2AX foci. B: Percentage of cells containing overlapping γH2AX foci in the control (n=40), MCI (n=18) and AD (n=20) groups. *P<0.05. Abbreviations: a.u., Arbitrary units; AD, Alzheimer's disease; MCI, Mild cognitive impairment. Data are means. Lines within data points indicate mean.

5.3.8 Receiver Operator Characteristic Curve

Receiver operation characteristic curves (ROC) were generated to determine the diagnostic value of these parameters for discriminating AD patients from controls. The accuracy of the test depends on how well the test distinguishes the group being tested from controls and AD patients. The area under the curve (AUC) quantifies the capacity of the test in discriminating between the control group and the AD group. An AUC value of 1 is considered to be a perfect test, while an AUC value of 0.5 is considered a low-efficiency test. Sensitivity represents the fraction of people within the AD group that the test correctly identifies as positive. On the other hand, specificity represents the fraction of people from the control group that the test correctly identifies as negative. Sensitivity and specificity were automatically calculated using each value from the data table. For each category of nuclei analysed by LSC, γH2AX parameters (e.g., integral, γH2AX MaxPixel, γH2AX area, γH2AX foci/nucleus) were significantly higher in AD compared to the control group. ROC curves were generated for the following

parameters: γH2AX integral, γH2AX MaxPixel, γH2AX area and γH2AX foci/nucleus. ROC curves for the γH2AX integral, γH2AX MaxPixel, γH2AX area, γH2AX foci/nucleus are shown in Figure 5.11 A–D, respectively. The ROC curve for the γH2AX integral yielded an AUC of 0.7638 (p=0.0001) for the AD group. The AUC values for the γH2AX MaxPixel, γH2AX area and γH2AX foci/nucleus were 0.7775 (p=0.0005), 0.6806 (p=0.03) and 0.7200 (p=0.0006) respectively (Figure 5.11 (A-D), Table 5.7). Of all parameters analysed by ROC curves, the γH2AX MaxPixel showed the highest likelihood for identification of AD with 85 % sensitivity and 67 % specificity.

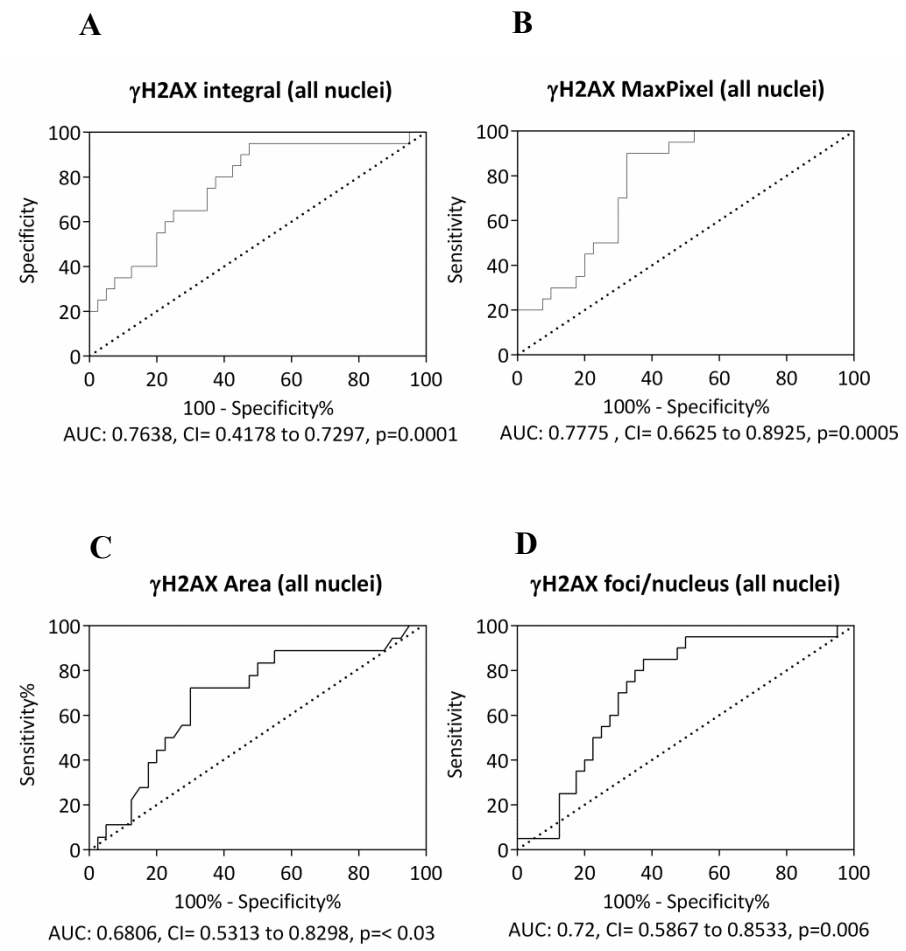

Figure 5.11: ROC curves for selected γH2AX parameters measured by LSC for control and AD nuclei. ROC curves were generated for the γH2AX integral, γH2AX MaxPixel, γH2AX area and γH2AX foci/nucleus in lymphocytes from control and AD groups.

Additionally, visually scored γH2AX signals were significantly higher in AD cells compared with those from the control group, as well as in MCI cells compared with those from the AD group. ROC curves were generated for the percentage of cells containing γH2AX foci and the percentage of cells containing overlapping γH2AX foci (Figure 5.12 (A-B), Table 5.7). The ROC curve of the % of cells containing γH2AX foci yielded an AUC of 0.8000 (p=0001), and for the percentage of cells containing overlapping γH2AX foci the AUC value was 0.9081 (p=<0001). Thus, the percentage of cells containing overlapping γH2AX foci showed the highest likelihood for

identification of AD, with 85 % sensitivity and 92 % specificity. In conclusion, visual scoring gave better AUC outcomes than LSC scoring.

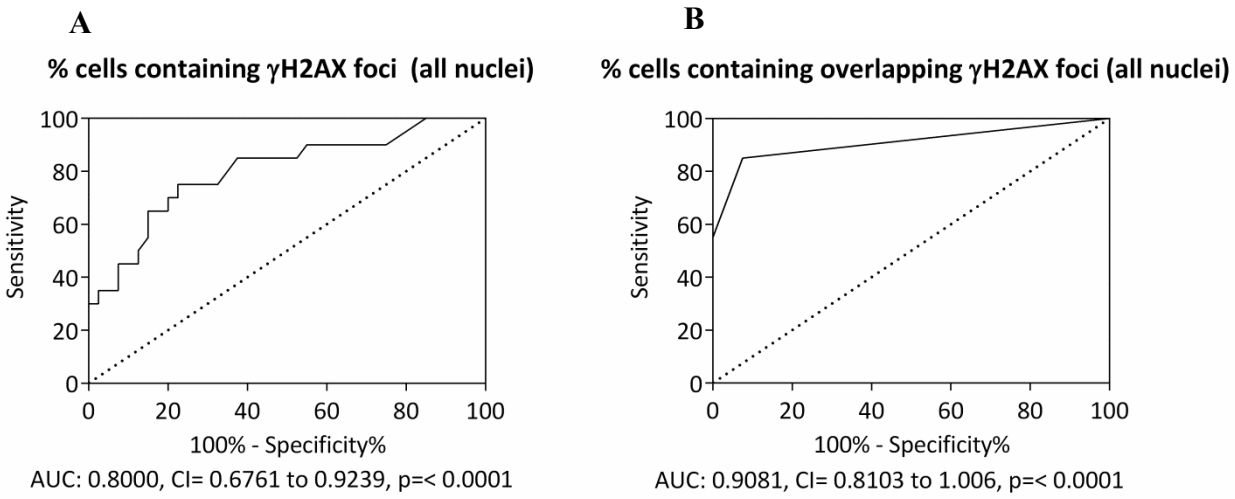

Figure 5.12: ROC curves for visually scored γH2AX parameters for controls and AD. ROC curves generated for the percentage of cells containing γH2AX foci and the percentage of cells containing overlapping γH2AX foci analysed by visual scoring in lymphocytes from the control and AD groups.

ROC curves were generated for the γH2AX integral, γH2AX MaxPixel, γH2AX area and γH2AX foci/nucleus in lymphocytes from control and AD groups. AUC, CI, P-value, sensitivity and specificity values are shown for each category of γH2AX parameters analysed using LSC or visual scoring. Abbreviations; AUC, Area under the curve; CI, Confidence interval.

Table 5.7: Data obtained from ROC curves generated for the different γH2AX parameters analysed in lymphocytes using LSC and visual scoring.

Parameters	AUC	CI	p-value	Sensitivity %	Specificity %
LSC					
γH2AX integral	0.7638	0.4-0.7	0.0001	75	62
γH2AX MaxPixel	0.7775	0.6-0.8	0.0005	85	67
γH2AX area	0.6806	0.5-0.8	0.0289	72	67
γH2AX foci/nucleus	0.7200	0.5-0.8	0.0006	75	67
Visual scoring					
% of cells with γH2AX foci	0.8000	0.6-0.9	<0.0001	75	77
% of cells with overlapping γH2AX foci	0.9081	0.8-1.0	<0.0001	85	92

5.3.9 Correlation of the γH2AX Integral and Other γH2AX Parameters by Laser Scanning Cytometry

Since the γH2AX integral is a function of both γH2AX total intensity and γH2AX area, the γH2AX integral in all nuclei was selected for investigating correlations with other γH2AX parameters measured by LSC. γH2AX MaxPixel, γH2AX area and γH2AX foci/nucleus strongly correlated with the γH2AX integral. Table 5.8 summarises the r and p-values obtained for each of the parameters examined. The parameters highlighted in bold correlated with the γH2AX integral.

Table 5.8: Summary of correlations tested between γH2AX integral and other γH2AX parameters in different types of nuclei from the SAND study

Cell types		LSC		
	Parameters	Correlation (r)	CI	p-value
All nuclei	γH2AX MaxPixel	0.74	0.6195–0.8265	**<0.0001**
	γH2AX area	0.9666	0.9480–0.9786	**<0.0001**
	γH2AX foci/nucleus	0.3986	0.1932–0.5706	**0.0003**
<2N	γH2AX MaxPixel	0.8165	0.7258–0.8793	**<0.0001**
	γH2AX area	0.982	0.9718–0.9885	**<0.0001**
	γH2AX foci/nucleus	0.3282	0.1139–0.5133	**0.0034**
2N nuclei	γH2AX MaxPixel	0.7425	0.6228–0.8282	**<0.0001**
	γH2AX area	0.9641	0.9441–0.9770	**<0.0001**
	γH2AX foci/nucleus	0.4076	0.2035–0.5778	**0.0002**
>2N nuclei	γH2AX MaxPixel	0.691	0.5536–0.7918	**<0.0001**
	γH2AX area	0.9096	0.8614–0.9415	**<0.0001**
	γH2AX foci/nucleus	0.4624	0.2673–0.6210	**<0.0001**
Senescent nuclei	γH2AX MaxPixel	0.7633	0.6514–0.8427	**<0.0001**
	γH2AX area	0.9268	0.8872–0.9528	**<0.0001**
	γH2AX foci/nucleus	0.4159	0.2131–0.5844	**0.0002**

Parameters highlighted in bold text were considered statistically significant.

5.3.10 Correlation of γH2AX Integral by LSC and Visually Scored γH2AX

The visually scored γH2AX parameters (percentage of cells containing γH2AX foci, percentage of cells containing overlapping γH2AX foci) were compared to the LSC scored γH2AX integrals. A strong positive correlation was observed between the γH2AX integral and each of the visually scored parameters. Table 5.9 summarises the r and p-values obtained for each of the visually scored parameters examined. The parameters highlighted in bold text correlated with the LSC scored γH2AX integral.

Table 5.9: Summary of correlations between γH2AX integral and other visually scored γH2AX parameters in different types of nuclei from the SAND study

Cell types	Visual scoring			
	Parameters	Correlation (r)	CI	p-value
All nuclei	% nuclei with γH2AX foci	0.7011	0.5670–0.7990	**<0.0001**
	% cell with diffuse γH2AX foci	0.3914	0.1849–0.5648	**0.0004**
<2N	% nuclei with γH2AX foci	0.2339	0.0119–0.4339	**0.0393**
	% cell with diffuse γH2AX foci	0.1908	-0.0331–0.3966	0.0942
2N	% nuclei with γH2AX foci	0.7041	0.5710–0.8011	**<0.0001**
	% cell with diffuse γH2AX foci	0.4111	0.2075–0.5805	**0.0002**
>2N nuclei	% nuclei with γH2AX foci	0.6349	0.4802–0.7513	**<0.0001**
	% cell with diffuse γH2AX foci	0.3636	0.1534–0.5423	**0.0011**
Senescent nuclei	% nuclei with γH2AX foci	0.5392	0.3598–0.6802	**<0.0001**
	% cell with diffuse γH2AX foci	0.2648	0.0448–0.4602	**0.0192**

Parameters highlighted in bold text were considered statistically significant.

5.3.11 Correlation of LSC and Visually Scored γH2AX with MMSE score

To investigate whether γH2AX measurements in lymphocytes were related to the extent of cognitive decline in the subjects, the correlation between γH2AX integral, γH2AX MaxPixel and MMSE scores was tested. Since γH2AX MaxPixel reached the strongest differences between AD and controls ($p=0.006$) of all the γH2AX parameters measured by LSC, and γH2AX MaxPixel was strongly correlated ($r=0.74$, $p<0.0001$, Table 5.8) with γH2AX integral, therefore the γH2AX MaxPixel value in all cells was selected for investigating any correlation with MMSE scores. Correlation tests were also carried out between each of visually scored parameters and MMSE scores to investigate whether the number of visually scored γH2AX foci/nucleus in lymphocytes was related to the advancement of cognitive decline in the subjects (Table 5.10).

Table 5.10: Summary of correlations between LSC scored γH2AX signals vs the MMSE score and between visually scored γH2AX signals and MMSE scores available from the SAND study

Parameters	Correlation (r)	CI	p-value
γH2AX integral	-0.1899	-0.4014 to 0.04083	0.0959
γH2AX MaxPixel	-0.2266	-0.4331 to 0.0024	**0.0460**
% cells containing γH2AX (visually scored)	-0.3188	-0.5105 to -0.09693	**0.0044**
% cells containing overlapping γH2AX foci (visually scored)	-0.5343	-0.6800 to -0.3479	**<0.0001**

Parameters highlighted in bold text were considered statistically significant. All are Spearman's rho correlation.

5.3.12 Correlation of LSC and Visually Scored γH2AX with Blood Parameters

Many blood parameters have been analysed in the SAND cohort that are known to be associated with AD. Correlation tests were carried out between each of these parameters and the γH2AX integral values as well as with γH2AX MaxPixel values. Table 5.11 summarises the r and p-values obtained for each of the parameters examined. Parameters highlighted in bold text correlated with the γH2AX integral as well as the γH2AX MaxPixel.

Table 5.11: Summary of correlations tested between γH2AX Integral and other blood parameters available from SAND study

	Parameters	Correlation (r)	CI	p-value
γH2AX Integral	B12	0.0551	-0.1696 to 0.2743	0.6319
	Folate	0.1913	-0.0327 to 0.3970	0.0934
	RCF	0.1153	-0.1131 to 0.3322	0.3212
	Homocysteine	0.0992	-0.1293 to 0.3175	0.3942
	Creatinine	**0.3007**	**0.0837 to 0.4904**	**0.0075**
	Albumin	-0.1566	-0.3690 to 0.07147	0.1768
	eGFR	**-0.2442**	**-0.4428 to -0.0229**	**0.0312**
	B2M	0.1089	-0.1166 to 0.3236	0.3428
	Cortisol	-0.0668	-0.2851 to 0.1582	0.5615
	CHI3L1	0.2089	-0.0389 to 0.4326	0.0976
γH2AX MaxPixel	B12	0.0246	-0.1991 to 0.2458	0.8309
	Folate	0.0868	-0.1385 to 0.3035	0.4502
	RCF	0.0995	-0.1289 to 0.3179	0.3926
	Homocysteine	0.0163	-0.2100 to 0.2409	0.8887
	Creatinine	0.2081	-0.0152 to 0.4116	0.0675
	Albumin	-0.1305	-0.3458 to 0.0979	0.2613
	GFR	-0.1925	-0.3980 to 0.0314	0.0913
	B2M	0.0889	-0.1363 to 0.3055	0.4387
	Cortisol	-0.0364	0.2569 to 0.1877	0.7517
	CHI3L1	**0.2939**	**0.0518 to 0.5034**	**0.0184**

Parameters highlighted in bold text were considered statistically significant. All are Pearson correlations. Parameters highlighted in bold text were considered statistically significant. All are Pearson correlations. Abbreviations: CHI3L1, Chitinase-3-like protein 1, eGFR, estimated glomerular filtration rate; ESR, erythrocyte sediment rate; Vitamin B12, B12. B2M, Beta-2 microglobulin, RCF, red cell folate.

Additional correlation test between visually scored γH2AX signals (percentage of cells containing γH2AX foci, percentage of cells containing diffuse γH2AX foci) and each of these blood parameters were also performed. Table 5.12 summarises the r and p-values obtained for each of the parameters examined. The parameters highlighted in bold text correlated with the percentage of cells containing γH2AX foci and the percentage of cells containing diffuse γH2AX foci. It is important to note that both LSC and visual scoring showed correlations between creatinine, GFR, and CHI3L1 and γH2AX signals, suggesting that visual and LSC scored γH2AX parameters may be used to identify abonarmalities in blood parameters of AD patients.

Table 5.12: Summary of correlations between visually scored γH2AX signals and other blood parameters available from the SAND study

Percentage of cells containing γH2AX foci			
Parameters	**Correlation (r)**	**CI**	**p-value**
B12	-0.0900	-0.3065 to 0.1353	0.4332
Folate	0.1120	- -0.1134 to 0.3264	0.3290
RCF	0.0583	-0.1695 to 0.2801	0.6172
Homocysteine	0.1920	-0.0351 to 0.4001	0.0967
Creatinine	**0.2884**	**0.0703 to 0.4801**	**0.0105**
Albumin	-0.0751	-0.2956 to 0.1530	0.5191
eGFR	-0.2189	-0.4209 to 0.0039	0.0542
B2M	0.1183	-0.1071 to 0.3322	0.3021
Cortisol	-0.0533	-0.2726 to 0.1713	0.6432
CHI3L1	**0.2734**	**0.0295 to 0.4865**	**0.0288**
Percentage of cells containing overlapping γH2AX foci			
Parameters	**Correlation (r)**	**CI**	**p-value**
B12	-0.0043	-0.2266 to 0.2185	0.9705
Folate	0.0304	-0.1935 to 0.2513	0.7918
RCF	0.0005	-0.2251 to 0.2259	0.9971
Homocysteine	**0.3606**	**0.1471 to 0.5421**	**0.0014**
Creatinine	0.1511	-0.0740 to 0.3615	0.1868
Albumin	0.1170	-0.1114 to 0.3337	0.3140
eGFR	**-0.2632**	**-0.4589 to -0.04311**	**0.0199**
B2M	0.0951	-0.1303 to 0.3111	0.4077
Cortisol	0.0087	-0.2143 to 0.2308	0.9401
CHI3L1	0.0706	-0.1784 to 0.3110	0.5797

Parameters highlighted in bold text were considered statistically significant. All are Pearson correlations. Abbreviations: CHI3L1, Chitinase-3-like protein 1, eGFR, estimated glomerular filtration rate; ESR, erythrocyte sediment rate; Vitamin B12, B12. B2M, Beta-2 microglobulin, RCF, red cell folate.

5.3.13 γH2AX response of lymphocytes population after exposure to X-irradiation

The levels of γH2AX were also tested in lymphocytes from the control, AD and MCI groups 30 min after exposure to X-irradiation. The γH2AX integral values increased significantly in the irradiated lymphocytes from the control (p=0.0001), MCI (p=0.0117) and AD (p=0.0210) group than in their respective non-irradiated lymphocytes (Figure 5.13). The results of X-irradiation treatment of lymphocytes were also calculated as the fold induction over the basal level of γH2AX signal. The γH2AX

integral increased approximately 6-fold in the irradiated control group; while in MCI and AD groups, the γH2AX integral increased approximately 2- and approximately 3-fold, respectively.

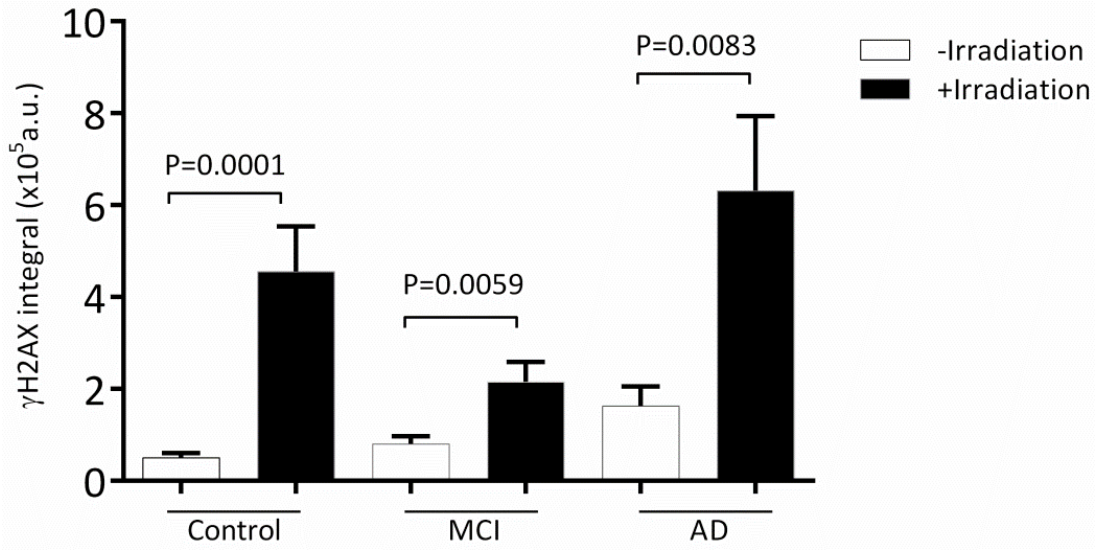

Figure 5.13: The effect of X-irradiation on the level of γH2AX signalling in the lymphocytes from Control, MCI and AD groups. Lymphocytes were exposed to 1 Gy X-irradiation. The γH2AX integral was measured by LSC after 30 min post-irradiation. Error bars represent the SEM for each group.

5.4 Discussion

The main objective of this study was to investigate whether MCI and AD patients have higher levels of endogenous DSBs than healthy controls, with the ultimate aim of identifying DSBs in lymphocytes for early AD diagnostic testing. The γH2AX assay was chosen for this analysis as it has been demonstrated to be a reliable and rapid measure of DNA DSBs for clinical purposes (Schurman et al. 2012, Banath, Macphail & Olive 2004, Scarpato et al. 2011). LSC and visual scoring methods were used to quantify endogenous γH2AX in peripheral blood lymphocytes of individuals who met clinical criteria for MCI and AD and in age-and gender-matched healthy controls. Both the LSC protocol and visual scoring showed increased levels of γH2AX in the lymphocytes of AD compared with control and MCI patients, and there was a concomitant increase with a significant trend for an increase in γH2AX from controls through MCI to AD. This result was further supported by the significant negative correlation between the γH2AX signals and MMSE score when the analysis included all subjects. The frequency of visually scored nuclei containing γH2AX signals showed a strong correlation with the LSC scored γH2AX integral. The LSC protocol developed here simultaneously quantifies the DNA content and different γH2AX parameters (integral, MaxPixel, area) in each nucleus in thousands of lymphocytes. Additionally, several significant correlations were observed between lymphocyte γH2AX signals and other blood parameters that were available from the SAND database (i.e., plasma homocysteine, creatinine, GFR, CHI3L1 that were previously shown to be increased in MCI and AD (Choi, Lee & Suk 2011, Zhuo, Wang & Pratico 2011, Wald, Kasturiratne & Simmonds 2011, Ng et al. 2014)). Finally, there was a blunted γH2AX response in the MCI and AD group compared to control group following X-ray exposure. These experimental results demonstrated that lymphocytes from AD patients exhibited

increased γH2AX levels relative to those in MCI patients and healthy controls, suggesting that this AD-associated increase in unrepaired DSBs may reflect a higher chronic induction of DSBs via oxidative or DNA replication stress, defective DNA repair, an inefficient processing of γH2AX.

In the visual scoring study, nuclei containing γH2AX foci were counted in lymphocytes from the control, MCI and AD groups. The results of the visual scoring demonstrated that the percentage of cells containing γH2AX foci was significantly higher in AD compared to the control group, and also significantly increased in AD compared to MCI. In previous studies, γH2AX immunocytochemical staining has been shown to be higher in the nuclei of hippocampal astrocytes from Alzheimer's disease patients relative to healthy controls as determined by immunocytochemical techniques, while another study reported no difference in astrocytes or neurons relative to AD progression (Myung et al. 2008, Simpson et al. 2010). Additionally, a recent study reported higher levels of expression of γH2AX in hippocampal tissues of individuals with both AD pathology and clinical dementia than in a normal ageing group (Silva et al. 2014). However, there is a lack of studies assessing the levels of γH2AX in peripheral blood cells of patients with AD relative to those seen in healthy controls and MCI patients. In line with other studies, the visually scored data suggest that the elevated levels of DNA DSBs in lymphocytes, as measured by the γH2AX assay, may be associated with a clinical diagnosis of AD and MCI. The results from the visual scoring also showed that the percentage of severely damaged nuclei (containing >10 foci) was significantly higher in AD compared to the control group and significantly increased in AD compared to MCI. These results are in agreement with other studies that show increased levels of endogenous γH2AX in lymphocytes from individuals with accelerated ageing disorders compared to healthy controls (e.g., Werner syndrome, obesity, diabetes, sleep

apnea, prostate cancer, cataract disease, hypertension and Hutchinson–Gilford progeria syndrome) (Schurman et al. 2012). Therefore, it is plausible that the accumulation of γH2AX foci is increased in individuals with accelerated ageing disorders and may be associated with the accumulation of DSBs in pathological ageing such as AD. In a study of obesity in children, severely damaged nuclei showing >50 γH2AX foci were also observed, and the levels of γH2AX in lymphocytes of obese children was 8-fold higher than those seen in non-obese children. It is likely that the severely damaged nuclei observed represent the necrotic or nonviable cell population with impaired DNA damage repair efficiency. For a complete understanding of the DNA damage response in lymphocytes isolated from control, MCI and AD cells, it would, therefore, be valuable in future studies to combine γH2AX detection with cellular markers of apoptosis in the different cell subtypes present (e.g., B and T lymphocytes).

One of the advantages of using automated quantitative LSC is the efficient, unbiased and quantifiable measure of γH2AX signals as well as determining DNA content in a large number of cells (thousands of cells per individual), making it a useful method to measure any subtle changes between individuals. Additionally, LSC allows scanning all samples with the same LSC setting and thus also reduces the possibility of scorer bias when counting individual γH2AX foci during visual scoring where multiple scorers are involved. LSC has previously been shown to be a useful tool to measure γH2AX induction after DNA damage when combined with the analysis of cellular DNA content for evaluation of the cell cycle stage (Zhao et al. 2009, Tanaka et al. 2007, Huang et al. 2004). DNA content (measured by nuclear DAPI integral) was therefore included as an additional measurement in the LSC protocol to allow the classification of nuclei as <2N, 2N and >2N. The results showed that majority of lymphocytes (~83 %) were post-mitotic 2N nuclei and that there was a significant increase in γH2AX signals in 2N

nuclei in AD patients compared with the control and MCI groups. Since DNA damage in the form of γH2AX has not been investigated in lymphocytes to assess the pathogenesis of AD, these findings support previous observations of stronger γH2AX staining in the nuclei of astrocytes from AD patients relative to healthy controls. However, the correlation of γH2AX in lymphocytes and astrocytes remains unknown. While the >2N nuclei showed a significant increase of all γH2AX parameters in AD lymphocytes compared to control cells, no significant increase was observed in <2N nuclei. Lymphocytes with <2N are likely to be apoptotic or necrotic cells or viable cells that are hypodiploid due to chromosome loss (Francois et al. 2014a, Kirsch-Volders, Fenech 2001). A further study with a larger patient cohort may provide new insights into mechanisms, especially if coupled with multiple types of nuclei and other complementary DNA damage parameters such as micronuclei and telomeres content and aggregation. Together, these results strongly suggest that the γH2AX assay has merits regarding differentiating AD from MCI and healthy controls. Although Migliore et al. (Migliore et al. 2005) reported a significant increase in oxidative DNA damage (oxidised DNA bases) and DNA strand breaks in lymphocytes from a MCI group compared with a control group, no significant increase of γH2AX was seen in MCI cells compared to control cells in this study. However, there was an increasing linear trend observed from control through MCI to AD cells, suggesting that lymphocytes from MCI patients are also more susceptible to DNA damage. The discrepancy between the results of this study and that of Migliore et al. (Migliore et al. 2005) may well reflect differences in the DNA strand breaks assays (i.e. comet vs. γH2AX) methodology, sample numbers and the populations under investigation. A more likely possibility is that the number of γH2AX molecules produced per DSB varies among individuals and may be reflected in the populations anlaysed in that study. It will be interesting to

examine in a larger cohort whether the lack of γH2AX formation per DSB is associated with MCI.

The LSC measurement of γH2AX signals in lymphocytes requires setting specific threshold values in the iCyte software for the blue and green channels (i.e., pixel values that were below these threshold values were not considered as DAPI and γH2AX signals but as background) which allow detection of small and dim γH2AX foci. This threshold in LSC may cause overestimation of γH2AX signals in contrast to visual scoring where there was no deal with counting small and faint γH2AX foci or counting γH2AX foci/nuclei but counting the number of nuclei with clear bright γH2AX foci to obtain % cell containing γH2AX foci or % cell containing overlapping γH2AX foci. The ability of visually scoring to differentiate AD group from MCI and control group was much better than measuring overall γH2AX signals using LSC. ROC curve analysis was carried out to assess the diagnostic accuracy of γH2AX assay in identifying individuals with AD from controls for both LSC and visual scoring. The visually scored % cell containing overlapping γH2AX foci displayed the best area under the ROC curve value of 0.9081 with 85 % sensitivity and 92 % specificity for the AD group while ROC curve for LSC scored γH2AX MaxPixel yielded the area under the ROC curve value of 0.7775 with 85% sensitivity and 67 % specificity for the AD group suggesting that measurement of % cell containing overlapping γH2AX foci by visual scoring in the buccal cell might be the best parameter in discriminating AD and control. This could, for instance, be due to counting the nuclei with overlapping γH2AX foci or counting the obvious bight γH2AX foci by eye. It will be interesting to examine in a large cohort whether visually scored parameters chosen in this study can be used as simple detection criteria to identify AD patients from MCI and control.

Accumulating evidence suggest that susceptibility of human cells to genotoxic compound (e.g. radiomimetic mutagen) may be useful to monitor disease status (Scarpato et al. 2011, Fernandez et al. 2013). In this study, the susceptibility of lymphocytes to genotoxic compound (e.g. ionizing radiation) was assessed by the treatment of lymphocytes from control, MCI, and AD groups with ionizing radiation. Interestingly, we observed that at 30 minutes after exposure to 1 Gy IR, lymphocytes from the control, MCI and AD groups exhibited different levels of induction of γH2AX expression. The highest level of γH2AX induction approximately 6-fold was observed in irradiated control lymphocytes as compared to non-irradiated control cells. There was an approximately 2-fold induction of γH2AX in irradiated lymphocytes from MCI patients compared to non-irradiated MCI cells, while γH2AX was induced approximately 3-fold in lymphocytes from irradiated AD lymphocytes compared to non-irradiated AD cells. It is possible that the high levels of endogenous γH2AX in AD compared to lymphocytes from the control group, may explain why the fold increase in γH2AX induction seen in AD cells after radiation exposure was lower than that in the control group. Similarly, the γH2AX induction in the MCI group was also lower than that in the control cells; however, the reason for the greater induction in AD cells compared to MCI cells remains unclear, and the difference was not statistically significant. These observations raise the question as to whether lymphocytes from AD and MCI patients are not only less able to respond to DNA damage in response to radiation, but are also less able to detect such damage, and show relatively lower levels of induction of γH2AX. There is a problem with just using one time-point post-radiation to measure γH2AX. It would have been better to do several time-points. Further research will provide valuable insight into this question. Nonetheless, these results clearly demonstrate that human peripheral lymphocytes from control, MCI and AD

patients respond differently to IR exposure, and this characteristic may provide the basis of a useful test for the early diagnosis of AD.

Senescent cells characterised by the presence of γH2AX, including the activity of senescence-associated β-galactosidase, accumulate in skin of aged animals, and are thought to increase in number during ageing and in age-related diseases (Dimri et al. 1995, Sikora et al. 2011). Previous studies have shown that senescent nuclei are flattened and larger in size. Using the features available in the iCys software of LSC, senescent nuclei from Mxt-treated cultured fibroblasts were isolated based on the criteria of decreased levels of DAPI staining (maximal pixel intensity) paralleled by an increased in nuclear size (area) and the simultaneous expression of senescence markers (e.g., the p21WAF1, p16INK4a or p27KIP1 cyclin kinase inhibitors) (Zhao, Darzynkiewicz 2013). Senescent nuclei were identified by plotting the ratio of the maximal pixel intensity of DAPI fluorescence per nucleus to the nuclear area versus the nuclear size (area), as described in Figure 4. A significant increase in the γH2AX signal was observed in senescent nuclei from AD cells for all individual γH2AX parameters measured by LSC, suggesting that senescent lymphocytes from AD patients have a reduced DNA repair capacity, leading to accumulation of DSBs. Alternatively, there was more γH2AX accumulation in cells of AD cases because of a higher frequency of DSBs in telomeres which are not repaired. The accumulation of DSBs and γH2AX in telomeres is a trigger for activation of the senescent process (Campisi 2013, Campisi et al. 2011). Although a previous study confirmed the presence of senescent cells using immunocytochemical analyses of the expression of additional senescence markers such as the p21WAF1, p16INK4a or p27KIP1 cyclin kinase inhibitors (Zhao, Darzynkiewicz 2013), this study did not confirm this, but rather attempted to identify senescent nuclei by their morphometric characteristics alone and is therefore a weakness that still needs

to be addressed. Hence, these results demonstrate for the first time that LSC can be used to identify the nuclear morphometric characteristics of senescent nuclei in lymphocytes from the control, MCI and AD groups. It will be interesting to investigate morphometric changes in senescent nuclei along with the expression of senescence markers in lymphocytes from MCI and AD patients compared to control cells by using LSC features and therefore LSC could be used to obtain valuable information of senescence-associated DNA damage in Alzheimer's patients.

Several significant correlations were observed between LSC and visually scored γH2AX parameters and the blood parameters that were measured in the SAND cohort samples. These significant correlations [i.e., creatinine levels, glomerular filtration rate (GFR): a measure of kidney function, homocysteine levels, and CHI3L1: an inflammation marker] suggest a possible mechanistic link between lymphocyte γH2AX and other blood markers measured in SAND. The LSC-scored γH2AX signals positively correlated with creatinine level, and negatively correlated with GFR. The percentage of cells containing γH2AX foci identified by visual scoring also showed significant positive correlations with creatinine levels and a negative correlation with GFR for nuclei with severe DNA damage (nuclei containing overlapping γH2AX foci). Previous studies have demonstrated that high serum creatinine levels and a low estimated GFR were significantly associated with poor episodic memory, considered the cognitive hallmark of developing AD (Ng et al. 2014). It is plausible that increased numbers of DSBs in lymphocytes coupled with renal dysfunction and its metabolic consequences may have a causative role in the development of dementia. Alternatively, there may a common risk factor such as the oxidative stress of DNA damage induced by malnutrition, accumulation of genotoxic metabolites, or due to poor kidney function. Thus, the γH2AX assay could be used to identify those at risk of developing AD using

LSC and visual scoring techniques, while the blood analytes simultaneously provide valuable information on the metabolic/nutrient profiles of those individuals on the risk of dementia. In this study, it was possible to find correlations between creatinine, GFR, CHI3l1 and γH2AX signals using both the visual and LSC scoring criteria. It will be interesting to examine if measuring a particular γH2AX parameter (i.e. either γH2AX MaxPixel by LSC or % of cells containing overlapping γH2AX foci by visual scoring) is a very sensitive and simple way to identify small changes in γH2AX signals related to AD and abnormalities in other routine blood parameters and therefore could be used for routine diagnostics to determine the AD patients from MCI and control.

Studies have shown that moderately elevated levels of plasma total homocysteine increase the risk of cognitive impairment in healthy ageing, with the progression of cognitive decline and development of AD (Smith 2008, Zhuo, Wang & Pratico 2011, Wald, Kasturiratne & Simmonds 2011, McIlroy et al. 2002). In this study, the percentage of nuclei with severe DNA damage (containing overlapping γH2AX foci) positively correlated with plasma homocysteine levels, indicating that individuals with high homocysteine levels may have a higher percentage of cells with severe DNA damage, suggesting a link between DNA damage and homocysteine levels in the blood. Lower status B vitamins (Folate, vitamin B6, and vitamin B12) are associated with increase DNA damage (uracil, micronuclei, DNA strand breaks) and contribute to the insufficient conversion of homocysteine to methionine and in turn homocysteine levels increase (Fenech 2012). Proof of concept for the protective effect of B vitamins has already been demonstrated in a small randomised controlled trial, which showed that B vitamin supplements delay brain atrophy and cognitive decline in people with MCI (Douaud et al. 2013). These authors also investigated whether lowering homocysteine by giving high doses of vitamin B supplements for two years could reduce the rate of

brain atrophy in people with pre-existing MCI. The results showed that treatment with B vitamins for 24 months led to a reduction in the rate of brain atrophy and the greater effect was observed in those who had the highest level of homocysteine. Previous study showed a reduction in DNA damage with folate and B12 supplementation (Fenech 2012). The current study showed a positive correlation between the percentage of severely damaged nuclei (nuclei containing overlapping γH2AX foci) and plasma homocysteine levels, suggesting that the plasma homocysteine levels may change with the progression of AD or it may mean more DNA damage induction on telomeres that is not repaired. A further prospective longitudinal study to determine whether the use of vitamin B can reduce γH2AX and homocysteine levels in blood and delay disease progression in people with MCI is warranted.

Elevated inflammation in AD patients is closely linked to disease pathology and is associated with functional disability and cognitive decline. Previous findings have shown elevated peripheral concentrations of inflammatory factors, including IL-1, IL-6, IL-12, IL-18, TNF-α, and TGF-β, in patients with AD compared to controls (Koyama et al. 2013, Swardfager et al. 2010). Plasma level of CHI3L1 (an inflammation marker (Kawada et al. 2007)) was significantly increased AD patients compared to control subjects and MCI patients (Choi, Lee & Suk 2011). In addition, increased plasma TNF-α has been associated with the development of AD in patients with MCI (Tobinick 2008). In a study of obesity in children, the relationship between DNA damage (measured by the presence of γH2AX) and obesity, as identified by specific plasma markers of inflammation, was investigated. A significant positive correlation was observed between the levels of γH2AX and plasma inflammatory markers (e.g., TNF-α, IL-6, and C-reactive protein) suggesting that obesity, involving altered metabolic conditions, triggers oxidative stress, which in turn augments the frequency of DNA

lesions in peripheral cells (Scarpato et al. 2011). In the current study, a weak positive correlation was observed between the LSC scored γH2AX MaxPixels and plasma levels of CHI3L1, as well as in the visually scored cells, the percentage of cells with γH2AX foci and plasma CHI3Ll levels, suggesting that the increased levels of DNA DSBs in lymphocytes may be linked to higher peripheral blood concentrations of inflammatory factors. It remains to be established whether this increased rate of DNA DSBs may indicate increased inflammation and ultimately the progression of dementia. Future investigations should include the measurement of γH2AX and CHI3L1 levels in blood from patients with MCI and AD to determine whether elevated γH2AX and CHI3L1 levels are unique to AD and associated with other more AD-specific biomarkers, such as amyloid beta 42 (Ab42), tau protein (tau), and phosphorylated p-tau.

Another important consideration is that lifestyle factors such as nutrition, physical exercise, tobacco smoking and alcohol consumption have an age-independent effect on the accumulation of DNA damage and telomere dysfunction in human blood cells (Song et al. 2010). In addition, previous studies found evidence that lifestyle interventions can contribute to reduced DNA damage and telomere shortening in vivo (Allgayer et al. 2008, Hofer et al. 2008, O'Callaghan et al. 2009). Another study reported significantly elevated levels of DNA 8-OHdG and decreased plasma antioxidants in patients with AD compared with controls, suggesting that the age-related increase in oxidative stress is related to a decline in antioxidant defenses and that DNA repair functions may be linked to the development of AD (Mecocci et al. 2002).

Many experimental studies suggest that the pathogenesis of AD is associated with oxidative DNA damage. 8-hydroxyguanine (8-OHG), a marker of DNA oxidation, was reported to be higher in several postmortem AD brain regions compared to control brains (Wang et al. 2005, Mecocci, MacGarvey & Beal 1994, Lyras et al. 1997).

Oxidative DNA damage has frequently been observed in peripheral tissues of AD patients and is thought to contribute to the development of AD. Increased 8-OHG was found in lymphocytes isolated from patients with AD compared to healthy controls, suggesting that oxidative DNA damage is also present in the peripheral cells of AD patients (Mecocci et al. 2002, Mecocci et al. 1998). In another study, increased oxidative DNA damage (oxidised DNA bases) was observed in lymphocytes from AD patients when measured using a modified version of the comet assay (Migliore et al. 2005, Mecocci et al. 1998, Morocz et al. 2002). Several studies reported altered DNA repair protein in specific regions of AD brain leading to inefficient repair of chronic or acute oxidative damage in AD brain (Bucholtz, Demuth 2013, Lovell, Xie & Markesbery 2000, Jacobsen et al. 2004, Canugovi et al. 2013). Since increased oxidative stress is associated with AD, the activity and abundance of DNA repair protein produced by oxidative stress may be associated with the pathogenesis of AD. It may be possible that the increased levels of DSBs observed in this study may be due to genetic factors, including DNA repair gene polymorphisms, contributing to a reduction in DNA repair protein abundance and activity. Analysing the impact of polymorphisms in DNA repair genes in conjunction with an accumulation of DSBs on the progression of AD in large case-control study would be desirable in order to increase the chance to identify AD and MCI patients from healthy controls.

DNA DSBs may accumulate during abnormal cellular processes, including DNA replication stress, cellular senescence, and chronic exposure to the excessive amount of reactive oxygen species. Therefore, endogenous γH2AX foci may be formed even in the absence of external DNA damaging agents such as radiation (Bonner et al. 2008). Humans and other mammals follow an intrinsic DNA repair mechanism to repair endogenous DNA DSBs. The repair of endogenous DSBs is continuous and rapid,

involving recurring transient γH2AX responses. However, small defects in the efficiency of repairing the chronic endogenous DNA DSBs for long periods (days, weeks, months and even years) may contribute to the accumulation of DSBs on telomeres which are not repaired, which can be reflected as persistent γH2AX and may be associated with the pathogenesis AD (Fumagalli et al. 2012, Hewitt et al. 2012). DSBs and γH2AX accumulate in telomere sequences within cells and may ultimately reach a threshold that triggers senescence-associated secretory phenotype (SASP) which put into action the senescence process by which such cells are eliminated (Campisi et al. 2011, Freund et al. 2010). Increased levels of γH2AX in the lymphocytes of AD patients as reported in this study may indicate that DSBs are either in the process of slow, ongoing repair, or DSBs that remain permanently unrepaired due to cellular senescence, apoptosis, or DSBs that remain unrepaired in specific genome sequences such as telomeres (Sedelnikova et al. 2004, Fumagalli et al. 2012, Hewitt et al. 2012).

Although a better understanding of the biology of the γH2AX response in the lymphocytes of AD and MCI individuals is needed, this study suggests that lymphocytes may be a tissue of interest to confirm an early diagnosis of MCI and AD. There is a clear need for the development of a simple, inexpensive and minimally invasive test for the diagnosis of AD, ideally at the onset of illness, or to predict the risk of developing MCI or AD. Use of the γH2AX assay to evaluate the levels of DNA DSBs in combination with the already established AD biomarkers may offer a potential route to more accurate biomarker panels and prove to be a more accurate test than any single marker to predict AD. Such high content analysis is made possible with the use of LSC. Indeed, the full automation of LSC offers an efficient, unbiased and quantifiable measure of multiple parameters in a large number of cells (thousands of

cells per individual) and should be considered as an alternative method to visual scoring in a large population-based study.

5.5 Acknowledgement

I thank Sau Lai for assisting with the preparation of preparation of lymphocytes. I thank all the participants who took part in this study and the clinicians who referred participants. Thanks to University of Adelaide registered editing service (Elite Editing) to help edit this chapter. I thank Maryam Hor for her work in assisting with recruiting, fractionating blood samples and helping out with keeping the SAND project going from its inception and maintaining the database.

Chapter 6: Summary of outcomes and conclusions

6.1 Summary of outcomes

The aim of this PhD thesis was to (i) investigate IR-induced persistent γH2AX response in Queensland fruit fly (Q-fly), (*Bactrocera tryoni*) and human buccal cells and (ii) investigate endogenous γH2AX level in buccal cells and lymphocytes of individuals with mild cognitive impairment (MCI) and AD relative to control. Knowledge of the induction, regulation and function of γH2AX foci in both *in vitro* and *in vivo* model systems is advanced, and there is an extensive literature relating to the short-term kinetics of the tissue- and cell-specific γH2AX response (Rogakou et al. 1998, Bhogal, Jalali & Bristow 2009, Madigan, Chotkowski & Glaser 2002, Roch-Lefevre et al. 2010, Sedelnikova et al. 2004, Qvarnstrom et al. 2004, Rube et al. 2008). However, much less is known about whether the presence of persistent γH2AX, as indicative of impaired DNA repair, can be used as an important parameter of retrospective irradiation exposure in insect and human cells. Linking radiation-induced DNA damage and persistent γH2AX signals is of fundamental importance to establish a molecular test capable of detecting/quantifying a prior radiation dose and the resulting DNA damage. Moreover, DNA damage has also been found to be associated with diseases of accelerated ageing and AD. However, comparatively few studies have investigated endogenous γH2AX levels in AD (Rogakou et al. 1998, Soto-Gordoa et al. 2015, Kivipelto et al. 2006, Sery et al. 2014, Suzuki et al. 2003). At present there is a need for non-invasive biomarkers and available and inexpensive diagnostic approaches, preferably using peripheral tissues. The identification of dietary risk factors for individuals at increased risk of developing MCI and AD is also essential for early diagnosis, and the initiation of

preventative treatment can be undertaken to reduce genome damage which may accelerate the onset of observable symptoms.

The results presented in this thesis offer new insight into γH2AX as a promising marker of DNA damage to measure prior radiation doses and diagnose AD. The study in Chapter 2 was designed to identify a persistent DNA damage marker in the commercially important pest Queensland fruit fly (Q-Fly; *Bactrocera tryoni*) as a model, which could be measured in tests to detect and quantify prior irradiation exposure. Q-fly are a very attractive test material because (i) Q-Fly samples can be easily irradiated with controlled conditions and (ii) the high radiation doses used for disinfestation (150 Gy) and sterile insect technique (SIT) (~70 Gy) may cause severe DNA damage, making live Q-fly samples containing severe DNA damage suitable for testing persistent DNA damage. Since there was no available γH2AX antibody specific for Q-fly at the time of initial screening (as the sequence was not known), we aimed to identify (phosphorylated) H2A sequence of *B. tryoni* using transcriptomics analysis by 454 sequencing. The Q-fly H2AX homologue was sequenced and named H2AvB (variant Bactrocera) and subsequently used to make specific γH2AvB antibodies. Persistent and dose-dependent γH2AB signals were detected and quantified either by Western blot or LSC for a significant period after irradiation treatment (up to 17 days) in histone extracts or isolated nuclei from adult Q-flies. The main findings of this study, as discussed in Chapter 2, are (i) H2AvB protein is 96.4% similar to that of the vinegar fly (a genetic model species) D. melanogaster (H2AvD), 54.8% similar to human H2AX, and identical to G. morsitans (the Savannah tsetse fly), (ii) γH2AvB is increased in crude pupal lysate following 24hr post-IR in a dose-dependent manner over 0–400 Gy and the dose dependence of this response was highly reproducible, (iii) although the γH2AvB signal in crude pupal lysate was reduced at 5 days post-IR, γH2AvB signal

significantly increased in semi-pure histone fractions and was also persistent in emergent adult Q-Fly irradiated at the pupal stage for up to 17 days, making H2AvB a good candidate for a commercial test, (v) removal of phosphorylation by treatment with alkaline phosphatase abolished the γH2AvB signal providing further evidence for the detection of the phosphorylated/active form of γH2AvB. γH2AvB signal was also detectable in eggs and larvae 24 hours after exposure to a disinfestation dose (150 Gy). A previous study in mini-pig skin cells showed that γH2AX was significantly elevated in irradiated cells after 70 days post-IR exposure compared to non-irradiated controls (Ahmed et al. 2012). Another study in mouse skin showed γH2AX signals up to 7 days post exposure and proposed that they may be used as a biodosimeter in accident scenarios (Bhogal et al. 2010). The persistent γH2AvB signals in Q-Fly could represent delayed or impaired DSB repair due to complex DNA damage involving cellular senescence, apoptosis, or DSBs that remain unrepaired in specific genome sequences, such as telomeres (Sedelnikova et al. 2004, Hewitt et al. 2012, Hewitt et al. 2012, Rogakou et al. 2000, Olive 2011). It may be possible that the clustering of damaged chromatin regions containing base lesions, DSBs, and abasic sites that are resistant to repair (Aten et al. 2004, Asaithamby, Hu & Chen 2011, Brenner, Ward 1992, Harding, Coackley & Bristow 2011). In summary, the outcomes from Chapter 2 indicated that IR exposure in Q-Fly at an early life-stage leads to persistent γH2AvB signals can easily be detected by Western blot, ELISA or quantitative immunofluorescence techniques. The γH2AvB assay has practical applications for confirming the irradiation status of live Q-Fly found in exported or imported fruits and testing irradiated flies captured during SIT eradication programmes. Indeed, the basis of this assay will be further investigated in Australian new “SITplus” consortium to identify whether γH2AvB can be used to

confirm whether unmarked flies caught in monitoring traps are released irradiated sterile fruit flies or are instead from wild type fruit flies (Merriman 2015).

Future studies should perhaps extend the time-course of the γH2AvB response following irradiation exposure to better characterise DNA repair in Q-fly. Since γH2AvB signal was detectable in the crude pupal lysate of Q-fly pupal brain and gonads, it may be worth investigating using immunohistochemistry in tissue sections or immunofluorescence techniques that detect whether γH2AvB signals in Q-Fly are the same or different in the other fabrics. Furthermore, understanding the kinetics of γH2AvB responses at different life stages (eggs, larvae, pupae, and adult) of Q-Fly after exposure to IR is warranted because if Q-Flies in the form of eggs or larvae or pupae or adult are found in exported or imported produce in quarantine facilities, the γH2AvB test may be used to confirm that the exported and imported produce had been treated with irradiation. This test may have potential to provide Australian producers with an advantage in facilitating broad use and confidence in irradiated produce. It is also important to investigate the confounding effect of other environmental challenges (such as toxins, chemicals, high and low temperature) on DNA damage in Q-fly when Q-flies are released in fruit fly epidemic areas as a part of a SIT programme or disinfestation with routine radiation doses. A key advantage of the test focusing on measuring the persistence γH2AvB is that the biomarker has been identified in many insect species and could form the basis of a similar test in other pest species such as Medfly. The next steps involve broadening the range of insects in which γH2AvB can be detected and validating/modifying the γH2AvB test for 'field conditions' so that it can be incorporated into commercial and quarantine facilities. Moreover, there is a scarcity of animal models to study the health risks of IR exposure in humans. The DSB repair kinetics (γH2AX foci loss) may be similar between humans and Q-fly. A comparative

assessment of DNA damage formation and repair kinetics using γH2AX assay in human and Q-Fly exposed *ex vivo* and *in vivo* to acute radiation doses may show similar DNA damage responses in human and Q-fly and may thus lay the ground for considering the use of common flies as an alternative animal model for γH2AX-based biodosimetry in the case of mass causality radiation exposure. It is important to note that in this study a linear dose–response of γH2AvB (0–400 Gy IR) was observed in whole Q-fly pupal lysates 24 h post-IR and was detected at doses as low as 20 Gy. It will be interesting to examine whether DNA DSB repair kinetics in Q-fly at low radiation dose (e.g. < 20 Gy or a wide range of acute doses of ionizing radiation.) based on the γ-H2AX assay, is similar to those observed in human counterparts and therefore Q-fly could be used for accurate estimations of radiation exposure during treatment decisions after accidental radiation exposure in human.

Scoring γH2AX foci has been proposed as an assay capable of quantifying DNA DSBs induced in buccal cells by IR in humans (Gonzalez et al. 2010, Yoon et al. 2009, Mondal, Ghosh & Ray 2011). Since buccal cells may be at different stages of differentiation and cell death, it is important to ensure a homogenous selection of the cells of interest to perform a reliable quantitative analysis of γH2AX signals. In all previous studies, most approaches to the γH2AX assay used a sub-population of buccal cells that were either manually scored by microscopy for the presence of individual γH2AX foci, or by measuring the relative intensity of γH2AX staining within a nucleus (Gonzalez et al. 2010, Yoon et al. 2009, Mondal, Ghosh & Ray 2011). Counting γH2AX foci by visual scoring is time-consuming and may become tiresome if many samples must be analysed and may cause variation when multiple scores are involved due to scorer fatigue. At the time of the studies reported in this thesis, there was no method available to quantify total γH2AX signals in large numbers of heterogeneous

buccal cell populations. In Chapter 3, buccal cells were separated based on their DNA content, and nuclear shape by LSC and a fully automated γH2AX quantification method was developed to quantify the levels of γH2AX in irradiated buccal cells. The hypothesis was that human buccal cells have different DNA contents and nuclear shapes and exhibit differences in their response to DNA damage induction and subsequent repair. LSC was used to analyse the γH2AX response in a large number of heterogeneous populations of buccal cells. The radiation-induced γH2AX response was shown to be persistent in human buccal cells when measured by LSC and visual scoring methods. γH2AX signals in human buccal cells following exposure to IR were detected and quantified either by visual scoring or LSC for up to 24 hours after exposure to IR. The main findings of this study, as discussed in Chapter 3, are as follows:

(i) γH2AX signals in human buccal cells increased in a dose-dependent manner for 30 minutes following exposure to 0, 1, 2 or 4 Gy of IR.

(ii) LSC and visual scoring methods correlated well when measuring γH2AX signals in non-irradiated and irradiated buccal cells

(iii) buccal cells exposed to IR exhibit elevated levels of γH2AX signal compared to the levels seen in non-irradiated controls for up to 24 h

(iv) the persistent γH2AX response remained dose-dependent and was measurable by both LSC and visual scoring methods

(v) buccal cells with different nuclear shapes (round, long, oval) were classified by visual scoring and LSC and the results showed that γH2AX responses vary in different nuclear shapes.

The number of baseline γH2AX foci number/cell varies greatly across publication and very few papers described their scoring limitation. For example, in non-irradiated buccal cells, using manual scoring on images the baseline γH2AX foci/nucleus varies from 0.08 to 4.08 foci/nucleus (Gonzalez et al. 2010). Therefore, the knowledge of baseline γH2AX foci response in a large population-based study is valuable in examining inter-individual radiosensitivity. In our study, the variation of baseline (0 Gy) γH2AX signals was substantial between individuals and indeed that reflected on IR-induced γH2AX signal (i.e. the individuals with the highest 2N γH2AX signals at baseline (0 Gy) showed the least IR-induced γH2AX response relative to the individuals with the lowest baseline γH2AX values showed the greatest IR-induced γH2AX signal). Since all published studies scored less number of buccal cells (e.g. 25-100 buccal cells) to obtain baseline γH2AX foci number (Gonzalez et al. 2010, Yoon et al. 2009), and the fact that heterogeneous populations of buccal cells may contain both diffuse and discrete foci, a method to quantify total γH2AX signal in a large population of buccal cells was needed. In chapter 3, using LSC and average of thousands of buccal nuclei were scored for detection of γH2AX signals (Gonzalez et al. 2010, Yoon et al. 2009). A significant amount of inter-individual variation, particularly at baseline (0 Gy) could be the reason why the IR group in 6 individuals had no significance in dose response. One potential explanation for high baseline level of γH2AX in human buccal cells may include decrease or increase in γH2AX kinases (DNA-PK, ATM, and ATR) / phosphatase (PP2A) activity among individuals. Genomic instability, repair deficiency (e.g. BRCA1 and DNA-PK deficient cells), P53 deficiency, cellular senescence and telomere dysfunction have been shown to be associated with increased level of baseline γH2AX signals (Yu et al. 2006, Warters et al. 2005, Nakamura et al. 2009, Bartkova et al. 2010). Further research is therefore needed to elucidate whether these factors also

contribute to inter-individual variation of baseline γH2AX signals in buccal cells. In addition, it is also important to investigate whether the γH2AX foci loss corresponds to the rate of DSBs repair in human buccal cells. The confounding effect of inter-individual variation of baseline γH2AX signals in buccal cells and its effect on IR–induced γH2AX response is most important since this may ultimately be the critical parameter affecting the radiation biodosimetry outcomes and limit the use of γH2AX in buccal cells for this purpose. Therefore, knowledge on baseline frequency of γH2AX signals in buccal cells from a large cohort would facilitate reliable dose estimation and radiation triage.

The LSC method developed and described in this thesis is capable of separating a large number of buccal cells based on their DNA content as well as nuclear shapes and simultaneously quantifying total γH2AX signal in non-irradiated and irradiated buccal cells. γH2AX signal increased significantly in all individual's 2N nuclei 30 min post-IR and was similar for round, long and oval shaped nuclei. Buccal cells with high nuclear to cytoplasm ratio have been categorized as basal buccal cells and separated from the differentiated cell (Gonzalez et al. 2010, Thomas et al. 2008). Further study should explore whether LSC is capable of quantifying γH2AX signals in the basal buccal cells. This could be achieved by incorporating antibody specific to basal cell marker combined with a multifluorescence analysis.

The first attempt to measure the relative intensity of γH2AX in buccal cells were made by Yoon et al. In that study buccal cells of individuals undergoing routine dental radiographic were examined (Yoon et al. 2009). The relative intensity of diffusive γH2AX foci intensity in 25-30 randomly selected buccal cells per individuals were measured using a high–power field (400 x magnifications) combined with a cell

measurement software package (Cell Analysis System CAS 200 optical microscope, Becton Dickinson, San Jose, CA). The method that we developed using LSC measured the total γH2AX signals within nuclei and simultaneously provided the DNA content information of individual nuclei. Individual data points of γH2AX integral, yH2AX area, γH2AX MaxPixel, nuclear integral and nuclear area of each nuclear event were automatically generated using the iCyte® 3.4 software.

It is unclear whether the number of buccal cells analysed to quantify radiation-induced DNA damage in previous studies is sufficient to obtain an accurate representation of the entire sample population's γH2AX response (Gonzalez et al. 2010, Yoon et al. 2009, Mondal, Ghosh & Ray 2011) or whether buccal cells from different sub-populations and with different nuclear shapes exhibit differences in their response to DNA damage and subsequent repair. In an attempt to provide a better understanding of the radiation-induced γH2AX response in human buccal cells, LSC was used to measure multiple parameters (area, integral, MaxPixel) of the γH2AX signals as well as the ploidy and nuclear shapes in thousands of cells, as shown in Chapter 3. Besides measuring γH2AX signals in nuclei with different DNA content, another novel finding of the study in Chapter 3 was that different shaped buccal cell nuclei (round, long, and oval) were classified, and the γH2AX signals were significantly increased in a dose-dependent manner in cells of all nuclear shapes, suggesting that regardless of the nuclear shapes analyzed, IR-induced γH2AX signals are present in all nuclei.

Visual scoring results showed a significantly higher frequency (%) of buccal cells containing 15–30 γH2AX foci up to 24 hours following exposure to 4 Gy of IR compared to than the non-irradiated control cells. Consistent with visual scoring, the LSC analysis also showed elevated levels of γH2AX than those seen in the non-

irradiated cells at 24 hours after exposure to IR. In a previous study, the longest time point to measure persistent γH2AX in buccal cells was 5 hours, whereas the current study showed for the first time that the DNA damage response as indicated by γH2AX signals after exposure to IR in the buccal cell is not fully repaired and may persist up to 24 hours. The persistent γH2AX signals in buccal cells 24 hours after 4 Gy IR are likely to be an indicator of delayed or impaired repair due to complex DNA damage, which may be lethal for the cell. Several studies reported that persistent γH2AX signals more than background levels (γH2AX signals in non-irradiated control) at 24 hours after IR exposure may be dead and dying cell (Tanaka et al. 2007, Bhogal et al. 2010, Olive 2011). In this study, 24 hours was considered long enough to provide adequate time for DNA damage repair. It is possible that the cells that scored positive for γH2AX foci 24 hours after IR exposure may be dying by apoptosis, or senescence (Olive 2011). It would be valuable in future studies to combine γH2AX detection with simultaneous expression of senescence cell markers (e.g. p21WAF1, p16INK4a or p27KIP1 cyclin kinase inhibitor) or apoptosis marker (e.g. caspase-3) for a better understanding of the biology of DNA damage response of buccal cells.

The persistent γH2AX signal in the buccal cell up to 24 hours after IR exposure has implications for biodosimetry following a radiation accident. Since human buccal cells are relatively easy to sample and sampling causes minimal discomfort, the presence of persistent γH2AX signals in buccal cells after accidental radiation exposure may enable retrospective estimation of the radiation dose exposure and extent of damage to cells. The same approach could be used to determine inter-individual variation in radiation sensitivity which would allow tailored treatment design for each patient. However, it is important to note that high background levels of γH2AX signals make it difficult to score radiation-induced persistent γH2AX foci accurately. It is also important to

determine the limitations of LSC to identify the weaknesses and advantages of this technique compared with previously published findings from buccal cells using visual scoring (Gonzalez et al. 2010, Mondal, Ghosh & Ray 2011). It is evident from this study that the major advantage of LSC is the automated γH2AX quantification, allowing the unbiased and objective analysis of hundreds or thousands of cells.

It will be of interest to investigate the threshold of γH2AX detection by the LSC technique, i.e., the minimum dose of IR that can produce a γH2AX signal detectable by LSC. A previous study has shown that the enumeration of γH2AX foci allowed the detection of DNA damage after dental x-ray examination (2.34 cGy) (Yoon et al. 2009). Thus, further studies should investigate whether the LSC method can detect γH2AX induced by doses of IR lower than 1 Gy in buccal cells (i.e., the radiation doses for x-rays, CT scans, and radiotherapy). It is important to determine further why the basal frequency of γH2AX foci differs between individuals and the extent to which it is affected by genetic, environmental, lifestyle and dietary factors. A previous study in leukapheresis derived mononuclear cells indicate that the average number of γH2AX foci per cell increases with age up to 57 years and then remained relatively stable up to the age of 83 (Schurman et al. 2012). A study investigating baseline γH2AX signals and the extended time-course kinetics of persistent γH2AX signals in buccal cells across a large range of ages in healthy participants from both genders would give new insight into the effects of age on γH2AX levels.

Chapters 4 and 5 explored the levels of endogenous γH2AX signals in combination with nuclear parameters using both multi-parameter LSC and visual scoring in buccal cells and lymphocytes of control, MCI and AD patients. Previous studies conducted in AD patients showed that the γH2AX signals are significantly elevated in the astrocytes of

AD patients in comparison to healthy controls, as well as being elevated in diseases related to accelerated ageing (e.g., Werner syndrome, obesity, diabetes, sleep apnea, prostate cancer, cataract disease, hypertension, and Hutchinson–Gilford progeria syndrome) (Myung et al. 2008, Sedelnikova et al. 2008, Schurman et al. 2012, Silva et al. 2014). The main findings described in Chapters 4 and 5 are that the levels of γH2AX signals in buccal cells and lymphocytes of AD patients were significantly elevated, compared with cells from MCI patients and healthy controls. Moreover, there was a linear trend in this increase from the control group through the MCI and AD groups. Increased nuclear circularity (i.e. irregular nuclear shape) was observed in buccal cells from AD patients compared to those from healthy controls, and a positive correlation was found between nuclear circularity and the γH2AX levels in the different types of nuclei analysed. Previous studies indicate that altered plasma homocysteine, creatinine, GFR, CHI3L1 levels is associated with the development of dementia and Alzheimer's disease (Smith 2008, Choi, Lee & Suk 2011, Zhuo, Wang & Pratico 2011, Wald, Kasturiratne & Simmonds 2011, Ng et al. 2014, McIlroy et al. 2002). Significant correlations were observed between lymphocyte γH2AX signals and other blood parameters (i.e., plasma homocysteine, creatinine, GFR, CHI3L1). Interestingly, there was a negative correlation between the γH2AX signals and MMSE scores. It is plausible that the increased levels of γH2AX signals in buccal cells of AD patients is a consequence of defective ability to efficiently repair endogenous DNA DSBs, leading to an accumulation of unrepaired DSBs on telomeres, genomic instability, repair deficiency, p53 mutation, replication stress, senescence, and telomere dysfunction that is reflected in persistent γH2AX signals and may be associated with the pathogenesis of AD (Fumagalli et al. 2012, Hewitt et al. 2012, Yu et al. 2006, Warters et al. 2005, Nakamura et al. 2009, Olive 2009, Rossiello et al. 2014). Therefore, the results from

Chapters 4 and 5 raise the intriguing possibility that the levels of γH2AX signals could provide an additional biomarker for identifying individuals with MCI and AD and possibly those at risk of developing dementia.

Of particular interest is that irregular nuclear shapes as measured by nuclear (circularity) in buccal cells were increased significantly in AD cells compared to control cells, and a significant positive correlation was also observed between nuclear circularity and γH2AX levels in the different types of nuclei analysed. The irregular nuclear shapes in AD cases could represent the accumulation of DNA damage which resulted in morphometric and cytometric alterations in the buccal mucosa cells of AD patients. It has been proposed previously that DNA damage increases in buccal cells from AD patients (Thomas et al. 2007); however, the link between accumulation and DNA damage and altered nuclear shape is unknown. It has been reported that nuclear and cell structure of buccal cells is altered with increasing age (Donald et al. 2013, Williams, Cruchley 1994) whilst this study suggests that irregular nuclear shapes of buccal cells is associated with MCI and AD patients which may result from the accumulation of DSBs that may cause instability in chromosome territories and interaction of DNA with the nuclear membrane. Additionally, the positive correlation between nuclear circularity and γH2AX in buccal cells of AD patients observed in this study could be primarily due to deficient nuclear lamina structure thus contributing to telomere dysfunction (Smogorzewska et al. 2002, Gonzalo 2014, Gonzalez-Suarez et al. 2009). Irregular nuclear shape and γH2AX should be investigated further and future studies should determine whether nuclear circularity coupled with multiple DNA damage markers (e.g., γH2AX, 8HOdG) is associated with telomere dysfunction and AD-specific markers (e.g., putative tau, Aβ) in buccal cells from a large patient cohort to improve

the predictive capacity of diagnosing risk for AD and MCI in apparently healthy controls.

Nutrients and metabolic biomarkers, including plasma homocysteine, creatinine, GFR and CHI3L1, have been shown to be associated with progression of cognitive decline and development of AD (Smith 2008, Choi, Lee & Suk 2011, Zhuo, Wang & Pratico 2011, Ng et al. 2014). Previous studies have reported that examining multiple biomarkers in combination improves the demarcation between healthy controls and memory-impaired individuals (Doecke et al. 2012, Faux et al. 2011, Mapstone et al. 2014). The study as described in Chapter 5 has shown significant correlations between lymphocyte γH2AX levels and other blood parameters that were available from the SAND database (i.e. plasma homocysteine, creatinine, GFR, CHI3L1). These results illustrate the strong link between various blood parameters and genome health and also support the notion of the usefulness of peripheral biomarkers of AD (Francois et al. 2014a, Francois et al. 2014b). Therefore, it would be necessary to incorporate several known nutrients and metabolic biomarkers, including plasma homocysteine, creatinine, GFR, and CHI3L1, with the γH2AX parameters in future studies. These could be combined to create a panel of biomarkers to improve the diagnostic power for the early detection of MCI and AD. This biomarker panel could also provide useful information on the nutritional and metabolic status of those at risk of developing AD, thus allowing preventive measures to be taken, including dietary and lifestyle interventions. It is important to test this biomarker panel in large prospective cohorts to access its suitability for the identification of those in the early stages of MCI and AD. Moreover, it would be valuable for future studies to test the biomarker panel in different cell sub-types (e.g., B and T lymphocytes) to improve the likelihood of identifying AD patients.

Chapters 4 and 5 report exciting preliminary data that show that there is an increased level of DNA damage, as measured by γH2AX, in buccal cells and lymphocytes of AD patients relative to those observed in cells from MCI patients and healthy controls, which opens the opportunity to consider using human buccal cells and lymphocytes as a reliable source of samples as an adjunct for the early diagnosis of AD. The effect of DNA damage in AD and response of cell to repair damaged DNA is of fundamental importance for better understanding of the molecular mechanisms involved in individuals prone to undergo neurodegeneration, such as AD individuals. The molecular mechanism of neurodegeneration in AD has been extensively investigated with a particular focus on oxidative DNA damage and repair. Reactive oxygen species (ROS) are produced during normal cellular metabolism as well as respiratory cycle in mitochondria. The consequence of ROS production involves modification of cellular biomolecules, such as DNA, protein, and lipids. The effects of ROS also include abnormal cellular function by impacting upon telomeres, microsatellite sequences, promoters and sites of methylation. (Evans, Cooke 2004, Evans, Dizdaroglu & Cooke 2004). It has been reported that lymphocytes of AD patients have significantly higher oxidized purine 8OHdG level than control (Mecocci et al. 1998, Gedik, Wood & Collins 1998). The elevated level of oxidized purines in AD patients may be due to either increased susceptibility of AD lymphocytes to ROS, or the increased oxidative stress. Repair of DNA DSBs in mammalian cells is accomplished through two major pathways (i) Non-Homologous End Joining (NHEJ) and (ii) Homologous Recombination (HR) (Khanna, Jackson 2001). In HR, a homologous DNA template is required for repair while NHEJ does not depend on sequence homology. Therefore, NHEJ tends to be a more error-prone repair pathway than HR. To repair DSB, initially, Ku70 and Ku80 form a heterodimer at the termini of the DSB. DNA-PKcs is then

recruited to form a complex with the Ku heterodimer and DNA ligase IV and XRCC4 then ligase the ends of the DSB (Khanna, Jackson 2001, Valerie, Povirk 2003). It has been reported that Ku DNA binding activity is reduced in the postmortem AD mid-frontal cortex (Love, Barber & Wilcock 1999). Poly (ADP-ribose) polymerase (PARP) is one of the DNA repair enzymes that is activated after DNA DSBs. A Higher proportion of PARP and poly(ADP-ribose) was observed in immunolabelled neurons of AD than in controls (Love, Barber & Wilcock 1999). The Mre11 protein complex consisting of Rad50, Mrel 1 and Nbsl plays an integral role in repairing damaged DNA (Jacobsen et al. 2004). The reduced level of Mre11 protein complex protein has been reported in the neuron of AD cortex suggesting that the elevated level of DNA damage in AD neuron may be associated with reduced level of Mre11 1 protein complexes (Jacobsen et al. 2004). Putting together literature data including oxidative-induced DNA damage and absence or failure of the repair enzymes in AD and our findings (the presence elevated level of DNA DSBs as measured by γH2AX assay) in lymphocytes and buccal cells of AD patients, lead us to consider that accumulation of DNA damage in cells may result in the loss of cellular function which may be the causative factor in the pathogenesis of AD. The next step is to perform a large cohort study to combine the γH2AX assays with other cellular markers of apoptosis and intracellular signaling into "high content assays" using the LSC protocol. Also, to better assess the impact of cell death and senescence resulting from increased chromosomal aberrations, tests measuring apoptosis, micronuclei and changes in the kinase and phosphatase activities that affect the endogenous γH2AX levels should be included in the γH2AX assays to define the precise mechanisms of DNA damage better.

Telomere dysfunction, resulting from erosion, breakage-fusion-bridge cycles, or other mechanisms, has been associated with chromosome instability and cancer progression

(Murnane 2012). A previous study in several melanoma cell lines showed that dysfunctional telomeres could be responsible for the elevated levels of endogenous γH2AX foci (Warters et al. 2005). DNA damage at telomeres is refractory to repair, whether the DNA damage is endogenously (e.g., from telomere shortening, replication stress) or exogenously (e.g., X-rays) induced (Fumagalli et al. 2012, Hewitt et al. 2012). Irreparable damage in telomeres is associated not only with replicative cellular senescence but also with oncogene- and DNA damage-induced cellular senescence (Rossiello et al. 2014). Increased background levels of γH2AX or the presence of DSBs on telomere ends may be indicative of replicative senescence, including premature senescence induced by anticancer drugs (Roninson 2003) or cancer progression. Future studies should investigate whether telomere shortening is linked with excessive endogenous γH2AX foci in buccal cells and lymphocytes of those individuals who are at increased risk of developing MCI and AD.

It is clear that more studies are required to establish baseline values of γH2AX as a marker of DNA damage in human populations. There is mounting evidence that two types of γH2AX foci exist, those that are transient in nature (up to several hours in duration), and those foci persist for weeks and months (Markova, Torudd & Belyaev 2011, Ahmed et al. 2012, Siddiqui et al. 2013). It is important to distinguish between each of these types of γH2AX foci in DNA damage repair kinetics since both provide very different information about the nature of DNA damage that the cell has experienced. For example, when lymphocytes are first isolated from the blood of patients it could be envisaged that transient foci are indicative of a recent acute damaging event, whether that be endogenous or exogenous, and demonstrates that the cell is currently in the process of repairing the double-stranded DNA lesion. On the other hand, accurately identifying those γH2AX foci that remain persistent may provide

information on DSBs that remain unresolvable, perhaps due to DNA repair defects or complexity of the lesion or DSBs in regions of the genome where repair of DSBs is limited, such as telomeres. Indeed, it is also essential to eliminate confounders such as cells undergoing apoptosis, although simple morphological criteria could be used to identify these cells. Determining whether a γH2AX focus indicates the site of a current or past DSB will require a reliable technique. It would be advantageous to build into the γH2AX assays some reporter of the transient vs. persistent DNA damage. Alternatively, upon isolation of lymphocytes from blood, the cells may be cultured for a further 24 hours to allow ample time for dephosphorylation and clearing of any existing transient γH2AX signals, potentially leaving only the residual (persistent) γH2AX foci associated with the DNA. Another possibility is to use confocal microscopy or other techniques to determine the size of γH2AX foci and genome location (e.g. co-localization with telomeres) as a marker for persistent damage. Furthermore, measuring the spatial proximity of γH2AX in nuclei may identify potential clustering of γH2AX foci at the nuclear envelope and therefore provide additional evidence of persistent DNA damage at telomeres given that telomere repeats have been located in the proximity of the nuclear envelope (Hoze et al. 2013).

The highly dynamic changes of foci number and foci size over time after treatment with radiation or cytotoxic compounds can make the visual scoring time-consuming, potentially subjective, operator-dependent, and may involve fluorescence bleaching due to extended evaluation time, and therefore unsuitable for high-throughput applications. One of the main issues when scoring multiple foci is the phenomenon of foci overlap that can lead to dose-response curves that give false saturation when γH2AX becomes more difficult to distinguish as discreet entities (foci). Therefore, counting overlapped γH2AX foci may not provide an accurate representation of the entire sample

population's γH2AX signal, and this needs to be accounted for in studies scoring γH2AX foci. LSC collects fluorescence signal through the nuclei, making it a useful method for obtaining total integral or intensity and can be used to measure any subtle changes among individuals. However, this approach may be somewhat less accurate for scoring individual γH2AX foci, particularly if two or more foci are spatially arranged in the same vertical plane. Several image analysis solutions for automated foci scoring have been developed, but are restricted to a low IR dose resulting in discrete scoreable foci within the nuclei. In this case, measurement of total γH2AX intensity using Western blot or flow cytometry techniques may be sufficient to measure the DNA damaging effects by quantifying the γH2AX signals. This thesis (Chapter 3) showed that in some buccal cell sub-types (unlike other cells types, such as lymphocytes, cultured cells etc.), γH2AX foci can be numerous at baseline, and as a result they tend to have a diffuse staining pattern, making the γH2AX foci completely indistinguishable (Siddiqui et al. 2015). Further, results in Chapter 5 showed that the overlapping γH2AX foci in some lymphocytes often lead to difficulty in obtaining an accurate number of the foci/nucleus in the entire sample population. It has been suggested that the large endogenous γH2AX foci observed in mouse embryonic stem cells may be a result of histone hyperacetylation and abundant chromatin-remodeling complexes (Banath et al. 2009).

While transient IR-induced γH2AX signals are rapidly lost over time by dephosphorylation processes, the persistent γH2AX signals are detectable for several days after IR exposure. Therefore, a simple, standardised γH2AX detection technique is required to rapidly identify individuals exposed to critically high radiation doses so that initial triage and medical treatment can be made. Although the confocal microscopy technique enables high-resolution 3D imaging thus allowing γH2AX detection for many

days after IR exposure (Bhogal et al. 2010), the time required for image analysis of individual γH2AX foci would need optimisation when using such techniques in radiation biodosimetry. In a recent study, a rapid '96-well lyse/fix' method was developed to measure γH2AX foci from finger-pricked blood samples with an estimated processing time of about 4 hours for 96 samples compared to 15 hours using the routine protocol (Moquet, Barnard & Rothkamm 2014). This protocol may be further modified by incorporating the simultaneous measurement of other cellular proteins/markers involved in DNA damage/repair signaling allowing accurate detection of persistent γH2AX in a large number of samples. The latter protocol may be better suited in the event of large-scale radiation emergency; since reliable measurement of prior radiation doses is required for population triage during the first few hours of a large-scale radiation emergency. Another study demonstrated that automated analysis of γH2AX using the AKLIDES platform is a rapid, efficient and reliable method to assess DNA DSB, requiring a minimum of 3 minutes for image acquisition and analysis of γH2AX foci for 100 cells per sample (Reddig et al. 2015). In the AKLIDES method, the threshold size of γH2AX foci was set in the range 0.25–1.2 μm. However, γH2AX foci that exceeded the maximum size of 1.2 μm were categorised as 'clusters'. To approximate individual foci, they took the area of the cluster and divided by the mean focus size to obtain the estimated average number of foci in a specific cluster. This feature of the AKLIDES platform in evaluating clusters or overlapping γH2AX foci appeared to work well under their assay conditions and may need to be further investigated to be able to be used reliably for the clinical diagnosis of persistent DNA DSBs (Reddig et al. 2015). The RABiT (Rapid Automated Biodosimetry Tool for Radiological Triage), is a fully automated high-throughput robotic system designed to measure γH2AX in lymphocytes present in a single drop of blood from a fingerstick in a

precise and fast manner (capable of processing up to 30,000 samples per day) (Turner et al. 2011, Garty et al. 2010) and could also be of interest to investigate persistent DNA DSBs.

Common immunofluorescence techniques allow the researcher to gain information on persistent γH2AX at equilibrium (essentially a snapshot in time). A better approach for analysing the persistence of these DSBs and also the origin and relative kinetics of endogenous foci is to generate cells (in vitro) with a fluorescent-tagged protein (such as GFP-labelled 53BP1). This protocol allows visualisation of the damaged site and enables one to monitor their repair in living cells (Bekker-Jensen et al. 2006, Mari et al. 2006). A novel approach to such imaging γH2AX quantification of DSBs in live mammalian cells has been described using bifragment luciferase reconstitution (Li et al. 2011). N- and C-terminal fragments of firefly luciferase genes were fused with H2AX and MDC1 genes, respectively. In mammalian cells following DSB formation, H2AX was rapidly phosphorylated and then physically associated with the MDC1 protein, thus joining N- and C-luciferase fragments together and ultimately resulting in reconstitution of luciferase activity which was assayed by analysing serial images at different time-points after radiation. This method for imaging γH2AX–MDC1 interaction was used for non-invasive evaluation of DSBs repair kinetics in vivo in tumour exposed to X-rays and 56Fe ions over 2 weeks (Li et al. 2011). This approach can be an alternative for experiments requiring observations of DSB induction and repair over an extended period of time (Li et al. 2011). Another method was developed that incorporated fluorophore- and radioisotope-labelled immunoconjugates which involved modification of anti-γH2AX antibodies to track in vivo damage in tumours (Cornelissen et al. 2011). Thus radioimmunoconjugates that target γH2AX as a real-time non-invasive imaging method to monitor DNA damage both in vivo and in vitro, would be useful to diagnose

susceptibility of cancer cells to DSB undergoing radiotherapy and to monitor treatment. A standard method in biological dosimetry includes cytogenetic analysis in which chromosome aberrations such as translocation, dicentric chromosomes, and micronuclei are scored in peripheral blood lymphocytes. These types of methods require growth stimulation of lymphocytes for at least 48-72 hours since chromosomal damage can only be measured following ex vivo cell division (Leonard et al. 2005, Kleinerman et al. 2006, Pinto, Santos & Amaral 2010). Thus, in the scenario of population triage during the first few hours after accidental catastrophic radiation exposure (when the physical dose is unavailable) a rapid enumeration of the level of exposure to the individual is required. The γH2AX assay has emerged as a useful measurement for the rapid identification of the retrospective estimation of IR dose exposure. Additionally, the γH2AX assay is highly sensitive to detect DNA damage induced by IR as low as 1.2 mGy (Rothkamm, Lobrich 2003). However, it is limited by inter-individual variability in kinetics of repair and results will vary depending on the time-frame of radiation exposure and blood collection. For this reason, it is more likely that an approach based on measuring persistent γH2AX may prove to be a superior diagnostic of radiation exposure. The levels of H2AX protein have been reported to vary by a factor of up to ten between different cell types; however, the level of variation in blood cells such as lymphocytes is not known (Rothkamm, Horn 2009). Thus, there is a possibility that biological variation occurs in the levels of induced phosphorylated H2AX (γH2AX) at DSB sites in individuals at risk of developing AD or exposed to accidental radiation exposure. This could for instance be due to difference in the number of γH2AX foci formed at a given DNA damage level or inefficiency of cell to convert DSBs to γH2AX foci. Another possibility could be the number of γH2AX molecules produced per DSB varies among individuals. Therefore, it is necessary to determine the baseline numbers

of γH2AX foci/nucleus prior to monitoring the number of radiation-induced or AD-related γH2AX foci level. Given the growing interest in the automation of counting γH2AX for practical applications (e.g., chemotherapy patient management), it is important to optimise the time required to process and analyse the assay results. However, it is yet to be determined whether this can be applied to routine clinical studies involving the diagnosis of AD or retrospectively assess if a living organism has been previously irradiated at precise radiation doses.

6.2 Conclusion

Quantification of the γH2AX response offers a highly sensitive and specific assay for detecting DNA DSB formation and repair. Although the available evidence supports the view that the majority of IR-induced DSBs are rapidly repaired, a small proportion may remain unrepaired, leading to a long-term persistent γH2AX response. This persistent expression of γH2AX varies in different tissues and may be affected by the genomic status and the type of DNA damage. Several studies have demonstrated that IR-induced γH2AX responses may persist for extended periods of time and that this persistent γH2AX expression tends to occur in the telomeric DNA and cells undergoing senescence. For the effective measurement of the γH2AX response, criteria are required to distinguish persistent γH2AX foci from transient foci. Furthermore, the variable γH2AX response to IR exposure between different cell/tissue samples should be taken into consideration when using the γH2AX assay for radiation biodosimetry and the estimation of persistent DNA damage. Understanding the impact of persistent DNA DSBs, the mechanisms that create and maintain them, and genomic instability in relation to the development of AD is an important area in the search for an early diagnostic test for AD. Moreover, the measurement of persistent γH2AX signals provides an indicator of unrepaired DNA DSBs, which is an important parameter to either determine prior radiation doses or predict the effect of radiation exposure at the genome level. This will allow the initiation of treatment and monitoring for the genotoxic effects of radiation.

This research study has opened up new opportunities in radiation biodosimetry and the early diagnosis of neurodegenerative diseases, such as MCI and AD, based on the findings that the γH2AX assay has the potential for the detection and quantification of

persistent γH2AX in pest fruit flies and human buccal cells. The γH2AX response and its subsequent decline detected in human buccal cells varies between individuals, but remains elevated above baseline levels and can be measured by automated LSC and visual scoring methods. Both lymphocytes and buccal cells of individuals with AD exhibited elevated levels of γH2AX, and it is feasible for the accurate diagnosis of genomic DNA damage, as indicated by DNA DSBs, to be correlated with different blood parameters in AD patients. Determining the levels of γH2AX in buccal cells and lymphocytes has potential clinical benefits, in that determining baseline γH2AX, expression levels may contribute to identifying individuals at risk of developing MCI and AD, as well as monitoring disease progression. A further potential application of quantifying γH2AX foci may be an early indicator of age-related disease risk, as an alteration in genomic integrity due to DSBs may accelerate ageing. The relationship between persistent γH2AX foci and telomere length and function requires further investigation to understand better telomere γH2AX biology and whether there are other regions of the genome (e.g. centromeres) where γH2AX accumulates and persists. With further research, it may be possible to determine baseline values of γH2AX in populations more reliably.

References

Abramoff, M.D., Magalhaes, P.J. & Ram, S.J. 2004, "Image processing with ImageJ", *Biophotonics International,* vol. 11, no. 7, pp. 36-42.

Ahmed, E.A., Agay, D., Schrock, G., Drouet, M., Meineke, V. & Scherthan, H. 2012, "Persistent DNA damage after high dose in vivo gamma exposure of minipig skin", *PloS one,* vol. 7, no. 6, pp. e39521.

Ahmed, E.A., van der Vaart, A., Barten, A., Kal, H.B., Chen, J., Lou, Z., Minter-Dykhouse, K., Bartkova, J., Bartek, J., de Boer, P. & de Rooij, D.G. 2007, "Differences in DNA double strand breaks repair in male germ cell types: lessons learned from a differential expression of Mdc1 and 53BP1", *DNA repair,* vol. 6, no. 9, pp. 1243-1254.

Alessio, N., Del Gaudio, S., Capasso, S., Di Bernardo, G., Cappabianca, S., Cipollaro, M., Peluso, G. & Galderisi, U. 2015, "Low dose radiation induced senescence of human mesenchymal stromal cells and impaired the autophagy process", *Oncotarget,* vol. 6, no. 10, pp. 8155-8166.

Allgayer, H., Owen, R.W., Nair, J., Spiegelhalder, B., Streit, J., Reichel, C. & Bartsch, H. 2008, "Short-term moderate exercise programs reduce oxidative DNA damage as determined by high-performance liquid chromatography-electrospray ionization-mass spectrometry in patients with colorectal carcinoma following primary treatment", *Scandinavian Journal of Gastroenterology,* vol. 43, no. 8, pp. 971-978.

Alzheimer's Association, Thies, W. & Bleiler, L. 2011, "2011 Alzheimer's disease facts and figures", *Alzheimer's & dementia : the journal of the Alzheimer's Association,* vol. 7, no. 2, pp. 208-244.

Anderson, L., Henderson, C. & Adachi, Y. 2001, "Phosphorylation and rapid relocalization of 53BP1 to nuclear foci upon DNA damage", *Molecular and cellular biology,* vol. 21, no. 5, pp. 1719-1729.

Andratschke, N., Blau, T., Schill, S. & Nieder, C. 2011, "Late residual gamma-H2AX foci in murine spinal cord might facilitate development of response-modifying strategies: a research hypothesis", *Anticancer Research,* vol. 31, no. 2, pp. 561-564.

Andrievski, A. & Wilkins, R.C. 2009, "The response of gamma-H2AX in human lymphocytes and lymphocytes subsets measured in whole blood cultures", *International journal of radiation biology,* vol. 85, no. 4, pp. 369-376.

Ant, T., Koukidou, M., Rempoulakis, P., Gong, H.F., Economopoulos, A., Vontas, J. & Alphey, L. 2012, "Control of the olive fruit fly using genetics-enhanced sterile insect technique", *BMC biology,* vol. 10, pp. 51-7007-10-51.

Armstrong, R.A. 2006, "Plaques and tangles and the pathogenesis of Alzheimer's disease", *Folia neuropathologica / Association of Polish Neuropathologists and Medical Research Centre, Polish Academy of Sciences,* vol. 44, no. 1, pp. 1-11.

Asaithamby, A., Hu, B. & Chen, D.J. 2011, "Unrepaired clustered DNA lesions induce chromosome breakage in human cells", *Proceedings of the National Academy of Sciences of the United States of America,* vol. 108, no. 20, pp. 8293-8298.

Aten, J.A., Stap, J., Krawczyk, P.M., van Oven, C.H., Hoebe, R.A., Essers, J. & Kanaar, R. 2004, "Dynamics of DNA double-strand breaks revealed by clustering of damaged chromosome domains", *Science (New York, N.Y.),* vol. 303, no. 5654, pp. 92-95.

Aubert, G. & Lansdorp, P.M. 2008, "Telomeres and aging", *Physiological Reviews,* vol. 88, no. 2, pp. 557-579.

Bader Lange, M.L., St Clair, D., Markesbery, W.R., Studzinski, C.M., Murphy, M.P. & Butterfield, D.A. 2010, "Age-related loss of phospholipid asymmetry in APP(NLh)/APP(NLh) x PS-1(P264L)/PS-1(P264L) human double mutant knock-in mice: Relevance to Alzheimer disease", *Neurobiology of disease, .*

Bae, N.S. & Baumann, P. 2007, "A RAP1/TRF2 complex inhibits nonhomologous end-joining at human telomeric DNA ends", *Molecular cell,* vol. 26, no. 3, pp. 323-334.

Baker, D.J., Wijshake, T., Tchkonia, T., LeBrasseur, N.K., Childs, B.G., van de Sluis, B., Kirkland, J.L. & van Deursen, J.M. 2011, "Clearance of p16Ink4a-positive senescent cells delays ageing-associated disorders", *Nature,* vol. 479, no. 7372, pp. 232-236.

Balcer-Kubiczek, E.K., Attarpour, M. & Edelman, M.J. 2007, "The synergistic effect of dimethylamino benzoylphenylurea (NSC #639829) and X-irradiation on human lung carcinoma cell lines", *Cancer chemotherapy and pharmacology,* vol. 59, no. 6, pp. 781-787.

Banath, J.P., Banuelos, C.A., Klokov, D., MacPhail, S.M., Lansdorp, P.M. & Olive, P.L. 2009, "Explanation for excessive DNA single-strand breaks and endogenous repair foci in pluripotent mouse embryonic stem cells", *Experimental cell research,* vol. 315, no. 8, pp. 1505-1520.

Banath, J.P., Klokov, D., MacPhail, S.H., Banuelos, C.A. & Olive, P.L. 2010, "Residual gammaH2AX foci as an indication of lethal DNA lesions", *BMC cancer,* vol. 10, pp. 4-2407-10-4.

Banath, J.P., Macphail, S.H. & Olive, P.L. 2004, "Radiation sensitivity, H2AX phosphorylation, and kinetics of repair of DNA strand breaks in irradiated cervical cancer cell lines", *Cancer research,* vol. 64, no. 19, pp. 7144-7149.

Bartkova, J., Hamerlik, P., Stockhausen, M.T., Ehrmann, J., Hlobilkova, A., Laursen, H., Kalita, O., Kolar, Z., Poulsen, H.S., Broholm, H., Lukas, J. & Bartek, J. 2010, "Replication stress and oxidative damage contribute to aberrant constitutive activation of DNA damage signalling in human gliomas", *Oncogene,* vol. 29, no. 36, pp. 5095-5102.

Baschnagel, A., Russo, A., Burgan, W.E., Carter, D., Beam, K., Palmieri, D., Steeg, P.S., Tofilon, P. & Camphausen, K. 2009, "Vorinostat enhances the radiosensitivity

of a breast cancer brain metastatic cell line grown in vitro and as intracranial xenografts", *Molecular cancer therapeutics,* vol. 8, no. 6, pp. 1589-1595.

Baynton, K., Otterlei, M., Bjoras, M., von Kobbe, C., Bohr, V.A. & Seeberg, E. 2003, "WRN interacts physically and functionally with the recombination mediator protein RAD52", *The Journal of biological chemistry,* vol. 278, no. 38, pp. 36476-36486.

Bekker-Jensen, S., Lukas, C., Kitagawa, R., Melander, F., Kastan, M.B., Bartek, J. & Lukas, J. 2006, "Spatial organization of the mammalian genome surveillance machinery in response to DNA strand breaks", *The Journal of cell biology,* vol. 173, no. 2, pp. 195-206.

Berkenkamp, B., Susnik, N., Baisantry, A., Kuznetsova, I., Jacobi, C., Sorensen-Zender, I., Broecker, V., Haller, H., Melk, A. & Schmitt, R. 2014, "In vivo and in vitro analysis of age-associated changes and somatic cellular senescence in renal epithelial cells", *PloS one,* vol. 9, no. 2, pp. e88071.

Bhogal, N., Jalali, F. & Bristow, R.G. 2009, "Microscopic imaging of DNA repair foci in irradiated normal tissues", *International journal of radiation biology,* vol. 85, no. 9, pp. 732-746.

Bhogal, N., Kaspler, P., Jalali, F., Hyrien, O., Chen, R., Hill, R.P. & Bristow, R.G. 2010, "Late residual gamma-H2AX foci in murine skin are dose responsive and predict radiosensitivity in vivo", *Radiation research,* vol. 173, no. 1, pp. 1-9.

Blennow, K. & Zetterberg, H. 2009, "Cerebrospinal fluid biomarkers for Alzheimer's disease", *Journal of Alzheimer's disease : JAD,* vol. 18, no. 2, pp. 413-417.

Bonner, W.M., Redon, C.E., Dickey, J.S., Nakamura, A.J., Sedelnikova, O.A., Solier, S. & Pommier, Y. 2008, "GammaH2AX and cancer", *Nature reviews.Cancer,* vol. 8, no. 12, pp. 957-967.

Bouquet, F., Muller, C. & Salles, B. 2006, "The loss of gammaH2AX signal is a marker of DNA double strand breaks repair only at low levels of DNA damage", *Cell cycle (Georgetown, Tex.),* vol. 5, no. 10, pp. 1116-1122.

Bourton, E.C., Plowman, P.N., Smith, D., Arlett, C.F. & Parris, C.N. 2011, "Prolonged expression of the gamma-H2AX DNA repair biomarker correlates with excess acute and chronic toxicity from radiotherapy treatment", *International journal of cancer.Journal international du cancer,* vol. 129, no. 12, pp. 2928-2934.

Braak, H. & Braak, E. 1991, "Demonstration of amyloid deposits and neurofibrillary changes in whole brain sections", *Brain pathology (Zurich, Switzerland),* vol. 1, no. 3, pp. 213-216.

Bracalente, C., Ibanez, I.L., Molinari, B., Palmieri, M., Kreiner, A., Valda, A., Davidson, J. & Duran, H. 2013, "Induction and persistence of large gammaH2AX foci by high linear energy transfer radiation in DNA-dependent protein kinase-deficient cells", *International journal of radiation oncology, biology, physics,* vol. 87, no. 4, pp. 785-794.

Brenner, D.J. & Ward, J.F. 1992, "Constraints on energy deposition and target size of multiply damaged sites associated with DNA double-strand breaks", *International journal of radiation biology,* vol. 61, no. 6, pp. 737-748.

Broers, J.L., Ramaekers, F.C., Bonne, G., Yaou, R.B. & Hutchison, C.J. 2006, "Nuclear lamins: laminopathies and their role in premature ageing", *Physiological Reviews,* vol. 86, no. 3, pp. 967-1008.

Brzozowska, K., Pinkawa, M., Eble, M.J., Muller, W.U., Wojcik, A., Kriehuber, R. & Schmitz, S. 2012, "In vivo versus in vitro individual radiosensitivity analysed in healthy donors and in prostate cancer patients with and without severe side effects after radiotherapy", *International journal of radiation biology,* vol. 88, no. 5, pp. 405-413.

Bucholtz, N. & Demuth, I. 2013, "DNA-repair in mild cognitive impairment and Alzheimer's disease", *DNA repair,* vol. 12, no. 10, pp. 811-816.

Burma, S., Chen, B.P., Murphy, M., Kurimasa, A. & Chen, D.J. 2001, "ATM phosphorylates histone H2AX in response to DNA double-strand breaks", *The Journal of biological chemistry,* vol. 276, no. 45, pp. 42462-42467.

Burns, A., Byrne, E.J. & Maurer, K. 2002, "Alzheimer's disease", *Lancet,* vol. 360, no. 9327, pp. 163-165.

Cairns, N.J., Ikonomovic, M.D., Benzinger, T., Storandt, M., Fagan, A.M., Shah, A.R., Reinwald, L.T., Carter, D., Felton, A., Holtzman, D.M., Mintun, M.A., Klunk, W.E. & Morris, J.C. 2009, "Absence of Pittsburgh compound B detection of cerebral amyloid beta in a patient with clinical, cognitive, and cerebrospinal fluid markers of Alzheimer disease: a case report", *Archives of Neurology,* vol. 66, no. 12, pp. 1557-1562.

Campisi, J. 2013, "Aging, cellular senescence, and cancer", *Annual Review of Physiology,* vol. 75, pp. 685-705.

Campisi, J., Andersen, J.K., Kapahi, P. & Melov, S. 2011, "Cellular senescence: a link between cancer and age-related degenerative disease?", *Seminars in cancer biology,* vol. 21, no. 6, pp. 354-359.

Campisi, J. & d'Adda di Fagagna, F. 2007, "Cellular senescence: when bad things happen to good cells", *Nature reviews.Molecular cell biology,* vol. 8, no. 9, pp. 729-740.

Cantor, S.B. & Brosh, R.M.,Jr 2014, "What is wrong with Fanconi anemia cells?", *Cell cycle (Georgetown, Tex.),* vol. 13, no. 24, pp. 3823-3827.

Canugovi, C., Misiak, M., Ferrarelli, L.K., Croteau, D.L. & Bohr, V.A. 2013, "The role of DNA repair in brain related disease pathology", *DNA repair,* vol. 12, no. 8, pp. 578-587.

Celeste, A., Fernandez-Capetillo, O., Kruhlak, M.J., Pilch, D.R., Staudt, D.W., Lee, A., Bonner, R.F., Bonner, W.M. & Nussenzweig, A. 2003, "Histone H2AX

phosphorylation is dispensable for the initial recognition of DNA breaks", *Nature cell biology,* vol. 5, no. 7, pp. 675-679.

Chiu, S.J., Chao, J.I., Lee, Y.J. & Hsu, T.S. 2008, "Regulation of gamma-H2AX and securin contribute to apoptosis by oxaliplatin via a p38 mitogen-activated protein kinase-dependent pathway in human colorectal cancer cells", *Toxicology letters,* vol. 179, no. 2, pp. 63-70.

Choi, J., Lee, H.W. & Suk, K. 2011, "Plasma level of chitinase 3-like 1 protein increases in patients with early Alzheimer's disease", *Journal of neurology,* vol. 258, no. 12, pp. 2181-2185.

Choudhuri, R., Degraff, W., Gamson, J., Mitchell, J.B. & Cook, J.A. 2011, "Guggulsterone-mediated enhancement of radiosensitivity in human tumor cell lines", *Frontiers in oncology,* vol. 1, pp. 19.

Chowdhury, D., Keogh, M.C., Ishii, H., Peterson, C.L., Buratowski, S. & Lieberman, J. 2005, "gamma-H2AX dephosphorylation by protein phosphatase 2A facilitates DNA double-strand break repair", *Molecular cell,* vol. 20, no. 5, pp. 801-809.

Chua, M.L., Somaiah, N., A'Hern, R., Davies, S., Gothard, L., Yarnold, J. & Rothkamm, K. 2011, "Residual DNA and chromosomal damage in ex vivo irradiated blood lymphocytes correlated with late normal tissue response to breast radiotherapy", *Radiotherapy and oncology : journal of the European Society for Therapeutic Radiology and Oncology,* vol. 99, no. 3, pp. 362-366.

Chung, H.Y., Cesari, M., Anton, S., Marzetti, E., Giovannini, S., Seo, A.Y., Carter, C., Yu, B.P. & Leeuwenburgh, C. 2009, "Molecular inflammation: underpinnings of aging and age-related diseases", *Ageing research reviews,* vol. 8, no. 1, pp. 18-30.

Citron, M., Vigo-Pelfrey, C., Teplow, D.B., Miller, C., Schenk, D., Johnston, J., Winblad, B., Venizelos, N., Lannfelt, L. & Selkoe, D.J. 1994, "Excessive production of amyloid beta-protein by peripheral cells of symptomatic and presymptomatic patients carrying the Swedish familial Alzheimer disease mutation", *Proceedings of the National Academy of Sciences of the United States of America,* vol. 91, no. 25, pp. 11993-11997.

Collins, S.R., Weldon, C.W., Banos, C. & Taylor, P.W. 2009, "Optimizing irradiation dose for sterility induction and quality of *Bactrocera tryoni*", *Journal of economic entomology,* vol. 102, no. 5, pp. 1791-1800.

Cornelissen, B., Kersemans, V., Darbar, S., Thompson, J., Shah, K., Sleeth, K., Hill, M.A. & Vallis, K.A. 2011, "Imaging DNA damage in vivo using gammaH2AX-targeted immunoconjugates", *Cancer research,* vol. 71, no. 13, pp. 4539-4549.

Cox, J.D., Stetz, J. & Pajak, T.F. 1995, "Toxicity criteria of the Radiation Therapy Oncology Group (RTOG) and the European Organization for Research and Treatment of Cancer (EORTC)", *International journal of radiation oncology, biology, physics,* vol. 31, no. 5, pp. 1341-1346.

d'Adda di Fagagna, F. 2008, "Living on a break: cellular senescence as a DNA-damage response", *Nature reviews.Cancer,* vol. 8, no. 7, pp. 512-522.

d'Adda di Fagagna, F., Reaper, P.M., Clay-Farrace, L., Fiegler, H., Carr, P., Von Zglinicki, T., Saretzki, G., Carter, N.P. & Jackson, S.P. 2003, "A DNA damage checkpoint response in telomere-initiated senescence", *Nature,* vol. 426, no. 6963, pp. 194-198.

Darzynkiewicz, Z., Smolewski, P., Holden, E., Luther, E., Henriksen, M., Francois, M., Leifert, W. & Fenech, M. 2011, "Laser scanning cytometry for automation of the micronucleus assay", *Mutagenesis,* vol. 26, no. 1, pp. 153-161.

de Lange, T. 2005, "Shelterin: the protein complex that shapes and safeguards human telomeres", *Genes & development,* vol. 19, no. 18, pp. 2100-2110.

de Oliveira, R.M., Lia, E.N., Guimaraes, R.M., Bocca, A.L., Cavalcante Neto, F.F. & da Silva, T.A. 2008, "Cytologic and cytometric analysis of oral mucosa in Alzheimer's disease", *Analytical and Quantitative Cytology and Histology / the International Academy of Cytology [and] American Society of Cytology,* vol. 30, no. 2, pp. 113-118.

de Vries, H.G., Collee, J.M., van Veldhuizen, M.H., Achterhof, L., Smit Sibinga, C.T., Scheffer, H., Buys, C.H. & ten Kate, L.P. 1996, "Validation of the determination of deltaF508 mutations of the cystic fibrosis gene in over 11 000 mouthwashes", *Human genetics,* vol. 97, no. 3, pp. 334-336.

Dechat, T., Pfleghaar, K., Sengupta, K., Shimi, T., Shumaker, D.K., Solimando, L. & Goldman, R.D. 2008, "Nuclear lamins: major factors in the structural organization and function of the nucleus and chromatin", *Genes & development,* vol. 22, no. 7, pp. 832-853.

Delledonne, A., Kouri, N., Reinstatler, L., Sahara, T., Li, L., Zhao, J., Dickson, D.W., Ertekin-Taner, N. & Leissring, M.A. 2009, "Development of monoclonal antibodies and quantitative ELISAs targeting insulin-degrading enzyme", *Molecular neurodegeneration,* vol. 4, pp. 39.

Denoyer, D., Lobachevsky, P., Jackson, P., Thompson, M., Martin, O.A. & Hicks, R.J. 2015, "Analysis of 177Lu-DOTA-Octreotate Therapy-Induced DNA Damage in Peripheral Blood Lymphocytes of Patients with Neuroendocrine Tumors", *Journal of nuclear medicine : official publication, Society of Nuclear Medicine,* vol. 56, no. 4, pp. 505-511.

Dikomey, E., Dahm-Daphi, J., Brammer, I., Martensen, R. & Kaina, B. 1998, "Correlation between cellular radiosensitivity and non-repaired double-strand breaks studied in nine mammalian cell lines", *International journal of radiation biology,* vol. 73, no. 3, pp. 269-278.

Dimri, G.P., Lee, X., Basile, G., Acosta, M., Scott, G., Roskelley, C., Medrano, E.E., Linskens, M., Rubelj, I. & Pereira-Smith, O. 1995, "A biomarker that identifies senescent human cells in culture and in aging skin in vivo", *Proceedings of the National Academy of Sciences of the United States of America,* vol. 92, no. 20, pp. 9363-9367.

Djuzenova, C.S., Elsner, I., Katzer, A., Worschech, E., Distel, L.V., Flentje, M. & Polat, B. 2013, "Radiosensitivity in breast cancer assessed by the histone gamma-H2AX and 53BP1 foci", *Radiation oncology (London, England),* vol. 8, pp. 98-717X-8-98.

Doai, M., Watanabe, N., Takahashi, T., Taniguchi, M., Tonami, H., Iwabuchi, K., Kayano, D., Fukuoka, M. & Kinuya, S. 2013, "Sensitive immunodetection of radiotoxicity after iodine-131 therapy for thyroid cancer using gamma-H2AX foci of DNA damage in lymphocytes", *Annals of Nuclear Medicine,* vol. 27, no. 3, pp. 233-238.

Doecke, J.D., Laws, S.M., Faux, N.G., Wilson, W., Burnham, S.C., Lam, C.P., Mondal, A., Bedo, J., Bush, A.I., Brown, B., De Ruyck, K., Ellis, K.A., Fowler, C., Gupta, V.B., Head, R., Macaulay, S.L., Pertile, K., Rowe, C.C., Rembach, A., Rodrigues, M., Rumble, R., Szoeke, C., Taddei, K., Taddei, T., Trounson, B., Ames, D., Masters, C.L., Martins, R.N. & for the Alzheimer's Disease Neuroimaging Initiative and Australian Imaging Biomarker and Lifestyle Research Group 2012, "Blood-based protein biomarkers for diagnosis of Alzheimer disease", *Archives of Neurology,* vol. 69, no. 10, pp. 1318-1325.

Doida, Y. & Okada, S. 1969, "Radiation-induced mitotic delay in cultured mammalian cells (L5178Y)", *Radiation research,* vol. 38, no. 3, pp. 513-529.

Donald, P.M., George, R., Sriram, G., Kavitha, B. & Sivapathasundharam, B. 2013, "Hormonal changes in exfoliated normal buccal mucosal cells", *Journal of cytology / Indian Academy of Cytologists,* vol. 30, no. 4, pp. 252-256.

Douaud, G., Refsum, H., de Jager, C.A., Jacoby, R., Nichols, T.E., Smith, S.M. & Smith, A.D. 2013, "Preventing Alzheimer's disease-related gray matter atrophy by B-vitamin treatment", *Proceedings of the National Academy of Sciences of the United States of America,* vol. 110, no. 23, pp. 9523-9528.

Downs, J.A., Lowndes, N.F. & Jackson, S.P. 2000, "A role for Saccharomyces cerevisiae histone H2A in DNA repair", *Nature,* vol. 408, no. 6815, pp. 1001-1004.

Dugle, D.L., Gillespie, C.J. & Chapman, J.D. 1976, "DNA strand breaks, repair, and survival in x-irradiated mammalian cells", *Proceedings of the National Academy of Sciences of the United States of America,* vol. 73, no. 3, pp. 809-812.

Durocher, D. & Jackson, S.P. 2001, "DNA-PK, ATM and ATR as sensors of DNA damage: variations on a theme?", *Current opinion in cell biology,* vol. 13, no. 2, pp. 225-231.

Ellis, K.A., Bush, A.I., Darby, D., De Fazio, D., Foster, J., Hudson, P., Lautenschlager, N.T., Lenzo, N., Martins, R.N., Maruff, P., Masters, C., Milner, A., Pike, K., Rowe, C., Savage, G., Szoeke, C., Taddei, K., Villemagne, V., Woodward, M., Ames, D. & AIBL Research Group 2009, "The Australian Imaging, Biomarkers and Lifestyle (AIBL) study of aging: methodology and baseline characteristics of 1112 individuals recruited for a longitudinal study of Alzheimer's disease", *International psychogeriatrics / IPA,* vol. 21, no. 4, pp. 672-687.

Endt, H., Sprung, C.N., Keller, U., Gaipl, U., Fietkau, R. & Distel, L.V. 2011, "Detailed analysis of DNA repair and senescence marker kinetics over the life span of a human fibroblast cell line", *The journals of gerontology.Series A, Biological sciences and medical sciences,* vol. 66, no. 4, pp. 367-375.

Evans, M.D. & Cooke, M.S. 2004, "Factors contributing to the outcome of oxidative damage to nucleic acids", *BioEssays : news and reviews in molecular, cellular and developmental biology,* vol. 26, no. 5, pp. 533-542.

Evans, M.D., Dizdaroglu, M. & Cooke, M.S. 2004, "Oxidative DNA damage and disease: induction, repair and significance", *Mutation research,* vol. 567, no. 1, pp. 1-61.

Fagan, A.M., Roe, C.M., Xiong, C., Mintun, M.A., Morris, J.C. & Holtzman, D.M. 2007, "Cerebrospinal fluid tau/beta-amyloid(42) ratio as a prediction of cognitive decline in nondemented older adults", *Archives of Neurology,* vol. 64, no. 3, pp. 343-349.

Fahrer, J., Huelsenbeck, J., Jaurich, H., Dorsam, B., Frisan, T., Eich, M., Roos, W.P., Kaina, B. & Fritz, G. 2014, "Cytolethal distending toxin (CDT) is a radiomimetic agent and induces persistent levels of DNA double-strand breaks in human fibroblasts", *DNA repair,* vol. 18, pp. 31-43.

Farias, S.T., Mungas, D., Reed, B.R., Harvey, D. & DeCarli, C. 2009, "Progression of mild cognitive impairment to dementia in clinic- vs community-based cohorts", *Archives of Neurology,* vol. 66, no. 9, pp. 1151-1157.

Faux, N.G., Ellis, K.A., Porter, L., Fowler, C.J., Laws, S.M., Martins, R.N., Pertile, K.K., Rembach, A., Rowe, C.C., Rumble, R.L., Szoeke, C., Taddei, K., Taddei, T., Trounson, B.O., Villemagne, V.L., Ward, V., Ames, D., Masters, C.L. & Bush, A.I. 2011, "Homocysteine, vitamin B12, and folic acid levels in Alzheimer's disease, mild cognitive impairment, and healthy elderly: baseline characteristics in subjects of the Australian Imaging Biomarker Lifestyle study", *Journal of Alzheimer's disease : JAD,* vol. 27, no. 4, pp. 909-922.

Faux, N.G., Rembach, A., Wiley, J., Ellis, K.A., Ames, D., Fowler, C.J., Martins, R.N., Pertile, K.K., Rumble, R.L., Trounson, B., Masters, C.L., AIBL Research Group & Bush, A.I. 2014, "An anemia of Alzheimer's disease", *Molecular psychiatry,* vol. 19, no. 11, pp. 1227-1234.

Feigelson, H.S., Rodriguez, C., Robertson, A.S., Jacobs, E.J., Calle, E.E., Reid, Y.A. & Thun, M.J. 2001, "Determinants of DNA yield and quality from buccal cell samples collected with mouthwash", *Cancer epidemiology, biomarkers & prevention : a publication of the American Association for Cancer Research, cosponsored by the American Society of Preventive Oncology,* vol. 10, no. 9, pp. 1005-1008.

Fenech, M. 2012, "Folate (vitamin B9) and vitamin B12 and their function in the maintenance of nuclear and mitochondrial genome integrity", *Mutation research,* vol. 733, no. 1-2, pp. 21-33.

Fenech, M. 2007, "Cytokinesis-block micronucleus cytome assay", *Nature protocols,* vol. 2, no. 5, pp. 1084-1104.

Fernandez, M., Gobartt, A.L., Balana, M. & COOPERA Study Group 2010, "Behavioural symptoms in patients with Alzheimer's disease and their association with cognitive impairment", *BMC neurology,* vol. 10, pp. 87.

Fernandez, M.I., Gong, Y., Ye, Y., Lin, J., Chang, D.W., Kamat, A.M. & Wu, X. 2013, "gamma-H2AX level in peripheral blood lymphocytes as a risk predictor for bladder cancer", *Carcinogenesis,* vol. 34, no. 11, pp. 2543-2547.

Fernandez-Capetillo, O., Lee, A., Nussenzweig, M. & Nussenzweig, A. 2004, "H2AX: the histone guardian of the genome", *DNA repair,* vol. 3, no. 8-9, pp. 959-967.

Ferri, C.P., Prince, M., Brayne, C., Brodaty, H., Fratiglioni, L., Ganguli, M., Hall, K., Hasegawa, K., Hendrie, H., Huang, Y., Jorm, A., Mathers, C., Menezes, P.R., Rimmer, E., Scazufca, M. & Alzheimer's Disease International 2005, "Global prevalence of dementia: a Delphi consensus study", *Lancet,* vol. 366, no. 9503, pp. 2112-2117.

Filion, T.M., Qiao, M., Ghule, P.N., Mandeville, M., van Wijnen, A.J., Stein, J.L., Lian, J.B., Altieri, D.C. & Stein, G.S. 2009, "Survival responses of human embryonic stem cells to DNA damage", *Journal of cellular physiology,* vol. 220, no. 3, pp. 586-592.

Firsanov, D., Vasilishina, A., Kropotov, A. & Mikhailov, V. 2012, "Dynamics of gammaH2AX formation and elimination in mammalian cells after X-irradiation", *Biochimie,* vol. 94, pp. 2416-2422.

Fischer, P., Jungwirth, S., Zehetmayer, S., Weissgram, S., Hoenigschnabl, S., Gelpi, E., Krampla, W. & Tragl, K.H. 2007, "Conversion from subtypes of mild cognitive impairment to Alzheimer dementia", *Neurology,* vol. 68, no. 4, pp. 288-291.

Fleckenstein, J., Kuhne, M., Seegmuller, K., Derschang, S., Melchior, P., Graber, S., Fricke, A., Rube, C.E. & Rube, C. 2011, "The impact of individual in vivo repair of DNA double-strand breaks on oral mucositis in adjuvant radiotherapy of head-and-neck cancer", *International journal of radiation oncology, biology, physics,* vol. 81, no. 5, pp. 1465-1472.

Follett, P.A. & Armstrong, J.W. 2004, "Revised irradiation doses to control melon fly, Mediterranean fruit fly, and oriental fruit fly (Diptera: Tephritidae) and a generic dose for tephritid fruit flies", *Journal of economic entomology,* vol. 97, no. 4, pp. 1254-1262.

Follett, P.A., Phillips, T.W., Armstrong, J.W. & Moy, J.H. 2011, "Generic phytosanitary radiation treatment for tephritid fruit flies provides quarantine security for Bactrocera latifrons (Diptera: Tephritidae)", *Journal of economic entomology,* vol. 104, no. 5, pp. 1509-1513.

Forlenza, O.V., Diniz, B.S., Stella, F., Teixeira, A.L. & Gattaz, W.F. 2013, "Mild cognitive impairment. Part 1: clinical characteristics and predictors of dementia",

Revista brasileira de psiquiatria (Sao Paulo, Brazil : 1999), vol. 35, no. 2, pp. 178-185.

Fraga, C.G., Shigenaga, M.K., Park, J.W., Degan, P. & Ames, B.N. 1990, "Oxidative damage to DNA during aging: 8-hydroxy-2'-deoxyguanosine in rat organ DNA and urine", *Proceedings of the National Academy of Sciences of the United States of America,* vol. 87, no. 12, pp. 4533-4537.

Franceschi, C. 2007, "Inflammaging as a major characteristic of old people: can it be prevented or cured?", *Nutrition reviews,* vol. 65, no. 12 Pt 2, pp. S173-6.

Francois, M., Leifert, W., Hecker, J., Faunt, J., Martins, R., Thomas, P. & Fenech, M. 2014a, "Altered cytological parameters in buccal cells from individuals with mild cognitive impairment and Alzheimer's disease", *Cytometry.Part A,* vol. 85A, no. 8, pp. 698-708.

Francois, M., Leifert, W., Martins, R., Thomas, P. & Fenech, M. 2014b, "Biomarkers of Alzheimer's Disease Risk in Peripheral Tissues; Focus on Buccal Cells", *Current Alzheimer research,* vol. 11, pp. 519-531.

Freund, A., Orjalo, A.V., Desprez, P.Y. & Campisi, J. 2010, "Inflammatory networks during cellular senescence: causes and consequences", *Trends in molecular medicine,* vol. 16, no. 5, pp. 238-246.

Friesner, J.D., Liu, B., Culligan, K. & Britt, A.B. 2005, "Ionizing radiation-dependent gamma-H2AX focus formation requires ataxia telangiectasia mutated and ataxia telangiectasia mutated and Rad3-related", *Molecular biology of the cell,* vol. 16, no. 5, pp. 2566-2576.

Fu, S., Yang, Y., Das, T.K., Yen, Y., Zhou, B.S., Zhou, M.M., Ohlmeyer, M., Ko, E.C., Cagan, R., Rosenstein, B.S., Chen, S.H. & Kao, J. 2012, "gamma-H2AX kinetics as a novel approach to high content screening for small molecule radiosensitizers", *PloS one,* vol. 7, no. 6, pp. e38465.

Fumagalli, M., Rossiello, F., Clerici, M., Barozzi, S., Cittaro, D., Kaplunov, J.M., Bucci, G., Dobreva, M., Matti, V., Beausejour, C.M., Herbig, U., Longhese, M.P. & d'Adda di Fagagna, F. 2012, "Telomeric DNA damage is irreparable and causes persistent DNA-damage-response activation", *Nature cell biology,* vol. 14, no. 4, pp. 355-365.

Furuta, T., Takemura, H., Liao, Z.Y., Aune, G.J., Redon, C., Sedelnikova, O.A., Pilch, D.R., Rogakou, E.P., Celeste, A., Chen, H.T., Nussenzweig, A., Aladjem, M.I., Bonner, W.M. & Pommier, Y. 2003, "Phosphorylation of histone H2AX and activation of Mre11, Rad50, and Nbs1 in response to replication-dependent DNA double-strand breaks induced by mammalian DNA topoisomerase I cleavage complexes", *The Journal of biological chemistry,* vol. 278, no. 22, pp. 20303-20312.

Garcia-Closas, M., Egan, K.M., Abruzzo, J., Newcomb, P.A., Titus-Ernstoff, L., Franklin, T., Bender, P.K., Beck, J.C., Le Marchand, L., Lum, A., Alavanja, M., Hayes, R.B., Rutter, J., Buetow, K., Brinton, L.A. & Rothman, N. 2001,

"Collection of genomic DNA from adults in epidemiological studies by buccal cytobrush and mouthwash", *Cancer epidemiology, biomarkers & prevention : a publication of the American Association for Cancer Research, cosponsored by the American Society of Preventive Oncology,* vol. 10, no. 6, pp. 687-696.

Garm, C., Moreno-Villanueva, M., Burkle, A., Petersen, I., Bohr, V.A., Christensen, K. & Stevnsner, T. 2013, "Age and gender effects on DNA strand break repair in peripheral blood mononuclear cells", *Aging cell,* vol. 12, no. 1, pp. 58-66.

Garty, G., Chen, Y., Salerno, A., Turner, H., Zhang, J., Lyulko, O., Bertucci, A., Xu, Y., Wang, H., Simaan, N., Randers-Pehrson, G., Yao, Y.L., Amundson, S.A. & Brenner, D.J. 2010, "The RABIT: a rapid automated biodosimetry tool for radiological triage", *Health physics,* vol. 98, no. 2, pp. 209-217.

Gasparini, L., Racchi, M., Binetti, G., Trabucchi, M., Solerte, S.B., Alkon, D., Etcheberrigaray, R., Gibson, G., Blass, J., Paoletti, R. & Govoni, S. 1998, "Peripheral markers in testing pathophysiological hypotheses and diagnosing Alzheimer's disease", *FASEB journal : official publication of the Federation of American Societies for Experimental Biology,* vol. 12, no. 1, pp. 17-34.

Gauthier, S., Reisberg, B., Zaudig, M., Petersen, R.C., Ritchie, K., Broich, K., Belleville, S., Brodaty, H., Bennett, D., Chertkow, H., Cummings, J.L., de Leon, M., Feldman, H., Ganguli, M., Hampel, H., Scheltens, P., Tierney, M.C., Whitehouse, P., Winblad, B. & International Psychogeriatric Association Expert Conference on mild cognitive impairment 2006, "Mild cognitive impairment", *Lancet,* vol. 367, no. 9518, pp. 1262-1270.

Gavrilov, B., Vezhenkova, I., Firsanov, D., Solovjeva, L., Svetlova, M., Mikhailov, V. & Tomilin, N. 2006, "Slow elimination of phosphorylated histone gamma-H2AX from DNA of terminally differentiated mouse heart cells in situ", *Biochemical and biophysical research communications,* vol. 347, no. 4, pp. 1048-1052.

Gedik, C.M., Grant, G., Morrice, P.C., Wood, S.G. & Collins, A.R. 2005, "Effects of age and dietary restriction on oxidative DNA damage, antioxidant protection and DNA repair in rats", *European journal of nutrition,* vol. 44, no. 5, pp. 263-272.

Gedik, C.M., Wood, S.G. & Collins, A.R. 1998, "Measuring oxidative damage to DNA; HPLC and the comet assay compared", *Free radical research,* vol. 29, no. 6, pp. 609-615.

Geisel, D., Heverhagen, J.T., Kalinowski, M. & Wagner, H.J. 2008, "DNA double-strand breaks after percutaneous transluminal angioplasty", *Radiology,* vol. 248, no. 3, pp. 852-859.

Giasson, B.I., Ischiropoulos, H., Lee, V.M. & Trojanowski, J.Q. 2002, "The relationship between oxidative/nitrative stress and pathological inclusions in Alzheimer's and Parkinson's diseases", *Free radical biology & medicine,* vol. 32, no. 12, pp. 1264-1275.

Giovannini, C., Piaggi, S., Federico, G. & Scarpato, R. 2014, "High levels of gamma-H2AX foci and cell membrane oxidation in adolescents with type 1 diabetes", *Mutation research,* vol. 770, pp. 128-135.

Goldstein, L.E., Muffat, J.A., Cherny, R.A., Moir, R.D., Ericsson, M.H., Huang, X., Mavros, C., Coccia, J.A., Faget, K.Y., Fitch, K.A., Masters, C.L., Tanzi, R.E., Chylack, L.T.,Jr & Bush, A.I. 2003, "Cytosolic beta-amyloid deposition and supranuclear cataracts in lenses from people with Alzheimer's disease", *Lancet (London, England),* vol. 361, no. 9365, pp. 1258-1265.

Goll, M.G. & Bestor, T.H. 2002, "Histone modification and replacement in chromatin activation", *Genes & development,* vol. 16, no. 14, pp. 1739-1742.

Gonzalez, J.E., Roch-Lefevre, S.H., Mandina, T., Garcia, O. & Roy, L. 2010, "Induction of gamma-H2AX foci in human exfoliated buccal cells after in vitro exposure to ionising radiation", *International journal of radiation biology,* vol. 86, no. 9, pp. 752-759.

Gonzalez-Suarez, I., Redwood, A.B., Perkins, S.M., Vermolen, B., Lichtensztejin, D., Grotsky, D.A., Morgado-Palacin, L., Gapud, E.J., Sleckman, B.P., Sullivan, T., Sage, J., Stewart, C.L., Mai, S. & Gonzalo, S. 2009, "Novel roles for A-type lamins in telomere biology and the DNA damage response pathway", *The EMBO journal,* vol. 28, no. 16, pp. 2414-2427.

Gonzalo, S. 2014, "DNA damage and lamins", *Advances in Experimental Medicine and Biology,* vol. 773, pp. 377-399.

Goodarzi, A.A., Jeggo, P. & Lobrich, M. 2010, "The influence of heterochromatin on DNA double strand break repair: Getting the strong, silent type to relax", *DNA repair,* vol. 9, no. 12, pp. 1273-1282.

Goodhead, D.T. 1994, "Initial events in the cellular effects of ionizing radiations: clustered damage in DNA", *International journal of radiation biology,* vol. 65, no. 1, pp. 7-17.

Gorbunova, V. & Seluanov, A. 2005, "Making ends meet in old age: DSB repair and aging", *Mechanisms of ageing and development,* vol. 126, no. 6-7, pp. 621-628.

Gotz, S., Garcia-Gomez, J.M., Terol, J., Williams, T.D., Nagaraj, S.H., Nueda, M.J., Robles, M., Talon, M., Dopazo, J. & Conesa, A. 2008, "High-throughput functional annotation and data mining with the Blast2GO suite", *Nucleic acids research,* vol. 36, no. 10, pp. 3420-3435.

Goukassian, D., Gad, F., Yaar, M., Eller, M.S., Nehal, U.S. & Gilchrest, B.A. 2000, "Mechanisms and implications of the age-associated decrease in DNA repair capacity", *The FASEB journal : official publication of the Federation of American Societies for Experimental Biology,* vol. 14, no. 10, pp. 1325-1334.

Goutham, H.V., Mumbrekar, K.D., Vadhiraja, B.M., Fernandes, D.J., Sharan, K., Kanive Parashiva, G., Kapaettu, S. & Bola Sadashiva, S.R. 2012, "DNA double-strand break analysis by gamma-H2AX foci: a useful method for determining the overreactors to radiation-induced acute reactions among head-and-neck cancer

patients", *International journal of radiation oncology, biology, physics,* vol. 84, no. 5, pp. e607-12.

Groesser, T., Chang, H., Fontenay, G., Chen, J., Costes, S.V., Helen Barcellos-Hoff, M., Parvin, B. & Rydberg, B. 2011, "Persistence of gamma-H2AX and 53BP1 foci in proliferating and non-proliferating human mammary epithelial cells after exposure to gamma-rays or iron ions", *International journal of radiation biology,* vol. 87, no. 7, pp. 696-710.

Grudzenski, S., Raths, A., Conrad, S., Rube, C.E. & Lobrich, M. 2010, "Inducible response required for repair of low-dose radiation damage in human fibroblasts", *Proceedings of the National Academy of Sciences of the United States of America,* vol. 107, no. 32, pp. 14205-14210.

Grundman, M., Petersen, R.C., Ferris, S.H., Thomas, R.G., Aisen, P.S., Bennett, D.A., Foster, N.L., Jack, C.R.,Jr, Galasko, D.R., Doody, R., Kaye, J., Sano, M., Mohs, R., Gauthier, S., Kim, H.T., Jin, S., Schultz, A.N., Schafer, K., Mulnard, R., van Dyck, C.H., Mintzer, J., Zamrini, E.Y., Cahn-Weiner, D., Thal, L.J. & Alzheimer's Disease Cooperative Study 2004, "Mild cognitive impairment can be distinguished from Alzheimer disease and normal aging for clinical trials", *Archives of Neurology,* vol. 61, no. 1, pp. 59-66.

Guangda, X., Bangshun, X., Xiujian, L. & Yangzhong, H. 1999, "Apovarepsilon(4) allele increases the risk for exercise-induced silent myocardial ischemia in non-insulin-dependent diabetes mellitus", *Atherosclerosis,* vol. 147, no. 2, pp. 293-296.

Hamasaki, K., Imai, K., Nakachi, K., Takahashi, N., Kodama, Y. & Kusunoki, Y. 2007, "Short-term culture and gammaH2AX flow cytometry determine differences in individual radiosensitivity in human peripheral T lymphocytes", *Environmental and molecular mutagenesis,* vol. 48, no. 1, pp. 38-47.

Hampel, H. & Prvulovic, D. 2012, "Are biomarkers harmful to recruitment and retention in Alzheimer's disease clinical trials? An international perspective", *The journal of nutrition, health & aging,* vol. 16, no. 4, pp. 346-348.

Harding, S.M., Coackley, C. & Bristow, R.G. 2011, "ATM-dependent phosphorylation of 53BP1 in response to genomic stress in oxic and hypoxic cells", *Radiotherapy and oncology : journal of the European Society for Therapeutic Radiology and Oncology,* vol. 99, no. 3, pp. 307-312.

Harley, C.B., Futcher, A.B. & Greider, C.W. 1990, "Telomeres shorten during ageing of human fibroblasts", *Nature,* vol. 345, no. 6274, pp. 458-460.

Harty, L.C., Garcia-Closas, M., Rothman, N., Reid, Y.A., Tucker, M.A. & Hartge, P. 2000, "Collection of buccal cell DNA using treated cards", *Cancer epidemiology, biomarkers & prevention : a publication of the American Association for Cancer Research, cosponsored by the American Society of Preventive Oncology,* vol. 9, no. 5, pp. 501-506.

Hastie, N.D., Dempster, M., Dunlop, M.G., Thompson, A.M., Green, D.K. & Allshire, R.C. 1990, "Telomere reduction in human colorectal carcinoma and with ageing", *Nature,* vol. 346, no. 6287, pp. 866-868.

Hattori, H., Matsumoto, M., Iwai, K., Tsuchiya, H., Miyauchi, E., Takasaki, M., Kamino, K., Munehira, J., Kimura, Y., Kawanishi, K., Hoshino, T., Murai, H., Ogata, H., Maruyama, H. & Yoshida, H. 2002, "The tau protein of oral epithelium increases in Alzheimer's disease", *The journals of gerontology.Series A, Biological sciences and medical sciences,* vol. 57, no. 1, pp. M64-70.

Hayney, M.S., Poland, G.A. & Lipsky, J.J. 1996, "A noninvasive 'swish and spit' method for collecting nucleated cells for HLA typing by PCR in population studies", *Human heredity,* vol. 46, no. 2, pp. 108-111.

Henriksen, M., Miller, B., Newmark, J., Al-Kofahi, Y. & Holden, E. 2011, "Laser scanning cytometry and its applications: a pioneering technology in the field of quantitative imaging cytometry", *Methods in cell biology,* vol. 102, pp. 161-205.

Henry, M.S., Passmore, A.P., Todd, S., McGuinness, B., Craig, D. & Johnston, J.A. 2012, "The development of effective biomarkers for Alzheimer's disease: a review", *International journal of geriatric psychiatry, .*

Herbig, U., Ferreira, M., Condel, L., Carey, D. & Sedivy, J.M. 2006, "Cellular senescence in aging primates", *Science (New York, N.Y.),* vol. 311, no. 5765, pp. 1257.

Hewitt, G., Jurk, D., Marques, F.D., Correia-Melo, C., Hardy, T., Gackowska, A., Anderson, R., Taschuk, M., Mann, J. & Passos, J.F. 2012, "Telomeres are favoured targets of a persistent DNA damage response in ageing and stress-induced senescence", *Nature communications,* vol. 3, pp. 708.

Hofer, T., Fontana, L., Anton, S.D., Weiss, E.P., Villareal, D., Malayappan, B. & Leeuwenburgh, C. 2008, "Long-term effects of caloric restriction or exercise on DNA and RNA oxidation levels in white blood cells and urine in humans", *Rejuvenation research,* vol. 11, no. 4, pp. 793-799.

Hosoya, A., Lee, J.M., Cho, S.W., Kim, J.Y., Shinozaki, N., Shibahara, T., Shimono, M. & Jung, H.S. 2008, "Morphological evidence of basal keratinocyte migration during the re-epithelialization process", *Histochemistry and cell biology,* vol. 130, no. 6, pp. 1165-1175.

Hozak, P., Sasseville, A.M., Raymond, Y. & Cook, P.R. 1995, "Lamin proteins form an internal nucleoskeleton as well as a peripheral lamina in human cells", *Journal of cell science,* vol. 108 (Pt 2), no. Pt 2, pp. 635-644.

Hoze, N., Ruault, M., Amoruso, C., Taddei, A. & Holcman, D. 2013, "Spatial telomere organization and clustering in yeast Saccharomyces cerevisiae nucleus is generated by a random dynamics of aggregation-dissociation", *Molecular biology of the cell,* vol. 24, no. 11, pp. 1791-800, S1-10.

Huang, S., Lee, L., Hanson, N.B., Lenaerts, C., Hoehn, H., Poot, M., Rubin, C.D., Chen, D.F., Yang, C.C., Juch, H., Dorn, T., Spiegel, R., Oral, E.A., Abid, M.,

Battisti, C., Lucci-Cordisco, E., Neri, G., Steed, E.H., Kidd, A., Isley, W., Showalter, D., Vittone, J.L., Konstantinow, A., Ring, J., Meyer, P., Wenger, S.L., von Herbay, A., Wollina, U., Schuelke, M., Huizenga, C.R., Leistritz, D.F., Martin, G.M., Mian, I.S. & Oshima, J. 2006, "The spectrum of WRN mutations in Werner syndrome patients", *Human mutation,* vol. 27, no. 6, pp. 558-567.

Huang, X., Halicka, H.D. & Darzynkiewicz, Z. 2004, "Detection of histone H2AX phosphorylation on Ser-139 as an indicator of DNA damage (DNA double-strand breaks)", *Current protocols in cytometry / editorial board, J.Paul Robinson, managing editor ...[et al.],* vol. Chapter 7, pp. Unit 7.27.

Huang, X., Okafuji, M., Traganos, F., Luther, E., Holden, E. & Darzynkiewicz, Z. 2004, "Assessment of histone H2AX phosphorylation induced by DNA topoisomerase I and II inhibitors topotecan and mitoxantrone and by the DNA cross-linking agent cisplatin", *Cytometry.Part A : the journal of the International Society for Analytical Cytology,* vol. 58, no. 2, pp. 99-110.

Hudson, D., Kovalchuk, I., Koturbash, I., Kolb, B., Martin, O.A. & Kovalchuk, O. 2011, "Induction and persistence of radiation-induced DNA damage is more pronounced in young animals than in old animals", *Aging,* vol. 3, no. 6, pp. 609-620.

Huerta, S., Gao, X., Livingston, E.H., Kapur, P., Sun, H. & Anthony, T. 2010, "In vitro and in vivo radiosensitization of colorectal cancer HT-29 cells by the smac mimetic JP-1201", *Surgery,* vol. 148, no. 2, pp. 346-353.

Humpel, C. 2011, "Identifying and validating biomarkers for Alzheimer's disease", *Trends in biotechnology,* vol. 29, no. 1, pp. 26-32.

Hye, A., Kerr, F., Archer, N., Foy, C., Poppe, M., Brown, R., Hamilton, G., Powell, J., Anderton, B. & Lovestone, S. 2005, "Glycogen synthase kinase-3 is increased in white cells early in Alzheimer's disease", *Neuroscience letters,* vol. 373, no. 1, pp. 1-4.

IAEA-TECDOC-1427 2004, "Irradiation as a phytosanitary treatment of food and agricultural commodities. Proceedings of a final research coordination meeting organized by the Joint FAO/IAEA Division of Nuclear Techniques in Food and Agriculture 2002", *International Atomic Energy Agency (IAEA),* , pp. 181pp.

Ingber, A.P., Hassenstab, J., Fagan, A.M., Benzinger, T.L., Grant, E.A., Holtzman, D.M., Morris, J.C. & Roe, C.M. 2016, "Cerebrospinal Fluid Biomarkers and Reserve Variables as Predictors of Future "Non-Cognitive" Outcomes of Alzheimer's Disease", *Journal of Alzheimer's disease : JAD,* .

Iqbal, K., Grundke-Iqbal, I., Smith, A.J., George, L., Tung, Y.C. & Zaidi, T. 1989, "Identification and localization of a tau peptide to paired helical filaments of Alzheimer disease", *Proceedings of the National Academy of Sciences of the United States of America,* vol. 86, no. 14, pp. 5646-5650.

Ismail, I.H., Wadhra, T.I. & Hammarsten, O. 2007, "An optimized method for detecting gamma-H2AX in blood cells reveals a significant interindividual variation in the

gamma-H2AX response among humans", *Nucleic acids research,* vol. 35, no. 5, pp. e36.

Ittner, L.M. & Gotz, J. 2011, "Amyloid-beta and tau--a toxic pas de deux in Alzheimer's disease", *Nature reviews.Neuroscience,* vol. 12, no. 2, pp. 65-72.

Ivashkevich, A., Redon, C.E., Nakamura, A.J., Martin, R.F. & Martin, O.A. 2012, "Use of the gamma-H2AX assay to monitor DNA damage and repair in translational cancer research", *Cancer letters,* vol. 327, no. 1-2, pp. 123-133.

Jacobsen, E., Beach, T., Shen, Y., Li, R. & Chang, Y. 2004, "Deficiency of the Mre11 DNA repair complex in Alzheimer's disease brains", *Brain research.Molecular brain research,* vol. 128, no. 1, pp. 1-7.

Janoshazi, A., Sellal, F., Marescaux, C., Danion, J.M., Warter, J.M. & de Barry, J. 2006, "Alteration of protein kinase C conformation in red blood cells: a potential marker for Alzheimer's disease but not for Parkinson's disease", *Neurobiology of aging,* vol. 27, no. 2, pp. 245-251.

Jeggo, P.A., Geuting, V. & Lobrich, M. 2011, "The role of homologous recombination in radiation-induced double-strand break repair", *Radiotherapy and oncology : journal of the European Society for Therapeutic Radiology and Oncology,* vol. 101, no. 1, pp. 7-12.

Jenkins, E.C., Velinov, M.T., Ye, L., Gu, H., Li, S., Jenkins, E.C.,Jr, Brooks, S.S., Pang, D., Devenny, D.A., Zigman, W.B., Schupf, N. & Silverman, W.P. 2006, "Telomere shortening in T lymphocytes of older individuals with Down syndrome and dementia", *Neurobiology of aging,* vol. 27, no. 7, pp. 941-945.

Joachim, C.L., Mori, H. & Selkoe, D.J. 1989, "Amyloid beta-protein deposition in tissues other than brain in Alzheimer's disease", *Nature,* vol. 341, no. 6239, pp. 226-230.

Kamentsky, L.A. & Kamentsky, L.D. 1991, "Microscope-based multiparameter laser scanning cytometer yielding data comparable to flow cytometry data", *Cytometry,* vol. 12, no. 5, pp. 381-387.

Kasten-Pisula, U., Windhorst, S., Dahm-Daphi, J., Mayr, G. & Dikomey, E. 2007, "Radiosensitization of tumour cell lines by the polyphenol Gossypol results from depressed double-strand break repair and not from enhanced apoptosis", *Radiotherapy and oncology : journal of the European Society for Therapeutic Radiology and Oncology,* vol. 83, no. 3, pp. 296-303.

Kataoka, Y., Bindokas, V.P., Duggan, R.C., Murley, J.S. & Grdina, D.J. 2006, "Flow cytometric analysis of phosphorylated histone H2AX following exposure to ionizing radiation in human microvascular endothelial cells", *Journal of radiation research,* vol. 47, no. 3-4, pp. 245-257.

Kawada, M., Hachiya, Y., Arihiro, A. & Mizoguchi, E. 2007, "Role of mammalian chitinases in inflammatory conditions", *The Keio journal of medicine,* vol. 56, no. 1, pp. 21-27.

Khan, S.S. & Bloom, G.S. 2016, "Tau: The Center of a Signaling Nexus in Alzheimer's Disease", *Frontiers in neuroscience,* vol. 10, pp. 31.

Khan, T.K. & Alkon, D.L. 2015, "Peripheral biomarkers of Alzheimer's disease", *Journal of Alzheimer's disease : JAD,* vol. 44, no. 3, pp. 729-744.

Khanna, K.K. & Jackson, S.P. 2001, "DNA double-strand breaks: signaling, repair and the cancer connection", *Nature genetics,* vol. 27, no. 3, pp. 247-254.

Kim, Y.B., Jeung, H.C., Jeong, I., Lee, K., Rha, S.Y., Chung, H.C. & Kim, G.E. 2013, "Mechanism of enhancement of radiation-induced cytotoxicity by sorafenib in colorectal cancer", *Journal of radiation research,* vol. 54, no. 1, pp. 52-60.

King, I.B., Satia-Abouta, J., Thornquist, M.D., Bigler, J., Patterson, R.E., Kristal, A.R., Shattuck, A.L., Potter, J.D. & White, E. 2002, "Buccal cell DNA yield, quality, and collection costs: comparison of methods for large-scale studies", *Cancer epidemiology, biomarkers & prevention : a publication of the American Association for Cancer Research, cosponsored by the American Society of Preventive Oncology,* vol. 11, no. 10 Pt 1, pp. 1130-1133.

Kinner, A., Wu, W., Staudt, C. & Iliakis, G. 2008, "Gamma-H2AX in recognition and signaling of DNA double-strand breaks in the context of chromatin", *Nucleic acids research,* vol. 36, no. 17, pp. 5678-5694.

Kirsch-Volders, M. & Fenech, M. 2001, "Inclusion of micronuclei in non-divided mononuclear lymphocytes and necrosis/apoptosis may provide a more comprehensive cytokinesis block micronucleus assay for biomonitoring purposes", *Mutagenesis,* vol. 16, no. 1, pp. 51-58.

Kivipelto, M., Ngandu, T., Laatikainen, T., Winblad, B., Soininen, H. & Tuomilehto, J. 2006, "Risk score for the prediction of dementia risk in 20 years among middle aged people: a longitudinal, population-based study", *The Lancet.Neurology,* vol. 5, no. 9, pp. 735-741.

Kleinerman, R.A., Romanyukha, A.A., Schauer, D.A. & Tucker, J.D. 2006, "Retrospective assessment of radiation exposure using biological dosimetry: chromosome painting, electron paramagnetic resonance and the glycophorin a mutation assay", *Radiation research,* vol. 166, no. 1 Pt 2, pp. 287-302.

Klokov, D., MacPhail, S.M., Banath, J.P., Byrne, J.P. & Olive, P.L. 2006, "Phosphorylated histone H2AX in relation to cell survival in tumor cells and xenografts exposed to single and fractionated doses of X-rays", *Radiotherapy and oncology : journal of the European Society for Therapeutic Radiology and Oncology,* vol. 80, no. 2, pp. 223-229.

Kobayashi, J. 2004, "Molecular mechanism of the recruitment of NBS1/hMRE11/hRAD50 complex to DNA double-strand breaks: NBS1 binds to gamma-H2AX through FHA/BRCT domain", *Journal of radiation research,* vol. 45, no. 4, pp. 473-478.

Kodym, R. & Horth, E. 1995, "Determination of radiation-induced DNA strand breaks in individual cells by non-radioactive labelling of 3' OH ends", *International journal of radiation biology,* vol. 68, no. 2, pp. 133-139.

Koo, E.H. 2002, "The beta-amyloid precursor protein (APP) and Alzheimer's disease: does the tail wag the dog?", *Traffic (Copenhagen, Denmark),* vol. 3, no. 11, pp. 763-770.

Kovalchuk, I.P., Golubov, A., Koturbash, I.V., Kutanzi, K., Martin, O.A. & Kovalchuk, O. 2014, "Age-dependent changes in DNA repair in radiation-exposed mice", *Radiation research,* vol. 182, no. 6, pp. 683-694.

Koyama, A., O'Brien, J., Weuve, J., Blacker, D., Metti, A.L. & Yaffe, K. 2013, "The role of peripheral inflammatory markers in dementia and Alzheimer's disease: a meta-analysis", *The journals of gerontology.Series A, Biological sciences and medical sciences,* vol. 68, no. 4, pp. 433-440.

Kuhne, M., Riballo, E., Rief, N., Rothkamm, K., Jeggo, P.A. & Lobrich, M. 2004, "A double-strand break repair defect in ATM-deficient cells contributes to radiosensitivity", *Cancer research,* vol. 64, no. 2, pp. 500-508.

Kumano, N., Haraguchi, D. & Kohama, T. 2008, "Effect of irradiation on mating ability in the male sweetpotato weevil (Coleoptera: Curculionidae)", *Journal of economic entomology,* vol. 101, no. 4, pp. 1198-1203.

Kummer, C., Wehner, S., Quast, T., Werner, S. & Herzog, V. 2002, "Expression and potential function of beta-amyloid precursor proteins during cutaneous wound repair", *Experimental cell research,* vol. 280, no. 2, pp. 222-232.

Ladd, B., O'Konek, J.J., Ostruszka, L.J. & Shewach, D.S. 2011, "Unrepairable DNA double-strand breaks initiate cytotoxicity with HSV-TK/ganciclovir", *Cancer gene therapy,* vol. 18, no. 10, pp. 751-759.

Lan, L., Nakajima, S., Komatsu, K., Nussenzweig, A., Shimamoto, A., Oshima, J. & Yasui, A. 2005, "Accumulation of Werner protein at DNA double-strand breaks in human cells", *Journal of cell science,* vol. 118, no. Pt 18, pp. 4153-4162.

Lang, J., Smetana, O., Sanchez-Calderon, L., Lincker, F., Genestier, J., Schmit, A.C., Houlne, G. & Chaboute, M.E. 2012, "Plant gammaH2AX foci are required for proper DNA DSB repair responses and colocalize with E2F factors", *The New phytologist,* vol. 194, no. 2, pp. 353-363.

Lassmann, M., Hanscheid, H., Gassen, D., Biko, J., Meineke, V., Reiners, C. & Scherthan, H. 2010, "In vivo formation of gamma-H2AX and 53BP1 DNA repair foci in blood cells after radioiodine therapy of differentiated thyroid cancer", *Journal of nuclear medicine : official publication, Society of Nuclear Medicine,* vol. 51, no. 8, pp. 1318-1325.

Lavker, R.M. & Sun, T.T. 1982, "Heterogeneity in epidermal basal keratinocytes: morphological and functional correlations", *Science (New York, N.Y.),* vol. 215, no. 4537, pp. 1239-1241.

Le Marchand, L., Lum-Jones, A., Saltzman, B., Visaya, V., Nomura, A.M. & Kolonel, L.N. 2001, "Feasibility of collecting buccal cell DNA by mail in a cohort study", *Cancer epidemiology, biomarkers & prevention : a publication of the American Association for Cancer Research, cosponsored by the American Society of Preventive Oncology,* vol. 10, no. 6, pp. 701-703.

Lee, E.J., Patten, G.S., Burnard, S.L. & McMurchie, E.J. 1994, "Osmotic and other properties of isolated human cheek epithelial cells", *The American Journal of Physiology,* vol. 267, no. 1 Pt 1, pp. C75-83.

Lee, S.L., Thomas, P., Hecker, J., Faunt, J. & Fenech, M. 2015, "Chromosomal DNA damage measured using the cytokinesis-block micronucleus cytome assay is significantly associated with cognitive impairment in South Australians", *Environmental and molecular mutagenesis,* vol. 56, no. 1, pp. 32-40.

Leifert, W.R., Francois, M., Thomas, P., Luther, E., Holden, E. & Fenech, M. 2011, "Automation of the buccal micronucleus cytome assay using laser scanning cytometry", *Methods in cell biology,* vol. 102, pp. 321-339.

Leinonen, V., Alafuzoff, I., Aalto, S., Suotunen, T., Savolainen, S., Nagren, K., Tapiola, T., Pirttila, T., Rinne, J., Jaaskelainen, J.E., Soininen, H. & Rinne, J.O. 2008, "Assessment of beta-amyloid in a frontal cortical brain biopsy specimen and by positron emission tomography with carbon 11-labeled Pittsburgh Compound B", *Archives of Neurology,* vol. 65, no. 10, pp. 1304-1309.

Leonard, A., Rueff, J., Gerber, G.B. & Leonard, E.D. 2005, "Usefulness and limits of biological dosimetry based on cytogenetic methods", *Radiation Protection Dosimetry,* vol. 115, no. 1-4, pp. 448-454.

Leskovac, A., Vujic, D., Guc-Scekic, M., Petrovic, S., Joksic, I., Slijepcevic, P. & Joksic, G. 2010, "Fanconi anemia is characterized by delayed repair kinetics of DNA double-strand breaks", *The Tohoku journal of experimental medicine,* vol. 221, no. 1, pp. 69-76.

Li, H., Mitchell, J.R. & Hasty, P. 2008, "DNA double-strand breaks: a potential causative factor for mammalian aging?", *Mechanisms of ageing and development,* vol. 129, no. 7-8, pp. 416-424.

Li, L. & Holscher, C. 2007, "Common pathological processes in Alzheimer disease and type 2 diabetes: a review", *Brain Research Reviews,* vol. 56, no. 2, pp. 384-402.

Li, W., Li, F., Huang, Q., Shen, J., Wolf, F., He, Y., Liu, X., Hu, Y.A., Bedford, J.S. & Li, C.Y. 2011, "Quantitative, noninvasive imaging of radiation-induced DNA double-strand breaks in vivo", *Cancer research,* vol. 71, no. 12, pp. 4130-4137.

Liu, S.K., Olive, P.L. & Bristow, R.G. 2008, "Biomarkers for DNA DSB inhibitors and radiotherapy clinical trials", *Cancer metastasis reviews,* vol. 27, no. 3, pp. 445-458.

Liu, Y., Rusinol, A., Sinensky, M., Wang, Y. & Zou, Y. 2006, "DNA damage responses in progeroid syndromes arise from defective maturation of prelamin A", *Journal of cell science,* vol. 119, no. Pt 22, pp. 4644-4649.

Lobo, A., Launer, L.J., Fratiglioni, L., Andersen, K., Di Carlo, A., Breteler, M.M., Copeland, J.R., Dartigues, J.F., Jagger, C., Martinez-Lage, J., Soininen, H. & Hofman, A. 2000, "Prevalence of dementia and major subtypes in Europe: A collaborative study of population-based cohorts. Neurologic Diseases in the Elderly Research Group", *Neurology,* vol. 54, no. 11 Suppl 5, pp. S4-9.

Lobrich, M., Rief, N., Kuhne, M., Heckmann, M., Fleckenstein, J., Rube, C. & Uder, M. 2005, "In vivo formation and repair of DNA double-strand breaks after computed tomography examinations", *Proceedings of the National Academy of Sciences of the United States of America,* vol. 102, no. 25, pp. 8984-8989.

Lobrich, M., Shibata, A., Beucher, A., Fisher, A., Ensminger, M., Goodarzi, A.A., Barton, O. & Jeggo, P.A. 2010, "gammaH2AX foci analysis for monitoring DNA double-strand break repair: strengths, limitations and optimization", *Cell cycle (Georgetown, Tex.),* vol. 9, no. 4, pp. 662-669.

Lopez-Otin, C., Blasco, M.A., Partridge, L., Serrano, M. & Kroemer, G. 2013, "The hallmarks of aging", *Cell,* vol. 153, no. 6, pp. 1194-1217.

Lou, Z., Minter-Dykhouse, K., Franco, S., Gostissa, M., Rivera, M.A., Celeste, A., Manis, J.P., van Deursen, J., Nussenzweig, A., Paull, T.T., Alt, F.W. & Chen, J. 2006, "MDC1 maintains genomic stability by participating in the amplification of ATM-dependent DNA damage signals", *Molecular cell,* vol. 21, no. 2, pp. 187-200.

Lovell, M.A., Xie, C. & Markesbery, W.R. 2000, "Decreased base excision repair and increased helicase activity in Alzheimer's disease brain", *Brain research,* vol. 855, no. 1, pp. 116-123.

Love, S., Barber, R. & Wilcock, G.K. 1999, "Increased poly(ADP-ribosyl)ation of nuclear proteins in Alzheimer's disease", *Brain : a journal of neurology,* vol. 122 (Pt 2), no. Pt 2, pp. 247-253.

Lum, A. & Le Marchand, L. 1998, "A simple mouthwash method for obtaining genomic DNA in molecular epidemiological studies", *Cancer epidemiology, biomarkers & prevention : a publication of the American Association for Cancer Research, cosponsored by the American Society of Preventive Oncology,* vol. 7, no. 8, pp. 719-724.

Lyras, L., Cairns, N.J., Jenner, A., Jenner, P. & Halliwell, B. 1997, "An assessment of oxidative damage to proteins, lipids, and DNA in brain from patients with Alzheimer's disease", *Journal of neurochemistry,* vol. 68, no. 5, pp. 2061-2069.

MacPhail, S.H., Banath, J.P., Yu, T.Y., Chu, E.H., Lambur, H. & Olive, P.L. 2003a, "Expression of phosphorylated histone H2AX in cultured cell lines following exposure to X-rays", *International journal of radiation biology,* vol. 79, no. 5, pp. 351-358.

MacPhail, S.H., Banath, J.P., Yu, Y., Chu, E. & Olive, P.L. 2003b, "Cell cycle-dependent expression of phosphorylated histone H2AX: reduced expression in unirradiated but not X-irradiated G1-phase cells", *Radiation research,* vol. 159, no. 6, pp. 759-767.

Madigan, J.P., Chotkowski, H.L. & Glaser, R.L. 2002, "DNA double-strand break-induced phosphorylation of Drosophila histone variant H2Av helps prevent radiation-induced apoptosis", *Nucleic acids research,* vol. 30, no. 17, pp. 3698-3705.

Mah, L.J., El-Osta, A. & Karagiannis, T.C. 2010, "gammaH2AX: a sensitive molecular marker of DNA damage and repair", *Leukemia : official journal of the Leukemia Society of America, Leukemia Research Fund, U.K,* vol. 24, no. 4, pp. 679-686.

Mapstone, M., Cheema, A.K., Fiandaca, M.S., Zhong, X., Mhyre, T.R., Macarthur, L.H., Hall, W.J., Fisher, S.G., Peterson, D.R., Haley, J.M., Nazar, M.D., Rich, S.A., Berlau, D.J., Peltz, C.B., Tan, M.T., Kawas, C.H. & Federoff, H.J. 2014, "Plasma phospholipids identify antecedent memory impairment in older adults", *Nature medicine,* vol. 20, no. 4, pp. 415-418.

Mari, P.O., Florea, B.I., Persengiev, S.P., Verkaik, N.S., Bruggenwirth, H.T., Modesti, M., Giglia-Mari, G., Bezstarosti, K., Demmers, J.A., Luider, T.M., Houtsmuller, A.B. & van Gent, D.C. 2006, "Dynamic assembly of end-joining complexes requires interaction between Ku70/80 and XRCC4", *Proceedings of the National Academy of Sciences of the United States of America,* vol. 103, no. 49, pp. 18597-18602.

Markova, E., Schultz, N. & Belyaev, I.Y. 2007, "Kinetics and dose-response of residual 53BP1/gamma-H2AX foci: co-localization, relationship with DSB repair and clonogenic survival", *International journal of radiation biology,* vol. 83, no. 5, pp. 319-329.

Markova, E., Torudd, J. & Belyaev, I. 2011, "Long time persistence of residual 53BP1/gamma-H2AX foci in human lymphocytes in relationship to apoptosis, chromatin condensation and biological dosimetry", *International journal of radiation biology,* vol. 87, no. 7, pp. 736-745.

Mastrangelo, T., Chaudhury, M.F., Skoda, S.R., Welch, J.B., Sagel, A. & Walder, J.M. 2012, "Feasibility of using a Caribbean screwworm for SIT campaigns in Brazil", *Journal of medical entomology,* vol. 49, no. 6, pp. 1495-1501.

May, M.S., Brand, M., Wuest, W., Anders, K., Kuwert, T., Prante, O., Schmidt, D., Maschauer, S., Semelka, R.C., Uder, M. & Kuefner, M.A. 2012, "Induction and repair of DNA double-strand breaks in blood lymphocytes of patients undergoing (1)(8)F-FDG PET/CT examinations", *European journal of nuclear medicine and molecular imaging,* vol. 39, no. 11, pp. 1712-1719.

McEachern, M.J., Krauskopf, A. & Blackburn, E.H. 2000, "Telomeres and their control", *Annual Review of Genetics,* vol. 34, pp. 331-358.

McIlroy, S.P., Dynan, K.B., Lawson, J.T., Patterson, C.C. & Passmore, A.P. 2002, "Moderately elevated plasma homocysteine, methylenetetrahydrofolate reductase genotype, and risk for stroke, vascular dementia, and Alzheimer disease in Northern Ireland", *Stroke; a journal of cerebral circulation,* vol. 33, no. 10, pp. 2351-2356.

McKenna, E., Traganos, F., Zhao, H. & Darzynkiewicz, Z. 2012, "Persistent DNA damage caused by low levels of mitomycin C induces irreversible cell senescence", *Cell cycle (Georgetown, Tex.),* vol. 11, no. 16, pp. 3132-3140.

McManus, K.J. & Hendzel, M.J. 2005, "ATM-dependent DNA damage-independent mitotic phosphorylation of H2AX in normally growing mammalian cells", *Molecular biology of the cell,* vol. 16, no. 10, pp. 5013-5025.

Mecocci, P., MacGarvey, U. & Beal, M.F. 1994, "Oxidative damage to mitochondrial DNA is increased in Alzheimer's disease", *Annals of Neurology,* vol. 36, no. 5, pp. 747-751.

Mecocci, P., Polidori, M.C., Cherubini, A., Ingegni, T., Mattioli, P., Catani, M., Rinaldi, P., Cecchetti, R., Stahl, W., Senin, U. & Beal, M.F. 2002, "Lymphocyte oxidative DNA damage and plasma antioxidants in Alzheimer disease", *Archives of Neurology,* vol. 59, no. 5, pp. 794-798.

Mecocci, P., Polidori, M.C., Ingegni, T., Cherubini, A., Chionne, F., Cecchetti, R. & Senin, U. 1998, "Oxidative damage to DNA in lymphocytes from AD patients", *Neurology,* vol. 51, no. 4, pp. 1014-1017.

Mendez-Acuna, L., Di Tomaso, M.V., Palitti, F. & Martinez-Lopez, W. 2010, "Histone post-translational modifications in DNA damage response", *Cytogenetic and genome research,* vol. 128, no. 1-3, pp. 28-36.

Menegakis, A., Yaromina, A., Eicheler, W., Dorfler, A., Beuthien-Baumann, B., Thames, H.D., Baumann, M. & Krause, M. 2009, "Prediction of clonogenic cell survival curves based on the number of residual DNA double strand breaks measured by gammaH2AX staining", *International journal of radiation biology,* vol. 85, no. 11, pp. 1032-1041.

Merriman, J. 2015, ***New biosecurity centre being established to stop fruit flies***. Available: http://www.theleadsouthaustralia.com.au/industries/primary-industries/new-biosecurity-centre-being-established-to-stop-fruit-flies/.

Meyn, R.E. & Jenkins, W.T. 1983, "Variation in normal and tumor tissue sensitivity of mice to ionizing radiation-induced DNA strand breaks in vivo", *Cancer research,* vol. 43, no. 12 Pt 1, pp. 5668-5673.

Michalczyk, A., Varigos, G., Smith, L. & Ackland, M.L. 2004, "Fresh and cultured buccal cells as a source of mRNA and protein for molecular analysis", *BioTechniques,* vol. 37, no. 2, pp. 262-4, 266-9.

Migliore, L., Botto, N., Scarpato, R., Petrozzi, L., Cipriani, G. & Bonuccelli, U. 1999, "Preferential occurrence of chromosome 21 malsegregation in peripheral blood lymphocytes of Alzheimer disease patients", *Cytogenetics and cell genetics,* vol. 87, no. 1-2, pp. 41-46.

Migliore, L. & Coppede, F. 2002, "Genetic and environmental factors in cancer and neurodegenerative diseases", *Mutation research,* vol. 512, no. 2-3, pp. 135-153.

Migliore, L., Coppede, F., Fenech, M. & Thomas, P. 2011, "Association of micronucleus frequency with neurodegenerative diseases", *Mutagenesis,* vol. 26, no. 1, pp. 85-92.

Migliore, L., Fontana, I., Trippi, F., Colognato, R., Coppede, F., Tognoni, G., Nucciarone, B. & Siciliano, G. 2005, "Oxidative DNA damage in peripheral leukocytes of mild cognitive impairment and AD patients", *Neurobiology of aging,* vol. 26, no. 5, pp. 567-573.

Minieri, V., Saviozzi, S., Gambarotta, G., Lo Iacono, M., Accomasso, L., Cibrario Rocchietti, E., Gallina, C., Turinetto, V. & Giachino, C. 2015, "Persistent DNA damage-induced premature senescence alters the functional features of human bone marrow mesenchymal stem cells", *Journal of Cellular and Molecular Medicine,* vol. 19, no. 4, pp. 734-743.

Mitchell, A.J. 2009, "A meta-analysis of the accuracy of the mini-mental state examination in the detection of dementia and mild cognitive impairment", *Journal of psychiatric research,* vol. 43, no. 4, pp. 411-431.

Mohapatra, S., Kawahara, M., Khan, I.S., Yannone, S.M. & Povirk, L.F. 2011, "Restoration of G1 chemo/radioresistance and double-strand-break repair proficiency by wild-type but not endonuclease-deficient Artemis", *Nucleic acids research,* vol. 39, no. 15, pp. 6500-6510.

Moll, R., Franke, W.W., Schiller, D.L., Geiger, B. & Krepler, R. 1982, "The catalog of human cytokeratins: patterns of expression in normal epithelia, tumors and cultured cells", *Cell,* vol. 31, no. 1, pp. 11-24.

Mondal, N.K., Ghosh, S. & Ray, M.R. 2011, "Micronucleus formation and DNA damage in buccal epithelial cells of Indian street boys addicted to gasp 'Golden glue'", *Mutation research,* vol. 721, no. 2, pp. 178-183.

Moquet, J., Barnard, S. & Rothkamm, K. 2014, "Gamma-H2AX biodosimetry for use in large scale radiation incidents: comparison of a rapid '96 well lyse/fix' protocol with a routine method", *PeerJ,* vol. 2, pp. e282.

Morgan, M.A., Parsels, L.A., Zhao, L., Parsels, J.D., Davis, M.A., Hassan, M.C., Arumugarajah, S., Hylander-Gans, L., Morosini, D., Simeone, D.M., Canman, C.E., Normolle, D.P., Zabludoff, S.D., Maybaum, J. & Lawrence, T.S. 2010, "Mechanism of radiosensitization by the Chk1/2 inhibitor AZD7762 involves abrogation of the G2 checkpoint and inhibition of homologous recombinational DNA repair", *Cancer research,* vol. 70, no. 12, pp. 4972-4981.

Morini, J., Babini, G., Mariotti, L., Baiocco, G., Nacci, L., Maccario, C., Rossler, U., Minelli, A., Savio, M., Gomolka, M., Kulka, U., Ottolenghi, A. & Danesino, C. 2015, "Radiosensitivity in Lymphoblastoid Cell Lines Derived from Shwachman-Diamond Syndrome Patients", *Radiation Protection Dosimetry,* .

Morocz, M., Kalman, J., Juhasz, A., Sinko, I., McGlynn, A.P., Downes, C.S., Janka, Z. & Rasko, I. 2002, "Elevated levels of oxidative DNA damage in lymphocytes from

patients with Alzheimer's disease", *Neurobiology of aging,* vol. 23, no. 1, pp. 47-53.

Moroni, M., Maeda, D., Whitnall, M.H., Bonner, W.M. & Redon, C.E. 2013, "Evaluation of the gamma-H2AX assay for radiation biodosimetry in a swine model", *International journal of molecular sciences,* vol. 14, no. 7, pp. 14119-14135.

Murnane, J.P. 2012, "Telomere dysfunction and chromosome instability", *Mutation research,* vol. 730, no. 1-2, pp. 28-36.

Mutika, G.N., Kabore, I., Seck, M.T., Sall, B., Bouyer, J., Parker, A.G. & Vreysen, M.J.B. 2013, "Mating performance of Glossina palpalis gambiensis strains from Burkina Faso, Mali, and Senegal", *Entomologia Experimentalis et Applicata,* vol. 146, no. 1, pp. 177-185.

Myerson, S., Hemingway, H., Budget, R., Martin, J., Humphries, S. & Montgomery, H. 1999, "Human angiotensin I-converting enzyme gene and endurance performance", *Journal of applied physiology (Bethesda, Md.: 1985),* vol. 87, no. 4, pp. 1313-1316.

Myung, N.H., Zhu, X., Kruman, I.I., Castellani, R.J., Petersen, R.B., Siedlak, S.L., Perry, G., Smith, M.A. & Lee, H.G. 2008, "Evidence of DNA damage in Alzheimer disease: phosphorylation of histone H2AX in astrocytes", *Age (Dordrecht, Netherlands),* vol. 30, no. 4, pp. 209-215.

Nakamura, A., Sedelnikova, O.A., Redon, C., Pilch, D.R., Sinogeeva, N.I., Shroff, R., Lichten, M. & Bonner, W.M. 2006, "Techniques for gamma-H2AX detection", *Methods in enzymology,* vol. 409, pp. 236-250.

Nakamura, A.J., Rao, V.A., Pommier, Y. & Bonner, W.M. 2010, "The complexity of phosphorylated H2AX foci formation and DNA repair assembly at DNA double-strand breaks", *Cell cycle (Georgetown, Tex.),* vol. 9, no. 2, pp. 389-397.

Nakamura, A.J., Redon, C.E., Bonner, W.M. & Sedelnikova, O.A. 2009, "Telomere-dependent and telomere-independent origins of endogenous DNA damage in tumor cells", *Aging,* vol. 1, no. 2, pp. 212-218.

Nelson, P.T., Alafuzoff, I., Bigio, E.H., Bouras, C., Braak, H., Cairns, N.J., Castellani, R.J., Crain, B.J., Davies, P., Del Tredici, K., Duyckaerts, C., Frosch, M.P., Haroutunian, V., Hof, P.R., Hulette, C.M., Hyman, B.T., Iwatsubo, T., Jellinger, K.A., Jicha, G.A., Kovari, E., Kukull, W.A., Leverenz, J.B., Love, S., Mackenzie, I.R., Mann, D.M., Masliah, E., McKee, A.C., Montine, T.J., Morris, J.C., Schneider, J.A., Sonnen, J.A., Thal, D.R., Trojanowski, J.Q., Troncoso, J.C., Wisniewski, T., Woltjer, R.L. & Beach, T.G. 2012, "Correlation of Alzheimer disease neuropathologic changes with cognitive status: a review of the literature", *Journal of neuropathology and experimental neurology,* vol. 71, no. 5, pp. 362-381.

Ng, A., Jion, Y.I., Zainal, N.H. & Kandiah, N. 2014, "Renal dysfunction contributes to episodic memory deficits and medial temporal atrophy in Alzheimer's disease: a pilot study", *Journal of the American Geriatrics Society,* vol. 62, no. 10, pp. 1981-1982.

Nunez, M.I., Villalobos, M., Olea, N., Valenzuela, M.T., Pedraza, V., McMillan, T.J. & Ruiz de Almodovar, J.M. 1995, "Radiation-induced DNA double-strand break rejoining in human tumour cells", *British journal of cancer,* vol. 71, no. 2, pp. 311-316.

O'Callaghan, N.J., Clifton, P.M., Noakes, M. & Fenech, M. 2009, "Weight loss in obese men is associated with increased telomere length and decreased abasic sites in rectal mucosa", *Rejuvenation research,* vol. 12, no. 3, pp. 169-176.

Oliva, C.F., Jacquet, M., Gilles, J., Lemperiere, G., Maquart, P.O., Quilici, S., Schooneman, F., Vreysen, M.J. & Boyer, S. 2012, "The sterile insect technique for controlling populations of Aedes albopictus (Diptera: Culicidae) on Reunion Island: mating vigour of sterilized males", *PloS one,* vol. 7, no. 11, pp. e49414.

Olive, P.L. 2011, "Retention of gammaH2AX foci as an indication of lethal DNA damage", *Radiotherapy and oncology : journal of the European Society for Therapeutic Radiology and Oncology,* vol. 101, no. 1, pp. 18-23.

Olive, P.L. 2009, "Endogenous DNA breaks: gammaH2AX and the role of telomeres", *Aging,* vol. 1, no. 2, pp. 154-156.

Olive, P.L. 1998, "The role of DNA single- and double-strand breaks in cell killing by ionizing radiation", *Radiation research,* vol. 150, no. 5 Suppl, pp. S42-51.

Olive, P.L. & Banath, J.P. 2004, "Phosphorylation of histone H2AX as a measure of radiosensitivity", *International journal of radiation oncology, biology, physics,* vol. 58, no. 2, pp. 331-335.

Panossian, L.A., Porter, V.R., Valenzuela, H.F., Zhu, X., Reback, E., Masterman, D., Cummings, J.L. & Effros, R.B. 2003, "Telomere shortening in T cells correlates with Alzheimer's disease status", *Neurobiology of aging,* vol. 24, no. 1, pp. 77-84.

Paris, L., Cordelli, E., Eleuteri, P., Grollino, M.G., Pasquali, E., Ranaldi, R., Meschini, R. & Pacchierotti, F. 2011, "Kinetics of gamma-H2AX induction and removal in bone marrow and testicular cells of mice after X-ray irradiation", *Mutagenesis,* vol. 26, no. 4, pp. 563-572.

Park, E.J., Chan, D.W., Park, J.H., Oettinger, M.A. & Kwon, J. 2003, "DNA-PK is activated by nucleosomes and phosphorylates H2AX within the nucleosomes in an acetylation-dependent manner", *Nucleic acids research,* vol. 31, no. 23, pp. 6819-6827.

Passos, J.F., Nelson, G., Wang, C., Richter, T., Simillion, C., Proctor, C.J., Miwa, S., Olijslagers, S., Hallinan, J., Wipat, A., Saretzki, G., Rudolph, K.L., Kirkwood, T.B. & von Zglinicki, T. 2010, "Feedback between p21 and reactive oxygen production is necessary for cell senescence", *Molecular systems biology,* vol. 6, pp. 347.

Patten, G.S., Leifert, W.R., Burnard, S.L., Head, R.J. & McMurchie, E.J. 1996, "Stimulation of human cheek cell Na+/H+ antiporter activity by saliva and salivary electrolytes: amplification by nigericin", *Molecular and cellular biochemistry,* vol. 154, no. 2, pp. 133-141.

Paull, T.T., Rogakou, E.P., Yamazaki, V., Kirchgessner, C.U., Gellert, M. & Bonner, W.M. 2000, "A critical role for histone H2AX in recruitment of repair factors to nuclear foci after DNA damage", *Current biology : CB,* vol. 10, no. 15, pp. 886-895.

Perry, G., Nunomura, A., Hirai, K., Zhu, X., Perez, M., Avila, J., Castellani, R.J., Atwood, C.S., Aliev, G., Sayre, L.M., Takeda, A. & Smith, M.A. 2002, "Is oxidative damage the fundamental pathogenic mechanism of Alzheimer's and other neurodegenerative diseases?", *Free radical biology & medicine,* vol. 33, no. 11, pp. 1475-1479.

Peters, R., Beckett, N., Forette, F., Tuomilehto, J., Clarke, R., Ritchie, C., Waldman, A., Walton, I., Poulter, R., Ma, S., Comsa, M., Burch, L., Fletcher, A., Bulpitt, C. & HYVET investigators 2008, "Incident dementia and blood pressure lowering in the Hypertension in the Very Elderly Trial cognitive function assessment (HYVET-COG): a double-blind, placebo controlled trial", *The Lancet.Neurology,* vol. 7, no. 8, pp. 683-689.

Petersen, R.C., Roberts, R.O., Knopman, D.S., Boeve, B.F., Geda, Y.E., Ivnik, R.J., Smith, G.E. & Jack, C.R.,Jr 2009, "Mild cognitive impairment: ten years later", *Archives of Neurology,* vol. 66, no. 12, pp. 1447-1455.

Pilch, D.R., Redon, C., Sedelnikova, O.A. & Bonner, W.M. 2004, "Two-dimensional gel analysis of histones and other H2AX-related methods", *Methods in enzymology,* vol. 375, pp. 76-88.

Pilch, D.R., Sedelnikova, O.A., Redon, C., Celeste, A., Nussenzweig, A. & Bonner, W.M. 2003, "Characteristics of gamma-H2AX foci at DNA double-strand breaks sites", *Biochemistry and cell biology = Biochimie et biologie cellulaire,* vol. 81, no. 3, pp. 123-129.

Pinto, M.M., Santos, N.F. & Amaral, A. 2010, "Current status of biodosimetry based on standard cytogenetic methods", *Radiation and environmental biophysics,* vol. 49, no. 4, pp. 567-581.

Porcedda, P., Turinetto, V., Lantelme, E., Fontanella, E., Chrzanowska, K., Ragona, R., De Marchi, M., Delia, D. & Giachino, C. 2006, "Impaired elimination of DNA double-strand break-containing lymphocytes in ataxia telangiectasia and Nijmegen breakage syndrome", *DNA repair,* vol. 5, no. 8, pp. 904-913.

Prince, M., Wimo, A., Guerchet, M., Claire Ali, G., Wu, Y. & Prina, M. 2015, "The Global Impact of Dementia", *The Journal of biological chemistry,* .

Purkis, P.E., Steel, J.B., Mackenzie, I.C., Nathrath, W.B., Leigh, I.M. & Lane, E.B. 1990, "Antibody markers of basal cells in complex epithelia", *Journal of cell science,* vol. 97 (Pt 1), no. Pt 1, pp. 39-50.

Qvarnstrom, O.F., Simonsson, M., Johansson, K.A., Nyman, J. & Turesson, I. 2004, "DNA double strand break quantification in skin biopsies", *Radiotherapy and oncology : journal of the European Society for Therapeutic Radiology and Oncology,* vol. 72, no. 3, pp. 311-317.

Raj, V. & Mahajan, S. 2011, "Dose response relationship of nuclear changes with fractionated radiotherapy in assessing radiosensitivity of oral squamous cell carcinoma", *J.Clin.Exp.Dent.,* vol. 3, no. 3, pp. e193-200.

Reddig, A., Lorenz, S., Hiemann, R., Guttek, K., Hartig, R., Heiserich, L., Eberle, C., Peters, V., Schierack, P., Sack, U., Roggenbuck, D. & Reinhold, D. 2015, "Assessment of modulated cytostatic drug resistance by automated gammaH2AX analysis", *Cytometry.Part A : the journal of the International Society for Analytical Cytology,* vol. 87, no. 8, pp. 724-732.

Redon, C., Pilch, D., Rogakou, E., Sedelnikova, O., Newrock, K. & Bonner, W. 2002, "Histone H2A variants H2AX and H2AZ", *Current opinion in genetics & development,* vol. 12, no. 2, pp. 162-169.

Redon, C.E., Dickey, J.S., Bonner, W.M. & Sedelnikova, O.A. 2009, "gamma-H2AX as a biomarker of DNA damage induced by ionizing radiation in human peripheral blood lymphocytes and artificial skin", *Advances in space research : the official journal of the Committee on Space Research (COSPAR),* vol. 43, no. 8, pp. 1171-1178.

Redon, C.E., Nakamura, A.J., Gouliaeva, K., Rahman, A., Blakely, W.F. & Bonner, W.M. 2010, "The use of gamma-H2AX as a biodosimeter for total-body radiation exposure in non-human primates", *PloS one,* vol. 5, no. 11, pp. e15544.

Riballo, E., Kuhne, M., Rief, N., Doherty, A., Smith, G.C., Recio, M.J., Reis, C., Dahm, K., Fricke, A., Krempler, A., Parker, A.R., Jackson, S.P., Gennery, A., Jeggo, P.A. & Lobrich, M. 2004, "A pathway of double-strand break rejoining dependent upon ATM, Artemis, and proteins locating to gamma-H2AX foci", *Molecular cell,* vol. 16, no. 5, pp. 715-724.

Richards, B., Skoletsky, J., Shuber, A.P., Balfour, R., Stern, R.C., Dorkin, H.L., Parad, R.B., Witt, D. & Klinger, K.W. 1993, "Multiplex PCR amplification from the CFTR gene using DNA prepared from buccal brushes/swabs", *Human molecular genetics,* vol. 2, no. 2, pp. 159-163.

Riches, L.C., Lynch, A.M. & Gooderham, N.J. 2008, "Early events in the mammalian response to DNA double-strand breaks", *Mutagenesis,* vol. 23, no. 5, pp. 331-339.

Roch-Lefevre, S., Mandina, T., Voisin, P., Gaetan, G., Mesa, J.E., Valente, M., Bonnesoeur, P., Garcia, O., Voisin, P. & Roy, L. 2010, "Quantification of gamma-H2AX foci in human lymphocytes: a method for biological dosimetry after ionizing radiation exposure", *Radiation research,* vol. 174, no. 2, pp. 185-194.

Rodier, F., Coppe, J.P., Patil, C.K., Hoeijmakers, W.A., Munoz, D.P., Raza, S.R., Freund, A., Campeau, E., Davalos, A.R. & Campisi, J. 2009, "Persistent DNA damage signalling triggers senescence-associated inflammatory cytokine secretion", *Nature cell biology,* vol. 11, no. 8, pp. 973-979.

Rogakou, E.P., Boon, C., Redon, C. & Bonner, W.M. 1999, "Megabase chromatin domains involved in DNA double-strand breaks in vivo", *The Journal of cell biology,* vol. 146, no. 5, pp. 905-916.

Rogakou, E.P., Nieves-Neira, W., Boon, C., Pommier, Y. & Bonner, W.M. 2000, "Initiation of DNA fragmentation during apoptosis induces phosphorylation of H2AX histone at serine 139", *The Journal of biological chemistry,* vol. 275, no. 13, pp. 9390-9395.

Rogakou, E.P., Pilch, D.R., Orr, A.H., Ivanova, V.S. & Bonner, W.M. 1998, "DNA double-stranded breaks induce histone H2AX phosphorylation on serine 139", *The Journal of biological chemistry,* vol. 273, no. 10, pp. 5858-5868.

Roninson, I.B. 2003, "Tumor cell senescence in cancer treatment", *Cancer research,* vol. 63, no. 11, pp. 2705-2715.

Rossiello, F., Herbig, U., Longhese, M.P., Fumagalli, M. & d'Adda di Fagagna, F. 2014, "Irreparable telomeric DNA damage and persistent DDR signalling as a shared causative mechanism of cellular senescence and ageing", *Current opinion in genetics & development,* vol. 26, pp. 89-95.

Rothkamm, K. & Horn, S. 2009, "gamma-H2AX as protein biomarker for radiation exposure", *Annali dell'Istituto Superiore di Sanita,* vol. 45, no. 3, pp. 265-271.

Rothkamm, K. & Lobrich, M. 2003, "Evidence for a lack of DNA double-strand break repair in human cells exposed to very low x-ray doses", *Proceedings of the National Academy of Sciences of the United States of America,* vol. 100, no. 9, pp. 5057-5062.

Rube, C.E., Dong, X., Kuhne, M., Fricke, A., Kaestner, L., Lipp, P. & Rube, C. 2008, "DNA double-strand break rejoining in complex normal tissues", *International journal of radiation oncology, biology, physics,* vol. 72, no. 4, pp. 1180-1187.

Rube, C.E., Fricke, A., Schneider, R., Simon, K., Kuhne, M., Fleckenstein, J., Graber, S., Graf, N. & Rube, C. 2010, "DNA repair alterations in children with pediatric malignancies: novel opportunities to identify patients at risk for high-grade toxicities", *International journal of radiation oncology, biology, physics,* vol. 78, no. 2, pp. 359-369.

Rube, C.E., Fricke, A., Widmann, T.A., Furst, T., Madry, H., Pfreundschuh, M. & Rube, C. 2011, "Accumulation of DNA damage in hematopoietic stem and progenitor cells during human aging", *PloS one,* vol. 6, no. 3, pp. e17487.

Runge, R., Hiemann, R., Wendisch, M., Kasten-Pisula, U., Storch, K., Zophel, K., Fritz, C., Roggenbuck, D., Wunderlich, G., Conrad, K. & Kotzerke, J. 2012, "Fully automated interpretation of ionizing radiation-induced gammaH2AX foci by the novel pattern recognition system AKLIDES(R)", *International journal of radiation biology,* vol. 88, no. 5, pp. 439-447.

Sak, A., Grehl, S., Erichsen, P., Engelhard, M., Grannass, A., Levegrun, S., Pottgen, C., Groneberg, M. & Stuschke, M. 2007, "gamma-H2AX foci formation in peripheral blood lymphocytes of tumor patients after local radiotherapy to different sites of the body: dependence on the dose-distribution, irradiated site and time from start of treatment", *International journal of radiation biology,* vol. 83, no. 10, pp. 639-652.

Savic, V., Yin, B., Maas, N.L., Bredemeyer, A.L., Carpenter, A.C., Helmink, B.A., Yang-Iott, K.S., Sleckman, B.P. & Bassing, C.H. 2009, "Formation of dynamic gamma-H2AX domains along broken DNA strands is distinctly regulated by ATM and MDC1 and dependent upon H2AX densities in chromatin", *Molecular cell,* vol. 34, no. 3, pp. 298-310.

Scarpato, R., Verola, C., Fabiani, B., Bianchi, V., Saggese, G. & Federico, G. 2011, "Nuclear damage in peripheral lymphocytes of obese and overweight Italian children as evaluated by the gamma-H2AX focus assay and micronucleus test", *FASEB journal : official publication of the Federation of American Societies for Experimental Biology,* vol. 25, no. 2, pp. 685-693.

Schurman, S.H., Dunn, C.A., Greaves, R., Yu, B., Ferrucci, L., Croteau, D.L., Seidman, M.M. & Bohr, V.A. 2012, "Age-related disease association of endogenous gamma-H2AX foci in mononuclear cells derived from leukapheresis", *PloS one,* vol. 7, no. 9, pp. e45728.

Schwartz, J.L., Muscat, J.E., Baker, V., Larios, E., Stephenson, G.D., Guo, W., Xie, T., Gu, X. & Chung, F.L. 2003, "Oral cytology assessment by flow cytometry of DNA adducts, aneuploidy, proliferation and apoptosis shows differences between smokers and non-smokers", *Oral oncology,* vol. 39, no. 8, pp. 842-854.

Sedelnikova, O.A., Horikawa, I., Redon, C., Nakamura, A., Zimonjic, D.B., Popescu, N.C. & Bonner, W.M. 2008, "Delayed kinetics of DNA double-strand break processing in normal and pathological aging", *Aging cell,* vol. 7, no. 1, pp. 89-100.

Sedelnikova, O.A., Horikawa, I., Zimonjic, D.B., Popescu, N.C., Bonner, W.M. & Barrett, J.C. 2004, "Senescing human cells and ageing mice accumulate DNA lesions with unrepairable double-strand breaks", *Nature cell biology,* vol. 6, no. 2, pp. 168-170.

Sedelnikova, O.A., Rogakou, E.P., Panyutin, I.G. & Bonner, W.M. 2002, "Quantitative detection of (125)IdU-induced DNA double-strand breaks with gamma-H2AX antibody", *Radiation research,* vol. 158, no. 4, pp. 486-492.

Selkoe, D.J. 2001, "Alzheimer's disease results from the cerebral accumulation and cytotoxicity of amyloid beta-protein", *Journal of Alzheimer's disease : JAD,* vol. 3, no. 1, pp. 75-80.

Sery, O., Hlinecka, L., Balcar, V.J., Janout, V. & Povova, J. 2014, "Diabetes, hypertension and stroke - does Alzheimer protect you?", *Neuro endocrinology letters,* vol. 35, no. 8, pp. 691-696.

Sharma, P.M., Ponnaiya, B., Taveras, M., Shuryak, I., Turner, H. & Brenner, D.J. 2015, "High Throughput Measurement of gammaH2AX DSB Repair Kinetics in a Healthy Human Population", *PloS one,* vol. 10, no. 3, pp. e0121083.

Sharpless, N.E. & DePinho, R.A. 2007, "How stem cells age and why this makes us grow old", *Nature reviews.Molecular cell biology,* vol. 8, no. 9, pp. 703-713.

Shechter, D., Dormann, H.L., Allis, C.D. & Hake, S.B. 2007, "Extraction, purification and analysis of histones", *Nature protocols,* vol. 2, no. 6, pp. 1445-1457.

Shukkur, E.A., Shimohata, A., Akagi, T., Yu, W., Yamaguchi, M., Murayama, M., Chui, D., Takeuchi, T., Amano, K., Subramhanya, K.H., Hashikawa, T., Sago, H., Epstein, C.J., Takashima, A. & Yamakawa, K. 2006, "Mitochondrial dysfunction and tau hyperphosphorylation in Ts1Cje, a mouse model for Down syndrome", *Human molecular genetics,* vol. 15, no. 18, pp. 2752-2762.

Siddiqui, M.S., Filomeni, E., Francois, M., Collins, S.R., Cooper, T., Glatz, R.V., Taylor, P.W., Fenech, M. & Leifert, W.R. 2013, "Exposure of insect cells to ionising radiation in vivo induces persistent phosphorylation of a H2AX homologue (H2AvB)", *Mutagenesis,* vol. 28, no. 5, pp. 531-541.

Siddiqui, M.S., Francois, M., Fenech, M.F. & Leifert, W.R. 2015, "gammaH2AX responses in human buccal cells exposed to ionizing radiation", *Cytometry.Part A : the journal of the International Society for Analytical Cytology,* vol. 87, no. 4, pp. 296-308.

Sikora, E., Arendt, T., Bennett, M. & Narita, M. 2011, "Impact of cellular senescence signature on ageing research", *Ageing research reviews,* vol. 10, no. 1, pp. 146-152.

Silva, A.R., Santos, A.C., Farfel, J.M., Grinberg, L.T., Ferretti, R.E., Campos, A.H., Cunha, I.W., Begnami, M.D., Rocha, R.M., Carraro, D.M., de Braganca Pereira, C.A., Jacob-Filho, W. & Brentani, H. 2014, "Repair of oxidative DNA damage, cell-cycle regulation and neuronal death may influence the clinical manifestation of Alzheimer's disease", *PloS one,* vol. 9, no. 6, pp. e99897.

Simpson, J.E., Ince, P.G., Haynes, L.J., Theaker, R., Gelsthorpe, C., Baxter, L., Forster, G., Lace, G.L., Shaw, P.J., Matthews, F.E., Savva, G.M., Brayne, C., Wharton, S.B. & MRC Cognitive Function and Ageing Neuropathology Study Group 2010, "Population variation in oxidative stress and astrocyte DNA damage in relation to Alzheimer-type pathology in the ageing brain", *Neuropathology and applied neurobiology,* vol. 36, no. 1, pp. 25-40.

Sinclair, D.A. & Oberdoerffer, P. 2009, "The ageing epigenome: damaged beyond repair?", *Ageing research reviews,* vol. 8, no. 3, pp. 189-198.

Sloane, P.D., Zimmerman, S., Suchindran, C., Reed, P., Wang, L., Boustani, M. & Sudha, S. 2002, "The public health impact of Alzheimer's disease, 2000-2050: potential implication of treatment advances", *Annual Review of Public Health,* vol. 23, pp. 213-231.

Smith, A.D. 2008, "The worldwide challenge of the dementias: a role for B vitamins and homocysteine?", *Food and nutrition bulletin,* vol. 29, no. 2 Suppl, pp. S143-72.

Smogorzewska, A., Karlseder, J., Holtgreve-Grez, H., Jauch, A. & de Lange, T. 2002, "DNA ligase IV-dependent NHEJ of deprotected mammalian telomeres in G1 and G2", *Current biology : CB,* vol. 12, no. 19, pp. 1635-1644.

Soininen, H., Syrjanen, S., Heinonen, O., Neittaanmaki, H., Miettinen, R., Paljarvi, L., Syrjanen, K., Beyreuther, K. & Riekkinen, P. 1992, "Amyloid beta-protein deposition in skin of patients with dementia", *Lancet (London, England),* vol. 339, no. 8787, pp. 245.

Song, Y.H. 2005, "Drosophila melanogaster: a model for the study of DNA damage checkpoint response", *Molecules and cells,* vol. 19, no. 2, pp. 167-179.

Song, Z., von Figura, G., Liu, Y., Kraus, J.M., Torrice, C., Dillon, P., Rudolph-Watabe, M., Ju, Z., Kestler, H.A., Sanoff, H. & Lenhard Rudolph, K. 2010, "Lifestyle impacts on the aging-associated expression of biomarkers of DNA damage and telomere dysfunction in human blood", *Aging cell,* vol. 9, no. 4, pp. 607-615.

Soopaya, R., Stringer, L.D., Woods, B., Stephens, A.E., Butler, R.C., Lacey, I., Kaur, A. & Suckling, D.M. 2011, "Radiation biology and inherited sterility of light brown apple moth (Lepidoptera: Tortricidae): developing a sterile insect release program", *Journal of economic entomology,* vol. 104, no. 6, pp. 1999-2008.

Soto-Gordoa, M., Arrospide, A., Moreno-Izco, F., Martinez-Lage, P., Castilla, I. & Mar, J. 2015, "Projecting Burden of Dementia in Spain, 2010-2050: Impact of Modifying Risk Factors", *Journal of Alzheimer's disease : JAD,* vol. 48, no. 3, pp. 721-730.

Spivack, S.D., Hurteau, G.J., Jain, R., Kumar, S.V., Aldous, K.M., Gierthy, J.F. & Kaminsky, L.S. 2004, "Gene-environment interaction signatures by quantitative mRNA profiling in exfoliated buccal mucosal cells", *Cancer research,* vol. 64, no. 18, pp. 6805-6813.

Stein, G.H., Drullinger, L.F., Robetorye, R.S., Pereira-Smith, O.M. & Smith, J.R. 1991, "Senescent cells fail to express cdc2, cycA, and cycB in response to mitogen stimulation", *Proceedings of the National Academy of Sciences of the United States of America,* vol. 88, no. 24, pp. 11012-11016.

Steller, H. 2008, "Regulation of apoptosis in Drosophila", *Cell death and differentiation,* vol. 15, no. 7, pp. 1132-1138.

Stiff, T., O'Driscoll, M., Rief, N., Iwabuchi, K., Lobrich, M. & Jeggo, P.A. 2004, "ATM and DNA-PK function redundantly to phosphorylate H2AX after exposure to ionizing radiation", *Cancer research,* vol. 64, no. 7, pp. 2390-2396.

Storandt, M. 1991, "Neuropsychological assessment in Alzheimer's disease", *Experimental aging research,* vol. 17, no. 2, pp. 100-101.

Sun, N.K., Sun, C.L., Lin, C.H., Pai, L.M. & Chao, C.C. 2010, "Damaged DNA-binding protein 2 (DDB2) protects against UV irradiation in human cells and Drosophila", *Journal of Biomedical Science,* vol. 17, pp. 27.

Suzuki, K., Ojima, M., Kodama, S. & Watanabe, M. 2003, "Radiation-induced DNA damage and delayed induced genomic instability", *Oncogene,* vol. 22, no. 45, pp. 6988-6993.

Suzuki, M., Suzuki, K., Kodama, S. & Watanabe, M. 2006, "Interstitial chromatin alteration causes persistent p53 activation involved in the radiation-induced senescence-like growth arrest", *Biochemical and biophysical research communications,* vol. 340, no. 1, pp. 145-150.

Swardfager, W., Lanctot, K., Rothenburg, L., Wong, A., Cappell, J. & Herrmann, N. 2010, "A meta-analysis of cytokines in Alzheimer's disease", *Biological psychiatry,* vol. 68, no. 10, pp. 930-941.

Tanaka, T., Halicka, D., Traganos, F. & Darzynkiewicz, Z. 2009, "Cytometric analysis of DNA damage: phosphorylation of histone H2AX as a marker of DNA double-strand breaks (DSBs)", *Methods in molecular biology (Clifton, N.J.),* vol. 523, pp. 161-168.

Tanaka, T., Huang, X., Halicka, H.D., Zhao, H., Traganos, F., Albino, A.P., Dai, W. & Darzynkiewicz, Z. 2007, "Cytometry of ATM activation and histone H2AX phosphorylation to estimate extent of DNA damage induced by exogenous agents", *Cytometry.Part A : the journal of the International Society for Analytical Cytology,* vol. 71, no. 9, pp. 648-661.

Taneja, N., Davis, M., Choy, J.S., Beckett, M.A., Singh, R., Kron, S.J. & Weichselbaum, R.R. 2004, "Histone H2AX phosphorylation as a predictor of radiosensitivity and target for radiotherapy", *The Journal of biological chemistry,* vol. 279, no. 3, pp. 2273-2280.

Tang, K., Hynan, L.S., Baskin, F. & Rosenberg, R.N. 2006, "Platelet amyloid precursor protein processing: a bio-marker for Alzheimer's disease", *Journal of the neurological sciences,* vol. 240, no. 1-2, pp. 53-58.

Thambisetty, M. & Lovestone, S. 2010, "Blood-based biomarkers of Alzheimer's disease: challenging but feasible", *Biomarkers in medicine,* vol. 4, no. 1, pp. 65-79.

Thomas, P. & Fenech, M. 2008, "Chromosome 17 and 21 aneuploidy in buccal cells is increased with ageing and in Alzheimer's disease", *Mutagenesis,* vol. 23, no. 1, pp. 57-65.

Thomas, P. & Fenech, M. 2007, "A review of genome mutation and Alzheimer's disease", *Mutagenesis,* vol. 22, no. 1, pp. 15-33.

Thomas, P., Harvey, S., Gruner, T. & Fenech, M. 2008, "The buccal cytome and micronucleus frequency is substantially altered in Down's syndrome and normal ageing compared to young healthy controls", *Mutation research,* vol. 638, no. 1-2, pp. 37-47.

Thomas, P., Hecker, J., Faunt, J. & Fenech, M. 2007, "Buccal micronucleus cytome biomarkers may be associated with Alzheimer's disease", *Mutagenesis,* vol. 22, no. 6, pp. 371-379.

Thomas, P., Holland, N., Bolognesi, C., Kirsch-Volders, M., Bonassi, S., Zeiger, E., Knasmueller, S. & Fenech, M. 2009, "Buccal micronucleus cytome assay", *Nature protocols,* vol. 4, no. 6, pp. 825-837.

Thomas, P., O'Callaghan, N.J. & Fenech, M. 2008, "Telomere length in white blood cells, buccal cells and brain tissue and its variation with ageing and Alzheimer's disease", *Mechanisms of ageing and development,* vol. 129, no. 4, pp. 183-190.

Tijms, B.M., Moller, C., Vrenken, H., Wink, A.M., de Haan, W., van der Flier, W.M., Stam, C.J., Scheltens, P. & Barkhof, F. 2013, "Single-subject grey matter graphs in Alzheimer's disease", *PloS one,* vol. 8, no. 3, pp. e58921.

Tobinick, E.L. 2008, "Re: Inflammatory markers and the risk of Alzheimer disease: the Framingham Study", *Neurology,* vol. 70, no. 14, pp. 1222-3; author reply 1223.

Tombaugh, T.N. & McIntyre, N.J. 1992, "The mini-mental state examination: a comprehensive review", *Journal of the American Geriatrics Society,* vol. 40, no. 9, pp. 922-935.

Torres-Bugarin, O., Zavala-Cerna, M.G., Nava, A., Flores-Garcia, A. & Ramos-Ibarra, M.L. 2014, "Potential uses, limitations, and basic procedures of micronuclei and nuclear abnormalities in buccal cells", *Disease markers,* vol. 2014, pp. 956835.

Torudd, J., Protopopova, M., Sarimov, R., Nygren, J., Eriksson, S., Markova, E., Chovanec, M., Selivanova, G. & Belyaev, I.Y. 2005, "Dose-response for radiation-induced apoptosis, residual 53BP1 foci and DNA-loop relaxation in human lymphocytes", *International journal of radiation biology,* vol. 81, no. 2, pp. 125-138.

Trippi, F., Botto, N., Scarpato, R., Petrozzi, L., Bonuccelli, U., Latorraca, S., Sorbi, S. & Migliore, L. 2001, "Spontaneous and induced chromosome damage in somatic cells of sporadic and familial Alzheimer's disease patients", *Mutagenesis,* vol. 16, no. 4, pp. 323-327.

Tucker, S.L., Geara, F.B., Peters, L.J. & Brock, W.A. 1996, "How much could the radiotherapy dose be altered for individual patients based on a predictive assay of normal-tissue radiosensitivity?", *Radiotherapy and oncology : journal of the European Society for Therapeutic Radiology and Oncology,* vol. 38, no. 2, pp. 103-113.

Turesson, I., Nyman, J., Holmberg, E. & Oden, A. 1996, "Prognostic factors for acute and late skin reactions in radiotherapy patients", *International journal of radiation oncology, biology, physics,* vol. 36, no. 5, pp. 1065-1075.

Turner, H.C., Brenner, D.J., Chen, Y., Bertucci, A., Zhang, J., Wang, H., Lyulko, O.V., Xu, Y., Shuryak, I., Schaefer, J., Simaan, N., Randers-Pehrson, G., Yao, Y.L., Amundson, S.A. & Garty, G. 2011, "Adapting the gamma-H2AX assay for automated processing in human lymphocytes. 1. Technological aspects", *Radiation research,* vol. 175, no. 3, pp. 282-290.

Turner, S.D., Wijnhoven, S.W., Tinwell, H., Lashford, L.S., Rafferty, J.A., Ashby, J., Vrieling, H. & Fairbairn, L.J. 2001, "Assays to predict the genotoxicity of the chromosomal mutagen etoposide -- focussing on the best assay", *Mutation research,* vol. 493, no. 1-2, pp. 139-147.

Vaidya, M.M., Borges, A.M., Pradhan, S.A., Rajpal, R.M. & Bhisey, A.N. 1989, "Altered keratin expression in buccal mucosal squamous cell carcinoma", *Journal of oral pathology & medicine : official publication of the International Association*

of Oral Pathologists and the American Academy of Oral Pathology, vol. 18, no. 5, pp. 282-286.

Valerie, K. & Povirk, L.F. 2003, "Regulation and mechanisms of mammalian double-strand break repair", *Oncogene,* vol. 22, no. 37, pp. 5792-5812.

Wald, D.S., Kasturiratne, A. & Simmonds, M. 2011, "Serum homocysteine and dementia: meta-analysis of eight cohort studies including 8669 participants", *Alzheimer's & dementia : the journal of the Alzheimer's Association,* vol. 7, no. 4, pp. 412-417.

Wang, C., Jurk, D., Maddick, M., Nelson, G., Martin-Ruiz, C. & von Zglinicki, T. 2009, "DNA damage response and cellular senescence in tissues of aging mice", *Aging cell,* vol. 8, no. 3, pp. 311-323.

Wang, H., Wang, M., Wang, H., Bocker, W. & Iliakis, G. 2005, "Complex H2AX phosphorylation patterns by multiple kinases including ATM and DNA-PK in human cells exposed to ionizing radiation and treated with kinase inhibitors", *Journal of cellular physiology,* vol. 202, no. 2, pp. 492-502.

Wang, J., Liu, Q. & Yang, Q. 2012, "Radiosensitization effects of berberine on human breast cancer cells", *International journal of molecular medicine,* vol. 30, no. 5, pp. 1166-1172.

Wang, J., Markesbery, W.R. & Lovell, M.A. 2006, "Increased oxidative damage in nuclear and mitochondrial DNA in mild cognitive impairment", *Journal of neurochemistry,* vol. 96, no. 3, pp. 825-832.

Wang, J., Xiong, S., Xie, C., Markesbery, W.R. & Lovell, M.A. 2005, "Increased oxidative damage in nuclear and mitochondrial DNA in Alzheimer's disease", *Journal of neurochemistry,* vol. 93, no. 4, pp. 953-962.

Wang, L., Raju, U., Milas, L., Molkentine, D., Zhang, Z., Yang, P., Cohen, L., Meng, Z. & Liao, Z. 2011, "Huachansu, containing cardiac glycosides, enhances radiosensitivity of human lung cancer cells", *Anticancer Research,* vol. 31, no. 6, pp. 2141-2148.

Ward, I. & Chen, J. 2004, "Early events in the DNA damage response", *Current topics in developmental biology,* vol. 63, pp. 1-35.

Ward, I.M. & Chen, J. 2001, "Histone H2AX is phosphorylated in an ATR-dependent manner in response to replicational stress", *The Journal of biological chemistry,* vol. 276, no. 51, pp. 47759-47762.

Ward, J.F. 1990, "The yield of DNA double-strand breaks produced intracellularly by ionizing radiation: a review", *International journal of radiation biology,* vol. 57, no. 6, pp. 1141-1150.

Ward, J.F. 1988, "DNA damage produced by ionizing radiation in mammalian cells: identities, mechanisms of formation, and reparability", *Progress in nucleic acid research and molecular biology,* vol. 35, pp. 95-125.

Warters, R.L., Adamson, P.J., Pond, C.D. & Leachman, S.A. 2005, "Melanoma cells express elevated levels of phosphorylated histone H2AX foci", *The Journal of investigative dermatology,* vol. 124, no. 4, pp. 807-817.

Wei, D., Parsels, L.A., Karnak, D., Davis, M.A., Parsels, J.D., Marsh, A.C., Zhao, L., Maybaum, J., Lawrence, T.S., Sun, Y. & Morgan, M.A. 2013, "Inhibition of protein phosphatase 2A radiosensitizes pancreatic cancers by modulating CDC25C/CDK1 and homologous recombination repair", *Clinical cancer research : an official journal of the American Association for Cancer Research,* vol. 19, no. 16, pp. 4422-4432.

Weintraub, S., Wicklund, A.H. & Salmon, D.P. 2012, "The neuropsychological profile of Alzheimer disease", *Cold Spring Harbor perspectives in medicine,* vol. 2, no. 4, pp. a006171.

Werbrouck, J., De Ruyck, K., Beels, L., Vral, A., Van Eijkeren, M., De Neve, W. & Thierens, H. 2010, "Prediction of late normal tissue complications in RT treated gynaecological cancer patients: potential of the gamma-H2AX foci assay and association with chromosomal radiosensitivity", *Oncology reports,* vol. 23, no. 2, pp. 571-578.

Williams, D.M. & Cruchley, A.T. 1994, "Structural aspects of ageing in the oral mucosa" in *The Effect of Ageing in the Oral Mucosa and Skin*, eds. C.A. Squier & M.W. Hill, Bocca Raton: CRC Press, London (UK), pp. 65-74.

Willitzki, A., Lorenz, S., Hiemann, R., Guttek, K., Goihl, A., Hartig, R., Conrad, K., Feist, E., Sack, U., Schierack, P., Heiserich, L., Eberle, C., Peters, V., Roggenbuck, D. & Reinhold, D. 2013, "Fully automated analysis of chemically induced gammaH2AX foci in human peripheral blood mononuclear cells by indirect immunofluorescence", *Cytometry.Part A : the journal of the International Society for Analytical Cytology,* vol. 83, no. 11, pp. 1017-1026.

Wilson, D.M.,3rd, Bohr, V.A. & McKinnon, P.J. 2008, "DNA damage, DNA repair, ageing and age-related disease", *Mechanisms of ageing and development,* vol. 129, no. 7-8, pp. 349-352.

Wu, J., Clingen, P.H., Spanswick, V.J., Mellinas-Gomez, M., Meyer, T., Puzanov, I., Jodrell, D., Hochhauser, D. & Hartley, J.A. 2013, "gamma-H2AX foci formation as a pharmacodynamic marker of DNA damage produced by DNA cross-linking agents: results from 2 phase I clinical trials of SJG-136 (SG2000)", *Clinical cancer research : an official journal of the American Association for Cancer Research,* vol. 19, no. 3, pp. 721-730.

Yoon, A.J., Shen, J., Wu, H.C., Angelopoulos, C., Singer, S.R., Chen, R. & Santella, R.M. 2009, "Expression of activated checkpoint kinase 2 and histone 2AX in exfoliative oral cells after exposure to ionizing radiation", *Radiation research,* vol. 171, no. 6, pp. 771-775.

Yoshida, K., Yoshida, S.H., Shimoda, C. & Morita, T. 2003, "Expression and radiation-induced phosphorylation of histone H2AX in mammalian cells", *Journal of radiation research,* vol. 44, no. 1, pp. 47-51.

Yu, T., MacPhail, S.H., Banath, J.P., Klokov, D. & Olive, P.L. 2006, "Endogenous expression of phosphorylated histone H2AX in tumors in relation to DNA double-strand breaks and genomic instability", *DNA repair,* vol. 5, no. 8, pp. 935-946.

Zalenskaya, I.A., Bradbury, E.M. & Zalensky, A.O. 2000, "Chromatin structure of telomere domain in human sperm", *Biochemical and biophysical research communications,* vol. 279, no. 1, pp. 213-218.

Zecevic, A., Menard, H., Gurel, V., Hagan, E., DeCaro, R. & Zhitkovich, A. 2009, "WRN helicase promotes repair of DNA double-strand breaks caused by aberrant mismatch repair of chromium-DNA adducts", *Cell cycle (Georgetown, Tex.),* vol. 8, no. 17, pp. 2769-2778.

Zengi, O., Karakas, A., Ergun, U., Senes, M., Inan, L. & Yucel, D. 2011, "Urinary 8-hydroxy-2'-deoxyguanosine level and plasma paraoxonase 1 activity with Alzheimer's disease", *Clinical chemistry and laboratory medicine : CCLM / FESCC,* vol. 50, no. 3, pp. 529-534.

Zetterberg, H. 2015, "Cerebrospinal fluid biomarkers for Alzheimer's disease: current limitations and recent developments", *Current opinion in psychiatry,* vol. 28, no. 5, pp. 402-409.

Zhao, H., Albino, A.P., Jorgensen, E., Traganos, F. & Darzynkiewicz, Z. 2009, "DNA damage response induced by tobacco smoke in normal human bronchial epithelial and A549 pulmonary adenocarcinoma cells assessed by laser scanning cytometry", *Cytometry.Part A : the journal of the International Society for Analytical Cytology,* vol. 75, no. 10, pp. 840-847.

Zhao, H. & Darzynkiewicz, Z. 2013, "Biomarkers of cell senescence assessed by imaging cytometry", *Methods in molecular biology (Clifton, N.J.),* vol. 965, pp. 83-92.

Zhao, H., Halicka, H.D., Traganos, F., Jorgensen, E. & Darzynkiewicz, Z. 2010, "New biomarkers probing depth of cell senescence assessed by laser scanning cytometry", *Cytometry.Part A : the journal of the International Society for Analytical Cytology,* vol. 77, no. 11, pp. 999-1007.

Zhao, H., Traganos, F. & Darzynkiewicz, Z. 2009, "Kinetics of the UV-induced DNA damage response in relation to cell cycle phase. Correlation with DNA replication", *Cytometry Part A,* vol. 77, no. 3, pp. 285-293.

Zhao, J., Guo, Z., Zhang, H., Wang, Z., Song, L., Ma, J., Pei, S. & Wang, C. 2013, "The potential value of the neutral comet assay and gammaH2AX foci assay in assessing the radiosensitivity of carbon beam in human tumor cell lines", *Radiology and oncology,* vol. 47, no. 3, pp. 247-257.

Zhuo, J.M., Wang, H. & Pratico, D. 2011, "Is hyperhomocysteinemia an Alzheimer's disease (AD) risk factor, an AD marker, or neither?", *Trends in pharmacological sciences,* vol. 32, no. 9, pp. 562-571.

Publications available online as PDF format

Mutation Research 766 (2015) 1–19

Contents lists available at ScienceDirect

Mutation Research/Reviews in Mutation Research

journal homepage: www.elsevier.com/locate/reviewsmr
Community address: www.elsevier.com/locate/mutres

Review

Persistent γH2AX: A promising molecular marker of DNA damage and aging

Mohammad Sabbir Siddiqui [a,b], Maxime François [a], Michael F. Fenech [a], Wayne R. Leifert [a,*]

[a] CSIRO Food and Nutrition Flagship, Genome Health and Healthy Aging, Adelaide, South Australia 5000, Australia
[b] University of Adelaide, School of Agriculture, Food & Wine, Urrbrae, South Australia 5064, Australia

ARTICLE INFO

Article history:
Received 27 March 2015
Received in revised form 13 July 2015
Accepted 14 July 2015
Available online 21 July 2015

Keywords:
γH2AX
Ionizing radiation
DNA damage
Aging

ABSTRACT

One of the earliest cellular responses to DNA double strand breaks (DSBs) is the phosphorylation of the core histone protein H2AX (termed γH2AX). Persistent γH2AX is the level of γH2AX above baseline, measured at a given time-point beyond which DNA DSBs are normally expected to be repaired (usually persist for days to months). This review summarizes the concept of persistent γH2AX in the context of exogenous source induced DNA DSBs (*e.g.* ionizing radiation (IR), chemotherapeutic drugs, genotoxic agents), and endogenous γH2AX levels in normal aging and accelerated aging disorders. Summary of the current literature demonstrates the following (i) γH2AX persistence is a common phenomenon that occurs in humans and animals; (ii) nuclei retain persistent γH2AX foci for up to several months after IR exposure, allowing for retrospective biodosimetry; (iii) the combination of various radiosensitizing drugs with ionizing radiation exposure leads to persistent γH2AX response, thus enabling the potential for monitoring cancer patients' response to chemotherapy and radiotherapy as well as tailoring cancer treatments; (iv) persistent γH2AX accumulates in telomeric DNA and in cells undergoing cellular senescence; and (v) increased endogenous γH2AX levels may be associated with diseases of accelerated aging. In summary, measurement of persistent γH2AX could potentially be used as a marker of radiation biodosimetry, evaluating sensitivity to therapeutic genotoxins and radiotherapy, and exploring the association of unrepaired DNA DSBs on telomeres with diseases of accelerated aging.

Contents

* Corresponding author at: CSIRO Food & Nutrition Flagship, Adelaide, South Australia 5000, Australia.
E-mail address: wayne.leifert@csiro.au (W.R. Leifert).

http://dx.doi.org/10.1016/j.mrrev.2015.07.001
1383-5742/

1. Introduction

Double strand breaks (DSBs) in DNA may lead to genetic instabilities and gene mutation resulting in reduced integrity of the genome and survival of the organism [1,2]. Replication stress, endogenous reactive oxygen species, exogenous sources of DNA damage such as ionizing radiation (IR), and genotoxic compounds are key causes of DNA breaks in living systems [3]. To repair these lesions, the DNA damage response (DDR) is initiated at the site of DNA damage [4,5]. An early known response to DNA DSBs in the cell is the phosphorylation of the C-terminal of the core histone protein H2AX (termed γH2AX when phosphorylated) [6,7]. The phosphorylation of H2AX occurs at the highly conserved amino acid Ser139 contained in the SQ (serine/glutamine) motif near the carboxy-terminus of H2AX [8,9]. The phosphoinositide 3-kinase-related protein kinase (PIKK) family which includes Ataxia Telangiectasia Mutated (ATM), Ataxia Telangiectasia and Rad3-related protein (ATR) and DNA protein kinase catalytic subunit (DNA-PKcs) have all been implicated in H2AX phosphorylation [8,9]. However, ATM is considered as the main kinase for H2AX phosphorylation in response to DSBs under normal physiological conditions and to a greater extent when a cell is exposed to ionizing radiation, such as γ-radiation [6,8,10]. On the other hand, during replication stress, ATR appears to be involved in H2AX phosphorylation at the site of stalled 'replication forks' and DNA-PKcs respond to DSBs during the non-homologous end joining process [10–13]. The role of γH2AX is to recruit associated DDR proteins and ensure the retention of those proteins in the vicinity of DSB sites [14–17]. γH2AX interacts with the mediator of DNA damage check point (MDC1), which in turn recruits p53 binding protein 1 (53BP1) at the vicinity of DNA DSB sites. MDC1 and 53BP1 then interact with the MRE11-RAD50-NBS1 (MRN) complex, and contribute to efficient ATM attachment at the DNA DSBs site [18]. Phosphorylation of H2AX is an important step in the DDR process and has widely been used as a marker of DNA damage [15–17,19–22].

It has been previously estimated in human fibroblasts that approximately 1% of H2AX becomes phosphorylated (γH2AX) per 1 Gy of IR [6]. This appears to approximate 35 DNA DSBs, and hence one might expect 35 γH2AX foci. An antibody for γH2AX was designed to recognize the last nine residues of H2AX, including the phosphorylated serine at position 139 [23]. γH2AX signals appear as individual foci when cells are immunostained against fluorescence-coupled antibodies and visualized by fluorescence microscopy. γH2AX is formed in the close vicinity to DSBs within seconds after cells are exposed to IR, and an individual γH2AX foci represents a single DSB with a ratio of 1:1 [6,24,25]. After successful repair of DSBs, the γH2AX molecules are dephosphorylated by protein phosphatase 2A (PP2A) and γH2AX foci are no longer detectable with the γH2AX antibody [17,26–28].

The kinetics of γH2AX foci formation and loss have been widely investigated in different cell and tissue types in the context of DSBs induced after exposure *ex vivo* and *in vivo* to exogenous DNA damaging agents [6,29–32]. Two types of γH2AX foci have been found in cells: Firstly, transient γH2AX foci that are associated with rapid DSB repair and dephosphorylation of γH2AX to H2AX, usually within minutes to hours. The second type of γH2AX foci are residual and tend to persist for days to months (Fig. 1). The long-term persistence of "residual γH2AX" has been also termed "excess γH2AX" foci by different groups [33,34]. In this review; we have chosen to use the term "persistent γH2AX" (*i.e.* the γH2AX level assessed at a given time-point beyond which DSBs are expected to be repaired after initial exposures to DNA damaging agents such as IR, chemotherapeutic drugs, and genotoxic agent minus the baseline γH2AX level). Persistent γH2AX may indicate DNA DSBs that are either in the process of slow, ongoing repair, or DSBs that remain permanently unrepaired due to cellular senescence, apoptosis, or DSBs that remain unrepaired in specific genome sequences such as telomeres [32,35–37]. DNA DSBs also occur during normal cellular processes, including DNA replication, cellular senescence, and exposure to reactive oxygen species. Therefore, endogenous γH2AX foci are formed even in the absence of external DNA damaging agents such as radiation [38]. Humans and other mammals follow an intrinsic DNA repair mechanism to

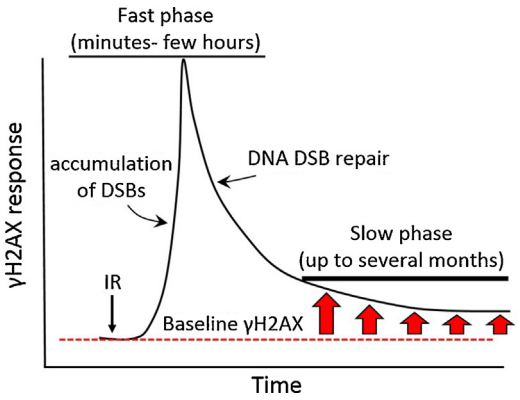

Fig. 1. Schematic representation of the short-term kinetics and persistent γH2AX response in relation to DSB repair. The kinetics of DNA DSB repair follows two phases, a fast phase lasting up to a few hours which is followed by a slower phase that may persist for several hours to days. Upon exposure to DNA damaging agents such as ionizing radiation (IR), the γH2AX foci appear in the fast phase within minutes after the DSBs are formed, and reach a maximum level after about 30 min. This level then declines rapidly, and corresponds to repair of DNA DSBs. A small portion of γH2AX (above baseline, as indicated by the dashed line) may persist for up to several months (slower phase) after the initial DSB-induction event and is known as the persistent γH2AX response (as indicated by the bold red arrows). Persistent γH2AX may represent unrepaired DSBs which are either in the process of slow ongoing repair, that are too complex to repair or associated with telomere DNA DSBs.

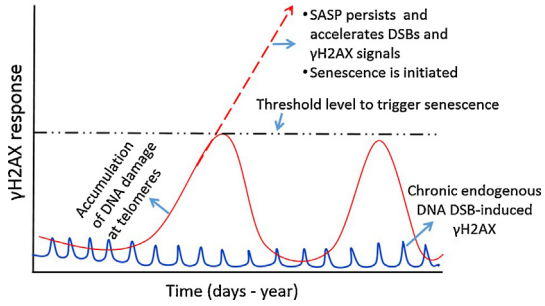

Fig. 2. Model depicting the possible cause of chronic endogenous DSB-induced persistent γH2AX. The intrinsic DNA repair mechanisms to repair endogenous DSBs occur during common cellular processes, including DNA replication, exposure to reactive oxygen species and cellular senescence. The repair of endogenous DSBs is continuous and rapid, involving recurring transient γH2AX responses. DSBs and γH2AX accumulate in telomere sequences within cells and may ultimately reach a threshold that triggers SASP which put into action the senescence process by which such cells are eliminated. There are therefore, two recurring waves of γH2AX foci expression in tissues: the first with short amplitude involving disappearance of γH2AX due to DSB repair and the second with wider amplitude involving elimination of cells with accumulated persistent γH2AX by cellular senescence processes. Abbreviations: DSBs, double-strand breaks; SASP, senescence associated secretory phenotype.

repair these endogenous DNA DSBs. However, small defects in the efficiency of repairing the chronic endogenous DNA DSBs for long periods (days, weeks, months and even years) may contribute to the accumulation of unrepaired DSBs on telomeres, which can be reflected as persistent γH2AX (Fig. 2). Measurement of persistent γH2AX in different cell and tissue types could therefore be used in radiation biodosimetry and cellular radiosensitivity responses during chemo- and radiotherapy, and to identify regions of the genome where DSB fails to repair.

IR-induced γH2AX foci formation and loss have been extensively investigated [6,29,30], whereas comparatively few studies have investigated endogenous γH2AX levels in normal aging and accelerated aging disorders. H2AX phosphorylation and DDR have been implicated in diseases of accelerated aging (*e.g.* Werner syndrome, Alzheimer's disease, obesity, diabetes, sleep apnoea, prostate cancer, cataract disease, hypertension, and Hutchinson–Gilford progeria syndrome) in recent studies [39–41], suggesting that lack of DNA integrity due to DNA damage progressively increases with age and may contribute to or be caused by these accelerated aging disorders. To date, no review has explored persistence of γH2AX in different cell and tissue types and discussed the importance of endogenous levels of γH2AX, in human aging and diseases of accelerated aging. The aims of this review are to summarize the findings of persistence of γH2AX in the context of exogenous source induced DSBs in different cell and tissue types, and to further discuss human diseases of accelerated aging that have reported endogenous γH2AX levels as a marker of unrepaired DNA damage.

2. Bibliographic search

The identification and selection of studies reported in this review was carried out through an extensive literature search using the PubMed database (National Library of Medicine, National Institutes of Health, Bethesda, MD, USA; http://www.ncbi.nih.gov/PubMed), and was up-to date as on April 30, 2015. The search strategy was based on the following keywords "persistent gammaH2AX", "residual gammaH2AX", "gammaH2AX kinetics", "unrepaired DNA damage", "irreparable DNA damage", "human endogenous gammaH2AX", "gammaH2AX in age-related diseases". Eligible studies included in this review were those conducted in humans, or animals, written in English, reporting long-term (>4 h) persistence of residual or excess γH2AX levels as a marker of either DNA damage or DNA repair (*i.e.* after *in vitro* or *in vivo* exposure to IR, and after chemotherapeutic or genotoxic drug treatment). Studies in blood cells or other surrogate cells, cancer tissues, biopsies, established cell lines or in cultured cells after treatments were included.

3. γH2AX detection methods

γH2AX foci can be observed with fluorescence microscopy by immunostaining cells with primary γH2AX antibodies coupled with fluorescent labeled secondary antibodies. The discernible hallmark of γH2AX foci counting is the ability to detect a single DSB in an individual cell [42–44]. The use of fluorescence can be extended to the measurement of total γH2AX protein level, in particular, types of cells and tissues using western blot and flow cytometry techniques [42–44]. The γH2AX foci counting approach has been used in numerous studies to assess the relationship between γH2AX foci removal and the rate of DSBs repair [25,45–48]. In radiation biology the number of DSBs positively correlates with γH2AX foci formation [6,23,24]. A linear increase of γH2AX foci per cell was proportional to the initial radiation dose 24 h and 48 h after exposure to IR doses ranging from 0.2 to 5 Gy in human blood samples and skin cells [49]. The highly dynamic changes of foci number and foci size over time after treatment with radiation or cytotoxic compounds can make the visual scoring time-consuming, potentially subjective, operator-dependent, and may involve fluorescence bleaching due to extended evaluation time, therefore, making visual scoring unsuitable for high-throughput applications. Several image analysis solutions for automated foci scoring have been developed, but were limited to low IR dose exposure resulting in discrete scoreable foci within the nuclei [50,51]. Visual and automated scoring of γH2AX foci formation in rat thyroid cells (PC Cl3) demonstrated a direct correlation between γH2AX foci and radiation dose but was restricted up to 1 Gy of IR [51]. Following exposure of cells to a dose of 5 Gy, visual scorers were unable to score γH2AX foci due to high density of DSBs which lead to γH2AX foci overlap (diffuse foci). Thus, one of the main issues when scoring multiple foci after exposure to a high radiation dose is the phenomenon of foci overlap that makes it more difficult to distinguish γH2AX as discrete entities (foci) [50]. In that case measurement of total γH2AX intensity using western blot or flow cytometry image analysis techniques may be sufficient to measure DNA damage levels by quantifying the total fluorescence for γH2AX signals.

Flow cytometry, allows rapid measurement of total γH2AX intensity in a large number of heterogeneous cell populations while enabling assessment of γH2AX intensity in different cell cycle phases and simultaneous measurement of other cellular proteins/markers involved in DNA damage/repair signaling process [52]. The γH2AX intensity in lymphocytes measured by flow cytometry quantitatively correlated with the number and size of γH2AX foci scored visually by fluorescence microscopy [52]. The IR-induced γH2AX quantification in the lymphocytes of prostate cancer patients during radiotherapy showed significant differences between patients and healthy donors by use of flow cytometry analysis; however, these results were not always in close agreement with results from fluorescence microscopy [52]. More recently, the use of laser scanning cytometry has also been proposed as a useful tool to measure cellular DNA content for cell cycle stage evaluation in conjunction with multiple γH2AX parameters (*e.g.* area, integral, MaxPixel) after inducing DNA damage [48,53,54]. The frequency of visually scored γH2AX in human buccal cell nuclei showed a strong correlation with LSC measured γH2AX integral [48]. Taken together, both microscopy and cytometry-based methods are suitable to evaluate γH2AX

formation and loss and the choice of the best γH2AX assay will depend on the purpose of the study. The image cytometry and LSC methods have an advantage over flow cytometry because they enable counting and sizing of γH2AX foci but they are slower to perform.

4. Long-term persistence of residual γH2AX

The decline kinetics of DNA DSB repair appears to follow two distinct phases: a fast phase generally lasting a few hours followed by a slower phase that may persist for several hours or days and may extend to several months [55,56] (a schematic is shown in Fig. 1). The majority of DSBs (~80%) are repaired during the first phase of the repair process and the remaining portion (~20%) repair at a slower pace during the slower phase [55,56]. The slow γH2AX repair kinetics reported in lymphocytes from healthy donors following exposure to IR is consistent with the findings that showed ~25% of residual γH2AX foci at 7 h after exposure to 4 Gy of IR in lymphocytes [57,58]. Evidence from several studies suggests that 60% of initial IR-induced DSBs are transient and repair in a relatively fast manner, often with half-lives of approximately 1–18 min [59,60]. The remaining 40% of DSBs repair slowly, with a repairing half-life in the range of 1.5–8 h [59–63]. DSBs measured several hours after an initial radiation exposure that still remain unrepaired, may be predictive of individual radiosensitivity to complex DNA lesions that can be lethal [64–66]. The rate of γH2AX foci loss and the presence of residual foci has also been correlated with cellular radiosensitivity and absorbed radiation dose [47,56,67–71]. Estimation of DSB repair rate from the decline kinetics of γH2AX foci was reported as a useful parameter to evaluate cellular radiosensitivity [58]. The persistent γH2AX foci may be present in the form of large foci. For example, in spermatids, the persistent γH2AX foci appeared as larger foci at 48 h after IR exposure [72]. Large persistent γH2AX foci were also observed in normal human fibroblasts (VH-10) and in HeLa cells after exposure to IR [73]. Additionally, a recent study reported the persistence and larger size of γH2AX foci 6 h after 3 Gy of high linear energy transfer radiation in a cell line lacking DNA-dependent protein kinase activity [74]. Clinical studies have demonstrated that the stochastic γH2AX foci induction and loss after external and internal radiation exposure in different types of cell depend on (i) the amount or type of IR (*e.g.* high dose (radiotherapy), low dose X-ray examination, or computed tomography (CT) scan), chemotherapeutic drug and genotoxic compound used; (ii) type of sample or part of body exposed to IR; (iii) duration or fractionation of exposure; (iv) inter individual radiosensitivity or damage response; (v) methods to measure γH2AX immunoreactivity; (vi) time-points for the kinetics of γH2AX foci formation and loss; (vii) time elapsed between the exposure and the γH2AX analysis, particularly if genotoxic exposure is acute rather than chronic [58,75,76].

In the following sections, we discuss persistence of γH2AX following *in vitro* and *in vivo* exposure to IR, chemotherapeutic drugs, and genotoxic agents among animals in different cell and tissue types (summarized in Table 1).

5. Persistent γH2AX in human cells

5.1. Peripheral blood mononuclear cells

Human blood lymphocytes have several advantages that make them suitable for evaluating γH2AX foci formation and loss: (i) a limited quantity of blood containing lymphocytes is required for γH2AX assay (1–2 ml) [77]; (ii) lymphocytes have low γH2AX background levels (0.05–0.1 foci/cell) [6,34,78]; (iii) the majority of cells are in the G_0 phase of the cell cycle [79]; (iv) there is minimal intra-individual variation in the level of γH2AX foci in different subsets of lymphocytes [80]; (v) there is minimal intra-individual variation in γH2AX foci number per lymphocytes, and therefore, the assay is relatively efficient at measuring differences in γH2AX between individuals [34,78,80].

Radiation therapy used in cancer treatment is applied either alone or in combination with chemotherapy; however, radiation therapy induces severe side-effects (acute effects such as erythema, edema, mucositis, dry or moist desquamation, severe skin changes, and late effects such as telangiectasia, fibrosis, cancer induction, brachial plexopathy, neurological effects) due to normal tissue toxicity (NTT) [81–85]. NTT has been graded by the Radiation Therapy Oncology Group into a standardized scale of acute and late responses after radiotherapy treatment for all tissue types, and these scales are used to avoid severe sequelae of radiotherapy [86]. Induction and persistence of γH2AX were assessed in peripheral blood lymphocytes (PBLs) of cancer patients with tumors in breast, thyroid, colon, brain, pituitary, prostate, cervix, and larynx for up to 24 h after 2 Gy of IR exposure [83]. The level of γH2AX response remained elevated in lymphocytes of cancer patients who had experienced acute NTT as a consequence of earlier radiotherapy compared to cancer patients who had little or no tissue toxicity as well as non-cancer controls, for up to 24 h after exposure to IR [83]. Persistence of γH2AX was significantly higher in lymphocytes from children with pediatric cancer compared with age-matched control children 8 h after exposure of whole blood with 1 Gy and 2 Gy of X-rays. While all healthy children exhibited efficient DNA repair, three children with pediatric cancer had impaired DNA repair capacity and two out of these three children developed acute normal tissue toxicity, which may be indicative of impaired DNA repair [87]. The measure of persistence of γH2AX can be a predictive assay in identifying those individuals at the greatest risk for the development of adverse effects to radiotherapy or chemotherapy. Additionally the γH2AX assay may be clinically useful to monitor NTT, thus will allow fine-tuning of the applied radiation dose during radiotherapy for improved cancer treatments. Another study reported higher levels of persistence of γH2AX foci per cell in lymphocytes of breast cancer patients with chronic late toxicities after radiotherapy compared with minimal late toxicities up to 24 h after exposure to 4 Gy of X-rays [88]. This result indicates that the persistence of γH2AX is likely associated with breast cancer patients' radiosensitivity. In another study, the mean number of γH2AX foci per cell analyzed in peripheral blood mononuclear cells (PBMCs) of breast cancer patients undergoing radiotherapy was significantly higher compared with untreated healthy controls with respect to the initial (30 min after 0.5 Gy of X-rays) and residual (24 h after exposure to 2 Gy X-rays) γH2AX foci, indicating potential use of γH2AX assay for screening radiosensitivity of breast cancer patients [66]. The level of γH2AX foci has also been previously measured to predict the side effects of radiotherapy among head and neck cancer patients [89]. Persistence of γH2AX was higher in lymphocytes of head and neck cancer patients compared with the untreated control group for up to 6 h after exposure to 2 Gy of X-rays [89]. Thus γH2AX would be a useful measure to identify individuals' radiosensitivity in advance so that customized radiation therapy may be applied to avoid severe side-effects due to radiation therapy. Persistence of γH2AX was also significantly higher in lymphocytes of Shwachman–Diamond syndrome individuals (an autosomal-recessive disorder characterized by bone marrow failure and a cumulative risk of progression to acute myeloid leukemia) compared to sham-irradiated cells 4 h after exposure to 4 Gy and 10 Gy of X-rays or γ-rays [90]. Interestingly, another group [84] found no difference in the persistence of γH2AX foci in T-lymphocytes 24 h after *ex vivo* exposure (up to 2.2 Gy) when comparing (1) none to mild and

Table 1
Persistent γH2AX response among animals in different cell and tissue types following ionizing radiation.

Cells/tissues analyzed	Treatment	Cohort/characteristic of cells	Outcome of γH2AX response	Technique used	Ref.
Human					
Lymphocytes	γ-rays 2 Gy	Cancer patients: (n = 12) with severe NTT after RT (n = 10) with little or no NTT and (n = 7) healthy, non-cancer control	*24 h post-IR* γH2AX ↑ by ∼4× in cancer patients with NTT compared with cancer patients with low NTT or non-cancer control	Flow cytometry	[83]
Lymphocytes	X-rays 1–2 Gy	Children with solid tumors received chemotherapy (n = 23), Healthy children (n = 24)	*24 h post-IR* ↑ foci/cell in children with solid tumors compared with age-matched healthy children ↑ foci/cell enables identification of children at risk with high-grade toxicities	Visually scored by fluorescence microscopy	[87]
Lymphocytes	γ-rays 2 Gy	Healthy donor (n = 4), AT (n = 6) and NBS (n = 4) patients	*72 h post IR* ↑ foci/cell by ∼4–8× in AT and NBS patient's cells	Visually scored by fluorescence microscopy	[91]
Lymphocytes	X-rays 4 Gy	Breast cancer patient after radiotherapy Control: very little or no damage in normal tissue (n = 7), Case: marked damage in normal tissue (n = 7)	*24 h post-IR* ↑ foci/cell in case compared with control	Visually scored by fluorescence microscopy	[88]
PBMCs	X-rays 4 Gy	Control: healthy donors (n = 12) Case: Breast cancer patients undergoing radiotherapy (n = 57)	*24 h post-IR* ↑ foci/cell in case compared with untreated healthy control	Visually scored using fluorescence images	[66]
Lymphocytes	X-rays 2 Gy	Head and neck cancer patients undergoing radiotherapy (n = 54) Untreated control (n = 26)	*6 h post IR* ↑ foci/cell in lymphocytes of head-and-neck cancer patients compared with untreated control group	Image captured by fluorescence microscopy followed by foci counting using Olympus microimage software	[89]
Lymphocytes	Low dose rate (14.7 cGy/h) and high dose rate (0.5 Gy/min)	Cervix cancer patients (n = 12) or endometrial cancer patients (n = 17)	*24 h post-IR* No significant changes in non to mild and moderate to severe late radiotoxicity	Visually scored using fluorescence images	[84]
Leucocytes	Radionuclide therapy with the isotope I^{131}	26 Patients with differentiated thyroid carcinoma (7 men, 19 women)	*6 days after administration* ↑ foci/cell	Visually scored using fluorescence images	[45]
Lymphocytes	Radionuclide therapy with the isotope I^{131}	15 patients with differentiated thyroid carcinoma (8 women, 7 men)	*4 days after administration* ↑ foci/cell	Visually scored using fluorescence images	[92]
Lymphocytes	X-rays 60–66 Gy (single dose 2 Gy, five fractions per week)	Head and nick cancer patients (n = 31)	*24 h post-IR* ↑ foci/cell predisposed to increased incidence of severe oral mucositis	Visually scored using fluorescence images	[82]
Lymphocytes	CT – 157 to 1514 mGy cm	Benign diseases (n = 13) and known malignant neoplasms (n = 10)	*24 h after CT* ↑ foci/cell in one patient with rectal cancer showed exceptionally severe side effects after radiotherapy	Visually scored using fluorescence images	[34]
Lymphocytes	PET involving the use of ^{18}F-fluorodeoxyglucose, and whole-body CT scan	Patients with history of lymphoma or leukemia (n = 33)	*24 h after combined PET/CT* ↑ foci/cell	Visually scored using fluorescence images	[93]
Lymphocytes	PRRT	Neuroendocrine tumors patients undergoing PRRT (n = 11)	*72 h after treatment* foci/cell ↓ close to baseline and correlated with absorbed dose to tumors and bone marrow ↓ number of lymphocytes	Visually scored using fluorescence images	[94]
Lymphocytes	CT – 7.78 per 1 Gy cm and PTA of lower limb arteries	Patients scheduled for CT (n = 5) and patients scheduled for PTA (n = 20)	*24 h after treatment* ↑ foci/cell	Visually scored using fluorescence images	[95]
Lymphocytes	γ rays 4 Gy	Healthy donors (n = 94)	*24 h after treatment* ↑ foci/cell	Fluorescence microscopy, ImageJ	[58]
Lymphocytes	γ rays 2 Gy	Healthy donors	*24 h to 4 weeks post-treatment* ↑foci/cell	Fluorescence microscopy, and LSM 510 software	[96]
Cell lines after isolation of lymphocytes from SDS patients	X-rays 4 10 Gy	SDS patients (n = 2) and SDS patient's heterozygous father (n = 1)	↑ foci/cell in SDS patients compared with sham irradiated control	Visually scored using fluorescence images	[90]
Fibroblasts	γ rays 0.6 Gy	Normal human fibroblast cells (IMR90)	*270 min post-IR* 4.5 foci/nucleus compared to 1.5 foci/nucleus at baseline	Laser scanning confocal microscopy	[23]

Table 1 (*Continued*)

Cells/tissues analyzed	Treatment	Cohort/characteristic of cells	Outcome of γH2AX response	Technique used	Ref.
Fibroblasts	γ rays 0.6 Gy	WS patients (n = 4) Control donors (n = 4)	*24 h post-IR* ↑ foci/cell by ∼1.5× in 60-year-old WS patients compared with controls	Visually scored by fluorescence microscopy	[40]
Fibroblasts	γ rays 2 Gy	FA patients (n = 10) Healthy donor (n = 6)	*24 h post-IR* foci/cell ↑ by ∼2.5–8× in FA cells compared with non-irradiated control and non-FABMF cells	Fluorescence microscopy, ImageJ	[102]
Fibroblasts	X-rays 10 Gy	Foreskin fibroblasts (HCA2)	*6 weeks post-exposure* ↑ foci/cell	Fluorescence microscopy, Photoshop CS2	[97]
Fibroblasts	Potent human carcinogen chromium Cr(VI) 20 μM	SV40-transformed WRN fibroblasts cell line (AG11395)	*24 h after treatment* ↑ foci/cell	Fluorescence microscopy, Phoenix software	[100]
Embryonic stem cells	γ rays 5 Gy	H1 hES cell lines	*24 h post-IR* dephosphorylation rate was slower in irradiated hES compared with normal somatic lung fibroblasts ↑ foci/cell in hES in irradiated hES compared with normal somatic lung fibroblasts	Western blot	[105]
Stem cells	X-rays 2 Gy	Healthy volunteers (n = 68) and umbilical cord blood (n = 34)	*24 h post-IR* Identical decline of foci/cell in all cells analyzed	Visually scored by fluorescence microscopy	[106]
Buccal cells	γ rays 2 Gy	5 healthy individuals (3 females, 2 males, aged 26–47 years)	*5 h post-IR* ↑ foci/cell by ∼4× in irradiated cells compared with non-irradiated control	Immunofluorescence and Histolab™ software	[104]
Buccal cells	γ rays 4 Gy	6 healthy individuals (3 females and 3 males, aged from 25 to 44 years)	*24 h post-IR* Visually scored: % of cell containing foci ↑ by ∼3× LSC: integral ↑ by ∼3×	Visually scored and laser scanning cytometry	[48]
Mouse					
Germ cells	X-rays 4 Gy	10- to 12-week-old C57Bl/6J male mice	% of cell containing foci ↑ by ∼6–10× 48 h post IR	Visually scored using fluorescence microscopy	[72]
Heart and kidney	X-rays 3 Gy	3 months old C57Bl/6 female mice	*23 h post-IR* % of nuclei containing foci ↑ by ∼5–10×	Confocal microscopy	[114]
Skin biopsies	γ rays 10 Gy	(n = 2) 4–6 week old radiosensitive strains (SCID and BALB/c) and (n = 2) radioresistant strains (C57BL/6 and C3H/HeJ) male mice	*7 days post-IR* Radioresistant strains (13–15 foci/100-μm^2 area) > Radiosensitive strains (∼4–6 γH2AX foci/100-μm^2 area)	Confocal microscopy	[65]
Spinal cord	X-rays 17 Gy followed by an immediate additional dose of 19 Gy	12 weeks old C3H/N female mice	*1 year post-IR* Foci were detected	Flow cytometry	[111]
Spleen, thymus, liver, lung, kidney, cerebellum, hippocampus, frontal cortex and olfactory bulb	*X-rays* 1 Gy	Very young (7 and 14 days old), adolescent (24 days old), young adult (30 days old) and sexually mature adult (45 days old) male and female mice	*24 h post-IR* Average number of foci/cell ↑ in Spleen ≫ Thymus > Liver > Lung Average number of foci/cell ↑ after 7 days > 14 days > 24 days > 30 days > 45 days	Visually scored using fluorescence microscopy	[115]
Small intestine, lung, brain, heart and kidney	Whole body X-rays 2 Gy	C57BL/6 mice	*48 h post-IR* ∼0.5 foci/cell, similar DNA repair kinetics were observed in all tissues.	Visually scored using fluorescence microscopy	[116]
Heart, small intestine, and kidney	X-rays 10 mGY, 100 mGy, and 1 Gy	C57BL/6 mouse	*24 h post-IR* 1 Gy: ∼<1 foci/cell 100 mGy: ∼<0.2 foci/cell 10 mGy: ∼<0.06 foci/cell	Visually scored using fluorescence images	[117]
Heart, brain, kidney and liver	Whole body X-rays 3 Gy	C57Bl/6 mice	*5 h post* γH2AX intensity ↑ in brain, kidney and liver compared with heart	Western blot	[120]
Minipig					
Skin biopsy	γ rays ∼50 Gy	14–16 months old (n = 7) female Göttingen minipig	*70 days post-IR* Irradiated cells: 0.14 foci/cell, non Irradiated cells: 0.05 foci/cell	Visually scored using fluorescence images	[118]

Table 1 (*Continued*)

Cells/tissues analyzed	Treatment	Cohort/characteristic of cells	Outcome of γH2AX response	Technique used	Ref.
(1) Lymphocytes (2) Fibroblasts	γ rays (1) 1.8 Gy (2) 2 Gy	4 months old male Göttingen minipigs	*24 h post-IR* (1) ↑ foci/cell by up to ~11× (2) ↑ foci/cell	Visually scored using fluorescence images	[33]
Fruit Fly					
Pupae	γ rays 0–400 Gy	Pupae were allowed to emerge as adults 17 days post-IR	*17 days post-IR* 25% of nuclei contained ↑ γH2AvB compared with non-irradiated controls	Western Blot, ImageJ and LSC	[119]
Syrian hamsters					
Heart, Brain, liver	X-rays 5 Gy	Male Syrian hamsters	*20 h post-IR* ↑ foci positive nuclei in heart, brain (not liver) by 3–4.5×	Visually scored following laser scanning confocal microscopy	[120]

Abbreviations: AT, ataxia telangiectasia; ATM, ataxia telangiectasia mutated; CT, computed tomography; FA, fanconic anemia; hES, human embryonic stem cells; IR, ionizing radiation; LSC, laser scanning cytometry; NTT, NORMAL tissue toxicity; NBS, Nijmegen breakage syndrome; Non-FABMF, non fanconic anemia bone marrow failure; PBMC, peripheral blood mononuclear cells; PET, positron emission tomography; PRRT, peptide receptor radionuclide therapy; PTA, percutaneous transluminal angioplasty; RT, radiotherapy; SDS, Shwachman–Diamond syndrome; WS, Werner syndrome.

(2) moderate to severe, late normal tissue radiotoxicity in gynecological cancer patients [84]. Persistent γH2AX was assessed in T lymphocytes from Ataxia Telangiectasia (AT) patients and patients with Nijmegen breakage syndrome (NBS), a disease associated with the mutation in nibrin proteins (coded by *NBN* gene). Seventy-two hours after exposure to 2 Gy of IR the number of γH2AX foci per cell increased in AT and NBS cells approximately 8- and 4-fold, respectively, compared with non-irradiated control cells [91].

γH2AX as a biomarker of toxicity and as a biodosimeter after systemic administration of radionuclide was investigated *in vivo* in several clinical studies [45,82]. For example, γH2AX induction and loss were assessed in a recent clinical study where radionuclide I^{131} therapy for thyroid cancer was used [45]. The leucocytes were irradiated *in vivo* by the β-particles emitting from circulating ^{131}I. γH2AX was quantified in leukocytes at different times and the highest number of γH2AX foci was observed at 2 h after administration of radionuclide therapy and thereafter declined with time; however, persistence of γH2AX was higher for up to 6 days compared with the number of γH2AX foci in the samples taken immediately before radionuclide therapy [45]. This result indicates that persistence of γH2AX is a promising marker to estimate the absorbed radiation dose *in vivo* after radionuclide therapy. Another study [92] reported elevated persistence of γH2AX foci in lymphocytes of thyroid cancer patients 4 days following *in vivo* isotope ^{131}I radionuclide therapeutic administration, allowing estimation of the radiation doses absorbed with this therapy. One important factor to consider on the interpretation of radionuclide induced *in vivo* γH2AX is that radionuclides may be continuously present in the body and induce DSBs chronically. Typically, other radiation exposures are acute and would likely represent a different kinetic profile of DSB formation and repair. It is also important to note that external irradiation treatment generally involves partial body irradiation whereas radionuclide therapy involves whole body exposure to irradiation. Another study showed that individuals who had higher levels of persistent γH2AX in PBMCs observed 24 h after *in vivo* exposure to X-rays (a single dose of 2 Gy, given once daily for 5 days per week) or RCT (radiotherapy in combination with chemotherapy) are likely to have an increased incidence of severe oral mucositis [82]. Following a CT examination, γH2AX levels in normal individuals reached baseline levels 24 h after the CT scan. However, one patient who had previously shown severe side effects after radiotherapy and had a DSB repair defect displayed a very much higher persistence of γH2AX foci [34]. This result suggests that individuals with a defect in DSB repair may exhibit impaired γH2AX foci loss thereby resulting in an increased persistence of γH2AX after CT [34]. The kinetics of γH2AX formation and loss were also assessed in blood lymphocytes of patients undergoing positron emission tomography (PET) involving the use of ^{18}F-Fluorodeoxyglucose (FDG), and whole body CT scan [93]. Radiation-induced γH2AX foci peaked 30 min after ^{18}F-FDG administration and 5 min after CT. After 24 h the number of γH2AX foci per cell decreased but remained higher compared to the pre-exposure level suggesting γH2AX as a useful marker to monitor radiation-induced *in vivo* DNA DSBs by ^{18}F-FDG and CT separately in patients undergoing combined PET/CT [93]. In a similar manner, the average number of γH2AX foci per lymphocyte increased in the first 30 min after LuTate administration (for neuroendocrine tumors) and peaked at 2 h [94]. The number of γH2AX foci decreased close to the baseline value 24–72 h after treatment. The γH2AX foci number in the interval from 10 min to 72 h after therapy correlated with the absorbed dose to tumor and bone marrow and subsequently resulted in a reduced number of lymphocytes. This result suggests γH2AX as a biomarker to assess lymphocyte cytotoxicity [94]. Immunofluorescence was used to demonstrate DSB induction (γH2AX foci) and repair in individuals exposed to IR during percutaneous transluminal angioplasty (PTA) [95]. γH2AX levels were approximately 1.7-fold higher in lymphocytes after PTA treatment compared to lymphocytes before PTA treatment. Thus γH2AX can be used as a marker to assess *in vivo* induction and repair of DSB in individuals exposed to radiation during PTA [95]. Persistence of 53BP1/γH2AX was also reported in human G_0 lymphocytes obtained from healthy volunteers 24 h to 4 weeks after exposure to 2 Gy of IR [96], indicating the potential use of γH2AX in biological dosimetry [96]. Therefore, persistence of γH2AX following the exposure to IR in human lymphocytes could be used as a maker to identify the radiosensitivity and the ability of individuals to recover from IR-related damage. The effect of age, gender, race, ethnicity, and alcohol use was investigated on IR-induced persistent γH2AX (24 h) in lymphocytes from healthy adults [58]. Of these demographic variables, there was a decline of persistent γH2AX in lymphocytes with increasing age, although age and race influenced the early γH2AX responses [58].

5.2. Fibroblasts

Persistence of γH2AX has been investigated in human fibroblasts after exposure to IR. In one study, γH2AX foci formed 3 min after exposure to 0.6 Gy of IR in human fibroblasts, γH2AX foci numbers then peaked at 30 min (11.6 foci/cell), and at 4.5 h this level declined to 4.5 foci/cell, which was higher compared to the level in non-irradiated control fibroblasts [23]. In another

study, persistence of γH2AX was reported in human diploid fibroblasts for up to 6 days after exposure to 10 Gy of IR (X-rays) [97]. However, the initial dose used in this study was very high [97]. The level of γH2AX was also tested in fibroblasts from Werner Syndrome patients (a disease associated with premature aging) to determine whether premature aging diseases is associated with a higher level of persistent γH2AX [40]. Twenty-four hours after exposure to 0.6 Gy of IR, the level of γH2AX foci in the fibroblasts from a 61-year-old healthy individual returned close to the values observed in non-irradiated controls. However, fibroblasts from a 60-year-old Werner Syndrome patient had approximately 1.5-fold increased levels of γH2AX foci/cell compared with the non-irradiated controls [40]. WRN protein exhibits both helicase and exonuclease activities and is mutated in Werner Syndrome [98,99]. WRN interacts with several proteins involved in the repair of DNA DSB and localizes to the sites of laser-induced DSB in live cells [100]. A recent study reported a higher persistence of γH2AX/53BP1 foci in human WRN-deficient fibroblasts compared with controls for up to 24 h after being treated with 20 μM of the potent human carcinogen, chromium Cr(VI), indicating impaired DSB repair due to abnormal mismatched repair [101]. This result suggests that the WRN protein may play an important role in repairing a specific class of DSB in human cells. Fanconi anemia is a blood disorder associated with a genetic defect in a cluster of proteins responsible for DNA repair and results in bone marrow failure [102]. The repair kinetics of radiation-induced DSBs were assessed in primary fibroblasts from Fanconi anemia, non-fanconic anemia bone marrow failure (non-FABMF) and control cell lines based on a γH2AX assay. Twenty-four hours after exposure to 2 Gy of IR, the level of γH2AX foci per cell in Fanconi anemia cell lines was approximately 2.5-fold higher compared to that in non-FABMF patients, and approximately 8-fold higher when compared with non-irradiated controls [103]. Fanconi anemia fibroblasts retained an elevated level of residual γH2AX foci after 24 h IR exposure, suggesting that the persistence of γH2AX foci could be a reliable measure to diagnose Fanconi anemia from non-FABMF and controls. These data suggest that persistence of γH2AX indicates impaired repair of a subset of IR-induced DNA DSBs in human fibroblasts and can be a useful marker to identify individuals with diseases of accelerated aging.

5.3. Buccal cells

Buccal cells are an easily accessible source of tissue and have been investigated for radiation biodosimetry [48,104]. The kinetics of γH2AX induction and loss in buccal cells were investigated by counting γH2AX foci for up to 5 h after exposure to 2 Gy of IR [104]. γH2AX signals in nuclei peaked at 30 min after exposure to IR, and subsequently declined over a period of 5 h. However, the level of γH2AX remained elevated in irradiated buccal cells for 5 h compared to non-irradiated control cells. In a recent study by our group, γH2AX levels remained elevated in γ-irradiated human buccal cells compared with non-irradiated control cells for up to 24 h following exposure to 4 Gy of IR as measured by quantitative laser scanning cytometry [48]. These results suggest that radiation induced γH2AX levels in human buccal cells may remain elevated above the baseline γH2AX level for a relatively long time (up to 24 h). Measurement of persistent γH2AX responses in human buccal cells could therefore be used as a powerful and reliable biomarker to assess DNA damage status of individuals exposed to IR during accidental catastrophic radiation exposure, or during radiation therapy, or possibly as a result of a DNA damaging disease process. However, the variable response to IR exposure between individuals should be taken into consideration when using the γH2AX assay for radiation biodosimetry.

5.4. Stem cells

The kinetics of DSB repair have been investigated in IR-induced human embryonic stem cells (hES) by measuring the persistence of γH2AX [105]. γH2AX levels decreased at a slower rate in hES after exposure to 5 Gy of IR, over a period of 24 h compared with normal somatic lung fibroblasts. This result suggests that hES retain persistent γH2AX and are possibly less efficient at repairing DSBs [105]. Another study quantified γH2AX foci numbers per cell after exposure to 2 Gy of IR in various subpopulations of stem cells (CD34+CD38−, CD34+CD38+, CD34−) derived from umbilical cord blood (newborn) and the bone marrow of healthy elderly individuals (>70 years) [106]. In all cell types examined, there was a similar increase in the frequency of γH2AX foci numbers per cell at both 8 h and 24 h after 2 Gy of IR exposure [106]. These results suggest that γH2AX response may persist in irradiated stem cells, and DSBs repair efficiency could be similar between the stem cell populations analyzed, irrespective of the wide difference in donor age.

5.5. Monitoring effects of radiotherapy on cell lines using persistent γH2AX response

Measurement of persistent γH2AX in human cell lines could be used as a powerful and reliable marker to identify the radiosensitivity of cells or to evaluate DNA damage repair capacity of cells undergoing radiotherapy treatment [107]. The combination of various radiosensitizing drugs with ionizing radiation exposure leads to persistent DNA damage compared with radiation or drug treatment alone (summarized in Table 2). The number of persistent γH2AX foci at 12 and 24 h after irradiation was found to correlate with clonogenic cell survival (an *in vitro* cell survival assay based on the ability of a single cell to grow into a colony) [108,109]. Since radiotherapy treatment of cancer cells is aimed to kill cancer cells with minimum side effects to normal cells, measurement of persistent γH2AX *in vitro* in different cell lines has a great potential for monitoring cancer patients' response to chemotherapy and radiotherapy as well as to enable tailored cancer treatments.

6. Persistent γH2AX in mouse cells and tissues

6.1. Germ cells

The persistence of γH2AX has been investigated in mouse germ cells after whole-body exposure to X-rays [72]. Round spermatids and primary spermatocytes had a higher proportion of cells containing γH2AX foci (around 50% and 30%, respectively) compared to non-irradiated controls, 48 h after exposure to 4 Gy IR. The pattern of γH2AX foci within these cells changed from many innumerable foci at early time points (1 h) to a pattern of fewer discrete foci at 48 h post-IR [72]. Another study showed the presence of Mdc1, 53BP1 and Rad51 proteins that are expressed in conjunction with γH2AX in male germ cell types for up to 16 h after exposure to 4 Gy of X-rays [110]. These results suggest that mouse germ cells display persistence of γH2AX following IR.

6.2. Skin biopsies

An *in vivo* investigation of persistent γH2AX as a biodosimeter of initial radiation dose has been carried out in keratinocytes within the epidermis of radiosensitive and radioresistant murine skin biopsies [65]. In this study, γH2AX foci/100 μm^2 areas of irradiated tissue sections were quantified for up to 7 days after exposure to a dose ranging from 1 to 10 Gy using 3D confocal microscopy. γH2AX foci were more persistent in radiosensitive strains compared with radioresistant strains and respective

Table 2
Persistent γH2AX response following exposure to IR, chemotherapeutic drugs and genotoxic agents in human cell lines.

Cell lines	Treatment	Outcome of γH2AX response	Technique used	Ref.
Cervical carcinoma (SiHa) Colon carcinoma (WiDr) SiHa and WiDr xenograft tumors	X-rays Single dose: 4 Gy, 6 Gy, and 10 Gy Fractionated dose: 1 Gy daily for 5 days 2 Gy daily for 5 days	24 h post-IR ↑foci/cell correlated with the clonogenic cell survival % of cells with <3 foci predicts cell survival	Visually scored by fluorescence microscopy Flow cytometry	[107]
Radiosensitive head and neck squamous cell carcinoma (SCC-61), and prostate cancer (PC-3) Radioresistant head and neck squamous cell carcinoma (SQ-20b) and prostate cancer (DU-145) (SCC-61) and (SQ-20b) xenograft tumors	X-rays 3 Gy	24 h post-IR ↑ foci & ↓ viability and clonogenic survival in radiosensitive cells compared with radioresistant cells	Immunoblot Fluorescence microscopy	[47]
Cervical cancer (HeLa, Caski, MS751, C33A, SW756, SiHA)	X-rays 2 Gy	24 h post-IR ↑ intensity and foci/cell correlated with clonogenic surviving fraction, indicates ↑ cellular radiosensitivity	Flow cytometry and Visually scored by fluorescence microscopy	[163]
Melanoma (HT144) Colon carcinoma (WiDr) Cervical carcinoma (SiHa) Glioma (U87) Breast cancer (HCC1937) Prostate cancer (DU145) B lymphoblastoid (WIL-2NS) Normal cell strains (HFL1)	X-rays 10 Gy	6 h post-IR ↑ γH2AX intensity in radiosensitive cells lines compared with radioresistant cells	Flow cytometry	[68]
Squamous cell carcinoma cells of head and neck (FaDu and SKX)	X-rays 4 Gy	24 h post-IR ↑ foci/cell correlated with the clonogenic cell survival % of cells with <3 foci predicts cell survival	Visually scored by fluorescence microscopy	[109]
Normal 48BR fibroblasts Patient-derived Artemis-deficient (CJ179 hTERT) fibroblasts	γ rays 2 Gy	18 h post-IR ↑ foci/cell in CJ179 hTERT compared with 48BR. Time dependent ↑ in γH2AX foci size (0.8 μm at 30 min to 1.4 μm at 12–18 h post-IR)	Confocal microscopy	[164]
Cervical carcinoma HeLa cells Hepatoma (HepG2) Mucoepidermoid carcinoma (MEC-1)	($^{12}C^{6+}$) and X-rays 2 and 4 Gy of radiation using carbon ions	24 h post-IR ↑ foci/cell ↓ clonogenic survival for ($^{12}C^{6+}$) radiation than for X-rays radiation indicates ↑ cellular radiosensitivity	Visually scored by fluorescence microscopy	[165]
Adenocarcinoma (A549) Squamous cell carcinoma (NCI-H226) Adenosquamous carcinoma (NCI-H596)	BPU + X-rays (4 Gy) 4 Gy alone	24 h post-treatment foci/cell ↑ ~2 times in cells pre-treated with BPU + X-rays compared with X-rays alone ↑ foci/cell, ↓ clonogenic survival, indicates ↑ cellular radiosensitivity	Flow cytometry	[166]
Bronchial carcinoma (A549) Squamous cell carcinoma head and neck (FaDu) Breast carcinoma (MCF7) Lung carcinoma (H1299) Prostate carcinoma (Du145)	Gossypol + X-ray (2–8) Gy 2–8 Gy alone	24 h post-treatment ↑ foci/cell in cells pre-treated with Gossypol + X-rays compared with X-rays alone ↑ foci/cell with ↓ clonogenic survival indicates ↑ cellular radiosensitivity	Visually scored by fluorescence microscopy	[78]
Breast cancer brain metastatic (MDA–MB-231-BR) Breast cancer brain metastatic (MDA–MB-231-BR) xenograft tumors	Vorinostat + X-rays (2 Gy) for 16 h 2 Gy alone	48 h post-treatment ↑ foci/cell with ↓ clonogenic survival in cells pre-treated with vorinostat + X-rays compared with X-rays alone	Visually scored by fluorescence microscopy	[167]
Breast cancer (MCF7) Astrocytoma (SF268)	γ rays 0.6 Gy	270 min post-IR 4.5 foci/nucleus compared to 1.5 foci/nucleus at baseline	Laser scanning confocal microscopy	[23]
SV40-transformed WRN fibroblast (AG11395)	Potent human carcinogen chromium Cr(VI) 20 μM	24 h after treatment ↑ foci/cell	Fluorescence microscopy, Phoenix software	[100]
Human colorectal cancer (HT-29) Human colorectal cancer (HT-29) xenograft tumors	JP-1201 + X-rays (2 Gy) 2 Gy alone	24 h post-treatment ↑ foci/cell with ↓ clonogenic survival in cells pre-treated with JP1201 + X-rays compared with X-rays alone	Visually scored by fluorescence microscopy	[168]

Table 2 (*Continued*)

Cell lines	Treatment	Outcome of γH2AX response	Technique used	Ref.
Colon carcinoma (HT29) Breast Carcinoma (MCF7) Pancreatic Carcinoma (MIA PaCa-2) Pancreatic carcinoma (Bx-PC3)	Guggulsterone + X-rays (6 Gy) 6 Gy alone	24 h post-treatment ↑ foci/cell with ↓ clonogenic survival in cells pre-treated with GS + X-rays compared with IR alone	Flow cytometry	[169]
Lung cancer: p53 wild-type (H460 and A549) p53 null (H1299)	HuaChanSu + γ rays (2 Gy)	24 h post-treatment ↑ foci/cell with ↓ clonogenic survival in cells treated with HCS + IR compared with IR alone	Visually scored by fluorescence microscopy	[170]
HeLa cells ATM deficient (AT5BIVA) DNA-PKcs deficient (M059J)	Wortmannin, caffeine or UCN-01 + X-rays (10 Gy)	24 h post-treatment ↑ foci/cell in HeLa and ATM deficient cell lines but not in DNA-PKcs cell lines	Western blot, Visually scored by fluorescence microscopy	[171]
Cervical carcinoma (SiHa)	DNA damaging drugs Camptothecin, cisplatin, doxorubicin, etoposide, hydrogen peroxide, MNNG, temozolomide, and tirapazamine	24 h post-treatment ↑ foci/cell with ↓ clonogenic survival	Visually scored by fluorescence microscopy	[64]
Prostate cancer (DU145)	Drugs + X-rays MS0019266 or MS0017509 + 4 Gy IR	6 and 24 h post-treatment ↑ foci/cell, ↓ cell survival in cells treated with MS0019266 or MS0017509 + X-rays compared with radiation alone	Visually scored by fluorescence microscopy	[172]
Primary skin fibroblasts: Wild-type – (48BR) ATM-deficient – (AT7BI) DNA ligase IV-deficient – (411BR) nonhomologous end-joining-deficient cells – (2BN)	γ rays 2 Gy IR	14 days post-IR ↑ level of foci/cell (representing 3–6% of unrepaired DSBs) in patient with mutation in ATM and DNA ligase IV	Visually scored by fluorescence microscopy	[173]
Colorectal adenocarcinomas cancer model (DLD-1 and HT-29) Colorectal adenocarcinomas cancer model (DLD-1 and HT-29) tumor xenograft	Sorafenib + X-rays (2 Gy) Sorafenib alone 2 Gy alone	6 and 24 h post-treatment ↑ foci/cell, ↓ cell survival in cells after treatment with Sorafenib + X-rays compared with radiation alone or drug alone cells	Visually scored by fluorescence microscopy	[174]
Bone marrow mesenchymal stem cells (U2OS and CALU-1)	Actinomycin D	21 days post-treatment ↑ foci/cell	Visually scored using fluorescence images	[175]
Pulmonary carcinoma (A549)	Mitomycin (0.01 and 0.02 μg/ml)	3–6 days after treatment Concentration dependent ↑ of γH2AX intensity	Laser scanning cytometry	[176]
Pancreatic cancer (Panc-1) Pancreatic cancer MiaPaCa-2 (PPP2R1A depleted by siRNA)	LB100 + X-rays 7.5 Gy + LB100 for 2 h	24 h post-treatment ↑ γH2AX intensity	Immunoblots	[177]
Breast cancer (MCF-7)	Barberine + X-rays 15 μM barberine for 24 h + 1 Gy	12 h post-treatment ↑ foci/cell in cells pre-treated with barberine + radiation compared with radiation alone	Visually scored using fluorescence images	[178]
Fibroblasts (GM637)	CDT + X-rays 0.5 μg/ml CDT and 5 Gy of IR	24 h post-treatment ↑ foci/cell and ↑ intensity in cells treated with CDT compared with IR treated cells	Western blot and Fluorescence microscopy, ImageJ	[179]
Colorectal cancer (HCT116)	Oxaliplatin (1–10 μM) treatment for 6–24 h	24 h post-treatment ↑ intensity in a time- and concentration dependent manner	Western blot	[180]
Human pancreatic cancer (MiaPaCa-2)	AZD7762 (Chk1/2 inhibitor) and gemcitabine	48 h post-treatment ↑ intensity in 56% of cells	Flow cytometry	[181]
The normal human fibroblasts AGO1522B (AGO) Normal peripheral blood lymphocytes from patients with advanced cancer	SJG-136 (crosslinking agent)	8 and 15 days post-treatment ↑ foci/cell	Visually scored using fluorescence images	[182]
Glioblastoma (U251)	HSV-TK + antiviral drug Ganciclovir	24 h post-treatment ↑ foci/cell	Visually scored using fluorescence images	[183]
Bone marrow mesenchymal stromal (MSC)	X-rays 40 and 2000 mGy	48 h post-treatment ↑ foci/cell	Visually scored using fluorescence images	[184]
Human mammary epithelial (HMEC)	Iron-ion and γ-rays 1 Gy and 2 Gy	72 h post-treatment ↑ foci/cell in non-proliferative cells compared with proliferative cells ↑ foci/cell after iron-ion exposure than after γ-rays exposure	Visually scored using fluorescence	[185]
Normal diploid cells (HE49)	X-rays 4 Gy	5 days post-IR ↑ foci size and ↑ % of positive nuclei	Fluorescence microscopy, IP lab software	[186]

Abbreviations: CDT, cytolethal distending toxin; BPU, dimethylamino benzoylphenylurea; GS, guggulsterone; HCS, HuaChanSu; HSV-TK, herpes simplex virus thymidine kinase; MMC, mitomycin C.

non-irradiated time-matched controls. Therefore, confocal microscopy may enable high resolution 3D image acquisition of γH2AX foci in different depths of skin biopsies, thereby making it possible to measure IR induced persistent γH2AX levels for many days after radiation exposure which could have practical application in radiation biodosimetry.

6.3. Spinal cord

γH2AX induction and loss have been investigated in murine spinal cord for 1 year after topical application of spinal cord to an acute IR dose of 17 Gy of X-rays followed by an immediate additional dose of 19 Gy of X-rays [111]. The frequency of γH2AX foci was higher in the blood vessel endothelium of irradiated spinal cord compared with non-irradiated controls where γH2AX was virtually absent. The higher levels of γH2AX foci were still detectable 1 year after IR exposure suggesting that the IR-induced γH2AX response can persist in murine spinal cord for a very long time after a radiation exposure event [111].

6.4. Other tissues and organs

Variations in IR-induced DNA breaks in different animal tissues were first observed in 1983 [112]. Although, the levels of H2AX protein have been reported in similar amounts among mouse thymus, testis and small intestine, the proportion of phosphorylated H2AX differed between tissues after 30 Gy IR exposure [113]. It was observed that 17% of H2AX were phosphorylated in the epithelial cells in the villi of the small intestine compared to 37% and 94% in thymus and testis respectively [113]. This result suggests that H2AX does not always phosphorylate to the same extent in all tissues after exposure to IR. γH2AX has been previously measured in heart and kidney sections of mice after their whole body was exposed to 3 Gy of X-rays [114]. The maximum frequency of γH2AX positive nuclei was found in heart and kidney sections at 20 and 40 min, respectively, then slowly declined. After a further 23 h the number of γH2AX positive nuclei (in about 50% of γH2AX positive nuclei in cardiomyocytes of heart) remained persistent; however γH2AX positive nuclei decreased in kidney cells to the values observed in the control [114]. Furthermore, the γH2AX response was tested in mouse heart, brain, kidney and liver tissues for up to 5 h after whole-body exposures to 3 Gy of IR. The amount of γH2AX observed was lowest in the heart compared with brain, kidney and liver at 5 h post-IR [120].

Persistence of γH2AX has been investigated in mouse spleen, thymus, liver, lung, kidney, cerebellum, hippocampus, frontal cortex and olfactory bulb of 7, 14, 24, 30 and 45 days old mice [115]. The number of γH2AX foci per cell peaked at 30 min after exposure to 1 Gy of X-rays, and then declined in most tissues within 24 h. However, IR-induced γH2AX foci were more persistent in the thymus and spleen of 7 and 14-day-old mice compared with mice from the older age categories.

One study has reported that the kinetics of γH2AX foci loss were almost similar in small intestine, lung, brain, heart, and kidney tissues of mice 48 h after whole-body exposure to 2 Gy of IR [116]. Similar results on the kinetics of γH2AX foci loss were also observed in mouse heart, small intestine, and kidney tissues for 24 h following whole-body exposure to 0.01, 0.1, and 1 Gy of X-rays [117]. Taken together, these data suggest that the rate of initial γH2AX induction as well as the rate of γH2AX loss after X-ray exposure significantly varies in non-proliferating mammalian tissues and should be taken into account when comparing radiation induced γH2AX responses between various tissues and species.

7. Persistent γH2AX in cells and tissues of other animals

7.1. Minipig skin, lymphocytes and fibroblasts

A recent study showed the presence of IR-induced γH2AX foci in ~60% of cells in keratinocytes within the epidermis of Göttingen minipig skin biopsies 4 h after exposure to 50 Gy of IR [118]. The average radiation induced γH2AX foci number per epidermal keratinocyte then declined after 70 days; however, the average numbers of residual γH2AX foci per epidermal keratinocyte at 70 days were significantly higher compared to non-irradiated controls [118]. Twenty-four hours after *ex vivo* exposure to 1.8 Gy of IR, both human and minipig lymphocytes exhibited ~15% of the maximal γH2AX response observed at 30 min [33]. Furthermore, approximately 3% residual γH2AX foci were found in human and minipig fibroblasts for up to 24 h after 2 Gy of IR exposure. γH2AX kinetics in minipig lymphocytes after exposure to different total body irradiation doses showed that persistent γH2AX foci per cell were proportional to the initial IR dose thus suggesting that a portion of IR-induced DSBs remains unrepaired [33].

7.2. Fruit fly pupae

Our previous study on the Queensland fruit fly (*Bactrocera tryoni*) demonstrated that IR exposure leads to a persistent γH2AvB response (a fruit fly variant of γH2AX) that could be assessed during the adult phase of the life cycle when the IR exposure was carried out at the pupal stage [119]. Queensland fruit flies are able to withstand high doses of IR, and we reported a linear dose–response of γH2AvB (0–400 Gy IR) 24 h after IR exposure. γH2AvB signal peaked at approximately 20 min after IR exposure. At 24 h post IR, the signal remained elevated but was substantially reduced after 5 days compared with 1-day post-IR exposure. γH2AvB response in adult Queensland fruit flies was persistent and dose-dependent up to 17 days after IR exposure. The persistent γH2AvB response can therefore be utilized as a biomarker of prior IR exposure of fruit flies [119]. This finding has several potential applications for the management of economically important insects, such as the sterile insect technique, where fruit flies are irradiated at ~70 Gy to induce reproductive sterility but not death of the organism or to determine whether fruit containing fruit fly larvae was irradiated with an appropriate dose of radiation [119].

7.3. Macaque lymphocytes and plucked hair bulbs

Persistence of γH2AX was observed in lymphocytes from macaque after whole body irradiation with doses from 1 to 8.5 Gy [70]. The number of γH2AX foci per cell were elevated in lymphocytes by approximately 16-fold for up to 14 days after exposure to 8.5 Gy of IR when compared with non-irradiated controls. Similarly, γH2AX foci from plucked hair bulbs of macaques were increased approximately 14-fold when compared with non-irradiated controls, up to 9 days after 8.5 Gy IR exposures [70]. This study suggests that plucked hair bulbs are an easily accessible source of sample to measure persistence of γH2AX for many days after radiation exposure and may be adopted as a strategy for early triage during accidental catastrophic radiation incidents.

7.4. Syrian hamster heart, brain, and liver tissues

The kinetics of γH2AX induction and loss were tested in heart, brain, and liver tissues of adult Syrian hamsters following whole-body exposure to 5 Gy of X-rays [120]. The γH2AX response 24 h after IR was more persistent in heart and brain tissues compared with liver [120]. These results suggest that the kinetics

of IR-induced γH2AX induction and loss are tissue specific, being less efficient in heart and brain in comparison with liver [120].

The results of these studies, suggest that (i) γH2AX persistence is a common phenomenon across species, and (ii) nuclei may retain persistent γH2AX foci for up to several months after IR exposure, allowing for retrospective biodosimetry.

8. Persistence of γH2AX associated with telomeres

Telomeres are evolutionarily conserved, specific, repetitive hexameric nucleotide sequences (TTAGGG) located at the end of each chromosome [75] and are responsible for protecting chromosomes from improper recombination and degradation [121]. These repetitive sequences bind to proteins forming a protein–DNA complex known as Shelterin [122]. This complex caps the end of the chromosome and prevents DNA repair machinery from misidentifying the overhang located at chromosome-ends as a DSB. A previous study reported that Shelterin components such as telomeric repeat-binding factor 2 inhibits DNA end-joining by DSB repair mechanisms and therefore, prevents end-to-end fusions of chromosomes, thus allowing DNA damage to accumulate at telomeres [108,121,123,124]. For this reason, it has been suggested that telomeric DNA may accumulate DSBs and could be a preferred location for formation of persistent DDR foci [35,36]. At 4 days post-IR exposure, approximately 10% of γH2AX foci were co-localized at telomeres, whilst at 10 and 30 days post-IR, 20% and 40% of γH2AX foci were co-localized at telomeres, respectively [35]. Co-localization between γH2AX foci and telomeres was also higher in X-ray-treated senescent human fibroblasts for up to 26 days after exposure to 20 Gy of IR [36]. Findings from this study suggest that while the mean number of γH2AX foci per cell in the non-telomeric region progressively declined, the percentage of γH2AX foci co-localizing with a telomere signal gradually increased for up to 26 days [36]. In order to demonstrate that γH2AX binds telomeric repeats and not only the sub-telomeric regions; quantitative real-time PCR of sub-telomeric regions were performed on chromatin immunoprecipitation of human diploid fibroblasts with an anti-γH2AX antibody 10 days after exposure to 20 Gy of IR. There was a strong enrichment of γH2AX at the sub-telomeric region of fibroblasts exposed to IR compared to non-irradiated controls. The enrichment of γH2AX increased from the centromere toward the direction of the chromosome terminal region and represented an approximate 14-fold enrichment of γH2AX at the telomere repeats, in irradiated human fibroblasts compared to non-irradiated human fibroblasts [36]. The enrichment of γH2AX at the telomere repeats has also been confirmed using a chromatin immunoprecipitation procedure followed by next generation sequencing and real-time PCR [35]. Both studies suggest that persistent γH2AX foci are not only associated with cytological close proximity with telomeres (the association observed when viewed by a microscope), but also physically associated (as measured by chromatin immunoprecipitation and real-time PCR) with telomeres. A schematic of the accumulation of γH2AX at telomeres is shown in Fig. 3. This result supports the paradigm that DNA damage at telomeres may not be repaired after exposure to DNA damaging agents such as IR. The irreparable telomeres may therefore, trigger persistent DDR (reflected by persistent γH2AX response) which is associated with the formation of cellular senescence processes.

9. Senescence-associated persistence of γH2AX

Unrepaired DSBs could result in either cell death or in a form of cell cycle arrest known as cellular senescence [125]. Cellular senescence is an irreversible process where cells remain alive but

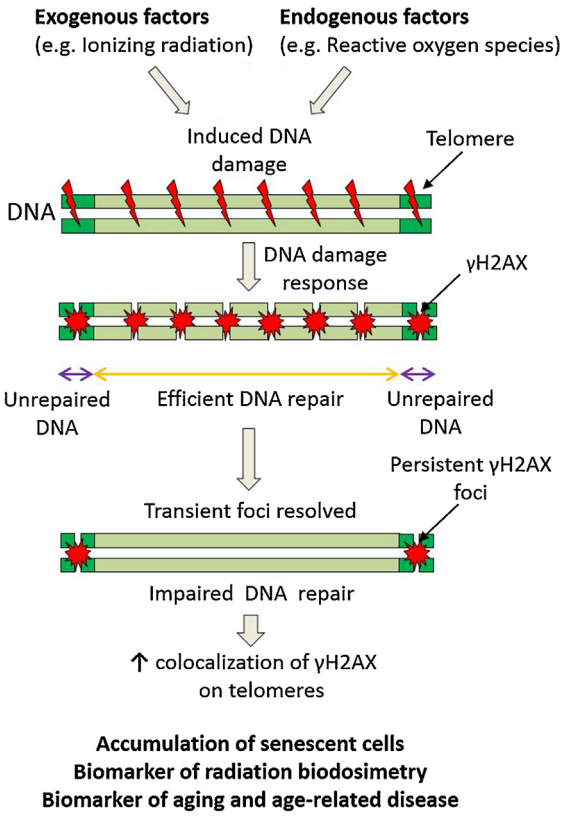

Fig. 3. Model of persistent γH2AX as a result of endogenous and exogenous factors. Exogenous and endogenous factors induce DNA damage throughout the genome. While the DNA DSBs in non-telomere regions are efficiently repaired, DNA DSBs generated in telomeres are not repaired leading to persistent γH2AX. These unrepaired DNA DSBs likely result in the accumulation of senescent cells. The accumulation of senescent cells may be involved in accelerated aging processes. Measurement of the persistent γH2AX could potentially be used as a biomarker of radiation biodosimetry, radiosensitivity and accelerated aging, adapted from [35].

are unable to proliferate [126]. Senescent cells can be detected by histochemical staining for senescence-associated β-galactosidase (SA-β-gal) activity [127]. Senescence-associated persistent γH2AX foci were present for up to 24 h after exposure to 1 Gy of IR in senescent cultured human fibroblasts, human prostate epithelial cells, human fibroblasts with elongated telomeres and in nuclei of whole tissues from mice (*i.e.* liver, testis, kidney, lung) [32]. To characterize persistent γH2AX foci, a further radiation dose was applied to the same cells (*i.e.* mouse and human cells already containing IR-induced foci). After 30 min post-IR, the newly formed γH2AX foci were eliminated 24 h post IR whilst the persistent foci, *i.e.* those from the first dose of IR, were still present 24 h after IR exposure [32]. Additionally, persistent γH2AX has been demonstrated in human diploid fibroblasts after exposure to 20 Gy of IR for up to 4 months [35]. In a separate experiment, senescent cells that already contained persistent γH2AX foci from prior IR as well as normal human diploid fibroblast cells (that were not exposed to IR) were irradiated to investigate the nature of persistent γH2AX foci. Whilst the newly formed IR-induced transient γH2AX foci were repaired, γH2AX foci in senescent cells (from prior treatment) remained unresolved [35]. This evidence suggests that senescent cells are associated with the accumulation of persistent γH2AX, which represents a subset of DSBs that are resistant to repair processes. The criteria of senescent-associated persistence of γH2AX after exposure to IR needs to be further investigated in order to be used as a potential marker of radiation biodosimetry.

10. γH2AX responses in aging

Aging is a process that alters cellular function of most living organisms and is influenced by environmental and genetic factors [128–130]. The aging process is regulated by the accumulation of genetic alterations and dysregulation in epigenetic fingerprints, which may ultimately contribute to genomic instability, cellular senescence, apoptosis and/or cancer [131,132]. Imperfections or defects in pathways repairing DNA DSBs may either trigger the aging process or indirectly regulate it by cellular senescence or apoptosis [128]. DSBs may cause progressive shortening or dysfunction of telomeres when left unrepaired and may play a major role in the aging process of somatic cells [133–135]. This accumulation of DSBs causes persistent DDR coupled with p53 activation and may contribute to cellular senescence [129,131,135,136], a key factor in healthy and pathological aging [126,137,138]. Senescent cells characterized by the presence of γH2AX, including activity of SA-β-gal, accumulate in tissues of aged animals and are thought to increase during aging and age-related diseases [127,139,140]. In addition to the arrest of cell proliferation, senescent cells display altered chromatin organization and gene expression. These changes involve the secretion of different proteins (such as proinflammatory cytokines, chemokines, growth factors, and proteases), the so-called senescence associated secretory phenotype (SASP) [141,142]. The secretion of SASP proteins by senescent cells ultimately results in chronic inflammation which is a cause of or important contributor to multiple age-related diseases [141,143,144]. It has been reported that persistent DDR signaling (observed by increased γH2AX levels) can fuel the secretion of SASP cytokines (*e.g.* IL-6) as compared with transient DDR signaling and is summarized in Fig. 4 [97]. It is likely that accumulation of persistent DSBs may be strongly involved during aging and diseases of accelerated aging.

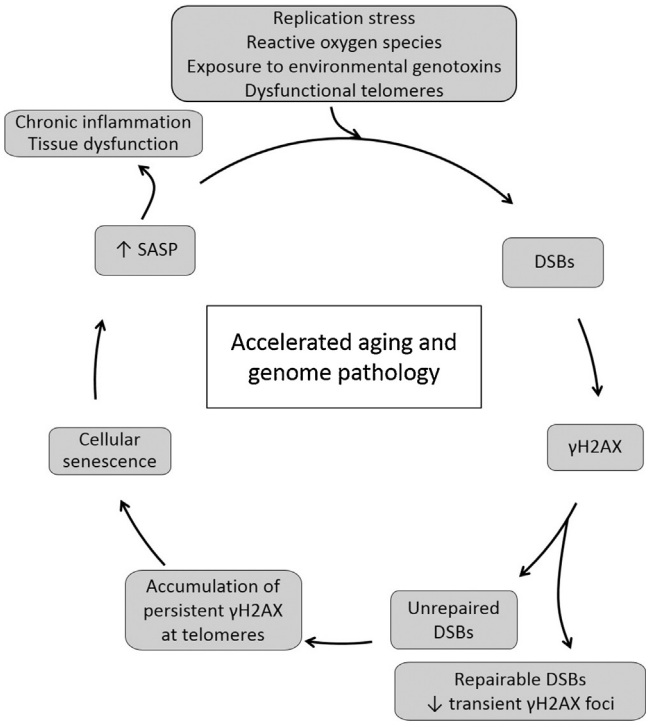

Fig. 4. Model depicting the possible role of persistent γH2AX/unrepaired DSBs in aging and diseases of accelerated aging. Replication stress, environmental genotoxins, dysfunctional telomeres and dysregulation in epigenetic fingerprints induce DSBs. When DSBs are repairable, transient γH2AX foci are removed; however, unrepaired DSBs marked by persistent γH2AX foci lead to cellular senescence. The persistence of γH2AX is also associated with increased expression of SASP. The deleterious effect of senescent cells and SASP includes chronic inflammation, tissue dysfunction promoting aging and fuelling the development of age-related disease. Abbreviations: DSBs, double-strand breaks; SASP, senescence associated secretory phenotype.

10.1. Endogenous levels of γH2AX in individuals of different ages

Several studies have examined whether endogenous levels of γH2AX is altered by the age of individuals [40,145]. For example, the frequency of γH2AX foci were measured to investigate the presence of unrepaired DSBs in human fibroblasts and lymphocytes from healthy young donors and older donors in the age range from 21 to 72 years [40]. The endogenous γH2AX foci per cell were higher in fibroblasts and lymphocytes from older donors compared with younger donors [40]. Studies on aging and senescing cell lines of epithelial and fibroblastic origin (including mice), also showed an increase in γH2AX foci with age [32,40,139,146]. Recently, a longitudinal study of aging also tested the hypothesis that the frequency of γH2AX foci correlates with age in leukapheresis-derived mononuclear cells from patients in the age range of 37–83 years; with 37 patients over the age of 50 and 13 patients over the age of 72 [41]. The average number of γH2AX foci per cell was increased with age up to 57 years and then remained relatively stable up to the age of 83. This result was in agreement with other observations whereby the number of γH2AX foci per cell increased with age up to approximately 50 years and then subsequently plateaued [40]. However, it is important to note in that study only 8 donors were examined in the 50-year-old group. A more recent study [58] reported a trend of a linear increase in endogenous γH2AX level with age in lymphocytes from 94 healthy adults with the age range from 19 to 50 years. Another study investigated the presence of endogenous levels of γH2AX in PBMCs from a population-based sample of twins ranging in age from 40 to 77 years [145]. In that study, γH2AX levels decreased with increasing donor age in human PBMCs. The reason for the discrepancies in the γH2AX levels with age is not known but may be partly due to the differences in the study populations. Interindividual variability of endogenous γH2AX response is known, although the effect of modulators such as age, genotype, ethnicity and race, hormonal responses, gender, environmental factors, and alcohol intake may impact on the base-line endogenous γH2AX responses, but this is not completely understood [58]. The endogenous γH2AX foci frequency (per cell) increased with age in CD34+ and CD34− stem/progenitor cells derived from both growth-factor mobilized peripheral blood and bone marrow cells compared to cells derived from umbilical cord blood [106]. Furthermore, endogenous γH2AX foci were approximately two times higher in CD34+CD38−, CD34+CD38+ and CD34− cells derived from bone marrow samples of healthy elderly individuals (>70 years) compared with cells from umbilical cord blood [106]. This indicates that different subtypes of stem cells and progenitor cells may accumulate unrepaired DSBs with age. Additionally, the frequencies of the senescent cell marker, *i.e.* SA-β-gal activity, and γH2AX foci positive cells increased in the heart, skeletal muscle, kidney, eye lens, testis, liver, skin, lung, spleen and small intestine of 42-month-old male mice compared with 12-month-old mice [139]. The levels of persistent γH2AX foci that co-localize with telomeres also increased with age in senescent primate fibroblasts [147]. These studies suggest that γH2AX response may be indirectly involved in the process of normal physiological aging but its use as a robust biomarker of biological aging remains uncertain.

10.2. γH2AX in chronic diseases of aging

The association between the levels of γH2AX foci and age-related disease have been investigated in several studies

[40,41]. For example, the frequency of γH2AX foci was apparently higher in PBMCs of hypertensive patients when compared to the cells from their respective controls [41]. However, the analysis was only significant when restricted to hypertensive patients that were aged more than 57 years old. In that study, the γH2AX foci per cell was 36% higher in hypertensive patients compared with non-hypertensive study participants [41]. A trend of increasing γH2AX foci per cell has also been reported in patients with sleep apnoea, prostate cancer and cataract disease patients compared to those without history of these respective conditions, although it should be noted that the increase observed did not reach statistical significance [41]. In another study, senescent fibroblasts from Werner Syndrome patients exhibited a higher number of γH2AX foci per cell compared to senescent fibroblasts from healthy donors [40]. The rate of recruitment of DDR proteins such as Mre11 and 53BP1 to γH2AX foci was inversely correlated with age in both healthy and Werner Syndrome donors [40]. Thus, recruitment of DDR proteins at the DSBs site may be less efficient with age, leading to accumulation of DSBs during the aging process [40,148]. In a study of obesity in children, γH2AX in lymphocytes of obese children ($n = 81$) and healthy controls ($n = 38$) was 8-fold higher in obese children compared with non-obese children [149]. The level of γH2AX was also measured in lymphocytes of adolescents with type 1 diabetes mellitus (T1DM) ($n = 35$) and healthy controls ($n = 19$) [150]. The number of γH2AX foci per nucleus was approximately 50-fold higher in T1DM patients compared with healthy controls [150]. γH2AX staining has been shown to be higher in the nuclei of astrocytes from Alzheimer's disease patients relative to healthy controls as determined by immunocytochemical techniques [39]. This result suggests that DSBs measured by γH2AX positive immunostaining in the nuclei of astrocytes may be associated with impaired neuronal function and contribute to the pathogenesis of Alzheimer's disease [39]. Fibroblasts from patients with Hutchinson–Gilford progeria syndrome (a disease associated with accelerated aging) also had increased amounts of endogenous γH2AX levels compared with controls [151]. Overall, these studies show that accumulation of γH2AX foci is marginally increased in individuals with increased morbidity and supports the hypothesis of accumulation of unrepaired DSBs in pathological aging.

11. Consideration of persistent γH2AX for future method development

It is clear that more studies are required to determine baseline values of γH2AX as a marker of DNA damage in human populations. There is evidence that two types of γH2AX foci exist, those that are transient in nature (up to several hours in duration), and those foci persist for weeks and months. It is important to distinguish between each of these types of γH2AX foci in DNA damage repair kinetics since both provide very different information about the nature of DNA damage that the cell has experienced. For example, when lymphocytes are first isolated from the blood of patients, it could be envisaged that transient foci are indicative of a recent acute damaging event, whether that be endogenous or exogenous, and demonstrates that the cell is currently in the process of repairing the double stranded DNA lesion. On the other hand, accurately identifying those γH2AX foci that remain persistent may provide information on DSBs that remain unresolvable, perhaps due to DNA repair defects or complexity of the lesion or DSBs in regions of the genome where repair of DSBs is limited such as telomeres. Indeed, it is also essential to eliminate confounders such as cells undergoing apoptosis, although simple morphological criteria could be used to identify these cells. It would be advantageous to build into the γH2AX assays some type of a reporter of the transient *vs.* persistent DNA damage. Alternatively, the cells may be cultured for a further 24 h after isolation to allow ample time for dephosphorylation and clearing of any existing transient γH2AX signals, leaving only the residual (persistent) γH2AX foci associated with the DNA. Another possibility is to use confocal microscopy or other techniques to determine the size of γH2AX foci and genome location (*e.g.* telomeres) as a marker for persistent damage. Furthermore, measuring the spatial proximity of γH2AX in nuclei may demonstrate that there is clustering of γH2AX foci at the nuclear envelope [152] and therefore, provide additional evidence of persistent DNA damage at telomeres given that telomere repeats have been located in the proximity of the nuclear envelope.

Whilst transient IR-induced γH2AX signals are rapidly lost over time, the persistent γH2AX signals are detectable for several days after IR exposure. Therefore, a simple standardized γH2AX detection technique is required to rapidly identify individuals exposed to critically high radiation doses so that initial triage and medical treatment can be made. Although the confocal microscopy technique enables high resolution 3D imaging thus allowing γH2AX detection for many days after IR exposure, the time required for image analysis of individual γH2AX foci would need optimization when using such techniques in radiation biodosimetry. In a recent study, a rapid "96-well lyse/fix" method was developed to measure γH2AX foci from finger pricked blood samples with an estimated processing time of about 4 h for 96 samples compared to 15 h using the routine protocol [153]. This protocol may be further modified by incorporating the simultaneous measurement of other cellular proteins/markers involved in DNA damage/repair signaling allowing accurate detection of persistent γH2AX in a large number of samples. This latter protocol may be better suited in radiation biodosimetry following a large-scale radiation emergency. The RABiT (Rapid Automated Biodosimetry Tool for Radiological Triage), is a fully automated high-throughput robotic system designed to measure γH2AX in lymphocytes present in a single drop of blood from a fingerstick in a precise and fast manner (capable of processing up to 30,000 samples per day) [154,155].

Common immunofluorescence techniques allow the researcher to gain information on persistent γH2AX at equilibrium (essentially a snapshot in time). A better approach for analyzing the persistence of these DSBs and also the origin and relative kinetics of endogenous foci is to generate cells (*in vitro*) with a fluorescent-tagged protein (such as GFP-labeled 53BP1). This protocol allows visualization of the damaged site and enables one to monitor their repair in living cells [156,157]. A novel approach to such imaging γH2AX quantification of DSBs in live mammalian cells has been described using bifragment luciferase reconstitution [158]. N- and C-terminal fragments of firefly luciferase genes were fused with H2AX and MDC1 genes, respectively. In mammalian cells following DSB formation, H2AX was rapidly phosphorylated and then physically associated with the MDC1 protein, thus joining N- and C-luciferase fragments together and ultimately resulting in reconstitution of luciferase activity, which was assayed by analyzing serial images at different time-points after radiation. This method for imaging γH2AX–MDC1 interaction was used for non-invasive evaluation of DSBs repair kinetics *in vivo* in tumor exposed to X-rays and ^{56}Fe ions over 2 weeks [158]. This approach can be an alternative for experiments requiring observations of DSB induction and repair over an extended period of time [158]. Another method was developed that incorporated fluorophore- and radioisotope-labeled immunoconjugates which involved modification of anti-γH2AX antibodies to track *in vivo* damage in tumors [159]. Thus radioimmunoconjugates that target γH2AX as a real-time noninvasive imaging method to monitor DNA damage both *in vivo* and *in vitro*, would be useful to diagnose susceptibility of cancer cells to DSB undergoing radiotherapy and to monitor treatment. A standard method in biological dosimetry

includes cytogenetic analysis in which chromosome aberrations such as translocation, dicentric chromosomes, and micronuclei are scored in PBLs. These types of methods require growth stimulation of lymphocytes for at least 48–72 h since chromosomal damage can only be measured following *ex vivo* cell division [160–162]. Thus in the scenario of population triage during the first few hours after accidental catastrophic radiation exposure (when the physical dose is unavailable) a rapid enumeration of the level of exposure to the individual is required. The γH2AX assay has emerged as a useful measurement for the rapid identification of the retrospective estimation of ionizing radiation dose exposure. Additionally the γH2AX assay is highly sensitive to detect DNA damage induced by ionizing radiation as low as 1.2 mGy [25]. However, it is limited by inter-individual variability in kinetics of repair, and results will vary depending on the time-frame of radiation exposure and blood collection. For this reason, it is more likely that an approach based on measuring persistent γH2AX may prove to be a superior diagnostic of radiation exposure.

12. Conclusion

Quantification of γH2AX response is a highly sensitive and specific assay for detecting DNA DSB formation and repair. Although available evidence supports the view that the majority of IR-induced DSBs are rapidly repaired, a small portion may remain unrepaired, leading to a long-term persistent γH2AX response. This persistent level of γH2AX also varies in different tissues and may be affected by genomic status and type of DNA damaging insult. Several studies have demonstrated that IR induced γH2AX responses may remain persistent for a long period of time and that persistent γH2AX tends to accumulate in telomeric DNA and in cells undergoing cellular senescence. For effective measurement of γH2AX responses, criteria to distinguish persistent from transient γH2AX foci are required. Furthermore, the variable γH2AX response to IR exposure among different cell/tissue samples should be taken into consideration when using the γH2AX assay for radiation biodosimetry and/or estimation of persistent DNA damage. A further application of quantifying γH2AX foci would be as an early indicator of age-related disease risk, as alteration in genomic integrity due to DSBs may accelerate aging. The relationship between persistent γH2AX foci and telomere length and function demand further investigation to better understand telomere γH2AX biology and whether there are other regions in the genome where γH2AX accumulates remains unknown. With further research, it may be possible to determine baseline values of γH2AX in populations more reliably. This will contribute to the increasing knowledge about the rate of DSBs and their repair in developmental and degenerative diseases and eventually help to identify the dietary, environmental, and life-style factors that may mitigate against excessive formation of DSBs.

Acknowledgements

Financial support from the CSIRO's Preventative Health Flagship is greatly acknowledged. MSS was supported by an Australian Postgraduate Award and a CSIRO Preventative Health Scholarship. Maxime François was supported by a CSIRO OCE post-doctoral fellowship.

References

[1] D.L. Dugle, C.J. Gillespie, J.D. Chapman, DNA strand breaks, repair, and survival in x-irradiated mammalian cells, Proc. Natl. Acad. Sci. U. S. A. 73 (1976) 809–812.
[2] P.L. Olive, The role of DNA single- and double-strand breaks in cell killing by ionizing radiation, Radiat. Res. 150 (1998) S42–S51.
[3] L.J. Mah, A. El-Osta, T.C. Karagiannis, gammaH2AX: a sensitive molecular marker of DNA damage and repair, Leukemia 24 (2010) 679–686.
[4] N.E. Sharpless, R.A. DePinho, How stem cells age and why this makes us grow old, Nat. Rev. Mol. Cell Biol. 8 (2007) 703–713.
[5] I. Ward, J. Chen, Early events in the DNA damage response, Curr. Top. Dev. Biol. 63 (2004) 1–35.
[6] E.P. Rogakou, D.R. Pilch, A.H. Orr, V.S. Ivanova, W.M. Bonner, DNA double-stranded breaks induce histone H2AX phosphorylation on serine 139, J. Biol. Chem. 273 (1998) 5858–5868.
[7] V. Savic, B. Yin, N.L. Maas, A.L. Bredemeyer, A.C. Carpenter, B.A. Helmink, K.S. Yang-Iott, B.P. Sleckman, C.H. Bassing, Formation of dynamic gamma-H2AX domains along broken DNA strands is distinctly regulated by ATM and MDC1 and dependent upon H2AX densities in chromatin, Mol. Cell 34 (2009) 298–310.
[8] C. Redon, D. Pilch, E. Rogakou, O. Sedelnikova, K. Newrock, W. Bonner, Histone H2A variants H2AX and H2AZ, Curr. Opin. Genet. Dev. 12 (2002) 162–169.
[9] A. Kinner, W. Wu, C. Staudt, G. Iliakis, Gamma-H2AX in recognition and signaling of DNA double-strand breaks in the context of chromatin, Nucleic Acids Res. 36 (2008) 5678–5694.
[10] S. Burma, B.P. Chen, M. Murphy, A. Kurimasa, D.J. Chen, ATM phosphorylates histone H2AX in response to DNA double-strand breaks, J. Biol. Chem. 276 (2001) 42462–42467.
[11] I.M. Ward, J. Chen, Histone H2AX is phosphorylated in an ATR-dependent manner in response to replicational stress, J. Biol. Chem. 276 (2001) 47759–47762.
[12] K.J. McManus, M.J. Hendzel, ATM-dependent DNA damage-independent mitotic phosphorylation of H2AX in normally growing mammalian cells, Mol. Biol. Cell 16 (2005) 5013–5025.
[13] D. Durocher, S.P. Jackson, DNA-PK, ATM and ATR as sensors of DNA damage: variations on a theme? Curr. Opin. Cell Biol. 13 (2001) 225–231.
[14] A. Celeste, O. Fernandez-Capetillo, M.J. Kruhlak, D.R. Pilch, D.W. Staudt, A. Lee, R.F. Bonner, W.M. Bonner, A. Nussenzweig, Histone H2AX phosphorylation is dispensable for the initial recognition of DNA breaks, Nat. Cell Biol. 5 (2003) 675–679.
[15] N. Bhogal, F. Jalali, R.G. Bristow, Microscopic imaging of DNA repair foci in irradiated normal tissues, Int. J. Radiat. Biol. 85 (2009) 732–746.
[16] A.J. Nakamura, V.A. Rao, Y. Pommier, W.M. Bonner, The complexity of phosphorylated H2AX foci formation and DNA repair assembly at DNA double-strand breaks, Cell Cycle 9 (2010) 389–397.
[17] T.T. Paull, E.P. Rogakou, V. Yamazaki, C.U. Kirchgessner, M. Gellert, W.M. Bonner, A critical role for histone H2AX in recruitment of repair factors to nuclear foci after DNA damage, Curr. Biol. 10 (2000) 886–895.
[18] A.A. Goodarzi, P. Jeggo, M. Lobrich, The influence of heterochromatin on DNA double strand break repair: getting the strong, silent type to relax, DNA Repair (Amst.) 9 (2010) 1273–1282.
[19] Z. Lou, K. Minter-Dykhouse, S. Franco, M. Gostissa, M.A. Rivera, A. Celeste, J.P. Manis, J. van Deursen, A. Nussenzweig, T.T. Paull, F.W. Alt, J. Chen, MDC1 maintains genomic stability by participating in the amplification of ATM-dependent DNA damage signals, Mol. Cell 21 (2006) 187–200.
[20] J. Kobayashi, Molecular mechanism of the recruitment of NBS1/hMRE11/hRAD50 complex to DNA double-strand breaks: NBS1 binds to gamma-H2AX through FHA/BRCT domain, J. Radiat. Res. 45 (2004) 473–478.
[21] L. Anderson, C. Henderson, Y. Adachi, Phosphorylation and rapid relocalization of 53BP1 to nuclear foci upon DNA damage, Mol. Cell. Biol. 21 (2001) 1719–1729.
[22] T. Furuta, H. Takemura, Z.Y. Liao, G.J. Aune, C. Redon, O.A. Sedelnikova, D.R. Pilch, E.P. Rogakou, A. Celeste, H.T. Chen, A. Nussenzweig, M.I. Aladjem, W.M. Bonner, Y. Pommier, Phosphorylation of histone H2AX and activation of Mre11, Rad50, and Nbs1 in response to replication-dependent DNA double-strand breaks induced by mammalian DNA topoisomerase I cleavage complexes, J. Biol. Chem. 278 (2003) 20303–20312.
[23] E.P. Rogakou, C. Boon, C. Redon, W.M. Bonner, Megabase chromatin domains involved in DNA double-strand breaks in vivo, J. Cell Biol. 146 (1999) 905–916.
[24] O.A. Sedelnikova, E.P. Rogakou, I.G. Panyutin, W.M. Bonner, Quantitative detection of (125)IdU-induced DNA double-strand breaks with gamma-H2AX antibody, Radiat. Res. 158 (2002) 486–492.
[25] K. Rothkamm, M. Lobrich, Evidence for a lack of DNA double-strand break repair in human cells exposed to very low X-ray doses, Proc. Natl. Acad. Sci. U. S. A. 100 (2003) 5057–5062.
[26] Y. Doida, S. Okada, Radiation-induced mitotic delay in cultured mammalian cells (L5178Y), Radiat. Res. 38 (1969) 513–529.
[27] D. Chowdhury, M.C. Keogh, H. Ishii, C.L. Peterson, S. Buratowski, J. Lieberman, Gamma-H2AX dephosphorylation by protein phosphatase 2A facilitates DNA double-strand break repair, Mol. Cell 20 (2005) 801–809.
[28] T. Stiff, M. O'Driscoll, N. Rief, K. Iwabuchi, M. Lobrich, P.A. Jeggo, ATM and DNA-PK function redundantly to phosphorylate H2AX after exposure to ionizing radiation, Cancer Res. 64 (2004) 2390–2396.
[29] J.P. Madigan, H.L. Chotkowski, R.L. Glaser, DNA double-strand break-induced phosphorylation of *Drosophila* histone variant H2Av helps prevent radiation-induced apoptosis, Nucleic Acids Res. 30 (2002) 3698–3705.
[30] S. Roch-Lefevre, T. Mandina, P. Voisin, G. Gaetan, J.E. Mesa, M. Valente, P. Bonnesoeur, O. Garcia, P. Voisin, L. Roy, Quantification of gamma-H2AX foci in human lymphocytes: a method for biological dosimetry after ionizing radiation exposure, Radiat. Res. 174 (2010) 185–194.

[31] P.L. Olive, J.P. Banath, Phosphorylation of histone H2AX as a measure of radiosensitivity, Int. J. Radiat. Oncol. Biol. Phys. 58 (2004) 331–335.
[32] O.A. Sedelnikova, I. Horikawa, D.B. Zimonjic, N.C. Popescu, W.M. Bonner, J.C. Barrett, Senescing human cells and ageing mice accumulate DNA lesions with unrepairable double-strand breaks, Nat. Cell Biol. 6 (2004) 168–170.
[33] M. Moroni, D. Maeda, M.H. Whitnall, W.M. Bonner, C.E. Redon, Evaluation of the gamma-H2AX assay for radiation biodosimetry in a swine model, Int. J. Mol. Sci. 14 (2013) 14119–14135.
[34] M. Lobrich, N. Rief, M. Kuhne, M. Heckmann, J. Fleckenstein, C. Rube, M. Uder, In vivo formation and repair of DNA double-strand breaks after computed tomography examinations, Proc. Natl. Acad. Sci. U. S. A. 102 (2005) 8984–8989.
[35] M. Fumagalli, F. Rossiello, M. Clerici, S. Barozzi, D. Cittaro, J.M. Kaplunov, G. Bucci, M. Dobreva, V. Matti, C.M. Beausejour, U. Herbig, M.P. Longhese, F. d'Adda di Fagagna, Telomeric DNA damage is irreparable and causes persistent DNA-damage-response activation, Nat. Cell Biol. 14 (2012) 355–365.
[36] G. Hewitt, D. Jurk, F.D. Marques, C. Correia-Melo, T. Hardy, A. Gackowska, R. Anderson, M. Taschuk, J. Mann, J.F. Passos, Telomeres are favoured targets of a persistent DNA damage response in ageing and stress-induced senescence, Nat. Commun. 3 (2012) 708.
[37] J. Torudd, M. Protopopova, R. Sarimov, J. Nygren, S. Eriksson, E. Markova, M. Chovanec, G. Selivanova, I.Y. Belyaev, Dose–response for radiation-induced apoptosis, residual 53BP1 foci and DNA-loop relaxation in human lymphocytes, Int. J. Radiat. Biol. 81 (2005) 125–138.
[38] W.M. Bonner, C.E. Redon, J.S. Dickey, A.J. Nakamura, O.A. Sedelnikova, S. Solier, Y. Pommier, GammaH2AX and cancer, Nat. Rev. Cancer 8 (2008) 957–967.
[39] N.H. Myung, X. Zhu, I.I. Kruman, R.J. Castellani, R.B. Petersen, S.L. Siedlak, G. Perry, M.A. Smith, H.G. Lee, Evidence of DNA damage in Alzheimer disease: phosphorylation of histone H2AX in astrocytes, Age (Dordr.) 30 (2008) 209–215.
[40] O.A. Sedelnikova, I. Horikawa, C. Redon, A. Nakamura, D.B. Zimonjic, N.C. Popescu, W.M. Bonner, Delayed kinetics of DNA double-strand break processing in normal and pathological aging, Aging Cell 7 (2008) 89–100.
[41] S.H. Schurman, C.A. Dunn, R. Greaves, B. Yu, L. Ferrucci, D.L. Croteau, M.M. Seidman, V.A. Bohr, Age-related disease association of endogenous gamma-H2AX foci in mononuclear cells derived from leukapheresis, PLoS ONE 7 (2012) e45728.
[42] D.R. Pilch, C. Redon, O.A. Sedelnikova, W.M. Bonner, Two-dimensional gel analysis of histones and other H2AX-related methods, Methods Enzymol. 375 (2004) 76–88.
[43] A. Nakamura, O.A. Sedelnikova, C. Redon, D.R. Pilch, N.I. Sinogeeva, R. Shroff, M. Lichten, W.M. Bonner, Techniques for gamma-H2AX detection, Methods Enzymol. 409 (2006) 236–250.
[44] K. Hamasaki, K. Imai, K. Nakachi, N. Takahashi, Y. Kodama, Y. Kusunoki, Short-term culture and gammaH2AX flow cytometry determine differences in individual radiosensitivity in human peripheral T lymphocytes, Environ. Mol. Mutagen. 48 (2007) 38–47.
[45] M. Lassmann, H. Hanscheid, D. Gassen, J. Biko, V. Meineke, C. Reiners, H. Scherthan, In vivo formation of gamma-H2AX and 53BP1 DNA repair foci in blood cells after radioiodine therapy of differentiated thyroid cancer, J. Nucl. Med. 51 (2010) 1318–1325.
[46] F. Bouquet, C. Muller, B. Salles, The loss of gammaH2AX signal is a marker of DNA double strand breaks repair only at low levels of DNA damage, Cell Cycle 5 (2006) 1116–1122.
[47] N. Taneja, M. Davis, J.S. Choy, M.A. Beckett, R. Singh, S.J. Kron, R.R. Weichselbaum, Histone H2AX phosphorylation as a predictor of radiosensitivity and target for radiotherapy, J. Biol. Chem. 279 (2004) 2273–2280.
[48] M.S. Siddiqui, M. Francois, M.F. Fenech, W.R. Leifert, gammaH2AX responses in human buccal cells exposed to ionizing radiation, Cytometry A 87 (2014) 296–308.
[49] C.E. Redon, J.S. Dickey, W.M. Bonner, O.A. Sedelnikova, Gamma-H2AX as a biomarker of DNA damage induced by ionizing radiation in human peripheral blood lymphocytes and artificial skin, Adv. Space Res. 43 (2009) 1171–1178.
[50] A. Willitzki, S. Lorenz, R. Hiemann, K. Guttek, A. Goihl, R. Hartig, K. Conrad, E. Feist, U. Sack, P. Schierack, L. Heiserich, C. Eberle, V. Peters, D. Roggenbuck, D. Reinhold, Fully automated analysis of chemically induced gammaH2AX foci in human peripheral blood mononuclear cells by indirect immunofluorescence, Cytometry A 83 (2013) 1017–1026.
[51] R. Runge, R. Hiemann, M. Wendisch, U. Kasten-Pisula, K. Storch, K. Zophel, C. Fritz, D. Roggenbuck, G. Wunderlich, K. Conrad, J. Kotzerke, Fully automated interpretation of ionizing radiation-induced gammaH2AX foci by the novel pattern recognition system AKLIDES(R), Int. J. Radiat. Biol. 88 (2012) 439–447.
[52] K. Brzozowska, M. Pinkawa, M.J. Eble, W.U. Muller, A. Wojcik, R. Kriehuber, S. Schmitz, In vivo versus in vitro individual radiosensitivity analysed in healthy donors and in prostate cancer patients with and without severe side effects after radiotherapy, Int. J. Radiat. Biol. 88 (2012) 405–413.
[53] H. Zhao, A.P. Albino, E. Jorgensen, F. Traganos, Z. Darzynkiewicz, DNA damage response induced by tobacco smoke in normal human bronchial epithelial and A549 pulmonary adenocarcinoma cells assessed by laser scanning cytometry, Cytometry A 75 (2009) 840–847.
[54] T. Tanaka, X. Huang, H.D. Halicka, H. Zhao, F. Traganos, A.P. Albino, W. Dai, Z. Darzynkiewicz, Cytometry of ATM activation and histone H2AX phosphorylation to estimate extent of DNA damage induced by exogenous agents, Cytometry A 71 (2007) 648–661.
[55] E. Riballo, M. Kuhne, N. Rief, A. Doherty, G.C. Smith, M.J. Recio, C. Reis, K. Dahm, A. Fricke, A. Krempler, A.R. Parker, S.P. Jackson, A. Gennery, P.A. Jeggo, M. Lobrich, A pathway of double-strand break rejoining dependent upon ATM, Artemis, and proteins locating to gamma-H2AX foci, Mol. Cell 16 (2004) 715–724.
[56] M. Lobrich, A. Shibata, A. Beucher, A. Fisher, M. Ensminger, A.A. Goodarzi, O. Barton, P.A. Jeggo, gammaH2AX foci analysis for monitoring DNA double-strand break repair: strengths, limitations and optimization, Cell Cycle 9 (2010) 662–669.
[57] D.T. Goodhead, Initial events in the cellular effects of ionizing radiations: clustered damage in DNA, Int. J. Radiat. Biol. 65 (1994) 7–17.
[58] P.M. Sharma, B. Ponnaiya, M. Taveras, I. Shuryak, H. Turner, D.J. Brenner, High throughput measurement of gammaH2AX DSB repair kinetics in a healthy human population, PLOS ONE 10 (2015) e0121083.
[59] R. Kodym, E. Horth, Determination of radiation-induced DNA strand breaks in individual cells by non-radioactive labelling of 3′ OH ends, Int. J. Radiat. Biol. 68 (1995) 133–139.
[60] M.I. Nunez, M. Villalobos, N. Olea, M.T. Valenzuela, V. Pedraza, T.J. McMillan, J.M. Ruiz de Almodovar, Radiation-induced DNA double-strand break rejoining in human tumour cells, Br. J. Cancer 71 (1995) 311–316.
[61] S.H. MacPhail, J.P. Banath, Y. Yu, E. Chu, P.L. Olive, Cell cycle-dependent expression of phosphorylated histone H2AX: reduced expression in unirradiated but not X-irradiated G1-phase cells, Radiat. Res. 159 (2003) 759–767.
[62] J.F. Ward, DNA damage produced by ionizing radiation in mammalian cells: identities, mechanisms of formation, and reparability, Prog. Nucleic Acid Res. Mol. Biol. 35 (1988) 95–125.
[63] J.F. Ward, The yield of DNA double-strand breaks produced intracellularly by ionizing radiation: a review, Int. J. Radiat. Biol. 57 (1990) 1141–1150.
[64] J.P. Banath, D. Klokov, S.H. MacPhail, C.A. Banuelos, P.L. Olive, Residual gammaH2AX foci as an indication of lethal DNA lesions, BMC Cancer 10 (2010) 4.
[65] N. Bhogal, P. Kaspler, F. Jalali, O. Hyrien, R. Chen, R.P. Hill, R.G. Bristow, Late residual gamma-H2AX foci in murine skin are dose responsive and predict radiosensitivity in vivo, Radiat. Res. 173 (2010) 1–9.
[66] C.S. Djuzenova, I. Elsner, A. Katzer, E. Worschech, L.V. Distel, M. Flentje, B. Polat, Radiosensitivity in breast cancer assessed by the histone gamma-H2AX and 53BP1 foci, Radiat. Oncol. 8 (2013) 98.
[67] P.A. Jeggo, V. Geuting, M. Lobrich, The role of homologous recombination in radiation-induced double-strand break repair, Radiother. Oncol. 101 (2011) 7–12.
[68] S.H. MacPhail, J.P. Banath, T.Y. Yu, E.H. Chu, H. Lambur, P.L. Olive, Expression of phosphorylated histone H2AX in cultured cell lines following exposure to X-rays, Int. J. Radiat. Biol. 79 (2003) 351–358.
[69] E. Dikomey, J. Dahm-Daphi, I. Brammer, R. Martensen, B. Kaina, Correlation between cellular radiosensitivity and non-repaired double-strand breaks studied in nine mammalian cell lines, Int. J. Radiat. Biol. 73 (1998) 269–278.
[70] C.E. Redon, A.J. Nakamura, K. Gouliaeva, A. Rahman, W.F. Blakely, W.M. Bonner, The use of gamma-H2AX as a biodosimeter for total-body radiation exposure in non-human primates, PLoS ONE 5 (2010) e15544.
[71] O.F. Qvarnstrom, M. Simonsson, K.A. Johansson, J. Nyman, I. Turesson, DNA double strand break quantification in skin biopsies, Radiother. Oncol. 72 (2004) 311–317.
[72] L. Paris, E. Cordelli, P. Eleuteri, M.G. Grollino, E. Pasquali, R. Ranaldi, R. Meschini, F. Pacchierotti, Kinetics of gamma-H2AX induction and removal in bone marrow and testicular cells of mice after X-ray irradiation, Mutagenesis 26 (2011) 563–572.
[73] E. Markova, N. Schultz, I.Y. Belyaev, Kinetics and dose–response of residual 53BP1/gamma-H2AX foci: co-localization, relationship with DSB repair and clonogenic survival, Int. J. Radiat. Biol. 83 (2007) 319–329.
[74] C. Bracalente, I.L. Ibanez, B. Molinari, M. Palmieri, A. Kreiner, A. Valda, J. Davidson, H. Duran, Induction and persistence of large gammaH2AX foci by high linear energy transfer radiation in DNA-dependent protein kinase-deficient cells, Int. J. Radiat. Oncol. Biol. Phys. 87 (2013) 785–794.
[75] I.A. Zalenskaya, E.M. Bradbury, A.O. Zalensky, Chromatin structure of telomere domain in human sperm, Biochem. Biophys. Res. Commun. 279 (2000) 213–218.
[76] I.H. Ismail, T.I. Wadhra, O. Hammarsten, An optimized method for detecting gamma-H2AX in blood cells reveals a significant interindividual variation in the gamma-H2AX response among humans, Nucleic Acids Res. 35 (2007) e36.
[77] A. Sak, S. Grehl, P. Erichsen, M. Engelhard, A. Grannass, S. Levegrun, C. Pottgen, M. Groneberg, M. Stuschke, Gamma-H2AX foci formation in peripheral blood lymphocytes of tumor patients after local radiotherapy to different sites of the body: dependence on the dose-distribution, irradiated site and time from start of treatment, Int. J. Radiat. Biol. 83 (2007) 639–652.
[78] U. Kasten-Pisula, S. Windhorst, J. Dahm-Daphi, G. Mayr, E. Dikomey, Radiosensitization of tumour cell lines by the polyphenol gossypol results from depressed double-strand break repair and not from enhanced apoptosis, Radiother. Oncol. 83 (2007) 296–303.
[79] A. Ivashkevich, C.E. Redon, A.J. Nakamura, R.F. Martin, O.A. Martin, Use of the gamma-H2AX assay to monitor DNA damage and repair in translational cancer research, Cancer Lett. 327 (2012) 123–133.
[80] A. Andrievski, R.C. Wilkins, The response of gamma-H2AX in human lymphocytes and lymphocytes subsets measured in whole blood cultures, Int. J. Radiat. Biol. 85 (2009) 369–376.
[81] I. Turesson, J. Nyman, E. Holmberg, A. Oden, Prognostic factors for acute and late skin reactions in radiotherapy patients, Int. J. Radiat. Oncol. Biol. Phys. 36 (1996) 1065–1075.

[82] J. Fleckenstein, M. Kuhne, K. Seegmuller, S. Derschang, P. Melchior, S. Graber, A. Fricke, C.E. Rube, C. Rube, The impact of individual in vivo repair of DNA double-strand breaks on oral mucositis in adjuvant radiotherapy of head-and-neck cancer, Int. J. Radiat. Oncol. Biol. Phys. 81 (2011) 1465–1472.
[83] E.C. Bourton, P.N. Plowman, D. Smith, C.F. Arlett, C.N. Parris, Prolonged expression of the gamma-H2AX DNA repair biomarker correlates with excess acute and chronic toxicity from radiotherapy treatment, Int. J. Cancer 129 (2011) 2928–2934.
[84] J. Werbrouck, K. De Ruyck, L. Beels, A. Vral, M. Van Eijkeren, W. De Neve, H. Thierens, Prediction of late normal tissue complications in RT treated gynaecological cancer patients: potential of the gamma-H2AX foci assay and association with chromosomal radiosensitivity, Oncol. Rep. 23 (2010) 571–578.
[85] S.L. Tucker, F.B. Geara, L.J. Peters, W.A. Brock, How much could the radiotherapy dose be altered for individual patients based on a predictive assay of normal-tissue radiosensitivity? Radiother. Oncol. 38 (1996) 103–113.
[86] J.D. Cox, J. Stetz, T.F. Pajak, Toxicity criteria of the Radiation Therapy Oncology Group (RTOG) and the European Organization for Research and Treatment of Cancer (EORTC), Int. J. Radiat. Oncol. Biol. Phys. 31 (1995) 1341–1346.
[87] C.E. Rube, A. Fricke, R. Schneider, K. Simon, M. Kuhne, J. Fleckenstein, S. Graber, N. Graf, C. Rube, DNA repair alterations in children with pediatric malignancies: novel opportunities to identify patients at risk for high-grade toxicities, Int. J. Radiat. Oncol. Biol. Phys. 78 (2010) 359–369.
[88] M.L. Chua, N. Somaiah, R. A'Hern, S. Davies, L. Gothard, J. Yarnold, K. Rothkamm, Residual DNA and chromosomal damage in ex vivo irradiated blood lymphocytes correlated with late normal tissue response to breast radiotherapy, Radiother. Oncol. 99 (2011) 362–366.
[89] H.V. Goutham, K.D. Mumbrekar, B.M. Vadhiraja, D.J. Fernandes, K. Sharan, G. Kanive Parashiva, S. Kapaettu, S.R. Bola, Sadashiva, DNA double-strand break analysis by gamma-H2AX foci: a useful method for determining the overreactors to radiation-induced acute reactions among head-and-neck cancer patients, Int. J. Radiat. Oncol. Biol. Phys. 84 (2012) e607–e612.
[90] J. Morini, G. Babini, L. Mariotti, G. Baiocco, L. Nacci, C. Maccario, U. Rossler, A. Minelli, M. Savio, M. Gomolka, U. Kulka, A. Ottolenghi, C. Danesino, Radiosensitivity in lymphoblastoid cell lines derived from Shwachman–Diamond syndrome patients, Radiat. Prot. Dosimetry (2015), http://dx.doi.org/10.1093/rpd/ncv152.
[91] P. Porcedda, V. Turinetto, E. Lantelme, E. Fontanella, K. Chrzanowska, R. Ragona, M. De Marchi, D. Delia, C. Giachino, Impaired elimination of DNA double-strand break-containing lymphocytes in ataxia telangiectasia and Nijmegen breakage syndrome, DNA Repair (Amst.) 5 (2006) 904–913.
[92] M. Doai, N. Watanabe, T. Takahashi, M. Taniguchi, H. Tonami, K. Iwabuchi, D. Kayano, M. Fukuoka, S. Kinuya, Sensitive immunodetection of radiotoxicity after iodine-131 therapy for thyroid cancer using gamma-H2AX foci of DNA damage in lymphocytes, Ann. Nucl. Med. 27 (2013) 233–238.
[93] M.S. May, M. Brand, W. Wuest, K. Anders, T. Kuwert, O. Prante, D. Schmidt, S. Maschauer, R.C. Semelka, M. Uder, M.A. Kuefner, Induction and repair of DNA double-strand breaks in blood lymphocytes of patients undergoing (1)(8)F-FDG PET/CT examinations, Eur. J. Nucl. Med. Mol. Imaging 39 (2012) 1712–1719.
[94] D. Denoyer, P. Lobachevsky, P. Jackson, M. Thompson, O.A. Martin, R.J. Hicks, Analysis of 177Lu-DOTA-octreotate therapy-induced DNA damage in peripheral blood lymphocytes of patients with neuroendocrine tumors, J. Nucl. Med. 56 (2015) 505–511.
[95] D. Geisel, J.T. Heverhagen, M. Kalinowski, H.J. Wagner, DNA double-strand breaks after percutaneous transluminal angioplasty, Radiology 248 (2008) 852–859.
[96] E. Markova, J. Torudd, I. Belyaev, Long time persistence of residual 53BP1/gamma-H2AX foci in human lymphocytes in relationship to apoptosis, chromatin condensation and biological dosimetry, Int. J. Radiat. Biol. 87 (2011) 736–745.
[97] F. Rodier, J.P. Coppe, C.K. Patil, W.A. Hoeijmakers, D.P. Munoz, S.R. Raza, A. Freund, E. Campeau, A.R. Davalos, J. Campisi, Persistent DNA damage signalling triggers senescence-associated inflammatory cytokine secretion, Nat. Cell Biol. 11 (2009) 973–979.
[98] K. Baynton, M. Otterlei, M. Bjoras, C. von Kobbe, V.A. Bohr, E. Seeberg, WRN interacts physically and functionally with the recombination mediator protein RAD52, J. Biol. Chem. 278 (2003) 36476–36486.
[99] S. Huang, L. Lee, N.B. Hanson, C. Lenaerts, H. Hoehn, M. Poot, C.D. Rubin, D.F. Chen, C.C. Yang, H. Juch, T. Dorn, R. Spiegel, E.A. Oral, M. Abid, C. Battisti, E. Lucci-Cordisco, G. Neri, E.H. Steed, A. Kidd, W. Isley, D. Showalter, J.L. Vittone, A. Konstantinow, J. Ring, P. Meyer, S.L. Wenger, A. von Herbay, U. Wollina, M. Schuelke, C.R. Huizenga, D.F. Leistritz, G.M. Martin, I.S. Mian, J. Oshima, The spectrum of WRN mutations in Werner syndrome patients, Hum. Mutat. 27 (2006) 558–567.
[100] L. Lan, S. Nakajima, K. Komatsu, A. Nussenzweig, A. Shimamoto, J. Oshima, A. Yasui, Accumulation of Werner protein at DNA double-strand breaks in human cells, J. Cell Sci. 118 (2005) 4153–4162.
[101] A. Zecevic, H. Menard, V. Gurel, E. Hagan, R. DeCaro, A. Zhitkovich, WRN helicase promotes repair of DNA double-strand breaks caused by aberrant mismatch repair of chromium-DNA adducts, Cell Cycle 8 (2009) 2769–2778.
[102] S.B. Cantor, R.M. Brosh Jr., What is wrong with Fanconi anemia cells? Cell Cycle 13 (2014) 3823–3827.
[103] A. Leskovac, D. Vujic, M. Guc-Scekic, S. Petrovic, I. Joksic, P. Slijepcevic, G. Joksic, Fanconi anemia is characterized by delayed repair kinetics of DNA double-strand breaks, Tohoku J. Exp. Med. 221 (2010) 69–76.
[104] J.E. Gonzalez, S.H. Roch-Lefevre, T. Mandina, O. Garcia, L. Roy, Induction of gamma-H2AX foci in human exfoliated buccal cells after in vitro exposure to ionising radiation, Int. J. Radiat. Biol. 86 (2010) 752–759.
[105] T.M. Filion, M. Qiao, P.N. Ghule, M. Mandeville, A.J. van Wijnen, J.L. Stein, J.B. Lian, D.C. Altieri, G.S. Stein, Survival responses of human embryonic stem cells to DNA damage, J. Cell. Physiol. 220 (2009) 586–592.
[106] C.E. Rube, A. Fricke, T.A. Widmann, T. Furst, H. Madry, M. Pfreundschuh, C. Rube, Accumulation of DNA damage in hematopoietic stem and progenitor cells during human aging, PLoS ONE 6 (2011) e17487.
[107] D. Klokov, S.M. MacPhail, J.P. Banath, J.P. Byrne, P.L. Olive, Phosphorylated histone H2AX in relation to cell survival in tumor cells and xenografts exposed to single and fractionated doses of X-rays, Radiother. Oncol. 80 (2006) 223–229.
[108] A. Smogorzewska, J. Karlseder, H. Holtgreve-Grez, A. Jauch, T. de Lange, DNA ligase IV-dependent NHEJ of deprotected mammalian telomeres in G1 and G2, Curr. Biol. 12 (2002) 1635–1644.
[109] A. Menegakis, A. Yaromina, W. Eicheler, A. Dorfler, B. Beuthien-Baumann, H.D. Thames, M. Baumann, M. Krause, Prediction of clonogenic cell survival curves based on the number of residual DNA double strand breaks measured by gammaH2AX staining, Int. J. Radiat. Biol. 85 (2009) 1032–1041.
[110] E.A. Ahmed, A. van der Vaart, A. Barten, H.B. Kal, J. Chen, Z. Lou, K. Minter-Dykhouse, J. Bartkova, J. Bartek, P. de Boer, D.G. de Rooij, Differences in DNA double strand breaks repair in male germ cell types: lessons learned from a differential expression of Mdc1 and 53BP1, DNA Repair (Amst.) 6 (2007) 1243–1254.
[111] N. Andratschke, T. Blau, S. Schill, C. Nieder, Late residual gamma-H2AX foci in murine spinal cord might facilitate development of response-modifying strategies: a research hypothesis, Anticancer Res. 31 (2011) 561–564.
[112] R.E. Meyn, W.T. Jenkins, Variation in normal and tumor tissue sensitivity of mice to ionizing radiation-induced DNA strand breaks in vivo, Cancer Res. 43 (1983) 5668–5673.
[113] K. Yoshida, S.H. Yoshida, C. Shimoda, T. Morita, Expression and radiation-induced phosphorylation of histone H2AX in mammalian cells, J. Radiat. Res. 44 (2003) 47–51.
[114] B. Gavrilov, I. Vezhenkova, D. Firsanov, L. Solovjeva, M. Svetlova, V. Mikhailov, N. Tomilin, Slow elimination of phosphorylated histone gamma-H2AX from DNA of terminally differentiated mouse heart cells in situ, Biochem. Biophys. Res. Commun. 347 (2006) 1048–1052.
[115] D. Hudson, I. Kovalchuk, I. Koturbash, B. Kolb, O.A. Martin, O. Kovalchuk, Induction and persistence of radiation-induced DNA damage is more pronounced in young animals than in old animals, Aging (Albany, NY) 3 (2011) 609–620.
[116] C.E. Rube, X. Dong, M. Kuhne, A. Fricke, L. Kaestner, P. Lipp, C. Rube, DNA double-strand break rejoining in complex normal tissues, Int. J. Radiat. Oncol. Biol. Phys. 72 (2008) 1180–1187.
[117] S. Grudzenski, A. Raths, S. Conrad, C.E. Rube, M. Lobrich, Inducible response required for repair of low-dose radiation damage in human fibroblasts, Proc. Natl. Acad. Sci. U. S. A. 107 (2010) 14205–14210.
[118] E.A. Ahmed, D. Agay, G. Schrock, M. Drouet, V. Meineke, H. Scherthan, Persistent DNA damage after high dose in vivo gamma exposure of minipig skin, PLoS ONE 7 (2012) e39521.
[119] M.S. Siddiqui, E. Filomeni, M. Francois, S.R. Collins, T. Cooper, R.V. Glatz, P.W. Taylor, M. Fenech, W.R. Leifert, Exposure of insect cells to ionising radiation in vivo induces persistent phosphorylation of a H2AX homologue (H2AvB), Mutagenesis 28 (2013) 531–541.
[120] D. Firsanov, A. Vasilishina, A. Kropotov, V. Mikhailov, Dynamics of gammaH2AX formation and elimination in mammalian cells after X-irradiation, Biochimie 94 (2012) 2416–2422.
[121] M.J. McEachern, A. Krauskopf, E.H. Blackburn, Telomeres and their control, Annu. Rev. Genet. 34 (2000) 331–358.
[122] T. de Lange, Shelterin: the protein complex that shapes and safeguards human telomeres, Genes Dev. 19 (2005) 2100–2110.
[123] N.S. Bae, P. Baumann, A RAP1/TRF2 complex inhibits nonhomologous end-joining at human telomeric DNA ends, Mol. Cell 26 (2007) 323–334.
[124] J.F. Passos, G. Nelson, C. Wang, T. Richter, C. Simillion, C.J. Proctor, S. Miwa, S. Olijslagers, J. Hallinan, A. Wipat, G. Saretzki, K.L. Rudolph, T.B. Kirkwood, T. von Zglinicki, Feedback between p21 and reactive oxygen production is necessary for cell senescence, Mol. Syst. Biol. 6 (2010) 347.
[125] F. d'Adda di Fagagna, Living on a break: cellular senescence as a DNA-damage response, Nat. Rev. Cancer 8 (2008) 512–522.
[126] J. Campisi, F. d'Adda di Fagagna, Cellular senescence: when bad things happen to good cells, Nat. Rev. Mol. Cell Biol. 8 (2007) 729–740.
[127] G.P. Dimri, X. Lee, G. Basile, M. Acosta, G. Scott, C. Roskelley, E.E. Medrano, M. Linskens, I. Rubelj, O. Pereira-Smith, A biomarker that identifies senescent human cells in culture and in aging skin in vivo, Proc. Natl. Acad. Sci. U. S. A. 92 (1995) 9363–9367.
[128] H. Li, J.R. Mitchell, P. Hasty, DNA double-strand breaks: a potential causative factor for mammalian aging? Mech. Ageing Dev. 129 (2008) 416–424.
[129] G. Aubert, P.M. Lansdorp, Telomeres and aging, Physiol. Rev. 88 (2008) 557–579.
[130] C. Lopez-Otin, M.A. Blasco, L. Partridge, M. Serrano, G. Kroemer, The hallmarks of aging, Cell 153 (2013) 1194–1217.
[131] D.A. Sinclair, P. Oberdoerffer, The ageing epigenome: damaged beyond repair? Ageing Res. Rev. 8 (2009) 189–198.
[132] C.M. Gedik, G. Grant, P.C. Morrice, S.G. Wood, A.R. Collins, Effects of age and dietary restriction on oxidative DNA damage, antioxidant protection and DNA repair in rats, Eur. J. Nutr. 44 (2005) 263–272.

[133] C.B. Harley, A.B. Futcher, C.W. Greider, Telomeres shorten during ageing of human fibroblasts, Nature 345 (1990) 458–460.
[134] N.D. Hastie, M. Dempster, M.G. Dunlop, A.M. Thompson, D.K. Green, R.C. Allshire, Telomere reduction in human colorectal carcinoma and with ageing, Nature 346 (1990) 866–868.
[135] J. Campisi, Aging, cellular senescence, and cancer, Annu. Rev. Physiol. 75 (2013) 685–705.
[136] F. d'Adda di Fagagna, P.M. Reaper, L. Clay-Farrace, H. Fiegler, P. Carr, T. Von Zglinicki, G. Saretzki, N.P. Carter, S.P. Jackson, A DNA damage checkpoint response in telomere-initiated senescence, Nature 426 (2003) 194–198.
[137] G.H. Stein, L.F. Drullinger, R.S. Robetorye, O.M. Pereira-Smith, J.R. Smith, Senescent cells fail to express cdc2, cycA, and cycB in response to mitogen stimulation, Proc. Natl. Acad. Sci. U. S. A. 88 (1991) 11012–11016.
[138] D.J. Baker, T. Wijshake, T. Tchkonia, N.K. LeBrasseur, B.G. Childs, B. van de Sluis, J.L. Kirkland, J.M. van Deursen, Clearance of p16Ink4a-positive senescent cells delays ageing-associated disorders, Nature 479 (2011) 232–236.
[139] C. Wang, D. Jurk, M. Maddick, G. Nelson, C. Martin-Ruiz, T. von Zglinicki, DNA damage response and cellular senescence in tissues of aging mice, Aging Cell 8 (2009) 311–323.
[140] E. Sikora, T. Arendt, M. Bennett, M. Narita, Impact of cellular senescence signature on ageing research, Ageing Res. Rev. 10 (2011) 146–152.
[141] J. Campisi, J.K. Andersen, P. Kapahi, S. Melov, Cellular senescence: a link between cancer and age-related degenerative disease? Semin. Cancer Biol. 21 (2011) 354–359.
[142] A. Freund, A.V. Orjalo, P.Y. Desprez, J. Campisi, Inflammatory networks during cellular senescence: causes and consequences, Trends Mol. Med. 16 (2010) 238–246.
[143] H.Y. Chung, M. Cesari, S. Anton, E. Marzetti, S. Giovannini, A.Y. Seo, C. Carter, B.P. Yu, C. Leeuwenburgh, Molecular inflammation: underpinnings of aging and age-related diseases, Ageing Res. Rev. 8 (2009) 18–30.
[144] C. Franceschi, Inflammaging as a major characteristic of old people: can it be prevented or cured? Nutr. Rev. 65 (2007) S173–S176.
[145] C. Garm, M. Moreno-Villanueva, A. Burkle, I. Petersen, V.A. Bohr, K. Christensen, T. Stevnsner, Age and gender effects on DNA strand break repair in peripheral blood mononuclear cells, Aging Cell 12 (2013) 58–66.
[146] H. Endt, C.N. Sprung, U. Keller, U. Gaipl, R. Fietkau, L.V. Distel, Detailed analysis of DNA repair and senescence marker kinetics over the life span of a human fibroblast cell line, J. Gerontol. A: Biol. Sci. Med. Sci. 66 (2011) 367–375.
[147] U. Herbig, M. Ferreira, L. Condel, D. Carey, J.M. Sedivy, Cellular senescence in aging primates, Science 311 (2006) 1257.
[148] V. Gorbunova, A. Seluanov, Making ends meet in old age: DSB repair and aging, Mech. Ageing Dev. 126 (2005) 621–628.
[149] R. Scarpato, C. Verola, B. Fabiani, V. Bianchi, G. Saggese, G. Federico, Nuclear damage in peripheral lymphocytes of obese and overweight Italian children as evaluated by the gamma-H2AX focus assay and micronucleus test, FASEB J. 25 (2011) 685–693.
[150] C. Giovannini, S. Piaggi, G. Federico, R. Scarpato, High levels of gamma-H2AX foci and cell membrane oxidation in adolescents with type 1 diabetes, Mutat. Res. 770 (2014) 128–135.
[151] Y. Liu, A. Rusinol, M. Sinensky, Y. Wang, Y. Zou, DNA damage responses in progeroid syndromes arise from defective maturation of prelamin A, J. Cell Sci. 119 (2006) 4644–4649.
[152] N. Hoze, M. Ruault, C. Amoruso, A. Taddei, D. Holcman, Spatial telomere organization and clustering in yeast *Saccharomyces cerevisiae* nucleus is generated by a random dynamics of aggregation–dissociation, Mol. Biol. Cell 24 (1791-800) (2013) S1–S10.
[153] J. Moquet, S. Barnard, K. Rothkamm, Gamma-H2AX biodosimetry for use in large scale radiation incidents: comparison of a rapid '96 well lyse/fix' protocol with a routine method, PeerJ 2 (2014) e282.
[154] H.C. Turner, D.J. Brenner, Y. Chen, A. Bertucci, J. Zhang, H. Wang, O.V. Lyulko, Y. Xu, I. Shuryak, J. Schaefer, N. Simaan, G. Randers-Pehrson, Y.L. Yao, S.A. Amundson, G. Garty, Adapting the gamma-H2AX assay for automated processing in human lymphocytes: 1. Technological aspects, Radiat. Res. 175 (2011) 282–290.
[155] G. Garty, Y. Chen, A. Salerno, H. Turner, J. Zhang, O. Lyulko, A. Bertucci, Y. Xu, H. Wang, N. Simaan, G. Randers-Pehrson, Y.L. Yao, S.A. Amundson, D.J. Brenner, The RABIT: a rapid automated biodosimetry tool for radiological triage, Health Phys. 98 (2010) 209–217.
[156] S. Bekker-Jensen, C. Lukas, R. Kitagawa, F. Melander, M.B. Kastan, J. Bartek, J. Lukas, Spatial organization of the mammalian genome surveillance machinery in response to DNA strand breaks, J. Cell Biol. 173 (2006) 195–206.
[157] P.O. Mari, B.I. Florea, S.P. Persengiev, N.S. Verkaik, H.T. Bruggenwirth, M. Modesti, G. Giglia-Mari, K. Bezstarosti, J.A. Demmers, T.M. Luider, A.B. Houtsmuller, D.C. van Gent, Dynamic assembly of end-joining complexes requires interaction between Ku70/80 and XRCC4, Proc. Natl. Acad. Sci. U. S. A. 103 (2006) 18597–18602.
[158] W. Li, F. Li, Q. Huang, J. Shen, F. Wolf, Y. He, X. Liu, Y.A. Hu, J.S. Bedford, C.Y. Li, Quantitative, noninvasive imaging of radiation-induced DNA double-strand breaks in vivo, Cancer Res. 71 (2011) 4130–4137.
[159] B. Cornelissen, V. Kersemans, S. Darbar, J. Thompson, K. Shah, K. Sleeth, M.A. Hill, K.A. Vallis, Imaging DNA damage in vivo using gammaH2AX-targeted immunoconjugates, Cancer Res. 71 (2011) 4539–4549.
[160] A. Leonard, J. Rueff, G.B. Gerber, E.D. Leonard, Usefulness and limits of biological dosimetry based on cytogenetic methods, Radiat. Prot. Dosimetry 115 (2005) 448–454.
[161] R.A. Kleinerman, A.A. Romanyukha, D.A. Schauer, J.D. Tucker, Retrospective assessment of radiation exposure using biological dosimetry: chromosome painting, electron paramagnetic resonance and the glycophorin a mutation assay, Radiat Res. 166 (2006) 287–302.
[162] M.M. Pinto, N.F. Santos, A. Amaral, Current status of biodosimetry based on standard cytogenetic methods, Radiat. Environ. Biophys. 49 (2010) 567–581.
[163] J.P. Banath, S.H. Macphail, P.L. Olive, Radiation sensitivity, H2AX phosphorylation, and kinetics of repair of DNA strand breaks in irradiated cervical cancer cell lines, Cancer Res. 64 (2004) 7144–7149.
[164] S. Mohapatra, M. Kawahara, I.S. Khan, S.M. Yannone, L.F. Povirk, Restoration of G1 chemo/radioresistance and double-strand-break repair proficiency by wild-type but not endonuclease-deficient artemis, Nucleic Acids Res. 39 (2011) 6500–6510.
[165] J. Zhao, Z. Guo, H. Zhang, Z. Wang, L. Song, J. Ma, S. Pei, C. Wang, The potential value of the neutral comet assay and gammaH2AX foci assay in assessing the radiosensitivity of carbon beam in human tumor cell lines, Radiol. Oncol. 47 (2013) 247–257.
[166] E.K. Balcer-Kubiczek, M. Attarpour, M.J. Edelman, The synergistic effect of dimethylamino benzoylphenylurea (NSC #639829) and X-irradiation on human lung carcinoma cell lines, Cancer Chemother. Pharmacol. 59 (2007) 781–787.
[167] A. Baschnagel, A. Russo, W.E. Burgan, D. Carter, K. Beam, D. Palmieri, P.S. Steeg, P. Tofilon, K. Camphausen, Vorinostat enhances the radiosensitivity of a breast cancer brain metastatic cell line grown in vitro and as intracranial xenografts, Mol. Cancer Ther. 8 (2009) 1589–1595.
[168] S. Huerta, X. Gao, E.H. Livingston, P. Kapur, H. Sun, T. Anthony, In vitro and in vivo radiosensitization of colorectal cancer HT-29 cells by the smac mimetic JP-1201, Surgery 148 (2010) 346–353.
[169] R. Choudhuri, W. Degraff, J. Gamson, J.B. Mitchell, J.A. Cook, Guggulsterone-mediated enhancement of radiosensitivity in human tumor cell lines, Front. Oncol. 1 (2011) 19.
[170] L. Wang, U. Raju, L. Milas, D. Molkentine, Z. Zhang, P. Yang, L. Cohen, Z. Meng, Z. Liao, Huachansu, containing cardiac glycosides, enhances radiosensitivity of human lung cancer cells, Anticancer Res. 31 (2011) 2141–2148.
[171] H. Wang, M. Wang, H. Wang, W. Bocker, G. Iliakis, Complex H2AX phosphorylation patterns by multiple kinases including ATM and DNA-PK in human cells exposed to ionizing radiation and treated with kinase inhibitors, J. Cell. Physiol. 202 (2005) 492–502.
[172] S. Fu, Y. Yang, T.K. Das, Y. Yen, B.S. Zhou, M.M. Zhou, M. Ohlmeyer, E.C. Ko, R. Cagan, B.S. Rosenstein, S.H. Chen, J. Kao, Gamma-H2AX kinetics as a novel approach to high content screening for small molecule radiosensitizers, PLoS ONE 7 (2012) e38465.
[173] M. Kuhne, E. Riballo, N. Rief, K. Rothkamm, P.A. Jeggo, M. Lobrich, A double-strand break repair defect in ATM-deficient cells contributes to radiosensitivity, Cancer Res. 64 (2004) 500–508.
[174] Y.B. Kim, H.C. Jeung, I. Jeong, K. Lee, S.Y. Rha, H.C. Chung, G.E. Kim, Mechanism of enhancement of radiation-induced cytotoxicity by sorafenib in colorectal cancer, J. Radiat. Res. 54 (2013) 52–60.
[175] V. Minieri, S. Saviozzi, G. Gambarotta, M. Lo Iacono, L. Accomasso, E. Cibrario Rocchietti, C. Gallina, V. Turinetto, C. Giachino, Persistent DNA damage-induced premature senescence alters the functional features of human bone marrow mesenchymal stem cells, J. Cell. Mol. Med. 19 (2015) 734–743.
[176] E. McKenna, F. Traganos, H. Zhao, Z. Darzynkiewicz, Persistent DNA damage caused by low levels of mitomycin C induces irreversible cell senescence, Cell Cycle 11 (2012) 3132–3140.
[177] D. Wei, L.A. Parsels, D. Karnak, M.A. Davis, J.D. Parsels, A.C. Marsh, L. Zhao, J. Maybaum, T.S. Lawrence, Y. Sun, M.A. Morgan, Inhibition of protein phosphatase 2A radiosensitizes pancreatic cancers by modulating CDC25C/CDK1 and homologous recombination repair, Clin. Cancer Res. 19 (2013) 4422–4432.
[178] J. Wang, Q. Liu, Q. Yang, Radiosensitization effects of berberine on human breast cancer cells, Int. J. Mol. Med. 30 (2012) 1166–1172.
[179] J. Fahrer, J. Huelsenbeck, H. Jaurich, B. Dorsam, T. Frisan, M. Eich, W.P. Roos, B. Kaina, G. Fritz, Cytolethal distending toxin (CDT) is a radiomimetic agent and induces persistent levels of DNA double-strand breaks in human fibroblasts, DNA Repair (Amst.) 18 (2014) 31–43.
[180] S.J. Chiu, J.I. Chao, Y.J. Lee, T.S. Hsu, Regulation of gamma-H2AX and securin contribute to apoptosis by oxaliplatin via a p38 mitogen-activated protein kinase-dependent pathway in human colorectal cancer cells, Toxicol. Lett. 179 (2008) 63–70.
[181] M.A. Morgan, L.A. Parsels, L. Zhao, J.D. Parsels, M.A. Davis, M.C. Hassan, S. Arumugarajah, L. Hylander-Gans, D. Morosini, D.M. Simeone, C.E. Canman, D.P. Normolle, S.D. Zabludoff, J. Maybaum, T.S. Lawrence, Mechanism of radiosensitization by the Chk1/2 inhibitor AZD7762 involves abrogation of the G2 checkpoint and inhibition of homologous recombinational DNA repair, Cancer Res. 70 (2010) 4972–4981.
[182] J. Wu, P.H. Clingen, V.J. Spanswick, M. Mellinas-Gomez, T. Meyer, I. Puzanov, D. Jodrell, D. Hochhauser, J.A. Hartley, Gamma-H2AX foci formation as a pharmacodynamic marker of DNA damage produced by DNA cross-linking agents: results from 2 phase I clinical trials of SJG-136 (SG2000), Clin. Cancer Res. 19 (2013) 721–730.
[183] B. Ladd, J.J. O'Konek, L.J. Ostruszka, D.S. Shewach, Unrepairable DNA double-strand breaks initiate cytotoxicity with HSV-TK/ganciclovir, Cancer Gene Ther. 18 (2011) 751–759.

[184] N. Alessio, S. Del Gaudio, S. Capasso, G. Di Bernardo, S. Cappabianca, M. Cipollaro, G. Peluso, U. Galderisi, Low dose radiation induced senescence of human mesenchymal stromal cells and impaired the autophagy process, Oncotarget 6 (2015) 8155–8166.
[185] T. Groesser, H. Chang, G. Fontenay, J. Chen, S.V. Costes, M. Helen Barcellos-Hoff, B. Parvin, B. Rydberg, Persistence of gamma-H2AX and 53BP1 foci in proliferating and non-proliferating human mammary epithelial cells after exposure to gamma-rays or iron ions, Int. J. Radiat. Biol. 87 (2011) 696–710.
[186] M. Suzuki, K. Suzuki, S. Kodama, M. Watanabe, Interstitial chromatin alteration causes persistent p53 activation involved in the radiation-induced senescence-like growth arrest, Biochem. Biophys. Res. Commun. 340 (2006) 145–150.

Mutagenesis vol. 28 no. 5 pp. 531–541
Advance Access publication 22 June 2013
doi:10.1093/mutage/get030

Exposure of insect cells to ionising radiation *in vivo* induces persistent phosphorylation of a H2AX homologue (H2AvB)

Mohammad S. Siddiqui[1,2], Erika Filomeni[1], Maxime François[1], Samuel R. Collins[3], Tamara Cooper[4,5], Richard V. Glatz[2,4], Phillip W. Taylor[3], Michael Fenech[1] and Wayne R. Leifert[1,*]

[1]CSIRO Animal, Food & Health Sciences, Nutritional Genomics & Genome Health Diagnostics, Adelaide, South Australia 5000, Australia, [2]School of Food, Agriculture and Wine, University of Adelaide, Urrbrae, South Australia 5064, Australia, [3]Department of Biological Sciences, Macquarie University, Sydney, New South Wales 2109, Australia and [4]SARDI Sustainable Systems, Entomology, Waite Building, Urrbrae, South Australia 5064, Australia
[5]Present address: Experimental Therapeutics Laboratory, School of Pharmacy and Medical Science, University of South Australia, Adelaide, South Australia 5000, Australia.

*To whom correspondence should be addressed. CSIRO Animal, Food & Health Sciences, Adelaide, South Australia 5000, Australia. Tel: +61 8 8303 8821; Fax: +61 8 8303 8899; Email: wayne.leifert@csiro.au

Received on March 7, 2013; revised on April 9, 2013; accepted on May 9, 2013

The response of eukaryotic cells to ionising radiation (IR)-induced double-strand DNA breaks is highly conserved and involves a DNA repair mechanism characterised by the early phosphorylation of histone protein H2AX (producing the active form γH2AX). Although the expression of an induced γH2AX variant has been detected in *Drosophila melanogaster*, the expression and radiation response of a γH2AX homologue has not been reported in economically important fruit flies. We use *Bactrocera tryoni* (Diptera: Tephritidae, Queensland fruit fly or 'Q-fly') to investigate this response with a view to developing molecular assays to detect/quantify exposure of fruit flies to IR and consequent DNA damage. Deep sequencing confirmed the presence of a H2AX homologue that we have termed H2AvB (i.e. variant *Bactrocera*) and has an identical sequence to a histone reported from the human disease vector *Glossina morsitans*. A linear dose–response of γH2AvB (0–400 Gy IR) was observed in whole Q-fly pupal lysates 24 h post-IR and was detected at doses as low as 20 Gy. γH2AvB signal peaked at ~20 min after IR exposure and at 24 h post-IR the signal remained elevated but declined significantly by 5 days. Persistent and dose-dependent γH2AvB signal could be detected and quantified either by western blot or by laser scanning cytometry up to 17 days post-IR exposure in histone extracts or isolated nuclei from adult Q-flies (irradiated as pupae). We conclude that IR exposure in Q-fly leads to persistent γH2AvB signals (over a period of days) that can easily be detected by western blot or quantitative immunofluorescence techniques. These approaches have potential as the basis for assays for detection and quantification of prior IR exposure in pest fruit flies.

Introduction

Double-strand breaks (DSBs) in chromosomal DNA may lead to genetic instabilities and gene mutations resulting in reduced integrity of the genome but also impaired health and survival (1,2). Phosphorylation of the C-terminal tails of H2AX histones in nucleosomes, which are located in the vicinity of the break (3,4), is one of the earliest known responses to DNA DSB formation in cells. The nucleosome complex comprises DNA wrapped around eight histone proteins, two from each of the four core histone families (H4, H3, H2B and H2A) and is essential for genome health in terms of normal regulation of gene expression and genome maintenance and replication (5–7). Induction of DSBs in live mammalian cells triggers the phosphorylation of Ser139 contained in the SQ motif near the carboxy terminus of H2AX, resulting in the formation of phosphorylated H2AX, termed γH2AX (8,9). While H2AX is distributed uniformly throughout chromatin, only H2AX molecules located in close vicinity to DSBs become phosphorylated (3,4,6). Several kinase proteins are known to phosphorylate H2AX including phosphatidylinositol 3-OH serine/threonine protein kinase-like kinases, ataxia telangiectasia mutated (ATM), ATM- and Rad-3-related and DNA-dependent protein kinase (DNA-PK). However, only ATM and DNA-PKs have been shown to phosphorylate H2AX in response to ionising radiation (IR) (3,8,10–14).

The SQ motif in H2AX is highly conserved among animals, plants and fungi (15–17). This evolutionary conservation of the phosphorylation of the core histone protein H2AX suggests the DSB damage-response mechanism is a fundamental process in DNA repair that arose prior to the evolutionary divergence of fungi, plants and animals. This is partly evidenced by the fact that SQ-specific antibodies raised against the mammalian γH2AX sequence can recognise DSBs in the frog *Xenopus laevis*, vinegar fly *Drosophila melanogaster* and bread/wine yeast *Saccharomyces cerevisiae*, after exposure to IR or other genotoxic agents (6,8). Antibodies that recognise phosphorylated H2AX in mammals have also been shown to recognise IR-induced H2Av (H2AX variant) in *D.melanogaster* (H2AvD) and binding has been shown to be dependent on the presence of the SQ motif (6,18).

Irradiation-induced genetic damage and repair processes involving γH2AX are relevant to two very different control measures applicable to management of Queensland fruit fly ('Q-fly' *Bactrocera tryoni*), Australia's most economically damaging insect pest of horticultural crops: post-harvest irradiation and sterile insect technique (SIT). Currently, a generic dose of 150 Gy is applied to exterminate fruit flies in infested produce (19,20); however, assurance of irradiation treatment of produce relies solely on certification. There are currently no routine assays available to detect and/or quantify prior IR exposure in economically important fruit flies or other insects. A direct and reliable assay to confirm irradiation would be of substantial value to export horticulture. In SIT, millions of Q-flies are irradiated as pupae (70 Gy) to induce reproductive sterility and released into the environment as adults where they mate with pest populations and induce reproductive failure, thereby reducing pest numbers in the next generation. Fruit flies captured in monitoring traps then need to be assessed as being part of the SIT release or part of the outbreak. A generic biomarker based on the distinctive

molecular processes of irradiation-induced DNA damage and repair would be a useful tool for this purpose. SIT is also the focus of various ongoing or proposed programs across the globe, aimed at a range of fly species (and other insects) of economic and medical concern (21–26) and so a biomarker for identifying sterilised insects would have internationally broad application. The aim of this study was to measure the phosphorylation of a H2AX homologue in the Q-fly as a marker of prior IR exposure.

In the present study, we identified the sequence of a H2AX protein variant from deep sequencing analysis of Q-fly transcripts and mass spectrometry of the irradiation-induced protein (we have termed this variant H2AvB and the sequence has been deposited into the NCBI Short Read Archive; BankIt1580860 isotig00988 KC161252). We found that H2AvB amino acid sequence is 96.4% similar to the homologue found in the genetic model *D.melanogaster*, 54.8% similar to human H2AX and identical in comparison with *Glossina morsitans morsitans* (the Savannah tsetse fly). Using western blotting and laser scanning cytometry (LSC) techniques, we demonstrate an irradiation-induced short-term rapid increase in γH2AvB followed by a long-term (persistent) and dose-dependent γH2AvB response in Q-fly. This assay has practical application to confirm irradiation status of live Q-fly found in exported fruits and to confirm the identity of unmarked flies captured in monitoring traps during SIT releases.

Materials and methods

Pupal and adult preparation and irradiation

Bactrocera tryoni (Q-fly) pupae were obtained from the NSW Department of Primary Industries Fruit Fly Production Facility at Elizabeth Macarthur Agricultural Institute (EMAI, New South Wales, Australia). Pupae from this facility are routinely sent to the Australian Nuclear Science and Technology Organisation (ANSTO, Lucas Heights, New South Wales, Australia) for irradiation as part of the SIT control program to suppress outbreak populations of wild Q-flies. Individual 'zip-lock' plastic bags (100×150 mm) containing ~8000 pupae were sealed and packed at EMAI and transported directly to ANSTO in an air-conditioned vehicle. All pupae were packed on the day of pupation and all irradiated pupae were treated 1 day post the onset of pupation. Bags of control and test pupae were packed together at all times during transport and storage to ensure that all pupae received similar conditions. To achieve a hypoxic atmosphere prior to irradiation, the sealed bags were held overnight at ANSTO in a temperature-controlled room at ~18°C. The following day, pupae were treated with IR using ANSTO's ^{60}Co GATRI facility delivering final doses of 0–400 Gy at a dose rate of 5 Gy/min. We investigated doses greater than the standard disinfestations dose of 150 Gy up to 400 Gy, since *Bactrocera* fruit flies appear to be considerably more tolerant to IR compared with other fruit fly genera such as *Ceratitis*, *Anastrepha* and *Rhagoletis* (20).

After irradiation, pupae were immediately transported in a closed styrofoam box in an air-conditioned vehicle to a laboratory at Macquarie University, Sydney, where they were housed to emerge in 5-l plastic cages, each with a large mesh-covered ventilation hole in the top. Pupae were held in a laboratory maintained at 25 ± 1°C and 70 ± 5% relative humidity, on a 14:10 day:night cycle including 1 h dawn and dusk periods during which the lights turned on and off intermittently. At 1 and 5 days post-IR, a sample of Q-fly pupae was frozen and stored at −80°C until required for assays. Other IR-treated pupae were allowed to emerge as adults, then collected using an aspirator and frozen at −80°C at 17 days post-IR. Adult flies were maintained on a standard diet of granular sucrose and yeast hydrolysate, with water provided in soaked cotton wool.

Egg collection and irradiation

Adult Q-flies were housed in 5-l plastic cages with one side replaced with mesh screen for ventilation. Approximately 150 flies were kept per cage. After observed mating (post 10 days of age), each cage was provided with an egging dish comprising of a 55-mm Petri dish containing a solution of lemon essence and water in a 140:1 ratio, covered with a layer of parafilm. The parafilm was pierced five to six times with an entomological pin to release the odour of lemon. After 2 days, the egging dishes were collected and a plastic 5-ml pipette was used to transfer eggs to a 10-ml vial of water. Each vial contained ~500 eggs. Vials were then exposed to either 0 or 150 Gy IR and then frozen at −80°C 2 h post-IR.

Larvae collection and irradiation

Adult Q-flies were housed in 5-l plastic cages with one side replaced with mesh screen for ventilation. Approximately 150 flies were kept per cage. After observed mating (post 10 days of age), each cage was provided a collection of fresh organic chillies resting on a 15-cm plate. After 4 days, the chillies were inspected for the presence of larvae. All chillies were then left a further 4 days to allow larvae to mature to third instar. Chillies were placed into separate 'zip-lock' bags and then exposed to 0 or 150 Gy IR and maintained at 25 ± 1°C and 70 ± 5% relative humidity for 24 h. Chillies were then sliced longitudinally in half and larvae were gently removed using a pair of forceps. Collected larvae were frozen at −80°C in 10-ml vials containing water.

Whole pupal lysate preparation for western blotting

Whole pupae were thawed from −80°C at room temperature (RT) for 5 min. Ten pupae of each IR dose being investigated were placed in cold (4°C) Tris-buffered saline (TBS) solution (50 mM Trizma base, 150 mM NaCl, pH 8.0) in a Petri dish on ice. The pupae were then added to 1 ml lysis buffer comprising radio-immune precipitation assay (RIPA) buffer (Sigma) with additional 0.9% sodium dodecyl sulphate, phosphatase inhibitors (25 mM NaF, 0.25 mM sodium orthovanadate, 1 mM EDTA, 1 mM phenylmethylsulphonyl fluoride, 1 mM dithiothreitol) and a protease inhibitor cocktail (Sigma) and their tissues disrupted in a glass tissue homogeniser on ice until a clear suspension was achieved (usually ~15 passes). Lysates were centrifuged at 4°C for 5 min at 300 × *g* to remove debris. Total protein from the pupal samples was quantified using the QuantiPro™ BCA Assay kit (Sigma) as per manufacturer's instructions, using bovine serum albumin (BSA) as a standard. Sample concentrations were adjusted to the same total protein concentration prior to gel electrophoresis. Samples were stored at −20°C until used for western blotting. Various amounts of total protein were added depending on the assay conducted and this is indicated in relevant figures.

Acid extraction of histone protein from pupae

To obtain histone proteins from pupal samples, an acid extraction technique was performed essentially as previously described (27) with some modification. Pupae were washed twice with TBS and placed in 3 ml of hypotonic lysis buffer (10 mM Trizma base pH 8.0, 1 mM KCl, 1.5 mM $MgCl_2$, 1 mM dithiothreitol), a commercial protease inhibitor cocktail and other phosphatase inhibitors (as above), in a glass homogeniser on ice. Pupae were then homogenised until a clear suspension was produced, followed by filtration with nylon net filters (filter type: 100 µm NY1H) and then incubation for 30 min (on a rotator at 4°C) to allow hypotonic swelling and lysis of cells. The crude extract was then centrifuged at 15 000 × *g* for 10 min at 4°C to separate the pellet (containing nuclei) from the soluble cytosol. The pellet was then resuspended in 400 µl of 0.8 M H_2SO_4 and vortexed thoroughly until aggregates were dispersed in the solution. This solution was vortexed gently overnight at 4°C using a minishaker. After centrifugation at 15 000 × *g* for 10 min at 4°C, the pellet was discarded and the acid-soluble histone proteins in the supernatant were then precipitated with a 33% trichloroacetic acid solution. The solution containing precipitated histones was mixed several times producing a milky suspension. Subsequently, the histone solution was incubated at 4°C overnight and then again centrifuged at 15 000 × *g* for 10 min at 4°C; the supernatant was then carefully discarded. The pellet of precipitated histones was washed three times with 1-ml ice-cold acetone to remove the acid from the protein sample. The acetone supernatant was removed and the protein pellet was air-dried for 30 min at RT and then dissolved in 150 µl of purified H_2O. Finally, the histone extract was stored at −20°C for subsequent analyses. In some experiments, dephosphorylation of the purified proteins was achieved by dissolving the extracted protein pellet in 100 mM NaCl, 50 mM Tris–HCl, 10 mM $MgCl_2$, 1 mM dithiothreitol (pH 7.9) and incubated with (or without for negative control) 1000 U/ml calf intestinal alkaline phosphatase (New England Biolabs, USA) overnight at 37°C.

Total lysates and histone extracts from individual pupae

Total lysates or histone extracts were prepared from individual pupae by a modification of the above method. For total lysates, the lysis volume was decreased to 150 µl of RIPA buffer (final volume), and for histone extracts of single pupae, the hypotonic buffer was decreased to 150 µl. For the single pupae total lysates, 180 µg total protein was used for sodium dodecyl sulphate-polyacrylamide gel electrophoresis and analysed by western blotting, while 1.3 µg total protein was loaded for the histone extracts from individual pupae.

Total lysates from irradiated eggs and larvae

Samples of irradiated Q-fly eggs were homogenised in liquid nitrogen and subsequently lysed in 150 µl RIPA buffer giving a final protein concentration of ~400 µg/ml. Third instar larvae (collected from 0 or 150 Gy irradiated chillies) were lysed (using the same method as for pupae) giving a final total protein concentration of ~7 mg/ml.

Antibodies

Anti-γH2AX was prepared by Biosensis Pty Ltd (Thebarton, South Australia, Australia). Affinity-purified KKAATQA[PSer]QEY (human sequence) peptide conjugated with KLH was used as antigen to generate high titre polyclonal antiserum in rabbit against γH2AX and this antibody was used in preliminary studies. *Drosophila* antihistone H2AvD pS137 (γH2AvD) rabbit polyclonal antibody (Rockland Immunochemicals Inc., Gilbertsville, PA, USA) (18) was routinely used to detect IR-induced histone in Q-fly. Both antibodies (γH2AX and H2AvD pS137) recognised a 15-kDa protein in western blot analyses. Cytochrome c oxidase subunit II and β-actin antibodies were from Abcam. Alexa Fluor 488-conjugated goat immunoglobulin G was from Invitrogen (Victoria, Australia) and horseradish peroxidase-labelled secondary antibodies were from PerkinElmer (Victoria, Australia).

Western blotting

Whole and histone-extracted lysates were diluted in Laemmli buffer (1:2 vol:vol) containing β-mercaptoethanol followed by heating at 95°C for 5 min, before being loaded on Criterion™-TGX™ precast polyacrylamide gels (BioRad) and subjected to electrophoresis. Gels were then stained with Coomassie Blue to ensure the electrophoresis had been successful and that similar amounts of protein were loaded in each well. A separate (duplicate) gel was used for western blotting onto a 0.2 µm pore nitrocellulose membrane (BioRad) for 1 h at 100 V in chilled transfer buffer (25 mM Trizma base, 190 mM glycine, 20% methanol, pH 8.5). The membrane was washed three times (5 min each) in TBST (TBS containing 0.5% Tween-20) and then blocked for 1 h at RT in TBST containing 5% BSA. Membranes were then incubated overnight at 4°C in primary antibody diluted 1:1000 in TBST containing 5% BSA. Membranes were then thoroughly washed three times in TBST for 5 min each time, then incubated with anti-rabbit horseradish peroxidase-linked secondary antibody (PerkinElmer) at a dilution of 1:2000 in TBST containing 5% BSA for 2 h at RT. Probed membranes were then finally washed three times with TBST prior to imaging by enhanced chemiluminescence (ECL) (Western Lightning® Plus-ECL, PerkinElmer) using an ImageQuant LAS 4000 imager (GE Health Care). Images were saved as 8-bit TIFF files and band intensities (as integrals) were quantified with ImageJ software (28). Data were normalised to β-actin (loading controls) where possible, i.e. in histone extracts, this was not possible since actin was removed during the processing of the samples. In western blots showing histone extracts containing γH2AvB where β-actin could not be used, we also show Coomassie-stained gel bands at ~15 kDa to demonstrate similar loading of histone proteins.

Immunofluorescence to quantify γH2AvB response in Q-fly nuclei

Cell nuclei obtained from adult Q-fly were extracted using a similar protocol as described above with the following modifications: adult Q-flies (17 days post-IR) were thawed from −80°C at RT for 5 min and suspended in 1.5 ml of hypotonic lysis buffer, containing 10 mM Tris–HCl pH 8.0, 1 mM KCl, 1.5 mM $MgCl_2$, phosphatase inhibitors (as above) and protease inhibitor cocktail, in a glass tissue homogeniser. Tissues were homogenised on ice until a clear suspension was achieved (usually five passes). The suspension was filtered using nylon net filters (filter type 100 µm NY1H) to remove most of the particles and then incubated for 30 min on a rotator at 4°C to allow the hypotonic swelling and lysis of cells, which were subsequently fixed in 1% formaldehyde in the same tube for 15 min at RT. Nuclei were then spotted on slides (using 10 µl of the suspension) and air-dried for 20 min at RT. Spotted nuclei were rehydrated in phosphate-buffered saline (PBS) for 15 min. Slides were then incubated in pre-chilled 70% ethanol for at least 20 min and washed in PBS for 15 min. Cell nuclei were 'blocked' using TBST containing 5% BSA for 30 min at RT, and slides were then washed once in PBS. Primary antibody (anti-H2AvB) was added at 1:500 dilution in TBST containing 5% BSA and slides were incubated overnight at 4°C under a parafilm cover. Slides were then washed three times in PBS for 5 min each to remove unbound antibody and then incubated with secondary antibody (Alexa Fluor 488 conjugated) at a dilution of 1:500 in TBST containing 5% BSA for 1 h at RT. Slides were again washed three times in PBS for 5 min each to remove unbound, or non-specifically bound, antibody. Nuclei staining was achieved using 4′,6-diamidino-2-phenylindole (DAPI) at a concentration of 0.2 µg/ml for 7 min at RT and then washed in a solution containing 300 mM NaCl and 30 mM trisodium citrate (pH 7.0). Spotted, DAPI-stained nuclei were subsequently mounted under a cover slip using mounting medium consisting of PBS and glycerol (1:1) and sealed to prevent desiccation prior to analysis by LSC.

Laser scanning cytometry

LSC is a very accurate cytometric method to colocalise and quantify fluorescent events in thousands of nuclei (29,30) (which is not practical with visual scoring techniques); therefore, we used LSC to quantify the γH2AvB signal in nuclei on microscope slides. Q-fly pupae were exposed to 0, 20 or 240 Gy IR and allowed to emerge as adults. At 17 days post-IR, the adult Q-flies were frozen at −80°C. Nuclei were subsequently extracted after hypotonic lysis and then fixed and stained on microscope slides. LSC was performed using an iCyte® Automated Imaging Cytometer (CompuCyte Corporation, Westwood, MA, USA) with full autofocus function and an inverted fluorescence microscope with laser excitation (Argon 488 nm, and Violet 405 nm) for quantitation of blue and green fluorescence emission. A total of 2656 (0 Gy), 3078 (20 Gy) or 3571 (240 Gy) nuclei were examined using iCyte cytometric analysis software version 3.4.10. The CompuColor feature in iCyte was used to provide nuclear staining as blue and γH2AX signal as green. The slides were scanned using a 40× objective and a 0.25 µm resolution step. Two lasers (405 and 488 nm) were used to excite the dyes DAPI and Alexa Fluor 488, respectively. The two lasers were scanned over the samples in separate passes, one immediately following the other, to prevent any overlapping (thus compensation) of fluorescence signals. The emitted and filtered fluorescence was then detected by photomultiplier tubes in separate channels (blue and green). The nuclei and γH2AvB events were contoured using empirically determined thresholds to exclude the scoring of false positives (e.g. small fluorescent debris). Any small debris or larger blue-emitting particulate matter (which was rarely observed) was excluded from the analyses. Individual data points for each nuclear event were automatically generated using the iCyte® software and transferred to statistical analysis software (see below).

mRNA isolation, cDNA synthesis and 454 sequencing

Frozen pupae that had been irradiated with 150 Gy were divided into three replicate groups, each weighing 0.1 g (10–11 pupae). mRNA was purified using a GenElute™ Direct mRNA miniprep kit (Sigma) according to the manufacturer's directions. Briefly, tissues were homogenised and lysed using liquid nitrogen with a mortar and pestle and 1 ml of lysis solution containing proteinase K. mRNA extraction proceeded using oligo(dT) beads and eluted mRNA was precipitated overnight at −20°C using 1 µl of 20 µg/µl glycogen, 0.1 volumes of 3 M sodium acetate pH 5.2 and three volumes of ice-cold ethanol. Precipitated mRNA was centrifuged and the pellet washed in 70% ethanol. mRNA was then resuspended in 19 µl of elution buffer and checked for quantity and quality using a NanoDrop 1000 spectrophotometer (Thermo Fisher, USA) and gel electrophoresis. The cDNA library was then generated according to the cDNA Rapid Library Preparation Method Manual (Roche). Each replicate group was ligated with different MID adaptors (RL 13, 14, 15; manufactured by Integrated DNA Technologies). Following library quantitation using a FLUOstar OPTIMA (BMG Labtech, Germany), 20 µl of each replicate was then pooled together and the combined library diluted to a final concentration of 1×10^6 molecules/µl. Emulsion PCR and bead enrichment were performed as per the emPCR amplification method manual, Lib-L (Roche Applied Science, USA), using two library molecules per bead. Approximately 500 000 of the enriched beads were loaded onto a PicoTiter-Plate (Roche Applied Science, USA) and pyrosequencing was performed using a 454 GS Junior (Roche Applied Science, USA) according to the manufacturer's sequencing method manual (Roche) using the default parameters for cDNA.

Sequence analysis and homology search

454 sequencing of the cDNA library generated 3 166 947 bases from 91 349 reads. These reads were assembled into 2512 contigs, 2258 isotigs and 21 950 singletons using *de novo* assembly by Newbler version 2.0.1 (Roche Applied Science). Isotig sequences were compared to sequences in the NCBI database by BLASTn using Blast2goPro (www.Blast2GO.org) (31). *E*-values lower than 1.0E-3 were considered significant. Isotig00988 (GenBank Acc No. KC161252) was found to be most similar to H2A of *G.morsitans*. Isotig00988 contained 748 bp and the nucleotide sequence was submitted to the ORF finder at NCBI (http://www.ncbi.nlm.nih.gov/gorf/gorf.html). The longest ORF was found to be the candidate H2A protein coding region. Clustal Omega (accessed through http://www.uniprot.org/) was used to compare the resulting amino acid sequence to *Drosophila* (accession no. P0895), human (accession no. P16104) and *Glossina* (accession no. D3PTWO) H2A sequences.

Statistical analyses

GraphPad Prism 5 was used to analyse data using the Student's *t*-test or to determine the correlation coefficients. Data were expressed as mean ± standard error of the mean (SEM). GraphPad InStat 3.1 was used for other statistical analyses.

Results

Our preliminary studies used an antibody that was prepared based on the human γH2AX sequence KKAATQA[PSer]QEY. The antibody recognised a nuclear protein of ~15 kDa that was evident in irradiated pupal samples (not shown) and is consistent with the molecular weight of γH2AX as observed in other species (6,8). Although the (human) antibody provided a clear band at ~15 kDa, there was some non-specific binding detected at ~75 kDa. Since there was no available γH2AX antibody specific to *B.tryoni*, we used an antibody specific to the *D.melanogaster* γH2AX sequence (γH2AvD) that resulted in a single band of ~15 kDa in irradiated samples. Figure 1 shows that 454 sequencing revealed a H2AX protein sequence that was identical to that found in *G.mortisans*, was 96.4% similar to *D.melanogaster* and only 54.8% similar to human H2AX. We have termed the *B.tryoni* H2AX homologue 'H2AvB'. The SQ motif of H2AvB was conserved as for all other species in which the histone has been sequenced.

Phosphorylated H2AvB (γH2AvB) was detected following exposure of pupae to doses as low as 10 Gy of IR (Figure 2A). The phosphorylation of H2AvB occurred rapidly and could be detected at 5 min post-IR exposure, peaking at ~20 min post-IR exposure (Figure 2B). There was a gradual decline of γH2AvB over a period of 24 h; however, there was still significant γH2AvB present 24 h post-IR exposure, indicating that only a proportion of γH2AvB was dephosphorylated within 24 h. As expected, 60 Gy IR exposure led to a higher level of γH2AvB relative to the pupae exposed to 10 Gy. Alkaline phosphatase treatment of a histone extract from IR-treated (70 Gy, 24 h post-IR) pupae abolished γH2AvB detection (Figure 2C), confirming the antibody was detecting only the phosphorylated form of the H2AvB, at the SQ motif. To confirm that irradiated samples at other life stages (egg versus larvae) of *B.tryoni* also elicit a γH2AvB response we have also shown an increase in γH2AvB response following IR exposure at 150 Gy, the standard dose used for Q-fly post-harvest disinfestation (Figure 2D).

The above data indicate a clear phosphorylation-dependent γH2AvB signal following IR exposure compared with non-irradiated samples. To further investigate the effect of IR on Q-fly pupae at different doses, particularly covering and exceeding the range most often used for SIT and to disinfest produce, pupae were exposed to a wide dose range (up to 400 Gy) and then frozen at −80°C 24 h post-IR. Figure 3A shows a representative western blot demonstrating a dose-dependent increase in the γH2AvB signal. The maximum signal was produced at the highest tested dose of 400 Gy and yielded an ~10-fold increase above non-irradiated pupae. γH2AvB signal was detected in Q-fly pupae at doses as low as 20 Gy; however, in Figure 3A, this is not particularly clear since this western blot was exposed for ECL under conditions that would clearly show the higher end doses (>80 Gy) of the western blot. To compare the results of three separate assays, data were normalised by using β-actin as a loading control. Since there were differences between imaging exposure times and therefore the band intensities between separate assays, the data were then further corrected to the 'maximum' signal (i.e. at 400 Gy) to account for these potential differences in imaging and incubation conditions. This allowed the slope and fit of the lines of γH2AvB responses to be compared appropriately in separate assays as shown in Figure 3B inset. This figure also demonstrates the high linear correlation of γH2AvB with IR dose ($r^2 > 0.9$).

Interestingly, our data show a very strong γH2AvB signal in Q-fly pupal lysates from exposures as low as 20 Gy, at least 24 h post-IR (Figure 3). This led us to examine whether the γH2AvB signal was evident at even longer time points post-IR, as this would potentially provide a useful biomarker to demonstrate prior IR exposure. Figure 4 demonstrates that the dose effect of IR on γH2AvB signal was clearly observed at 24 h post-IR (for doses of 0, 70 and 240 Gy); however, at 5 days post-IR, the γH2AvB signal in pupal lysates was substantially reduced compared with 1 day post-IR (the same amount of total protein was loaded in all samples to allow direct comparisons). It should be noted that in some of our earlier western blot assays we did occasionally observe a very low amount of γH2AvB signal (~15 kDa) after 70 Gy exposure at 5 days post-IR, when higher amounts of total protein were loaded and when longer ECL exposure times were used. These preliminary observations led us to believe that there was indeed a measureable persistent γH2AvB signal even 5 days post-IR exposure. Figure 4A (lower right panel, labelled 'overexposed') shows a longer development time on the same western blot membrane and a dose-responsive γH2AvB signal became more evident, albeit not as intensely as achieved when analyzed at 1 day post-IR. This suggests that despite a large decline in phosphorylated γH2AvB levels between 1 and 5 days post-IR exposure in Q-fly pupae, a persistent or residual γH2AvB signal remained.

To further examine whether we could detect γH2AvB signal at least 5 days after IR exposure (at the standard dose used

```
1   MAGGKAGKDSGKAKAKAVSRSARAGLQFPVGRIHRHLKSRTTSHGRVGATAAVYSAAILE  B. tryoni
1   MAGGKAGKDSGKAKAKAVSRSARAGLQFPVGRIHRHLKSRTTSHGRVGATAAVYSAAILE  G. morsitans (D3TPW0)
1   MAGGKAGKDSGKAKAKAVSRSARAGLQFPVGRIHRHLKSRTTSHGRVGATAAVYSAAILE  D. melanogaster (P0895)
1   --MSGRGKTGGKARAKAKSRSSRAGLQFPVGRVHRLLRKG-HYAERVGAGAPVYLAAVLE  Human (P16104)

61  YLTAEVLELAGNASKDLKVKRITPRHLQLAIRGDEELDSLIK-ATIAGGGVIPHIHKSLI  B. tryoni
61  YLTAEVLELAGNASKDLKVKRITPRHLQLAIRGDEELDSLIK-ATIAGGGVIPHIHKSLI  G. morsitans (D3TPW0)
61  YLTAEVLELAGNASKDLKVKRITPRHLQLAIRGDEELDSLIK-ATIAGGGVIPHIHKSLI  D. melanogaster (P0895)
58  YLTAEILELAGNAARDNKKTRIIPRHLQLAIRNDEELNKLLGGVTIAQGGVLPNIQAVLL  Human (P16104)

120 GKKEDNVQDPQRKN----TVILSQGY  B. tryoni
120 GKKEDNVQDPQRKN----TVILSQGY  G. morsitans (D3TPW0)
120 GKKEETVQDPQRKG----NVILSQAY  D. melanogaster (P0895)
118 PKKTSATVGPKAPSGGKKATQASQEY  Human (P16104)
```

Fig. 1. Amino acid sequence and alignment of H2A histone variants. The conserved SQ motif is highlighted in red text. The sequence of a H2AX homologue protein was identified from deep sequencing transcript analyses and mass spectrometry of Q-fly (*Bactrocera tryoni*) cells. The Q-fly H2A variant is termed H2AvB (GenBank Accession #KC161252). We found that H2AvB is 96.4% similar to that of the vinegar fly (genetic model species) *Drosophila melanogaster* (H2AvD), 54.8% similar to human H2AX and identical to *Glossina morsitans* (the Savannah tsetse fly). The numbers in parentheses represent the UniProtKB accession numbers for each sequence. Figures at the left of sequences represent the first amino acid position of each line.

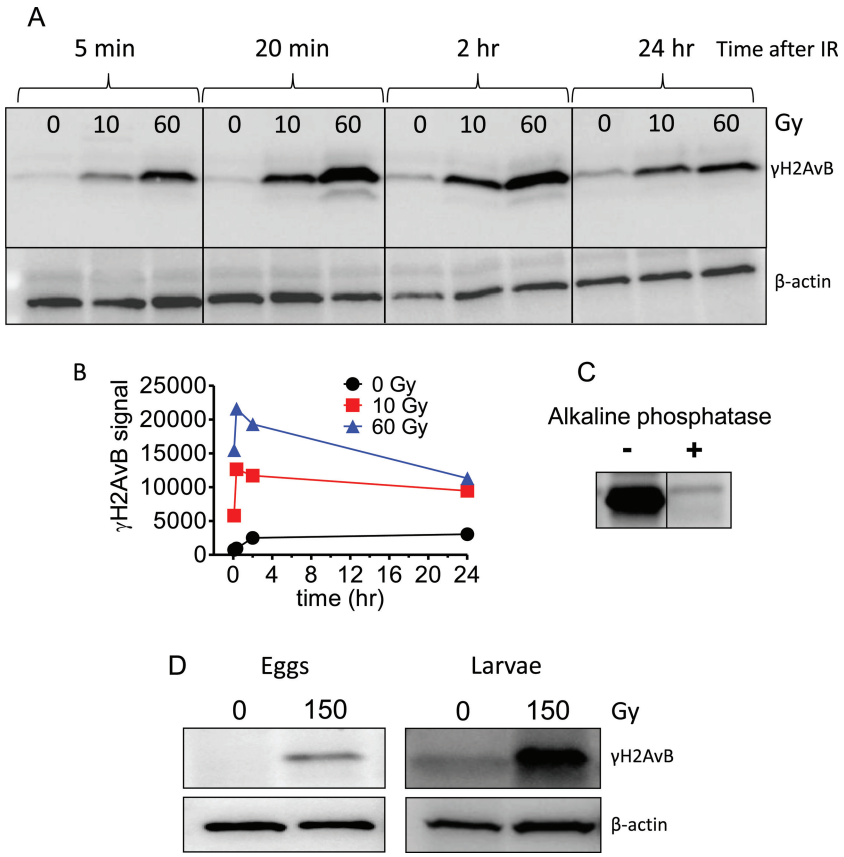

Fig. 2. Short-term kinetics of H2AvB phosphorylation in Q-fly. (**A**) Total pupae lysates were prepared and γH2AvB responses are shown to 0, 10 and 60 Gy IR at 5 min, 20 min, 2 h or 24 h following IR exposure. β-Actin is shown on the lower panels to demonstrate loading controls (225 µg protein on each lane). (**B**) The γH2AvB signal from (A) was quantified using ImageJ and the data were plotted with the following symbols: 0 Gy (filled circles), 10 Gy (filled squares) and 60 Gy (filled triangles). (**C**) Post-IR-exposed (24 h) pupae were subjected to the acid precipitation method to extract histones. Treatment of samples with alkaline phosphatase (+) abolished the γH2AvB signal, which remained in non-treated samples (−). The data shown confirmed the IR-induced H2AvB is in the phosphorylated form that is detected by the primary antibody. (**D**) Western blot analyses of Q-fly eggs (73 µg protein loaded; left panel) or larvae (105 µg protein loaded; right panel) demonstrating detectable γH2AvB signal in different Q-fly life stages.

for SIT), we investigated the effect of 70 Gy IR on γH2AvB signal using whole Q-fly pupal lysates 1 day and 5 days post-IR. The γH2AvB response was quantified by western blot as shown in Figure 5A (left 'pupal lysate' panels, lanes 1 and 2) demonstrating a significant γH2AvB signal at ~15 kDa. β-Actin and cytochrome c oxidase subunit II were used as loading controls and confirmed that equivalent amounts of protein had been loaded for each treatment. To confirm the specific association of the γH2AvB signal with cell nuclei and to improve the γH2AvB signal, we isolated nuclear proteins by an acid precipitation method as described previously (27). When 15 µg total nuclear protein extract was examined by western blot analysis (shown in lanes 5 and 6 of Figure 5A, labelled 'histone extract'), the γH2AvB signal following 70 Gy IR clearly yielded a higher signal than that of the equivalent amount of protein from the whole 'pupal lysate' when either 15 or 150 µg protein was loaded (Figure 5A). This enrichment of nuclear γH2AvB protein observed was also associated with a higher γH2AvB signal at 0 Gy. Nevertheless, the IR response of γH2AvB signal was clearly distinguishable from background levels and several fold more intense at 70 Gy compared with 0 Gy. The absence of any detectable signal coming from β-actin (cytoplasm) and cytochrome c oxidase subunit II (a mitochondrial protein) in the histone extract (Figure 5A, lanes 5 and 6) demonstrates that the histone extract was relatively free from these latter proteins as expected and confirms that the nuclear extract method employed did not result in significant cytoplasmic or mitochondrial contamination, while significantly enriching the histone fraction. Therefore, it appears that the nuclear histone extraction method offers a convenient way to partially purify and concentrate low levels of persistent IR-induced γH2AvB signal from Q-fly. Since our objective was to detect any long-term persistent γH2AvB signal in irradiated Q-fly pupae, we subsequently used the histone extract method to concentrate the γH2AvB signal as outlined earlier. Figure 5B shows a representative western blot experiment using whole lysate from Q-fly pupae (120 µg protein) and nuclear extracts (6 µg protein), 5 days post-IR. Under the same duration of exposure times using ECL, left panels in Figure 5B (lanes 1 and 2) show no apparent γH2AvB signal response to 70 Gy IR using 120 µg total protein loaded, compared to a strong signal using the histone extract with only 6 µg total nuclear protein loaded (i.e. 20 times less protein, compare lanes 2 and 4 of Figure 5B). The IR-induced signal (70 Gy) was clearly evident and significantly higher than the background (0 Gy) signal. Since Q-fly are able to survive and withstand relatively high doses of IR, we hypothesised that adult Q-fly specimens produced from irradiated pupae would contain persistent γH2AvB (as has been observed recently with minipig skin samples after receiving a dose of 50 Gy IR) (32). Figure 5C demonstrates that persistent IR-responsive γH2AvB signal was observed in adult Q-fly at 17 days post-IR, in nuclear extract samples.

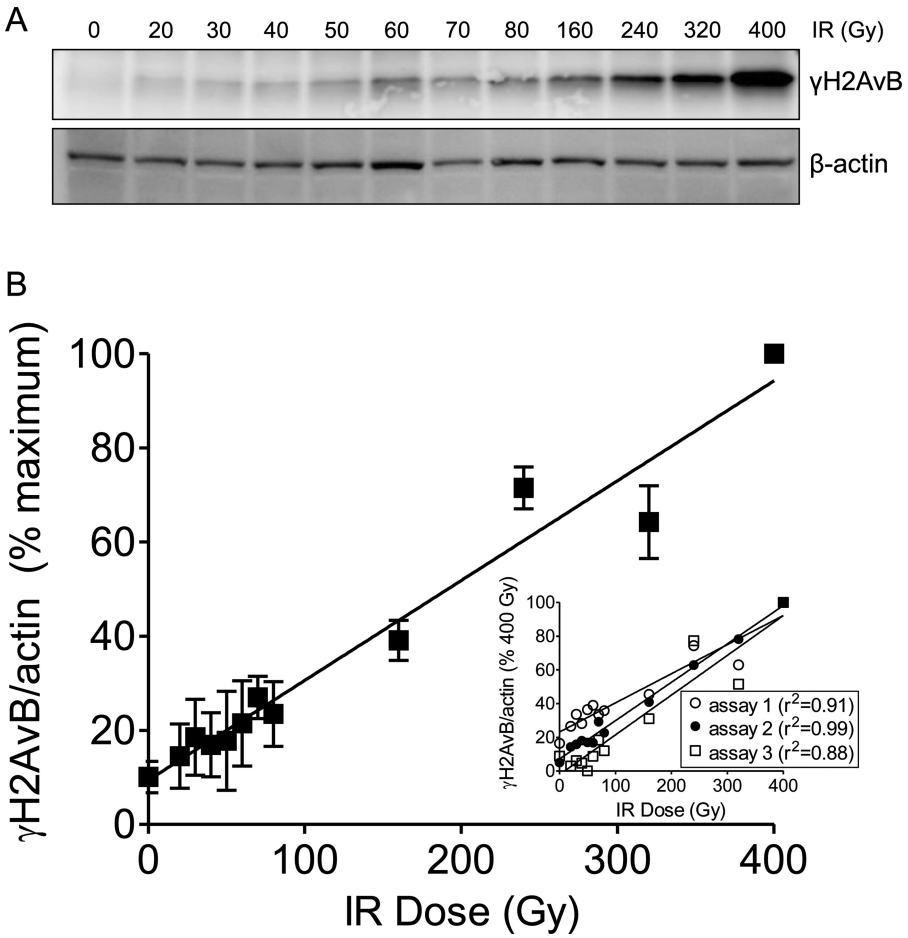

Fig. 3. The intensity of γH2AvB signal in Q-fly pupae (24 h post-IR) is proportional to IR exposure. (**A**) Western blot showing the γH2AvB signal at ~15 kDa (upper panel) increases in proportion to the IR dose up to the maximum exposure of 400 Gy tested for this assay. The lower panel shows the β-actin loading controls. (**B**) ImageJ software was used to quantify the integral of the bands in (A) upper and lower panels. γH2AvB signal from three independent assays (see inset) was corrected for the amount of β-actin loaded and data (as percentage of maximum) were plotted against IR dose to allow for differences in incubating conditions and imaging exposure times. Data are mean ± SEM.

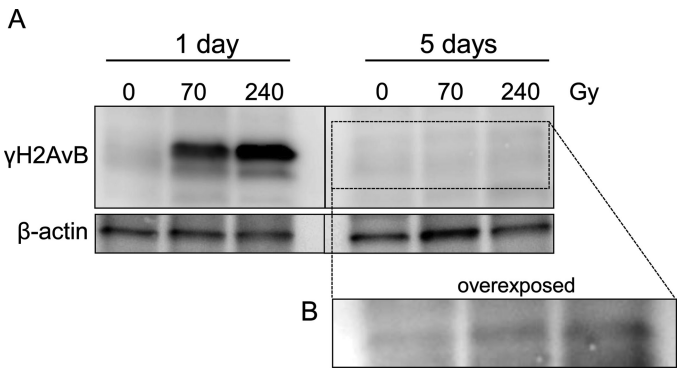

Fig. 4. γH2AvB signal in Q-fly pupae was reduced at 5 days post-IR. (**A**) Western blot showing a dose-dependent increase in γH2AvB signal 1 day after IR exposure (0, 70 and 240 Gy). However, at 5 days post-IR, the γH2AvB response was not easily visible in this representative assay until the western blot membrane was allowed to develop with a longer imaging time ('overexposed') as shown in (**B**). Protein (100 µg) was loaded in all lanes.

Although we did not investigate later time points, this may be a convenient method to identify prior IR exposure of Q-fly pupae and therefore may have application for SIT. To address whether individual pupae show variation in their γH2AvB response following IR exposure, we scaled down the total lysate and histone extraction techniques in order to examine γH2AvB responses of individual pupae. Figure 5D demonstrates that when replicate individual pupae were lysed and used for western blot analyses, there was some variation of the γH2AvB produced in response to IR as would be expected. However, on the whole, all pupae from the 0 Gy group (individual pupae lysates were loaded in lanes 1–6, Figure 5D) had significantly less γH2AvB signal compared with individual pupae exposed to 70 Gy IR (24 h post-IR), as shown in Figure 5D, lanes 7–12. The γH2AvB signal was quantified using ImageJ and results are shown on the right panel of Figure 5D, with 70 Gy ($n = 6$) significantly higher ($P < 0.001$) than 0 Gy ($n = 6$). Furthermore, we were able to scale down the histone extraction method in

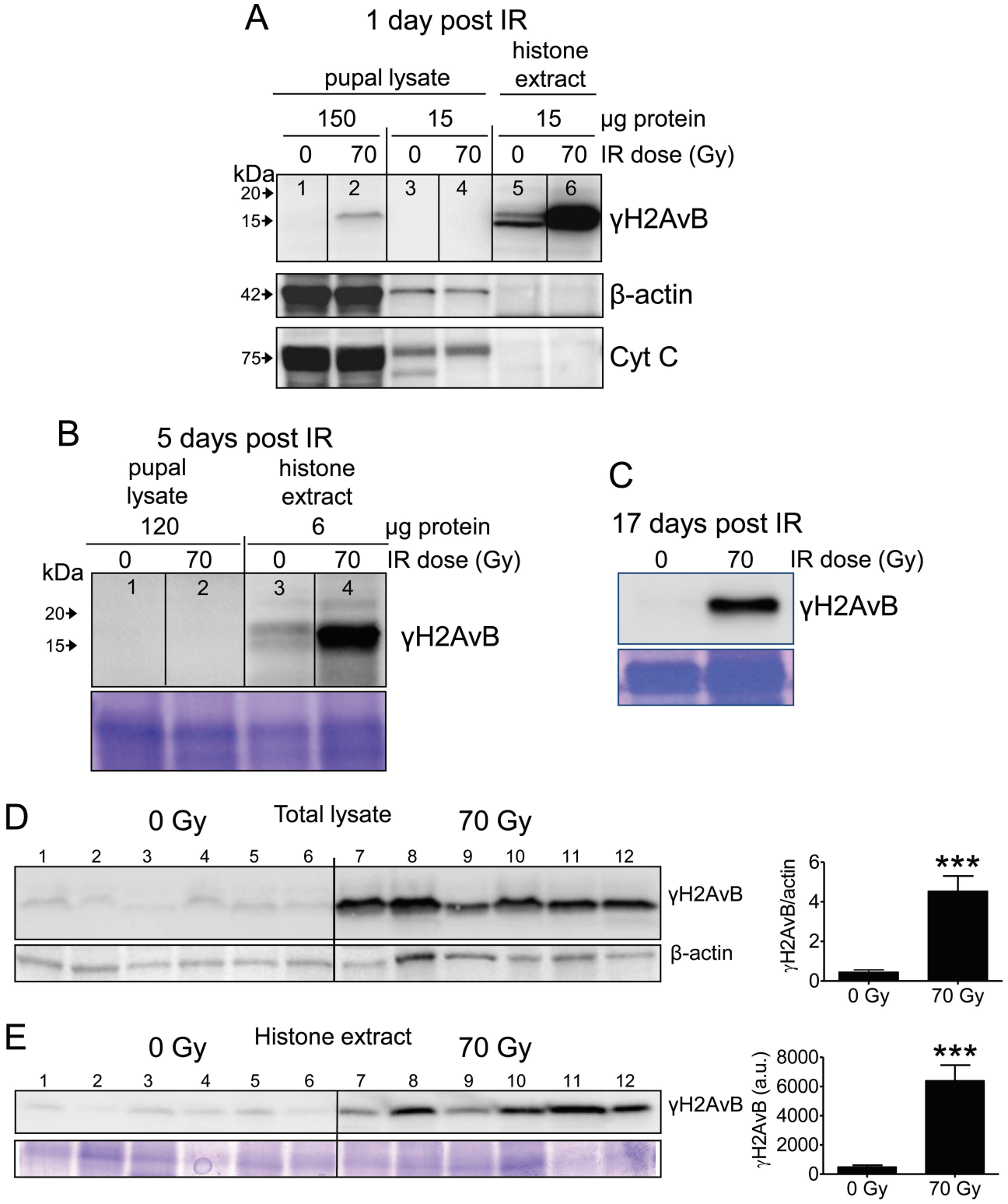

Fig. 5. γH2AvB response in Q-fly pupae following 70 Gy exposure at different times post-IR. (**A**) Left panel shows γH2AvB response from whole pupal lysates (150 µg protein loaded; 0 versus 70 Gy; lanes 1 and 2). γH2AvB was not observed in the same western blot membrane when the sample was diluted 10-fold to 15 µg protein (lanes 3 and 4). However, when 15 µg total protein from the histone extract was loaded, the 70 Gy sample (lane 6) showed an intense signal exceeding that observed from the total pupal lysates at 70 Gy (lane 2). The absence of cytoplasmic proteins (as observed in lanes 5 and 6, lower panels) including β-actin and cytochrome c oxidase subunit II confirmed the relative purity of the histone extract. (**B**) γH2AvB signal in Q-fly pupae was reduced at 5 days post-IR as confirmed by analyses of total pupal lysates (lanes 1 and 2). However, significant γH2AvB signal was observed in the histone extract from Q-fly pupae 5 days post-IR (0 and 70 Gy in lanes 3 and 4, respectively). (**C**) Histone fraction showing significant γH2AvB signal 17 days post-IR (70 Gy) compared with 0 Gy. (**D**) Variability of the γH2AvB response in individual pupae is shown for 0 Gy ($n = 6$; lanes 1–6) or 70 Gy ($n = 6$; lanes 7–12) in the upper panel. The lower panel shows the β-actin loading controls. (**E**) Variability of the γH2AvB response in histone extracts from individual pupae that were exposed to 0 Gy ($n = 6$; lanes 1–6) or 70 Gy ($n = 6$; lanes 7–12). For both (D) and (E), all samples shown were run on the same western blot to allow direct comparison. Bar charts to the right of (D) and (E) represent the mean ± SEM of the band intensities (integral) as determined by ImageJ analyses. Lower panels in (B), (C) and (E) are loading controls showing the Coomassie-stained gels have equivalent amount of protein. ***$P < 0.001$.

a similar manner so that individual pupae could be subjected to the nuclear extraction method to increase the γH2AvB signal per total protein tested. Pupae exposed to 70 Gy had a significantly higher amount of γH2AvB signal ($P < 0.001$) in the individual histone preparations as demonstrated by the western blot from the single pupae replicates compared with 0 Gy (Figure 5E).

To further validate the long-term (17 days) post-IR γH2AvB response (as shown in the western blot in Figure 5C), we employed immunofluorescence methods using nuclear extracts in combination with LSC. Representative LSC images of adult Q-fly nuclei stained with DAPI (blue) and demonstrating the γH2AvB signal are shown in Figure 6A–C. To determine whether long-term persistent γH2AvB signal could be observed at low and high doses, Q-fly pupae were exposed to 0, 20 or 240 Gy and then allowed to emerge as adults. The γH2AvB signal (green) was observed within nuclei 17 days post-IR, in doses as low as 20 Gy. Figure 6D shows the mean (±SEM) integral fluorescence (from LSC) was significantly increased ($P < 0.001$) following 20 Gy IR ($n = 3078$ nuclei) or 240 Gy IR ($n = 3571$ nuclei) compared with 0 Gy IR ($n = 2656$ nuclei). Figure 6E demonstrates that both 20 and 240 Gy IR exposure resulted in a significantly higher percentage of nuclei containing a γH2AvB signal compared with 0 Gy (control). The fluorescence integrals of those nuclei with a positive γH2AvB signal identified from Figure 6E were quantified and then reported in Figure 6F (as mean ± SEM). Figure 6F demonstrates that the γH2AvB signal (integral) was also significantly elevated in adult Q-fly nuclei 17 days post-IR at the low dose of 20 Gy ($P < 0.01$) as well as the higher dose of 240 Gy ($P < 0.05$). The area of the γH2AvB signal in nuclei was examined as shown in Figure 6G. Although the area of γH2AvB signal appeared to be dose dependent at 20 and 240 Gy, this increase was not statistically significant. The overall findings illustrated in Figure 6 further confirmed that γH2AvB signals persisted in emergent adult Q-flies for at least 17 days post-IR (irradiated as pupae).

Discussion

Phosphorylation of the C-terminal tail of H2AX proteins in nucleosomes located in the vicinity of DSBs is one of the earliest responses to IR-induced DNA damage (3,14). A γH2AX homologue has not been reported previously in tephritid fruit flies, including the commercially important

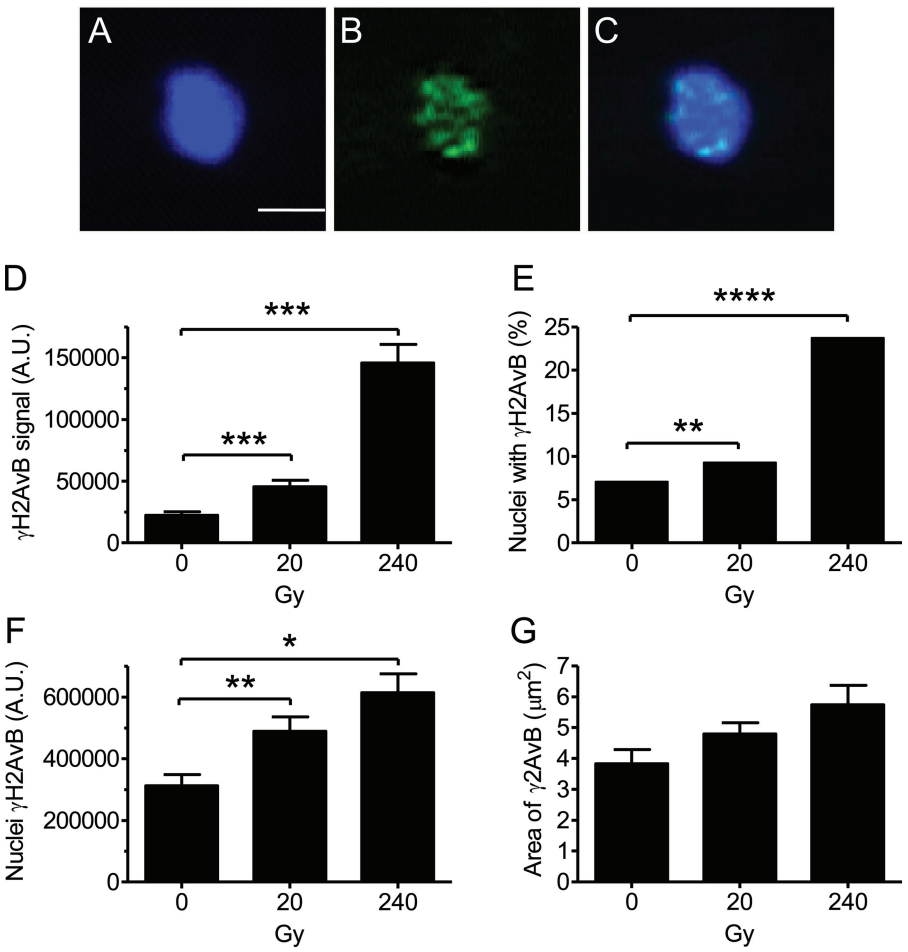

Fig. 6. Quantification of γH2AvB signal in isolated adult Q-fly nuclei by LSC. Representative LSC images of Q-fly nuclei showing (**A**) DAPI only (blue), (**B**) γH2AvB signal only (green) and (**C**) 'merged' images that show the DAPI and γH2AvB signal overlaid. The scale bar in (A) represents 5 μm. (**D**) Mean ± SEM of the integral fluorescence per nucleus of all nuclei examined including nuclei that lacked any measurable γH2AvB signal; $n = 2656$, 3078 and 3571 nuclei for 0, 20 and 240 Gy samples, respectively. (**E**) The percentage of nuclei examined that contain a measurable γH2AvB signal above background, increased significantly from ~7% in 0 Gy samples to 9.3% in 20 Gy samples ($P < 0.01$) and to 23.7% of nuclei in 240 Gy samples ($P < 0.0001$ by chi-square test). To further examine if there was a greater γH2AvB signal in the 20 and 240 Gy samples compared with 0 Gy samples, only those nuclei with a measurable γH2AvB signal were analyzed and this is reported in (**F**) as the mean integral (±SEM). Finally, the mean contoured areas of the total γH2AvB signal per nucleus are shown in (**G**). $^{*}P < 0.05$, $^{**}P < 0.01$, $^{***}P < 0.001$ and $^{****}P < 0.0001$.

Q-fly (*B.tryoni*), although the expression of a H2AX variant (H2AvD) has been reported in the vinegar fly *D.melanogaster* (18). In this study, we show that Q-fly pupae exposed to IR had an elevated level of phosphorylated H2A protein (termed γH2AvB). Consistent with reports for other species (6), irradiated Q-fly pupae showed a strong γH2AvB signal of ~15 kDa when examined using western blot. The γH2AvB sequence was identified using 454 sequencing and found to be identical to *G.morsitans*. The identity and partial sequence of the IR-induced, phosphorylated histone was also confirmed by liquid chromatography–electrospray ionization–tandem mass spectrometry (data not shown, mass spectrometry was carried out by the Adelaide Proteomics Centre, University of Adelaide, South Australia, Australia). Twenty-four hours post-IR, we observed a linear dose–response of γH2AvB up to our maximum tested dose of 400 Gy in Q-fly pupae. However, after 5–17 days post-IR, the γH2AvB signal had declined significantly when analysing whole pupal lysates. In contrast, the persistent (5 days post-IR and beyond) γH2AvB response remained dose responsive and was easily measurable by either western blot or immunofluorescence methods such as LSC when analysing enriched histone extracts. The dose-dependent response over doses used for SIT (70 Gy) and disinfestation of fruit (up to 400 Gy) shows that γH2AvB may be useful as a marker of previous IR exposure in assays that support these commercially important applications.

γH2AX is highly conserved across a wide taxonomic range of organisms (8,16) and is a well-characterised histone protein that is known to be responsive to IR-induced DSBs (14,33,34). We identified the sequence of a H2AX homologue protein in the Q-fly, *B.tryoni* (termed H2AvB; GenBank Accession #KC161252). We found that H2AvB is ~96% similar to the vinegar fly *D.melanogaster* H2AvD, ~54.8% similar to human H2AX and, interestingly, identical to the human disease vector *G.morsitans* (which is also the subject of SIT) (24). Our preliminary experiments demonstrated that an antibody designed to the human C-terminal tail sequence of γH2AX, KKAATQA[PSer]QEY, showed similar IR-induced γH2AvB signal compared with the antibody used for detection of *D.melanogaster* γH2Av as used in this study, which revealed a protein of ~15 kDa. The C-terminal amino acid sequence of human histone H2AX consists of ASQEY, whereas for *D.melanogaster*, the equivalent sequence is LSQAY. Although the C-terminal sequence for *B.tryoni* is slightly different from both human and *Drososphila*, it therefore appears that the antibody recognition site is likely to be mostly targeted towards recognising the SQ phosphorylation motif, which is conserved across species. Indeed, others have used antibodies based on the human sequence of phosphorylated H2AX and found that it cross-reacts with histone H2A (phosphorylated) variants from many diverse taxa, including plants (6,16). Therefore, it was not surprising in this study that the H2AvD antibody (based on the *Drosophila* sequence) yielded a single intense band on western blots (following IR) corresponding to phosphorylated H2AvB in the *B.tryoni* samples.

Many studies have analyzed the kinetics of phosphorylation and dephosphorylation of H2AX, with IR shown to induce maximal amounts of γH2AX in cells at times often <10 min after exposure to IR followed by a decline in γH2AX signal over a period of hours (3,14,18,33). Previous reports using *Drosophila* S2 tissue culture cells have suggested that the phosphorylation of H2Av increases within minutes following IR exposure but then declines significantly after several hours (18). The rapid loss of the phosphorylated H2Av was likely due to regulated dephosphorylation of H2Av and was similar to that reported for radiation-induced phosphorylation/dephosphorylation kinetics in mammals (3). Indeed, γH2AX quantification assays have been proposed as the basis of protocols for biological dosimetry following IR events (33). Although the absolute number of phosphorylated γH2AX molecules declines over a period of hours and days post-IR, a recent study in mice showed a dose-dependent response of γH2AX foci in nuclei up to 7 days after exposure to IR (35). The residual γH2AX foci at 24–72 h post-IR are believed to represent misrepaired DSBs, unrepaired DNA with ongoing genomic instability, S-phase cells or apoptotic cells (36). In *Drosophila* S2 cultured cells, the percentage of phosphorylated H2AX variant (H2Av) was shown to have reduced almost to non-irradiated levels within 3 h after the initial IR dose (18). Similarly, in cultured human microvascular endothelial cells exposed to 2–16 Gy IR, a transient increase in γH2AX signal was observed to peak at 1 h post-IR and return to background levels 24 h post-IR (37). The γH2AvB response we observed in whole tissue displayed kinetics that were less transient than that of cultured cells and persisted at measurable levels for at least 17 days, although the signal was considerably reduced even 1–5 days post-IR. It should be noted that doses used in human studies are generally much less than applied here, as the doses used for SIT and disinfestation of insects are well beyond what can be tolerated by humans. Thus, the persistence of the phosphorylated protein may be related to the higher IR doses we have tested. The basis for the relatively high IR tolerance of insects is not clear; however, it is conceivable that it may be partly related to the persistence of the phosphorylated histone. A recent study that used Göttingen minipig skin biopsies found that radiation-induced γH2AX foci (50 Gy) were observed in ~60% of cells 4 h after IR. The number of γH2AX foci was found to be significantly less after 70 days following IR exposure; however, there remained a significantly higher number of γH2AX foci per epidermal keratinocyte compared with controls (32). In our study, there was a strong positive linear correlation ($r^2 > 0.9$) in γH2AX signal over a dose range of 0–400 Gy, corresponding to a 10-fold increase in signal above the background (non-irradiated) level. It is, therefore, likely that high IR doses are necessary to observe the long-term persistent γH2AX or γH2AvB signals. Indeed, after 17 days post-IR (240 Gy), we found that ~25% of nuclei had a measurable γH2AvB signal as determined by LSC. Although LSC detected a small amount of measurable background signal in 0 Gy Q-fly adults in ~7% of nuclei, we did not observe a 0 Gy γH2AvB signal by western blotting (Figure 5C). Therefore, it appears LSC may prove to be a more sensitive method to detect and quantify γH2AvB signal in nuclei that are persistent many days after exposure to the IR event. Rogakou *et al.* (6) previously suggested there is potentially a low level of γH2AX in non-irradiated cells. This is in agreement with our study (see discussion below) in which we additionally confirmed the necessity for the phosphorylation of putative Ser137 within the SQ motif of γH2AvB to allow detection by our primary antibody, through abolishing the signal via treatment of the histone extract with alkaline phosphatase.

At 5 days post-IR exposure, we occasionally observed an IR-induced γH2AvB signal in whole pupal lysates via western blotting (depending on amount of protein loaded on gels and imaging exposure times). Therefore, the nucleosome (histone) extraction procedure was used and this resulted in a substantial enrichment of the γH2AvB signal compared with the use of the whole pupal lysates. In the non-irradiated whole pupal lysate,

we did not detect any γH2AvB. However, in the nonirradiated histone fraction, we observed a basal γH2AvB signal in the non-irradiated 5-day samples.

LSC was a successful technique for quantitation of IR-induced γH2AvB signal in Q-fly showing the localisation within nuclei as well as its quantitative increase in adult Q-fly 17 days post-IR as pupae. Our LSC results support data obtained by western blot analyses and also provide a visualisation of the signal although visual scoring of foci was not practical. The iCyte® software allows for automated scoring and quantitation of nuclei and events within them, and therefore LSC could be useful for future studies to investigate additional parameters associated with IR induction of γH2AvB (e.g. γH2AvB signal related to cell cycle phases) at a tissue-specific level. Additionally, LSC could be used to simultaneously detect γH2AvB signal with a dependent DNA repair mechanism protein such as ATM or other markers such as caspases (for apoptosis) to yield more information on cell cycle dynamics.

Our work has identified γH2AvB as a potential biomarker and biodosimeter of prior IR exposure in Q-fly. This finding has several potential applications for the management of these economically important insects. First, with chemical approaches facing increasing restrictions, IR treatment is quickly becoming an internationally accepted alternative for disinfestation of horticultural produce (38). Second, doses of 70 Gy applied to pupae are used to induce reproductive sterility in flies released during SIT pest management programs that are used to reduce Q-fly populations (39). The γH2AvB assay presented here (or modifications thereof) may have applications in both these contexts for detecting IR-induced DNA damage in Q-fly specimens. Given that *G.mortisans* is an important human disease vector for which SIT is being investigated and that its homologous histone protein is apparently identical to γH2AvB, the assays developed here may also be applicable for monitoring in *G.mortisans* SIT programs. In addition, given that many of the DNA repair and apoptotic biochemical pathways are conserved between mammals and insects (40–42), insect-based assays may be useful for detecting DNA damage processes occurring in the environment as insects are widespread and abundant, and some species can be efficiently trapped using highly specific chemical lures. Tephritid fruit flies also generally meet these criteria. Future studies that focus on γH2AvB as a potential biomarker of IR-induced DNA damage in Q-fly should extend the time course following IR exposure and use tissue section immunohistochemistry or immunofluorescence techniques that will allow identification of tissue specificity of γH2AvB signals in Q-fly. The kinetics of γH2AvB phosphorylation/dephosphorylation in different life stages of Q-fly would also be of benefit.

Funding

This work was supported by Horticulture Australia Limited (project number VG09160) using the vegetable levy, voluntary contributions from industry (Bowen District Growers Association) and matched funds from the Australian Government.

Acknowledgements

Q-flies were generously provided from the stock used by New South Wales Department of Primary Industries for Sterile Insect Technique releases.

Conflict of interest statement: None declared.

References

1. Dugle, D. L., Gillespie, C. J. and Chapman, J. D. (1976) DNA strand breaks, repair, and survival in x-irradiated mammalian cells. *Proc. Natl Acad. Sci. U. S. A.*, **73**, 809–812.
2. Olive, P. L. (1998) The role of DNA single- and double-strand breaks in cell killing by ionizing radiation. *Radiat. Res.*, **150**, S42–S51.
3. Rogakou, E. P., Pilch, D. R., Orr, A. H., Ivanova, V. S. and Bonner, W. M. (1998) DNA double-stranded breaks induce histone H2AX phosphorylation on serine 139. *J. Biol. Chem.*, **273**, 5858–5868.
4. Savic, V., Yin, B., Maas, N. L., Bredemeyer, A. L., Carpenter, A. C., Helmink, B. A., Yang-Iott, K. S., Sleckman, B. P. and Bassing, C. H. (2009) Formation of dynamic gamma-H2AX domains along broken DNA strands is distinctly regulated by ATM and MDC1 and dependent upon H2AX densities in chromatin. *Mol. Cell*, **34**, 298–310.
5. Goll, M. G. and Bestor, T. H. (2002) Histone modification and replacement in chromatin activation. *Genes Dev.*, **16**, 1739–1742.
6. Rogakou, E. P., Boon, C., Redon, C. and Bonner, W. M. (1999) Megabase chromatin domains involved in DNA double-strand breaks in vivo. *J. Cell Biol.*, **146**, 905–916.
7. Méndez-Acuña, L., Di Tomaso, M. V., Palitti, F. and Martínez-López, W. (2010) Histone post-translational modifications in DNA damage response. *Cytogenet. Genome Res.*, **128**, 28–36.
8. Redon, C., Pilch, D., Rogakou, E., Sedelnikova, O., Newrock, K. and Bonner, W. (2002) Histone H2A variants H2AX and H2AZ. *Curr. Opin. Genet. Dev.*, **12**, 162–169.
9. Kinner, A., Wu, W., Staudt, C. and Iliakis, G. (2008) Gamma-H2AX in recognition and signaling of DNA double-strand breaks in the context of chromatin. *Nucleic Acids Res.*, **36**, 5678–5694.
10. Park, E. J., Chan, D. W., Park, J. H., Oettinger, M. A. and Kwon, J. (2003) DNA-PK is activated by nucleosomes and phosphorylates H2AX within the nucleosomes in an acetylation-dependent manner. *Nucleic Acids Res.*, **31**, 6819–6827.
11. Stiff, T., O'Driscoll, M., Rief, N., Iwabuchi, K., Löbrich, M. and Jeggo, P. A. (2004) ATM and DNA-PK function redundantly to phosphorylate H2AX after exposure to ionizing radiation. *Cancer Res.*, **64**, 2390–2396.
12. Burma, S., Chen, B. P., Murphy, M., Kurimasa, A. and Chen, D. J. (2001) ATM phosphorylates histone H2AX in response to DNA double-strand breaks. *J. Biol. Chem.*, **276**, 42462–42467.
13. Fernandez-Capetillo, O., Lee, A., Nussenzweig, M. and Nussenzweig, A. (2004) H2AX: the histone guardian of the genome. *DNA Repair (Amst.)*, **3**, 959–967.
14. Olive, P. L. and Banáth, J. P. (2004) Phosphorylation of histone H2AX as a measure of radiosensitivity. *Int. J. Radiat. Oncol. Biol. Phys.*, **58**, 331–335.
15. Downs, J. A., Lowndes, N. F. and Jackson, S. P. (2000) A role for *Saccharomyces cerevisiae* histone H2A in DNA repair. *Nature*, **408**, 1001–1004.
16. Friesner, J. D., Liu, B., Culligan, K. and Britt, A. B. (2005) Ionizing radiation-dependent gamma-H2AX focus formation requires ataxia telangiectasia mutated and ataxia telangiectasia mutated and Rad3-related. *Mol. Biol. Cell*, **16**, 2566–2576.
17. Lang, J., Smetana, O., Sanchez-Calderon, L., Lincker, F., Genestier, J., Schmit, A. C., Houlné, G. and Chabouté, M. E. (2012) Plant γH2AX foci are required for proper DNA DSB repair responses and colocalize with E2F factors. *New Phytol.*, **194**, 353–363.
18. Madigan, J. P., Chotkowski, H. L. and Glaser, R. L. (2002) DNA double-strand break-induced phosphorylation of *Drosophila* histone variant H2Av helps prevent radiation-induced apoptosis. *Nucleic Acids Res.*, **30**, 3698–3705.
19. Follett, P. A. and Armstrong, J. W. (2004) Revised irradiation doses to control melon fly, Mediterranean fruit fly, and oriental fruit fly (Diptera: Tephritidae) and a generic dose for tephritid fruit flies. *J. Econ. Entomol.*, **97**, 1254–1262.
20. Follett, P. A., Phillips, T. W., Armstrong, J. W. and Moy, J. H. (2011) Generic phytosanitary radiation treatment for tephritid fruit flies provides quarantine security for *Bactrocera latifrons* (Diptera: Tephritidae). *J. Econ. Entomol.*, **104**, 1509–1513.
21. Oliva, C. F., Jacquet, M., Gilles, J., Lemperiere, G., Maquart, P. O., Quilici, S., Schooneman, F., Vreysen, M. J. and Boyer, S. (2012) The sterile insect technique for controlling populations of *Aedes albopictus* (Diptera: Culicidae) on Reunion Island: mating vigour of sterilized males. *PLoS One*, **7**, e49414.
22. Mastrangelo, T., Chaudhury, M. F., Skoda, S. R., Welch, J. B., Sagel, A. and Walder, J. M. (2012) Feasibility of using a Caribbean screwworm for SIT campaigns in Brazil. *J. Med. Entomol.*, **49**, 1495–1501.

23. Ant, T., Koukidou, M., Rempoulakis, P., Gong, H. F., Economopoulos, A., Vontas, J. and Alphey, L. (2012) Control of the olive fruit fly using genetics-enhanced sterile insect technique. *BMC Biol.*, **10**, 51.
24. Mutika, G. N., Kabore, I., Seck, M. T., Sall, B., Bouyer, J., Parker, A. G. and Vreysen, M. J. B. (2013) Mating performance of *Glossina palpalis gambiensis* strains from Burkina Faso, Mali, and Senegal. *Entomol. Exp. Appl.* **146**, 177–185.
25. Kumano, N., Haraguchi, D. and Kohama, T. (2008) Effect of irradiation on mating ability in the male sweetpotato weevil (Coleoptera: Curculionidae). *J. Econ. Entomol.*, **101**, 1198–1203.
26. Soopaya, R., Stringer, L. D., Woods, B., Stephens, A. E., Butler, R. C., Lacey, I., Kaur, A. and Suckling, D. M. (2011) Radiation biology and inherited sterility of light brown apple moth (Lepidoptera: Tortricidae): developing a sterile insect release program. *J. Econ. Entomol.*, **104**, 1999–2008.
27. Shechter, D., Dormann, H. L., Allis, C. D. and Hake, S. B. (2007) Extraction, purification and analysis of histones. *Nat. Protoc.*, **2**, 1445–1457.
28. Abramoff, M. D., Magalhaes, P. J. and Ram, S. J. (2004) Image processing with ImageJ. *Biophoton. Int.* **11**, 36–42.
29. Zhao, H., Traganos, F. and Darzynkiewicz, Z. (2010) Kinetics of the UV-induced DNA damage response in relation to cell cycle phase. Correlation with DNA replication. *Cytometry A*, **77**, 285–293.
30. Zhao, H., Albino, A. P., Jorgensen, E., Traganos, F. and Darzynkiewicz, Z. (2009) DNA damage response induced by tobacco smoke in normal human bronchial epithelial and A549 pulmonary adenocarcinoma cells assessed by laser scanning cytometry. *Cytometry A*, **75**, 840–847.
31. Götz, S., García-Gómez, J. M., Terol, J. *et al.* (2008) High-throughput functional annotation and data mining with the Blast2GO suite. *Nucleic Acids Res.*, **36**, 3420–3435.
32. Ahmed, E. A., Agay, D., Schrock, G., Drouet, M., Meineke, V. and Scherthan, H. (2012) Persistent DNA damage after high dose in vivo gamma exposure of minipig skin. *PLoS One*, **7**, e39521.
33. Roch-Lefèvre, S., Mandina, T., Voisin, P. *et al.* (2010) Quantification of gamma-H2AX foci in human lymphocytes: a method for biological dosimetry after ionizing radiation exposure. *Radiat. Res.*, **174**, 185–194.
34. Huang, X., Halicka, H. D. and Darzynkiewicz, Z. (2004) Detection of histone H2AX phosphorylation on Ser-139 as an indicator of DNA damage (DNA double-strand breaks). *Curr. Protoc. Cytom.*, **Chapter 7**, Unit 7.27.
35. Bhogal, N., Kaspler, P., Jalali, F., Hyrien, O., Chen, R., Hill, R. P. and Bristow, R. G. (2010) Late residual gamma-H2AX foci in murine skin are dose responsive and predict radiosensitivity in vivo. *Radiat. Res.*, **173**, 1–9.
36. Liu, S. K., Olive, P. L. and Bristow, R. G. (2008) Biomarkers for DNA DSB inhibitors and radiotherapy clinical trials. *Cancer Metastasis Rev.*, **27**, 445–458.
37. Kataoka, Y., Bindokas, V. P., Duggan, R. C., Murley, J. S. and Grdina, D. J. (2006) Flow cytometric analysis of phosphorylated histone H2AX following exposure to ionizing radiation in human microvascular endothelial cells. *J. Radiat. Res.*, **47**, 245–257.
38. IAEA. (2004) Irradiation as a phytosanitary treatment of food and agricultural commodities. IAEA-TECDOC-1427. In *Proceedings of a Final Research Coordination Meeting Organized by the Joint FAO/IAEA Division of Nuclear Techniques in Food and Agriculture 2002*. International Atomic Energy Agency (IAEA), Vienna, Austria. p. 181.
39. Collins, S. R., Weldon, C. W., Banos, C. and Taylor, P. W. (2009) Optimizing irradiation dose for sterility induction and quality of *Bactrocera tryoni*. *J. Econ. Entomol.*, **102**, 1791–1800.
40. Song, Y. H. (2005) *Drosophila melanogaster*: a model for the study of DNA damage checkpoint response. *Mol. Cells*, **19**, 167–179.
41. Steller, H. (2008) Regulation of apoptosis in *Drosophila*. *Cell Death Differ.*, **15**, 1132–1138.
42. Sun, N. K., Sun, C. L., Lin, C. H., Pai, L. M. and Chao, C. C. (2010) Damaged DNA-binding protein 2 (DDB2) protects against UV irradiation in human cells and *Drosophila*. *J. Biomed. Sci.*, **17**, 27.

Cytometry
PART A
Journal of the International Society for Advancement of Cytometry

γH2AX Responses in Human Buccal Cells Exposed to Ionizing Radiation

Mohammad Sabbir Siddiqui,[1,2] Maxime François,[1] Michael F. Fenech,[1] Wayne R. Leifert[1]*

[1]CSIRO Food & Nutrition Flagship, Nutrigenomics & DNA Damage, Adelaide, South Australia, 5000, Australia

[2]University of Adelaide, School of Agriculture, Food & Wine, Urrbrae, South Australia, 5064, Australia

Received 30 July 2014; Revised 15 October 2014; Accepted 27 November 2014

Grant sponsor: Australian Postgraduate Award (APA)

Correspondence to: Dr Wayne R. Leifert, CSIRO Food & Nutrition Flagship, Adelaide, South Australia, 5000, Australia. E-mail: wayne.leifert@csiro.au

Published online 16 December 2014 in Wiley Online Library (wileyonlinelibrary.com)

DOI: 10.1002/cyto.a.22607

Abstract

DNA double strand breaks are induced by ionizing radiation (IR), leading to the phosphorylation of the core histone protein H2AX (termed γH2AX). The understanding of the γH2AX responses in irradiated human buccal cells is still very limited. We used visual scoring and laser scanning cytometry (LSC) methods to investigate γH2AX signaling following exposure of human buccal cells (from six individuals) to ionizing radiation at 0–4 Gy. The frequency of nuclei containing 15–30 γH2AX foci was significantly elevated 30 min post-IR exposure (by visual scoring). Concomitantly, there was a significant decrease in the frequency of cells without foci following exposure to IR. IR-induced γH2AX signal as determined by laser scanning cytometry (which included γH2AX integral and MaxPixel value) increased significantly in all individual's 2N nuclei 30 min post-IR and was similar for all three nuclear shapes identified. Individuals with the lowest baseline γH2AX integral (i.e., in nonirradiated cells) showed the greatest fold stimulation of γH2AX and significant dose-responses to IR doses of 1, 2, and 4 Gy. In 5 out of 6 individuals, the frequency of visually scored γH2AX in nuclei showed a strong correlation (up to $r = 0.999$) with LSC scored γH2AX integrals. The γH2AX response and subsequent decline varied between individuals but remained elevated above baseline levels 24 h post IR exposure. γH2AX response in irradiated human buccal cells has potential to be used as an index of baseline DNA damage in population studies. The variable response to IR exposure between individuals should be taken into consideration when using the γH2AX assay for radiation biodosimetry. © 2014 International Society for Advancement of Cytometry

Key terms

γH2AX; buccal cells; ionizing radiation

Introduction

DNA Double strand breaks (DSBs) are one of the most biologically significant DNA damage lesions that leads to chromosome breakage and/or rearrangement, mutagenesis, and loss or gain of genetic information (1,2). DSBs are directly generated by exogenous agents such as ionizing radiation (IR) (3,4), antitumor drugs (bleomycin, mitoxantrone, etoposide) (5,6) or by endogenously generated reactive oxygen species (7). Mammalian cells respond to DSBs by activating a multitude of proteins involved in signaling and DNA repair pathways. Although the majority of lesions are efficiently repaired, the very nature of DSBs poses such a threat to cell survival that DNA damage checkpoint proteins may be activated to initiate cellular division arrest. This provides time for DNA repair to proceed before mitosis is completed or in the case of overwhelming damage, apoptosis ensues (8). Therefore, DSBs in chromosomal DNA may lead to reduced integrity of the genome but also impaired health and survival of mammalian cells (1,2).

The histone proteins are intricate components of the nucleosome complex and are essential for genome integrity in terms of normal regulation of gene expression, genome maintenance, and replication (9–11). Induction of DNA DSBs in live mam-

ISAC
International Society for Advancement of Cytometry

malian cells triggers the phosphorylation of Ser139 in the SQ motif near the C-terminal of H2AX, which results in the phosphorylated form of H2AX, termed γH2AX (12,13). The phosphorylation of H2AX histone proteins which are located in the vicinity of the DSBs (14,15) is known as one of the earliest responses to DNA DSBs in cells. Therefore, γH2AX quantification may prove to be a sensitive biomarker of DNA DSBs in human cells.

Studies of the kinetics of phosphorylation and dephosphorylation of H2AX after exposure of cells to IR have shown induction of maximal amounts of γH2AX in cells in a few minutes after exposure to IR (14,16–18). Subsequently, the γH2AX signals decline over a period of hours. However, radiation-induced γH2AX signals have been observed to persist after 70 days post IR exposure to skin cells (19). Our previous study using Queensland fruit fly (*Bactrocera tryoni*) demonstrated that IR exposure leads to persistent γH2AvB signals (a variant of γH2AX) that could be measured during the adult stage of the life cycle when the IR exposure was conducted at the pupal stage (20). Therefore, it is plausible that persistent γH2AX may represent prior DNA damage due to misrepaired DSBs, unrepaired DSBs in specific sequences such as telomeric DNA, S-phase cells or apoptotic cells (21).

Human buccal mucosa has considerable potential as an easily accessible source of cells to determine endogenous- or exogenous-induced DNA damage (22,23) and has been used successfully to measure IR-induced γH2AX signals (24,25). In one recent study, a sub-population of 50–100 buccal cells were scored from microscope images by semi-automation for the presence of γH2AX foci (24). Another study measured the absorbance of diffuse γH2AX staining in nuclei from individuals exposed to a low dose of ionizing radiation by examining only 25–30 cells from each individual (25). However, our previous studies have demonstrated that there are multiple subpopulations of buccal cell types present (26–28) and therefore in both of those earlier studies (24,25), it was likely that insufficient cells were scored to give an accurate representation of the entire sample population's γH2AX response. Moreover, different nuclear shapes have been used as criteria to identify nuclear abnormalities in buccal cells (29). The aim of this study was to determine whether LSC could be used to measure multiple parameters (area, integral, MaxPixel) of γH2AX signals as well as the ploidy and nuclear shapes in thousands of cells. Use of the proposed LSC γH2AX method can overcome limitations of visual scoring methods by increasing scoring speed, increasing cell number measured, eliminating variation due to differences between scorers and scorer fatigue, and enabling the possibility of higher statistical power and high content analysis of multiple nuclear parameters.

Materials and Methods

Chemicals and Reagents

Roswell Park Memorial Institute (RPMI)−1640, Fetal Bovine Serum (FBS), sodium pyruvate, L-glutamine/penicillin/streptomycin mix and all other chemicals were purchased from Sigma-Aldrich (Castle Hill, NSW, Australia) unless otherwise stated. Mouse monoclonal antibody anti-γH2AX (clone JBW301) was obtained from Millipore (Kilsyth, VIC, Australia). Dulbecco's Phosphate Buffered Saline (DPBS) and secondary antibody Alexa Fluor 488 Goat anti-mouse were purchased from Life Technologies (Mulgrave, VIC, Australia).

Participants

Buccal cells were collected from six healthy individuals (three females and three males) aged from 25 to 44 years. Participants were healthy nonsmokers, not taking vitamin supplements and were informed of the purpose of the study. Approval for this study was obtained from the CSIRO Human Research Ethics Committee.

Buccal Cell Collection

Prior to buccal cell collection, each participant was first required to rinse their mouth twice with water. Small flat headed toothbrushes were rotated 20 times against the inner part of the cheeks in a circular motion. Both cheeks were sampled using separate toothbrushes. Heads of the brushes were transferred into 20 ml conical screw cap tubes (one tube per participant) each containing 15 ml of fresh prewarmed complete medium (RPMI with 10% FBS, 2 mM L-Glutamine, 1 mM sodium pyruvate, 100 U penicillin and 100 μg/ml streptomycin) and vigorously agitated to dislodge the cells. Cells were centrifuged at 1000*g* for 10 min before discarding and replacing supernatant with fresh DPBS. This washing procedure was carried out twice. The cells were then resuspended in 10 ml of fresh prewarmed (37°C) complete medium. Cell concentration was assessed using a haemocytometer and diluted with complete medium to reach a final concentration of 50,000 cells/ml. The cell suspension was then divided into four 10-ml aliquots in 20-ml conical screw cap tubes.

Buccal Cell Irradiation

Cell aliquots were exposed to 0, 1, 2, or 4 Gy ionizing radiation (IR) using a ^{137}Cs-γ IBL 437 irradiator 5 Gy/min at 25°C (Shering CIS bio international) and immediately incubated for 30 min at 37°C in complete medium using a portable tissue incubator. For kinetics experiments, post-irradiated cells (4 Gy) and nonirradiated cells (0 Gy) were incubated at 37°C in complete medium for 30 min, 3 h, or 24 h. Following incubation, cells were centrifuged at 1,000*g* for 10 min and supernatant was discarded. Cells were then resuspended in 10 ml of 4% formaldehyde in DPBS for 15 min at room temperature. Following fixation cells were centrifuged at 1,000*g* for 10 min and supernatant was removed before washing cells in 10 ml of buccal cell buffer (10 mM Tris, 0.1 M ethylenediaminetetraacetic, 20 mM NaCl, pH 7.0). The washing procedure was carried out twice, and cells were then cytocentrifuged for 5 min at 600 rpm onto microscopic slides to a final number of 5,000 cells per cytospot using a Shandon Cytospin®4 (Thermo Scientific, USA). Slides were washed once with distilled water and air-dried for 15 min at room temperature.

Staining of Buccal Cells

A circle was drawn around each cytospot using a hydrophobic PAP pen (Dako, Australia) and air-dried for 10 min.

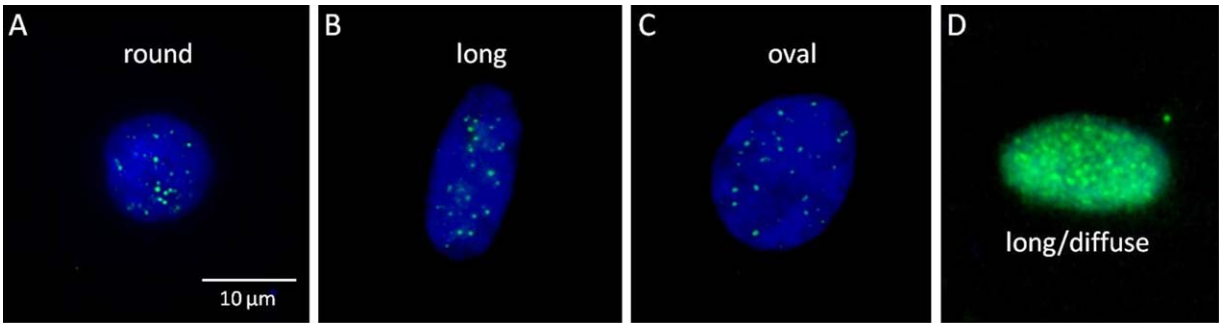

Figure 1. Fluorescence images of buccal cell nuclei containing discrete or diffuse γH2AX foci. Buccal cell nuclei were visualised (stained with DAPI) with a fluorescence microscope as described in the Materials and Methods section. Nuclei were classified into three categories i.e. round nuclei (**A**), long nuclei (**B**), and oval nuclei (**C**). Discrete γH2AX foci were observed in A–C; however, ~25% of nuclei at baseline demonstrated a diffuse pattern of γH2AX signal within nuclei (**D**). [Color figure can be viewed in the online issue, which is available at wileyonlinelibrary.com.]

Slides were rinsed in DBPS for 15 min, incubated in chilled 70% ethanol for 20 min and washed in DPBS for 15 min. Buccal cell cytospots were then treated with 150 µl of prewarmed (37°C) pepsin solution (containing 750 U/ml of porcine gastric mucosa pepsin) in 0.01 M HCl and then covered with parafilm for 30 min at 37°C in a humidified box. The slides were then washed twice with DPBS for 5 min. Buccal cells were then permeabilized with 1% Triton X-100 for 15 min at room temperature and subsequently quenched of any trace of formaldehyde by dipping slides into 0.1 M glycine in DPBS twice for 2 min. Slides were then rinsed three times in DPBS and a blocking step was performed by incubating cells in 10% goat serum for 1 h at room temperature before being washed once with DPBS. The anti-γH2AX antibody was added to each cytospot at a dilution of 1:100 in DPBS containing 10% goat serum and covered with parafilm overnight at 4°C in a humidified box. Slides were washed three times in DPBS for 5 min and a secondary antibody Alexa Fluor 488 Goat anti-mouse was added to each cytospot at a dilution of 1:500 in DPBS containing 10% FBS and covered with parafilm for 1 h at room temperature. Slides were washed three times in DPBS for 5 min and nuclei were counterstained with 4,6-diamidino-2-phenylindole (DAPI) at a concentration of 1 µg/ml for 10 min at room temperature. The excess DAPI was removed by rinsing the slides with a solution containing 300 mM NaCl and 34 mM sodium citrate. Slides were then mounted with coverslips and DPBS:glycerol (1:1) medium. The edges of coverslips were sealed with nail polish to prevent drying prior to performing LSC and visual scoring.

Visual Scoring of γH2AX Foci

Visual scoring of γH2AX foci was performed immediately after the staining procedure was applied using a fluorescence microscope (ZEISS Metasystems, Althusheim, Germany) under a 63x oil objective. DAPI (nuclei) and Alexa Fluor 488 (γH2AX) fluorescence was viewed using a blue and green filter, respectively. A minimum of 375 cells per cytospot were scored for γH2AX foci. Since we observed three distinct shapes of nuclei (which may represent different stages of postmitotic differentiation), they were classified into three groups based upon their morphological features i.e., round nuclei, long nuclei, and oval nuclei. γH2AX appeared as discrete foci or as diffuse staining within nuclei (see Fig. 1), therefore we categorized γH2AX scores for each nucleus as follows; no foci, 1–14 foci per nucleus, 15–30 foci per nucleus and diffuse foci (either >30 foci or diffuse nuclear staining of γH2AX i.e., wide-spread and uniform presence of γH2AX signal within the nucleus).

Laser Scanning Cytometry Measurements of γH2AX

Laser scanning cytometry (LSC) measurements were carried out with an iCyte® Automated Imaging Cytometer (Thorlabs, Sterling Virginia, USA) with full autofocus function as well as 405 nm and 488 nm lasers for excitation of DAPI and Alexa Fluor 488, respectively. Fluorescence from DAPI (blue) and Alexa Fluor 488 (green) was collected with a photomultiplier tube. Samples were scanned in separate passes (consecutively) to prevent spectral overlap. The nuclei and γH2AX events were contoured using empirically determined thresholds to exclude the scoring of false positives (e.g., small fluorescent debris). The frequency (%) of nuclei containing γH2AX signal was recorded as well as multiple parameters within each nucleus; including the total γH2AX integral (a function of γH2AX intensity and size) and the MaxPixel value (the value of the most intense γH2AX signal/pixel within nuclei). These parameters were generated using the iCyte® 3.4 software and subsequently transferred into excel for further statistical analyses. Nuclei were also classified into round, long, or oval shapes (Fig. 2) by utilizing the iCyte software parameters which included area, circularity, perimeter and diameter as described in detail of figure legend (Fig. 2). Additionally, all nuclei were separated according to their ploidy status (DNA content) as follows; <2N, 2N, and >2N, where 2N was defined as the mean integral signal of the population of nuclei ± 1 standard deviation. For 2N nuclei, the peak of the nuclei count coincided with the mean DAPI integral.

Statistical Analyses

GraphPad Prism 6.01 (GraphPad Prism, San Diego, CA) was used to analyse data. For visual scoring comparison of the frequency of DNA damaged cells at IR doses 1, 2, and 4 Gy were compared with control (0 Gy) using one-way ANOVA

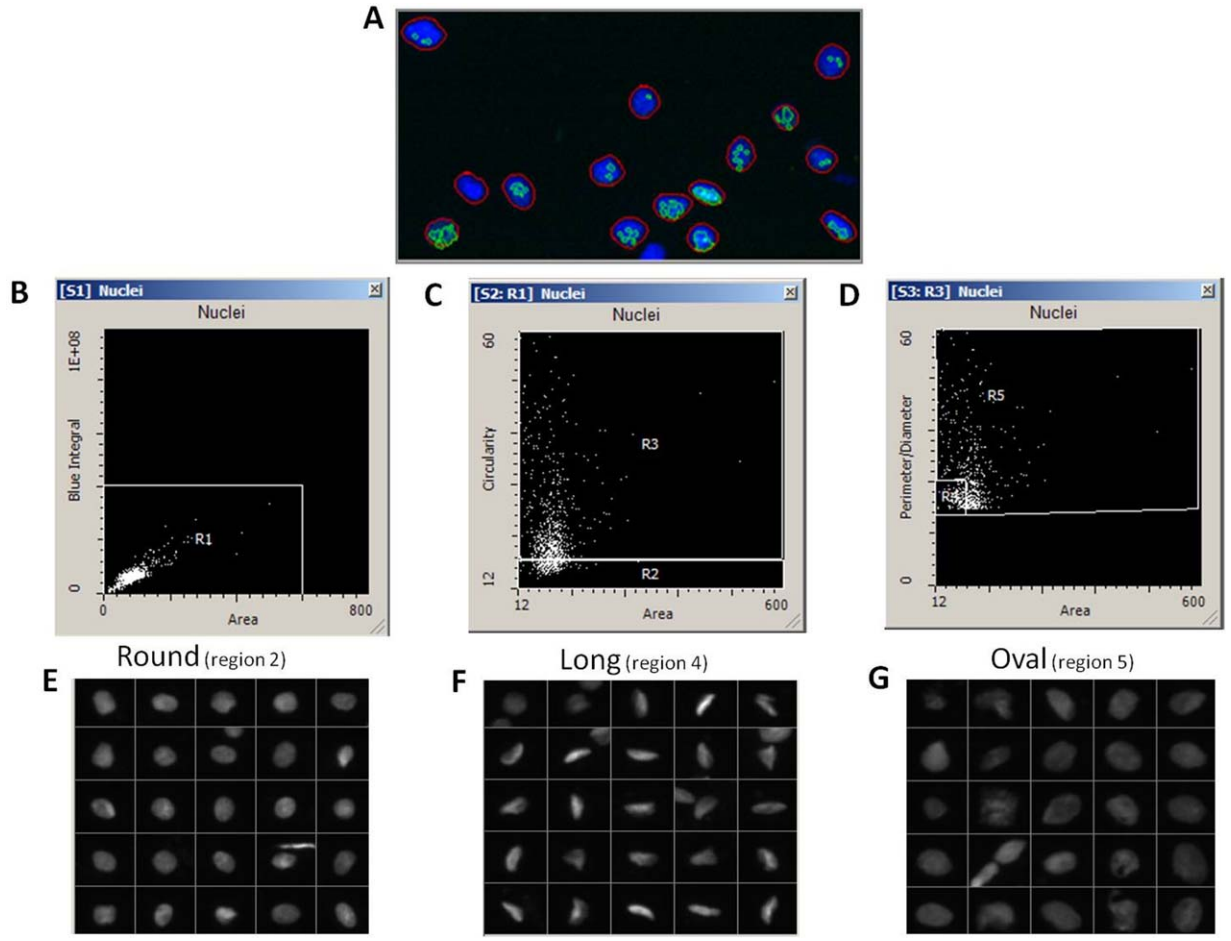

Figure 2. Identification of buccal cell nuclear shapes; round, long, and oval, by laser scanning cytometry. The events from different scattergram regions were relocated and imaged (using an imaging gallery) to empirically identify the three different nuclear shapes present. **A**: Individual nuclei were automatically contoured (red contour lines) as described in methods based on a thresholding procedure. γH2AX signal (green contour lines) was detected and quantified (integral or MaxPixel) within the nuclei following exposure to 0–4 Gy. **B**: Nuclei having area values that ranged from 0 to 600 μm and blue integral values that ranged from 0 to 4×10^7 (arbitrary units) in Region 1 (R1) were analyzed in (**C**) by plotting their circularity (*y*-axis) versus nuclear area (*x*-axis) where "Round" nuclei were identified in Region 2 (R2). **D**: Nuclei from Region 3 (R3) were further analyzed by plotting their perimeter/diameter ratio (*y*-axis) versus nuclear area (*x*-axis). Two new groups were established from R3; long nuclei were identified in R4 and oval nuclei in R5. Representative galleries of nuclear shape are shown for (**E**) round, (**F**) long, and (**G**) oval nuclei. [Color figure can be viewed in the online issue, which is available at wileyonlinelibrary.com.]

followed by Dunnett's multiple comparison test. For LSC analyses, yH2AX data were checked for normality using D'Agostino and Pearson omnibus normality test. Comparison of the frequency of DNA damaged cells at IR doses 1, 2, and 4 Gy were compared with control (0 Gy) using the Kruskal-Wallis test followed by the Dunn's multiple comparisons test. Correlation coefficients were obtained using the Pearson correlation coefficient (r). Data were expressed as mean ± standard error of the mean (SE). $P < 0.05$ was considered statistically significant.

Results

Visual Scoring of γH2AX in Buccal Cells

Representative images of nuclei are shown in Figure 1. Nuclei were classified into three groups based upon the nuclear shape; either round, long or oval as shown in Figures 1A–1C, respectively. γH2AX foci were observed in buccal cell nuclei as shown in Figures 1A–1D, even at baseline i.e., 0 Gy. The frequency (%) of buccal cell nuclei in six individuals that had no γH2AX foci at baseline (0 Gy) was $11.70 \pm 3.52\%$, $13.60 \pm 3.92\%$, and $10.89 \pm 2.80\%$ for round, long, and oval nuclei, respectively (totaling 36% of all nuclei) as shown in Table 1. Following exposure to IR the frequency of nuclei (all three types) containing no foci significantly decreased with increasing dose of IR exposure (Table 1). This suggested that IR exposure caused an increase in the levels of γH2AX in the buccal cell nuclei. On further examination, the frequency of long nuclei containing 15–30 γH2AX foci was significantly increased following IR exposure to 1 Gy ($P < 0.05$), 2 Gy ($P < 0.001$), and 4 Gy ($P < 0.0001$) as shown in Table 1. Additionally, there was a significant increase in the frequency of round nuclei containing 15–30 γH2AX foci at 2 Gy ($P < 0.05$) and 4 Gy ($P < 0.01$).

Table 1. Visually scored γH2AX in buccal cells

NUCLEUS SHAPE	γH2AX FOCI	RADIATION DOSE			
Round		0 Gy	1 Gy	2 Gy	4 Gy
	0 foci	11.70 ± 3.52	4.13 ± 0.90[A]	1.82 ± 0.39[B]	1.20 ± 0.23[B]
	1−14 foci	3.20 ± 0.86	2.40 ± 0.91	1.69 ± 0.38	1.24 ± 0.64
	15−30 foci	10.20 ± 2.33	12.40 ± 2.54	17.87 ± 1.57[A]	20.00 ± 1.74[B]
	>30 diffuse foci	9.09 ± 1.52	10.71 ± 1.75	8.18 ± 1.70	7.78 ± 1.61
Long		0 Gy	1 Gy	2 Gy	4 Gy
	0 foci	13.60 ± 3.92	6.76 ± 1.97	2.49 ± 0.89[B]	0.71 ± 0.21[B]
	1−14 foci	1.92 ± 0.48	2.67 ± 0.93	1.82 ± 0.45	0.93 ± 0.33
	15−30 foci	9.14 ± 2.94	19.02 ± 1.40[A]	24.62 ± 1.36[C]	28.27 ± 2.64[D]
	>30 diffuse foci	8.93 ± 1.47	11.96 ± 1.67	12.40 ± 2.67	9.20 ± 3.07
Oval		0 Gy	1 Gy	2 Gy	4 Gy
	0 foci	10.89 ± 2.80	4.04 ± 0.92[A]	2.22 ± 0.54[B]	1.69 ± 0.59[B]
	1−14 foci	2.73 ± 0.55	2.18 ± 0.62	2.62 ± 0.69	0.76 ± 0.27
	15−30 foci	11.45 ± 2.91	14.22 ± 2.95	17.56 ± 1.37	15.73 ± 3.11
	>30 diffuse foci	7.15 ± 0.95	9.51 ± 1.30	6.71 ± 1.98	12.49 ± 3.46
All nuclei types		0 Gy	1 Gy	2 Gy	4 Gy
(round + long + oval)	0 foci	36.17 ± 9.94	14.93 ± 2.80[A]	6.53 ± 0.90[B]	3.6 ± 0.60[C]
	1−14 foci	7.85 ± 1.66	7.23 ± 1.97	6.13 ± 1.39	2.93 ± 0.98
	15−30 foci	30.80 ± 7.72	45.63 ± 2.81	60.03 ± 2.55[B]	64.00 ± 6.45[C]
	>30 diffuse foci	25.18 ± 2.84	32.18 ± 1.97	27.28 ± 1.99	29.46 ± 7.54

Frequency (%) of the different nuclear types classified (round, long, and oval nuclei) containing γH2AX signals ($n = 6$ individuals, 375 cells scored for each individual) at 0, 1, 2, and 4 Gy in the 6 individuals A−E is shown. Data are presented as Mean ± SE. [A]$P < 0.05$, [B]$P < 0.01$, [C]$P < 0.001$, [D]$P < 0.0001$.

The frequency of oval nuclei containing no foci (10.89 ± 2.80%) significantly decreased to 4.04 ± 0.92%, 2.22 ± 0.54%, and 1.69 ± 0.59% for 1 Gy ($P < 0.05$), 2 Gy ($P < 0.01$), and 4 Gy ($P < 0.01$), respectively, i.e., there were dose-related increases in the frequency of nuclei with 15–30 γH2AX foci across all nuclear types. However, there was no statistically significant increase in the frequency of oval nuclei containing 1–14 γH2AX foci, 15–30 γH2AX foci or diffuse γH2AX. In fact, regardless of nuclear type, there was no significant change in the frequency of nuclei containing diffuse γH2AX or 1–14 γH2AX foci following IR exposure (Table 1).

Scoring of γH2AX in Buccal Cells by LSC

Figure 3 shows a representative example of the data obtained from a single individual's preliminary LSC assay (from "individual B"). To demonstrate the distribution of DNA content in the buccal cells, nuclei count versus DAPI integral (equivalent to DNA content) was plotted as shown in Figure 2A, whereby 2,634 nuclei were examined. Nuclei were then classified as <2N, 2N, or >2N prior to further analyses. Figure 2B shows the DAPI integral was correlated with nuclear area for the same 2,634 nuclei as in Figure 2A. Figures 2C and 2D shows the γH2AX integral of individual B when plotted against DNA content (DAPI integral) for 0 Gy (mean = 0.131 × 10^6 a.u., $n = 2{,}634$ nuclei) and 4 Gy (mean = 3.25 × 10^6 a.u., $n = 1{,}060$ nuclei), respectively.

2N Nuclei

Table 2 summarizes γH2AX integral measurements in buccal cells exposed to 0, 1, 2, or 4 Gy for six individuals. All six individuals demonstrated a significant increase in γH2AX integral in buccal nuclei following exposure to IR as low as 1 Gy. The variation of baseline (0 Gy) γH2AX signals were variable between individuals. For example, two individuals (B and E) had γH2AX signals that were less than 1 × 10^6 a.u. at 0 Gy, whereas the remaining 4 individuals had values that ranged from 1.209 to 6.067 × 10^6 a.u. There was also considerable variation in the response of buccal cells to radiation exposure; indeed, the individuals with the lowest baseline γH2AX values (B and E) also showed the greatest fold increase in IR-induced γH2AX signal. For example, the γH2AX integral in individual B significantly increased from 0.132 × 10^6 a.u. at 0 Gy to 1.009 × 10^6 a.u. ($P < 0.0001$) at 1 Gy, 1.954 × 10^6 a.u. ($P < 0.0001$) at 2 Gy and 2.673 × 10^6 a.u. at 4 Gy ($P < 0.0001$), representing up to a 20-fold increase of γH2AX signal in 2N nuclei. Conversely, the individuals with the highest γH2AX integral at baseline (0 Gy) showed the least IR-induced γH2AX signal response, although the responses were statistically significant. Each individual had a significantly increased γH2AX integral following IR exposure; however, when the 4 IR doses were averaged ($n = 6$ per IR dose), there was no significant difference between IR exposure doses compared with 0 Gy, which was likely due to the large amount of inter-individual variation, particularly at baseline (0 Gy).

Consistent with the increase in γH2AX integral post-IR as discussed above, both the γH2AX area (data not shown) and γH2AX MaxPixel values also increased significantly with IR dose (Table 3). Additionally, both parameters (γH2AX area and MaxPixel) correlated well with the γH2AX integral values (γH2AX integral and γH2AX area correlation coefficients were $R^2 = 0.979$ and $R^2 = 0.960$ for γH2AX area and γH2AX

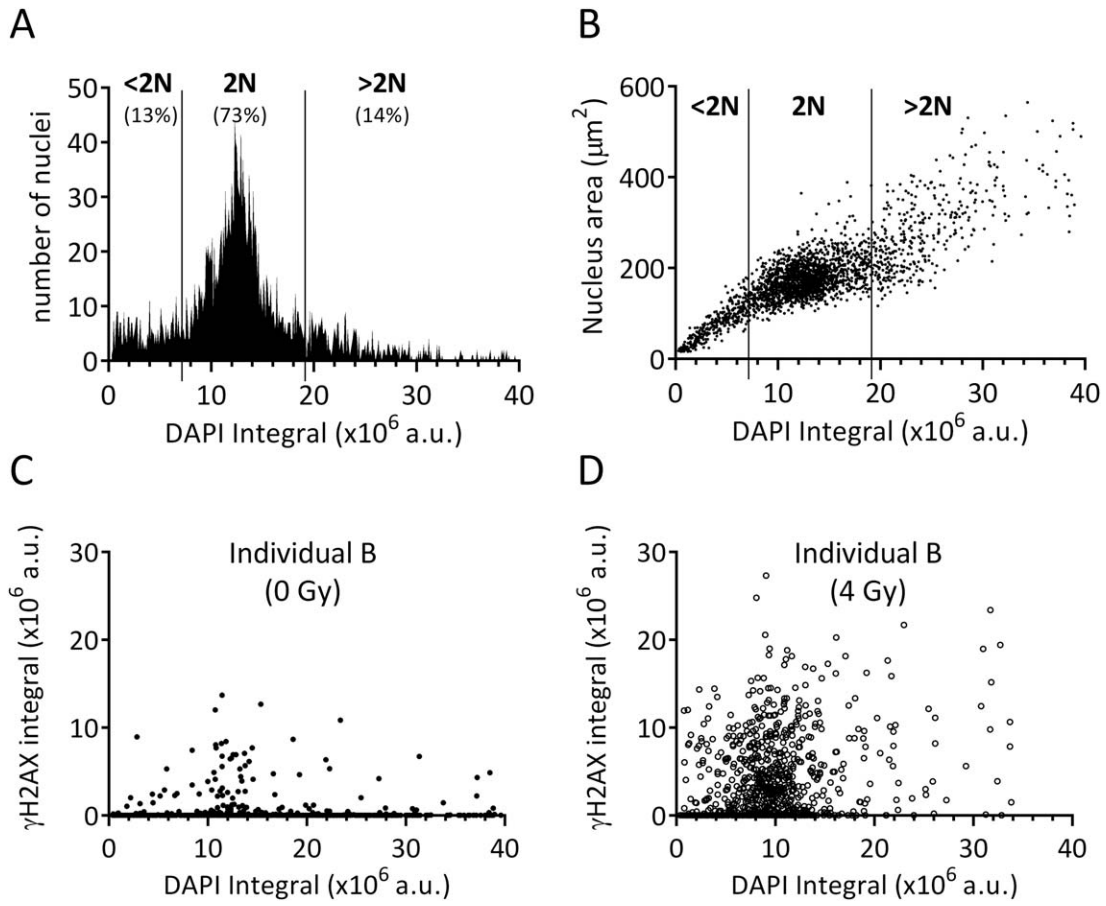

Figure 3. DNA content and γH2AX quantification in buccal cell nuclei by laser scanning cytometry (LSC). A representative example from individual B showing: **A**: buccal cell DNA content was calculated automatically from all nuclei by using the DAPI integral feature within the iCyte software; the DNA content was determined by categorizing nuclei as <2N, 2N, and >2N. 2N was defined as the mean integral ± 1 S.D. Sub-2N and >2N were less and greater than 1 S.D. from the mean, respectively. Numbers in parentheses represent the percentage of nuclei. **B**: The correlation of DAPI integral with nuclear area. γH2AX integral in buccal cells from individual B exposed to either 0 Gy (**C**) or 4 Gy (**D**) IR and γH2AX signal was plotted for all nuclei versus DNA content; the number of nuclei examined by LSC was $n = 2{,}634$ at 0 Gy and $n = 1{,}060$ nuclei at 4 Gy.

MaxPixel, respectively) in buccal cell nuclei exposed to 0, 1, 2, and 4 Gy in all individuals ($n = 6$) (Fig. 4).

<2N Nuclei and >2N Nuclei

Tables 2 and 3 summarize γH2AX integral and MaxPixel, respectively for <2N and >2N nuclei from six individuals. For <2N nuclei, 3 out of 6 individuals showed a significant increase in γH2AX integral (Table 2) whereas for >2N nuclei 4 out of 6 individuals had significantly increased γH2AX integral values at 4 Gy compared with 0 Gy. As expected, both the γH2AX area (not shown) and γH2AX MaxPixel (Table 3) values also increased significantly with IR dose.

Inter- and Intra-Individual Variation

The variation between the six individuals examined for 2N nuclei ranged from 2.326 to 8.942 $\times$ 10^6 a.u. at 4 Gy (Table 2). When a single individual's γH2AX integral (2N) was measured on six separate occasions (individual B), the 4 Gy γH2AX integral ranged from 2.67 to 4.74 $\times$ 10^6 a.u. with a coefficient of variation of 20.5%.

Nuclear Shape

In an attempt to score nuclear shape by LSC (as was done for visual scoring of buccal cell nuclei), we categorized nuclei as either round, long, or oval by using several iterative processes in iCyte as shown in Figure 2. By using some of the features available within the iCyte software (area, perimeter, diameter, and circularity) we empirically classified the buccal cell nuclei shapes and quantified the γH2AX MaxPixel values as shown in (Table 4). For each individual, the dose-response data for each nuclear shape are shown at 0–4 Gy. For round nuclei, all six individuals showed a significant IR-induced increase in γH2AX MaxPixel values. For long nuclei, three out of six individuals showed a significant increase, while for oval nuclei, four out of six individuals showed significant increases in MaxPixel values at 4 Gy compared with 0 Gy.

Correlation of Visually Scored γH2AX and γH2AX Integral by LSC

The frequency of visually scored long nuclei (containing 15–30 foci) was strongly correlated with LSC scored γH2AX

Table 2. Summary of γH2AX integral (a.u. X10^6) by LSC in <2N, 2N, or >2N buccal cells exposed to 0, 1, 2, or 4 Gy

NUCLEAR PLOIDY	INDIVIDUALS	0 GY	1 GY	2 GY	4 GY
<2N	A	1.967 ± 0.293 (n=108)	3.509 ± 0.663 (n=88)	3.127 ± 0.518 (n=102)	4.152 ± 0.491^A (n=111)
	B	0.092 ± 0.033 (n=353)	0.438 ± 0.101^D (n=70)	1.984 ± 0.203^D (n=320)	2.724 ± 0.540^D (n=101)
	C	2.902 ± 0.570 (n=102)	3.500 ± 0.399 (n=187)	2.814 ± 0.264 (n=366)	2.278 ± 0.340 (n=122)
	D	1.121 ± 0.119 (n=313)	2.915 ± 0.825 (n=33)	2.153 ± 0.237^A (n=216)	2.641 ± 0.332^D (n=215)
	E	1.528 ± 0.873 (n = 155)	2.090 ± 0.906 (n = 129)	2.958 ± 2.327 (n = 70)	1.057 ± 0.239 (n = 85)
	F	4.388 ± 0.516 (n = 74)	5.227 ± 1.065 (n = 25)	3.657 ± 0.458 (n = 99)	6.440 ± 0.715 (n = 73)
	Mean ± SE	2.000 ± 0.610	2.946 ± 0.655	2.782 ± 0.255	3.215 ± 0.761
	Individuals	0 Gy	1 Gy	2 Gy	4 Gy
2N	A	6.067 ± 0.298 (n = 586)	7.484 ± 0.395^A (n = 397)	7.745 ± 0.352^C (n = 498)	8.942 ± 0.455^D (n = 388)
	B	0.132 ± 0.021 (n = 1,913)	1.009 ± 0.076^D (n = 751)	1.954 ± 0.078^D (n = 2,466)	2.673 ± 0.122^D (n = 1,312)
	C	3.337 ± 0.191 (n = 810)	5.469 ± 0.179^D (n = 1,626)	4.333 ± 0.119^D (n = 3,218)	4.329 ± 0.229^B (n = 777)
	D	1.209 ± 0.059 (n = 1,847)	2.059 ± 0.221^D (n = 209)	2.619 ± 0.114^D (n = 1,444)	3.877 ± 0.170^D (n = 976)
	E	0.511 ± 0.073 (n = 433)	0.913 ± 0.105^B (n = 473)	1.242 ± 0.418^A (n = 213)	2.326 ± 0.622^D (n = 211)
	F	4.998 ± 0.337 (n = 379)	6.122 ± 0.546^B (n = 148)	5.627 ± 0.323^A (n = 433)	8.872 ± 0.490^D (n = 326)
	Mean ± SE	2.709 ± 1.010	3.843 ± 1.168	3.920 ± 1.007	5.170 ± 1.220
	Individuals	0 Gy	1 Gy	2 Gy	4 Gy
>2N	A	10.620 ± 1.536 (n = 58)	12.040 ± 2.190 (n = 44)	8.364 ± 1.147 (n = 73)	9.229 ± 1.550 (n = 56)
	B	0.164 ± 0.047 (n = 368)	3.052 ± 0.738^D (n = 59)	3.478 ± 0.270^D (n = 441)	7.388 ± 1.103^D (n = 108)
	C	5.389 ± 0.834 (n = 89)	9.216 ± 1.053^B (n = 122)	8.329 ± 0.624^B (n = 326)	7.520 ± 0.952 (n = 89)
	D	1.070 ± 0.229 (n = 262)	2.019 ± 0.527^C (n = 30)	3.567 ± 0.456^D (n = 276)	3.829 ± 0.451^D (n = 177)
	E	0.762 ± 0.286 (n = 61)	0.640 ± 0.193 (n = 69)	1.088 ± 0.612 (n = 33)	2.739 ± 1.138^A (n = 34)
	F	4.367 ± 0.804 (n = 55)	4.349 ± 0.941 (n = 30)	8.736 ± 1.957 (n = 65)	7.250 ± 0.854^B (n = 58)
	Mean ± SE	3.729 ± 1.625	5.219 ± 1.818	5.594 ± 1.341	6.326 ± 1.015

Letters denote the *P*-values when comparing 1, 2, or 4 Gy IR relative to 0 Gy for each individual. Data are presented as Mean ± SE. Numbers in parentheses represent the total number of nuclei that were scored at each IR dose. $^A P < 0.05$, $^B P < 0.01$, $^C P < 0.001$, $^D P < 0.0001$.

integrals in five out of six individuals (Fig. 5). The Pearson correlation coefficients from individuals A–E were $r = 0.999$, 0.930, 0.964, 0.608, and 0.945 while one individual (individual F) showed no correlation. Indeed for individual F, the LSC measured γH2AX integrals (including area and MaxPixel) significantly increased with IR dose (see Table 2, 2N nuclei, individual F). However, using the visual scoring criteria used here, we were unable to demonstrate significant differences between the frequency (%) of nuclei containing 15–30 foci at the different IR doses for individual F. This suggests that LSC was more sensitive to quantifying the small changes in IR-induced γH2AX signals in nuclei.

Kinetics of γH2AX in Buccal Cells

The time course of γH2AX was monitored at 0, 0.5, 3, and 24 h after the exposure of buccal cells to 4 Gy IR in 3

Table 3. Summary of γH2AX MaxPixel (a.u.) by LSC in <2N, 2N, or >2N buccal cells exposed to 0, 1, 2, or 4 Gy

NUCLEAR PLOIDY	INDIVIDUALS	0 GY	1 GY	2 GY	4 GY
<2N	A	2,994 ± 337 (n = 108)	4,241 ± 485 (n = 88)	3,728 ± 473 (n = 102)	5,614 ± 544[B] (n = 111)
	B	332 ± 100 (n = 353)	1,820 ± 283[D] (n = 70)	2,373 ± 217[D] (n = 320)	2,698 ± 352[D] (n = 101)
	C	4,092 ± 524 (n = 102)	5,356 ± 431[A] (n = 187)	4,148 ± 263 (n = 366)	4,520 ± 460 (n = 122)
	D	2,289 ± 203 (n = 313)	3,436 ± 782 (n = 33)	2,768 ± 241 (n = 216)	3,820 ± 323[C] (n = 215)
	E	2023 ± 325 (n = 155)	1913 ± 326 (n = 129)	1897 ± 470 (n = 70)	2279 ± 356 (n = 85)
	F	4,680 ± 475 (n = 74)	6,560 ± 981 (n = 25)	3,932 ± 381 (n = 99)	7,449 ± 605[B] (n = 73)
	Mean ± SE	2,735 ± 636	3,887 ± 770	3,141 ± 376	4,396 ± 785
	Individuals	0 Gy	1 Gy	2 Gy	4 Gy
2N	A	5,874 ± 206 (n = 586)	6,552 ± 247 (n = 397)	7,381 ± 250[D] (n = 498)	8,124 ± 303[D] (n = 388)
	B	445 ± 54 (n = 1913)	3,085 ± 152[D] (n = 751)	2,593 ± 79[D] (n = 2466)	3,062 ± 103[D] (n = 1312)
	C	3,598 ± 150 (n = 810)	5,484 ± 120[D] (n = 1626)	5,185 ± 87[D] (n = 3218)	5,064 ± 178[D] (n = 777)
	D	2,163 ± 84 (n = 1847)	3,242 ± 251[C] (n = 209)	3,141 ± 100[D] (n = 1444)	4,738 ± 142[D] (n = 976)
	E	1,092 ± 132 (n = 433)	1,498 ± 126[B] (n = 473)	1,989 ± 289[A] (n = 213)	3,274 ± 344[D] (n = 211)
	F	5,195 ± 274 (n = 379)	6,886 ± 414[C] (n = 148)	5,673 ± 202 (n = 433)	8,199 ± 306[D] (n = 326)
	Mean ± SE	3,121 ± 909	4,457 ± 884	4,327 ± 851	5,410 ± 927
	Individuals	0 Gy	1 Gy	2 Gy	4 Gy
>2N	A	9,212 ± 804 (n = 58)	8,786 ± 1025 (n = 44)	8,161 ± 819 (n = 73)	9,451 ± 1,194 (n = 56)
	B	587 ± 120 (n = 368)	6,664 ± 984[D] (n = 59)	4,012 ± 232[D] (n = 441)	6,316 ± 583[D] (n = 108)
	C	6,575 ± 572 (n = 89)	10,772 ± 814[C] (n = 122)	10,690 ± 426[D] (n = 326)	10,658 ± 1060[A] (n = 89)
	D	1,793 ± 244 (n = 262)	3,632 ± 609 [C] (n = 30)	3,759 ± 292[D] (n = 276)	5,311 ± 440[D] (n = 177)
	E	1,608 ± 380 (n = 61)	1,841 ± 431 (n = 69)	2,182 ± 959 (n = 33)	5,027 ± 1,410[A] (n = 34)
	F	4,938 ± 536 (n = 55)	5,210 ± 798 (n = 30)	6,983 ± 695 (n = 65)	8,133 ± 603[C] (n = 58)
	Mean ± SE	4,118 ± 1376	6,150 ± 1,346	5,964 ± 1306	7,482 ± 939

Letters denote the *P*-values when comparing 1, 2, or 4 Gy IR relative to 0 Gy for each individual. Data are presented as Mean ± SE. Numbers in parentheses represent the total number of nuclei that were scored at each IR dose. [A]$P < 0.05$, [B]$P < 0.01$, [C]$P < 0.001$, [D]$P < 0.0001$.

individuals (B, D, and E). These individuals were chosen for γH2AX kinetics analyses since they had the greatest dose-response to irradiation at 0–4 Gy. Figure 6A demonstrates that the mean frequency (%) of nuclei containing 15–30 γH2AX foci, when scored visually, remained elevated for a period of up to 24 h post IR. A peak was reached at 30 min post IR exposure (4 Gy) and subsequently declined by 40% at 24 h post IR (4 Gy); however, this remained significantly ($P < 0.0001$) higher than the baseline value. A similar result was obtained by LSC as shown in Figure 6B. The γH2AX integral significantly increased ($P < 0.05$) 30 min post IR exposure and then subsequently declined by 82% 24 h post IR, which was not significantly different from the baseline value.

Discussion

The objective of the present study was to investigate the induction and persistence of DNA DSBs in irradiated human

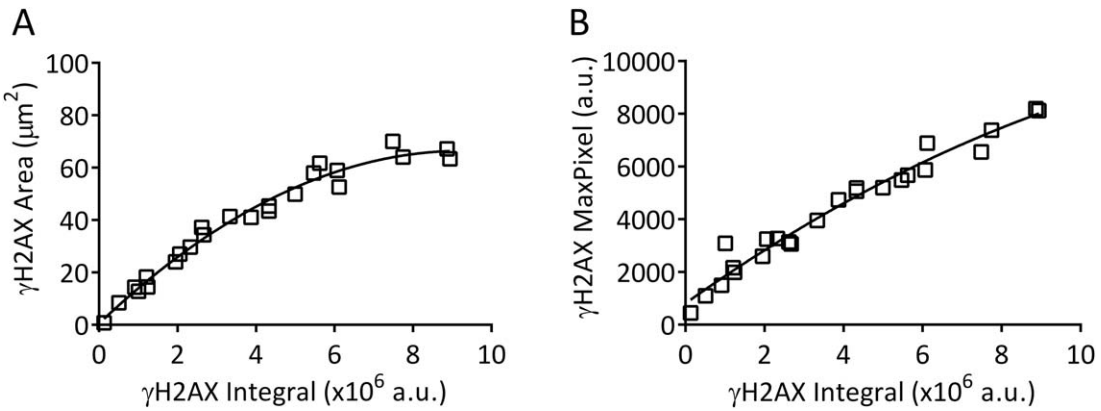

Figure 4. Correlation of γH2AX integral with γH2AX area and γH2AX MaxPixel by LSC. **A**: Correlation of γH2AX foci area and γH2AX integral or (**B**) correlation of γH2AX MaxPixel and γH2AX integral, per nucleus scored by LSC in buccal cell nuclei exposed to 0, 1, 2, and 4 Gy in all individuals ($n = 6$). The relationship of the two parameters fitted a second order polynomial (quadratic) resulting in correlation coefficients (R^2) for γH2AX foci area = 0.979 and for γH2AX MaxPixel = 0.960.

buccal cells. We used two scoring protocols to quantify ionizing radiation-induced γH2AX, a marker of DNA DSBs. Visual scoring of nuclei was correlated with the automated laser scanning cytometry (LSC) method developed here to quantify γH2AX integral (and MaxPixel) in each nucleus examined in thousands of buccal cells for each individual. Additionally, these LSC measurements were combined with quantitation of nuclear DNA content to classify cells depending on their DNA content (ploidy status) as well as nuclear shapes based on their area, perimeter, diameter, and circularity. Our experimental results demonstrated that buccal cells exposed to IR have the capacity to accumulate γH2AX which partially remained up to 24 h post IR exposure suggesting buccal cells have diminished capacity to repair DNA DSBs. We also observed a large variation in baseline levels of γH2AX and in γH2AX response to IR exposure.

In the visual scoring study, we aimed to classify buccal cells into separate groups based upon their nuclear shapes. Since the buccal mucosa is known to consist of heterogeneous cell types that may have discrete functions within the mucosa (22,23,27,29–33); we therefore hypothesized that our defined categories may also exhibit differences in their response to DNA damage induction and subsequent repair. In fact, our results demonstrated that γH2AX could be measured in buccal cells and that γH2AX response following IR varied between nuclei types as has been observed in previous studies (24,25,34). Long nuclei, for instance, showed the largest dose response (up to 3-fold) to increasing radiation exposure (0, 1, 2, and 4 Gy) with a higher frequency of nuclei containing 15–30 foci. In contrast, no significant difference was observed for oval shaped nuclei, and a weaker dose response (up to 2-fold) was found in round nuclei containing 15–30 foci. Interestingly, there was no change in the frequency of cells with diffuse foci following exposure to IR. It is likely that these "diffuse" nuclei we categorized here (∼25%) represent the necrotic or nonviable cell population expressing a phenotype of reduced response efficiency to DNA damage. This notion is consistent with previous studies showing that a relatively high proportion (up to 20%) of buccal cells are nonviable, necrotic, or apoptotic at baseline (24,35,36). For a more complete understanding of the DNA damage response biology of buccal cells, it would therefore be valuable in future studies to combine γH2AX detection with a cytoplasmic marker of cell subtypes present (if compatible with the current immunofluorescence protocol). Such markers could be met, for example, by the detection of cytokeratin proteins or other markers of epithelial cells, which are expressed differentially between buccal mucosa cell types depending on their differentiation status (32,37–39).

LSC has previously been shown as a useful tool to measure cellular DNA content for cell cycle stage evaluation in conjunction with γH2AX after inducing DNA damage (40–42). It was therefore decided to include DNA content (measured by nuclear DAPI integral) as an additional measurement in our LSC protocol allowing us to classify nuclei as <2N, 2N, or >2N. Previously, we demonstrated that ∼60% of buccal cells are likely to be post-mitotic 2N nuclei (27) which is similar to the results obtained in this study (see Fig. 3A). Our current findings support previous observations in that significant increases of γH2AX in buccal cell nuclei are induced by exposure to IR (24). A significant increase in γH2AX signal in 2N nuclei up to 4 Gy was observed in all individuals and dose responses measured by LSC correlated with those measured visually. For <2N nuclei only three out of six individuals showed a significant increase in γH2AX at a dose of 4 Gy. Alternatively, four out of six individuals showed a significant increase in γH2AX at a dose of 4 Gy in >2N nuclei. We believe that the buccal cell <2N and >2N populations are mainly composed of apoptotic cells, condensed chromatin cells or cells immobilized at a cell cycle check point due to mitotic defects or abnormal nuclear DNA content (27,43). The nature of the <2N and >2N population of cells may partly explain their somewhat lower response to radiation compared to the 2N cell population.

Although all individuals showed an increase in γH2AX following IR exposure, when the individual data obtained for

Table 4. Summary of γH2AX MaxPixel (a.u.) by LSC in round-, long-, and oval-shaped nuclei of buccal cells exposed to 0, 1, 2, or 4 Gy

NUCLEAR SHAPE	INDIVIDUALS	0 GY	1 GY	2 GY	4 GY
Round	A	6,435 ± 200 ($n = 576$)	7,443 ± 306[A] ($n = 277$)	7,619 ± 256[B] ($n = 429$)	8,376 ± 312[D] ($n = 366$)
	B	1,319 ± 54 ($n = 623$)	3,450 ± 143[D] ($n = 494$)	3,686 ± 83[D] ($n = 1817$)	5,223 ± 157[D] ($n = 625$)
	C	4,093 ± 131 ($n = 792$)	5,453 ± 117[D] ($n = 1484$)	5,409 ± 82[D] ($n = 3227$)	5,382 ± 134[D] ($n = 1227$)
	D	2,510 ± 52 ($n = 1963$)	3,339 ± 352 ($n = 60$)	3,534 ± 107[D] ($n = 866$)	5,315 ± 136[D] ($n = 1015$)
	E	1,912 ± 88 ($n = 431$)	2,193 ± 105 ($n = 323$)	2,170 ± 140 ($n = 133$)	3,115 ± 184[D] ($n = 227$)
	F	5,372 ± 284 ($n = 282$)	7,727 ± 653[B] ($n = 62$)	5,876 ± 220 ($n = 378$)	8,878 ± 305[D] ($n = 322$)
	Mean ± SE	3,667 ± 857	4,934 ± 942	4,716 ± 800	6,050 ± 888
	Individuals	0 Gy	1 Gy	2 Gy	4 Gy
Long	A	4,286 ± 638 ($n = 34$)	5,941 ± 633 ($n = 60$)	5,662 ± 690 ($n = 55$)	7,061 ± 714[A] ($n = 53$)
	B	1,400 ± 90 ($n = 60$)	2,846 ± 236[B] ($n = 137$)	3,690 ± 259[D] ($n = 198$)	3,169 ± 281[C] ($n = 148$)
	C	4,334 ± 872 ($n = 25$)	5,207 ± 695 ($n = 46$)	5,541 ± 411 ($n = 133$)	3,870 ± 453 ($n = 56$)
	D	2,519 ± 373 ($n = 55$)	4,150 ± 473 ($n = 57$)	4,537 ± 340[B] ($n = 116$)	4,671 ± 427[B] ($n = 84$)
	E	2,473 ± 375 ($n = 44$)	3,666 ± 494 ($n = 44$)	2,894 ± 554 ($n = 30$)	2,753 ± 318 ($n = 34$)
	F	6,951 ± 951 ($n = 26$)	6,936 ± 827 ($n = 40$)	4,682 ± 705 ($n = 28$)	8,880 ± 949 ($n = 34$)
	Mean ± SE	3,672 ± 803	4,791± 621	4,501 ± 436	5,280 ± 984
	Individuals	0 Gy	1 Gy	2 Gy	4 Gy
Oval	A	6,049 ± 464 ($n = 124$)	6,855 ± 388 ($n = 167$)	7,000 ± 450 ($n = 155$)	7,334 ± 545 ($n = 106$)
	B	1,456 ± 50 ($n = 1812$)	2,698 ± 175[D] ($n = 210$)	3,626 ± 114[D] ($n = 1030$)	3,989 ± 234[D] ($n = 240$)
	C	5,418 ± 339 ($n = 162$)	6,371 ± 259 ($n = 341$)	6,774 ± 228[B] ($n = 478$)	6,564 ± 298[A] ($n = 268$)
	D	2,578 ± 125 ($n = 353$)	4,030 ± 316[D] ($n = 115$)	3,703 ± 106[D] ($n = 866$)	4,656 ± 293[D] ($n = 220$)
	E	2,469 ± 166 ($n = 143$)	2,540 ± 142 ($n = 249$)	2,426 ± 247 ($n = 128$)	2,988 ± 339 ($n = 54$)
	F	4,627 ± 284 ($n = 178$)	6,282 ± 551[B] ($n = 84$)	5,071 ± 279 ($n = 158$)	7,836 ± 561[D] ($n = 91$)
	Mean ± SE	3,310 ± 673	4,384 ± 762	4,320 ± 678	5,206 ± 803

Letters denote the *P*-values when comparing 1, 2, or 4 Gy IR relative to 0 Gy for each individual. Data are presented as Mean ± SE. Numbers in parentheses represent the total number of nuclei that were scored at each IR dose. [A]$P < 0.05$, [B]$P < 0.01$, [C]$P < 0.001$, [D]$P < 0.0001$.

the six individuals was averaged, the significant differences between IR exposure doses compared to 0 Gy was absent in all three populations of nuclei (i.e., <2N, 2N, and >2N). However, we believe this is due to the substantial differences observed in the γH2AX baseline levels at 0 Gy between the individuals in this study. Such variation in baseline γH2AX signal in human buccal cells has been observed previously when the γH2AX foci were scored. Indeed, values ranged from 0.08 γH2AX foci/nucleus (24) to 4.08 γH2AX foci/nucleus (34); however, the former study excluded some buccal cell types from their analyses, which may partly explain the differences observed between previous studies. In our study, the LSC protocol was also utilized to extract data on γH2AX integral, MaxPixel and area measurements from within the contoured nuclei. Both γH2AX MaxPixel and area correlated well with the γH2AX integral as expected, since the integral is a

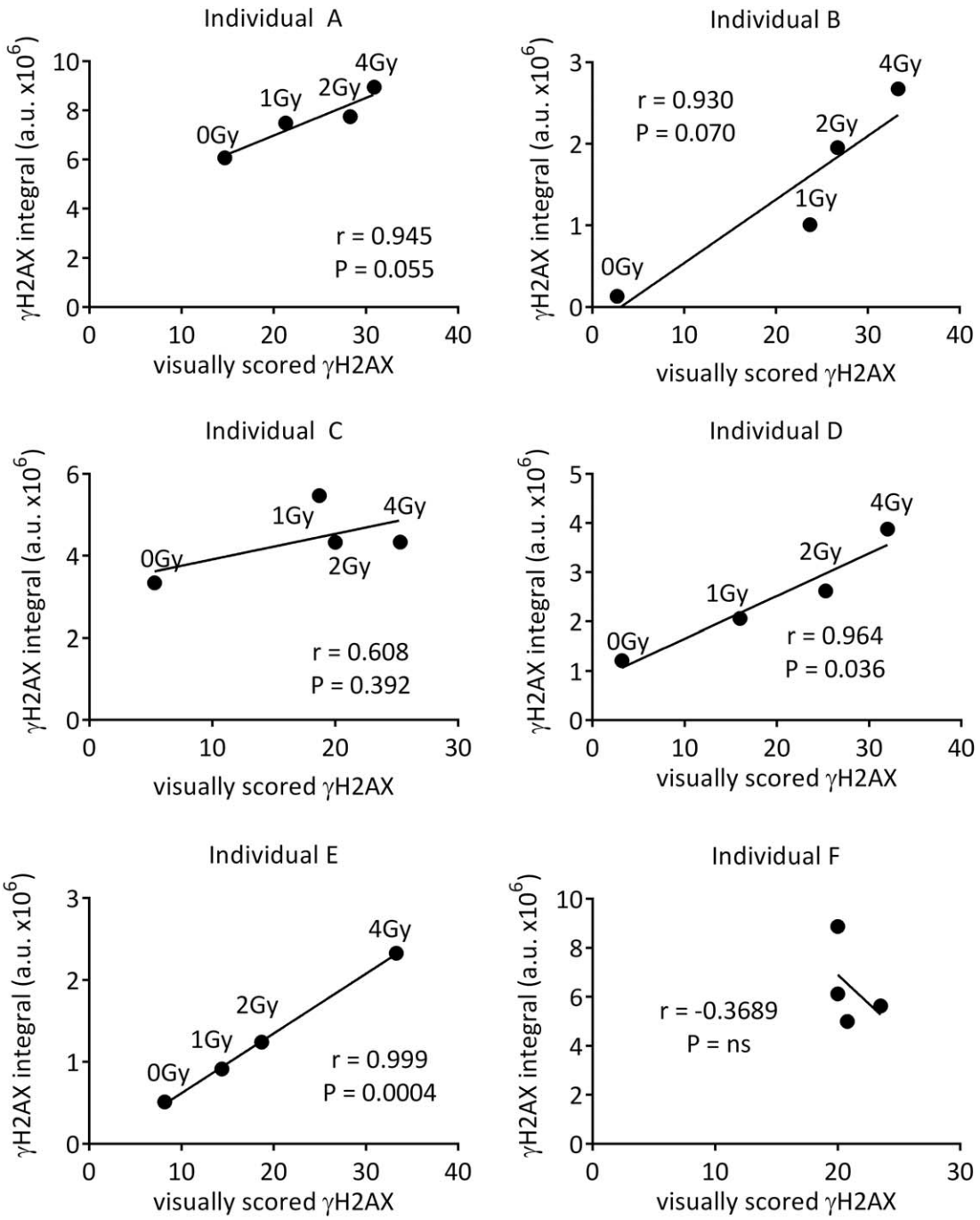

Figure 5. Correlation of visually scored and LSC quantified γH2AX signals in buccal cell nuclei exposed to 0, 1, 2, or 4 Gy IR. The frequency (%) of visually scored buccal nuclei containing 15–30 γH2AX foci are shown on the *x*-axis and the mean γH2AX integrals (by LSC) per 2N nuclei are shown on the *y*-axis for all individuals A–E ($n = 6$). Pearson correlation coefficients (r) and *P*-values are shown as insets within each graph.

function of both γH2AX total intensity and γH2AX area. Furthermore, the increase in γH2AX MaxPixel and area indicates that the abundance of phosphorylated histone H2AX proteins accumulated at sites of DNA breakage, and that the accumulation of γH2AX was dose-dependent and readily quantifiable by LSC. Therefore, these types of quantifiable parameters could prove useful as alternative measures to quantify γH2AX responses within buccal cells that may be achieved with the use of other automated imaging platforms.

Different nuclear shape morphology has been used as one of the criteria to distinguish nuclear abnormalities and has been used in patients with oral squamous cell carcinoma to assess radiosensitivity (29,44). In this study, we assessed the γH2AX MaxPixel response to IR in different shaped buccal

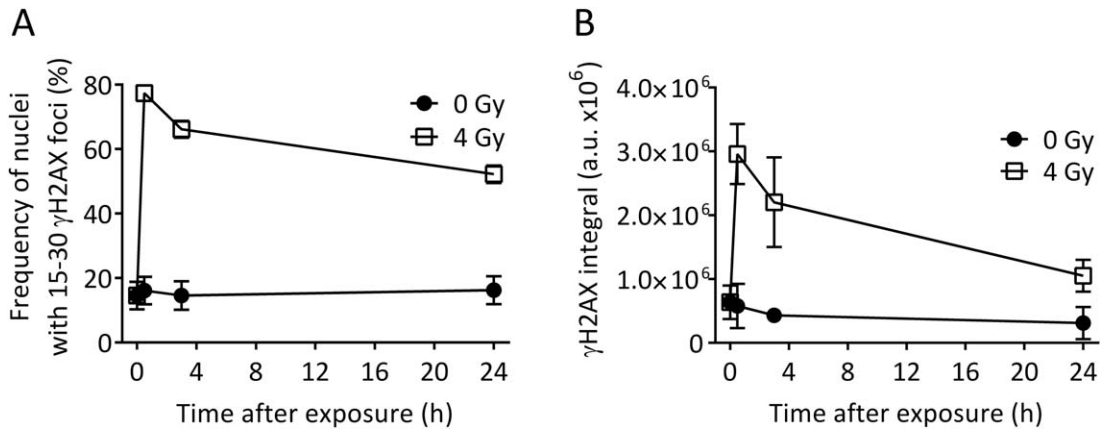

Figure 6. Twenty-four hour kinetics of γH2AX foci in buccal cell nuclei assessed by visual scoring method or LSC. Buccal cells were exposed to 4 Gy IR and then subsequently incubated for 0, 0.5, 3, or 24 h prior to fixation. **A**: The frequency (%) of buccal cell nuclei containing 15–30 γH2AX foci per nucleus was visually scored as described in methods. **B**: γH2AX integral in 2N nuclei was determined by LSC.

cell nuclei (round, long, and oval). Although γH2AX MaxPixel dose-dependently increased there appeared to be no particular nuclear shape that was more responsive than the other. Nuclear shape could be a parameter used in future studies when comparing buccal cell nuclei at "baseline" (e.g., in studies comparing populations or disease states) as it may provide information on long-term (chronic) DNA damage. One advantage of LSC (compared with visual scoring) is that multiple parameters can be examined and quantified in cells (high content) simultaneously which may provide more information on cellular signaling. Ideally, this approach could be combined with cell morphology parameters to accurately identify the buccal cell-subtypes present.

The kinetics of γH2AX response in buccal cells were investigated by measuring DNA damage levels up to 24 h post-IR. LSC and visual scoring demonstrated that γH2AX signals in nuclei peaked at 30 min after exposure to IR, which subsequently declined over a period of 24 h. In some individuals the level of γH2AX remained higher than baseline levels 24 h after exposure, suggesting persistent DNA damage occurred. In a previous study investigating DNA DSBs in buccal cells, the longest time point following IR exposure was 5 h (24). Our study, therefore, demonstrates for the first time that buccal cells express variable but persistent γH2AX responses up to 24 h post-IR. The kinetics of γH2AX can be rapid, with γH2AX declining over a period of hours (14,16–18). Persistence of DNA damage has also been observed in different models. For instance, a recent study that used Göttingen minipig skin biopsies found that IR-induced γH2AX foci was found to be significantly lower after 70 days post-IR exposure; however, a significantly higher number of γH2AX foci still remained in irradiated epidermal keratinocytes compared with controls (19). Most recently, γH2AX formation and removal in heart, brain, and liver tissue following X-ray exposure was tested in adult Syrian hamsters; it was found that all tissues accumulated γH2AX but heart and brain tissues contained more persistent γH2AX 24 h post-IR indicating the presence of unrepaired DNA DSBs. This result suggested that kinetics of IR-induced H2AX phosphorylation (and γH2AX dephosphorylation) is tissue specific, being less efficient in heart and brain in comparison with liver and kidney (45). Since different tissues can have distinct γH2AX responses, it may not be possible to extrapolate buccal cell data generated from our study to investigations carried out on other tissues. Moreover, the high level of γH2AX still present in cells after 24 h suggest that buccal cells may simply not repair DNA damage as efficiently as other cell types. The persistent γH2AX signal after 24 h could be explored for radiation biodosimetry purpose following a radiation accident. However, this may be limited by the large variation in baseline γH2AX signal in cells not exposed to IR between individuals. Understanding the dietary, life-style, genotoxic exposure, and genetic factors is essential prior to considering the possibility of using γH2AX assay in buccal cells for human biodosimetry.

Although a better understanding of the biology of γH2AX response in buccal cells is needed, our findings suggest that buccal mucosa may be a tissue of interest in monitoring radiation exposure in humans or monitoring levels of DNA damage in patients undergoing radiotherapy. Such large-scale monitoring may be made possible with the use of LSC. Indeed, the full automation of this LSC method offers an efficient unbiased and quantifiable measure of γH2AX abundance in a large number of cells (thousands of cells per individual) and should be considered as an alternative method to visual scoring, which is labor-intensive and subject to bias. Additionally, the LSC protocol presented here can combine accurate measurement of γH2AX signal with nuclei ploidy status and by its design, can potentially incorporate the simultaneous measurement of other cellular proteins/markers involved in DNA damage/repair signaling processes.

Literature Cited

1. Dugle DL, Gillespie CJ, Chapman JD. DNA strand breaks, repair, and survival in x-irradiated mammalian cells. Proc Natl Acad Sci USA 1976;73:809–812.
2. Olive PL. The role of DNA single- and double-strand breaks in cell killing by ionizing radiation. Radiat Res 1998;150:S42–S51.

3. Riches LC, Lynch AM, Gooderham NJ. Early events in the mammalian response to DNA double-strand breaks. Mutagenesis 2008;23:331–339.
4. Ismail IH, Wadhra TI, Hammarsten O. An optimized method for detecting gamma-H2AX in blood cells reveals a significant interindividual variation in the gamma-H2AX response among humans. Nucleic Acids Res 2007;35:e36.
5. Tanaka T, Halicka D, Traganos F, Darzynkiewicz Z. Cytometric analysis of DNA damage: Phosphorylation of histone H2AX as a marker of DNA double-strand breaks (DSBs). Methods Mol Biol 2009;523:161–168.
6. Turner SD, Wijnhoven SW, Tinwell H, Lashford LS, Rafferty JA, Ashby J, Vrieling H, Fairbairn LJ. Assays to predict the genotoxicity of the chromosomal mutagen etoposide—Focussing on the best assay. Mutat Res 2001;493:139–147.
7. Pilch DR, Sedelnikova OA, Redon C, Celeste A, Nussenzweig A, Bonner WM. Characteristics of gamma-H2AX foci at DNA double-strand breaks sites. Biochem Cell Biol 2003;81:123–129.
8. Rogakou EP, Nieves-Neira W, Boon C, Pommier Y, Bonner WM. Initiation of DNA fragmentation during apoptosis induces phosphorylation of H2AX histone at serine 139. J Biol Chem 2000;275:9390–9395.
9. Goll MG, Bestor TH. Histone modification and replacement in chromatin activation. Genes Dev 2002;16:1739–1742.
10. Rogakou EP, Boon C, Redon C, Bonner WM. Megabase chromatin domains involved in DNA double-strand breaks in vivo. J Cell Biol 1999;146:905–916.
11. Mendez-Acuna L, Di Tomaso MV, Palitti F, Martinez-Lopez W. Histone post-translational modifications in DNA damage response. Cytogenet Genome Res 2010; 128:28–36.
12. Redon C, Pilch D, Rogakou E, Sedelnikova O, Newrock K, Bonner W. Histone H2A variants H2AX and H2AZ. Curr Opin Genet Dev 2002;12:162–169.
13. Kinner A, Wu W, Staudt C, Iliakis G. Gamma-H2AX in recognition and signaling of DNA double-strand breaks in the context of chromatin. Nucleic Acids Res 2008;36: 5678–5694.
14. Rogakou EP, Pilch DR, Orr AH, Ivanova VS, Bonner WM. DNA double-stranded breaks induce histone H2AX phosphorylation on serine 139. J Biol Chem 1998;273: 5858–5868.
15. Savic V, Yin B, Maas NL, Bredemeyer AL, Carpenter AC, Helmink BA, Yang-Iott KS, Sleckman BP, Bassing CH. Formation of dynamic gamma-H2AX domains along broken DNA strands is distinctly regulated by ATM and MDC1 and dependent upon H2AX densities in chromatin. Mol Cell 2009;34:298–310.
16. Madigan JP, Chotkowski HL, Glaser RL. DNA double-strand break-induced phosphorylation of Drosophila histone variant H2Av helps prevent radiation-induced apoptosis. Nucleic Acids Res 2002;30:3698–3705.
17. Roch-Lefevre S, Mandina T, Voisin P, Gaetan G, Mesa JE, Valente M, Bonnesoeur P, Garcia O, Voisin P, Roy L. Quantification of gamma-H2AX foci in human lymphocytes: A method for biological dosimetry after ionizing radiation exposure. Radiat Res 2010;174:185–194.
18. Olive PL, Banath JP. Phosphorylation of histone H2AX as a measure of radiosensitivity. Int J Radiat Oncol Biol Phys 2004;58:331–335.
19. Ahmed EA, Agay D, Schrock G, Drouet M, Meineke V, Scherthan H. Persistent DNA damage after high dose in vivo gamma exposure of minipig skin. PLoS One 2012;7: e39521.
20. Siddiqui MS, Filomeni E, Francois M, Collins SR, Cooper T, Glatz RV, Taylor PW, Fenech M, Leifert WR. Exposure of insect cells to ionising radiation in vivo induces persistent phosphorylation of a H2AX homologue (H2AvB). Mutagenesis 2013;28: 531–541.
21. Liu SK, Olive PL, Bristow RG. Biomarkers for DNA DSB inhibitors and radiotherapy clinical trials. Cancer Metastasis Rev 2008;27:445–458.
22. Leifert WR, Francois M, Thomas P, Luther E, Holden E, Fenech M. Automation of the buccal micronucleus cytome assay using laser scanning cytometry. Methods Cell Biol 2011;102:321–339.
23. Darzynkiewicz Z, Smolewski P, Holden E, Luther E, Henriksen M, Francois M, Leifert W, Fenech M. Laser scanning cytometry for automation of the micronucleus assay. Mutagenesis 2011;26:153–161.
24. Gonzalez JE, Roch-Lefevre SH, Mandina T, Garcia O, Roy L. Induction of gamma-H2AX foci in human exfoliated buccal cells after in vitro exposure to ionising radiation. Int J Radiat Biol 2010;86:752–759.
25. Yoon AJ, Shen J, Wu HC, Angelopoulos C, Singer SR, Chen R, Santella RM. Expression of activated checkpoint kinase 2 and histone 2AX in exfoliative oral cells after exposure to ionizing radiation. Radiat Res 2009;171:771–775.
26. Thomas P, Holland N, Bolognesi C, Kirsch-Volders M, Bonassi S, Zeiger E, Knasmueller S, Fenech M. Buccal micronucleus cytome assay. Nat Protoc 2009;4: 825–837.
27. Francois M, Leifert W, Hecker J, Faunt J, Martins R, Thomas P, Fenech M. Altered cytological parameters in buccal cells from individuals with mild cognitive impairment and Alzheimer's disease. Cytometry A 2014;85A:698–708.
28. Thomas P, Hecker J, Faunt J, Fenech M. Buccal micronucleus cytome biomarkers may be associated with Alzheimer's disease. Mutagenesis 2007;22:371–379.
29. Torres-Bugarin O, Zavala-Cerna MG, Nava A, Flores-Garcia A, Ramos-Ibarra ML. Potential uses, limitations, and basic procedures of micronuclei and nuclear abnormalities in buccal cells. Dis Markers 2014;2014:956835.
30. Thomas P, Harvey S, Gruner T, Fenech M. The buccal cytome and micronucleus frequency is substantially altered in Down's syndrome and normal ageing compared to young healthy controls. Mutat Res 2008;638:37–47.
31. Patten GS, Leifert WR, Burnard SL, Head RJ, McMurchie EJ. Stimulation of human cheek cell Na+/H+ antiporter activity by saliva and salivary electrolytes: Amplification by nigericin. Mol Cell Biochem 1996;154:133–141.
32. Hosoya A, Lee JM, Cho SW, Kim JY, Shinozaki N, Shibahara T, Shimono M, Jung HS. Morphological evidence of basal keratinocyte migration during the re-epithelialization process. Histochem Cell Biol 2008;130:1165–1175.
33. Lavker RM, Sun TT. Heterogeneity in epidermal basal keratinocytes: morphological and functional correlations. Science 1982;215:1239–1241.
34. Mondal NK, Ghosh S, Ray MR. Micronucleus formation and DNA damage in buccal epithelial cells of Indian street boys addicted to gasp 'Golden glue'. Mutat Res 2011; 721:178–183.
35. Schwartz JL, Muscat JE, Baker V, Larios E, Stephenson GD, Guo W, Xie T, Gu X, Chung FL. Oral cytology assessment by flow cytometry of DNA adducts, aneuploidy, proliferation and apoptosis shows differences between smokers and non-smokers. Oral Oncol 2003;39:842–854.
36. de Oliveira RM, Lia EN, Guimaraes RM, Bocca AL, Cavalcante Neto FF, da Silva TA. Cytologic and cytometric analysis of oral mucosa in Alzheimer's disease. Anal Quant Cytol Histol 2008;30:113–118.
37. Moll R, Franke WW, Schiller DL, Geiger B, Krepler R. The catalog of human cytokeratins: patterns of expression in normal epithelia, tumors and cultured cells. Cell 1982;31:11–24.
38. Vaidya MM, Borges AM, Pradhan SA, Rajpal RM, Bhisey AN. Altered keratin expression in buccal mucosal squamous cell carcinoma. J Oral Pathol Med 1989;18:282–286.
39. Purkis PE, Steel JB, Mackenzie IC, Nathrath WB, Leigh IM, Lane EB. Antibody markers of basal cells in complex epithelia. J Cell Sci 1990;97 (Part 1):39–50.
40. Zhao H, Albino AP, Jorgensen E, Traganos F, Darzynkiewicz Z. DNA damage response induced by tobacco smoke in normal human bronchial epithelial and A549 pulmonary adenocarcinoma cells assessed by laser scanning cytometry. Cytometry A 2009;75A:840–847.
41. Tanaka T, Huang X, Halicka HD, Zhao H, Traganos F, Albino AP, Dai W, Darzynkiewicz Z. Cytometry of ATM activation and histone H2AX phosphorylation to estimate extent of DNA damage induced by exogenous agents. Cytometry A 2007; 71A:648–661.
42. Huang X, Okafuji M, Traganos F, Luther E, Holden E, Darzynkiewicz Z. Assessment of histone H2AX phosphorylation induced by DNA topoisomerase I and II inhibitors topotecan and mitoxantrone and by the DNA cross-linking agent cisplatin. Cytometry A 2004;58A:99–110.
43. Kirsch-Volders M, Fenech M. Inclusion of micronuclei in non-divided mononuclear lymphocytes and necrosis/apoptosis may provide a more comprehensive cytokinesis block micronucleus assay for biomonitoring purposes. Mutagenesis 2001;16:51–58.
44. Raj V, Mahajan S. Dose response relationship of nuclear changes with fractionated radiotherapy in assessing radiosensitivity of oral squamous cell carcinoma. J Clin Exp Dent 2011;3:e193–200.
45. Firsanov D, Vasilishina A, Kropotov A, Mikhailov V. Dynamics of gammaH2AX formation and elimination in mammalian cells after X-irradiation. Biochimie 2012;94: 2416–2422.